

FNP-FSAR-4

4.0 REACTOR

TABLE OF CONTENTS

	<u>Page</u>
4.1 SUMMARY DESCRIPTION	4.1-1
4.2 MECHANICAL DESIGN	4.2-1
4.2.1 Fuel	4.2-2
4.2.1.1 Design Bases	4.2-2
4.2.1.2 Description and Design Drawings	4.2-6
4.2.1.3 Design Evaluation	4.2-16
4.2.1.4 Testing and Inspection Plan	4.2-29
4.2.2 Reactor Vessel Internals	4.2-34
4.2.2.1 Design Bases	4.2-34
4.2.2.2 Description and Drawings	4.2-34
4.2.2.3 Design Loading Conditions	4.2-38
4.2.2.4 Design Loading Categories	4.2-39
4.2.2.5 Design Criteria Basis	4.2-40
4.2.3 Reactivity Control System	4.2-41
4.2.3.1 Design Bases	4.2-41
4.2.3.2 Description and Drawings	4.2-44
4.2.3.3 System Evaluation	4.2-54
4.2.3.4 Testing and Inspection Plan	4.2-63
4.2.3.5 Instrumentation	4.2-65
4.3 NUCLEAR DESIGN	4.3-1
4.3.1 Design Bases	4.3-1
4.3.1.1 Fuel Burnup	4.3-2
4.3.1.2 Negative Reactivity Feedbacks (Reactivity Coefficient)	4.3-2
4.3.1.3 Control of Power Distribution	4.3-3
4.3.1.4 Maximum Controlled Reactivity Insertion Rate	4.3-4
4.3.1.5 Shutdown Margins	4.3-4
4.3.1.6 Stability	4.3-5
4.3.1.7 Anticipated Transients Without Scram (ATWS)	4.3-6
4.3.1.8 Long-Term Shutdown for Large Break LOCA	4.3-6

TABLE OF CONTENTS

	<u>Page</u>
4.3.2 Description	4.3-7
4.3.2.1 Nuclear Design Description	4.3-7
4.3.2.2 Power Distributions	4.3-8
4.3.2.3 Reactivity Coefficients	4.3-19
4.3.2.4 Control Requirements	4.3-23
4.3.2.5 Control	4.3-25
4.3.2.6 Control Rod Patterns and Reactivity Worth	4.3-27
4.3.2.7 Criticality of the Reactor During Refueling	4.3-29
4.3.2.8 Stability	4.3-42
4.3.2.9 Vessel Irradiation	4.3-46
4.3.3 Analytical Methods	4.3-47
4.3.3.1 Fuel Temperature Doppler Calculations.	4.3-47
4.3.3.2 Macroscopic Group Constants	4.3-48
4.3.3.3 Spatial Few-Group Diffusion Calculations	4.3-49
4.4 THERMAL AND HYDRAULIC DESIGN	4.4-1
4.4.1 Design Bases	4.4-1
4.4.1.1 Departure From Nucleate Boiling (DNB) Design Basis	4.4-1
4.4.1.2 Fuel Temperature Design Basis	4.4-3
4.4.1.3 Core Flow Design Basis	4.4-3
4.4.1.4 Hydrodynamic Stability Design Bases	4.4-3
4.4.1.5 Other Considerations	4.4-4
4.4.2 Description	4.4-4
4.4.2.1 Summary Comparison	4.4-4
4.4.2.2 Fuel and Cladding Temperatures (Including Densification)	4.4-4
4.4.2.3 Critical Heat Flux Ratio or Departure from Nucleate Boiling Ratio and Mixing Technology	4.4-7
4.4.2.4 Flux Tilt Considerations	4.4-13
4.4.2.5 Void Fraction Distribution	4.4-13
4.4.2.6 Core Coolant Flow Distribution	4.4-14
4.4.2.7 Core Pressure Drops and Hydraulic Loads	4.4-14
4.4.2.8 Correlation and Physical Data	4.4-15
4.4.2.9 Thermal Effects of Operational Transients	4.4-17
4.4.2.10 Uncertainties in Estimates	4.4-18
4.4.2.11 Plant Configuration Data	4.4-19

TABLE OF CONTENTS

	<u>Page</u>
4.4.3 Evaluation	4.4-20
4.4.3.1 Core Hydraulics	4.4-20
4.4.3.2 Influence of Power Distribution	4.4-22
4.4.3.3 Core Thermal Response	4.4-23
4.4.3.4 Analytical Techniques	4.4-23
4.4.3.5 Hydrodynamic and Flow Power Coupled Instability	4.4-25
4.4.3.6 Temperature Transient Effects Analysis	4.4-27
4.4.3.7 Potentially Damaging Temperature Effects During Transients	4.4-27
4.4.3.8 Energy Release During Fuel Element Burnout	4.4-28
4.4.3.9 Energy Release or Rupture of Water-Logged Fuel Elements	4.4-28
4.4.3.10 Fuel Rod Behavior Effects from Coolant Flow Blockage	4.4-28
4.4.4 Testing and Verification	4.4-30
4.4.4.1 Tests Prior to Initial Criticality	4.4-30
4.4.4.2 Initial Power and Plant Operation	4.4-30
4.4.4.3 Component and Fuel Inspections	4.4-30
4.4.5 Instrumentation Application	4.4-30
4.4.5.1 Incore Instrumentation	4.4-30
4.4.5.2 Overtemperature and Overpower DT Instrumentation	4.4-31
4.4.5.3 Instrumentation to Limit Maximum Power Output.	4.4-31
4.4.5.4 Instrumentation to Measure Reactor Vessel Head Plenum Coolant Temperature	4.4-32
4.4.5.5 Instrumentation to Measure Reactor Coolant Inventory	4.4-32

LIST OF TABLES

4.1-1	Comparison of Design Parameters
4.1-2	Analytic Techniques In Core Design
4.1-3	Design Loading Conditions for Reactor Core Components
4.2-1	Maximum Deflections Specified for Reactor Internal Support Structures
4.3-1	Reactor Core Description
4.3-2	Nuclear Design Parameters (First Cycle)
4.3-3	Reactivity Requirements for Rod Cluster Control Assemblies
4.3-4	Axial Stability Index PWR Core With A 12-Foot Height
4.3-5	Typical Neutron Flux Levels (n/cm ² -s) At Full Power
4.3-6	Comparison of Measured and Calculated Doppler Defects
4.3-7	Benchmark Critical Experiments (25,34,35) LEOPARD Comparison
4.3-8	Saxton Core II Isotopics Rod My+, Axial Zone 6
4.3-9	Critical Boron Concentrations (ppm), HZP, BOL
4.3-10	Comparison of Measured and Calculated Ag-In-Cd Rod Worth
4.3-11	Comparison of Measured and Calculated Moderator Coefficients at HZP, BOL
4.3-12	95/95 K _{eff} for Spent Fuel Rack Storage Configurations
4.3-13	95/95 K _{eff} for Spent Fuel Cask Loading Operations
4.4-1	Thermal and Hydraulic Comparison Table for FNP Units 1 and 2
4.4-2	Void Fractions at Nominal Reactor Conditions
4.4-3	Deleted

LIST OF FIGURES

4.2-1 (sheet 1)	Fuel Assembly Outline 17 x 17 LOPAR
4.2-1 (sheet 2)	Fuel Assembly Cross-Section 17 x 17 VANTAGE 5
4.2-2 (sheet 1)	Pre Unit 2 Cycle 3 and Unit 1 Cycle 6 Fuel Assembly Cross-Section 17 x 17 LOPAR
4.2-2 (sheet 2)	Unit 2 Cycles 3-5, Unit 1 Cycles 6-8 and Assembly Cross-Section 17 x 17 LOPAR
4.2-2 (sheet 3)	Unit 2 Cycle 6, Unit 1 Cycle 9 Fuel Assembly Cross-Section 17 x 17 LOPAR
4.2-2 (sheet 4)	Unit 2 Cycle 7, Unit 1 Cycle 10 Fuel Assembly Cross-Section 17 x 17 LOPAR
4.2-2 (sheet 5)	Unit 2 Cycle 8, Unit 1 Cycle 11 Fuel Assembly Cross-Section 17 x 17 LOPAR
4.2-2 (sheet 6)	Unit 2 Cycle 9, 10, 11, 12, 13, Unit 1 Cycle 12, 13, 14, 15 Fuel Assembly 17 x 17 VANTAGE 5
4.2-2 (sheet 7)	Unit 1 Cycle 16, 17 and Unit 2 Cycle 14 and After Fuel Assembly Outline 17 x 17 VANTAGE w/Protective Grid ZIRLO Fuel Rods
4.2-2 (sheet 8)	Unit 2 Cycle 15 and Unit 1 Cycle 18 and After Fuel Assembly Outline 17 x 17 VANTAGE+ with Low Pressure ZIRLO Fuel Rods and Low force Holddown Spring
4.2-3 (sheet 1)	Pre Unit 2 Cycle 3 and Unit 1 Cycle 6 Fuel Rod Schematic
4.2-3 (sheet 2)	Unit 2 Cycle 3, 4, 5 and Unit 1 Cycle 6, 7, and 8 Fuel Rod Schematic
4.2-3 (sheet 3)	Unit 2 Cycle 6 and Unit 1 Cycle 9 Fuel Rod Schematic
4.2-3 (sheet 4)	Unit 2 Cycle 7, Unit 1 Cycle 10 Fuel Rod Schematic
4.2-3 (sheet 5)	Unit 2 Cycle 8, Unit 1 Cycle 11 Fuel Rod Schematic
4.2-3 (sheet 6)	Unit 2 Cycle 9, 10, 11, 12, 13 and Unit 1 Cycle 12, 13, 14, 15
4.2-3 (sheet 7)	Unit 1 Cycle 16 and Unit 2 Cycle 14 Fuel Rod Schematic
4.2-3 (sheet 8)	Unit 2 Cycle 15 and Unit 1 Cycle 18 and After Fuel Rod Schematic

LIST OF FIGURES

4.2-4	Grid Plan View
4.2-5 (sheet 1)	Pre Unit 2 Cycle 6 and Unit 1 Cycle 9 Top Grid-to-Nozzle Attachment
4.2-5 (sheet 2)	Unit 2 Cycle 6, 7, and 8, Unit 1 Cycle 9, 10, and 11 Top Grid-to-Nozzle Attachment
4.2-5 (sheet 3)	Unit 2 Cycle 9 through 25, Unit 1 Cycle 12 through 28 Top Grid-to-Nozzle Attachment Detail
4.2-5 (sheet 4)	Unit 2 Cycle 26, Unit 1 Cycle 29 and Later Top Grid-to-Nozzle Attachment Detail
4.2-6 (sheet1)	Elevation View, Grid-to-Thimble Attachment for LOPAR Fuel
4.2-6 (sheet 2)	Elevation View, Grid-to-Thimble Attachment
4.2-7	Guide Thimble to Bottom Nozzle Joint
4.2-8	Typical Clad and Pellet Dimensions as a Function of Exposure (Deleted)
4.2-9	Representative Fuel Rod Internal Pressure and Linear Power Density for the Lead Burnup Rod as a Function of Time (Deleted)
4.2-10	Lower Core Support Assembly (Core Barrel Assembly)
4.2-11	Upper Core Support Assembly
4.2-12	Plan View of Upper Core Support Structure
4.2-13	Full-Length Rod Cluster Control and Drive Rod Assembly with Interfacing Components
4.2-14	Full-Length Rod Cluster Control Assembly Outline
4.2-15	Full-Length Absorber Rod
4.2-16 (sheet 1)	Burnable Absorber Assembly (Standard Borosilicate Glass)
4.2-16 (sheet 2)	Unit 1 Cycles 8 and 9, Unit 2 Cycles 6 and 7 Burnable Absorber Assembly (Wet Annular)
4.2-16 (sheet 3)	Unit 1 Cycle 10, Unit 2 Cycle 8 and After Absorber Assembly (Wet Annular)

LIST OF FIGURES

4.2-17 (sheet 1)	Burnable Absorber Rod (Standard Borosilicate Glass)
4.2-17 (sheet 2)	Burnable Absorber Rod (Wet Annular)
4.2-18	Primary Source Assembly
4.2-19A	Secondary Source Assembly for Unit 1 Cycles 1 and 2 Only
4.2-19B	Secondary Source Assembly for Unit 1 Cycles 2 to 12 and Unit 2 Cycles 1 to 9
4.2-19C	Double Encapsulated Secondary Source Assembly for Unit 2 Cycle 9 and After and Unit 1 Cycle 12 and After
4.2-20 (sheet 1)	Thimble Plug Assembly
4.2-20 (sheet 2)	Standardized Thimble Plug Assembly (sheet 2)
4.2-21	Full-Length Control Rod Drive Mechanism
4.2-22	Full-Length Control Rod Drive Mechanism Schematic
4.2-23	Nominal Latch Clearance at Minimum and Maximum Temperature
4.2-24	Control Rod Drive Mechanism Latch Clearance Thermal Effect
4.2-25	Removable Rod Compared to Standard Rod
4.2-26	Removable Fuel Rod Assembly Outline
4.2-27	Location of Removable Rods Within an Assembly
4.2-28	Schematic Representation of Reactor Core Model
4.2-29	Westinghouse Integral Nozzle (WIN)
4.3-1 (sheet 1)	Fuel Loading Arrangement for Initial Core
4.3-1 (sheet 2)	Typical Reload Fuel Loading Arrangement
4.3-2	Production and Consumption of Higher Isotopes
4.3-3	Boron Concentration Versus Cycle Burnup With Burnable Absorbers, Typical

LIST OF FIGURES

4.3-4 (sheet 1)	Typical Discrete Burnable Absorber Rod Arrangements Within an Assembly
4.3-4 (sheet 2)	IFBA Arrangement Within an Assembly
4.3-5	Unit 1 Cycle 1 Burnable Absorber Loading Pattern
4.3-6 (sheet 1)	Unit 2 Cycle 1 Burnable Absorber Loading Pattern
4.3-6 (sheet 2)	Typical Discrete Burnable Absorber Loading Pattern
4.3-6 (sheet 3)	Typical IFBA Loading Pattern
4.3-7 (sheet 1)	Cycle 1 Normalized Power Density Distribution Near Beginning of Life, Unrodded Core, Hot Full Power, No Xenon
4.3-7 (sheet 2)	Typical Reload Normalized Power Density Distribution Near Beginning of Life, Unrodded Core, Hot Full Power, No Xenon
4.3-8 (sheet 1)	Cycle 1 Normalized Power Density Distribution Near Beginning of Life, Unrodded Core, Hot Full Power, Equilibrium Xenon
4.3-8 (sheet 2)	Typical Reload Normalized Power Density Distribution Near Beginning of Life, Unrodded Core, Hot Full Power, Equilibrium Xenon
4.3-9 (sheet 1)	Cycle 1 Normalized Power Density Distribution Near Beginning of Life, Bank D at Insertion Limit, Hot Full Power, Equilibrium Xenon
4.3-9	Typical Reload Normalized Power Density Distribution Near Beginning of Life, Bank D at Insertion Limit, Hot Full Power, Equilibrium Xenon
4.3-10 (sheet 1)	Cycle 1 Normalized Power Density Distribution Near Middle of Life, Unrodded Core, Hot Full Power, Equilibrium Xenon
4.3-10 (sheet 2)	Typical Reload Normalized Power Density Distribution Near Middle of Life, Unrodded Core, Hot Full Power, Equilibrium Xenon
4.3-11 (sheet 1)	Cycle 1 Normalized Power Density Distribution Near End of Life, Unrodded Core, Hot Full Power, Equilibrium Xenon
4.3-11 (sheet 2)	Typical Reload Normalized Power Density Distribution Near End of Life, Unrodded Core, Hot Full Power, Equilibrium Xenon
4.3-12 (sheet 1)	Cycle 1 Rodwise Power Distribution in a Typical Assembly (Assembly G-9) Near Beginning of Life, Hot Full Power, Equilibrium Xenon, Unrodded Core

LIST OF FIGURES

4.3-12 (sheet 2)	Typical Reload Rodwise Power Distribution in a Typical Assembly (Assembly E-10) Near Beginning of Life, Hot Full Power, Equilibrium Xenon, Unrodded Core
4.3-13	Cycle 1 Rodwise Power Distribution in a Typical Assembly (Assembly G-9) Near End of Life, Hot Full Power, Equilibrium Xenon, Unrodded Core
4.3-13	Typical Reload Rodwise Power Distribution in a Typical Assembly (Assembly E-10) Near End of Life, Hot Full Power, Equilibrium Xenon, Unrodded Core
4.3-14	Typical HFP Axial Power Shape Occurring at Beginning of Life
4.3-15	Typical HFP Axial Power Shape Occurring at Middle of Life
4.3-16	Typical HFP Axial Power Shape Occurring at End of Life
4.3-17	Deleted
4.3-18	Flow Chart for Determining Spike Model (Deleted)
4.3-19	Predicted Power Spike Due to Single Nonflattened Gap in the Adjacent Fuel
4.3-20	Power Spike Factor as a Function of Axial Position
4.3-21	Maximum $F_Q X$ Power Versus Axial Height During Normal Operation
4.3-22	Peak Power During Control Rod Malfunction Overpower Transients
4.3-23	Peak Power During Boration/Dilution Overpower Transient
4.3-24	Comparison Between Calculated and Measured Relative Fuel Assembly Power Distribution
4.3-25	Comparison of Calculated and Measured Axial Shape
4.3-26	Measured Values of F_Q for Full Power Rod Configurations
4.3-27	Doppler Temperature Coefficient at BOL and EOL Versus T_{eff} for Cycle 1
4.3-28	Doppler Only Power Coefficient Versus Power Level at BOL and EOL Cycle 1

LIST OF FIGURES

4.3-29	Doppler Only Power Defect Versus Percent Power, BOL and EOL Cycle 1
4.3-30	Moderator Temperature Coefficient, BOL, Cycle 1, No Rods
4.3-31	Moderator Temperature Coefficient, EOL, Cycle 1
4.3-32	Moderator Temperature Coefficient as a Function of Boron Concentration - BOL Cycle 1, No Rods
4.3-33	Hot Full Power Moderator Temperature Coefficient During Cycle 1 for the Critical Boron Concentration
4.3-34	Total Power Coefficient Versus Percent Power for BOL and EOL, Cycle 1
4.3-35	Total Power Defect BOL, EOL, Cycle 1
4.3-36	Rod Cluster Control Assembly Pattern
4.3-37	Accidental Simultaneous Withdrawal of Two Control Banks EOL, HZP Banks D and B Moving in the Same Plane, Typical
4.3-38	Design - Trip Curve
4.3-39	Normalized Rod Worth Versus Rod Insertion All Rods But One
4.3-40	Axial Offset Versus Time, PWR Core With a 12-ft Height and 121 Assemblies
4.3-41	XY Xenon Test Thermocouple Response Quadrant Tilt Difference Versus Time
4.3-42	Calculated and Measured Doppler Defect and Coefficients at BOL Two-Loop Plant, 121 Assemblies, 12-ft Core
4.3-43	Comparison of Calculated and Measured Boron Concentration for 2-Loop Plant, 121 Assemblies, 12-ft Core
4.3-44	Comparison of Calculated and Measured C_B 2-Loop With 121 Assemblies, 12-ft Core
4.3-45	Comparison of Calculated and Measured C_B in 3-Loop Plant, 157 Assemblies, 12-ft Core
4.3-46	DELETED
4.4-1 (sheet 1)	Deleted

LIST OF FIGURES

4.4-1 (sheet 2)	Deleted	
4.4-2 (sheet 1)	Deleted	
4.4-2 (sheet 2)	Deleted	
4.4-3	Deleted	
4.4-4	Deleted	
4.4-5 (sheet 1)	Measured vs. Predicted Critical Heat Flux ABB-NV Correlation	
4.4-5 (sheet 2)	Measured vs. Predicted Critical Heat Flux WLOP Correlation	
4.4-6	TDC Versus Reynolds Number for 26-in. Grid Spacing	
4.4-7	Normalized Radial Flow and Enthalpy Distribution at 4-ft Elevation	
4.4-8	Normalized Radial Flow and Enthalpy Distribution at 8-ft Elevation	
4.4-9	Normalized Radial Flow and Enthalpy Distribution at 12-ft Elevation - Core Exit	
4.4-10	Deleted	
4.4-11	Deleted	
4.4-12	Deleted	
4.4-13	Deleted	
4.4-14	Deleted	
4.4-15	Deleted	
4.4-16	Unit 1 Distribution of Incore Instrumentation	
4.4-17	Unit 2 Distribution of Incore Instrumentation	
4.4-18	Unit 1 Upper Head Thermocouple Schematic	
4.4-19	Unit 1 Upper Head Thermocouple Schematic	
4.4-20	Typical HJTC Probe/Sensor Configuration	

LIST OF FIGURES

4.4-21 Electrical Diagram of HJTC

4.0 - REACTOR

The Farley Nuclear Plant (FNP) described in this report is designed to operate at the NSSS power rating of 2841 MWt with sufficient margins to allow for transient operation and instrument error without causing damage to the core and without exceeding the pressure of the safety valve settings in the coolant system. The core power is 2831 MWt. The 10 MWt difference is the net contribution of heat to the reactor coolant system (RCS) from the reactor coolant pumps and other sources.

This chapter describes the design of the reactor and presents an evaluation of the design. The evaluation demonstrates the capability of the reactor to perform its intended functions without releasing other than minimal amounts of fission products to the coolant. In addition, this chapter provides supporting information for the safety analyses discussed in chapter 15. Analyses have been performed using inputs which are considered to be conservative for the FNP.

4.1 SUMMARY DESCRIPTION

The mechanical components of the reactor described in this chapter include the fuel rods and fuel assemblies, burnable absorber and source rod assemblies, reactor internals, rod cluster control assemblies (RCCA), and the control rod drive mechanisms (CRDM). The nuclear design and thermal hydraulic design are also described.

Reload cases are comprised of 17 x 17 LOPAR, VANTAGE+ and/or VANTAGE 5 fuel assemblies. The original referenced design described herein consisted of LOPAR fuel assemblies arranged in a checkered, low-leakage core loading pattern.

The LOPAR fuel is not analyzed for use at the power uprate. The LOPAR design parameters at 2775 MWt are maintained in Table 4.1-1 for historical purposes.

The significant new mechanical design features of the VANTAGE+/VANTAGE 5 design, as described in reference 1, relative to the LOPAR fuel design include the following: integral fuel burnable absorbers (IFBA), intermediate flow mixer (IFM) grids, reconstitutable top nozzle (RTN), extended burnup capability, and axial blankets. In addition, a debris filter bottom nozzle (DFBN) has been implemented replacing the standard nozzle. The RTN and extended burnup capability were introduced previously in both FNP Units 1 and 2. Fuel reloads subsequent to the implementation of the VANTAGE+/VANTAGE 5 fuel design contain an advanced zirconium alloy clad fuel material known as ZIRLO®, reference 2, and improved design features including: annular blanket pellets, protective bottom grid, longer fuel rod end plugs, and ZIRLO guide thimbles, instrumentation tube mid-grid and IFM grid. Recent fuel reloads contain advanced features such as the Standardized DFBN (SDFBN), the Robust Protective Grid, and the Westinghouse Integral Top Nozzle (WIN), as described herein. Optimized ZIRLO™ clad material (reference 4) has also been approved for use by the NRC (reference 5).

The core is cooled and moderated by light water at a pressure of 2250 psia in the RCS. The moderator coolant contains boron as a neutron absorber. The concentration of boron in the coolant is varied as required to control relatively slow reactivity changes, including the effects of fuel burnup. Additional boron, in the form of burnable absorber (BA) rods and/or IFBAs, is

FNP-FSAR-4

employed to establish the desired reactivity and limit the moderator temperature coefficient and local power peaking that can be achieved. Standard borosilicate glass rods were used in the first cycle. Either the standard burnable absorber, wet annular burnable absorbers (WABAs), and/or IFBAs are used in subsequent reloads.

Two hundred sixty-four fuel rods are mechanically joined in a square array to form a fuel assembly. The fuel rods are supported at intervals along their lengths by grid assemblies which maintain the lateral spacing between the rods throughout the design life of the assembly. The grid assembly consists of an "egg-crate" arrangement of interlocked straps. The grid straps contain spring fingers and dimples for fuel rod support, as well as coolant mixing vanes.

The fuel rods consist of slightly enriched uranium dioxide ceramic cylindrical pellets contained in slightly cold-worked zircaloy-4 tubing which is plugged and seal welded at the ends to encapsulate the fuel. Commencing with Farley Unit 2 Cycle 12 and Unit 1 Cycle 15, the fresh fuel region uses an advanced zirconium alloy tubing known as ZIRLO to provide improved fuel performance, reference 2. Additionally, Optimized ZIRLO is approved for use by the NRC (reference 5). An axial blanket of natural mid-enriched, or fully-enriched solid or annular UO_2 fuel pellets may be placed at the ends of the enriched fuel pellet stack. The natural or mid-enriched axial blanket pellets are used to reduce the neutron leakage and to improve fuel utilization. The annular blanket pellets are used to increase the void volume for gas accommodation within the fuel rod. A second fuel rod type is utilized to varying degrees within some fuel assemblies. These rods use thin boride coated fuel pellets in the central portion of the fuel stack. These are the IFBAs which are described in paragraph 4.2.1.2.1. To increase fatigue life during operation, all fuel rods are pressurized with helium during fabrication to reduce stresses and strains.

A fuel assembly may be reconstituted with limited substitutions of zirconium alloy, zircaloy-4, ZIRLO, or stainless steel filler rods to replace fuel rods, in accordance with the NRC-approved methodology in reference 3.

The center position in a fuel assembly is reserved for the incore instrumentation, while an additional 24 positions in the array are equipped with guide thimbles mechanically attached to the grids and to the top and bottom nozzles. Depending upon the position of the assembly in the core, the guide thimbles are used as core locations for rod cluster control assemblies, neutron source assemblies, and burnable absorber rods. Otherwise, the guide thimbles may be fitted with plugging devices to limit bypass flow.

The bottom nozzle is a box-like structure which serves as a bottom structural element of the fuel assembly and directs the coolant flow distribution to the assembly.

The top nozzle assembly functions as the upper structural element of the fuel assembly, in addition to providing a partially protective housing for the rod cluster control assembly or other components.

The rod cluster control assemblies each consist of a group of individual absorber rods fastened at the top end to a common hub, or spider, assembly. These assemblies contain absorber material to control the reactivity of the core under operating conditions.

FNP-FSAR-4

The control rod drive mechanisms for the rod cluster control assemblies are of the magnetic latch type. The latches are controlled by three magnetic coils. They are so designed that, upon a loss of power to the coils, the rod cluster control assembly is released and falls by gravity to shut down the reactor.

The components of the reactor internals are divided into three parts, consisting of the lower core support structure (including the entire core barrel and neutron shield pad assembly), the upper core support structure, and the incore instrumentation support structure. The reactor internals support the core, maintain fuel alignment, limit fuel assembly movement, maintain alignment between fuel assemblies and control rod drive mechanisms, direct coolant flow past the fuel elements and to the pressure vessel head, provide gamma and neutron shielding, and provide guides for the incore instrumentation.

The nuclear design analyses and evaluations establish physical locations for control rods and burnable absorbers, and establish physical parameters for factors such as fuel enrichments and boron concentrations in the coolant. Using the values obtained through these calculations, the reactor core is given inherent characteristics which, in combination with corrective actions of the reactor's control, protective, and emergency cooling systems, provide adequate reactivity control even if the highest reactivity-worth rod cluster control assembly is stuck in the fully withdrawn position.

The thermal hydraulic design analyses and evaluations establish coolant flow parameters which assure that adequate heat transfer takes place between the fuel cladding and the reactor coolant. The thermal design takes into account local variations in fuel rod dimensions, power generation, flow distribution, and mixing. The mixing vanes incorporated into the fuel assembly spacer grid design and the VANTAGE+/VANTAGE 5 fuel assembly IFMs induce additional flow mixing between the various flow channels within a fuel assembly, as well as between adjacent assemblies.

Instrumentation is provided in and out of the core to monitor the nuclear, thermal hydraulic, and mechanical performance of the reactor and to provide inputs to automatic control functions.

The reactor core design (mechanical, nuclear, and thermal hydraulics) together with corrective actions of the reactor control, protection, and emergency cooling systems can meet the reactor performance and safety criteria specified in section 4.2.

The analysis techniques employed in the core design are tabulated in table 4.1-2. The loading conditions considered in general for the core internals and components are tabulated in table 4.1-3. Specific, or limiting, loads of the various components, as considered for design purposes, are listed as follows: fuel assemblies in paragraph 4.2.1.1.2; reactor internals in paragraph 4.2.2.3 and table 5.2-2; neutron absorber rods, burnable absorber rods, neutron source rods and thimble plug assemblies in paragraph 4.2.3.1.3; and full-length control rod drive mechanisms in paragraph 4.2.3.1.4. The dynamic analyses, input forcing functions, and response loadings are presented in section 3.9.

REFERENCES

1. Davidson, S. L. and Kramer, W. R., eds., "Reference Core Report VANTAGE 5 Fuel Assembly," WCAP-10445-NP-A, September 1985.
2. Davidson, S. L., Nuhfer, D. L., eds., "VANTAGE+ Fuel Assembly Reference Core Report," WCAP-12610-P-A and Appendices A through D, June 1990.
3. Slagle, W. H. (ed.), "Westinghouse Fuel Assembly Reconstitution Evaluation Methodology," WCAP-13060-P-A, July 1993.
4. Shah, H., "Optimized ZIRLO™," WCAP-12610-P-A & CENPD-404-P-A Addendum 1-A, July 2006.
5. USNRC Letter to C. R. Pierce, "Joseph M. Farley Nuclear Plant, Units 1 and 2, and Vogtle Electric Generating Plant, Units 1 and 2 - Issuance of Amendments Regarding Use of Optimized ZIRLO™", August 4, 2016 (ML16179A386).
6. O. Linsuain, et al., "Westinghouse Performance Analysis and Design Model (PAD5)," WCAP-17642-P-A, Revision 1, November 2017.

FNP-FSAR-4

TABLE 4.1-1 (SHEET 1 OF 4)
COMPARISON OF DESIGN PARAMETERS

	<u>LOPAR^(e)</u>	<u>VANTAGE 5+/ VANTAGE 5</u>	
THERMAL AND HYDRAULIC DESIGN PARAMETERS			
Reactor core heat output (MWt)	2775	2821	
Total core heat output (Btu/h)	9469 x 10 ⁶	9626 x 10 ⁶	
Heat generated in fuel (%)	97.4	97.4	
System pressure, nominal (psia)	2250	2250	
System pressure, min. steady-state (psia)	2200	2200	
Minimum DNBR for design transients - Thimble	1.24	1.24	
- Typical	1.25	1.24	
<u>Coolant Flow</u>			
Total flowrate, (lb/h)	99.4 - 98.1 x 10 ⁶	99.5 - 98.2 x 10 ⁶	
Effective flow area for heat transfer (ft ²)	41.55	44.04	
Effective flowrate for heat transfer (lb/h)	92.3 - 91.1 x 10 ⁶	92.5 - 91.2 x 10 ⁶	
Average velocity along fuel rods (ft/s)	13.5	12.8	
Average mass velocity (lb/h-ft ²)	2.22 - 2.19 x 10 ⁶	2.10 - 2.07 x 10 ⁶	
<u>Coolant Temperatures (°F) at 100% Power</u>			
Reactor inlet temperature	530.6 - 541.1	530.0 - 541.5	
Average rise in vessel	73.2 - 72.2	74.4 - 73.4	
Average rise in core	78.2 - 77.0	79.4 - 78.3	
Average in core	571.7 - 581.8	571.8 - 582.0	
Average in vessel	567.2 - 577.2	567.2 - 577.2	
<u>Heat Transfer at 100% Power</u>			
Active heat transfer surface area (ft ²)	48,598	46,779	
Average heat flux (Btu/h-ft ²)	189,820	200,426	
Maximum heat flux (Btu/h-ft ²) (normal operation)	440,380	501.065	
Average thermal output (kW/ft)	5.45	5.54	
Maximum thermal output (kW/ft)	12.63	13.85	
Peak linear power for determination of protection setpoints (kW/ft)	22.4	^(f)	
Heat flux hot channel factor (F _Q)	2.32	2.50 ^(b)	

FNP-FSAR-4

TABLE 4.1-1 (SHEET 2 OF 4)

	<u>LOPAR^(e)</u>	<u>VANTAGE 5+/ VANTAGE 5</u>	
<u>Fuel Centerline Temperature</u>			
Maximum at 100% power (°F)	3039	(f)	
Maximum at peak linear power for determination of protection setpoints (°F)	4700	(f)	
<u>17 x 17 Fuel Assembly</u>			
CORE MECHANICAL DESIGN PARAMETERS			
<u>Fuel Assemblies</u>			
Design	RCC Canless		
Rod pitch (in.)	0.496		
Overall dimensions (in.)	8.426 x 8.426		
Number of grids per assembly	LOPAR: 8-R type ^(e)		
	VANTAGE 5: 2-non-mixing vane type		
	6-mixing vane type		
	3-IFM		
	1-Protective grid		
<u>Fuel Rods</u>			
Number	41,448		
Outside diameter (in.)	LOPAR: 0.374 ^(e)		
	VANTAGE5+/VANTAGE 5: 0.360		
Diametral gap (in.)	LOPAR: 0.0065 ^(e)		
	VANTAGE5+/VANTAGE 5: 0.0062		
Clad thickness (in.)	0.0225		
Clad material	LOPAR: Zircaloy-4 ^(e)		
	VANTAGE5+/VANTAGE 5: Zircaloy-4, ZIRLO, or Optimized ZIRLO		
<u>Fuel Pellets</u>			
Material	UO ₂ sintered		
Density (percent of theoretical)	95		
Length (in.) - enriched fuel	LOPAR: 0.387 ^{(d)(e)}		
	VANTAGE5+/VANTAGE 5: 0.370/0.462 or 0.500 (blanket pellet)		
Diameter (in.)	LOPAR: 0.3225 ^(e)		
	VANTAGE5+/VANTAGE 5: 0.3088 (non-IFBA)		

FNP-FSAR-4

TABLE 4.1-1 (SHEET 3 OF 4)

17 x 17 Fuel Assembly

Rod Cluster Control Assemblies

Material	Ag-In-Cd
Number of RCC Assemblies (full-length)	48
Number of absorber rods per RCC assembly	24
Clad material	Type 304
	SS: cold-worked
Clad thickness (in.)	0.0185

Core Structure

Core barrel I.D./O.D. (in.)	133.85/137.875
Thermal shield	Neutron pads

NUCLEAR DESIGN DATA

Structure Characteristics

Fuel weight (as UO ₂)(lb) ^(c)	LOPAR: 181,205 ^(e)
	VANTAGE 5+/VANTAGE 5: 166,111
Zircaloy-4, ZIRLO, or Optimized ZIRLO weight (lb) (active fuel)	LOPAR: 41,416 ^(e)
	VANTAGE 5+/VANTAGE 5: 37,350
Core diameter (in.) (equiv.)	119.7
Core height (in.) (active fuel)	143.7
Number of fuel assemblies	157
UO ₂ rods per assembly	264

[HISTORICAL]

[Performance Characteristics, First Cycle]

<i>Loading technique</i>	<i>3 region</i>
	<i>Nonuniform</i>

Feed Enrichments, wt/%, First Cycle

<i>Region 1</i>	<i>2.10</i>
<i>Region 2</i>	<i>2.60</i>
<i>Region 3</i>	<i>3.10]</i>

FNP-FSAR-4

TABLE 4.1-1 (SHEET 4 OF 4)

17 x 17 Fuel Assembly

Reflector Thickness and Composition

Top - water plus steel (in.)	~10
Bottom - water plus steel (in.)	~10
Side - water plus steel (in.)	~15
H ₂ O/U, cold molecular ratio lattice	LOPAR: 2.41 ^(e) VANTAGE 5+/VANTAGE 5: 2.73

- a. This limit is associated with the value of $F_Q = 2.32$ for LOPAR fuel and $F_Q = 2.50$ for VANTAGE 5+/VANTAGE 5 fuel.
- b. See paragraph 4.3.2.2.6.
- c. Values are without fuel pellet chamfer. The chamfered pellet increases the fuel weight less than 1 percent. The decrease in fuel weight due to annular pellets is not considered.
- d. Farley 1 cycle 9 and Farley 2 cycle 7 and following. Pellet length prior to Farley 1 cycle 9 and Farley 2 cycle 7 is 0.530 in.
- e. LOPAR fuel is not analyzed for the power uprate. The LOPAR values are retained for historical purposes.
- f. Fuel centerline temperatures and power to melt limits are calculated based on methods and fuel melt limits defined in Reference 6.

FNP-FSAR-4

TABLE 4.1-2 (SHEET 1 OF 2)

<u>Analysis</u>	<u>Technique</u>	<u>Computer Code</u>	<u>Subsection Referenced</u>
Mechanical Design of Core Components			
Loads, deflections, and stress analysis	Static and dynamic modeling	Blowdown code, FORCE, finite element structural analysis code, and others	3.7.2.1 3.9.1 3.9.3
Fuel Rod Design			
Fuel performance characteristics (temperature, internal pressure, clad stress, etc.)	Semiempirical thermal model of fuel with consideration of fuel density changes, heat transfer, fission gas release, etc.	Westinghouse fuel rod design model	4.2.1.3.1 4.3.3.1 4.4.2.2 4.4.3.4.2
Nuclear Design			
Cross-sections and group constants	Microscopic data Macroscopic constants for homogenized core regions	Modified ENDF/B (library) LEOPARD/CINDER type or PHOENIX-P or NEXUS/PARAGON	4.3.3.2 4.3.3.2 4.3.2.7
	Group constants for control rods with self-shielding	HAMMER-AIM or PHOENIX-P or NEXUS/PARAGON	4.3.3.2
X-Y and X-Y-Z power distributions, fuel depletion, critical boron concentrations, x-y and x-y-z xenon distributions, reactivity coefficients	2-group diffusion theory	TURTLE (2-D) or ANC (2-D or 3-D)	4.3.3.3 4.3.3.3
Axial power distributions, control rod worths, and axial xenon distribution	1-D, 2-group diffusion theory, 2-group nodal theory	APOLLO	4.3.3.3
Fuel rod power	Integral transport theory	LASER	4.3.3.1
Effective resonance temperature	Monte Carlo weighting function	REPAD	

FNP-FSAR-4

TABLE 4.1-2 (SHEET 2 OF 2)

<u>Analysis</u>	<u>Technique</u>	<u>Computer Code</u>	<u>Subsection Referenced</u>
Thermal-Hydraulic Design			
Steady state	Subchannel analysis of local fluid conditions in rod bundles, including inertial cross-flow resistance terms	VIPRE-01*	4.4.3.4.1
Transient DNB analysis	Subchannel analysis of local fluid conditions in rod bundles during transients by including accumulation terms in conservation equations. The solution is based on a one-pass model which simulates the core and hot channels	VIPRE-01*	4.4.3.4.1

TABLE 4.1-3

DESIGN LOADING CONDITIONS FOR REACTOR CORE COMPONENTS

1. Fuel assembly weight
2. Fuel assembly spring forces
3. Internals weight
4. Control rod scram (equivalent static load)
5. Differential pressure
6. Spring preloads
7. Coolant flow forces (static)
8. Temperature gradients
9. Differences in thermal expansion
 - a. Because of temperature differences
 - b. Because of expansion of different materials
10. Interference between components
11. Vibration (mechanically or hydraulically induced)
12. One or more loops out of service
13. All operational transients listed in table 5.2-2
14. Pump overspeed
15. Seismic loads (operation basis earthquake and design basis earthquake)
16. Blowdown forces (due to cold and hot leg break)

4.2 **MECHANICAL DESIGN**

The plant conditions for design are divided into four categories according to their anticipated frequency of occurrence and risk to the public. The categories are as follows: Condition I - Normal Operation; Condition II -Incidents of Moderate Frequency; Condition III – Infrequent Incidents; Condition IV - Limiting Faults.

Chapter 15 describes bases and plant operation and events involving each condition.

The reactor is designed so that its components meet the following performance and safety criteria:

- A. The mechanical design of the reactor core components and their physical arrangement, together with corrective actions of the reactor control protection and emergency cooling systems (when applicable), ensure that:
 - 1. Fuel damage^(a) is not expected during Condition I and Condition II events. Although it is not possible to preclude a very small number of rod failures, these are within the capability of the plant cleanup system and are consistent with the plant design bases.
 - 2. The reactor can be brought to a safe state following a Condition III event with only a small fraction of fuel rods damaged.^(a) The fraction of fuel rods damaged must be limited to meet the dose guidelines of 10 CFR 100, although sufficient fuel damage might occur to preclude immediate resumption of operation.
 - 3. The reactor can be brought to a safe state and the core can be kept subcritical with acceptable heat transfer geometry following transients arising from Condition IV events.
- B. The fuel assemblies are designed to accommodate expected conditions for handling during assembly inspection and refueling operations and shipping loads.
- C. The fuel assemblies are designed to accept control rod insertions in order to provide the required reactivity control for power operations and reactivity shutdown conditions.
- D. All fuel assemblies have provisions for the insertion of incore instrumentation necessary for plant operation.

a. Fuel damage as used here is defined as penetration of the fission product barrier; i.e., the fuel rod clad.

- E. The reactor internals, in conjunction with the fuel assemblies, direct reactor coolant through the core to achieve acceptable flow distribution and to restrict bypass flow so that the heat transfer performance requirements can be met for all modes of operation. In addition, the internals provide core support and distribute coolant flow to the pressure vessel head so that the temperature differences between the vessel flange and head do not result in leakage from the flange during the Condition I and II modes of operation. Inservice inspection can be carried out as required because the internals are removable and provide access to the inside of the pressure vessel.
- F. Consistent with the growth in technology, Westinghouse modified and licensed fuel system advanced designs. These modifications utilized NRC-approved methods. Fuel design criteria to be satisfied by these advanced fuel designs were issued to the NRC in reference 28, and are also presented below in section 4.2.1.1.1.

4.2.1 FUEL

4.2.1.1 Design Bases

The fuel rod and fuel assembly design bases are established to satisfy the general performance and safety criteria presented in section 4.2 and specific criteria noted below. The fuel rods are designed for extended burnup as described in the Extended Burnup Evaluation Report (references 15 and 28).

4.2.1.1.1 Fuel Rods

The integrity of the fuel rods is ensured by proper fuel rod design. This is achieved by designing the fuel rods so that specific design criteria are satisfied. The design process must consider the effects of variations and fluctuations in core and local power, and in reactor coolant temperature, pressure, and flow which occur during normal operation and anticipated operational occurrences (AOOs).

To ensure reliable operation, established fuel rod design criteria must be satisfied for all operating conditions consistent with normal operation and AOOs. The fuel rod design is judged to have met these criteria when it is demonstrated that the performance of a fuel region is within the limits specified by the criteria for these events. This is generally accomplished by demonstrating that the limiting fuel rod performance with appropriate allowance for uncertainties is within the limits specified by each criterion. These evaluations are performed using the Performance Analysis and Design (PAD5) code and models (reference 28).

- Clad Stress
 - Design Basis - The fuel system will not be damaged due to excessive fuel clad stress.
 - Acceptance Limit - Maximum cladding stress intensities excluding pellet-cladding interaction (PCI) induced stress shall be evaluated based on American Society of Mechanical Engineers (ASME) Boiler and Pressure Vessel Code

guidelines. Stresses in the cladding are combined to calculate a maximum stress intensity which is then compared to the criteria described in reference 28.

- Clad Strain
 - Design Basis - The fuel rod will not fail due to excessive fuel clad strain.
 - Acceptance Limit - The design limit for the fuel rod clad strain is that the total tensile strain, elastic plus plastic, due to uniform cylindrical fuel pellet deformation during any single Condition I or II transient shall be less than 1% from the pre- transient value.
- Rod Internal Pressure
 - Design Basis - The fuel system will not be damaged due to excessive fuel rod internal pressure.
 - Acceptance Limit - The internal pressure of the lead fuel rod in the reactor will (1) be limited to a value below that which could cause the diametral gap to increase (cladding liftoff) due to outward cladding creep during normal operation; (2) be limited to a value below that which could result in cladding hydride reorientation in the radial direction; and (3) be limited to preclude extensive departure from nucleate boiling (DNB) propagation.
- Clad Fatigue
 - Design Basis - The fuel system will not be damaged due to fatigue.
 - Acceptance Limit - The fatigue life usage factor is limited to prevent reaching the material fatigue limit.
- Clad Oxidation
 - Design Basis - The fuel system will not be damaged due to excessive fuel clad oxidation.
 - Acceptance Limit - The predicted oxide thickness shall be no greater than 100 microns.
- Clad Hydrogen Pickup
 - Design Basis - The fuel system will be operated to prevent significant degradation of mechanical properties of the clad at low temperatures as a result of hydrogen embrittlement caused by the formation of zirconium hydride platelets.
 - Acceptance Limit - The best estimate hydrogen pickup in the cladding shall not exceed 600 ppm on a volume-average basis at end of life through the entire clad wall.
- Fuel Rod Axial Growth
 - Design Basis - The fuel system will not be damaged due to excessive axial interference between the fuel rods and the fuel assembly structure.
 - Acceptance Limit - The fuel rods shall be designed with adequate clearance between the fuel rod and the top and bottom nozzles to accommodate the differences in the growth of fuel rods and the growth of the assembly without interference.
- Clad Flattening
 - Design Basis - Fuel rod failures will not occur due to clad flattening.
 - Acceptance Limit - The fuel rod design shall preclude clad flattening during projected exposure.
- Clad Free Standing
 - Design Basis - The fuel system will not be damaged due to excessive fuel clad

- stress.
 - Acceptance Limit - The cladding shall be short-term free standing at beginning of life, at power, and during hot hydrostatic testing.
- Fuel Pellet Overheating (Power-to-Melt)
 - Design Basis - The fuel rods will not fail due to fuel centerline melting for normal operation or AOOs.
 - Acceptance Limit - The fuel rod centerline temperature shall not exceed the fuel melt temperature during Condition I and II operation, accounting for degradation of the melt temperature due to burnup and the addition of integral burnable absorbers.
- Pellet/Clad interaction (PCI)
 - Design Basis - The fuel rod will not fail due to pellet clad interaction.
 - Acceptance Limit – The NRC SRP does not require a specific design criterion for PCI. Two related criteria, the one percent clad strain criterion and the fuel overheating (no centerline fuel melt) criterion, must be met.

Reference 28 is the basis for performing these fuel performance criteria, which are evaluated on a cycle-specific basis as part of each fuel reload.

The detailed fuel rod design establishes such parameters as pellet size and density, clad/pellet diametral gap, gas plenum size, and helium prepressure. The design considers both Condition I and II modes of operation and accounts for effects such as fuel density changes (including swelling), fission gas release, clad creep, and other physical properties which vary with burnup and temperature as described in references 18, 20, 24, and 28. As part of the measurement uncertainty recapture (MUR) program, the NRC approved fuel performance model, PAD 5 (reference 28) is acceptable for use with fuel rod design reload criterion and supporting input to the non-LOCA analyses. Fuel performance evaluations at extended burnups will identify any cycle-specific safety issues with operation to the burnup values given in reference 15.

Fuel experience and testing results, as they become available, are used to improve fuel rod design and manufacturing processes and to assure that the design bases and safety criteria are satisfied.

4.2.1.1.2 Fuel Assembly Structure

Structural integrity of the fuel assemblies is assured by setting limits on stresses and deformations caused by various loads and by determining that the assemblies do not interfere with the functioning of other components. Three types of loads are considered.

- A. Nonoperational loads, such as those caused by shipping and handling.
- B. Normal and abnormal loads which are defined for Conditions I and II.
- C. Abnormal loads which are defined for Conditions III and IV.

FNP-FSAR-4

These criteria are applied to the design and evaluation of the top and bottom nozzles, the guide thimbles, the grids, and the thimble joints.

The design bases for evaluating the structural integrity of the fuel assemblies are as follows:

- A. Nonoperational - 4 g axial and 6 g lateral loading with dimensional stability.⁽¹⁶⁾
- B. Normal Operation (Condition I) and Incidents of Moderate Frequency (Condition II).

For the normal operating (Condition I) and upset (Condition II) conditions, the fuel assembly component structural design criteria are classified into two material categories: austenitic steels and zircaloy or ZIRLO. The stress categories and strength theory presented in the ASME Boiler and Pressure Vessel Code, Section III, are used as general guides. The maximum shear theory (Tresca criterion) for combined stresses is used to determine the stress intensities for the austenitic steel components. The stress intensity is defined as the numerically largest difference between the various principal stresses in a three-dimensional field. The allowable stress intensity value for austenitic steels, such as nickel chromium iron alloys, is given by the lower of the following:

1. One-third of the specified minimum tensile strength or two-thirds of the specified minimum yield strength at room temperature.
2. One-third of the tensile strength or 90 percent of the yield strength at room temperature, but not to exceed two-thirds of the specified minimum yield strength at room temperature.

The stress limits for the austenitic steel components are given below. All stress nomenclature is per the ASME Code, Section III.

Stress Intensity Limits

<u>Categories</u>	<u>Limits</u>
General primary membrane stress intensity	Sm
Local primary membrane stress intensity	1.5 Sm
Primary membrane plus bending stress intensity	1.5 Sm
Total primary plus secondary stress intensity	3.0 Sm

The zircaloy/ ZIRLO structural components which consist of guide thimble and fuel tubes are in turn subdivided into two categories because of material differences and functional requirements. Note that zircaloy/ ZIRLO structural components also include the mid grids, which are discussed in paragraph 4.2.1.2.1. The fuel tube design criteria are covered separately in paragraph 4.2.1.3.1. The maximum

shear theory is used to evaluate the guide thimble design. The zircaloy/ZIRLO unirradiated properties are used to define the stress limits.

- C. Abnormal loads during Conditions III or IV-worst cases represented by combined seismic and blowdown loads.
 - 1. Deflections of components cannot interfere with the reactor shutdown or emergency cooling of the fuel rods.
 - 2. The fuel assembly structural component stresses under faulted conditions are evaluated using primarily the methods outlined in Appendix F of the ASME Pressure Vessel Code, Section 3. Since the current analytical methods utilize elastic analysis, the stress allowables are defined as the smaller value of 2.4 Sm or 70 Su for primary membrane and 3.6 Sm or 1.05 Su for primary membrane plus primary bending. For the austenitic steel fuel assembly components, the stress intensity is defined in accordance with the rules described in the previous section for normal operating conditions. For the zircaloy/ ZIRLO components the stress limits are set at two-thirds of the material yield strength, S_y , at reactor operating temperature. This results in zircaloy/ ZIRLO stress intensity limits being the smaller of 1.6 S_y or .70 Su for primary membrane and 2.4 S_y or 1.05 Su for primary membrane plus bending. For conservative purposes, the zircaloy/ ZIRLO unirradiated properties are used to define the stress limits. The grid component strength criteria are based on experimental tests. The limit is established at 0.9 P_c , where P_c is the experimental collapse load.

4.2.1.2 Description and Design Drawings

The fuel assembly and fuel rod design data are given in Table 4.3-1.

The VANTAGE 5 fuel assembly has the same cross-sectional envelope as the LOPAR fuel assembly. The VANTAGE 5 fuel assembly has the same overall length as the current LOPAR assembly design for both units. Note that earlier LOPAR assemblies had other lengths. See figure 4.2-2 for the various lengths. The grid centerline elevations of the VANTAGE 5 (except for the intermediate flow mixer (IFM) grids) are essentially identical to those of the region 10/cycle 8 LOPAR assembly for Unit 2 and region 13/cycle 11 LOPAR assembly for Unit 1. Furthermore, by matching grid elevations, any crossflow maldistribution between the LOPAR and VANTAGE 5 fuel assemblies is minimized. The effect of the zircaloy IFM grids and inconel grid elevation differences on hydraulic compatibility has been addressed and found to be acceptable.

Commencing with Region 15 in Unit 2 Cycle 13 and Region 18 in Unit 1 Cycle 16, the fuel assembly skeleton includes ZIRLO fabricated guide thimble tubes, instrumentation tubes, IFM grids, and mid-grids. The ZIRLO guide thimble tube and instrumentation tube lengths have been reduced, resulting in a slightly shorter overall fuel assembly height to allow for additional growth at high burnup. The top nozzle hold-down spring design for the shorter ZIRLO fuel assembly was maintained the same as the current top nozzle hold-down spring design on the

FNP-FSAR-4

fuel assemblies with zircaloy-4 guide tubes. This change reduces the hold-down spring force margin; however, the design still meets all current design criteria. The top Inconel grid was lowered by 0.2 inch because of the shorter overall height of the ZIRLO skeleton.

The ZIRLO mid-grid and IFM grid designs are identical to the previous zircaloy-4 designs except that the ZIRLO grid sleeves are 0.1 inch shorter than the zircaloy-4 grid sleeves. The shorter sleeves are for the purpose of identification during fuel fabrication and have a negligible effect on the thermal/hydraulic performance of the grids. The bulge locations for the grid-to-thimble attachment are unchanged for the ZIRLO grids. The mechanical performance of the ZIRLO grids and the fuel assembly remains the same as for the previous zircaloy-4 grid designs.

Commencing with Region 17 in Unit 2 Cycle 15 and Region 20 in Unit 1 Cycle 18, the length of the ZIRLO fuel assembly skeleton has been restored to the same length as the VANTAGE 5 design with the zircaloy-4 skeleton. The increased length for the ZIRLO fuel assembly skeleton is based on the current NRC-approved growth model for ZIRLO. The top Inconel grid for the longer ZIRLO skeleton design has been returned to the same elevation as in the VANTAGE 5 design with the zircaloy-4 skeleton. The top nozzle holddown spring on the longer ZIRLO fuel assembly has been reduced in height to maintain the assembly holddown force at approximately the current level. All design criteria regarding the fuel assembly holddown springs continue to be met for the reduced height holddown spring design.

Two hundred sixty-four fuel rods, 24 guide thimble tubes, and one instrumentation thimble tube are arranged within a supporting structure to form a fuel assembly. The instrumentation thimble is located in the center position and provides a channel for insertion of an incore neutron detector if the fuel assembly is located in an instrumented core position. The guide thimbles provide channels for insertion of either a rod cluster control assembly (RCCA), a neutron source assembly, a burnable absorber assembly, or a plugging device, depending on the position of the particular fuel assembly in the core. Figure 4.2-1 shows a cross-section of the fuel assembly array, and figure 4.2-2 shows fuel assembly full-length views for feed fuel in each cycle. The fuel rods are loaded into the fuel assembly structure so that there is clearance between the fuel rod ends and the top and bottom nozzles. All fuel assemblies in the core are similar in mechanical construction.

A fuel assembly may be reconstituted with limited substitutions of zirconium alloy, zircaloy-4, ZIRLO, or stainless steel filler rods to replace fuel rods, in accordance with the NRC-approved methodology in reference 25.

Each fuel assembly is installed vertically in the reactor vessel and stands upright on the lower core plate, which is fitted with alignment pins to locate and orient the assembly. After all fuel assemblies are set in place, the upper support structure is installed. Alignment pins built into the upper core plate engage and locate the upper ends of the fuel assemblies. The upper core plate then bears downward against the fuel assembly top nozzle via the holddown springs to hold the fuel assemblies in place.

Improper orientation of fuel assemblies within the core is prevented by the use of an indexing hole in one corner of the top nozzle top plate. The assembly is oriented with respect to the handling tool and the core by means of a pin inserted into this indexing hole. Visual

confirmation of proper orientation is also provided by an engraved identification number on the opposite corner clamp.

4.2.1.2.1 Fuel Rods

The fuel rods consist of uranium dioxide ceramic pellets contained in slightly cold-worked zircaloy-4, ZIRLO, or Optimized ZIRLO tubing which is plugged and seal welded at the ends to encapsulate the fuel. Schematics of the fuel rods are shown in figure 4.2-3 for feed fuel in each cycle. The fuel pellets are right circular cylinders consisting of slightly enriched uranium dioxide powder which has been compacted by cold pressing and then sintered to the required density. The ends of each pellet are dished slightly to allow greater axial expansion at the center of the pellets. The ends of each pellet also have a small chamfer at the outer cylindrical surface which improves manufacturability.

The VANTAGE 5 fuel rod has the same clad wall thickness as the LOPAR fuel rod, but the VANTAGE 5 fuel rod diameter is reduced to optimize the water-to-uranium ratio. The VANTAGE 5 fuel rod length is greater than the LOPAR fuel rod length to provide a longer plenum and bottom end plug. The bottom end plug has an internal-grip feature to facilitate rod loading on both designs and is longer to provide a longer lead-in for the removable top nozzle reconstitution feature.

Commencing with the Region 18 fuel rods in Unit 1 Cycle 16 and the Region 16 fuel rods in Unit 2 Cycle 14, the fuel rod bottom end plug was elongated for use with the protective bottom grid. In conjunction with the elongated bottom end plug, the fuel rod top end plug was elongated and fitted with an external gripper.

Commencing with the Region 17 fuel rods in Unit 2 Cycle 15 and the Region 20 fuel rods in Unit 1 Cycle 18, the ZIRLO fuel rod length has been increased based on the approved growth model at the time for ZIRLO. In addition, the fuel rod top end plug was reduced in length by eliminating the external gripper feature. The reduced top end plug length allowed a further increase in the fuel rod tube length, and, consequently, an increase in the fuel rod plenum.

The VANTAGE 5 fuel rod may include an integral fuel burnable absorber (IFBA) and may include axial blankets which are new features relative to the LOPAR fuel rod design. The axial blanket region is the nominal 6 in. of fuel pellets located at each end of the fuel rod pellet stack. The fuel pellets in the axial blanket region may be natural, mid-enriched or fully-enriched solid or annular pellets. The natural or mid-enriched axial blankets reduce neutron leakage and improve fuel utilization. The annular blanket pellets are used to increase the void volume for gas accommodation within the fuel rod. The axial blankets utilize chamfered pellets which are physically different (in length) from the enriched pellets to help prevent accidental mixing during manufacturing.

The IFBA coated fuel pellets are identical to the enriched uranium dioxide pellets except for the addition of a thin boride coating on the pellet cylindrical surface. Coated pellets occupy the central portion of the fuel stack. The number and pattern of IFBA rods within an assembly may vary depending on specific application. The ends of the enriched coated pellets are dished to

allow for greater axial expansion at the pellet centerline and to increase the void volume for fission gas release.

(Historical)

Commencing with Region 15 in Unit 2 Cycle 13 and Region 18 in Unit 1 Cycle 16, the fuel rods incorporate fully-enriched annular axial blanket pellets in the top six inches of the fuel stack in the IFBA rods only. Commencing with Region 16 in Unit 2 Cycle 14 and Region 19 in Unit 1 Cycle 17, the fuel rods incorporate fully-enriched annular axial blanket pellets in the bottom and top six inches of the fuel stack in the IFBA rods only. The enrichment in the fully-enriched annular axial blanket pellets is the same as that of the enriched solid fuel pellet stack within the fuel rod. The fully-enriched annular axial blanket pellets have the same pellet outside diameter and pellet edge chamfer as the current enriched solid fuel pellets, but have no dish on the pellet ends. The fully-enriched annular axial blanket pellets are also longer than the solid fuel pellets (see table 4.1-1). The diameter of the annulus is 0.155 inches which results in a 25% annular volume to accommodate gas release in the IFBA rods. The fully-enriched annular axial blanket pellets in the IFBA rods increase the void volume for gas accommodation within the fuel rod compared to the previous IFBA fuel rod design, thereby providing margin to meet the rod internal pressure criterion.

Commencing with Region 15 in Unit 2 Cycle 13 and Region 18 in Unit 1 Cycle 16, the fuel incorporates 1.25X IFBA rods with a B-10 loading of 1.88 mg/in. The 1.25X IFBA B-10 loading is a new loading that was developed to reduce rod internal pressure concerns while still providing peaking factor hold-down as with the 1.0X and 1.5X IFBA loadings used in previous regions. The 1.25X IFBA design continues to use an enriched boron coating.

The B-10 loading in the 1.25X IFBA design represents approximately a 16% decrease in the amount of B-10 atoms per inch in an IFBA rod compared to the 1.5X IFBA design. The 1.25X IFBA rods continue to use a backfill pressure of 100 psig, which is the same as the 1.5X design. The use of 1.25X IFBA decreases the amount of helium generated in the IFBA fuel rod, thereby providing margin to meet the rod internal pressure criterion.

To avoid overstressing of the cladding or seal welds, void volume and clearances are provided within the rods to accommodate fission gases released from the fuel, differential thermal expansion between the cladding and the fuel, and fuel density changes during burnup. Shifting of the fuel within the cladding during handling or shipping prior to core loading is prevented by a stainless steel spring which bears on the top of the fuel. During assembly the pellets are stacked in the cladding to the required fuel height, the spring is then inserted into the top end of the fuel tube, and the end plugs are pressed into the ends of the tube and welded. All fuel rods are internally pressurized with helium during the welding process in order to minimize compressive clad stresses and creep caused by coolant operating pressures. The helium prepressurization may be different for each fuel region.

Fuel rod pressurization is dependent on the planned fuel burnup, as well as other fuel design parameters and fuel characteristics (particularly densification potential). The fuel rods are designed such that: the internal gas pressure of the lead rod will not exceed the value which causes the fuel/clad diametral gap to increase because of outward cladding creep during steady-state operation; extensive DNB propagation will not occur; the cladding stress and strain

limits (paragraph 4.2.1.1.1) are not exceeded for condition I and II events; and clad flattening will not occur during the fuel core life.

A 1.5X coating was introduced in Region 16 for Unit 1 and 14 for Unit 2, and continues to be used for all Farley fuel.

4.2.1.2.2 Fuel Assembly Structure

The fuel assembly structure consists of a bottom nozzle, top nozzle, guide thimbles, and grids, as shown in figure 4.2-2.

Bottom Nozzle

The bottom nozzle serves as a bottom structural element of the fuel assembly and directs the coolant flow distribution to the assembly. The square nozzle is fabricated from type 304 stainless steel and consists of a perforated plate and four angle legs with bearing plates, as shown in figure 4.2-2. Starting with Farley Unit 2 Cycle 10 and Unit 1 Cycle 13, the fuel assembly bottom nozzles will be a two-piece design, known as a composite nozzle, incorporating a high machining stainless steel adapter plate welded to a low cobalt investment casting. This casting replaces the current eight-piece weldment comprised of four cast legs and four rolled skirt plates. The new design is functionally interchangeable with the old design while providing additional design margin, since welding at the skirt-to-leg interface has been eliminated and replaced with a solid joint. The legs form a plenum for the inlet coolant flow to the fuel assembly. The plate itself acts to prevent a downward ejection of the fuel rods from their fuel assembly. The bottom nozzle is fastened to the fuel assembly guide tubes by locked thimble screws which penetrate through the nozzle and mate with an inside fitting in each guide tube.

Coolant flow through the fuel assembly is directed from the plenum in the bottom nozzle upward through the penetrations in the plate to the channels between the fuel rods. The penetrations in the plate are positioned between the rows of fuel rods.

Axial loads (holddown) imposed on the fuel assembly and the weight of the fuel assembly are transmitted through the bottom nozzle to the lower core plate. Indexing and positioning of the fuel assembly is controlled by alignment holes in two diagonally opposite bearing plates which mate with locating pins in the lower core plate. Any lateral loads on the fuel assembly are transmitted to the lower core plate through the locating pins.

A debris filter bottom nozzle (DFBN) was introduced as a functional replacement to the nozzle design described above to inhibit debris from entering the active fuel region of the core. This nozzle utilized the same material, geometry, and welding requirements as the previous bottom nozzle, with the exception of the differences associated with the composite nozzle, as described above. The revised end plate flow hole pattern is shown on figure 4.2-2 to illustrate the increased number of smaller flow holes that reduce the passage of debris into the active region of the fuel assembly. The DFBN was initially used in Farley Unit 1 cycle 10. Starting with Unit 2 cycle 8 and Unit 1 cycle 11, a modification adding a skirt to the standard DFBN was made to

FNP-FSAR-4

improve the structural integrity of the bottom nozzle. In addition, five holes were placed on each face of this skirt to allow lateral flow communication.

Commencing with the fresh fuel installed in Farley Unit 2 Cycle 23, Unit 1 Cycle 26, and subsequent Farley reloads, the standardized debris filter bottom nozzle (SDFBN), which was developed for 17 x 17 fuel and is designed to have a loss coefficient that is the same, independent of supplier, will be implemented. The SDFBN has eliminated the side skirt communication flow holes as a means of improving the debris mitigation performance of the bottom nozzle, as shown in figure 4.2-2. This nozzle has been extensively evaluated and analyzed and it was demonstrated that it meets all of the applicable mechanical design criteria. In addition, specific testing was performed to demonstrate that there is no adverse effect on the thermal hydraulic performance of the SDFBN, either with respect to the pressure drop or with respect to DNB.

Standard Top Nozzle

The top nozzle assembly functions as the upper structural element of the fuel assembly in addition to providing a partially protective housing for the rod cluster control assembly or other components. The top nozzle assembly is installed on the guide thimble tubes and consists of an adapter plate, enclosure, top plate, and pads. The integral welded assembly has four sets of holddown spring packs mounted to the top plate with bolts. The springs and bolts are made of Inconel 718 and Inconel 600, respectively; other components are made of type 304 stainless steel.

The adapter plate is provided with round and slotted (with semicircular ends) penetrations to permit the flow of coolant upward through the top nozzle. Other round holes are provided to accept the sleeves, which are welded to the adapter plate and mechanically attached to the thimble tubes (figure 4.2-5, sheet 1). The ligaments in the plate cover the tops of the fuel rods and prevent their upward ejection from the fuel assembly. The enclosure is a box-like plate structure shroud which sets the distance between the adapter plate and the nozzle top plate. The top plate has a large square hole in the center to permit access for the control rods and the control rod spiders. Holddown springs are mounted on the top plate and are fastened in place by bolts and clamps located at two diagonally opposite corners. On the other two corners of the top plate integral pads are positioned which contain alignment holes for locating the upper end of the fuel assembly.

Reconstitutable Top Nozzle

A reconstitutable top nozzle (RTN) design feature was incorporated beginning with J. M. Farley Unit 1 Cycle 9 and J. M. Farley Unit 2 Cycle 6. Use of the RTN will continue in subsequent cycles for each unit.

The RTN design differs from the above standard nozzle design in two ways: a groove is provided in each thimble thru-hole in the nozzle plate to facilitate attachment and removal, and the nozzle plate thickness is reduced to provide additional axial space for fuel rod growth. The sleeves are mechanically fitted to the top nozzle using a finger arrangement and a lock tube.

FNP-FSAR-4

A composite top nozzle was introduced in Farley Unit 2 Cycle 12 and Unit 1 Cycle 15, and replaces the integral welded assembly. This design change for manufacturing process improvement reduces the total number of component parts required to fabricate and assemble the top nozzle. However, use of the composite top nozzle does not preclude reverting to a welded design.

Commencing with Region 17 in Unit 2 Cycle 15 and Region 20 in Unit 1 Cycle 18, the material used for the fuel assembly holddown spring screws on the RTN is Alloy 718 instead of Alloy 600 to improve resistance to primary water stress corrosion cracking.

To remove the top nozzle assembly, a tool is first inserted through a lock tube (figure 4.2-5, sheets 2 and 3) and expanded radially to engage the bottom edge of the tube. An axial force is then exerted on the tool which overrides local lock tube deformations and withdraws the lock tube from the insert. After the lock tubes have been withdrawn, the nozzle assembly is removed by raising it off the upper slotted ends of the nozzle inserts, which deflect inwardly under the axial lift load.

With the top nozzle assembly removed, direct access is provided for fuel rod examination or replacement. Reconstitution is completed by the remounting of the nozzle assembly and the insertion of lock tubes. Additional details of this design feature, the design bases, and evaluation of the RTN are given in reference 17.

Westinghouse Integral Nozzle

Commencing with Farley Unit 1, Cycle 28, the Westinghouse Integral Nozzle (WIN) will replace the RTN. The WIN top nozzle functions as the upper structural element of the fuel assembly in addition to providing a partial protective housing for the RCCA or other core components. The top nozzle consists of an adapter plate, enclosure, top plate, and pads. Holddown springs are mounted on the assembly, as shown in figure 4.2-29. For the WIN, the springs are made of Alloy 718 and the main nozzle body and the pins are made of Type 304 stainless steel. The WIN design, while similar to the RTN, incorporates design and manufacturing improvements to eliminate the Alloy 718 spring screws for attachment of the holddown springs. In the WIN nozzle, the springs are assembled into the nozzle pad and pinned in place, as shown in figure 4.2-29. The WIN design provides a wedged rather than a clamped (bolted) joint for transfer of the fuel assembly holddown forces into the top nozzle structure. Integral pads which contain alignment holes for locating the upper end of the fuel assembly are positioned on the other two corners for the WIN. The flow plate, thermal characteristics, and method of attachment of the nozzle are all unchanged from the RTN top nozzle design.

Replacement Reconstitutable Top Nozzle (RRTN)

A replacement reconstitutable top nozzle (RRTN) design may be used in a reload cycle to replace the original reconstitutable top nozzle (RTN) or WIN on an irradiated fuel assembly. The mechanical features of the RRTN are the same as those for the RTN (see figure 4.2-5) or WIN with some minor dimensional differences in the top nozzle adapter plate thimble hole to facilitate attachment to an irradiated fuel assembly.

The RRTN may be manufactured by either the composite (cast) process or the integral welded process. The cast and integral welded top nozzles are interchangeable. Therefore, either of these RRTN designs may be used to replace an RTN or WIN regardless of whether the original RTN or WIN on the assembly was the composite (cast) design or the integral welded design. The material used for the fuel assembly hold-down spring screws on the RRTN may be either Alloy 718 or Alloy 600.

Guide Thimble and Instrument Tubes

The guide thimbles are structural members which provide channels for the neutron absorber rods, burnable absorber rods, neutron source assemblies, or thimble plugs. With the exception of a reduction in the guide thimble diameter and length above the dashpot, the VANTAGE 5 guide thimbles are identical to those in the LOPAR design. A reduction to the guide thimble OD and ID is required due to the thicker zircaloy/ ZIRLO grid straps and reduced cell size. The VANTAGE 5 thimble tube is shorter than the LOPAR thimble tube due to the RTN and insert features. Each guide thimble is fabricated from zircaloy/ ZIRLO tubing having two different diameters. The larger diameter at the top provides a relatively large annular area to permit rapid insertion of the control rods during a reactor trip, as well as to accommodate the flow of coolant during normal operation. The lower portion of the guide thimbles has a reduced diameter to produce a dashpot action near the end of the control rod travel during normal operation and to accommodate the outflow of water from the dashpot during a reactor trip. Four holes are provided on the thimble tube above the dashpot to reduce the rod drop time.

The dashpot is closed at the bottom by means of an end plug which is provided with a small flow port to avoid fluid stagnation in the dashpot volume during normal operation. The top end of the guide thimble is fastened to a tubular sleeve by three expansion swages. The sleeve fits into and is welded to the top nozzle adapter plate. For fuel assemblies with the RTN feature, the top of the sleeve, or insert, engages with a groove in the top nozzle adapter plate and is secured with a lock tube. The lower end of the guide thimble is fitted with an end plug which is then fastened into the bottom nozzle by a crimp locking screw.

Fuel rod support grids are fastened to the guide thimble assemblies to create an integral structure. Attachment of the inconel and zircaloy/ ZIRLO grids to the zircaloy/ ZIRLO thimble tubes is performed using the fastening technique depicted in figures 4.2-4, 4.2-5, and 4.2-6, except for the bottom grid, which is fastened securely between the guide thimble end plug and bottom nozzle.

An expanding tool is inserted into the inner diameter of the zircaloy thimble tube at the elevation of stainless steel grid sleeves that have been brazed into the Inconel grid assembly. For zircaloy grids, the sleeves are welded to the grid. The four-lobed tool forces the thimble and sleeve outward to a predetermined diameter, thus joining the two components.

The top grid-to-thimble attachment is shown in figure 4.2-5 for welded top nozzle assemblies. The 304L stainless steel sleeves are brazed into the Inconel grid assembly. The zircaloy/ ZIRLO guide thimbles are fastened to the long sleeves by expanding the two members as shown in figures 4.2-4 and 4.2-5. Finally, the top ends of the sleeves are mechanically fitted to the top nozzle adapter plate as shown in figure 4.2-5.

FNP-FSAR-4

In assemblies with reconstitutable top nozzles, the guide thimbles are fastened inside the top grid sleeves and nozzle inserts as shown in figure 4.2-5. A bulge in the nozzle insert is then captured in a corresponding groove in the hole in the top-nozzle plate. The insert is fixed in place by the insertion of a lock tube into the insert, thus providing a mechanical connection between the guide thimble and the top nozzle.

The top inconel grid sleeve, top nozzle insert, and thimble of the VANTAGE 5 design are joined together using bulge joint mechanical attachments as shown in figure 4.2-5. This bulge joint connection was mechanically tested and found to meet all applicable design criteria.

The VANTAGE 5 intermediate mixing vane and IFM zircaloy/ ZIRLO grids employ a single bulge connection (figure 4.2-6, sheet 2) to the sleeve and thimble as compared to a two bulge connection used in the top Inconel grid (figure 4.2-5). Mechanical testing of this bulge joint connection was also found to be acceptable.

The bottom grid assembly is joined to the assembly as shown in figure 4.2-7. The stainless steel insert is spot welded to the bottom grid and later captured between the guide thimble end plug and the bottom nozzle by means of a stainless steel thimble screw.

The described methods of grid fastening are standard and have been used successfully since the introduction of zircaloy guide thimbles in 1969.

The central instrumentation tube in each fuel assembly is constrained by seating in counterbores in each nozzle. This tube is a constant diameter and guides the incore neutron detectors. This thimble is expanded at the top and mid-grids in the same manner as the previously discussed expansion of the guide thimbles to the grids.

The VANTAGE 5 instrumentation tube has a reduction in diameter when compared to the LOPAR instrumentation tube; the wall thickness remains the same. This decrease still allows sufficient diametral clearance for the flux thimble to traverse the tube without binding.

Grid Assemblies

The fuel rods, as shown in figure 4.2-2, are supported laterally at intervals along their lengths by grid assemblies which maintain the lateral spacing between the rods throughout the design life of the assembly. Each fuel rod is afforded lateral support at six contact points within each grid by the combination of support dimples and springs. The grid assembly consists of individual slotted straps interlocked and brazed in an "egg-crate" arrangement to join the straps permanently at their points of intersection. The straps contain spring fingers, support dimples, and mixing vanes.

Because of its corrosion resistance and high strength properties, the grid material chosen for the LOPAR fuel assembly design is Inconel 718. The magnitude of the grid restraining force on the fuel rod is set high enough to minimize possible fretting, without overstressing the cladding at the points of contact between the grids and fuel rods. The grid assemblies are designed to allow axial thermal expansion of the fuel rods without imposing restraint sufficient to develop buckling or distortion of the fuel rods.

Two types of structural grid assemblies are used in each LOPAR fuel assembly. One type, with mixing vanes projecting from the edges of the straps into the coolant stream, is used in the high heat flux region of the fuel assemblies to promote mixing of the coolant. The other type, located at the ends of the assembly, does not contain mixing vanes on the internal straps. The outside straps on all grids contain mixing vanes which, in addition to their mixing function, aid in guiding the grids and fuel assemblies past projecting surfaces during handling or during loading and unloading of the core. Starting with the Farley Unit 1 Cycle 10 and Farley Unit 2 Cycle 7 reload, a vane has been added to the existing vanes and tabs on both the top and bottom of the outside grid strap to prevent hangup from the grid strap interference during fuel assembly removal. Also, to counter the effects of extended burnup, the bottom Inconel grid was modified starting with Farley Unit 2, Region 12 (Cycle 10) and Unit 1, Region 15 (Cycle 13) to give a higher spring force. This increase in spring force leads to a lower propensity for grid-to-fuel rod fretting. The top and bottom Inconel (nonmixing vane) grids for VANTAGE 5 fuel assemblies are similar in design to the Inconel grids of the typical LOPAR fuel assembly design. The six intermediate (mixing vane) grids on VANTAGE 5 are made of zircaloy-4/ ZIRLO material rather than Inconel, which is currently used on the LOPAR design.

The zircaloy/ ZIRLO grids have thicker straps than the Inconel grids. Also, the zircaloy grid height is higher compared to the Inconel mixing vane grids. These dimensional changes were made to compensate for differences in material strength properties. The zircaloy/ ZIRLO grid incorporates the same grid cell support configuration as the Inconel grid. The zircaloy/ ZIRLO interlocking strap joints and grid/sleeve joints are fabricated by laser welding, whereas the Inconel grid joints are brazed. The mixing vanes incorporated in the six zircaloy/ ZIRLO mid-grids induce additional flow mixing among the various flow channels in a fuel assembly as well as between adjacent fuel assemblies, and thus improve thermal performance.

The IFM grids shown in figure 4.2-2 are located in the three uppermost spans between the zircaloy/ ZIRLO mixing vane structural grids and incorporate a similar mixing vane array. Their prime function is mid-span flow mixing in the hottest fuel assembly spans. Each IFM grid cell contains four dimples which are designed to prevent mid-span channel closure in the spans containing IFMs and fuel rod contact with the mixing vanes. This simplified cell arrangement allows short grid cells so that the IFM grid can accomplish its flow mixing objective with minimal pressure drop.

The IFM grids, like the VANTAGE 5 mixing vane grids, are fabricated from zircaloy/ ZIRLO. This material was selected to take advantage of the material's inherent low neutron capture cross-section. The zircaloy/ ZIRLO IFM grid straps are manufactured using the same basic techniques as the zircaloy/ ZIRLO grid assemblies used for the Westinghouse OFA design and are joined to the guide thimbles via sleeves which are welded at the bottom of appropriate grid cells.

Grid impact testing has been performed on Zircaloy-4/ ZIRLO structural grids indicative of the VANTAGE 5 design. The purpose of the testing was to determine the dynamic crush strength of the grids. The grid impact testing was performed at an elevated temperature of 600°F. This temperature is a conservative value representing the core average temperature at the mid-grid locations.

The IFM grids are not intended to be structural members. The IFM grids do, however, share the loads of the structural grids during faulted loading and, as such, contribute to enhance the load carrying capability of the VANTAGE 5 fuel assembly. Grid impact testing has been performed on VANTAGE 5 zircaloy/ ZIRLO (structural) and IFM grids.

Commencing with the Region 18 fuel assemblies in Unit 1 Cycle 16 and the Region 16 fuel assemblies in Unit 2 Cycle 14, the fuel incorporated a protective bottom grid (figure 4.2-2, sheet 7 of 9) and modifications to the top and bottom fuel rod end plug (figure 4.2-3, sheet 7 of 7). The protective bottom grid is a partial height grid similar in configuration to the intermediate flow mixing grid, but fabricated of Inconel without mixing vanes. It is positioned on the top plate of the bottom nozzle. The fuel rod bottom end plug positioned within the protective grid is an elongated version of the previous fuel rod bottom end plug design. The protective bottom grid and elongated end plug together provide a zone below the active fuel in which debris can be entrapped.

As part of the addition of the protective bottom grid, a bottom Inconel grid with longer inserts and a bottom grid span reduction were also incorporated. The bottom Inconel grid was raised and the first ZIRLO grid was lowered to reduce the lower most span length in the fuel assembly. This change increases the resistance of the fuel assembly to flow induced fuel rod vibration to preclude excessive clad wear.

Commencing with the fresh fuel installed in Farley Unit 2 Cycle 23, Unit 1 Cycle 26, and subsequent Farley reload, the robust protective grid (RPG) which was developed as a result of observed failures in the field as noted in post irradiation exams (PIE) performed at several different plants, will be implemented. It was determined that observed failures were the result of two primary issues: 1) fatigue failure within the protective grid itself at the top of the end strap and 2) stress corrosion cracking (SCC) primarily within the rod support dimples. The RPG implements design changes such as increasing the maximum nominal height of the grid, increasing the ligament length and the radii of the ligament cutouts, and the use of four additional spacers for a total of eight spacers to help strengthen the grid. The nominal height of the grid was increased to allow "V-notch" window cutouts to be added to help minimize flow-induced vibration caused by vortex shedding at the trailing edge of the inner grid straps. These design changes incorporated into the RPG design help address the issues of fatigue failures and failures due to SCC. It was demonstrated that the above changes do not impact the thermal hydraulic performance of the RPG as there is no change to the pressure loss coefficient. In addition, the RPG retains the original protective grid function as a debris mitigation feature.

4.2.1.3 Design Evaluation

4.2.1.3.1 Fuel Rods

The fuel rods are designed to assure that the design bases are satisfied for Condition I and II events. This assures that the fuel performance and safety criteria (section 4.2) are satisfied.

Materials - Fuel Cladding

The desired fuel rod cladding is a material which has a superior combination of neutron economy (low absorption cross-section), high strength (to resist deformation caused by differential pressures and mechanical interaction between fuel and clad), high corrosion resistance (to coolant, fuel, and fission products), and high reliability. Zircaloy-4 has this desired combination of cladding properties. In Farley Unit 2 Cycle 12 and Unit 1 Cycle 15, ZIRLO was introduced as a fuel rod cladding material to provide added corrosion resistance and fuel reliability. The ZIRLO material was submitted for NRC review in reference 20 and received NRC approval. Clad hydriding has not been a significant cause of clad perforation since current controls on fuel-contained moisture levels were instituted.

Additionally, the use of Optimized ZIRLO clad material to improve corrosion resistance has been approved by the NRC (reference 27).

Metallographic examination of irradiated commercial fuel rods have shown occurrences of fuel/clad chemical interaction. Reaction layers of <1 mil in thickness have been observed between fuel and clad at limited points around the circumference. Westinghouse metallographic data indicate that this interface layer remains very thin even at high burnup. Thus, there is no indication of propagation of the layer and eventual clad penetration.

Stress corrosion cracking is another postulated phenomenon related to fuel/clad chemical interaction. Out-of-reactor tests have shown that in the presence of high clad tensile stress, relatively large concentrations of iodine, or cadmium in solution in liquid cesium, can stress-corrode zircaloy tubing and lead to eventual clad cracking. This mechanism is discussed in reference 15.

Materials - Fuel Pellets

Sintered, high density uranium dioxide fuel is chemically inert, with respect to the cladding, at core operating temperatures and pressures. In the event of cladding defects, the high resistance of uranium dioxide to attack by water protects against fuel deterioration, although limited fuel erosion can occur. As has been shown by operating experience and extensive experimental work, the thermal design parameters conservatively account for changes in the thermal performance of the fuel elements caused by pellet fracture which may occur during power operation. The consequences of defects in the cladding are greatly reduced by the ability of uranium dioxide to retain fission products, including those which are gaseous or highly volatile.

Observations from several operating Westinghouse PWRs (reference 8) have shown that fuel pellets can densify under irradiation to a density higher than the manufactured values. Fuel densification and subsequent incomplete settling of the fuel pellets result in local and distributed gaps in the fuel rods. Fuel densification has been minimized by improvements in the fuel manufacturing process and by specifying a nominal 95-percent initial fuel density.

The effects of fuel densification have been taken into account in the nuclear and thermal hydraulic design of the reactor described herein in sections 4.3 and 4.4, respectively.

The evaluation of fuel densification effects and the treatment of fuel swelling and fission gas release are described in references 18, 22, 24, and 28.

Materials - Strength Considerations

One of the most important limiting factors in fuel element duty is the mechanical interaction of fuel and cladding. This fuel/cladding interaction produces cyclic stresses and strains in the cladding, and these in turn consume cladding fatigue life. The reduction of fuel cladding interaction is therefore a principal goal of design. In order to achieve this goal and to enhance the cyclic operational capability of the fuel rod, the technology for using prepressurized fuel rods in Westinghouse PWRs has been developed.

Initially, the gap between the fuel and cladding is sufficient to prevent contact between the two. However, during power operation, a gradual compressive creep of the cladding onto the fuel pellet occurs because of the external pressure exerted on the rod by the coolant. Cladding compressive creep eventually results in the fuel/cladding contact. During this period of fuel/cladding contact, changes in power level could result in significant changes in cladding stresses and strains. By using prepressurized fuel rods to partially offset the effect of the coolant external pressure, the rate of cladding creep toward the surface of the fuel is reduced. Fuel rod prepressurization delays the time at which substantial fuel/cladding interaction and contact occur and, hence, significantly reduces the number and extent of cyclic stresses and strains experienced by the cladding both before and after fuel/cladding contact. These factors result in an increase in the fatigue life margin of the cladding and lead to greater cladding reliability. If gaps should form in the fuel stacks, clad flattening will be prevented by the rod prepressurization so that the flattening time will be greater than the fuel core life.

Steady-State Performance Evaluation

In the calculation of the steady-state performance of a nuclear fuel rod, the following interacting factors must be considered:

- A. Cladding creep and elastic deflection.
- B. Pellet density changes, fuel relocation, thermal expansion, gas release, and thermal properties as functions of temperature and fuel burnup.
- C. Internal pressure as a function of fission gas release, rod geometry, and temperature distribution.

These effects are evaluated using fuel rod design models ^(18, 24, 28) which include appropriate models for time-dependent fuel densification. With these interacting factors considered, the model determines the fuel rod performance characteristics for a given rod geometry, power history, and axial power shape. In particular, internal gas pressure, fuel and cladding temperatures, and cladding deflections are calculated. The fuel rod is divided lengthwise into several sections and radially into a number of annular zones. Fuel density changes, cladding stresses, strains and deformations, and fission gas releases are calculated separately for each segment. The effects are integrated to obtain the internal rod pressure.

FNP-FSAR-4

The initial rod internal pressure is selected to delay fuel/clad mechanical interaction and to avoid the potential for flattened rod formation. It is limited, however, by the design criteria for the rod internal pressure. The plenum height of the fuel rod has been designed to ensure that the maximum internal pressure of the fuel rod will not exceed the value which would cause the fuel/clad diametral gap to increase during steady-state operation.

Fuel rod design methodology has been introduced, reference 22, that reduces the densification power spike factor to 1.0 and demonstrates that clad flattening will not occur in Westinghouse fuel designs.

The gap conductance between the pellet surface and the cladding inner diameter is calculated as a function of the composition, temperature, and pressure of the gas mixture and the gap size or contact pressure between clad and pellet. After computing the fuel temperature for each pellet annular zone, the fractional fission gas released is assessed using an empirical model derived from experimental data.^(18, 24, 28) The total amount of gas released is based on the average fractional release within each axial and radial zone and the gas generation rate which, in turn, is a function of burnup. Finally, the gas released is summed over all zones and the pressure is calculated.

The model shows good agreement in fit for a variety of published and proprietary data on fission gas release, fuel temperatures, and clad deflections.^(18, 24, 28) Included in this spectrum are variations in power, time, fuel density, and geometry. The in-pile fuel temperature measurement comparisons used are shown in references 18, 24, and 28.

Transient Evaluation Method

Pellet thermal expansion caused by power increases is considered the only mechanism by which significant stresses and strains can be imposed on the clad. Power increases in commercial reactors can result from fuel shuffling (e.g., region 3 positioned near the center of the core for cycle 2 operation after operating near the periphery during cycle 1), reactor power escalation following extended reduced power operation, and full-length control rod movement. In the mechanical design model, lead rods are depleted using best estimate power histories as determined by core physics calculations. During the depletion, the amount of diametral gap closure is evaluated based upon the pellet expansion cracking model, clad creep model, and fuel swelling model. At various times during the depletion, the power is increased locally on the rod to the burnup-dependent attainable power density as determined by core physics calculation.

Slow, transient power increases can result in large clad strains without exceeding the clad yield stress because of clad creep and stress relaxation. Based upon high strain rate burst and tensile test data on irradiated tubing, 1-percent transient strain was determined to be the lower limit on irradiated clad ductility and thus was adopted as a design criterion.

In addition to the mechanical design models and design criteria, Westinghouse relies on performance data accumulated through transient power test programs in experimental and commercial reactors, and through normal operation in commercial reactors.

It is recognized that a possible limitation to the satisfactory behavior of the fuel rods in a reactor which is subjected to daily load follow is the failure of the cladding by low-cycle strain fatigue. During their normal residence time in the reactor, the fuel rods may be subjected to ~1000 cycles, with typical changes in power level from 50 to 100 percent of their steady state values.

The assessment of the fatigue life of the fuel rod cladding is subjected to considerable uncertainty because of the difficulty of evaluating the strain range which results from the cyclic interaction of the fuel pellets and claddings. This difficulty arises, for example, from such highly unpredictable phenomena as pellet cracking, fragmentation, and relocation. Nevertheless, since early 1968, Westinghouse has been investigating this particular phenomenon both analytically and experimentally. Strain fatigue tests on irradiated and nonirradiated hydrided Zr-4 claddings were performed which permitted the definition of a conservative fatigue-life limit and recommendation of a methodology to treat the strain fatigue evaluation of the Westinghouse-referenced fuel rod designs.

However, Westinghouse is convinced that the final proof of the adequacy of a given fuel rod design to meet the load follow requirements can come only from in-pile experiments performed on actual reactors. The Westinghouse experience in load follow operation dates back to early 1970 with the load follow operation of the Saxton reactor. More recently, successful load follow operation has been performed on reactor A (300 load follow cycles) and reactor B (150 load follow cycles). In both cases, there was no significant coolant activity increase that could be associated with the load follow mode of operation.

The following paragraphs present briefly the Westinghouse analytical approach to strain fatigue.

A comprehensive review of the available strain fatigue models was conducted by Westinghouse as early as 1968. This included the Langer-O'Donnel model⁽¹¹⁾, the Yao-Munse model, and the Manson-Halford model.

Upon completion of this review, and using the results of the Westinghouse experimental programs discussed below, it was concluded that the approach defined by Langer-O'Donnel would be retained and the empirical factors of their correlation modified in order to conservatively bound the results of the Westinghouse testing program.

The Langer-O'Donnel empirical correlation has the following form:

$$S_a = \frac{E}{\sqrt[4]{N_f}} \ln \left(\frac{100}{100 - RA} \right) + S_e$$

where:

$$S_a = \frac{1}{2} E \Delta \epsilon_t = \text{pseudo-stress amplitude which causes failure in } N_f \text{ cycles (lb/in.}^2\text{)}$$

$$\Delta \epsilon_t = \text{total strain range (in./in.)}$$

FNP-FSAR-4

- E = Young's Modulus (lb/in.²)
- N_f = number of cycles to failure
- RA = reduction in area at fracture in a uniaxial tensile test (percent)
- S_e = endurance limit (lb/in.²)

Both RA and S_e are empirical constants which depend on the type of material, the temperature, and the irradiation. The Westinghouse testing program was subdivided into the following subprograms:

- A. A rotating bend fatigue experiment on unirradiated Zr-4 specimens at room temperature and at 725°F. Both hydrided and nonhydrided Zr-4 claddings were tested.
- B. A biaxial fatigue experiment in gas autoclave on unirradiated Zr-4 claddings, both hydrided and non-hydrided.
- C. A fatigue test program on irradiated claddings from the Carolina Virginia Test Reactor (CVTR) and Yankee Core V conducted at Battelle Memorial Institute.

The results of these test programs provided information on different cladding conditions, including the effect of irradiation, of hydrogen level, and of temperature.

The Westinghouse design equations followed the concept for the fatigue design criterion according to Section III of the ASME Boiler and Pressure Vessel code, namely:

- A. The calculated pseudo-stress amplitude (S_a) has to be multiplied by a factor of 2 in order to obtain the allowable number of cycles (N_f).
- B. The allowable cycles for a given S_a is 5 percent of N_f, or a safety factor of 20 on cycles.

The lesser of the two allowable numbers of cycles is selected. The cumulative fatigue life fraction is then computed as:

$$\sum_1^k \frac{n_k}{N_{fk}} \leq 1$$

where:

- n_k = number of diurnal cycles of mode k.
- N_{fk} = number of allowable cycles.

The potential effects of operation with waterlogged fuel are discussed in paragraph 4.4.3.6. Waterlogging is not considered to be a concern during operational transients.

4.2.1.3.2 Fuel Assembly Structure

Stresses and Deflections

The potential sources of high stresses in the assembly are avoided by the design. For example, stresses in the fuel rod caused by thermal expansion and zircaloy, ZIRLO, or Optimized ZIRLO irradiation growth are limited by the relative motion of the rod as it slips over the grid spring and dimple surfaces. Clearances between the fuel rod ends and nozzles are provided so that zircaloy, ZIRLO, or Optimized ZIRLO irradiation growth will not result in end interferences. As another example, stresses caused by hold-down springs in opposition to the hydraulic lift force are limited by the deflection characteristic of the springs. Stresses in the fuel assembly caused by tripping of the rod cluster control assembly have little influence on fatigue because of the small number of events during the life of an assembly. Welded joints in the fuel assembly structure are considered in the structural analysis of the assembly. Appropriate material properties of welds are used to ensure that the design bases are met. Assembly components and prototype fuel assemblies made from production parts have been subjected to structural tests to verify that the design bases requirements are met.

The fuel assembly design loads for shipping have been established at 6 g laterally and 4 g axially while maintaining dimensional stability.⁽¹⁶⁾ Accelerometers are permanently placed into the shipping cask to monitor and detect fuel assembly displacements that would result from loads in excess of the criteria. Past history/experience has indicated that loads that exceed the allowable limits rarely occur. Exceeding the limits requires reinspection of the fuel assembly for damage. Tests on various fuel assembly components, such as the grid assembly, sleeves, inserts, and structure joints have been performed to ensure that the shipping design limits do not result in impairment of fuel assembly function.

Seismic analysis methodology of the fuel assembly is presented in references 10 and 17.

Dimensional Stability

A prototype fuel assembly has been subjected to column loads in excess of those expected in normal service and faulted conditions.^(10, 17)

The coolant flow channels are established and maintained by the structure composed of grids and guide thimbles. The lateral spacing between fuel rods is provided and controlled by the support dimples of adjacent grid cells. Contact of the fuel rods on the dimples is assured by the clamping force provided by the grid springs. Lateral motion of the fuel rods is opposed by the spring force and the internal moments generated between the spring and the support dimples. Grid testing is discussed in references 10 and 17.

No interference with control rod insertion into thimble tubes will occur during a postulated loss-of-coolant accident (LOCA) transient caused by fuel rod swelling, thermal expansion, or bowing. In the early phase of the transient following the coolant break, the high axial loads

which potentially could be generated by the difference in thermal expansion between fuel clad and thimbles are relieved by slippage of the fuel rods through the grids. The relatively low drag force restraint on the fuel rods will only induce minor thermal bowing not sufficient to close the fuel rod-to-thimble tube gap. This rod-to-grid slip mechanism occurs simultaneously with control rod drop.

Vibration and Wear

The effect of a flow-induced vibration of the fuel assembly and individual fuel rods is minimal. The cyclic stress range associated with deflections of such small magnitude is insignificant and has no effect on the structural integrity of the fuel rod.

The conclusion that the effect of flow-induced vibrations on the LOPAR fuel assembly and fuel rod is minimal is based on test results and analysis documented in the Hydraulic Flow Test of the 17-x-17 Fuel Assembly Report,⁽¹²⁾ which takes into consideration the conditions normally encountered in reactor operation. Hydraulic flow testing of the VANTAGE 5 fuel assembly is given in reference 17.

The reaction on the grid support because of vibration motions is also correspondingly small and much less than the spring preload. Firm contact is therefore maintained. No significant wear of the cladding or grid supports is expected during the life of the fuel assembly, based on out-of-pile flow tests, performance of similarly designed fuel in operating reactors,⁽⁸⁾ and design analyses.

Due to the current LOPAR and VANTAGE 5 fuel assembly designs employing different grid designs, there is a potential for unequal axial pressure distribution between the assemblies. Hydraulic testing (reference 17) was performed to verify hydraulic compatibility of the LOPAR and VANTAGE 5 designs. The VANTAGE 5 fuel assembly was flow tested adjacent to the most limiting fuel assembly design. Upon completion of the elevated temperature hydraulic test, the VANTAGE 5 fuel assemblies were removed from the baffle enclosure and the fuel rods were inspected for wear. Results of the wear inspection and analysis revealed that the VANTAGE 5 fuel assembly wear characteristic was similar to that of a previously (hot) tested 17-x-17 OFA and would not exceed design criteria established for 48 months of full flow operation.

Evaluation of the Reactor Core for LOCA

The 17-x-17 VANTAGE 5 IFM fuel assembly responses resulting from a LOCA were analyzed using time history numerical integration techniques. Since the resulting vessel motion induces primarily lateral loads on the reactor core, the seismic model described in references 10 and 17 was used to assess the fuel assembly deflections and impact forces. The model simulates the fuel assembly interaction during planar array with interassembly gaps. For the Farley plants, all fuel assemblies across the core diameter were modeled.

The reactor vessel motions resulting from the LOCA transient loadings are not symmetric with respect to the geometric center of the reactor core; therefore, a full fuel assembly model is used to determine the fuel assembly deflections and grid impact forces. The methodology for evaluating the faulted condition loads is described in references 10 and 17.

A series of 3, 7, 9, 11, 13, and 15 fuel assembly elements, as shown in figure 4.2-28, was used to represent the core. The time histories representing the coolant pipe rupture transient were obtained from the time history analysis of the reactor vessel and internals finite element model. The time history motions of the barrel at the upper core plate elevation and the upper and lower core plates (F_3 , F_2 , and F_1 , respectively) are applied simultaneously to the reactor core model.

The fuel assembly responses, namely, fuel assembly deflections and grid impact forces, are obtained from the reactor core model using the core plate motions. The fuel assembly stresses resulting from the maximum deflection were evaluated and indicate adequate margins compared to the allowable values.

The fuel assembly grid impact forces were also obtained from the reactor core time history response. To comply with the requirements in the USNRC 4.2 Standard Review Plan (SRP), the maximum grid impact responses obtained from the LOCA and seismic analyses are combined at the grid elevations using the square-root-of-sum-of-squares (SRSS) method. The grid spacer strengths were determined based on the 95-percent confidence level of the true mean as taken from the distribution of measurements at operating temperature. The analysis results show that the calculated grid impact forces are less than the grid strength at all locations except at the IFMs at the corner fuel assembly locations along the three-wide fuel assembly rows. These locations do not correspond to control rod locations. A coolable geometry assessment has been performed for these locations. Results demonstrate that the core remains amenable to cooling. All applicable fuel assembly design basis criteria and acceptance limits are satisfied for the LOCA; i.e., fuel rod fragmentation does not occur, control rod insertability is maintained, and a coolable geometry is maintained.

4.2.1.3.3 [HISTORICAL] [Operational Experience]

Westinghouse has had considerable experience with zircaloy-clad fuel since its introduction in the Jose Cabrera plant in June 1968, and with ZIRLO, since its introduction in the V. C. Summer plant in 1991. This experience is extensively described in reference 8. More than 70-million megawatt hours of energy have been generated through October 1973. While region 3 of both Beznau Unit 1 and Ginna had cladding defect caused by moisture, and although densification and rod flattening have received a great deal of attention, these problems have been successfully and promptly solved, and Westinghouse zircaloy-clad fuel is now operating in accordance with expectations. More importantly, there has been no instance in which fuel performance problems have in any way endangered the plant or public safety.

The Jose Cabrera plant had its initial startup in 1968. The first cycle (16 GWD/MTU) showed good performance with coolant activity stable at low levels, indicating possible leakage from a few rods. Visual examination during refueling showed three partially damaged rods in a peripheral assembly. It was judged at the time that a handling mishap prior to loading may have been responsible for the damage. All other assemblies were in good condition. The plant operated normally during its second cycle (7 GWD/MTU) until scheduled shutdown. The coolant activity was well within limits of acceptability, but slightly higher than in Cycle 1. A visual examination made during refueling disclosed three damaged rods at the same peripheral

location where the damaged rods had been observed after Cycle 1. The second refueling also showed a failed rod in a peripheral assembly on the opposite side of the core. A detailed investigation concluded that the damage was caused by higher than normal cross-flow velocities in these locations, identified as high velocity coolant cross-flow leaking through gaps in the corner joints in the core baffle. The cross-flow caused excessive rod vibration and eventual fretting through the cladding in the grid support areas. Corrective action was taken during the 1972 refueling, in which the baffle joints were repaired to eliminate the leakage. The absence of damage during the recent Cycle 3 refueling inspections confirms the efficiency of this repair.

A small number of high-power test rods in special assemblies also experienced cladding defect during Cycle 2, but their power level burnup condition is not typical of current design. The performance of the remaining standard fuel assemblies was excellent. The core performed as expected during the third cycle (9.3 GWD/MTU) with no further indication of fuel difficulties.

The Beznau Unit I plant had its initial startup in 1969. Normal power runs were conducted for several weeks after first cycle (11.5 GWD/MTU) startup. Then, over a period of eight weeks, the coolant activity slowly increased, indicating clad defect in several rods. Continuing surveillance of the activity, always below established limits, confirmed that almost all clad defect developed early in life. Operation of the plant continued without restriction until scheduled refueling.

After shutdown, a detailed investigation was launched. Both direct examination and leak tests were performed. Their study disclosed that cladding defects were mainly in region 3. Close inspection revealed that localized cladding hydriding was caused by excessive moisture in the as-built fuel pellets. All affected fuel was replaced.

The thorough fuel inspection also disclosed that several rods contained flattened sections, ranging from about 0.5-in. to 2.5-in. long. This condition had not been observed before in Westinghouse fuel. Hot cell examination of such rods showed that the flattened sections had undergone creep collapse. It was subsequently shown that this occurred because in-pile densification of the UO_2 , coupled with pellet stack hangup, had left gaps in the pellet column. The lack of pellet support for the cladding had allowed it to locally distort to oval shape, creep, then collapse under the force of coolant pressure. Clad flattening was confined to unpressurized fuel.

Reload fuel containing pressurized rods was placed in the core along with previously irradiated unpressurized fuel for the second cycle (8 GWD/MTU). The latter was reloaded after detailed nuclear, thermal hydraulic, and mechanical design analysis proved that safety was not compromised. Throughout the cycle, coolant activity remained stable and substantially below first cycle values. At the normal conclusion of the cycle, fuel surveillance showed that additional clad flattening had occurred as predicted in the unpressurized rods, but not in the pressurized fuel assemblies.

The Ginna plant had its initial startup in 1969. During normal Cycle 1A (8 GWD/MTU) power operations in the spring of 1970, increases in the primary coolant activity were observed.

Although the activity stabilized after a short time at acceptably low levels (within the technical specifications), there were indications that several fuel rods had undergone clad defect. This experience was similar to that of Beznau Unit 1. Because of their similarity it was decided to take advantage of a scheduled shutdown for turbine inspection to also inspect the fuel.

Leak testing and visuals confirmed that clad defect caused by hydriding had occurred and was confined to region 3. Twelve assemblies containing rods with this condition were replaced.

After nearly a year of operation in Cycle 1B (8 GWD/MTU), the plant was uprated to 1520 MWt. During the 1-month operating period, coolant activity increased from a low level, indicating some additional clad defect.

Examination conducted during the scheduled refueling revealed a number of fuel rods containing locally flattened sections. These varied in length from 0.5 in. to 3 in. This condition was seen only in unpressurized fuel.

Though clad flattening is not necessarily a cause of cladding defect, there is an operational concern because of flux peaking in rods adjacent to the collapses. The fuel containing collapses was allowed to remain in the core for the next cycle, but at a reduced core power of 1266 MWt.

At the end of the short second cycle (215 GWD/MTU), 48 of the remaining unpressurized assemblies were replaced with pressurized fuel. The twelve pressurized fuel assemblies that had been placed in the core after Cycle 1A had achieved a burnup of 12 GWD/MTU with no evidence of clad flattening or defect.

The core during the third cycle (8 GWD/MTU) contained only pressurized fuel. The reactor logged a record 189 days of continuous operation, while coolant activity levels remained low and stable. Partly because of this excellent performance, approval was given to return to the rated power of 1520 MWt.

The Beznau Unit II plant had its initial startup in 1971. Scheduled shutdown for refueling in July 1973 followed a successful first cycle (14.2 GWD/MTU), including a period of 159 consecutive days of operation. During refueling, an underwater TV examination revealed all three regions of pressurized fuel to be in good condition with no flattened cladding.

Startup of cycle 2 occurred in September 1973 and The Mihama Unit I plant had its initial startup in 1970. The core performed well throughout the entire first cycle (13 GWD/MTU). Coolant activity remained at a low level, indicating the presence of very little clad defect. During a mid-cycle shutdown for the required annual pressure vessel inspection, the fuel was found to be in excellent condition.

During the latter half of the cycle the coolant activity was also low, though somewhat higher than during the first half.

FNP-FSAR-4

Examination after shutdown for scheduled refueling showed that about one percent of the region 1 nonpressurized rods had flattened sections, ranging from 0.5-to 1.5-inches long. No clad flattening was seen in prepressurized regions 2 and 3. Cycle 2 burnup as of October 1973 was 1 GWD/MTU.

The Mihama Unit II plant had its initial startup in 1972. Core operation during the first cycle (10.5 GWD/MTU) was satisfactory with coolant activity at low levels. Examination during the annual inspection revealed a few assemblies with clad defect. They were removed.

The annual 3-month inspection began in September 1973. Thus, the plant had not completed its first cycle as of October 1973.

The Point Beach Unit I plant had its initial startup in 1971. The core performed well throughout the first cycle (17 GWd/Mtu) with gradually increasing coolant activity only toward the end. Visual examination at refueling showed clad flattening confined to nonpressurized fuel.

All of the nonpressurized assemblies (region 1) were removed. It was noted that clad defect and flattening were highly correlated for the first time. Neither clad flattening nor defect were observed in the prepressurized fuel, which was consistent with other observations on Westinghouse fuel.

This core loading went critical in March 1973 and contained only prepressurized fuel rods. Operation has been near rated power during the second cycle (5 GWd/Mtu).

The H. B. Robinson II plant had its initial startup in 1970. This, the first of the large three-loop plants to use zircaloy-clad, RCC-type fuel, performed well during its first cycle (15 GWd/Mtu). Low level coolant activity observed during operation indicated some clad defect. As in other cases, visual examination at refueling disclosed the defective clad (three rods) was confined to the nonpressurized region 1 fuel.

Also confined to the region 1 fuel, which is normally discharged after the first cycle, were assemblies containing flattened cladding. The approximate frequency of 1 percent flattened rods was consistent with other observations on Westinghouse fuel.

Operation has been normal during the first 5 months of the second cycle (1 GWd/Mtu).

Three plants went online during 1972 with an accumulated burnup of 16 GWd/Mtu through October 1973. Cladding defect, as indicated from coolant activity level, is less than .01 percent.

Four additional plants went online prior to October 1973 and accumulated approximately 10 GWd/Mtu burnup as of October 1973. Coolant activity at these plants has indicated cladding defect at barely detectable levels.

To demonstrate early performance of the VANTAGE 5 design product features in a commercial reactor, 4 VANTAGE 5 demonstration assemblies (17 x 17) were loaded into the V. C. Summer cycle 2 core and began power production in December 1984. These assemblies completed 1 cycle of irradiation in October 1985 with an average burnup of 11,357 MWd/Mtu. Post-irradiation examinations showed all four demonstration assemblies were of good mechanical integrity. No mechanical damage or wear was evident on any of the VANTAGE 5 components. Likewise, the IFM grids on the VANTAGE 5 demonstration assemblies had no effect on the adjacent fuel assemblies. All four demonstration assemblies were reinserted into V. C. Summer for a second cycle of irradiation. This cycle was completed in March 1987, at which time the demonstration assemblies achieved an average burnup of about 30,000 MWd/Mtu. The observed behavior of the four assemblies at the end of 2 cycles of irradiation was as good as that observed at the end of the first cycle of irradiation. The 4 assemblies were reinserted for a third cycle of irradiation, which was completed in November 1988 (EOC burnup 46,000 MWd/Mtu). The observed behavior of the four assemblies was again as good as that observed at the end of the first and second cycles of irradiation.

In addition to V. C. Summer, individual VANTAGE 5 product features have been demonstrated at other nuclear plants. IFBA demonstration fuel rods have been irradiated in Turkey Point Units 3 and 4 for two reactor cycles. Unit 4 contained 112 fuel rods equally distributed in four demonstration assemblies. The IFBA coating performed well with no loss of coating integrity or adherence. The IFM grid feature has been demonstrated at McGuire Unit 1. The demonstration assembly at McGuire was irradiated for three reactor cycles and showed good mechanical integrity.

The following plants are currently operating with full regions of VANTAGE 5 fuel assemblies: Callaway, V. C. Summer, Shearon Harris, Diablo Canyon, Byron/Braidwood, and D. C. Cook.

The improved corrosion resistance of ZIRLO cladding under irradiation has been demonstrated. Beginning in the early 1970s in the BR-3 Test Reactor Demonstration Program, fuel rods containing cladding fabricated from ZIRLO alloy were irradiated at linear power levels of up to 17 kw/ft to rod average burnups of 68 GWd/Mtu (peak pellet burnups of approximately 80 GWd/Mtu). Post-irradiation examinations have demonstrated that ZIRLO alloy exhibited a reduction in corrosion rate and improved dimensional stability as compared to Zircaloy-4 rods having similar power histories, which were irradiated as controls in the same assemblies.

Full-length ZIRLO rods were fabricated for a second demonstration program at the North Anna 1 commercial reactor, with operation beginning in June 1987. The first post-irradiation examination of the assemblies was completed after 18 months of irradiation to a rod average burnup of over 21 GWd/Mtu (completed in February 1989). Visual and dimensional inspection during refueling showed no abnormalities.

Continued corrosion resistance and dimensional stability with no abnormalities was shown in the visual and dimensional inspections performed on another assembly having rods operating for a second cycle to a rod burnup approaching 40 GWd/Mtu (completed in January 1991).

Cladding corrosion measurements showed that the reduced corrosion exhibited by the ZIRLO rods was significantly better than anticipated on the basis of licensing analyses.

Two demonstration fuel assemblies containing selected ZIRLO clad fuel rods were introduced in Vogtle Unit 1 Cycle 4. These assemblies were irradiated for three cycles and removed for Cycle 7 operation. Visual examinations during refueling indicated no abnormalities in the assemblies containing the ZIRLO clad fuel rods.

On-site inspections (visual examination, rod and assembly length measurements, and corrosion measurement) of selected assemblies from V. C. Summer Region 9 VANTAGE+ fuel (containing ZIRLO clad and ZIRLO guide thimbles and instrumentation tubes) after one and two cycles of irradiation have supported the good performance observed in prior examinations of ZIRLO clad fuel.

Since the first commercial region application of VANTAGE+ fuel in the V. C. Summer Cycle 7 core, experience with ZIRLO alloy components has continued to increase.]

4.2.1.3.4 High Power Fuel Rod Development (Historical)

Test rod and test assembly experience is presented in sections 8 and 23 of reference 5.

4.2.1.4 Testing and Inspection Plan

4.2.1.4.1 Quality Assurance Program

The quality assurance program plan of the Westinghouse Nuclear Fuel Division for the FNP is summarized in reference 6.

The program provides for control over all activities affecting product quality, commencing with design and development and continuing through procurement, materials handling, fabrication, testing and inspection, storage, and transportation. The program also provides for the indoctrination and training of personnel and for the auditing of activities affecting product quality through a formal auditing program.

Westinghouse drawings and product, process, and material specifications identify the inspections to be performed.

4.2.1.4.2 Quality Control

Quality control (QC) philosophy is generally based on the following inspections being performed to a 95-percent confidence level that at least 95 percent of the product meets specifications, unless otherwise noted.

FNP-FSAR-4

A. Fuel system components and parts

The characteristics inspected depend upon the component parts. The QC program includes dimensional and visual examinations, check audits of test reports, material certification, and nondestructive examination, such as X-ray and ultrasonic.

All material used in this core is accepted and released by QC.

B. Pellets

Inspection is performed for dimensional characteristics such as diameter, density, length, and squareness of ends. Additional visual inspections are performed for cracks, chips, and surface conditions according to approved standards.

Density is determined in terms of weight-per-unit-length and is plotted on zone charts used in controlling the process. Chemical analyses are taken on a specified sample basis throughout pellet production.

C. Rod inspection

The fuel rod, control rod, burnable absorber, and source rod inspections consist of the following nondestructive examination techniques and methods, as applicable:

1. Each fuel, burnable absorber, and secondary source rod is leak tested using a calibrated mass spectrometer, with helium being the detectable gas.
2. Rod welds are inspected by ultrasonic test or x-ray in accordance with a qualified technique and Westinghouse specifications.
3. All rods are dimensionally inspected prior to final release. The requirements include such items as length, camber, visual appearance, and weld diameter.
4. All fuel rods are inspected by gamma scanning and/or other approved methods to ensure proper plenum dimensions.
5. All burnable absorber rods are inspected by x-ray and/or other approved methods to ensure proper plenum dimensions.
6. All fuel rods are inspected by gamma scanning or other approved methods to ensure that no significant gaps exist between pellets.
7. All fuel rods are active-gamma scanned to verify enrichment control prior to acceptance for assembly loading.
8. Traceability of rods and associated rod components is established by QC.

D. Assemblies

Each fuel, control rod, burnable absorber, and source rod assembly is inspected for compliance with drawing and/or specification requirements. Other in-core control component inspection and specification requirements are given in paragraph 4.2.3.4.

E. Other inspections

The following inspections are performed as part of the routine inspection operation:

1. Tool and gauge inspection and control, including standardization to primary and/or secondary working standards. Tool inspection is performed at prescribed intervals on all serialized tools. Complete records are kept of calibration and conditions of tools.
2. Audits of inspection activities and records are performed to ensure that prescribed methods are followed and that records are correct and properly maintained.
3. Surveillance inspection, where appropriate, and audits of outside contractors are performed to ensure conformance with specified requirements.

F. Process control

To prevent the possibility of mixing enrichments during fuel manufacture and assembly, strict enrichment segregation and other process controls are exercised.

The UO₂ powder is kept in sealed containers. The contents are fully identified by an item control system bar code label. Isotopic content is confirmed by analysis.

Powder withdrawal from storage can be made by only one authorized group, which directs the powder to the correct pellet production line. All pellet production lines are physically separated from each other and pellets of only a single, nominal enrichment are produced in a given production line at any given time.

Finished pellets are placed on trays and are transferred to segregated storage racks within the confines of the pelleting area. Samples from each pellet lot are tested for isotopic content and impurity levels prior to acceptance by QC. Physical barriers prevent mixing of pellets of different nominal densities and enrichments in this storage area. Discrepant and unused powder and pellets are labeled and returned to the appropriate controlled area.

Loading of pellets into the clad is performed in isolated production lines and, again, only one enrichment is loaded on a line at a time.

A serialized traceability code is placed on each fuel tube to provide unique identifications. The end plugs are inserted and then inert-welded to seal the tube. The fuel tube remains coded and traceability identified until just prior to installation in the fuel assembly.

Before an assembly is Quality Control Released, the traceability codes are checked against computer records to assure that the fuel rods in the assembly are from the correct core region. Traceability of all fuel assembly components in an assembly are permanently maintained and identified by a unique identification number engraved on the fuel assembly top nozzle.

Similar traceability is provided for burnable absorber (BA), source rods, and control rodlets, as required.

4.2.1.4.3 Onsite Inspection

Onsite inspection programs for fuel, control rods, and internals are based on the manufacturer's detailed procedures. The following program is based on Westinghouse procedures for the internals and initial core. In the event reloads or other components are supplied by other manufacturers, similar programs will be developed based on that manufacturer's procedures.

Loaded fuel containers, when received onsite, are externally inspected to ensure that labels and markings are intact and seals are unbroken. After the containers are opened, the shock indicators attached to the suspended internals are inspected to determine if movement during transit exceeded design limitations.

Following removal of the fuel assembly from the container in accordance with detailed procedures from the fuel fabricator, the polyethylene wrapper is then removed and a visual inspection of the entire bundle is performed. The polyethylene wrapper is then replaced for dry storage, if desired.

Control rod assemblies are usually shipped in fuel assemblies and are inspected when assembly is removed (during fuel inspection). The control rod assembly is withdrawn a few inches from the fuel assembly using the fuel handling tool to ensure free and unrestricted movement. The exposed section is then visibly inspected for mechanical integrity, replaced in the fuel assembly, and stored with the fuel assembly. Control rod assemblies can be shipped individually in their own transport containers and will be similarly inspected and tested for unrestricted movement in a fuel assembly. Control rod assemblies may be stored separately or within fuel assemblies in the new fuel storage area.

Reactor internals are visually inspected and manually checked for tightness upon receipt at the site. Clearance measurements performed during assembly and installation in accordance with the manufacturer's detailed procedures also serve to verify the mechanical integrity of the internals.

Surveillance of fuel and reactor performance is routinely conducted on Westinghouse reactors. Power distribution is monitored using ex-core fixed and incore movable detectors. Coolant activity and chemistry are followed to permit early detection of any fuel clad defects.

Visual fuel inspection is routinely conducted during refueling. Additional fuel inspections are dependent on the results of the operational monitoring and the visual inspections.

4.2.1.4.4 Removable Fuel Rod Assembly

A fuel assembly, containing 88 removable fuel rods, is included in region 3 of the initial core loading Unit 1. There are no plans to inspect these rods.

The overall dimensions, rod pitch, number of rods, and materials are the same as for other region 3 assemblies. These fuel rods will be fabricated in parallel with the regular region 3 rods, using selected region 3 clad and pellets, assembled and then released to the same manufacturing tolerance limits. Mechanically, the special assemblies differ only slightly from other region 3 assemblies. These differences are:

- A. The end plugs on the removable rods are designed to facilitate removal and reinsertion.
- B. The upper nozzle adapter plate on the assembly is modified to allow access to the removable rods.
- C. The base plate on the thimble plug assembly is modified to provide axial restraint of the fuel rods normally provided by the upper nozzle adapter plate for standard assemblies. The distances between the top of the rods and the restraining plates, for both types of rods in the removable rod assembly, are identical to those of the standard assembly.

Figure 4.2-25 compares the mechanical design of a removable fuel rod to that of a standard rod. Figure 4.2-26 shows the removable rod fuel assembly, the modified upper nozzle adapter plate and thimble plug assembly, to compare to a standard assembly shown in figure 4.2-2. The location of the removable rods within the fuel assembly is shown in figure 4.2-27.

Previous experience with removable rods has been attained at Saxton, Yankee, San Onofre, Zorita, Zion Units 1 and 2, Point Beach Unit 1, H. B. Robinson Unit 2, and Trojan and Surry Units 1 and 2 reactors. Handling of removable rods has been done routinely and without difficulty.

The same fuel rod design limits indicated in subsection 4.2.1 for standard fuel rods and assemblies are maintained for these removable rods. Over the active fuel length, the removable rod clad and pellet dimensions and enrichment are identical to other rods in the same fuel region. Therefore, there is no reduction in margin to DNB or other thermal limits. Their inclusion in the initial core loading introduces no additional safety considerations and in no way changes the safeguard analyses and related engineering information presented in previously submitted material in support of the license application.

4.2.2 REACTOR VESSEL INTERNALS

4.2.2.1 Design Bases

The design bases for the mechanical design of the reactor vessel internals components are as follows:

- A. The reactor internals in conjunction with the fuel assemblies shall direct reactor coolant through the core to achieve acceptable flow distribution and to restrict bypass flow so that the heat transfer performance requirements are met for all modes of operation. In addition, required cooling for the pressure vessel head shall be provided so that the temperature differences between the vessel flange and head do not result in leakage from the flange during reactor operation.
- B. In addition to neutron shielding provided by the reactor coolant, a separate neutron pad assembly is provided to limit the exposure of the pressure vessel in order to maintain the required ductility of the material for all modes of operation.
- C. Provisions shall exist for installing incore instrumentation useful for the plant operation and vessel material test specimens required for a pressure vessel irradiation surveillance program.
- D. The core internals are designed to withstand mechanical loads arising from the SSE, 1/2 SSE, and pipe ruptures and meet the requirement of Item E below.
- E. The reactor shall have mechanical provisions sufficient to adequately support the core and internals, and sufficient to assure that the core is intact with acceptable heat transfer geometry following transients arising from abnormal operating conditions.
- F. Following the design basis accident (DBA), the plant shall be capable of being shutdown and cooled in an orderly fashion so that fuel/clad temperature is kept within specified limits. This implies that the deformation of certain critical reactor internals must be kept sufficiently small to allow core cooling.

The functional limitations for the core structures during the design basis accident are shown in table 4.2-1. To ensure no column loading of rod cluster control guide tubes, the upper core plate deflection is limited to not exceed the value shown in table 4.2-1.

Details of the dynamic analyses, input forcing functions, and response loadings are presented in section 3.9.

4.2.2.2 Description and Drawings

The components of the reactor internals consist of the lower core support structure (including the entire core barrel and neutron shield pad assembly), the upper core support structure and the incore instrumentation support structure. The reactor internals support the core, maintain fuel alignment, limit fuel assembly movement, maintain alignment between fuel assemblies and control rod drive mechanisms (CRDM), direct coolant flow past the fuel elements, direct coolant flow to the pressure vessel head, provide gamma and neutron shielding, and provide guides for the incore instrumentation. The coolant flows from the vessel inlet nozzles down the annulus between the core barrel and the vessel wall and then into a plenum at the bottom of the vessel. It then reverses and flows up through the core support and through the lower core plate. The lower core plate is sized to provide the desired inlet flow distribution to the core. After passing through the core, the coolant enters the region of the upper support structure and then flows radially to the core barrel outlet nozzles and directly through the vessel outlet nozzles. A small amount of the entering flow is directed into the vessel head plenum and exits through the vessel outlet nozzles. Similarly, a small portion of the coolant flows between the baffle plates and the core barrel to provide additional cooling of the barrel. Both units were originally designed to direct coolant flow downward between the baffle plates and core barrel. However, both units' reactor vessel internals were modified to direct the coolant flow upward between the baffle plates and core barrel to minimize the effects of water jetting between the baffle plates.

All reactor internals are removable from the vessel for inspection, as well as for the inspection of the vessel's internal surface.

All the major material for the reactor internals is type 304 stainless steel. Parts not fabricated from type 304 stainless steel include bolts and dowel pins which are fabricated from type 316 stainless steel. The clevis insert and radial support key bolts are fabricated of Inconel. The only stainless steel materials used in the reactor core support structures which have yield strengths greater than 90,000 lb are the 403 series used for holddown springs. The use of these materials is compatible with the reactor coolant and is acceptable based on the 1971 ASME Boiler and Pressure Vessel Code, Case No. 1337.

Lower Core Support Structure

The major containment and support member of the reactor internals is the lower core support structure, shown in figure 4.2-10. This support structure assembly consists of the core barrel; the core baffle; the lower core plate and support columns; the neutron shield pads; and the core support, which is welded to the core barrel. The major material for this structure is type 304 stainless steel. The lower core support structure is supported at its upper flange from a ledge in the reactor vessel and, at its lower end, is restrained in its transverse movement by a radial support system attached to the vessel wall. Within the core barrel are an axial baffle and a lower core plate, both of which are attached to the core barrel wall and form the enclosure periphery of the core. The lower core support structure and core barrel provide passageways and direct the coolant flow. The lower core plate is positioned at the bottom level of the core, below the baffle plates, and provides support and orientation for the fuel assemblies.

The lower core plate is a 1.75-inch-thick member through which the necessary flow distribution holes for each fuel assembly are machined. Fuel assembly locating pins (two for each assembly) are also inserted into this plate. Columns are placed between the lower core plate and the core support of the core barrel to provide stiffness and to transmit the core load to the

FNP-FSAR-4

core support. Adequate coolant distribution is obtained through the use of the lower core plate and core support.

The neutron shield pad assembly consists of four pads that are bolted and pinned to the outside of the core barrel. These pads are constructed of type 304 stainless steel and are approximately 36- to 48-in. wide by 148 in. long by 2.7 in. thick. The pads are located azimuthally to provide the required degree of vessel protection. Rectangular specimen guides in which material surveillance samples are inserted and irradiated during reactor operation are bolted and pinned to the pads. The samples are held in the rectangular tubing by a preloaded spring device at the top and bottom to prevent sample movement. Additional details of the neutron shielding pads and irradiation specimen holders are given in reference 7.

Vertically downward loads from weight, fuel assembly preload, control rod dynamic loading, hydraulic loads and earthquake acceleration are carried by the lower core plate into the lower core plate support flange on the core barrel shell and through the lower support columns to the core support and thence through the core barrel shell to the core barrel flange supported by the vessel flange. Transverse loads from earthquake acceleration, coolant cross-flow, and vibration are carried by the core barrel shell and distributed by the lower radial support to the vessel wall, and to the vessel flange. Transverse loads of the fuel assemblies are transmitted to the core barrel shell by direct connection of the lower core plate to the barrel shell by direct connection of the lower core plate to the barrel wall and by upper core plate alignment pins which are welded into the core barrel.

The radial support system of the core barrel is accomplished by "key" and "keyway" joints to the reactor vessel wall. At four equally spaced points around the circumference, an Inconel block is welded to the vessel inner diameter. Another Inconel block is bolted to each of these clevis blocks, and has a "keyway" geometry. Opposite each of these is a "key" which is welded to the lower core supports. At assembly, as the internals are lowered into the vessel, the keys engage the keyways in the axial direction. With this design, the internals are provided with a support at the furthest extremity, and may be viewed as a beam fixed at the top and simply supported at the bottom.

Radial and axial expansions of the core barrel are accommodated, but transverse movement of the core barrel is restricted by this design. With this system, cyclic stresses in the reactor internals are within the ASME Section III limits. In the event of an abnormal downward vertical displacement of the internals following a hypothetical failure, energy-absorbing devices limit the displacement after contacting the vessel bottom head. The load is then transferred through the energy-absorbing devices of the internals to the vessel.

The energy absorbers, cylindrical in shape, are mounted on a base plate, which is contoured on its bottom surface to the reactor vessel bottom internal geometry. Their number and design are determined so as to limit the stresses imposed on all components except the energy absorber to less than yield. Assuming a downward vertical displacement, the potential energy of the system is absorbed mostly by the strain energy of the energy absorbing device.

Upper Core Support Assembly

The upper core support assembly, shown in figures 4.2-11 and 4.2-12, consists of the upper support assembly and the upper core plate between which are contained support columns and guide tube assemblies. The support columns establish the spacing between the top support plate assembly and the upper core plate and are fastened at top and bottom to these plates. The support columns transmit the mechanical loadings between the upper support and the upper core plate. The guide tube assemblies shield and guide the control rod drive shafts and control rods. They are fastened to the top support plate and are guided by pins in the upper core plate for proper orientation and support. Additional guidance for the control rod drive shafts is provided by the upper guide tube which is attached to the upper support.

The upper core support assembly, which is removed as a unit during refueling operation, is positioned in its proper orientation with respect to the lower support structure by slots in the upper core plate which engage flat-sided upper core plate alignment pins welded into the core barrel. At an elevation in the core barrel where the upper core plate is positioned, the flat-sided pins are located at angular positions of 90 degrees from each other. Four slots are milled into the core plate at the same positions. As the upper support structure is lowered into the lower internals, the slots in the plate engage the flat-sided pins in the axial direction. Lateral displacement of the plate and of the upper support assembly is restricted by this design. Fuel assembly locating pins protrude from the bottom of the upper core plate and engage the fuel assemblies as the upper assembly is lowered into place. Proper alignment of the lower core support structure, the upper core support assembly, the fuel assemblies, and the control rods is thereby assured by this system of locating pins and guidance arrangement. The upper core support assembly is restrained from any axial movements by a large circumferential spring which rests between the upper barrel flange and the upper core support assembly and is compressed when the reactor vessel head is installed on the pressure vessel.

Vertical loads from weight, earthquake acceleration, hydraulic loads and fuel assembly preload are transmitted through the upper core plate via the support columns to the upper support plate assembly and then the reactor vessel head. Transverse loads from coolant cross-flow, earthquake acceleration, and possible vibrations are distributed by the support columns to the upper support plate and upper core plate. The upper support structure is particularly stiff in order to minimize deflection.

Incore Instrumentation Support Structures

The incore instrumentation support structures consist of an upper system to convey and support thermocouples penetrating the vessel through the head and a lower system to convey and support flux thimbles penetrating the vessel through the bottom. Figure 7.7-9 shows the basic flux mapping system.

The upper system utilizes the reactor vessel head penetrations. Instrumentation port columns are slip-connected to inline columns that are in turn fastened to the upper support plate. These port columns protrude through the head penetrations. The thermocouples are carried through these port columns and the upper support plate at positions above their readout locations. The thermocouple conduits are supported from the columns of the upper core support system. The thermocouple conduits are type 304 stainless steel tubes.

In addition to the upper incore instrumentation, there are reactor vessel bottom port columns (see figure 4.2-10) which carry the retractable, cold-worked stainless steel flux thimbles that are pushed upward into the reactor core. Conduits extend from the bottom of the reactor vessel down through the concrete shield area and up to a thimble seal line. The minimum bend radii are about 144 in. and the trailing ends of the thimbles (at the seal line) are extracted approximately 15 ft during refueling of the reactor in order to avoid interference within the core. The thimbles are closed at the leading ends and serve as the pressure barrier between the reactor pressurized water and the containment atmosphere.

Mechanical seals between the retractable thimbles and the conduits are provided at the seal line. During normal operation, the retractable thimbles are stationary and move only during refueling or for maintenance, at which time a space of approximately 15 ft above the seal line is cleared for the retraction operation.

The incore instrumentation support structure is designed for adequate support of instrumentation during reactor operation and is rugged enough to resist damage or distortion under the conditions imposed by handling during the refueling sequence. These are the only conditions that affect the incore instrumentation support structure. Reactor vessel surveillance specimen capsules are covered in subsection 5.2.4.4, and all the necessary details with regard to irradiation surveillance are added, including a cross-section of the reactor showing the capsule identity and location.

4.2.2.3 Design Loading Conditions

The design loading conditions that provide the basis for the design of the reactor internals are:

- A. Fuel assembly weight.
- B. Fuel assembly spring forces.
- C. Internals weight.
- D. Control rod trip (equivalent static load).
- E. Differential pressure.
- F. Spring preloads.
- G. Coolant flow forces (static).
- H. Temperature gradients.
- I. Differences in thermal expansion.
 - 1. Because of temperature differences.
 - 2. Because of expansion of different materials.

- J. Interference between components.
- K. Vibration (mechanically or hydraulically induced).
- L. One or more loops out of service.
- M. All operational transients listed in table 5.2-2.
- N. Pump overspeed.
- O. Seismic loads (1/2 SSE and SSE).
- P. Blowdown forces (because of cold and hot leg break).

Combined seismic and blowdown forces are included in the stress analysis as a design loading condition by assuming the maximum amplitude of each force to act concurrently.

The main objective of the design analysis is to satisfy allowable stress limits, to assure an adequate design margin, and to establish deformation limits which are concerned primarily with the functioning of the components. The stress limits are established not only to assure that peak stresses will not reach unacceptable values, but also to limit the amplitude of the oscillatory stress component in consideration of fatigue characteristics of the materials. Both low- and high-cycle fatigue stresses are considered when the allowable amplitude of oscillation is established. Dynamic analysis on the reactor internals is provided in section 3.9.

As part of the evaluation of design loading conditions, extensive testing and inspections are performed from the initial selection of raw materials up to and including component installation and plant operation. Among these tests and inspections are those performed during component fabrication, plant construction, startup and checkout, and during plant operation.

4.2.2.4 Design Loading Categories

The combination of design loadings fits into either the normal, upset, or faulted conditions as defined in the ASME Section III Code.

Loads and deflections imposed on components because of shock and vibration are determined analytically and experimentally in both scaled models and operating reactors. The cyclic stresses caused by these dynamic loads and deflections are combined with the stresses imposed by loads from component weights, hydraulic forces and thermal gradients for the determination of the total stresses of the internals.

The reactor internals are designed to withstand stresses originating from various operating conditions as summarized in table 5.2-2.

The scope of the stress analysis problem is very large, requiring many different techniques and methods, both static and dynamic. The analysis performed depends on the mode of operation under consideration.

Allowable Deflections

For normal operating conditions, downward vertical deflection of the lower core support plate is negligible.

For the loss-of-coolant accident plus the SSE condition, the deflection criteria of critical internal structures are the limiting values given in table 4.2-1. The corresponding no-loss-of-function limits are included in table 4.2-1 for comparison purposes with the allowed criteria.

The criteria for the core drop accident is based upon analyses which have been performed to determine the total downward displacement of the internal structures following a hypothesized core drop resulting from loss of the normal core barrel supports. The initial clearance between the secondary core support structures and the reactor vessel lower head in the hot condition is approximately 1/2 in. An additional displacement of approximately 3/4 in. would occur because of the strain of the energy-absorbing devices of the secondary core support. Thus, the total drop distance is about 1-1/4 in., which is insufficient to permit the grips of the rod cluster control assembly to come out of the guide thimble in the fuel assemblies.

Specifically, the secondary core support is a device which will never be used, except during a hypothetical accident of the core support (core barrel, barrel flange, etc.). There are four supports in each reactor. The core support limits the fall of the core and absorbs the energy of the fall, which otherwise would be imparted to the vessel. The energy of the fall is calculated assuming a complete and instantaneous failure of the primary core support and is absorbed during the plastic deformation of the controlled volume of stainless steel, loaded in tension. The maximum deformation of this austenitic stainless steel piece is limited to approximately 15 percent, after which a positive step is provided to ensure support.

For additional information on design loading categories see section 3.9.

4.2.2.5 Design Criteria Basis

The basis for the design stress and deflection criteria is identified below:

Allowable Stresses

For normal operating conditions, Section III of the ASME Boiler and Pressure Vessel Code is used as a basis for evaluating acceptability of calculated stresses. Both static and alternating stress intensities are considered. Under Code Case 1618, bolt material type 316 stainless steel is now covered in ASME Section III and is so treated. It should be noted that the allowable stresses in Section III of the ASME Code are based on unirradiated material properties. In view of the fact that irradiation increases the strength of the type 304 stainless steel used for the internals, although decreasing its elongation, it is considered that use of the allowable stresses in Section III is appropriate and conservative for irradiated internal structures.

The allowable stress limits during the design basis accident (DBA) used for the core support structures are based on the January 1971 draft of the ASME Code for Core Support Structures, Subsection NG, and the Criteria for Faulted Conditions.

Design of the replaced baffle-former bolts in the Units 1 and 2 reactor vessels is based on the 1989 ASME Code, Subsection NG, as a guideline for allowable stress limits during the design basis accident.

4.2.3 REACTIVITY CONTROL SYSTEM

4.2.3.1 Design Bases

4.2.3.1.1 Design Stresses

A basis for temperature, stress on structural members, and material compatibility are imposed on the design of the reactivity control components. The reactivity control system is designed to withstand stresses originating from various operating conditions as summarized in Table 5.2-2.

Allowable Stresses: For normal operating conditions, Section III of the ASME Boiler and Pressure Vessel Code is used as a general guide. Stress and deformation limits for the reactivity control system are as follows:

ANS N18.2 Conditions I and II

Section III of the ASME Code is used as a general guide.

ANS N18.2 Condition III and IV

Full-length control rods - Full-length control rods must not be prevented from performing their function.

Other reactivity control systems - The reactivity control system must not interfere with reactor shutdown or emergency cooling of the fuel rods.

Dynamic Analysis: The cyclic stresses caused by dynamic loads and deflections are combined with the stresses imposed by loads from component weights, hydraulic forces, and thermal gradients for the determination of the total stresses of the reactivity control system.

4.2.3.1.2 Material Compatibility

Materials are selected for compatibility in a PWR environment, for adequate mechanical properties at room and operating temperature, for resistance to adverse property changes in a radioactive environment, and for compatibility with interfacing components.

4.2.3.1.3 Reactivity Control Components

The reactivity control components are subdivided into two categories:

- A. Permanent devices used to control or monitor the core.
- B. Temporary devices used to control or monitor the core.

The permanent components are the full-length rod cluster control assemblies, control rod drive mechanism assemblies, neutron source assemblies, and thimble plug assemblies. Although the thimble plug assembly does not directly contribute to the reactivity control of the reactor, it is presented as a reactivity control system component in this document because it is needed to restrict bypass flow through those thimbles not occupied by absorber, source, or burnable absorber rods.

The temporary component is the burnable absorber assembly. The design bases for each of the mentioned components are in the following paragraphs.

Absorber Rods

The following are considered design conditions under Sections NG and NB of the ASME Boiler and Pressure Vessel Code Section III:

The control rod which is cold rolled type 304 stainless steel is the only noncode material used in the control rod assembly.

The stress intensity limit S_m for this material is defined as two-thirds of the 0.2 percent offset yield stress.

- A. The external pressure equal to the reactor coolant system (RCS) operating pressure.
- B. The wear allowance equivalent to 1,000 reactor trips.
- C. Bending of the rod because of a misalignment in the guide tube.
- D. Forces imposed on the rods because of rod trip.
- E. Loads caused by accelerations imposed by the control rod drive mechanism.
- F. Radiation exposure for maximum core life.
- G. Temperature effects at operating condition.

The absorber material temperature shall not exceed its melting temperature (1470°F for Ag-In-Cd absorber material).⁽²⁾

Burnable Absorber Rods (Standard and WABA)

The burnable absorber rod clad is designed using Sections NG and NB of the ASME Boiler and Pressure Vessel code, Section III, 1973 as a guide for Conditions I and II. For abnormal loads during Conditions III and IV, code stresses are not considered limiting. Failures of the burnable absorber rods during these conditions must not interfere with reactor shutdown or emergency cooling of the fuel rods. The burnable absorber material is nonstructural. The structural elements of the burnable absorber rod are designed to maintain the absorber geometry even if the absorber material is fractured. In addition, the structural elements are designed to prevent excessive slumping.

The standard burnable absorber material is borosilicate glass and is designed so that the absorber material is below its softening temperature of $1510^{\circ}\text{F} + 18^{\circ}\text{F}$ for 12.5 w/o boron rods. The softening temperature for borosilicate glass is defined in ASTM C 338.

The wet annular burnable absorber (WABA) material is B_4C contained in an alumina matrix. Thermal-physical and gas release properties of $\text{Al}_2\text{O}_3 - \text{B}_4\text{C}$ are described in reference 9. The WABA rods are designed so that the absorber temperature does not exceed 1200°F during normal operation or an overpower transient. The 1200°F maximum temperature helium gas release in a WABA rod will not exceed 30 percent.⁽⁹⁾

Neutron Source Rods

The neutron source rods are designed to withstand the following:

- A. The external pressure equal to the RCS operating pressure.
- B. An internal pressure equal to the pressure generated by released gases over the source rod life.

Thimble Plug Assembly

When used, the thimble plug assemblies satisfy the following:

- A. Accommodate the differential thermal expansion between the fuel assembly and the core internals.
- B. Maintain positive contact with the fuel assembly and the core internals.
- C. Limit the flow through each occupied thimble to the acceptable design value.

4.2.3.1.4 Control Rod Drive Mechanisms (CRDM)

The pressure vessel assembly consists of Class I components designed to meet the stress requirements for normal operating conditions of Section III of the ASME Boiler and Pressure

Vessel Code. Both static and alternating stress intensities are considered. The stresses originating from the required design transients are included in the analysis.

A dynamic seismic analysis is required on the full-length control rod drive mechanism when a seismic disturbance has been postulated to confirm the ability of the mechanism to meet ASME Code, Section III allowable stresses and to confirm its ability to trip when subjected to the seismic disturbance.

The control rod drive mechanism design used for the 17 x 17 fuel assembly control rod is identical to the 15 x 15 CRDM. The seismic analysis and response of the 17 x 17 CRDM will be identical to those of the 15 x 15 mechanism.

Full-Length Control Rod Drive Mechanism Operational Requirements

The basic operational requirements for the full-length CRDMs are as follows:

- A. 5/8-in. step.
- B. 144-in. travel.
- C. 360-lb maximum load.
- D. Step in-or-out at 45 in./min (72 steps/min) maximum.
- E. Power interruption shall initiate release of drive rod assembly.
- F. Trip delay of < 150 ms. Free fall of drive rod assembly shall begin < 150 ms after power interruption no matter what holding or stepping action is being executed with any load and coolant temperatures of 100°F to 550°F.
- G. 40-year design life with normal refurbishment.^(a)
- H. 28,000 complete travel excursions which is 13×10^6 steps with normal refurbishment.^(a)

4.2.3.2 Description and Drawings

Reactivity control is provided by neutron absorbing rods and a soluble chemical neutron absorber (boric acid). Design drawings and flow diagrams for the chemical injection system are given in subsection 9.3.4. The boric acid concentration is varied to control long-term reactivity changes such as:

- A. Fuel depletion and fission product buildup.
- B. Cold to hot, zero power reactivity change.
- C. Reactivity change produced by intermediate-term fission products such as xenon and samarium.

FNP-FSAR-4

- D. Burnable absorber depletion.

The rod cluster control assemblies provide reactivity control for:

- A. Shutdown.
- B. Reactivity changes caused by coolant temperature changes in the power range.
- C. Reactivity changes associated with the power coefficient of reactivity.
- D. Reactivity changes caused by void formation.

For the initial cycle and reload cycles, if soluble boron was the sole means of control, the moderator temperature coefficient would be above its technical specification limit at beginning of life. The moderator temperature coefficient is kept within its technical specification limit by installation of burnable absorbers and by rod withdrawal limits, when necessary.

The neutron source assemblies provide neutrons to assure the source range detectors are responding and operable. With natural sources in the burned fuel, these assemblies are not necessary.

a. The renewed operating licenses authorize an additional 20-year period of extended operation for both FNP units, resulting in a plant operating life of 60 years. In accordance with 10 CFR Part 54, appropriate aging management programs and activities have been initiated to manage the detrimental effects of aging to maintain functionality during the period of extended operation (see chapter 18).

The most effective reactivity control components are the full-length rod cluster control assemblies and their corresponding drive rod assemblies which are the only kinetic parts in the reactor. Figure 4.2-13 identifies the full-length rod cluster control and drive rod assembly, in addition to the arrangement of these components in the reactor relative to the interfacing fuel assembly, guide tubes, and control rod drive mechanism.

The guidance system for the full-length control rod cluster is provided by the guide tube as shown on figure 4.2-13. The guide tube provides two regimes of guidance: First, in the lower section, a continuous guidance system provides support immediately above the core, which protects the rod against excessive deformation and wear caused by hydraulic loading. Second, the region above the continuous section provides support and guidance at uniformly spaced intervals.

The envelope of support is determined by the pattern of the control rod cluster as shown on figure 4.2-14. The guide tube ensures alignment and support of the control rods, spider body,

and drive rod while maintaining trip times at or below required limits. In the following paragraphs, each reactivity control component is described in detail.

4.2.3.2.1 Reactivity Control Components

Full-Length Rod Cluster Control Assembly

The full-length rod cluster control assemblies are divided into two groups: control and shutdown. The control group compensates for reactivity changes due to variations in operating conditions of the reactor, i.e., power and temperature variations. Two criteria have been employed for selection of the control group. First, the total reactivity worth must be adequate to meet the nuclear requirements of the reactor. Second, in view of the fact that these rods may be partially inserted at power operation, the total power peaking factor should be low enough to ensure that the power capability is met. The control and shutdown groups provide adequate shutdown margin which is defined as the amount by which the core would be subcritical at hot shutdown if all rod cluster control assemblies are tripped assuming that the highest-worth assembly remains fully withdrawn and assuming no changes in xenon or boron concentration. With any RCCA not capable of being fully inserted, the reactivity worth of the RCCA must be accounted for in the determination of SDM; and in Modes 1 and 2, the fuel and moderator temperatures are changed to the hot zero power temperatures.

A rod cluster control assembly comprises a group of individual neutron absorber rods fastened at the top end to a common spider assembly, as illustrated in figure 4.2-14.

The absorber material used in the control rods is silver-indium-cadmium alloy which is essentially "black" to thermal neutrons and has sufficient additional resonance absorption to significantly increase its worth. The alloy is in the form of extruded rods which are sealed in stainless steel tubes to prevent the rods from coming in direct contact with the coolant. In construction, the silver-indium-cadmium rods are inserted into cold worked stainless steel tubing which is then sealed at the bottom and the top by welded end plugs as shown in figure 4.2-15. Sufficient diametral and end clearance is provided to accommodate relative thermal expansions.

Commencing with Cycle 16 in Unit 1 and subsequent cycles enhanced performance rod cluster control assemblies (EP-RCCAs) are being phased into use as replacements for the original RCCAs. The EP-RCCA design uses cold worked, high purity stainless steel tubes for the absorber rodlet cladding. A thin chrome electroplate may be applied to the outer surface over a specified length of the absorber rodlet cladding in contact with the reactor internal guides to provide increased resistance to cladding wear. In addition, the absorber diameter is reduced slightly at the lower extremity of the rodlets in order to accommodate absorber swelling and minimize cladding interaction.

The bottom plugs are made bullet nosed to reduce the hydraulic drag during reactor trip and to guide smoothly into the dashpot section of the fuel assembly guide thimbles. The upper plug is threaded for assembly to the spider and has a reduced end section to make the joint more flexible.

FNP-FSAR-4

The material used in the absorber rod end plugs is type 308 stainless steel. The design stresses used for the type 308 material are the same as those defined in the ASME Code, Section III, for type 304 stainless steel. At room temperature the yield and ultimate stresses per American Society of Testing Materials (ASTM) 580 are exactly the same for the two alloys. In view of the similarity of composition of the alloys, the temperature dependence of strength for the two materials is also assumed to be the same.

The allowable stresses used as a function of temperature are listed in Table 1-1.2 of Section III of the ASME Code. The fatigue strength for the type 308 material is based on the S-N curve for austenitic stainless steels in figure 1-9.2 of Section III.

The spider assembly is in the form of a central hub with radial vanes containing cylindrical fingers from which the absorber rods are suspended. Handling detents and detents for connection to the drive rod assembly are machined into the upper end of the hub. A spring pack is assembled into a skirt integral to the bottom of the hub to stop the rod cluster control assembly and absorb the impact energy at the end of a trip insertion. The radial vanes are joined to the hub and the fingers are joined to the vanes by furnace brazing. A centerpost which holds the spring pack and its retainer is threaded into the hub within the skirt and welded to prevent loosening in service. All components of the spider assembly are made from type 304 and type 308 stainless steel except for the retainer, which is of 17-4 pH material, and the springs, which are Inconel X-718 alloy or oil tempered carbon steel where the springs do not contact the coolant.

The absorber rods are fastened securely to the spider to assure trouble-free service. The rods are first threaded into the spider fingers and then pinned to maintain joint tightness, after which the pins are welded in place. The end plug below the pin position is designed with a reduced section to permit flexing of the rods to correct for small operating or assembly misalignments.

The overall length is such that when the assembly is withdrawn through its full travel the tips of the absorber rods remain engaged in the guide thimbles so that alignment between rods and thimbles is always maintained. Since the rods are long and slender, they are relatively free to conform to any small misalignments with the guide thimble.

Burnable Absorber Assembly

Each burnable absorber assembly consists of burnable absorber rods attached to a holddown assembly. The burnable absorber assemblies are shown in figure 4.2-16 for standard and WABA design.

The standard absorber rods consist of borosilicate glass tubes contained within type 304 stainless steel tubular cladding which is plugged and seal welded at the ends to encapsulate the glass. The glass is also supported along the length of its inside diameter by a thin-wall, tubular, inner liner of type 304 stainless steel. The top end of the liner is open to permit the diffused helium to pass into the void volume, and the liner extends beyond the forward end of the glass tube to assure the liner always overhangs the glass. The liner has an outward flange at the bottom end to maintain the position of the liner with the glass. The clad in the rod assemblies is slightly cold worked 304 stainless steel. All other structural materials are 304 or 308 stainless steel except for the springs which are Inconel X-718. The borosilicate glass tube provides

sufficient boron content to meet the criteria discussed in subsection 4.3.1. A typical burnable absorber rod is shown in longitudinal and transverse cross-sections in figure 4.2-17.

The WABA rod consists of annular pellets of aluminaboron carbide $\text{Al}_2\text{O}_3 - \text{B}_4\text{C}$ burnable absorber material contained within two concentric zircaloy tubes. These zircaloy tubes, which form the inner and the outer clad for the WABA rod, are pressurized with helium and plugged and seal welded at each end to encapsulate the stack of absorber material. The absorber stack length (figure 4.2-16) is positioned axially within the WABA rod by the use of zircaloy bottom end spacers. An annular plenum is provided within the rod to accommodate the helium gas released from the absorber material as it depletes during irradiation. The reactor coolant flows inside the inner tube and outside the outer tube of the annular rod. A typical WABA burnable absorber rod is shown in longitudinal and transverse cross-sections in figure 4.2-17. Additional design details are given in Section 3.0 of reference 9.

The rods are statically suspended and positioned in selected guide thimbles within specified fuel assemblies. The absorber rods in each fuel assembly are grouped and attached together at the top end of the rods to a holddown assembly by a flat, perforated retaining plate which fits within the fuel assembly top nozzle and rests on the adaptor plate. The retaining plate (and the absorber rods) is held down and restrained against vertical motion through a spring pack which is attached to the plate and is compressed by the upper core plate when the reactor upper internals assembly is lowered into the reactor. This arrangement assures that the absorber rods cannot be ejected from the core by flow forces. Through Farley Unit 1 cycle 9 and Farley Unit 2 cycle 7, each rod is permanently attached to the base plate by a nut which is lock welded into place. Starting with Farley Unit 1 cycle 10 and Farley Unit 2 cycle 8, each rod is permanently attached to the base plate by a crimped attaching nut.

Neutron Source Assembly

The purpose of the neutron source assembly is to provide base neutron level to ensure that the detectors are operational and responding to core multiplication neutrons. Since in the first core there is very little neutron activity during loading, refueling, shutdown, and approach to criticality, a neutron source is placed in the reactor to provide a positive neutron count of at least 2 counts per second on the source range detectors attributable to core neutrons. Subsequent cores have enough of a neutron source in their burned fuel to not require a source assembly to meet these operability requirements. The detectors, called source range detectors, are used primarily when the core is subcritical and during special subcritical modes of operation.

The source assembly also permits detection of changes in the core multiplication factor during core loading refueling and approach to criticality. This can be done since the multiplication factor is related to an inverse function of the detector count rate. Therefore, a change in the multiplication factor can be detected during addition of fuel assemblies while loading the core, a change in control rod positions, and changes in boron concentration.

Both primary and secondary neutron source rods are used in the initial core. The primary source rod, containing a radioactive material, spontaneously emits neutrons during initial core loading and reactor startup. After the primary source rod decays beyond the desired neutron flux level, neutrons are then supplied by the secondary source rod. The secondary source rod, containing stable material, must be activated by neutron bombardment during reactor operation.

FNP-FSAR-4

This activation results in the subsequent release of neutrons and a source of neutrons during periods of low neutron activity, such as refueling and the following startups.

The secondary source assemblies can be eliminated from reload cores if sufficient neutron activity is available from the fuel to maintain the reactivity monitoring capability.

The initial reactor core employs four source assemblies: two primary source assemblies and two secondary source assemblies. Each primary source assembly contains one primary source rod and between 0 and 19 burnable absorber rods. Each secondary source assembly contains a symmetrical grouping of four secondary source rods and burnable absorber rods for Unit 1 cycles 1 and 2 only (figure 4.2-19a). For Unit 1 cycles 2 to 12 and Unit 2 cycles 1 to 9, each secondary source assembly contains a symmetrical grouping of four secondary source rods with no burnable absorber rods (figure 4.2-19b). Starting from Unit 2 cycle 9 and Unit 1 cycle 12, a new double encapsulated secondary source design has been introduced (reference 19). The new secondary source assembly also contains a symmetrical grouping of four secondary source rods with no burnable absorber rods (figure 4.2-19c). The location of the secondary source assemblies in the Unit 1 and Unit 2 initial cores is shown in figures 4.3-5 and 4.3-6, respectively. Locations not filled with a source or burnable absorber rod contain a thimble plug. Conceptual source assemblies are shown in figures 4.2-18 and -19. For subsequent reloads, the primary sources are removed, and the secondary sources continue functioning. Commencing with Cycle 17 in Unit 2 and Cycle 20 in Unit 1, the secondary source assemblies are eliminated from the core.

The primary and secondary source rods both utilize the same type of cladding material as the absorber rods. The secondary source rods contain Sb-Be pellets stacked to a height of approximately 88 inches. The primary source rods contain capsules of californium source material and alumina spacer rods to position the source material within the cladding. The rods in each assembly are permanently fastened at the top end to a holddown assembly, which is similar to that of the burnable absorber assemblies.

The other structural members are constructed of type 304 stainless steel except for the springs. The springs exposed to the reactor coolant are wound from an age-hardened, nickel-based alloy for corrosion resistance and high strength. The springs, when contained within the rods where corrosion resistance is not necessary, are of an oil-tempered carbon steel.

Thimble Plug Assembly

In order to limit bypass flow through the rod cluster control (RCC) guide thimbles in fuel assemblies which do not contain either control rods, source rods, or burnable absorber rods, the fuel assemblies at those locations may be fitted with thimble plug assemblies. The effect of thimble plug removal is incorporated into the thermal-hydraulic analysis which bounds either conditions with or without thimble plugs.

The thimble plug assemblies as shown in figure 4.2-20 consist of a flat base plate with short rods suspended from the bottom surface and a spring pack assembly. The 24 short rods, called thimble plugs, project into the upper ends of the guide thimbles to reduce the bypass flow area. Similar short rods are also used on the source assemblies and burnable absorber assemblies to fill the ends of all vacant fuel assembly guide thimbles. At installation in the core, the thimble

plug assemblies interface with both the upper core plate and with the fuel assembly top nozzles by resting on the adaptor plate. The spring pack is compressed by the upper core plate when the upper internals assembly is lowered into place. Each thimble plug is permanently attached to the base plate by a nut which is lock-welded or crimped to the threaded end of the plug.

All components in the thimble plug assembly, except for the springs, are constructed from type 304 stainless steel. The springs are wound from an age-hardened, nickel-based alloy for corrosion resistance and high strength.

4.2.3.2.2 Control Rod Drive Mechanism

All parts exposed to reactor coolant are made of metals which resist the corrosive action of the water. Three types of metals are used exclusively: stainless steels, Inconel-X, and cobalt-based alloys. Wherever magnetic flux is carried by parts exposed to the main coolant, 400 series stainless steel is used. Cobalt-based alloys are used for the pins and latch tips. Inconel-X is used for the springs of latch assemblies, and type 304 stainless steel is used for all pressure-retaining components. Hard chrome plating provides wear surfaces on the sliding parts and prevents galling between mating parts.

A rod position coil stack indicator assembly slides over the full-length control rod drive mechanism rod travel housing. It detects the drive rod assembly position by means of 42 discrete coils that magnetically sense the entry and presence of the drive rod assembly through its center line over the normal length of the drive rod assembly travel.

Full-Length Control Rod Drive Mechanism

Control rod drive mechanisms are located on the dome of the reactor vessel head. Full-length control rod drive mechanisms are coupled to rod cluster control assemblies which have neutron absorber material over the entire length of the control rods and derive their name from this feature. The full-length control rod drive mechanism is shown on figure 4.2-21 and schematically on figure 4.2-22.

The primary function of the full-length control rod drive mechanism is to insert, withdraw, or hold RCCAs within the core to control average core temperature and to shut down the reactor.

The full-length control rod drive mechanism is a magnetically operated jack. A magnetic jack is an arrangement of three electromagnets which are energized in a controlled sequence by a power cycler to insert or withdraw RCCAs in the reactor core in discrete steps.

The control rod drive mechanism consists of four separate subassemblies. They are the pressure vessel assembly, the coil stack assembly, the latch assembly, and the drive rod assembly.

- A. The pressure vessel assembly includes a latch housing and a one-piece rod travel housing which are connected by a butt welded joint which facilitates replacement of the latch assembly.

FNP-FSAR-4

The latch housing is the lower portion of the pressure vessel and encloses the latch assembly. The rod travel housing is the upper portion of the pressure vessel and provides space for the drive rod assembly during its upward movement as the control rods are withdrawn from the core.

- B. The coil stack assembly includes the coil housings, an electrical conduit and connector, and three operating coils: the stationary gripper coil, the moveable gripper coil, and the lift coil.

The coil stack assembly is a separate unit which is installed on the control rod drive mechanism by sliding it over the outside of the latch housing. It rests on the base of the latch housing without mechanical attachment.

Energizing of the operation coils causes movement of the pole pieces and latches in the latch assembly.

- C. The latch assembly includes the guide tube, stationary pole pieces, moveable pole pieces, and two sets of latches: the moveable gripper latch, and the stationary gripper latch.

The latches engage grooves in the drive rod assembly. The moveable gripper latches are moved up or down in 5/8-inch steps by the lift pole to raise or lower the drive rod assembly. The stationary gripper latches hold the drive rod assembly while the moveable gripper latches are repositioned for the next 5/8-inch step.

- D. The drive rod assembly includes a flexible coupling, a drive rod, a disconnect button, a disconnect rod assembly, and a locking button.

The drive rod is machined with grooves on a 5/8-inch pitch which receive the latches during holding or moving of the drive rod assembly. The flexible coupling is attached to the drive rod and produces the means for coupling to the rod cluster control assembly.

The disconnect button, disconnect rod assembly, and locking button provide positive locking of the coupling to the rod cluster control assembly and permits remote disconnection of the drive rod assembly.

The control rod drive mechanism is a trip design. Tripping can occur during any part of the power-cycler sequencing if power to the coils is interrupted.

The control rod drive mechanism is threaded and seal welded on a head adaptor on top of the reactor vessel head and is coupled to the rod cluster control assembly directly below.

The mechanism is capable of handling a 360-pound load, including the drive rod assembly weight, at a maximum rate of 45 inches/minute. Withdrawal of the rod cluster control assembly is accomplished by magnetic forces while insertion is by gravity.

FNP-FSAR-4

The mechanism internals are designed to operate in 650°F reactor coolant. The pressure vessel assembly is designed to contain reactor coolant at 650°F and 2500 psia. The three operating coils are designed to operate at 392°F with forced-air cooling required to maintain that temperature.

The full-length control rod drive mechanism shown schematically in figure 4.2-22 withdraws and inserts its control rod as electrical pulses are received by the operator coils. An ON-or-OFF sequence, repeated by silicon controlled rectifiers in the power programmer, causes either withdrawal or insertion of the control rod. The position of the drive rod assembly is measured by 42 discrete coils mounted on the rod position indicator coil stack assembly surrounding the rod travel housing. Each coil magnetically senses the entry and presence of the top of the ferro-magnetic drive rod assembly as it moves through the coil center line.

During plant operation the stationary gripper coil of the control rod drive mechanism holds the control rod withdrawn from the core in a static position until the movable gripper coil is energized.

Rod Cluster Control Assembly Withdrawal

The control rod is withdrawn by repetition of the following sequence of events:

A. Movable Gripper Coil - ON

The latch locking plunger raises and swings the movable gripper latches into the drive rod assembly groove. A 1/16-inch axial clearance exists between the latch teeth and the drive rod.

B. Stationary Gripper Coil - OFF

The force of gravity, acting upon the drive rod assembly and attached control rod, causes the stationary gripper latches and plunger to move downward 1/16-inch until the load of the drive rod assembly and attached control rod is transferred to the movable gripper latches. The plunger continues to move downward and swings the stationary gripper latches out of the drive rod assembly groove.

C. Lift Coil - ON

The 5/8-inch gap between the movable gripper pole and the lift pole closes and the drive rod assembly with attached control rod raises one step length (5/8-inch).

D. Stationary Gripper Coil - ON

The plunger raises and closes the gap below the stationary gripper pole. The three links, pinned to the plunger, swing and the stationary gripper latches into a drive rod assembly groove. The latches contact the drive rod assembly and lift it (and the attached control rod) 1/16-inch. The 1/16-inch vertical drive rod assembly movement transfers the drive rod assembly load from the movable gripper latches to the stationary gripper latches.

FNP-FSAR-4

E. Movable Gripper Coil - OFF

The latch locking plunger separates from the movable gripper pole under the force of a spring and gravity. Three links, pinned to the plunger, swing the three movable gripper latches out of the drive rod assembly groove.

F. Lift Coil - OFF

The gap between the movable gripper pole and lift pole opens. The movable gripper latches drop 5/8-inch to a position adjacent to a drive rod assembly groove.

G. Repeat Step A

The sequence described above (A thru F) is termed as one step or one cycle. The control rod moves 5/8-inch for each step or cycle. The sequence is repeated at a rate of up to 72 steps per minute and the drive rod assembly (which has a 5/8-inch groove pitch) is raised 72 grooves per minute. The control rod is thus withdrawn at a rate up to 45 inches per minute.

Rod Cluster Control Assembly Insertion

The sequence for control rod insertion is similar to that for control rod withdrawal, except the timing of lift coil ON and OFF is changed to permit lowering the control rod .

A. Lift Coil - ON

The 5/8-inch gap between the movable gripper and lift pole closes. The movable gripper latches are raised to a position adjacent to a drive rod assembly groove.

B. Movable Gripper Coil - ON

The latch locking plunger raises and swings the movable gripper latches into a drive rod assembly groove. A 1/16-inch axial clearance exists between the latch teeth and the drive rod assembly.

C. Stationary Gripper Coil - OFF

The force of gravity, acting upon the drive rod assembly and attached control rod, causes the stationary gripper latches and plunger to move downward 1/16-inch until the load of the drive rod assembly and attached control rod is transferred to the movable gripper latches. The plunger continues to move downward and swings the stationary gripper latches out of the drive rod assembly groove.

D. Lift Coil - OFF

The force of gravity separates the movable gripper pole from the lift pole and the drive rod assembly and attached control rod drop down 5/8-inch.

E. Stationary Gripper - ON

The plunger raises and closes the gap below the stationary gripper pole. The three links, pinned to the plunger, swing the three stationary gripper latches into a drive rod assembly groove. The latches contact the drive rod assembly and lift it (and the attached control rod) 1/16 inch. The 1/16-inch vertical drive rod assembly movement transfers the drive rod assembly load from the movable gripper latches to the stationary gripper latches.

F. Movable Gripper Coil - OFF

The latch locking plunger separates from the movable gripper pole under the force of a spring and gravity. Three links, pinned to the plunger, swing the three movable gripper latches out of the drive rod assembly groove.

G. Repeat Step A

The sequence is repeated, as for control rod withdrawal, up to 72 steps per minute which gives a control rod insertion rate of 45 inches per minute.

Holding and Tripping of the Control Rods

During most of the plant operating time, the control rod drive mechanisms hold the control rods withdrawn from the core in a static position. In the holding mode, only one coil, the stationary gripper coil, is energized on each mechanism. The drive rod assembly and attached control rod hang suspended from the three latches.

If power to the stationary gripper coil is cut off, the combined weight of the drive rod assembly and the rod cluster control assembly is sufficient to move latches out of the drive rod assembly groove. The control rod falls by gravity into the core. The trip occurs as the magnetic field, holding the stationary gripper plunger half against the stationary gripper pole, collapses and the stationary gripper plunger half is forced down by the weight acting upon the latches. After the drive rod assembly is released by the mechanism, it falls freely until the control rods enter the buffer section of their thimble tubes.

4.2.3.3 System Evaluation

4.2.3.3.1 **Reactivity Control Components**

The components are analyzed for loads corresponding to normal, upset, emergency, and faulted conditions. The analysis performed depends on the mode of operation under consideration.

The scope of the analysis requires many different techniques and methods, both static and dynamic. An explanation of the techniques and analytical methods used is included in section 3.9.

FNP-FSAR-4

Some of the loads that are considered on each component where applicable are as follows:

- A. Control rod trip (equivalent static load).
- B. Differential pressure.
- C. Spring preloads.
- D. Coolant flow forces (static).
- E. Temperature gradients.
- F. Differences in thermal expansion.
 - a. Because of temperature differences.
 - b. Because of expansion of different materials.
- G. Interference between components.
- H. Vibration (mechanically or hydraulically induced).
- I. All operational transients listed in table 5.2-2.
- J. Pump overspeed.
- K. Seismic loads (1/2 SSE and SSE).

The main objective of the analysis is to satisfy allowable stress limits, to assure an adequate design margin, and to establish deformation limits which are concerned primarily with the functioning of the components. The stress limits are established not only to assure that peak stresses will not reach unacceptable values, but also to limit the amplitude of the oscillatory stress component in consideration of fatigue characteristics of the materials. Standard methods of strength of materials are used to establish the stresses and deflections of these components. The dynamic behavior of the reactivity control components has been studied using experimental test data (D loop, reference 12) and experience from operating reactors.

The design of reactivity component rods provides a sufficient cold void volume within the standard and WABA burnable absorber and the source rods to limit the internal pressures to a value which satisfies the criteria in paragraph 4.2.3.1. The void volume for the helium in the standard burnable absorber rods is obtained through the use of glass in tubular form which provides a central void along the length of the rods. Helium gas is not released by the neutron absorber rod material, thus the absorber rod only sustains an external pressure during operating conditions. The internal pressure of source rods continues to increase from ambient until end of life (EOL) at which time the internal pressure never exceeds that allowed by the criteria in paragraph 4.2.3.1. The stress analysis of reactivity component rods assumes 100 percent gas release to the rod void volume, considers the initial pressure within the rod, and assumes that the pressure external to the component rod is zero.

Based on available data for properties of the borosilicate glass and on nuclear and thermal calculations for the burnable absorber rods, gross swelling or cracking of the glass tubing is not expected during operation. Some minor creep of the glass at the hot spot on the inner surface of the tube is expected to occur, but continues only until the glass comes in contact with the inner liner. The wall thickness of the inner liner is sized to provide adequate support in the event of slumping and to collapse locally before rupture of the exterior cladding if unexpected, large volume changes caused by swelling or cracking should occur. The top of the inner liner is open to receive the helium which diffuses out of the glass. The Al_2O_3 - B_4C WABA pellets are designed such that gross swelling or crumbling of the pellets is not expected during reactor operation. Some minor cracking of the pellets may occur, but this cracking should not affect the overall absorber stack integrity.

Sufficient diametral and end clearances have been provided in the neutron absorber, burnable absorber, and source rods to accommodate the relative thermal expansions between the enclosed material and the surrounding clad and end plugs. Analysis has shown that there is no apparent reason for bending or warping of the long flexible rods to occur. The generous clearance offered by the guide thimble would permit a postulated warpage to occur possibly without restraint on the rods. The radial and axial temperature profiles have been determined by considering gap conductance, thermal expansion, and neutron and/or gamma heating of the contained material, as well as gamma heating of the clad. The maximum neutron absorber material temperature was found to be less than 900°F, which occurs axially at only the highest flux region. The maximum borosilicate glass temperature in the standard burnable absorber was found to be less than 1100°F and takes place following the initial rise to power. The maximum temperature of the Al_2O_3 - B_4C burnable absorber pellet is calculated to be less than 1200°F which takes place following the initial rise to power. The glass and pellet temperature then decreases rapidly for the following reasons: reduction in heat generation due to B10 depletion; better gap conductance as the helium produced diffuses to the gap; and, for the standard burnable absorber, external gap reduction because of borosilicate glass creep. The rod, guide thimble, and dashpot flow analysis performed indicates that the flow is sufficient to prevent coolant boiling while maintaining low cladding temperatures at which the clad material has adequate strength to resist coolant operating pressures and rod internal pressures.

Analysis and experimental tests on the full-length rod cluster control spider indicate that the spider is structurally adequate to withstand the various operating condition loads, especially the higher loads occurring during the drive mechanism stepping action and rod drop.

The evaluation of the materials used in the reactivity control components includes considerations such as material adequacy throughout the design lifetime of the control system. The materials selected were (and still are) considered to be the best available from the standpoint of resistance to irradiation damage and compatibility to the reactor environment. (In fact, the materials selected partially dictate the reactor environment, e.g., C1 control in the coolant.) Thus far, the current design-type reactivity controls have been in service for as much as six years with no apparent degradation of construction materials.

Specifically with regard to the aspect of the materials of construction exhibiting satisfactory resistance to adverse property changes in a radioactive environment, it should be noted that in current design work on breeder reactors, similar materials are being applied because better materials are not known. At high fluences the austenitic materials increase in strength with a

corresponding decrease in ductility (as measured by tensile tests), but energy absorption (as measured by impact tests) remains quite high. The mechanism for this apparent conflict is not clear, but it would appear that the ductility loss is not in itself an indication of drastically reduced fracture-energy requirements. With regard to degradation of materials by corrosion, it should be noted that the general corrosion of the materials exposed to the coolant is quite low and that proper control of C_1 and O_2 in the coolant will prevent the occurrence of stress corrosion. All of the austenitic stainless steel base materials used are processed and fabricated to preclude sensitization. Although the control rod spiders are fabricated by furnace brazing, the procedure used requires that the pieces be rapidly cooled so that the time-at-temperature is minimized. The time that is spent by the control rod spiders in the sensitization range, 800-1500°F, is not more than 0.2 hours, as a maximum, during fabrication to preclude sensitization. The 17-4 PH parts are all aged at the highest standard aging temperature of 1100°F to avoid stress corrosion problems exhibited by aging at lower temperatures.

Analysis of the full-length rod cluster control assemblies shows that if the drive mechanism housing ruptures, the rod cluster control assembly will be ejected from the core by the pressure differential of the operating pressure and ambient pressure across the drive rod assembly. The ejection is also predicted on the failure of the drive mechanism to retain the drive rod/rod cluster control assembly position. It should be pointed out that a drive mechanism housing rupture will cause the ejection of only one rod cluster control assembly with the other assemblies remaining in the core. Analysis also showed that a pressure drop in excess of 4000 psi must occur across a two-fingered vane to break the vane/spider body joint causing ejection of two neutron absorber rods from the core. Since the greatest pressure drop in the system is only 2250 psi, a pressure drop in excess of 4000 psi is incredible. Thus, the ejection of the neutron absorber rods is not possible.

Ejection of a burnable absorber or thimble plug assembly is conceivable based on the postulation that the holddown bar fails and that the base plate and burnable absorber rods severely deform. In the unlikely event that failure of the holddown bar occurs, the upward displacement of the burnable absorber assembly only permits the base plate to contact the upper core plate. Since this displacement is small, the major portion of the burnable absorber remains positioned within the core. In the case of the thimble plug assembly, the thimble plugs will partially remain in the fuel assembly guide thimbles, thus maintaining a majority of the desired flow impedance. Further displacement or complete ejection would necessitate that the square base plate and burnable absorber rods be forced, thus plastically deformed, to fit up through a smaller diameter hole. It is expected that this condition requires a substantially higher force or pressure drop than that of the holddown bar failure.

Experience with control rods, burnable absorber rods, and source rods is discussed in reference 8.

The mechanical design of the reactivity control components provides for the protection of the active elements to prevent the loss of control capability and functional failure of critical components. The components have been reviewed for potential and consequences of a functional failure of critical parts. The results of the review are summarized below.

Full-Length Rod Cluster Control Assembly

- A. The basic absorbing material is sealed from contact with the primary coolant and the fuel assembly and guidance surfaces by a high quality stainless steel clad. Potential loss of absorber mass or reduction in reactivity control material due to mechanical or chemical erosion or wear is therefore reliably prevented.
- B. A breach of the cladding for any postulated reason does not result in serious consequences. The absorber material silver-indium-cadmium is relatively inert and would still remain remote from high coolant velocity regions. Rapid loss of material resulting in significant loss of reactivity control material would not occur.
- C. The individually clad absorber rods are doubly secured to the retaining spider finger by a threaded joint and a welded lock pin. A redundant fastening system is therefore achieved. No failure of this joint has ever been experienced in functional testing or in years of actual service in operating plants such as San Onofre, Connecticut Yankee, Zorita, Beznau No. 1, Robert Emmett Ginna, etc.

It should also be noted that in several instances of control rod jamming caused by foreign particles, the individual rods at the site of the jam have borne the full capacity of the control rod drive mechanism and higher impact loads to dislodge the jam without failure. The guide tube card/guide thimble arrangement is such that large loads are required to buckle individual control rods. The conclusion to be drawn from this experience is that this joint is extremely insensitive to potential mechanical damage. A failure of the joint would result in the insertion of the individual rod into the core. This results in reduced reactivity which is a fail-safe condition. Further information is given in reference 8.

- D. The spider finger braze joint by which the individual rods are fastened to the vanes has also experienced the service described above and been subjected to the same jam-freeing procedures, also without failure. A failure of this joint would also result in insertion of the individual rod into the core.
- E. The radial vanes are attached to the spider body, again by a brazed joint. The joints are designed to a theoretical strength in excess of that of the components joined. The diagonal vanes each carry two individual absorber rods. It is a feature of the design that the guidance of the rod cluster control is accomplished by the inner fingers of these vanes. They are therefore the most susceptible to mechanical damage. Since these vanes carry two rods, failure of the vane-to-hub joint, such as the isolated incidents at Connecticut Yankee, does not prevent the free insertion of the rod pair.⁽⁸⁾ Neither does such a failure interfere with the continuous free operation of the drive line, also as experienced at Connecticut-Yankee.⁽⁸⁾

Failure of the vane-to-hub joint of a single rod vane could potentially result in failure of the separated vane and rod to insert. This could occur only at withdrawal elevations where the spider is above the continuous guidance section of the guide tube (in the upper internals). A rotation of the disconnected vane could cause it to

hang on one of the guide cards in the intermediate guide tube. Such an occurrence would be evident from the failure of the rod cluster control to insert below a certain elevation, but with free motion above this point.

This possibility is considered extremely remote because the single rod vanes are subjected to only vertical loads and very light lateral reactions from the rods. The lateral loads are light even during a seismic event because the guide tube/guide thimble arrangement allows very limited lateral motion. The consequences of such a failure are not considered critical since only one drive line of the reactivity control system would be involved. This condition is readily observed and can be cleared at shutdown.

- F. The spider hub, being of single-unit cylindrical construction, is very rugged and of extremely low potential for damage. It is difficult to postulate any condition to cause failure. Should some unforeseen event cause fracture of the hub above the vanes, the lower portion with the vanes and rods attached would insert by gravity into the core, causing reactivity decrease. The rod could then not be removed by the drive line, again a fail-safe condition. Fracture below the vanes cannot be postulated since all loads, including trip impact, are taken above the vane elevation.
- G. The rod cluster control rods are provided a clear channel for insertion by the guide thimbles of the fuel assemblies. All fuel rod failures, passive or violent, are protected against by providing this physical barrier between the fuel rod and the intended insertion channel. Distortion of the fuel rods by bending cannot apply sufficient force to damage or significantly distort the guide thimble. Fuel rod distortion by swelling should have terminated by fracture before contact with the guide thimble occurs. If such were not the case, it would be expected that a force reaction at the point of contact would cause a slight deflection of the guide thimble. The radius of curvature of the deflected shape of the guide thimbles would be sufficiently large to have a negligible influence on rod cluster control insertion.

Burnable Absorber Assemblies

The burnable absorber assemblies, containing either standard or WABA rods, are static, temporary reactivity control elements whose positional integrity is conservatively maintained in the core. The axial position is assured by the holddown assembly which bears against the upper core plate. Their lateral position is maintained by the guide thimbles of the fuel assemblies.

The individual rods are shouldered against the underside of the retainer plate and securely fastened at the top by a threaded nut which is then locked in place by a welded pin. The square dimension of the retainer plate is larger than the diameter of the flow holes through the core plate. Failure of the holddown bar or spring pack therefore does not result in ejection of the burnable absorber rods from the core.

The only incident that could potentially result in ejection of the burnable absorber rods is a multiple fracture of retainer plate. This is not considered credible considering the light loads

borne by this component. During normal operation the loads borne by the plate are approximately 5 lb/rod, or a total of 100 lb distributed at the points of attachment. Even a multiple fracture of the retainer plate should result in jamming of the plate segments against the upper core plate, again preventing ejection. Excessive reactivity increase because of burnable absorber ejection is therefore prevented.

The same type of stainless steel clad used on rod cluster controls is also used on the standard burnable absorber rods. In this application there is even less susceptibility to mechanical damage since these are static assemblies. The guide thimbles of the fuel assembly afford the same protection from damage caused by fuel rod failures as that described for the rod cluster control rods.

The consequences of clad breach are also similarly small. For the standard burnable absorber, the borosilicate glass is maintained in position by a central hollow tube. In the event of a hole developing in the clad for any postulated reason, the expected consequence is only the loss of the helium produced by the absorption process into the primary coolant. The glass is chemically inert and remains remote from high coolant velocities. Therefore, significant loss of absorber material resulting in reactivity increase is not expected. Rods of this design have performed very well in actual service, with very few failures observed through full life of one full cycle.

For the WABA, in the unlikely event that the zircaloy clad is breached, the B4C in the affected rod(s) could be leached out by the coolant water. If this occurred early in the cycle, incore instruments could detect large peaking factor changes, and corrective action would be taken if warranted. A postulated clad breach after substantial irradiation would have no significant effect on peaking factors since the B10 will have been burned-out. Breaching of the zircaloy clad by internal hydriding is not expected due to moisture controls employed during fabrication. Rods of this design have also performed very well, with no failures observed through full life of one fuel cycle.⁽⁸⁾

Drive Rod Assemblies

All postulated failures of the drive rod assemblies, either by fracture or uncoupling, lead to the fail safe conclusion. If the drive rod assembly fractures at any elevation, that portion remaining coupled falls with, and is guided by, the rod cluster control assembly. This always results in reactivity decrease.

4.2.3.3.2 Control Rod Drive Mechanism

Material Selection

All pressure-retaining materials comply with Section III of the ASME Pressure Vessel Code and are fabricated from austenitic (type 304) stainless steel.

Magnetic pole pieces are fabricated from type 410 stainless steel. All nonmagnetic parts, except pins and springs, are fabricated from type 304 stainless steel. Haynes 25 is used to fabricate link pins. Springs are made from Inconel-X. Latch arm tips are clad with Stellite 6 to

FNP-FSAR-4

provide improved wearability. Hard chrome plate and Stellite 6 are used selectively for bearing and wear surfaces.

At the start of the development program, a survey was made to determine whether a material better than type 410 stainless steel was available for the magnetic pole pieces. Ideal material requirements are as follows:

- A. High magnetic saturation value.
- B. High permeability.
- C. Low coercive force.
- D. High resistivity.
- E. High curie temperature.
- F. Corrosion resistant.
- G. High impact strength.
- H. Nonoriented.
- I. High machinability.
- J. Radiation damage.

After a comprehensive material trade-off study was made, it was decided that the type 410 stainless steel was satisfactory for this application.

The cast coil housings require a magnetic material. Both low-carbon cast steel and ductile iron have been successfully tested for this application. Ductile iron will be specified for the control rod drive mechanism. The finished housings are zinc plated to provide corrosion resistance.

Coils are wound on bobbins of molded Dow Corning 302 material, with double-glass insulated copper wire. Coils are then vacuum-impregnated with silicon varnish. A wrapping of mica sheet is secured to the coil's outer surface. The result is a well insulated coil capable of sustained operation at 200°C.

The drive rod assembly utilizes a type 410 stainless steel drive rod. The coupling is machined from type 403 stainless steel. Other parts are type 304 stainless steel with the exception of the springs, which are Inconel-X, and the locking button, which is Haynes 25.

Radiation Damage

As required by the equipment specification, the control rod drive mechanisms are designed to meet a radiation requirement of 10 Rad/h. Materials have been selected to meet this requirement. The above radiation level, which amounts to 1.753×10^6 Rads in twenty years, will

FNP-FSAR-4

not limit control rod drive mechanism life. Control rod drive mechanisms at Yankee Rowe which have been in operation since 1960 have not experienced problems due to radiation.

Positioning Requirements

The mechanism has a step length of five-eighths of an inch, which determines the positioning capabilities of the control rod drive mechanism. (Note: Positioning requirements are determined by reactor physics.)

Evaluation of Materials Adequacy

The ability of the pressure housing components to perform throughout the design lifetime as defined in the equipment specification is confirmed by the stress analysis report required by the ASME Boiler and Pressure Vessel Code, Section III. Internal components subjected to wear will withstand a minimum of 2,500,000 steps without refurbishment as confirmed by life tests.

Dimensional and Tolerance Analysis

With respect to the control rod drive mechanism, critical clearances are present in the following areas:

- A. Latch assembly (diametral clearances).
- B. Latch arm-drive rod clearances.
- C. Coil stack assembly thermal clearances.
- D. Coil fit in coil housing.

The following section defines clearances that are designed to provide reliable operation in the control rod drive mechanism in these four critical areas. These clearances have been proven by life tests and actual field performance at operating plants.

Latch Assembly - Thermal Clearances

The magnetic jack has several clearances where parts made of type 410 stainless steel fit over parts made from type 304 stainless steel. Differential thermal expansion is therefore important. Minimum clearances of these parts at 68°F is 0.011 inches. At the maximum design temperature of 650°F minimum clearance is 0.0045 inches and at the maximum expected operating temperatures of 550°F is .0057 inches.

Latch Arm - Drive Rod Clearances

The control rod drive mechanism incorporates a load transfer action. The movable and stationary gripper latches are not under load during engagement, as previously explained, because of load transfer action.

Figure 4.2-23 shows latch clearance variation with the drive rod as a result of minimum and maximum temperatures. Figure 4.2-24 shows clearance variations over the design temperature range.

Coil Stack Assembly - Thermal Clearances

The assembly clearance of the coil stack assembly over the latch housing was selected so that the assembly could be removed under all anticipated conditions of thermal expansion.

At 70°F the inside diameter of the coil stack is 7.428/7.438 inches. The outside diameter of the latch housing is 7.39/7.38 inches.

Thermal expansion of the mechanism operating temperature of the control rod drive mechanism results in minimum inside diameter of the coil stack being 7.440 inches at 222°F and the maximum latch housing diameter being 7.426 inches at 650°F.

Under the extreme tolerance conditions listed above, it is necessary to allow time for a 70°F coil housing to heat during a replacement operation.

Four similar coil stack assemblies were removed from four hot control rod drive mechanisms mounted on 11.035-inch centers on a 550°F test loop, allowed to cool, and then replaced without incident as a test to prove the preceding.

Coil Fit in Coil Housing

Control rod drive mechanism and coil housing clearances are selected so that coil heat-up results in a close-to-tight fit. This is done to facilitate thermal transfer and coil cooling in a hot control rod drive mechanism.

4.2.3.4 Testing and Inspection Plan

4.2.3.4.1 Reactivity Control Components

Tests and inspections are performed on each reactivity control component to verify the mechanical characteristics. In the case of the full-length rod cluster control assembly, prototype testing has been conducted and both manufacturing test/inspections and functional testing at the plant site are performed.

During the component manufacturing phase, the following requirements apply to the reactivity control components to assure the proper functioning during reactor operation:

- A. All materials are procured to specifications to attain the desired standard of quality.
- B. All spider assemblies are proof tested by applying a 5000-lb load to the spider body so that approximately 310 lb are applied to each vane. This proof load provides a bending moment at the spider body equivalent to approximately 1.4 times the load caused by the acceleration imposed by the CRDM.

- C. All clad/end plug welds are checked for integrity by visual inspection and by X-ray, and are helium leak-checked. All the seal welds in the neutron absorber rods, burnable absorber rods, and source rods are checked in this manner.
- D. To assure proper fitup with the fuel assembly, the rod cluster control, burnable absorber, and source assemblies are installed in the fuel assembly and checked for binding in the dry condition.

The RCCAs are functionally tested following each core loading but prior to criticality to demonstrate reliable operation of the assemblies.

To demonstrate continuous free movement of the RCCAs and to ensure acceptable core power distributions during operations, partial movement checks are performed on every RCCA, as required by the Technical Specifications. Following each refueling, drop tests of the full-length RCCAs are performed at hot full-flow conditions to demonstrate continued ability to meet trip time requirements.

If an RCCA cannot be moved by its mechanism, adjustments in the boron concentration of the coolant ensure that adequate shutdown margin would be achieved following a trip. Thus, inability to move one RCCA can be tolerated. More than one inoperable RCCA could be tolerated, but would impose additional demands on the plant operator. Therefore, the number of inoperable RCCAs has been limited to one.

4.2.3.4.2 Control Rod Drive Mechanisms

Quality assurance procedures during production of control rod drive mechanisms include material selection, process control, mechanism component tests during production, and hydrotests.

After all manufacturing procedures had been developed, several prototype control rod drive mechanisms and drive rod assemblies were life tested with the entire drive line under environmental conditions of temperature, pressure, and flow. All acceptance tests were of duration equal to or greater than service required for the plant operation. All drive rod assemblies tested in this manner have shown minimal wear damage.

These tests include verification that the trip time achieved by the full-length control rod drive mechanisms meets the design requirement of 2.7 seconds from start of rod cluster control assembly motion to dashpot entry. This trip time requirement will be confirmed for each control rod drive mechanism prior to initial reactor operation and at periodic intervals after initial reactor operation. In addition, a technical specification has been set to ensure that the trip time requirement is met. The Technical Requirements Manual contains requirements for rod drop testing following maintenance or modification.

It is expected that all control rod drive mechanisms will meet specified operating requirements for the duration of plant life with normal refurbishment. However, a technical specification pertaining to an inoperable rod cluster control assembly has been set.

If a rod cluster control assembly cannot be moved by its mechanism, adjustments in the boron concentration ensure that adequate shutdown margin would be achieved following a trip. Thus, inability to move one rod cluster control assembly can be tolerated. More than one inoperable rod cluster control assembly could be tolerated, but would impose additional demands on the plant operator. Therefore, the number of inoperable rod cluster control assemblies has been limited to one.

In order to demonstrate continuous free movement of the full-length rod cluster control assemblies and to ensure acceptable core power distributions during operation, partial movement checks are performed on every full-length rod cluster control assembly as required by the technical specifications. In addition, periodic drop tests of the full-length rod cluster control assemblies are performed at each refueling shutdown to demonstrate continued ability to meet trip time requirements, to ensure core subcriticality after reactor trip, and to limit potential reactivity insertions from a hypothetical rod cluster control assembly ejection. During these tests the acceptable drop time of each assembly is not greater than 2.7 seconds, at full flow and operating temperature, from the beginning of decay of stationary gripper voltage to dashpot entry.

To confirm the mechanical adequacy of the fuel assembly and full-length rod cluster control assembly, functional test programs have been conducted on a full scale control rod. The prototype assembly was tested under simulated conditions of reactor temperature, pressure, and flow for approximately 1000 hours. The prototype mechanism accumulated about 3,000,000 steps and 600 trips. At the end of the test the control rod drive mechanism was still operating satisfactorily.

Actual experience on the Ginna, Mihama No. 1, Point Beach No. 1 and H.B. Robinson plants indicates excellent performance of control rod drive mechanisms.

All units are production tested prior to shipment to confirm ability of the control rod drive mechanism to meet design specification operational requirements.

4.2.3.5 Instrumentation

Instrumentation for determining reactor coolant average temperature (T_{avg}) is provided to create demand signals for moving groups of full-length rod cluster control assemblies. Automatic movement of full-length rod cluster assemblies can be used for load follow (determined as a function of turbine impulse pressure) during normal operation and to counteract operational transients. Normally, the full-length rod cluster control assemblies are operated in the fully withdrawn position or positioned as necessary to control neutron flux. Reactor coolant average temperature changes are controlled by adjusting boron concentration levels to compensate for load changes and core burnup. Hot- and cold-leg resistance temperature detectors (RTDs) are located in the reactor coolant loops as described in section 5.5.3. The protection functions of the RTDs are described in sections 7.2 and 7.3. The reactor control system which controls the reactor coolant average temperature by regulation of control rod bank position is described in section 7.7.

FNP-FSAR-4

Rod position indication instrumentation is provided to sense the actual position of each control rod so that the actual position of the individual rod may be displayed to the operator. Signals are also supplied by this system as input to the rod deviation comparator. The rod position indication system is described in chapter 7.

The reactor makeup control system, whose functions are to permit adjustment of the reactor coolant boron concentration for reactivity control (as well to maintain the desired operating fluid inventory in the volume control tank), consists of a group of instruments arranged to provide a manually preselected makeup composition that is borated or diluted as required to the charging pump suction header or the volume control tank. This system, as well as other systems including boron sampling provisions that are part of the chemical and volume control system, is described in section 9.3.

When the reactor is critical, the normal indication of reactivity status in the core is the position of the control bank in relation to reactor power (as indicated by the reactor coolant system loop ΔT) and coolant average temperature. These parameters are used to calculate insertion limits for the control banks to give warning to the operator of excessive rod insertion. Monitoring of the neutron flux for various phases of reactor power operation as well as of core loading, shutdown, startup, and refueling is by means of the nuclear instrumentation system. The monitoring functions and readout and indication characteristics for the following means of monitoring reactivity are included in the discussion on safety-related display instrumentation in section 7.5.

- A. Nuclear instrumentation system.
- B. Temperature indicators.
 - 1. T average (measured).
 - 2. ΔT (measured).
 - 3. Auctioneered T average.
 - 4. T reference.
- C. Demand position of rod cluster control assembly group.
- D. Actual rod position indicator.

The above means of monitoring reactivity provides the reactor operator sufficient indication to ensure that he can maintain the rate of change of reactivity or power level within safe limits. He must also be aware of any chemical additions (batch or continuous) which may dilute the reactor coolant system.

REFERENCES

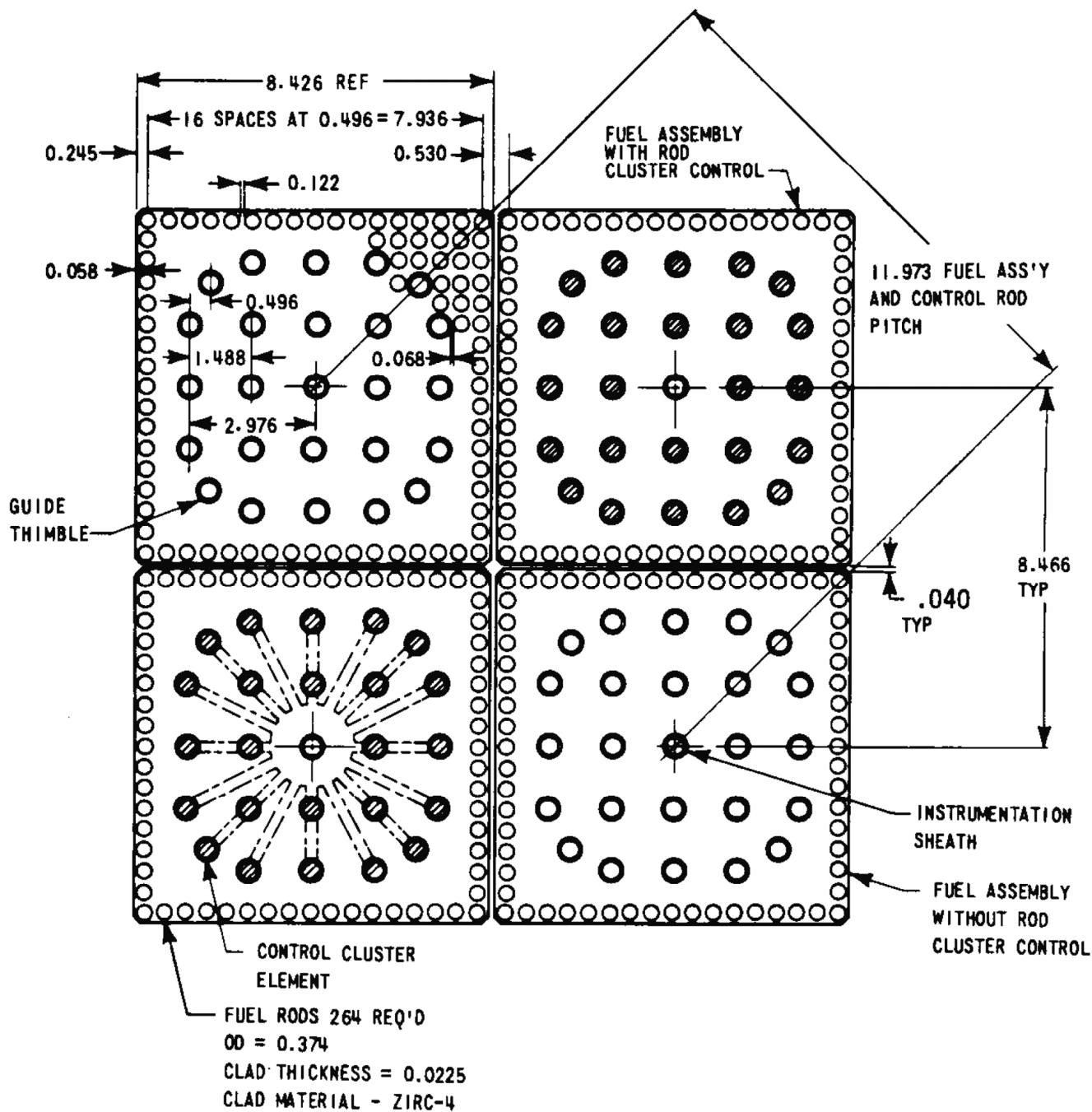
1. Deleted
2. Cohen, J., "Development and Properties of Silver-Based Alloys as Control Rod Materials for Pressurized Water Reactors," WAPD-214, December 1959.
3. Deleted
4. Deleted
5. Eggleston, E. T., "Safety-Related Research and Development for Westinghouse Pressurized Water Reactors, Program Summaries - Winter 1976 - Summer 1978," WCAP-8768, Revision 2, October 1977.
6. Woodson, N. and Bakos, F., "Westinghouse Electric Corporation Energy System; Business Unit Quality Management System," Revision 1, January 1996.
7. Kraus, S., "Neutron Shielding Pads," WCAP-7870, May 1972.
8. Slagle, W., "Operational Experience with Westinghouse Cores," WCAP-8183 (updated annually).
9. Skaritka, J., et al., "Westinghouse Wet Annular Burnable Absorber Evaluation Report," WCAP-10021-P-A, Revision, (Proprietary), October 1983.
10. Gesinski, L., Chiang, D., and Nakazato, S., "Safety Analysis of the 17 x 17 Fuel Assembly for Combined Seismic and Loss-of-Coolant Accident," WCAP-8288, December 1973.
11. O'Donnell, W. J. and Langer, B. F., "Fatigue Design Basis for Zircaloy Components," Nuclear Science and Engineering 20, pp 1-12, 1964.
12. Demario, E. E. and Nakazato, S., "Hydraulic Flow Test of the 17 x 17 Fuel Assembly," WCAP-8279, February 1974.
13. Deleted
14. Deleted
15. Davidson, S. L., ed., et al., "Extended Burnup Evaluation of Westinghouse Fuel," WCAP-10125-P-A, December 1985.
16. Letter from E. P. Rahe, Jr. (Westinghouse) to L. E. Phillips (NRC) dated April 12, 1984, NS-EPR-2893; Subject: "Fuel Handling Load Criteria (6g vs 4g)."
17. Davidson, S. L., ed., et al., "Reference Core Report VANTAGE 5 Fuel Assembly," WCAP-10444-P-A, September 1985.

FNP-FSAR-4

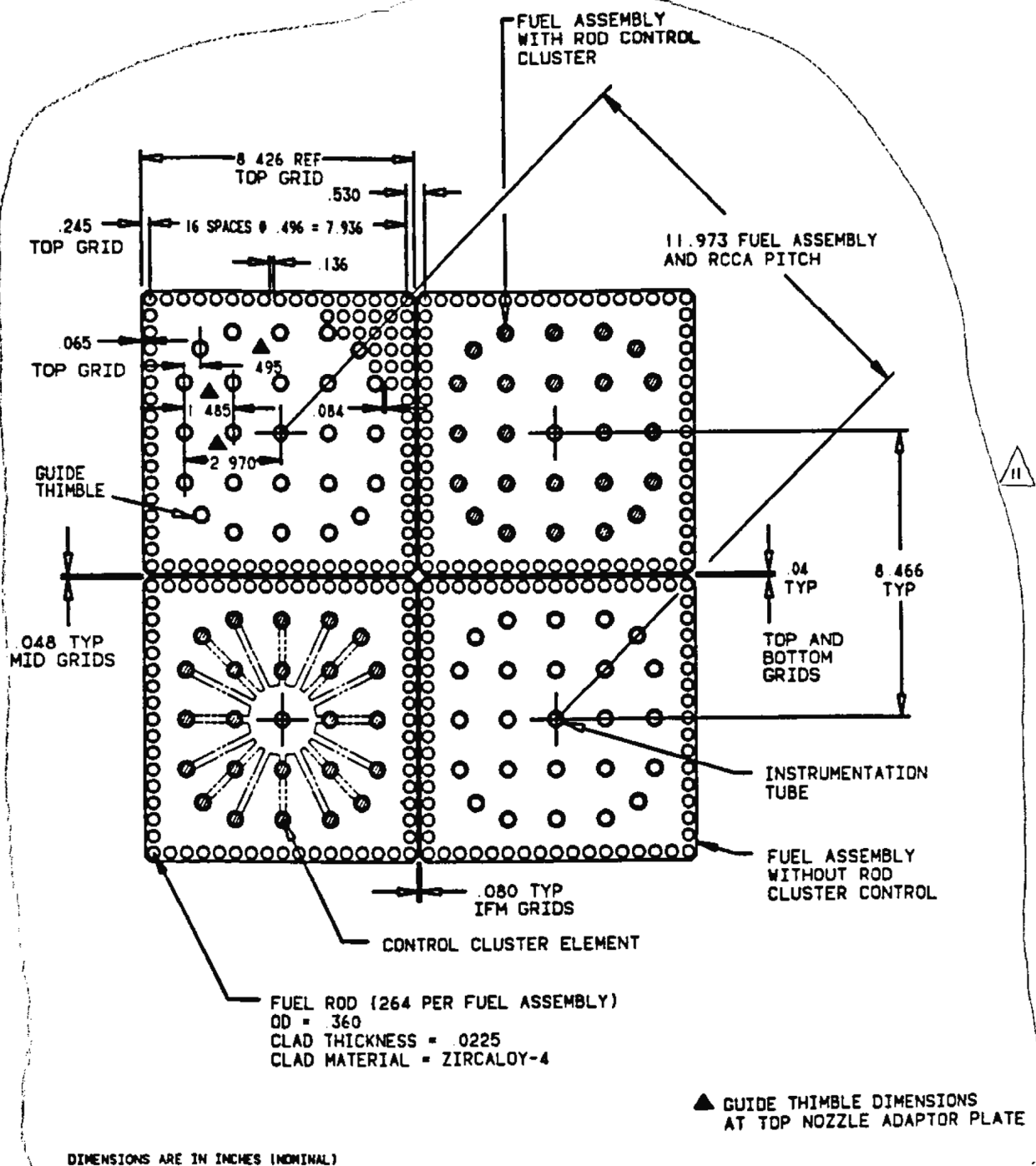
18. Weiner, R. A., et al., "Improved Fuel Performance Models for Westinghouse Fuel Rod Design and Safety Evaluations," WCAP-10851-P-A (Proprietary) and WCAP-11873-A (Nonproprietary), August 1988.
19. Letter from D. E. McKinnon (Westinghouse) to R. G. Cocherell (SNC) dated October 28, 1991, Subject: "Joseph M. Farley Nuclear Plant Units 1 and 2 Secondary Source Assemblies," 91AP*-G-0064.
20. Davidson, S. L., and Nuhfer, D. L., eds., "VANTAGE+ Fuel Assembly Reference Core Report," WCAP-12610-P-A, and Appendices A through D, June 1990.
21. Deleted
22. Kersting, P. J., et al., "Assessment of Clad Flattening and Densification Power Spike Factor Elimination in Westinghouse Nuclear Fuel," WCAP-13589-A, March 1995.
23. Deleted
24. Foster, J. P., et al., "Westinghouse Improved Performance Analysis and Design Model (PAD 4.0)," WCAP-15063-P-A, Revision 1, with Errata, July, 2000.
25. Slagle, W. H., ed., "Westinghouse Fuel Assembly Reconstitution Evaluation Methodology," WCAP-13060-P-A, July 1993.
26. Shah, H., "Optimized ZIRLO™," WCAP-12610-P-A & CENPD-404-P-A Addendum 1-A, July 2006.
27. USNRC Letter to C. R. Pierce, "Joseph M. Farley Nuclear Plant, Units 1 and 2, and Vogtle Electric Generating Plant, Units 1 and 2 - Issuance of Amendments Regarding Use of Optimized ZIRLO™", August 4, 2016 (ML16179A386).
28. O. Linsuain, et al., "Westinghouse Performance Analysis and Design Model (PAD5)," WCAP-17642-P-A, Revision 1, November 2017.

TABLE 4.2-1
MAXIMUM DEFLECTIONS SPECIFIED
FOR REACTOR INTERNAL SUPPORT STRUCTURES

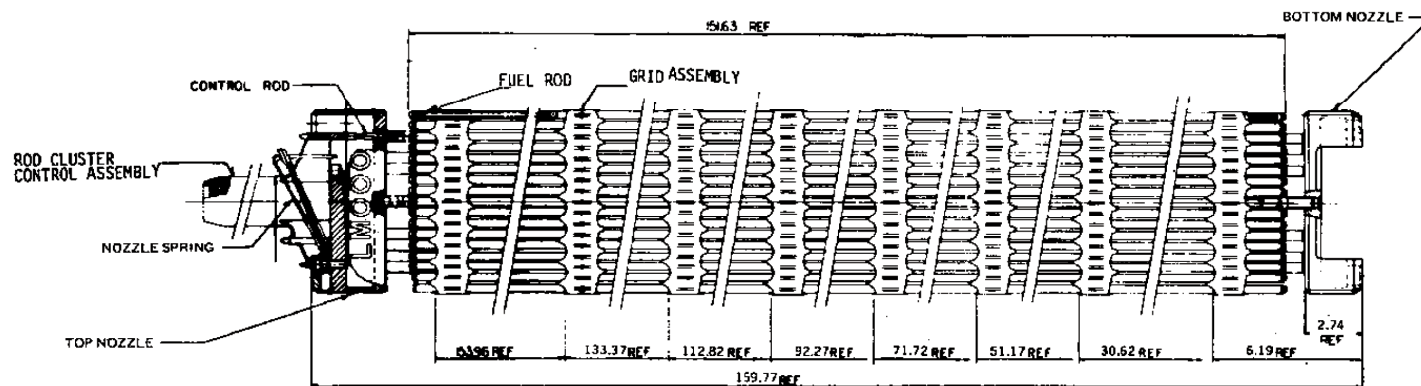
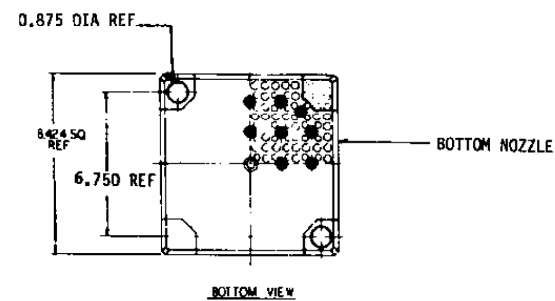
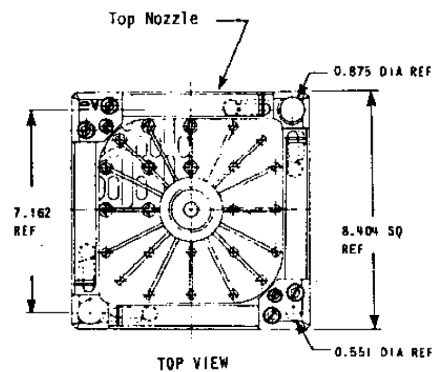
<u>Component</u>	<u>Allowable Deflections (in.)</u>	<u>No Loss of Function Deflections (in.)</u>
Upper Barrel		
radial inward	4.38	8.77
radial outward	0.5	1.0
Upper Package	0.1	0.15
Rod Cluster Guide		
tubes	1.0	1.75



REV 21 5/08

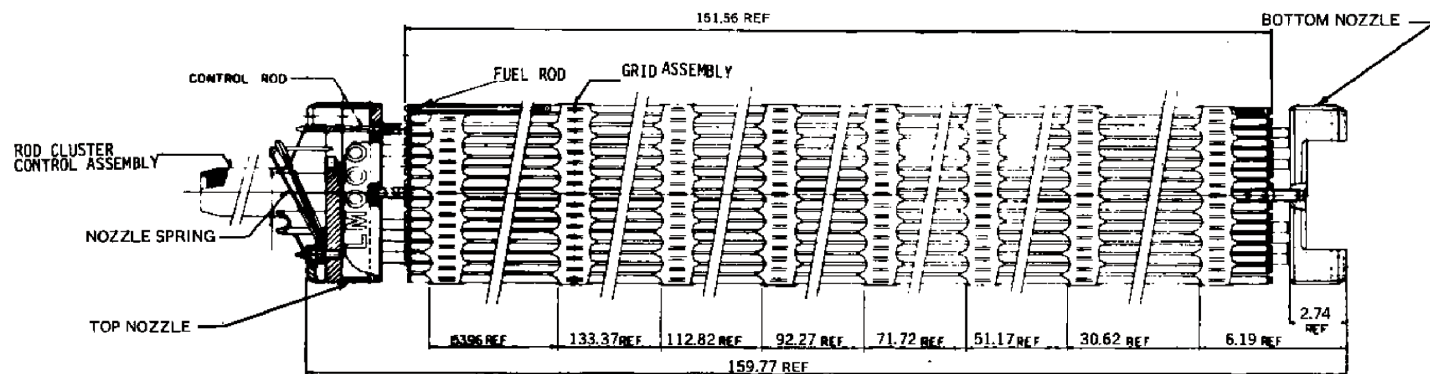
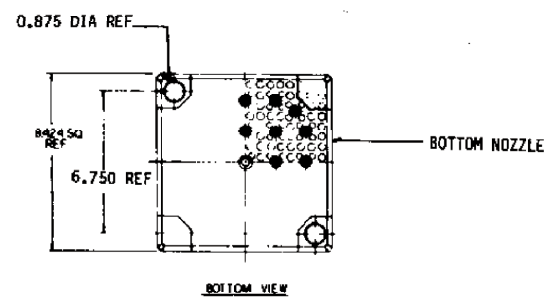
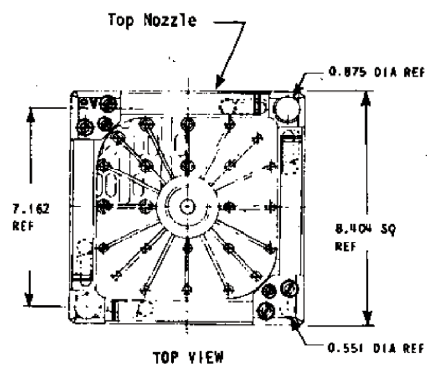


REV 21 5/08



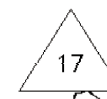
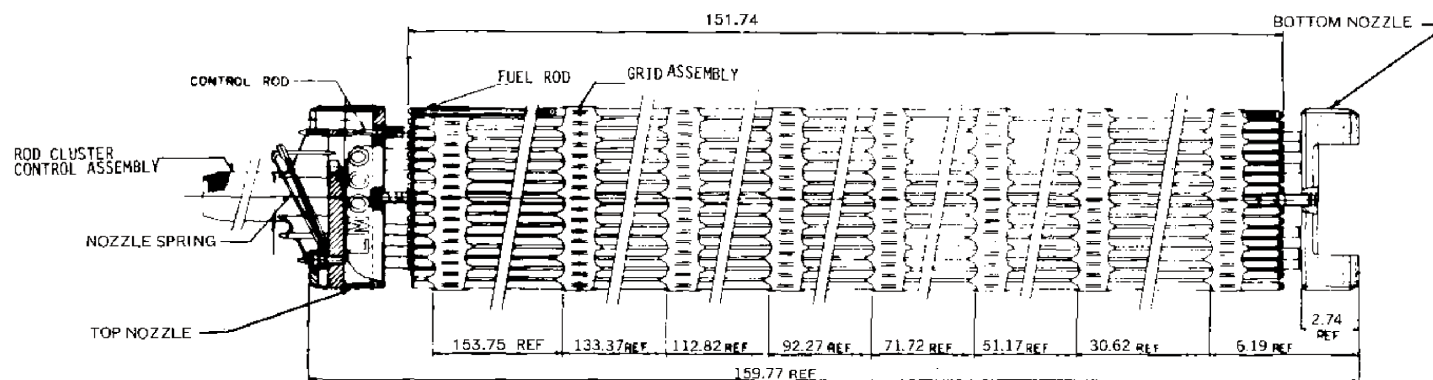
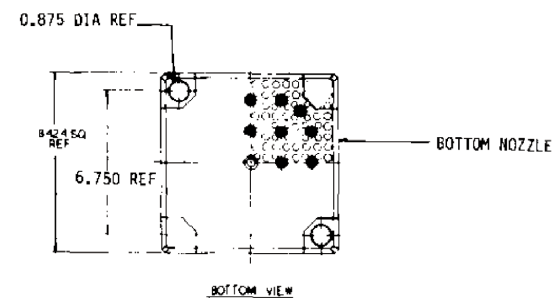
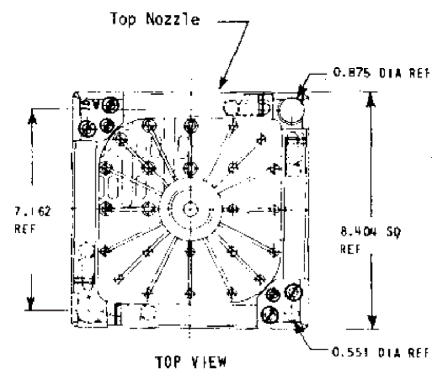
17

REV 25 4/14



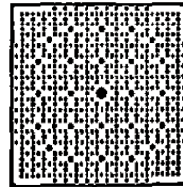
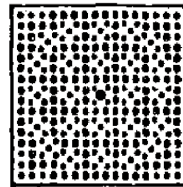
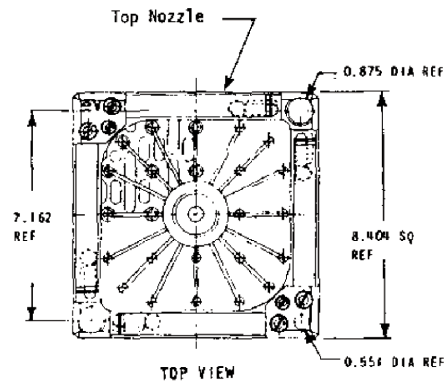
17

REV 25 4/14

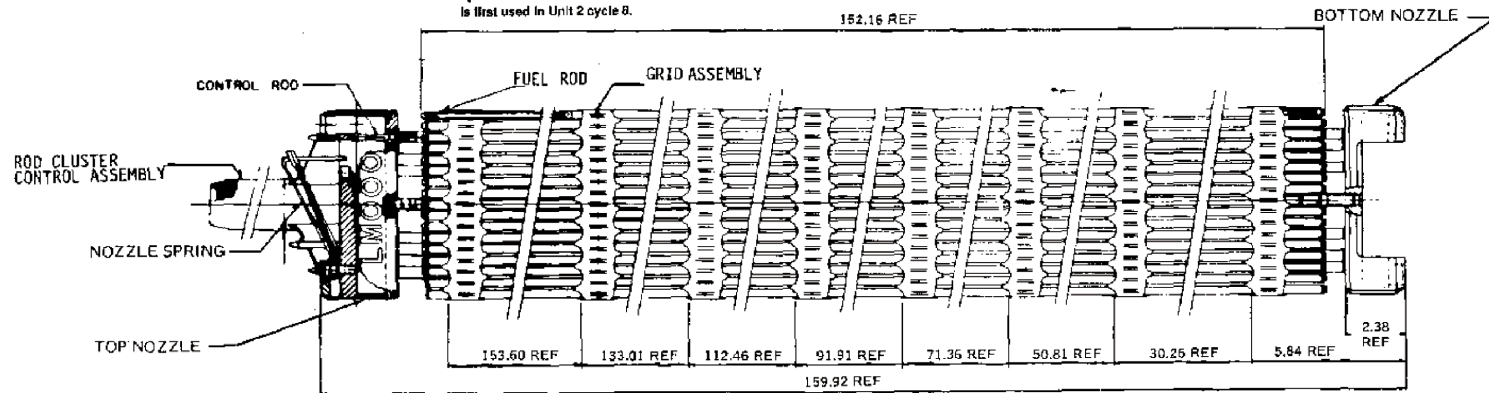
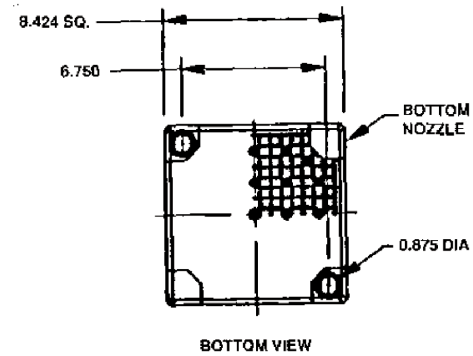


REV 25 4/14

DEBRIS FILTER BOTTOM NOZZLE FLOW HOLE COMPARISON

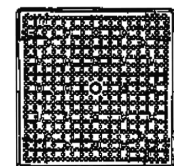
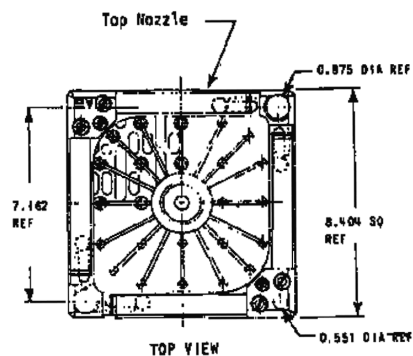


Note: The debris filter bottom nozzle is first used in Unit 1 cycle 10. The modified debris filter bottom nozzle is first used in Unit 2 cycle 8.



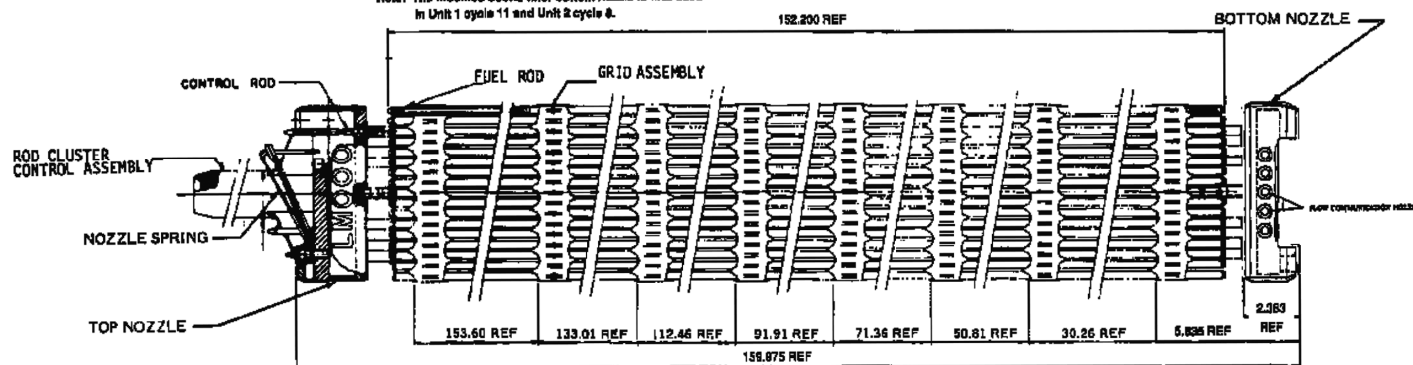
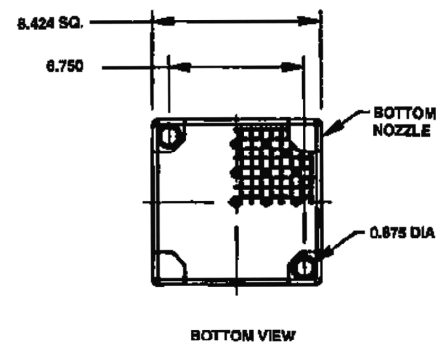
17

REV 25 4/14



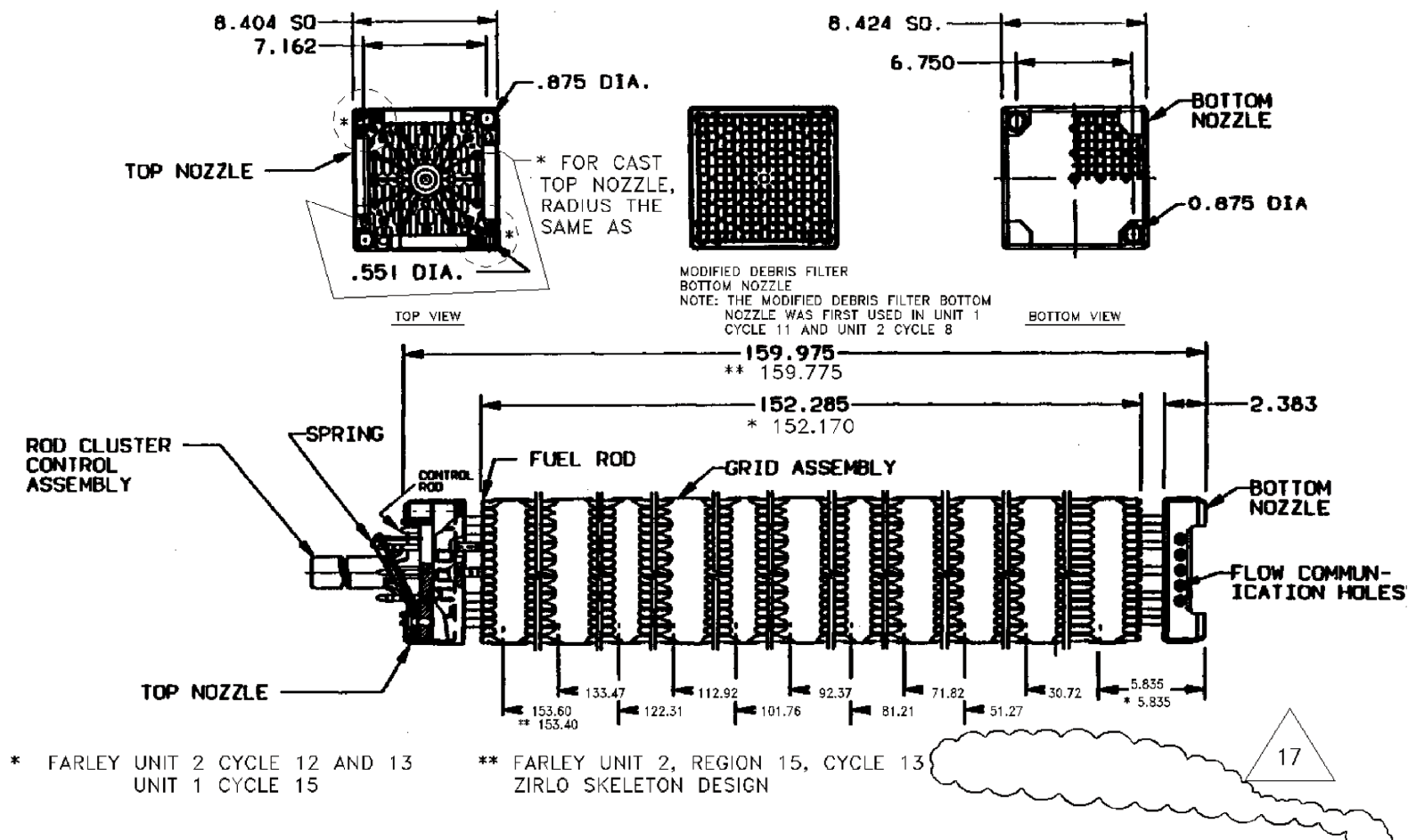
MODIFIED FILTER BOTTOM NOZZLE

Note: This modified debris filter bottom nozzle is first used in Unit 1 cycle 11 and Unit 2 cycle 8.



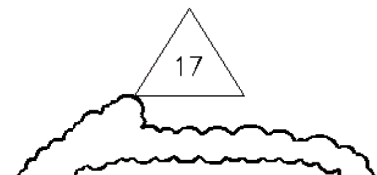
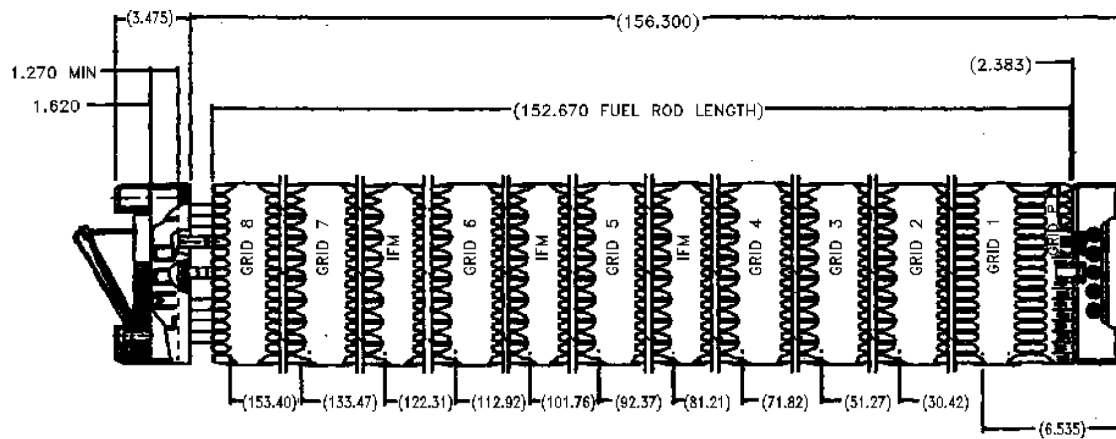
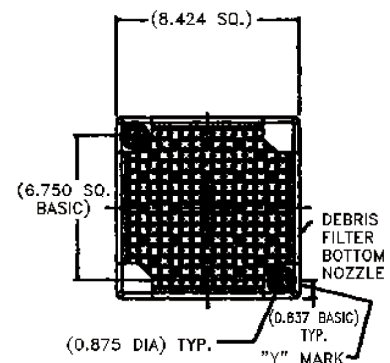
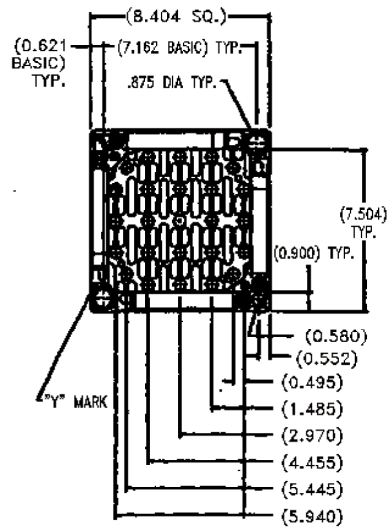
17

REV 25 4/14

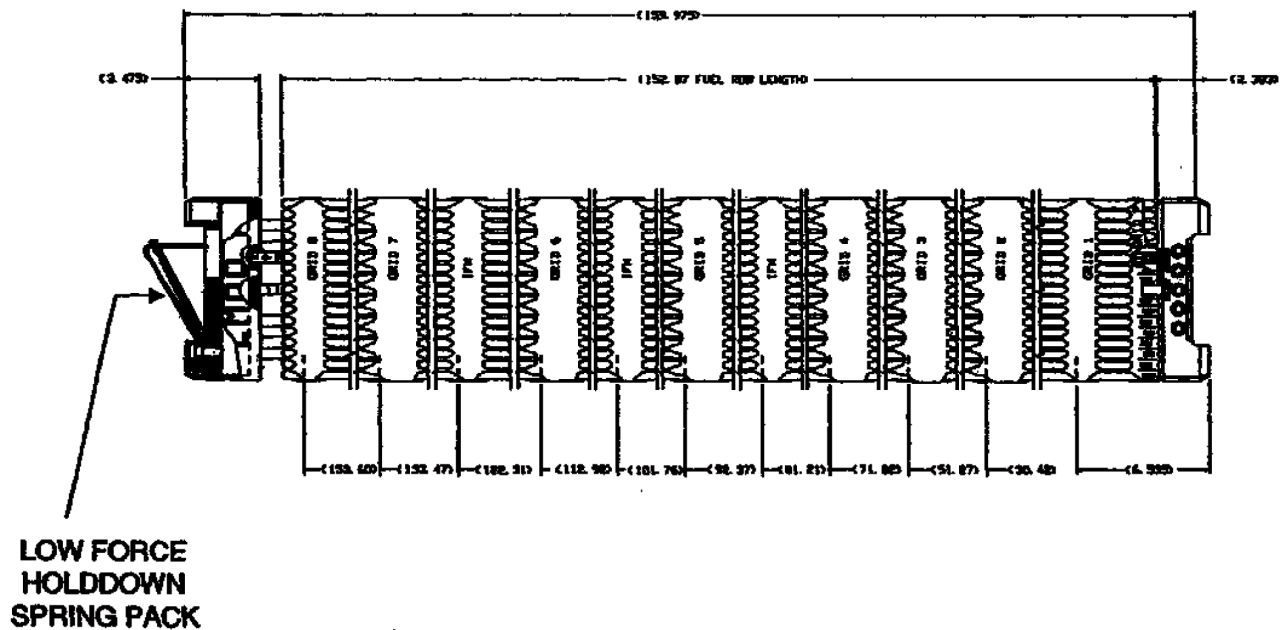
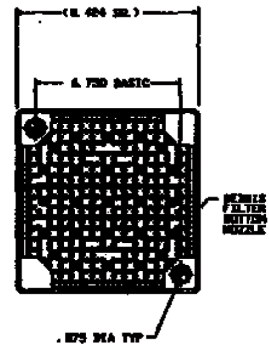
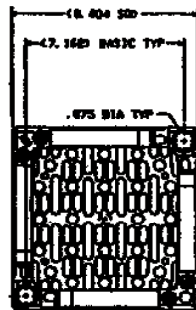


NOTE: ALL DIMENSIONS
ARE REFERENCE

REV 25 4/14



REV 25 4/14



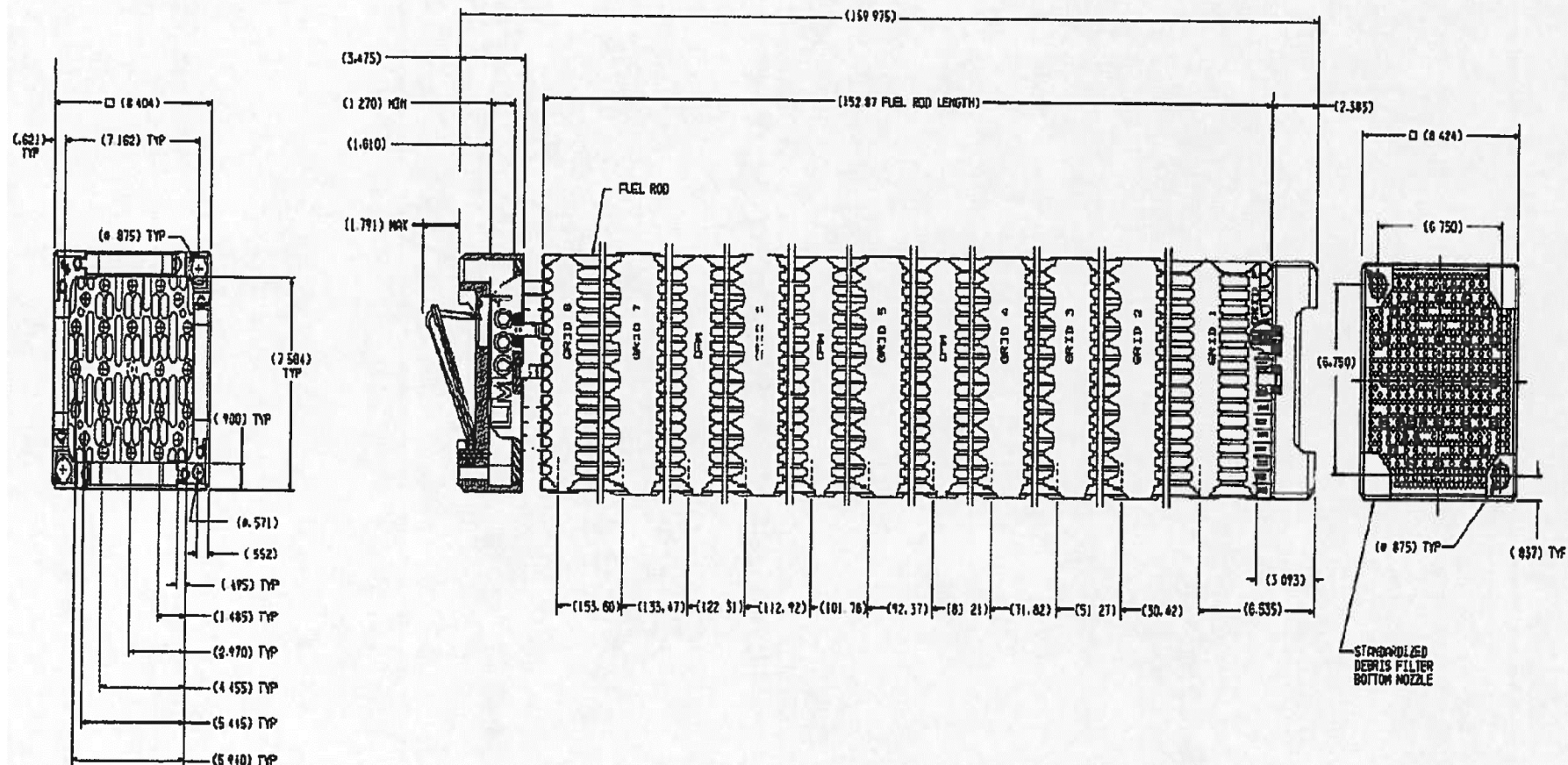
REV 25 4/14



JOSEPH M. FARLEY
NUCLEAR PLANT
UNIT 1 AND UNIT 2

UNIT 2 CYCLE 15 - CYCLE 22 AND UNIT 1 CYCLE 18 -
CYCLE 25 FUEL ASSEMBLY OUTLINE 17 X 17 VANTAGE+
WITH LOW PRESSURE ZIRLO FUEL RODS, AND
LOW FORCE HOLDDOWN SPRING

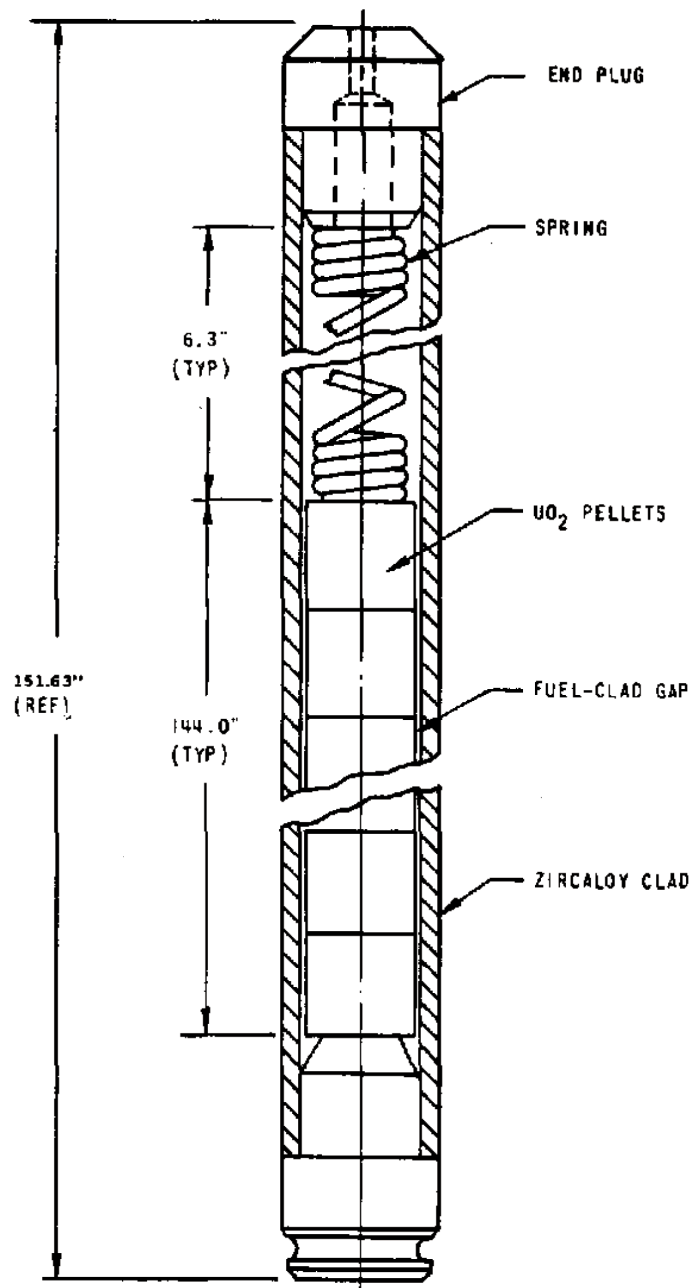
FIGURE 4.2-2 (SHEET 8 OF 9)



REV 25 4/14

UNIT 1 CYCLE 26 AND AFTER; UNIT 2 CYCLE 23 AND AFTER
FUEL ASSEMBLY OUTLINE 17 X 17 VANTAGE+ FUEL FIGURE
WITH ROBUST PROTECTIVE GRID (RPG) AND
STANDARDIZED DEBRIS FILTER BOTTOM NOZZLE (SDFBN)

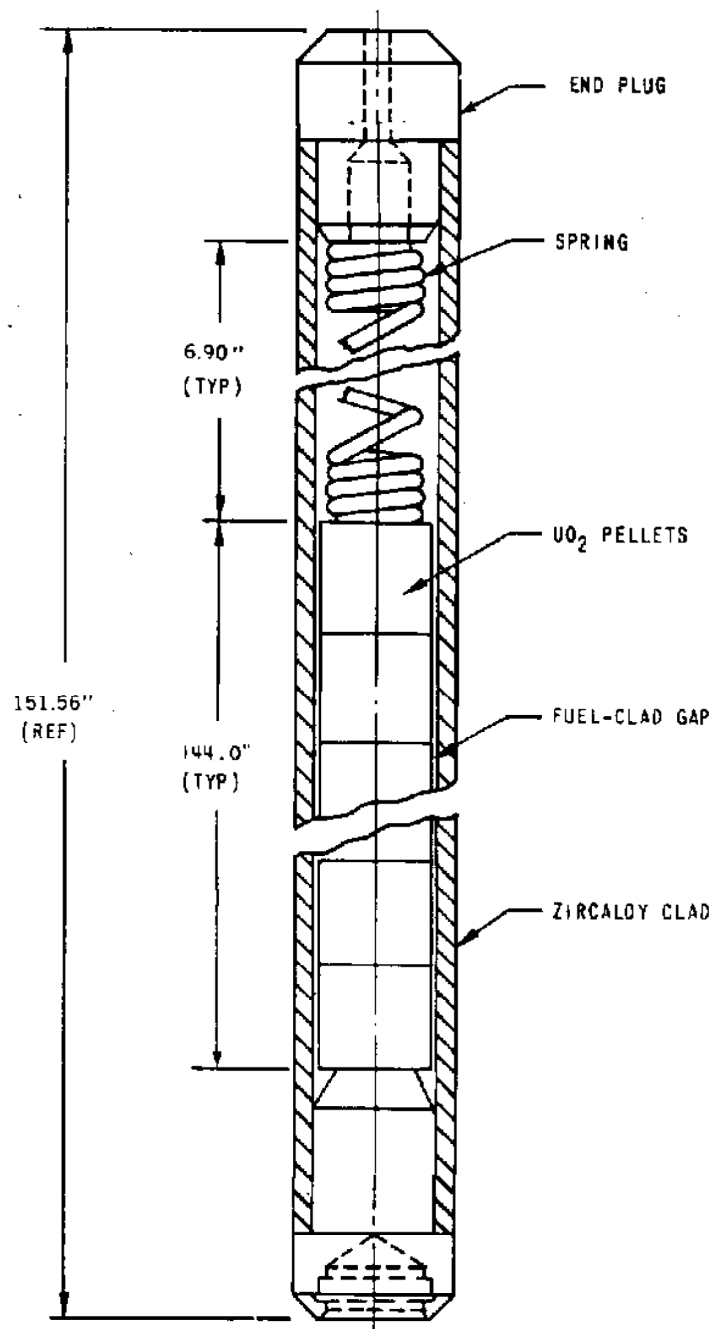
FIGURE 4.2-2 (SHEET 9 OF 9)



SPECIFIC DIMENSIONS DEPEND ON DESIGN VARIABLES SUCH AS
PRE-PRESSURIZATION, POWER HISTORY, AND DISCHARGE BURNUP

17

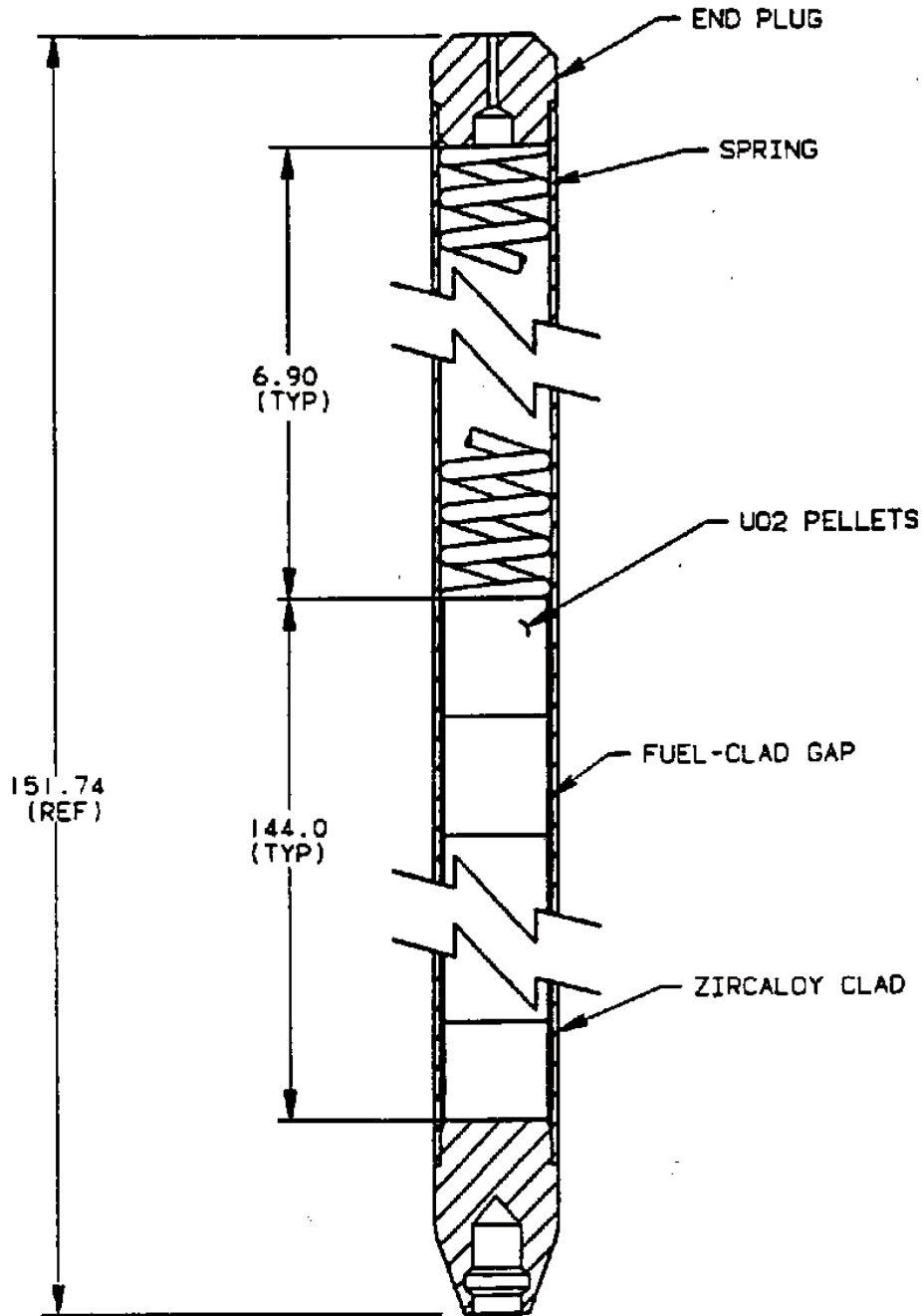
REV 21 5/08



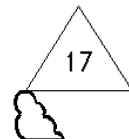
SPECIFIC DIMENSIONS DEPEND ON DESIGN VARIABLES SUCH AS
PRE-PRESSURIZATION, POWER HISTORY, AND DISCHARGE BURNUP



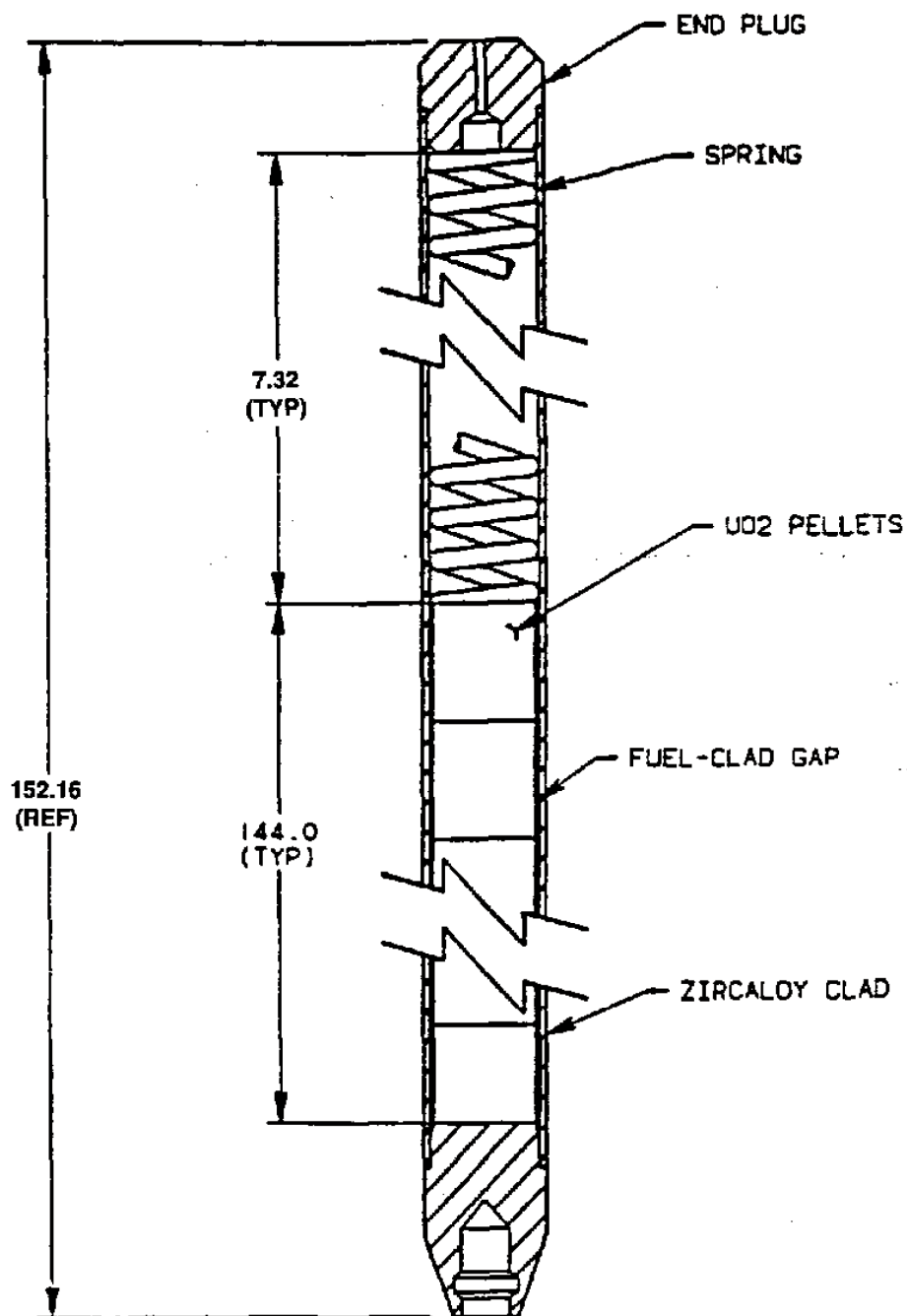
REV 21 5/08



SPECIFIC DIMENSIONS DEPEND ON DESIGN VARIABLES SUCH AS
PRE-PRESSURIZATION, POWER HISTORY, AND DISCHARGE BURNUP



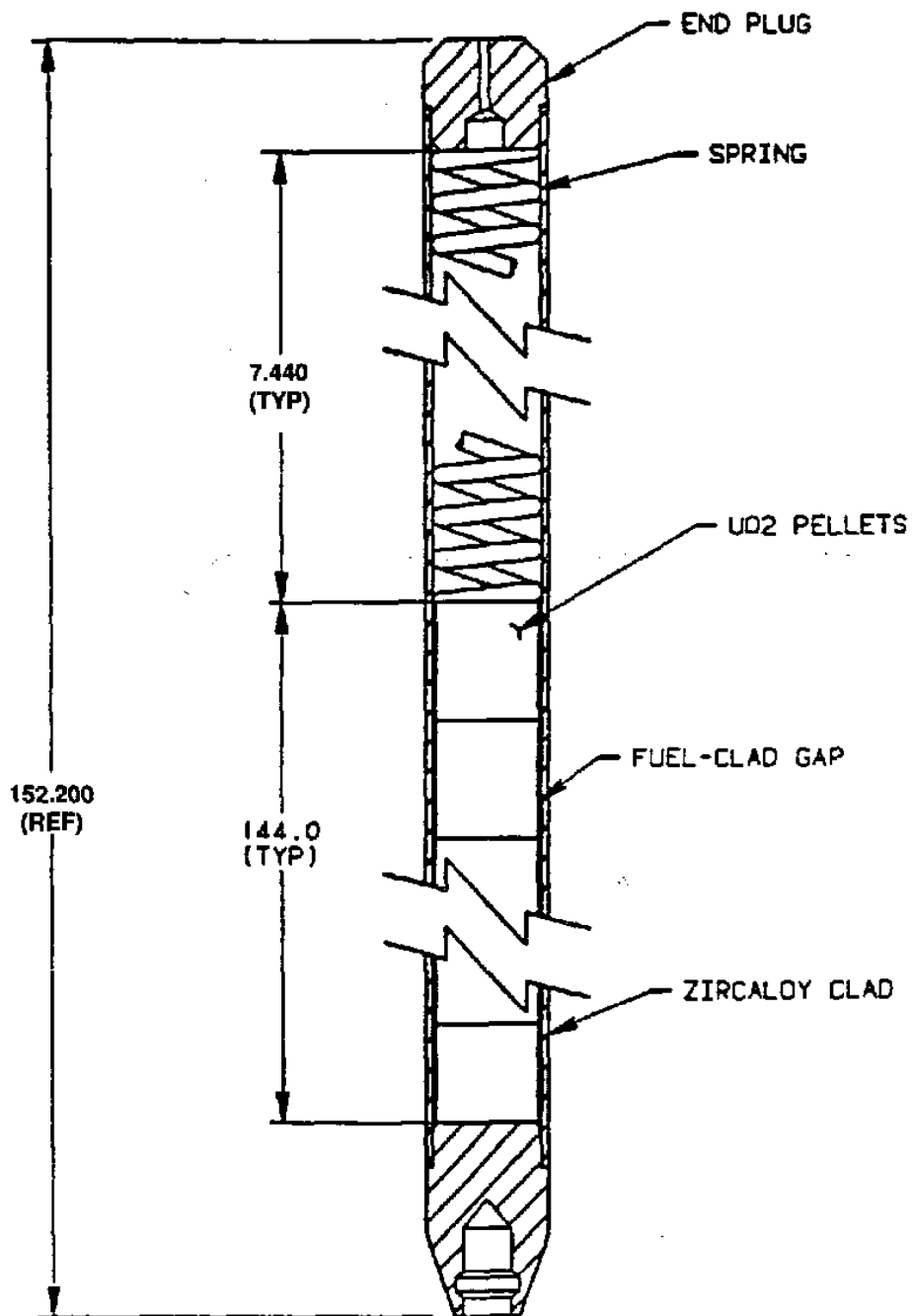
REV 21 5/08



SPECIFIC DIMENSIONS DEPEND ON DESIGN VARIABLES SUCH AS
PRE-PRESSURIZATION, POWER HISTORY, AND DISCHARGE BURNUP



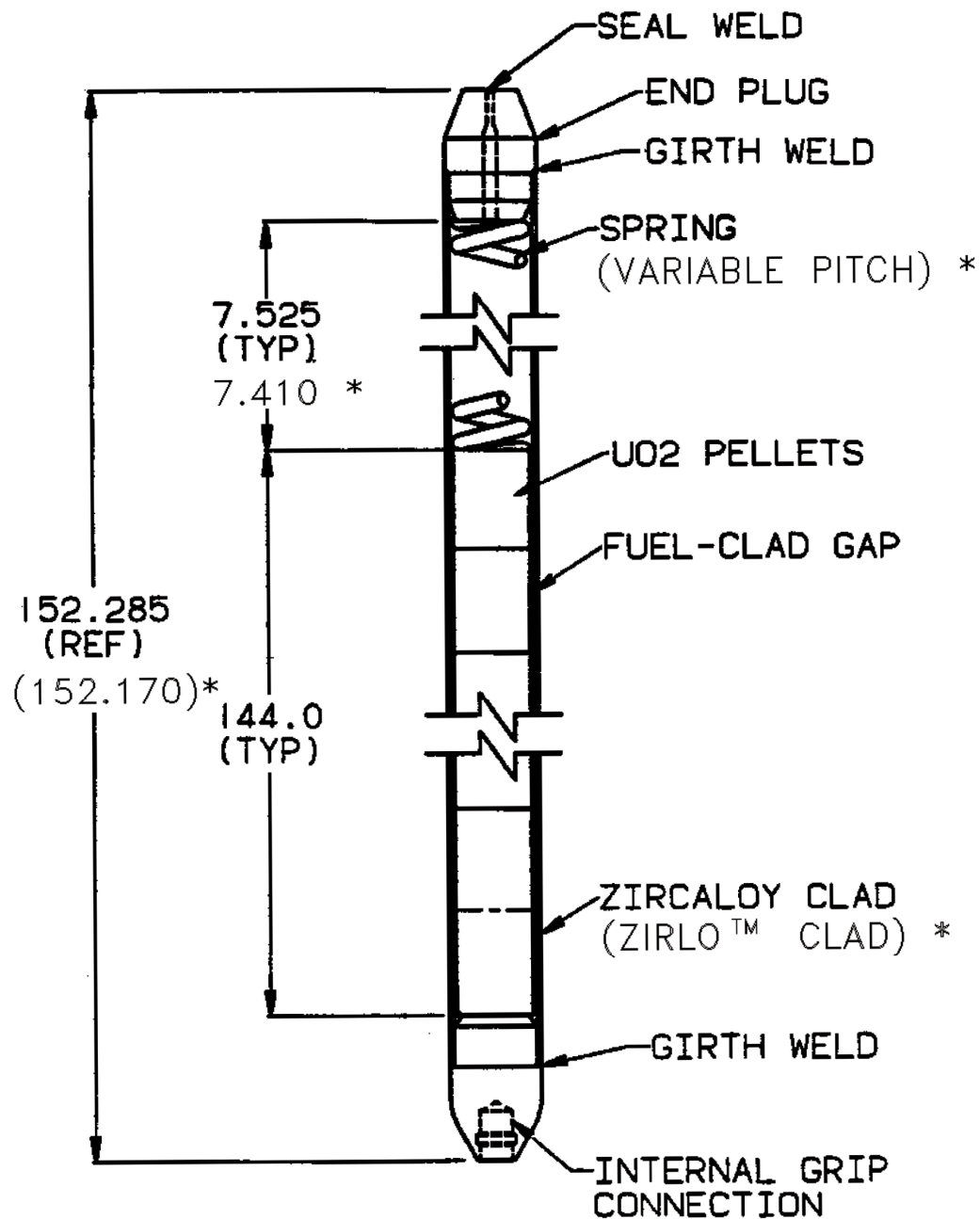
REV 21 5/08



SPECIFIC DIMENSIONS DEPEND ON DESIGN VARIABLES SUCH AS
PRE-PRESSURIZATION, POWER HISTORY, AND DISCHARGE BURNUP



REV 21 5/08

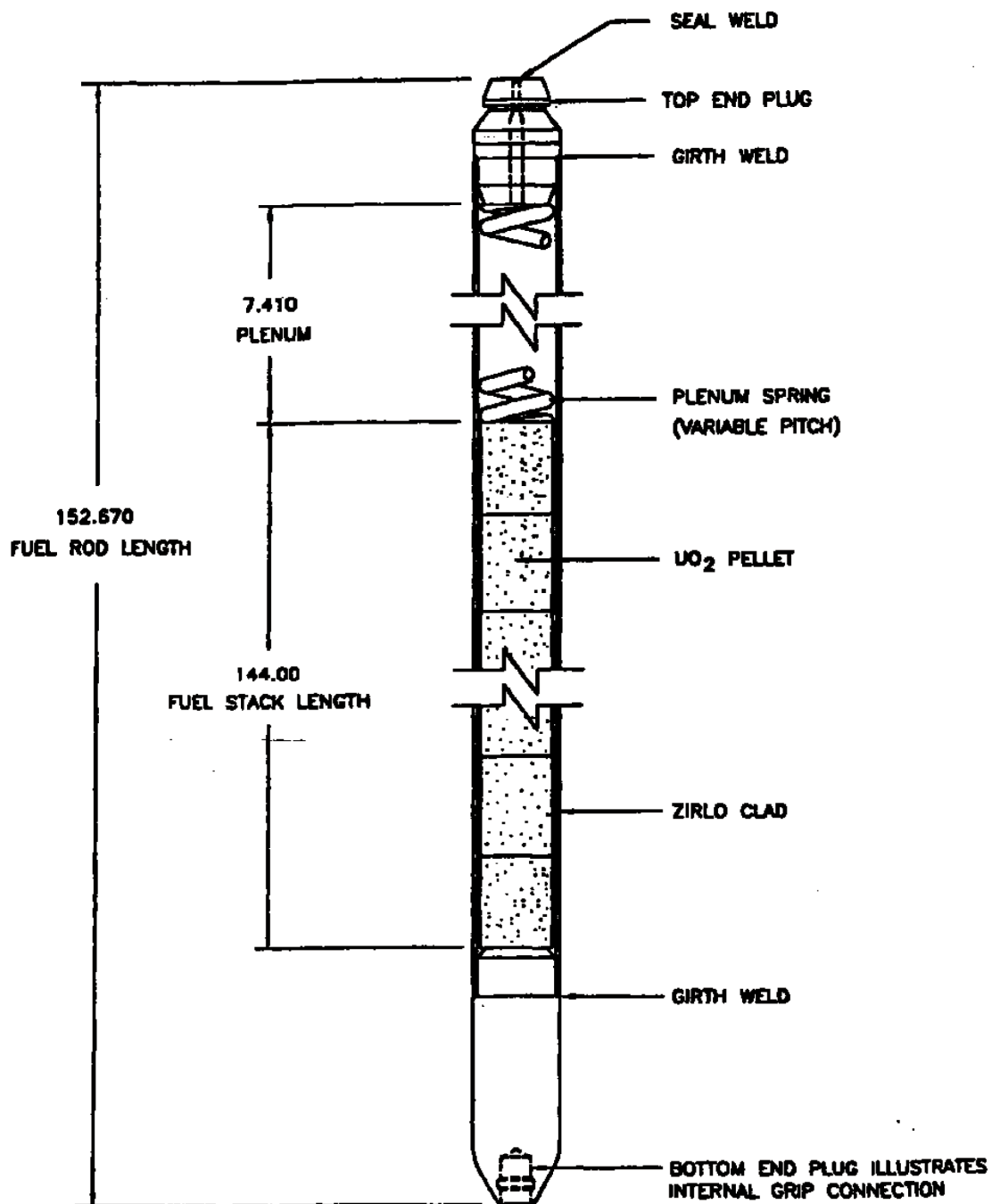


* FARLEY UNIT 2 CYCLE 12 AND 13
UNIT 1 CYCLE 15

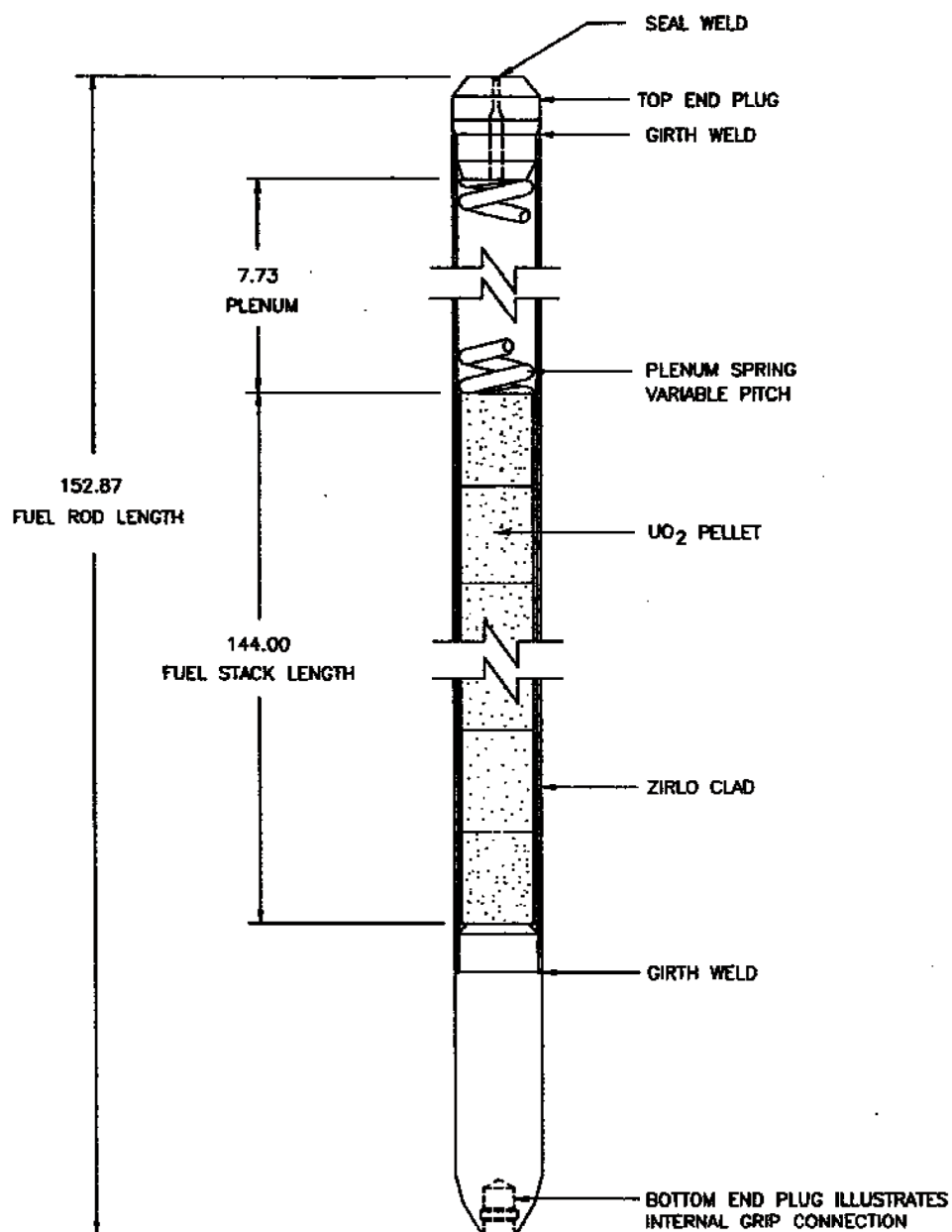
SPECIFIC DIMENSIONS DEPEND ON DESIGN VARIABLES SUCH AS
PRE-PRESSURIZATION, POWER HISTORY, AND DISCHARGE BURNUP

17

REV 21 5/08



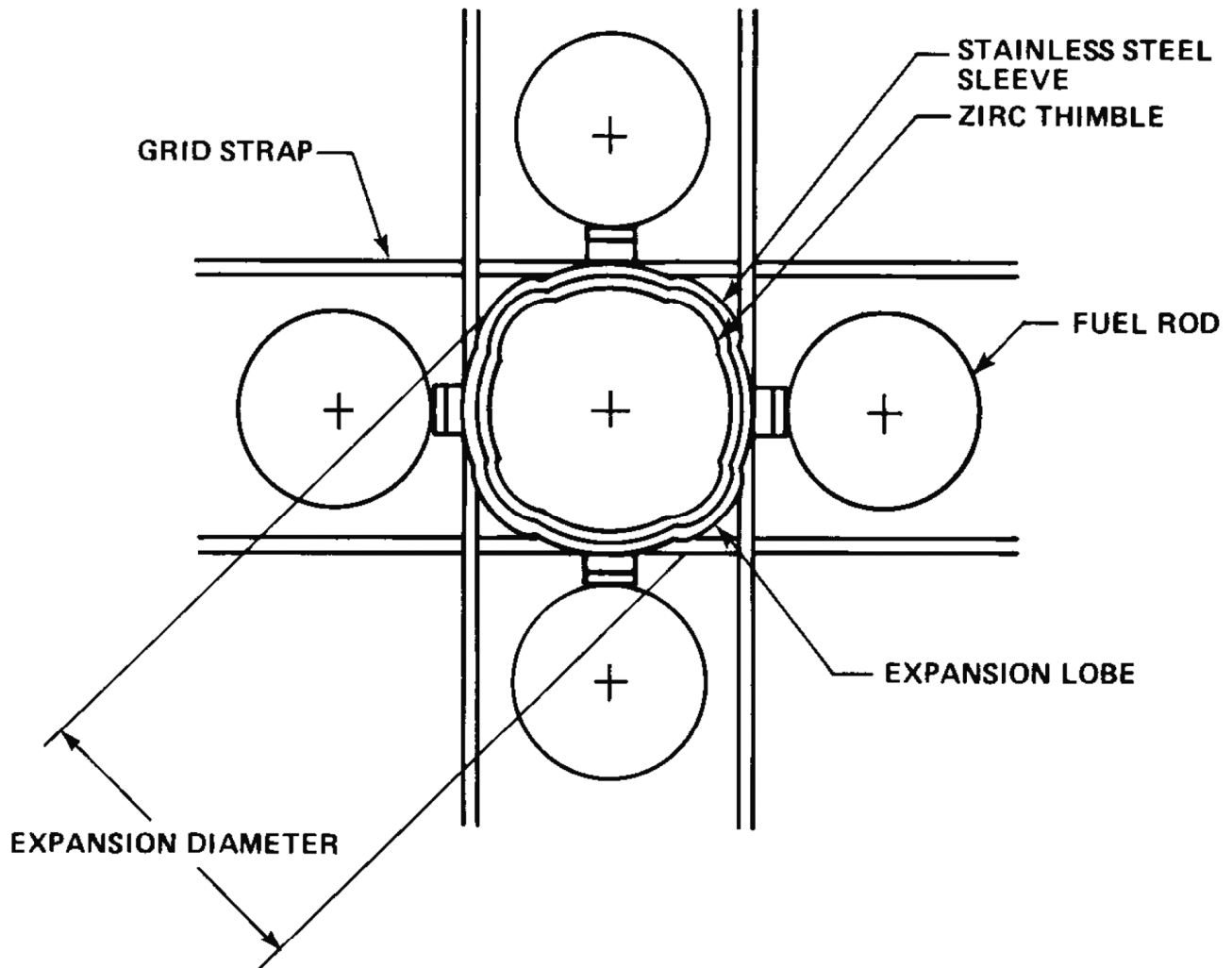
REV 21 5/08



SPECIFIC DIMENSIONS DEPEND ON DESIGN VARIABLES SUCH AS PRE-PRESSURIZATION, POWER HISTORY, AND DISCHARGE BURNUP

REV 21 5/08

INTERMEDIATE GRID EXPANSION JOINT DESIGN



REV 21 5/08

BUTT WELD ALL AROUND

ZIRCALOY THIMBLE

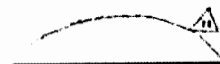
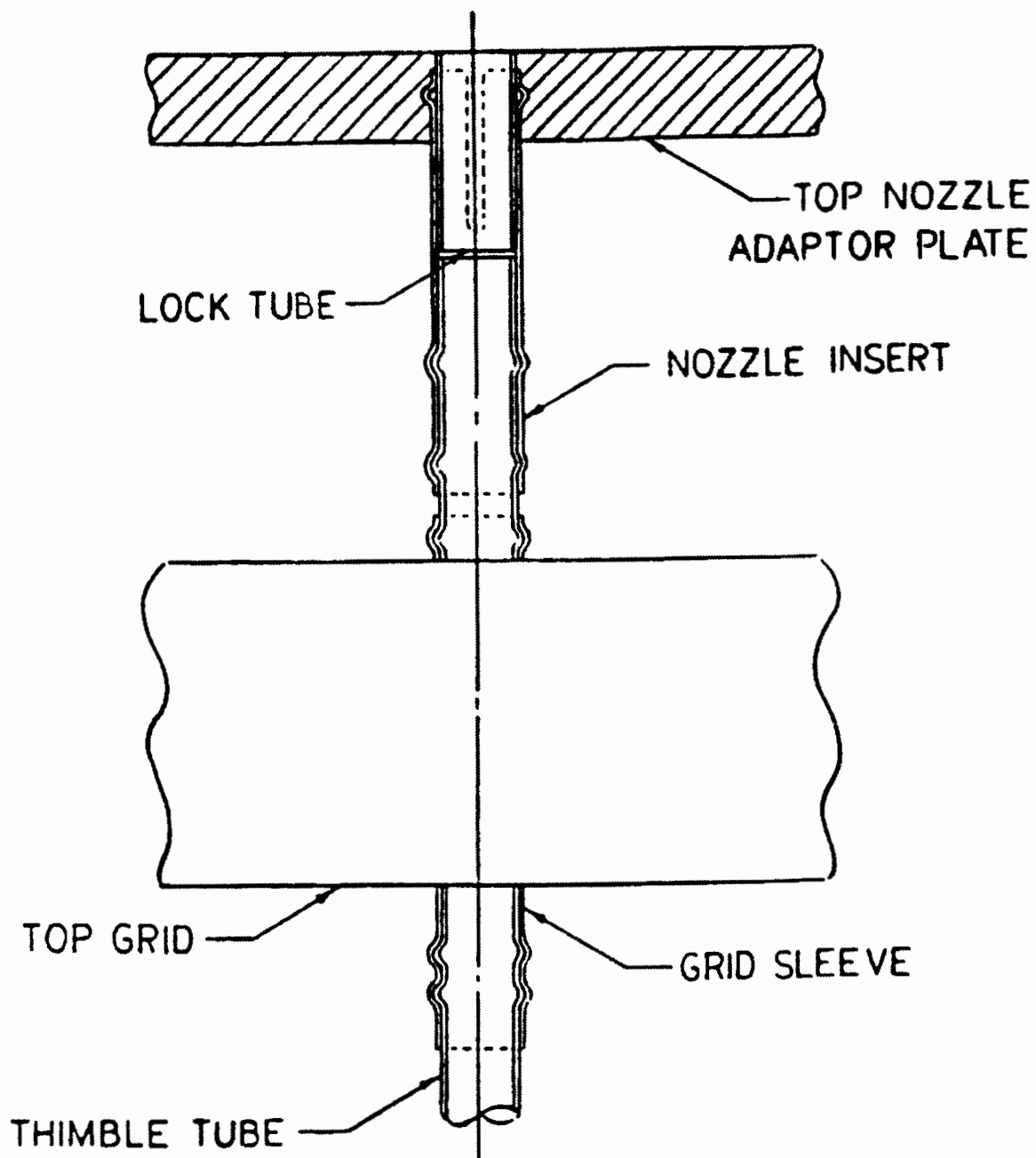
TOP NOZZLE ADAPTER PLATE

STAINLESS STEEL SLEEVE

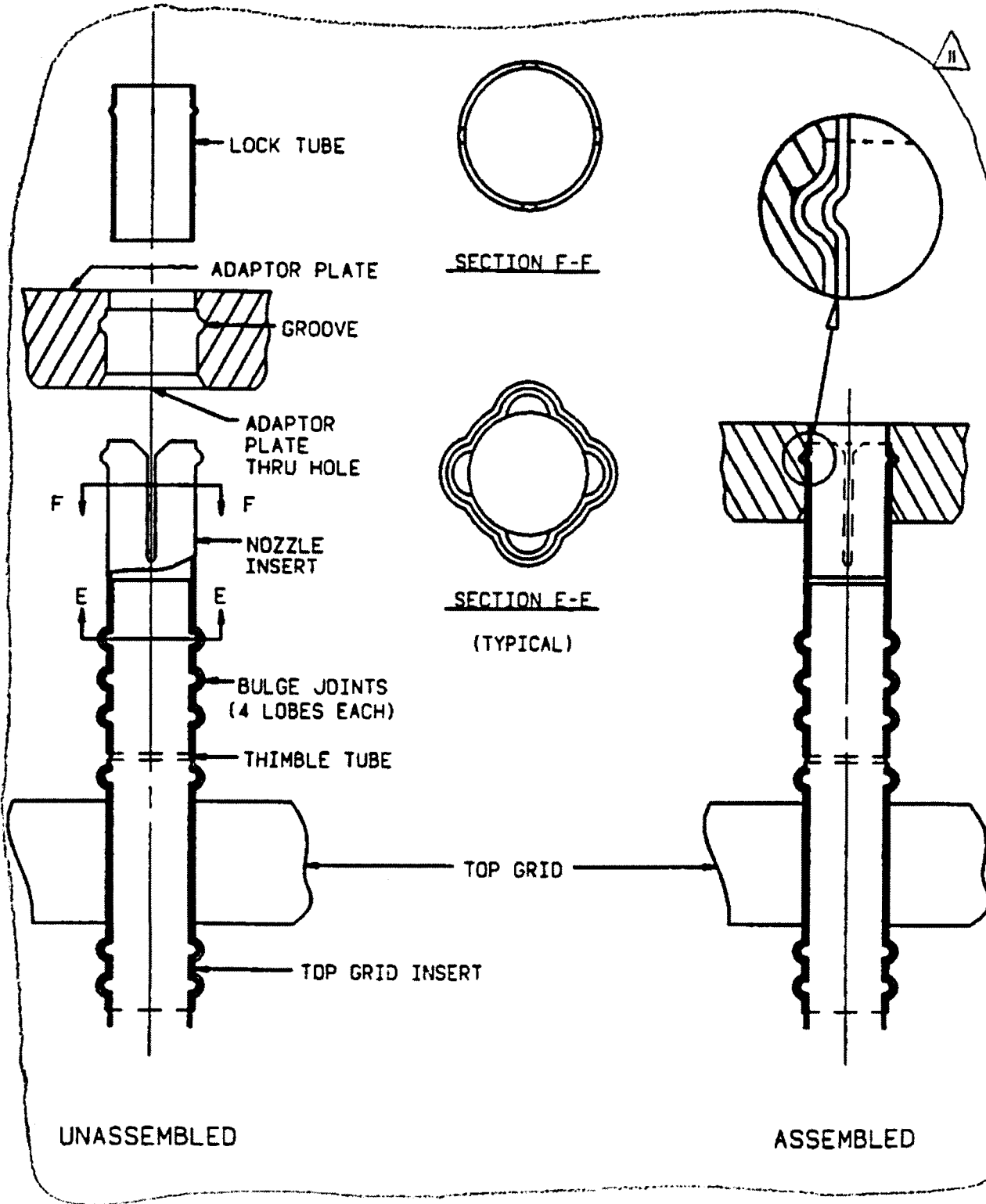
EXPANSION LOBE

TOP GRID

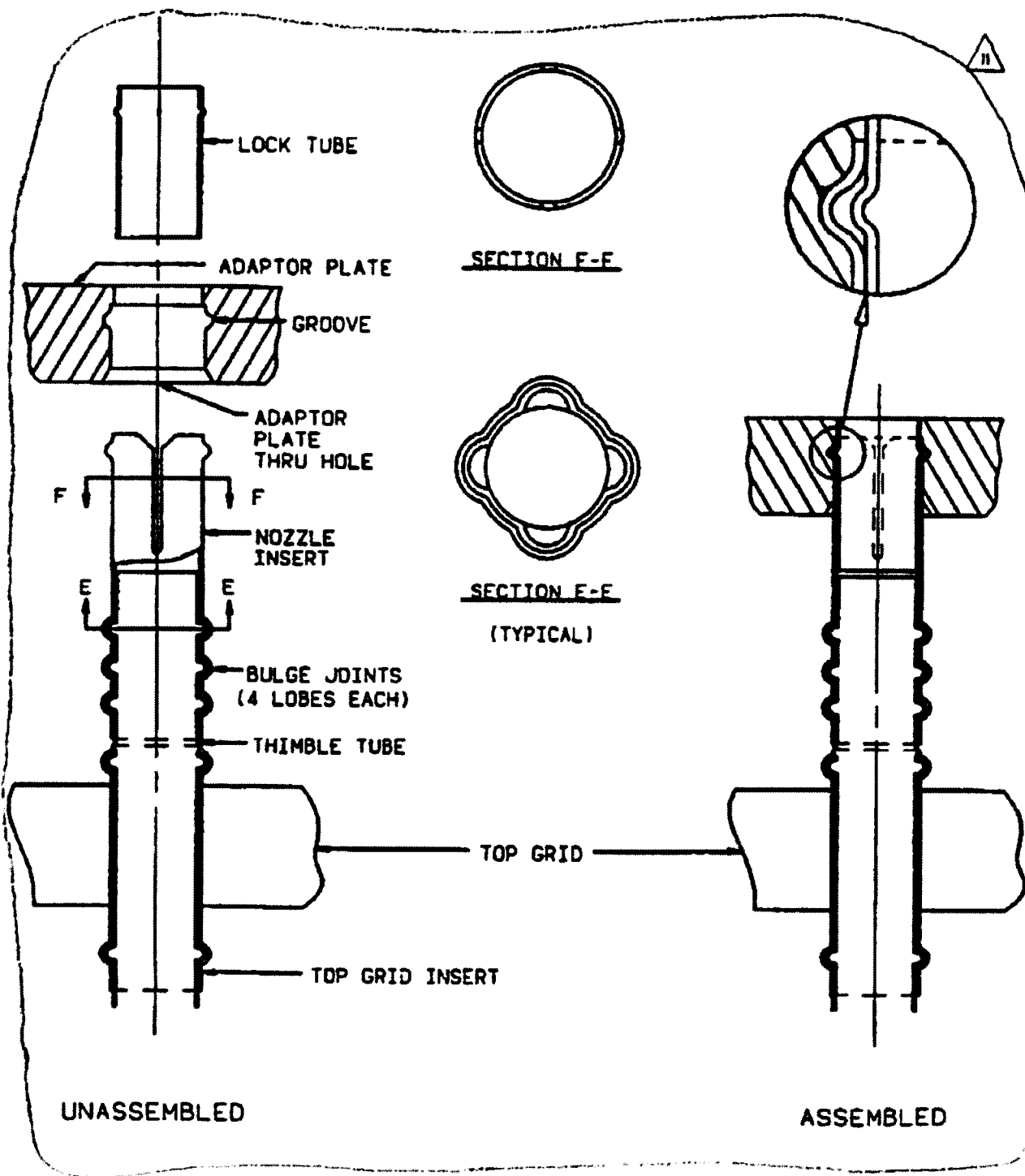
REV 28 10/18



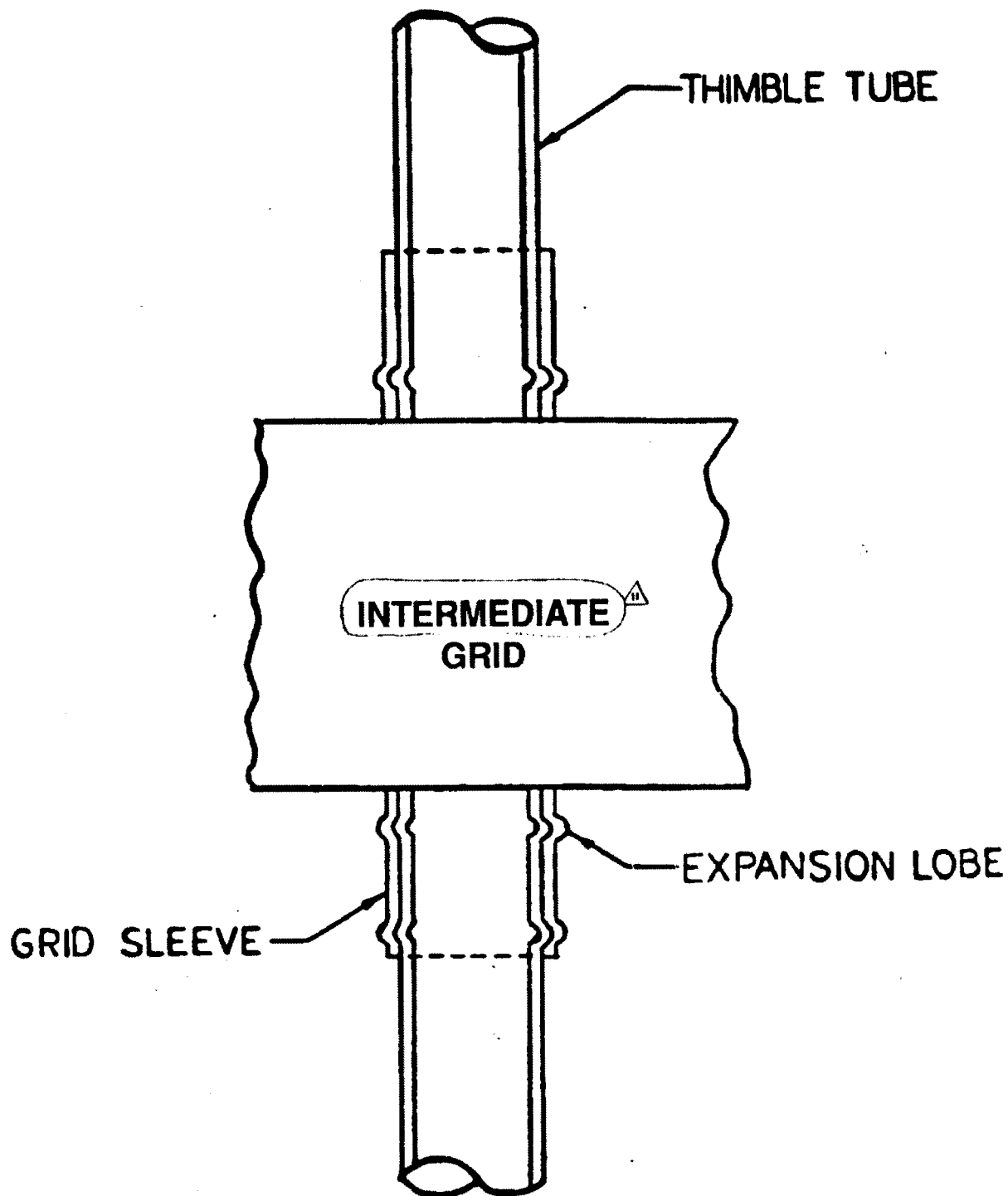
REV 28 10/18



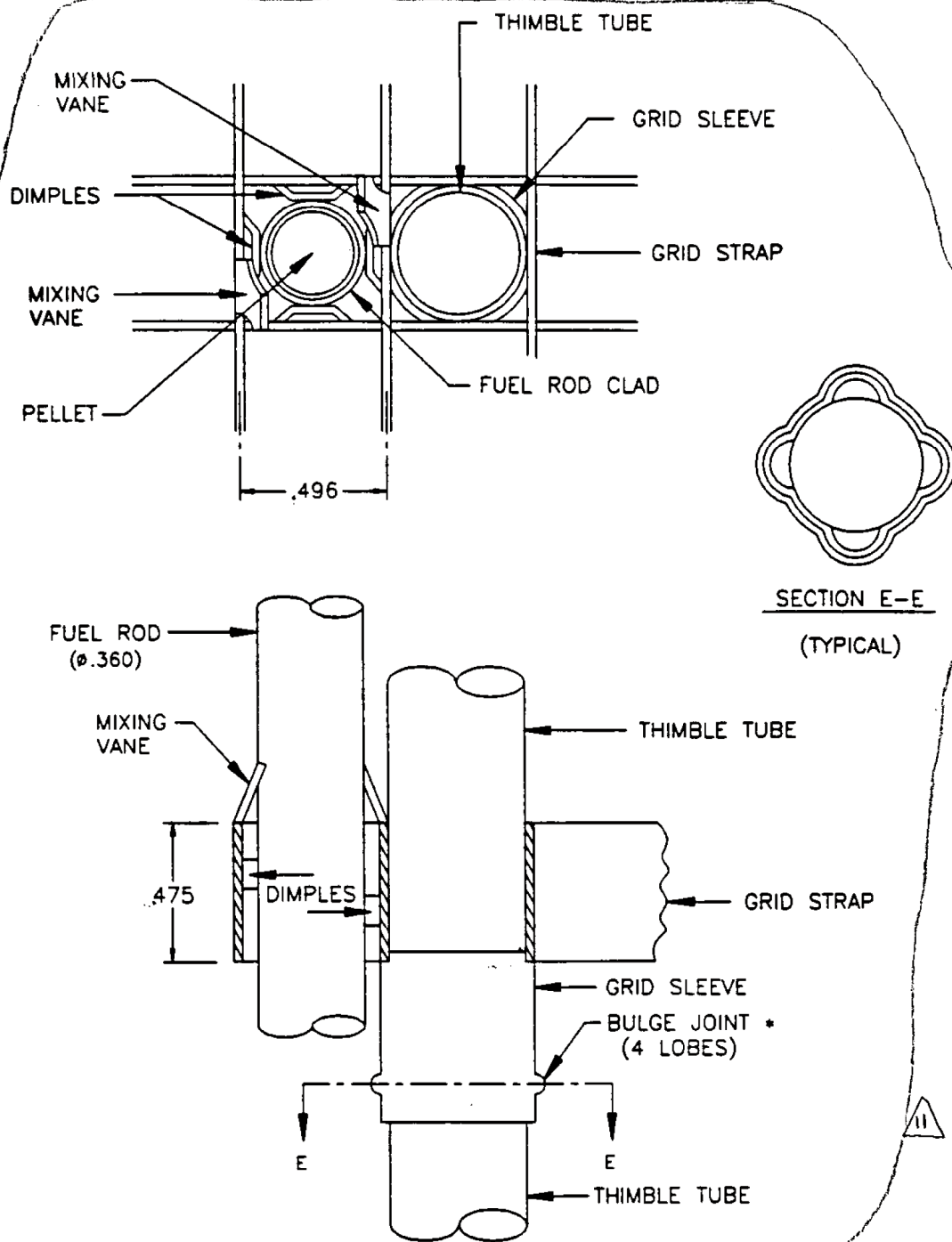
REV 28 10/18



REV 28 10/18



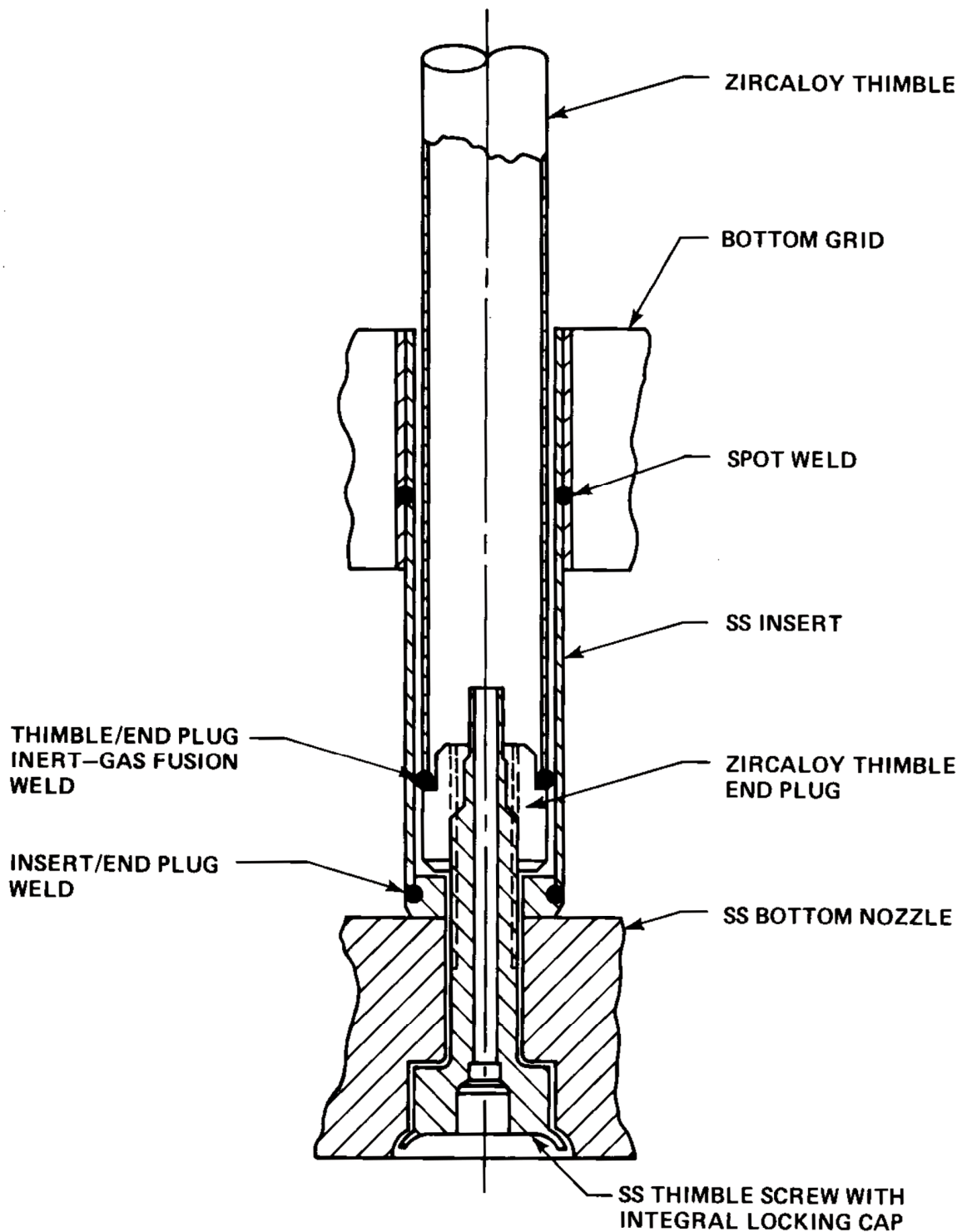
REV 28 10/18



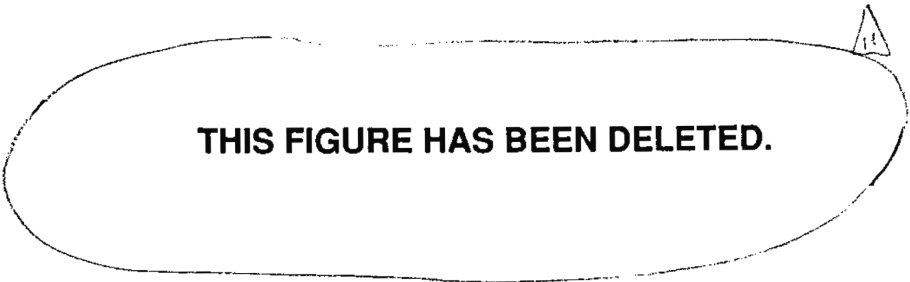
VANTAGE 5 ATTACHMENT DETAIL

DIMENSIONS ARE IN INCHES (NOMINAL)
 • TYPICAL FOR INTERMEDIATE GRIDS

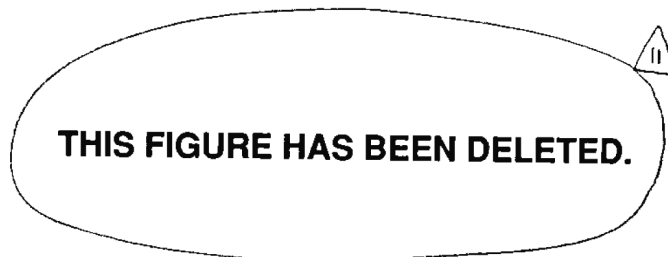
REV 21 5/08



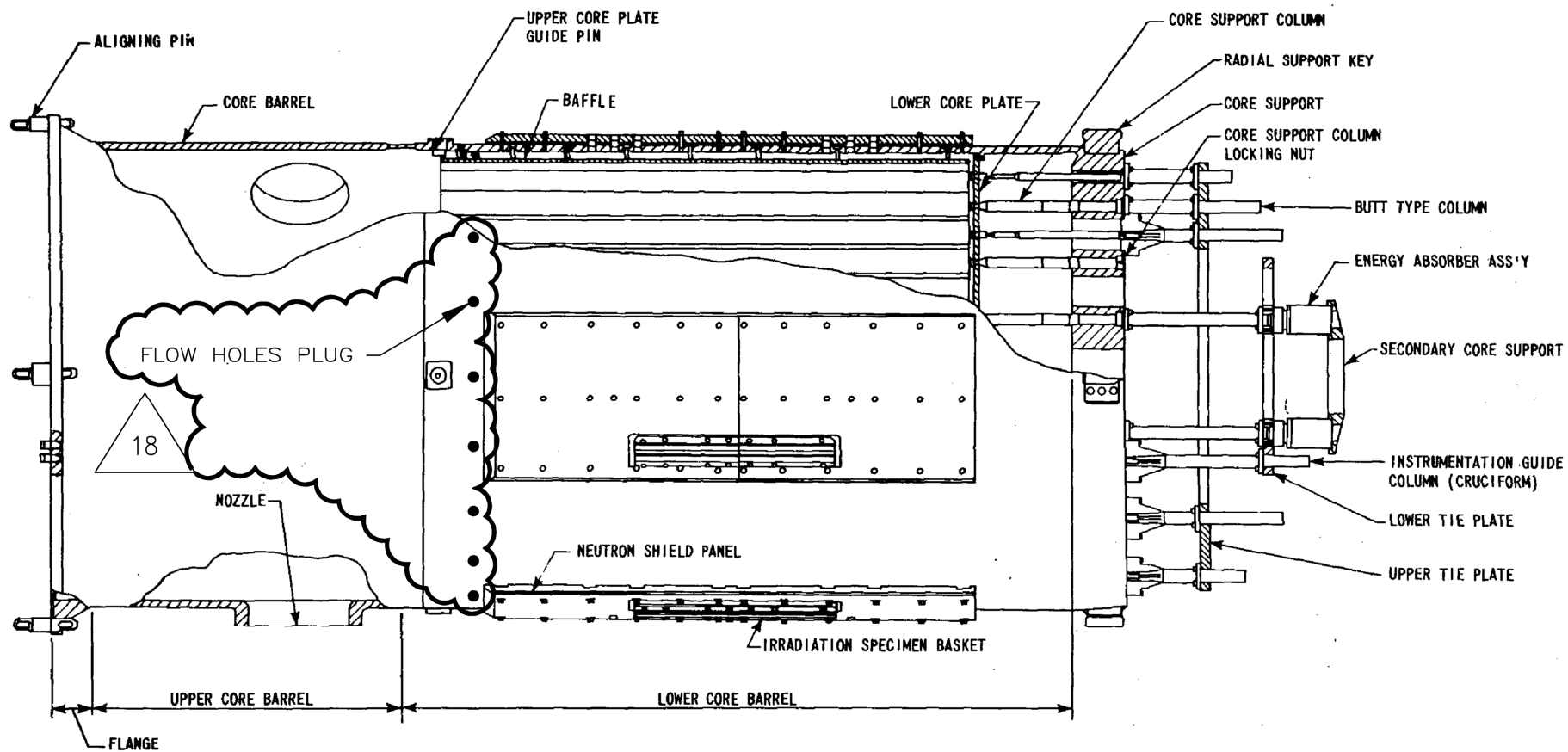
REV 21 5/08



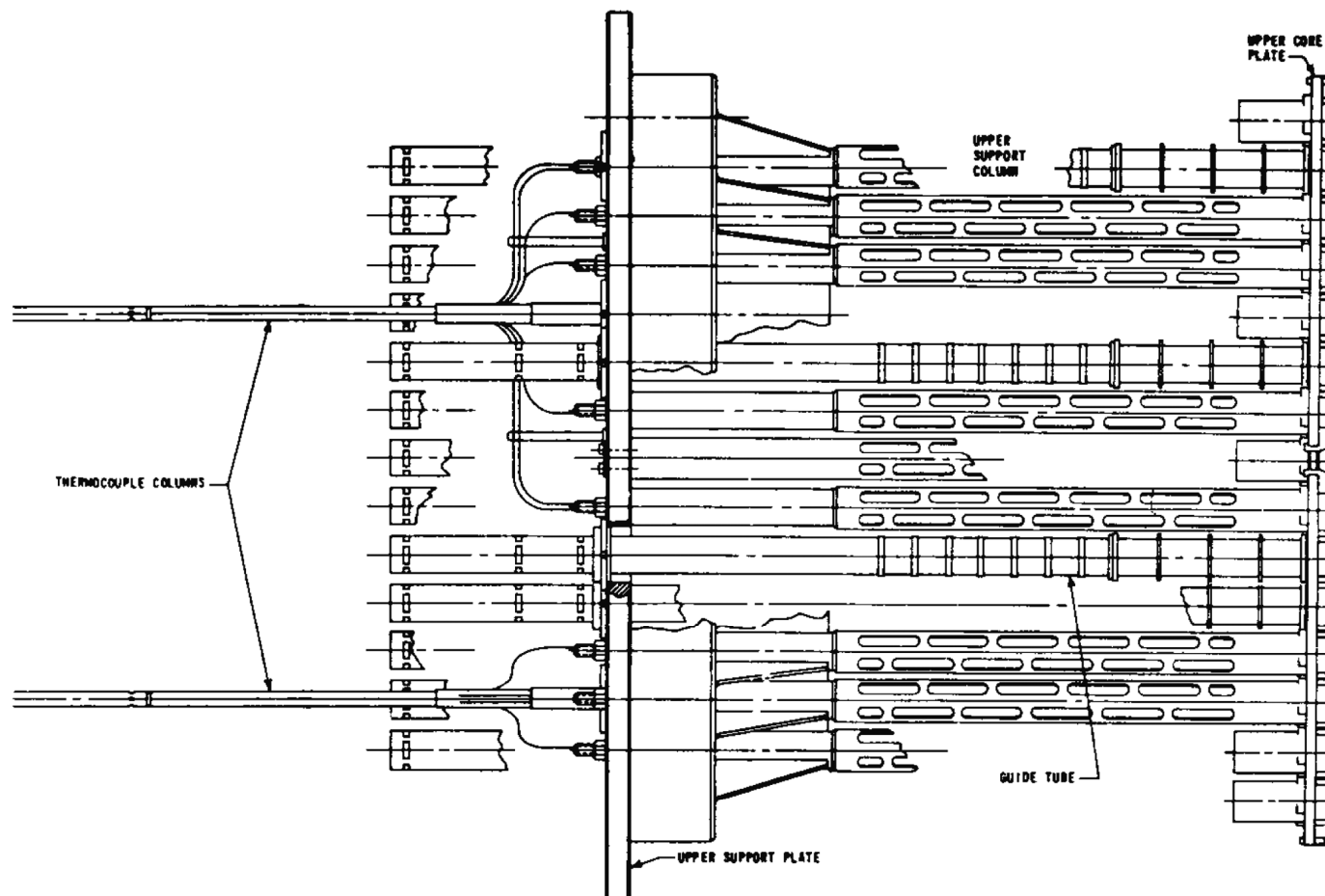
REV 21 5/08



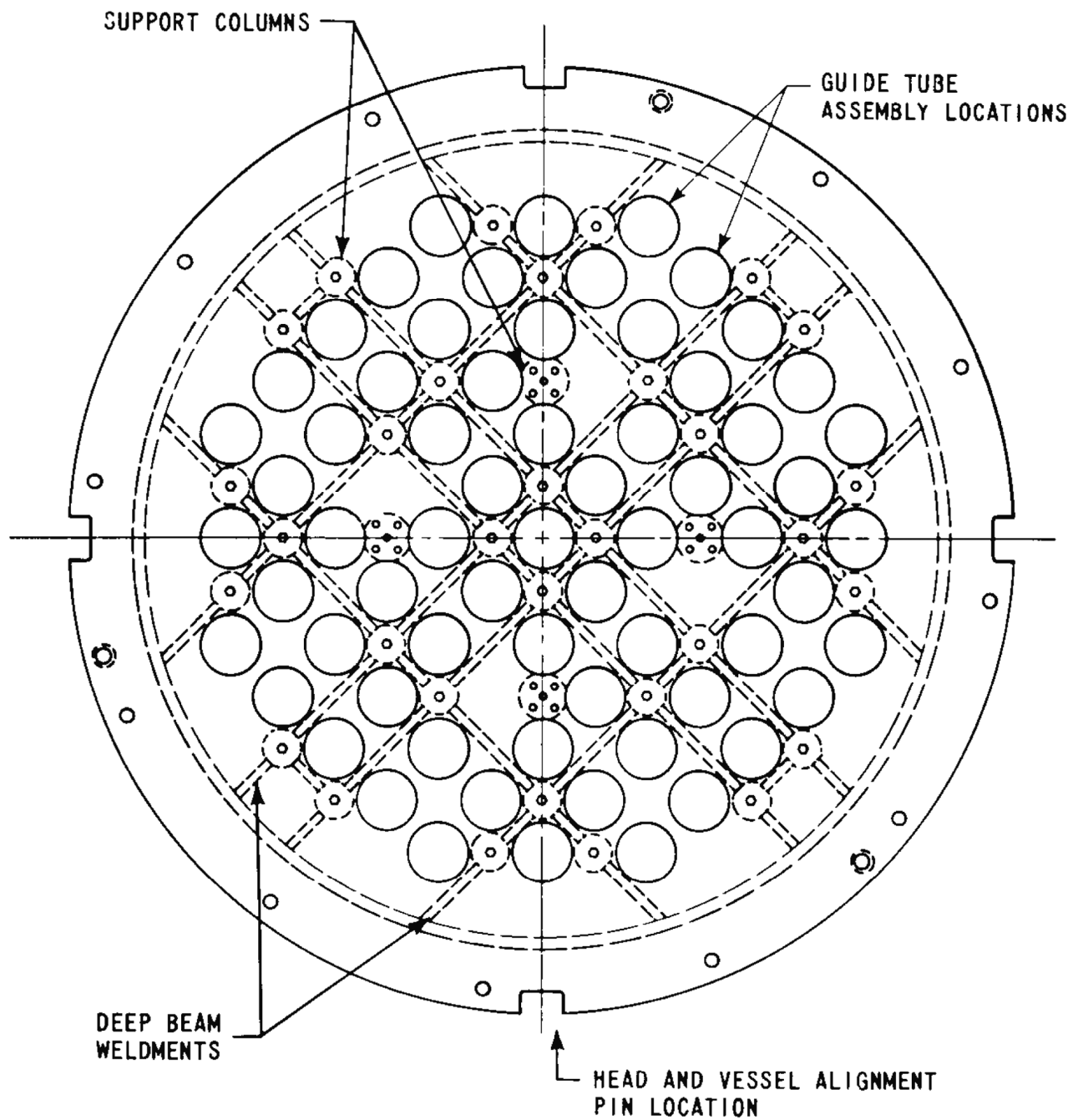
REV 21 5/08



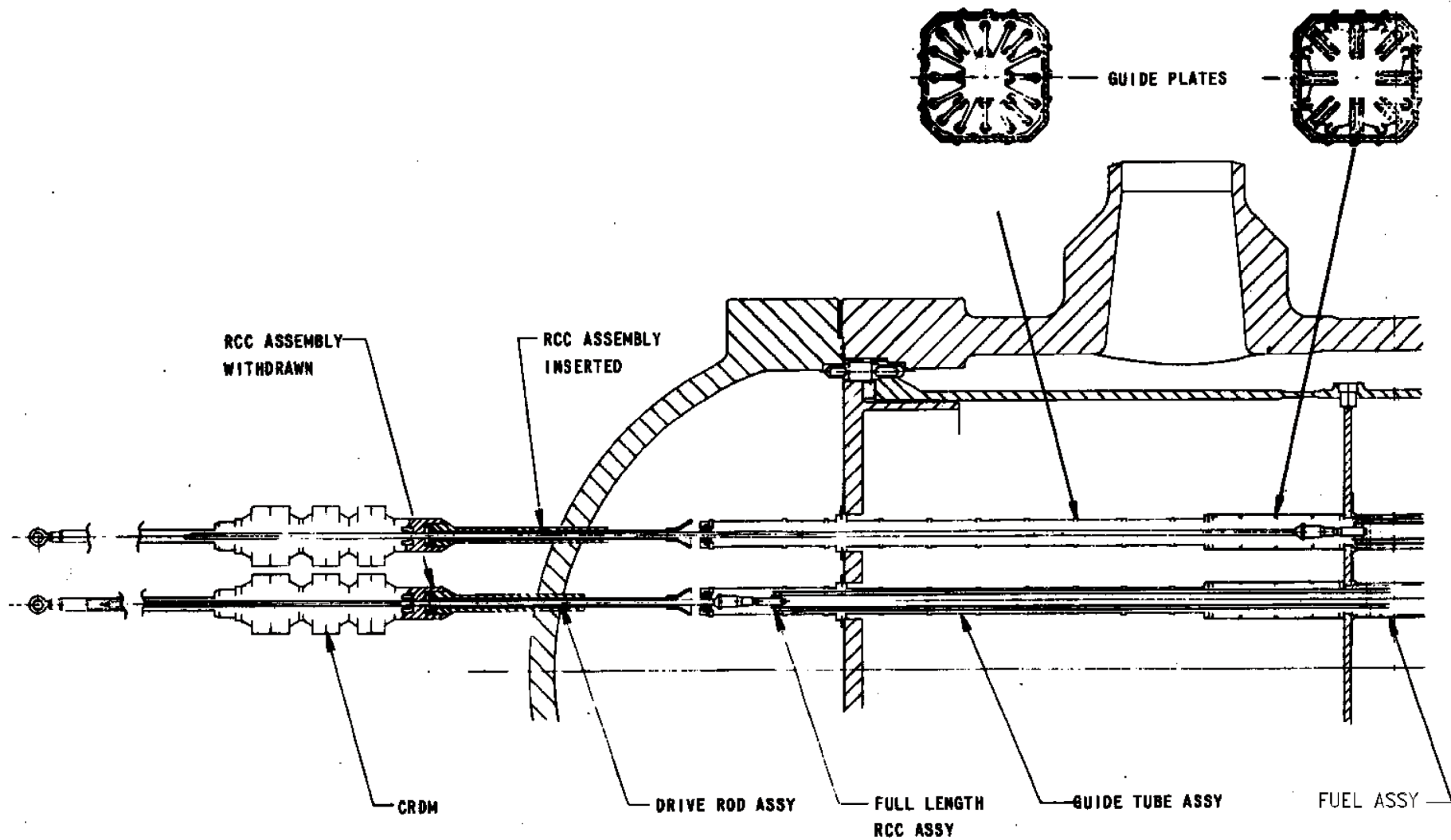
REV 21 5/08



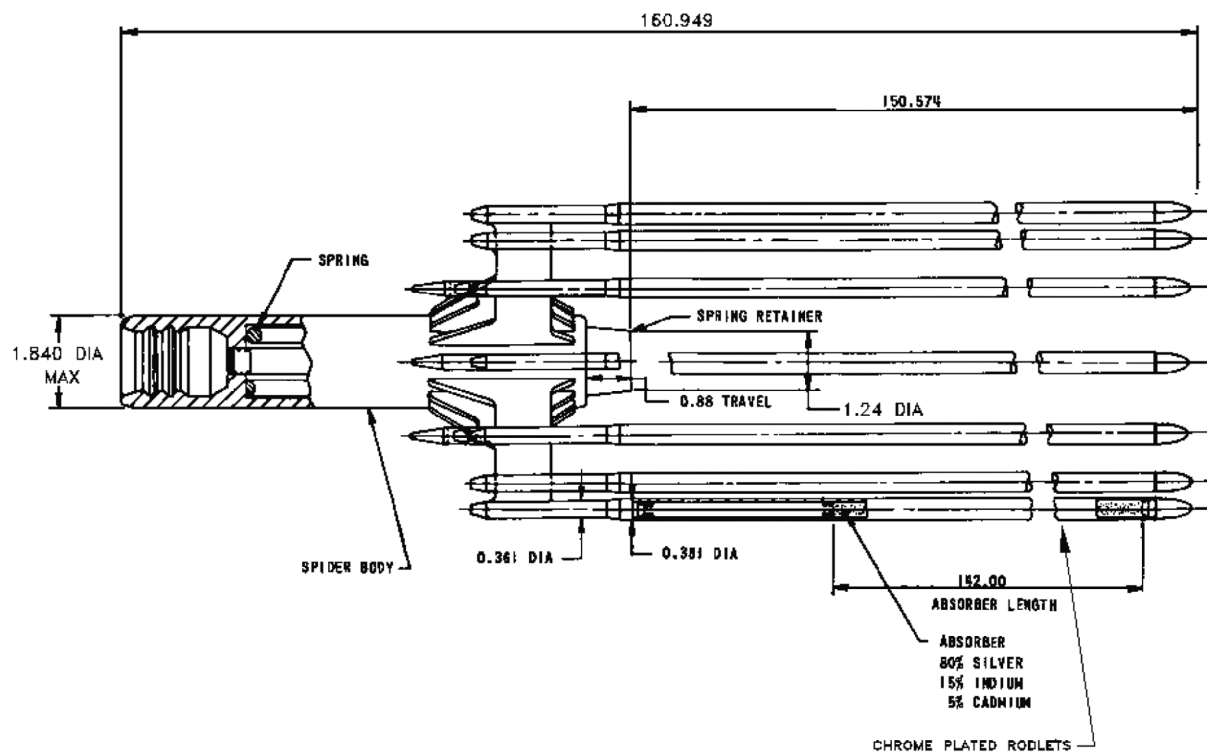
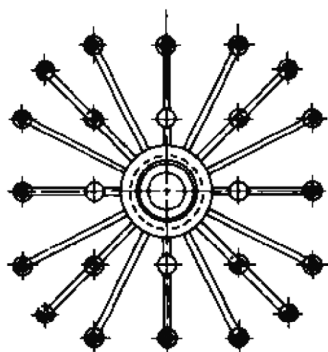
REV 21 5/08



REV 21 5/08

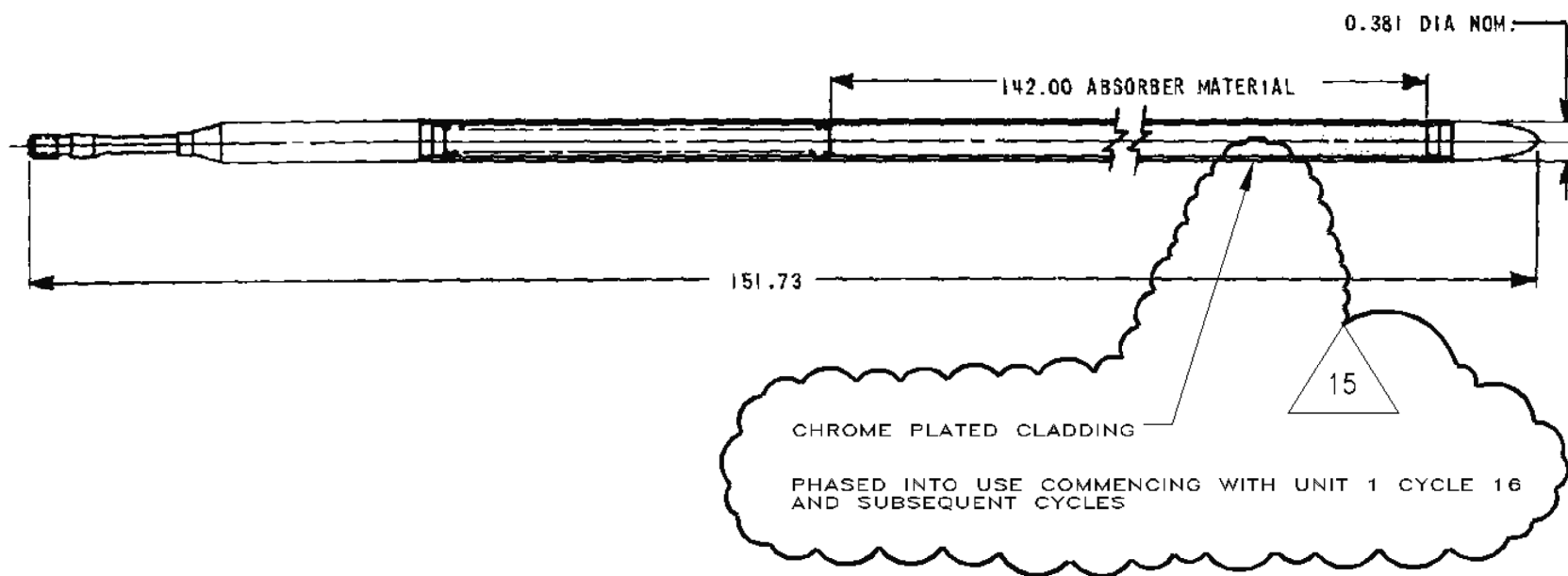


REV 21 5/08

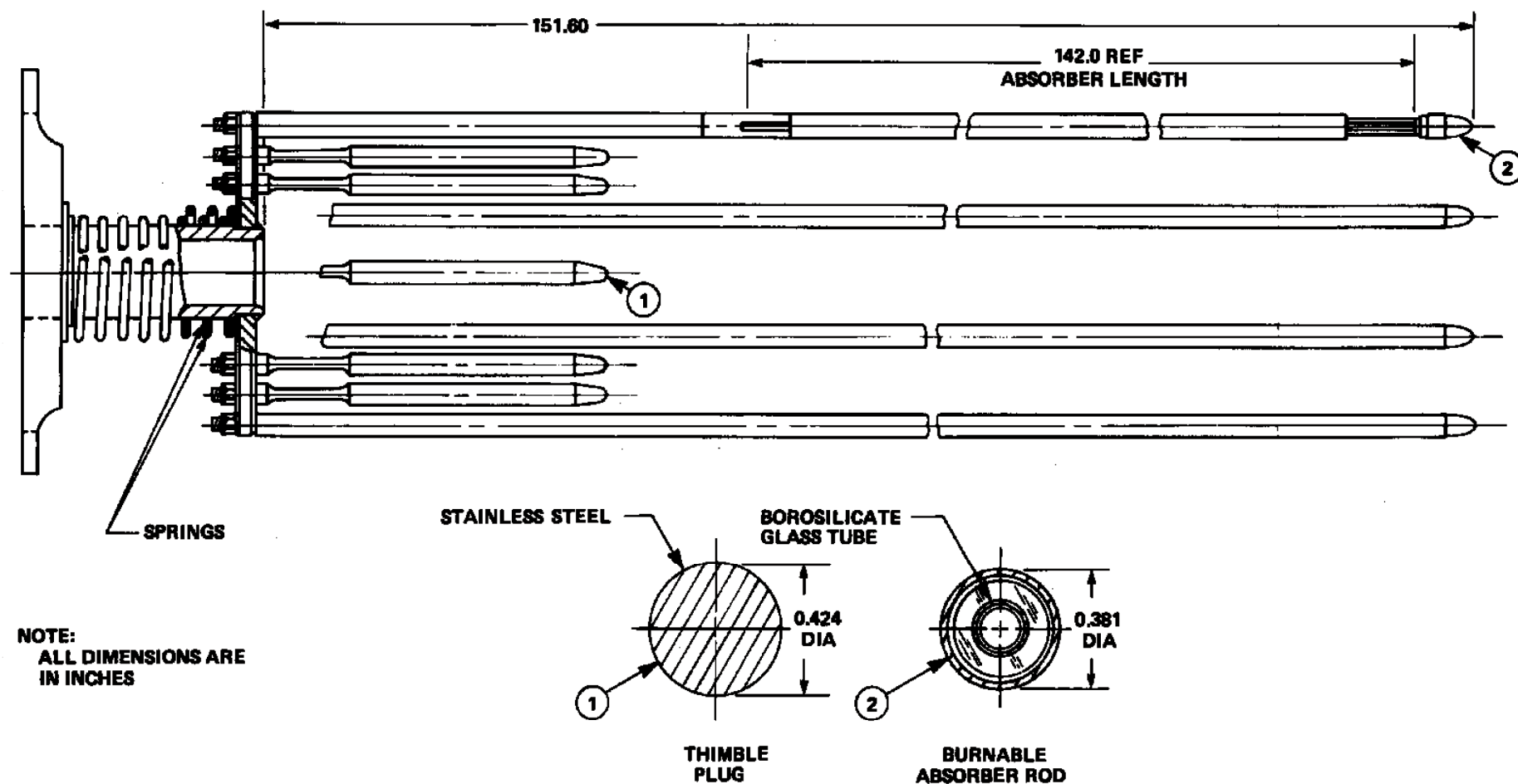


PHASED INTO USE COMMENCING WITH UNIT 1 CYCLE 16
AND SUBSEQUENT CYCLES

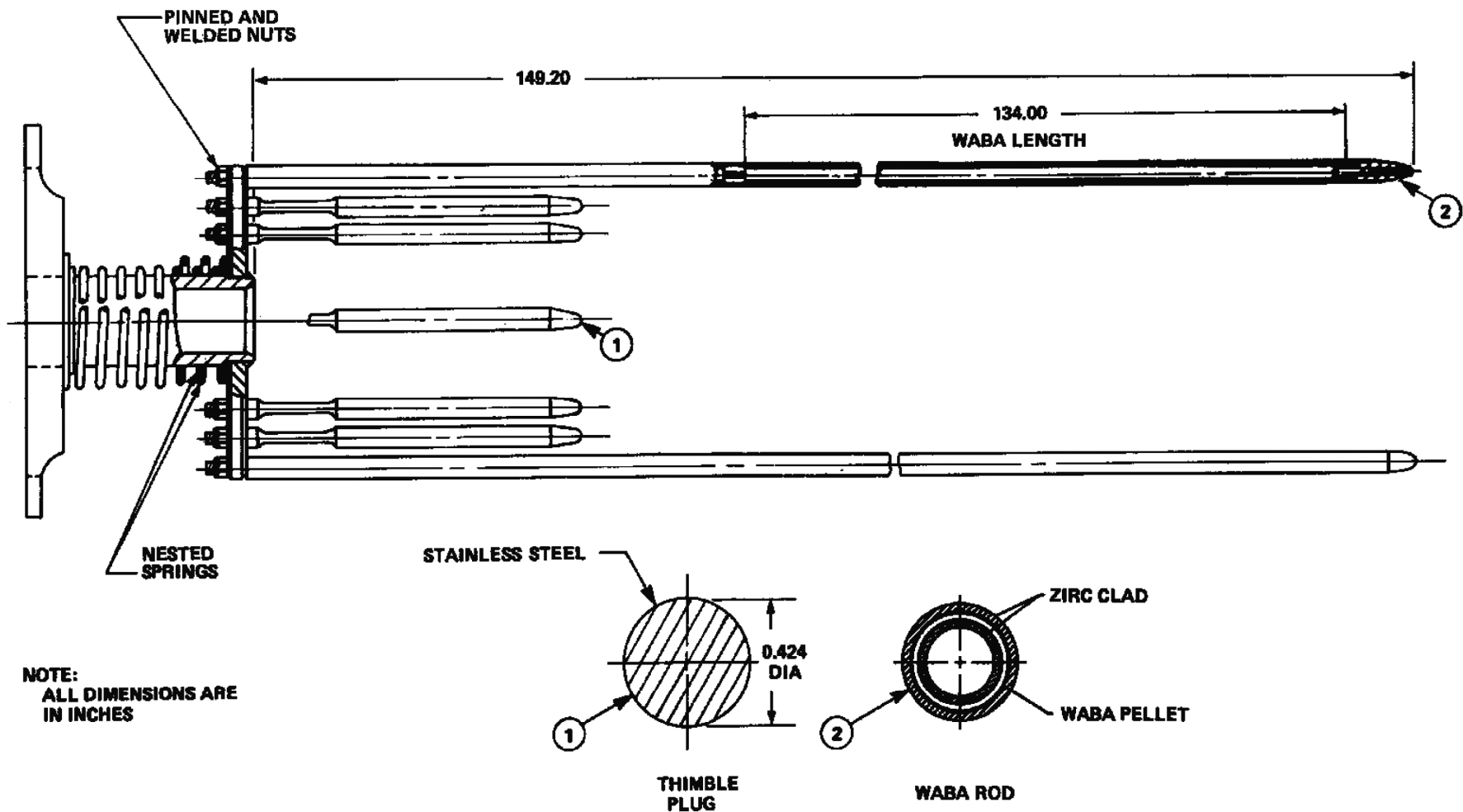
REV 21 5/08



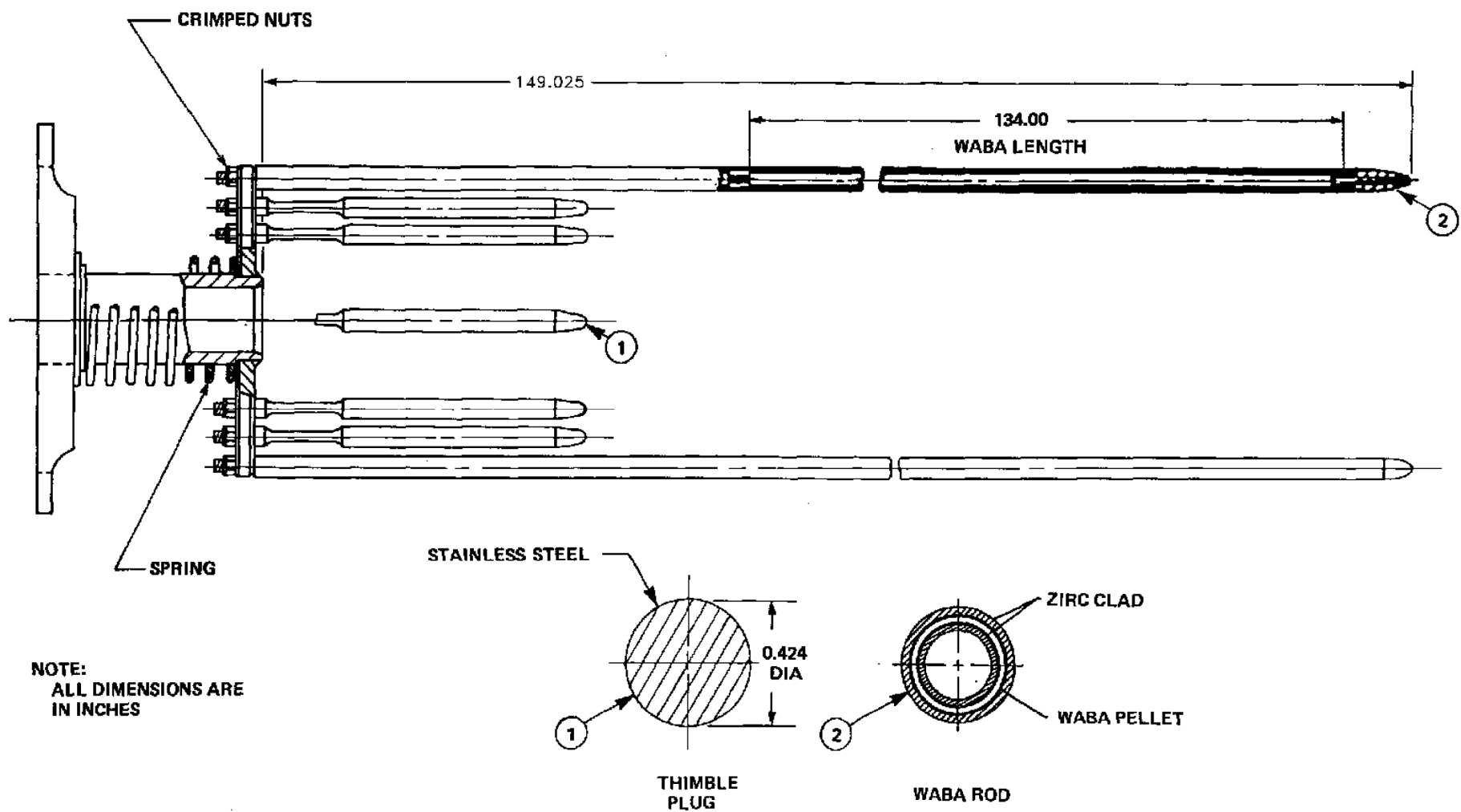
REV 21 5/08



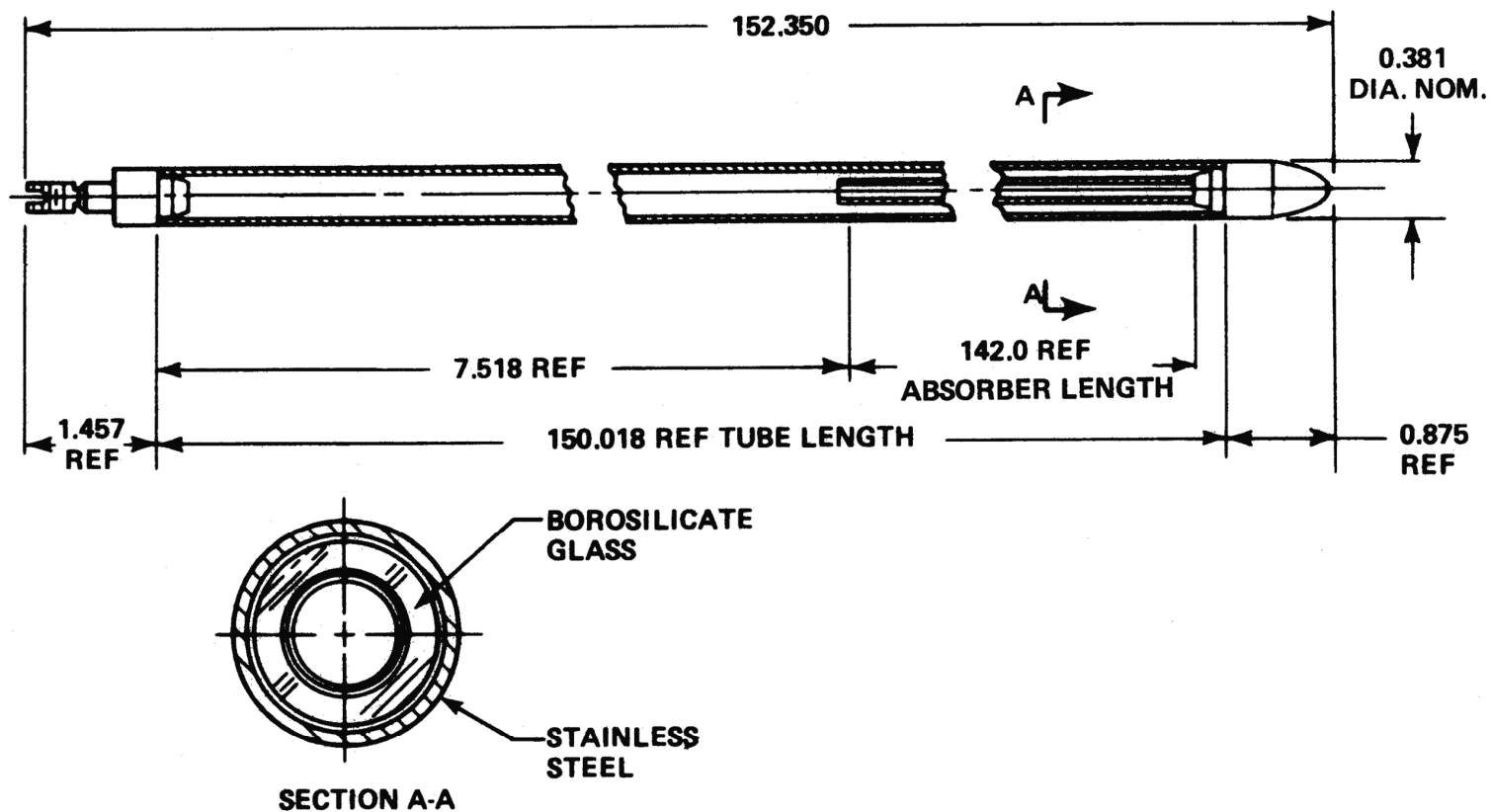
REV 21 5/08



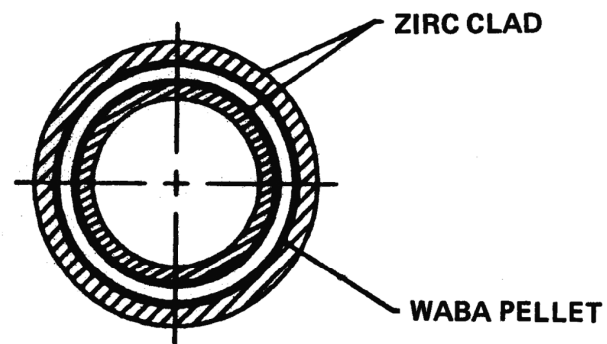
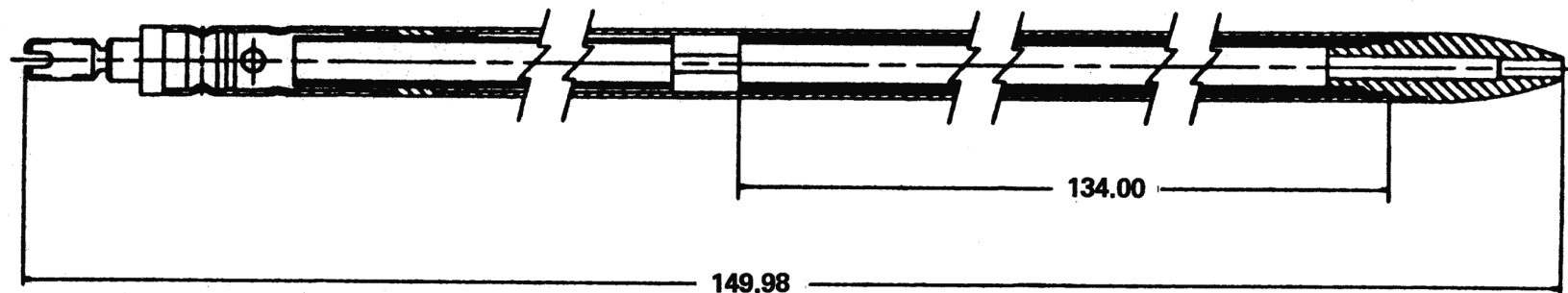
REV 21 5/08



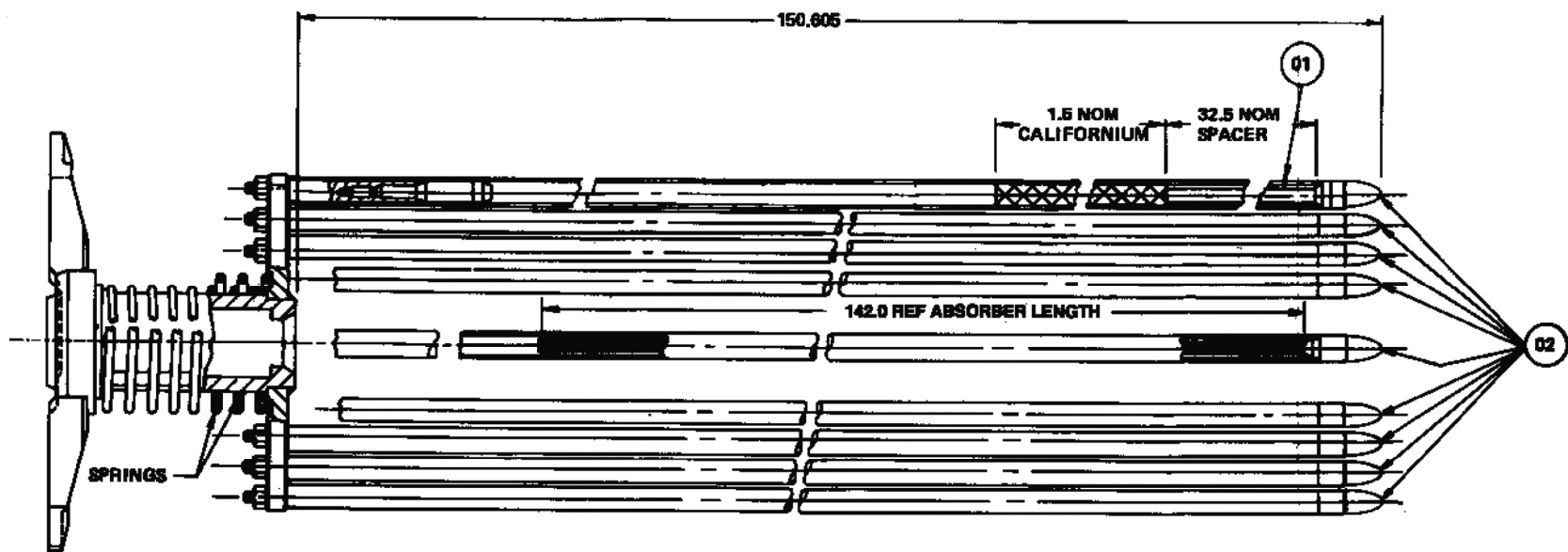
REV 21 5/08



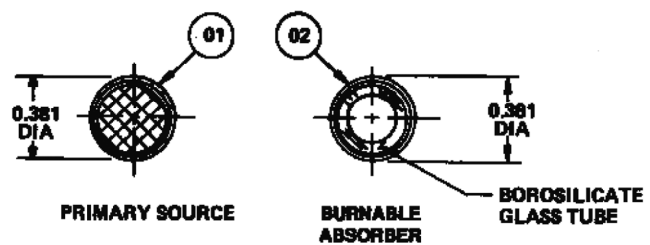
REV 21 5/08



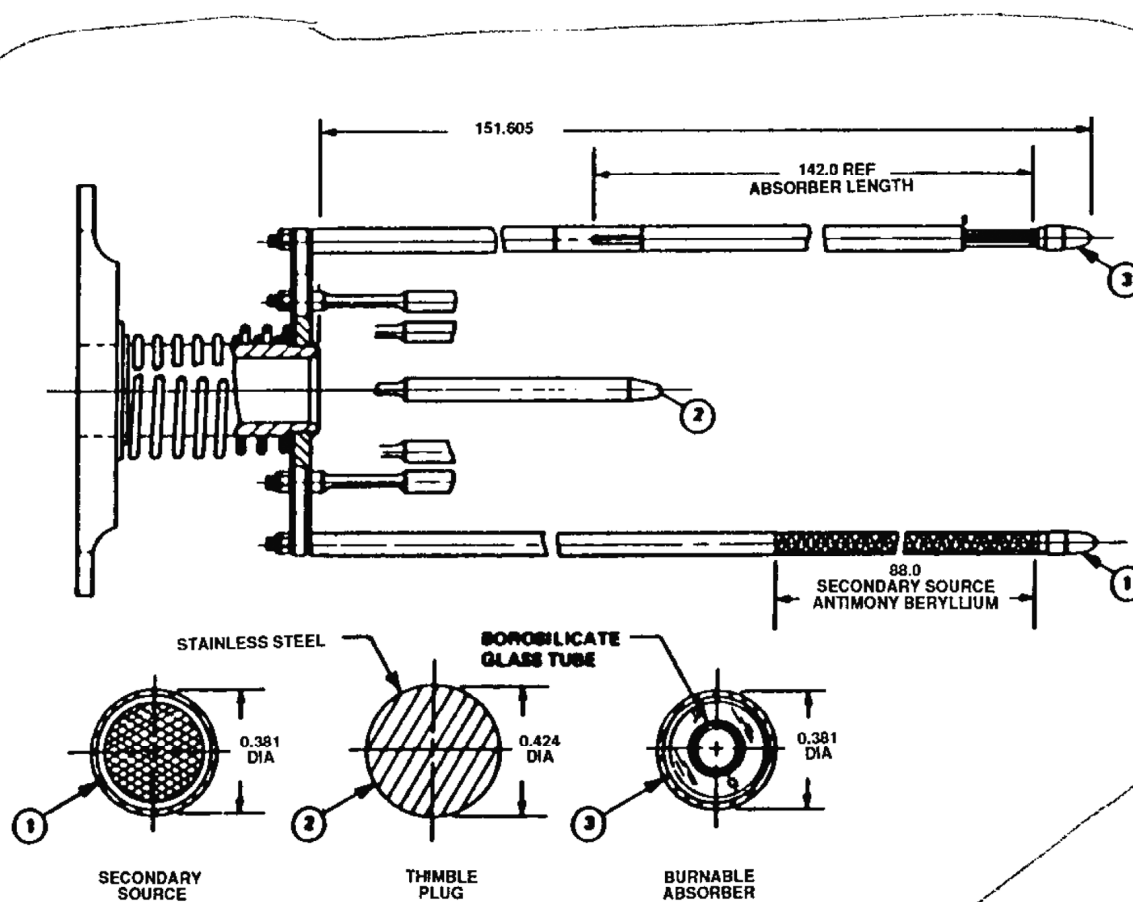
REV 21 5/08



NOTE: ALL DIMENSIONS ARE IN INCHES

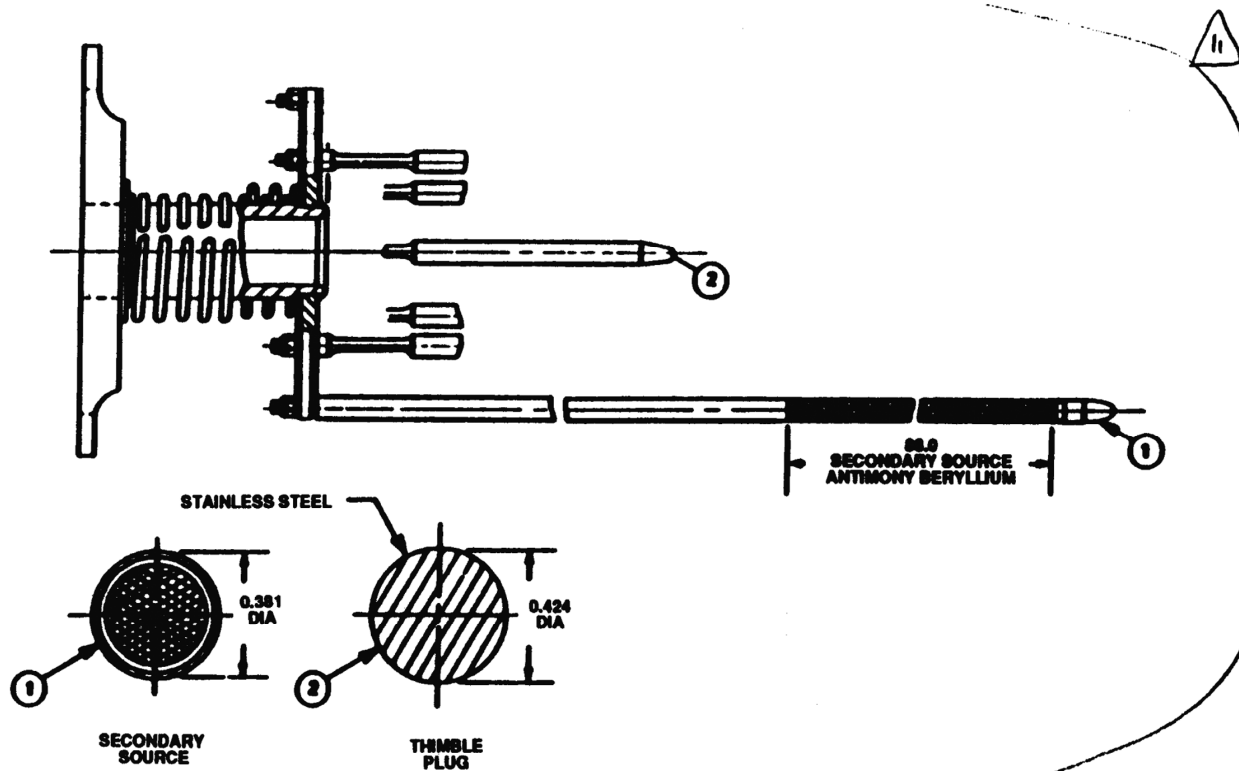


REV 21 5/08

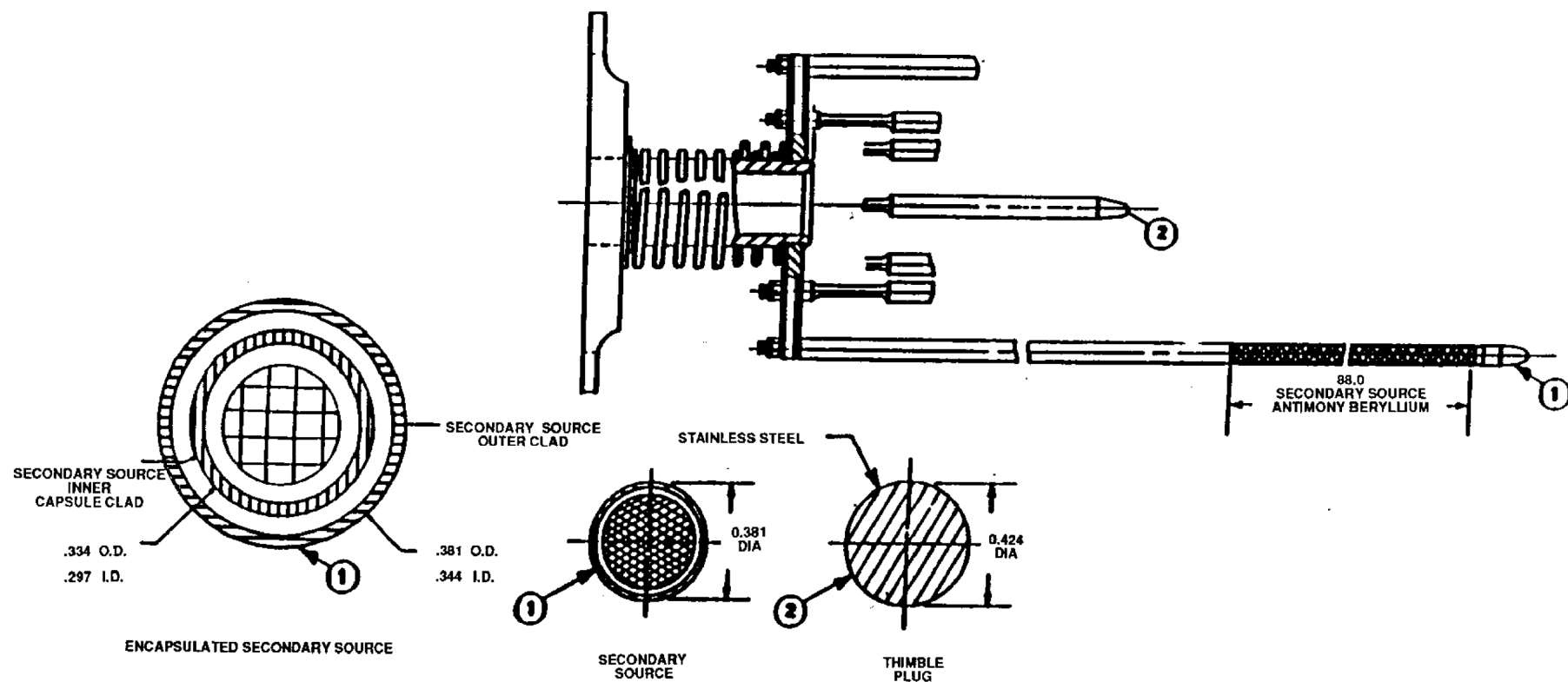


NOTE: ALL DIMENSIONS ARE IN INCHES.

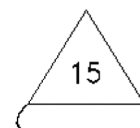
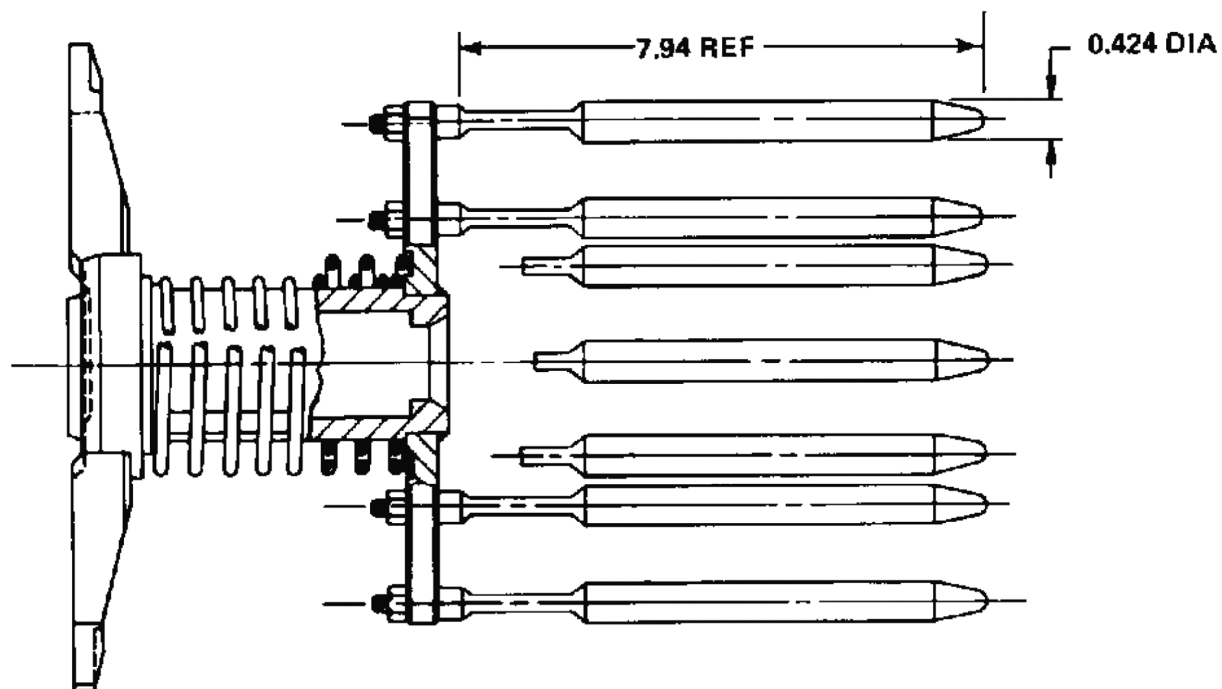
REV 21 5/08



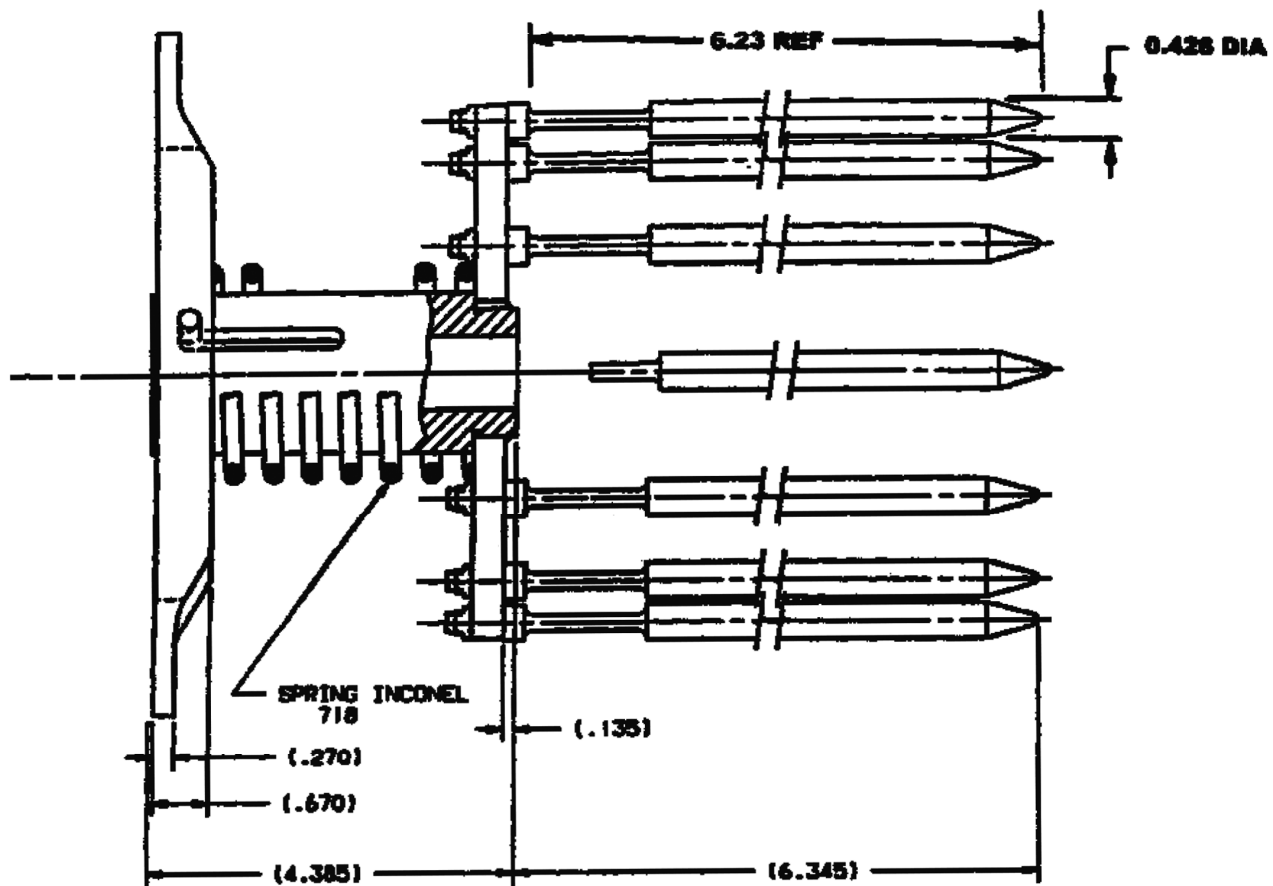
REV 21 5/08



REV 21 5/08

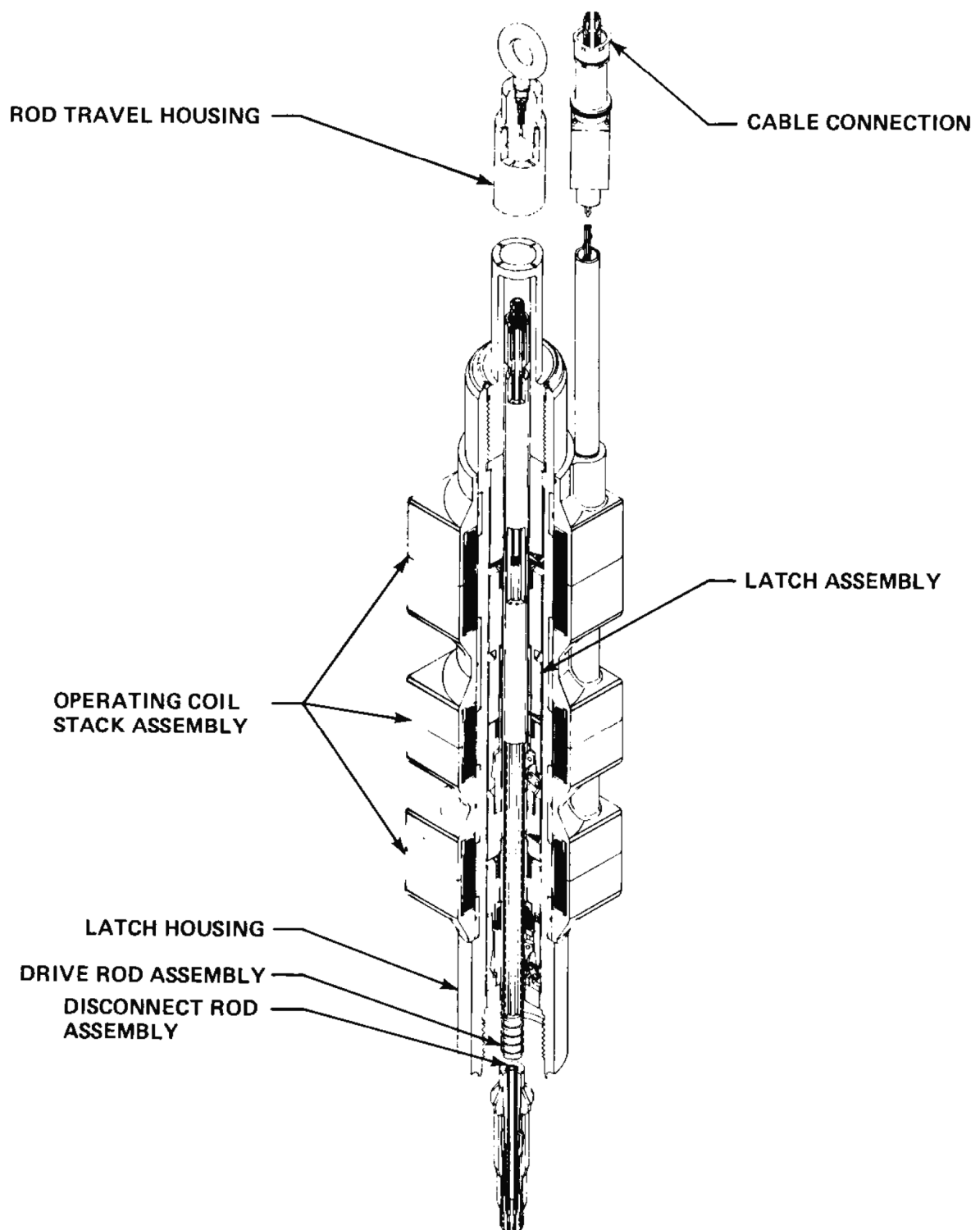


REV 21 5/08

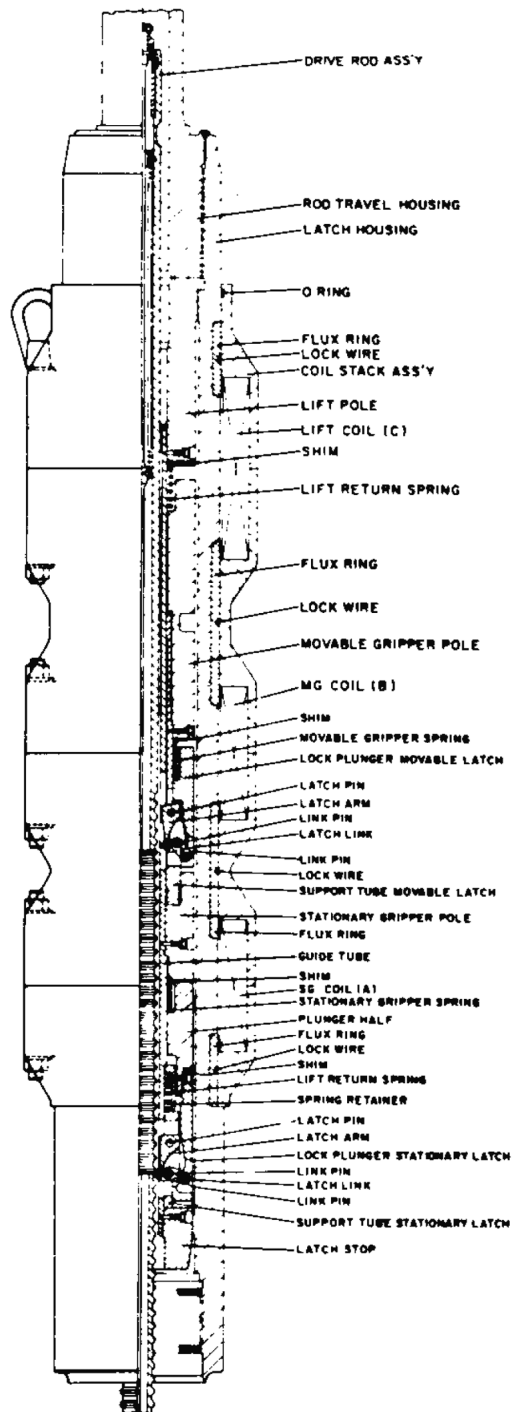


FARLEY UNIT 2 CYCLE 13 AND AFTER
FARLEY UNIT 1 CYCLE 16 AND AFTER

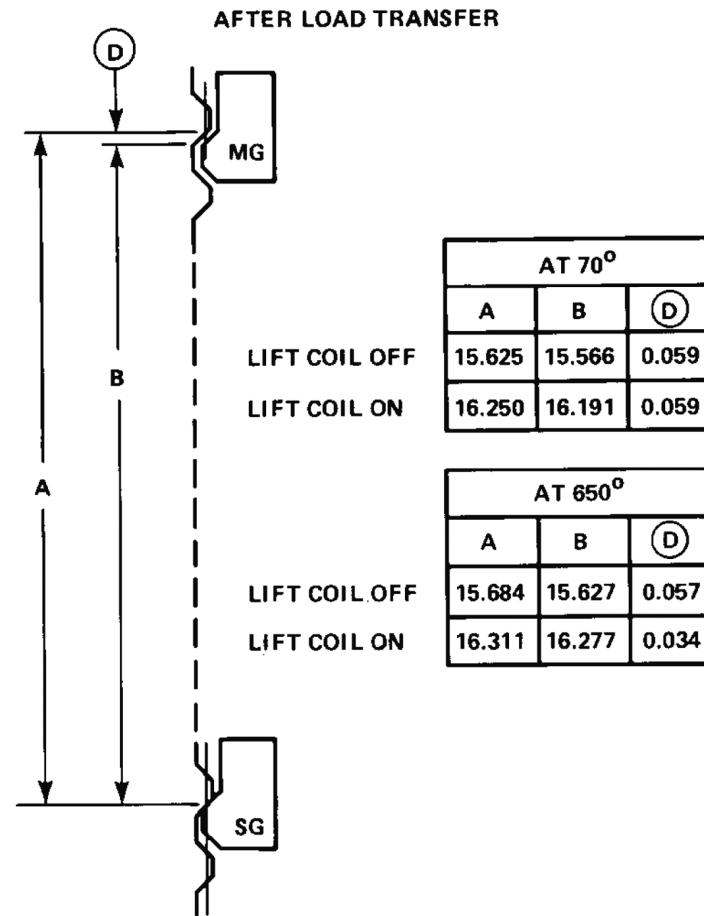
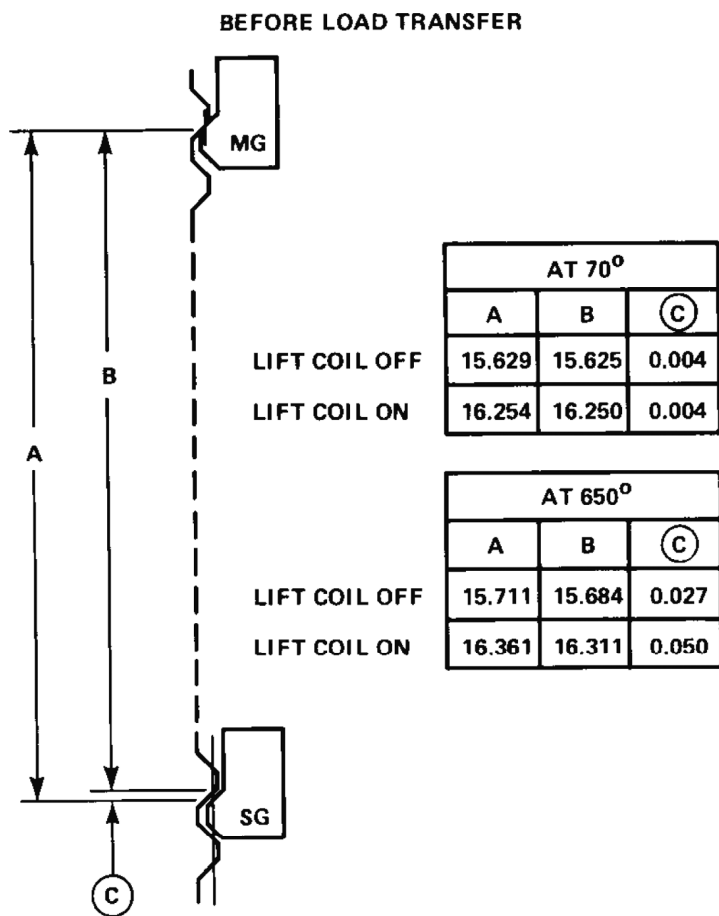
REV 21 5/08



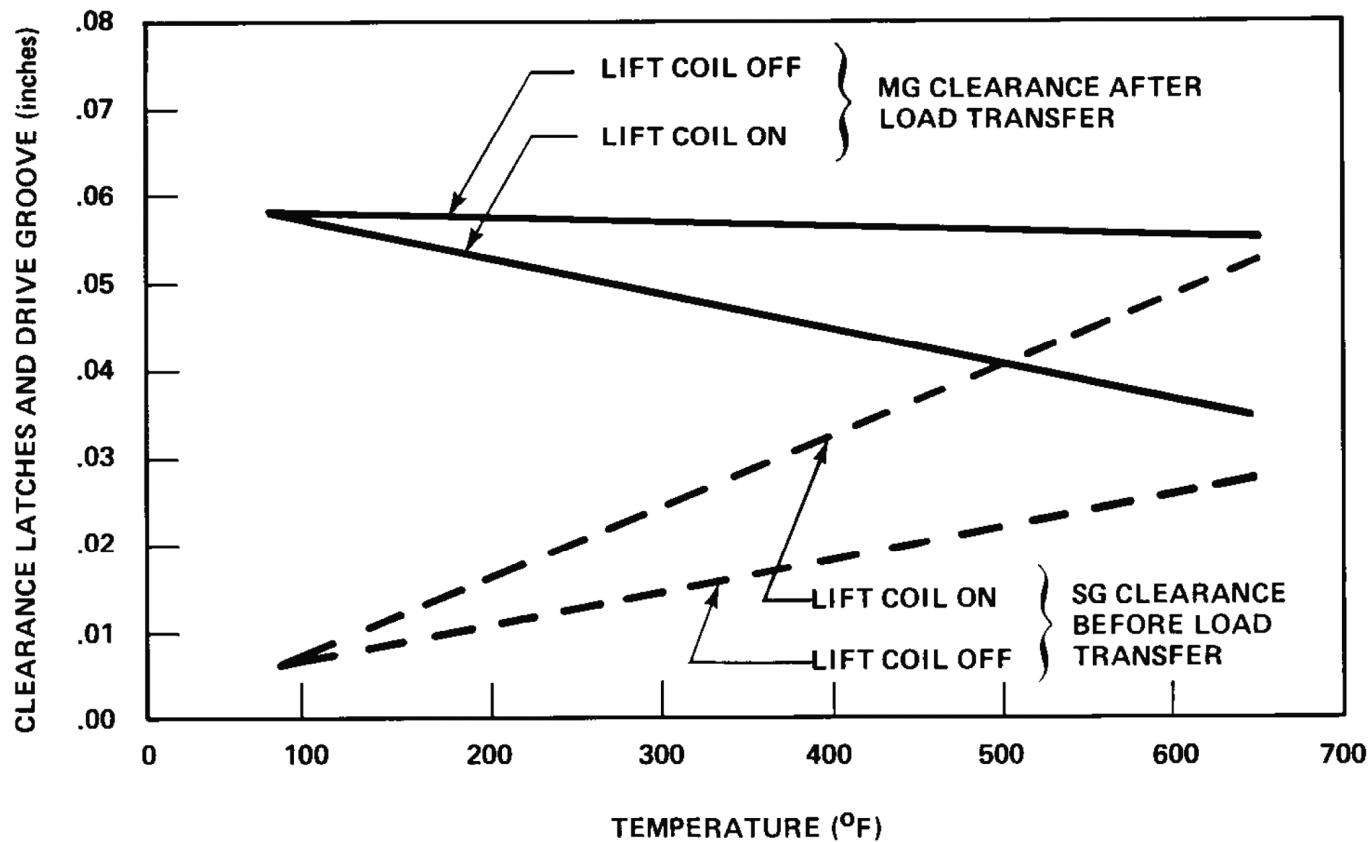
REV 21 5/08



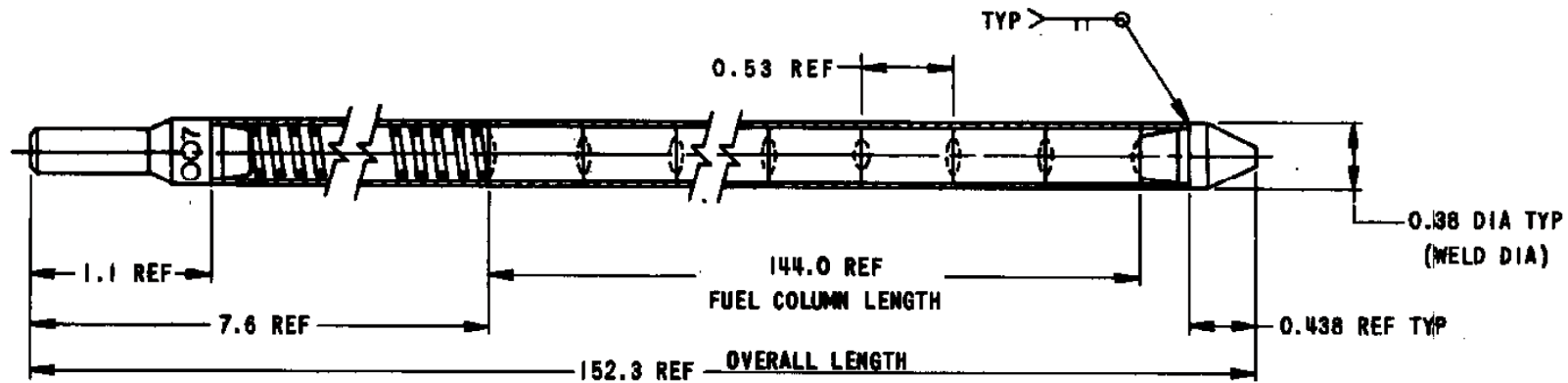
REV 21 5/08



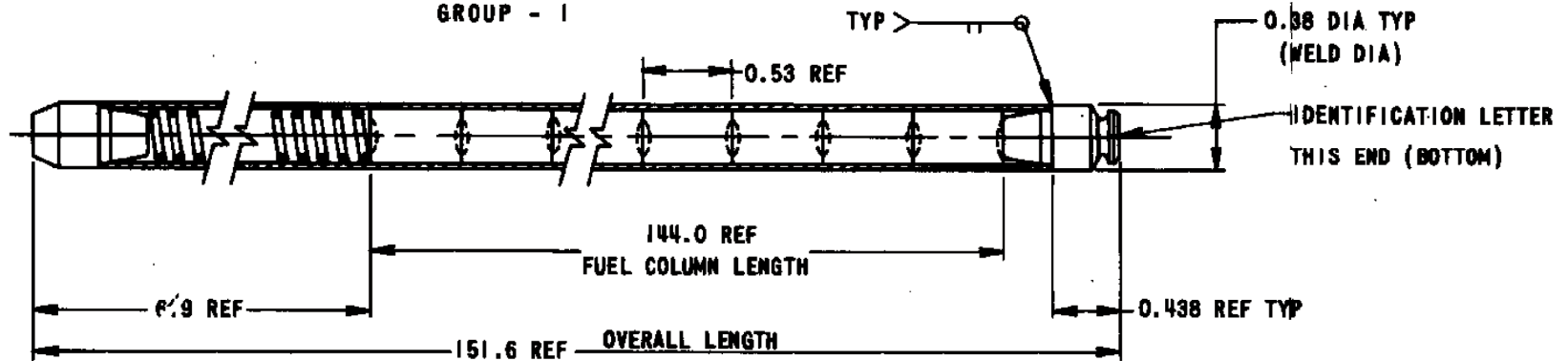
REV 21 5/08



REV 21 5/08

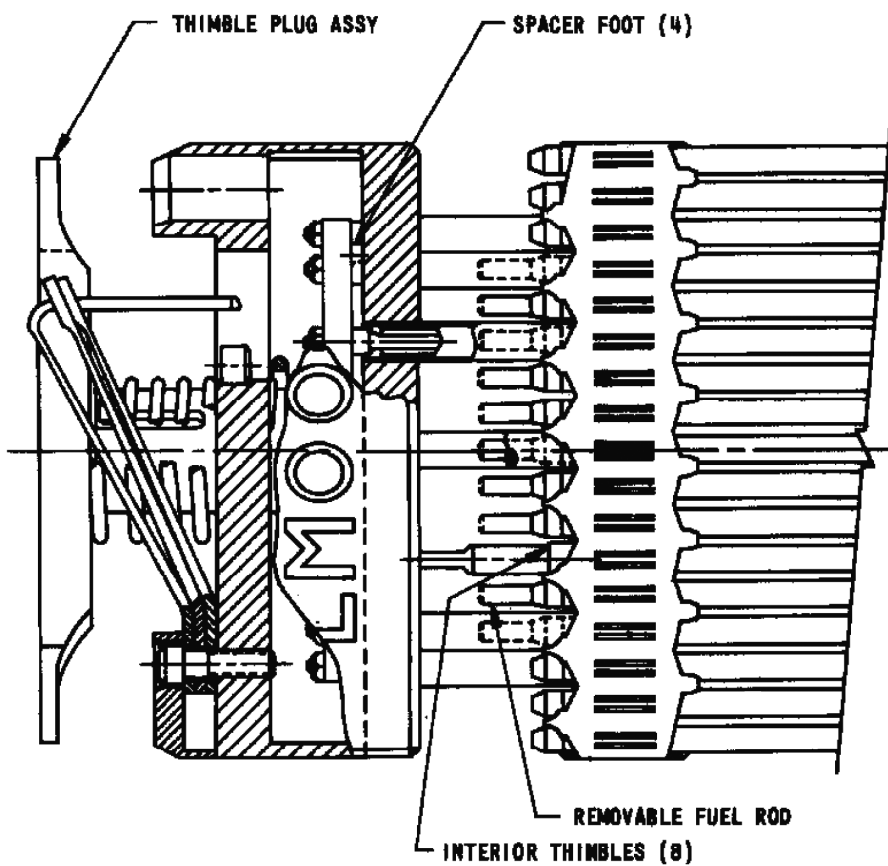
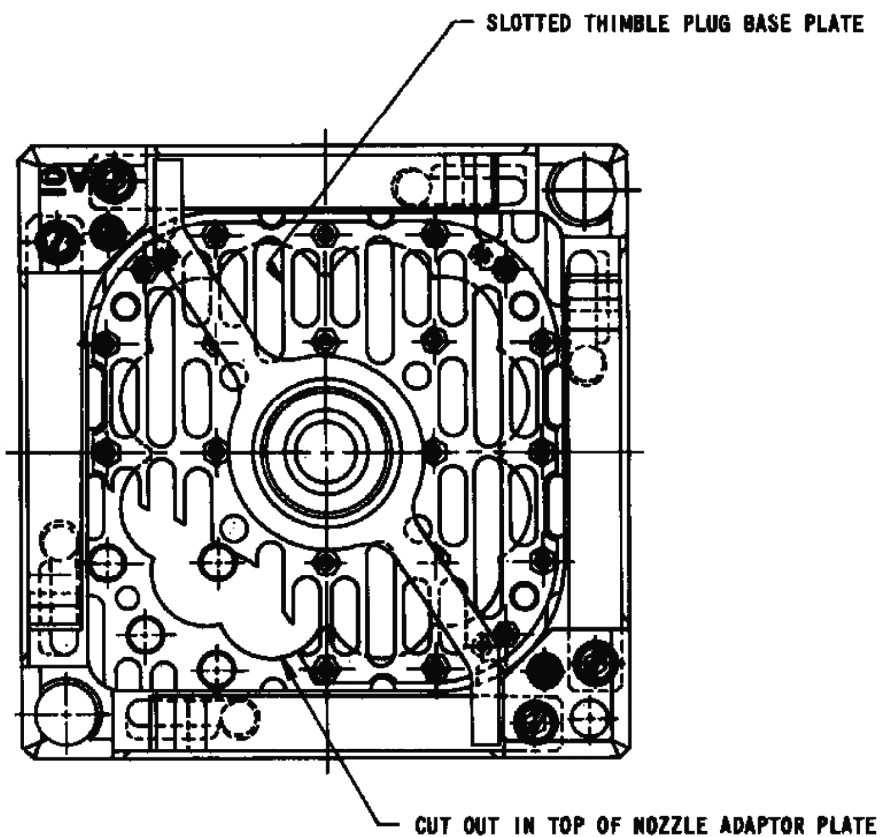


REMOVABLE FUEL ROD
GROUP - 1

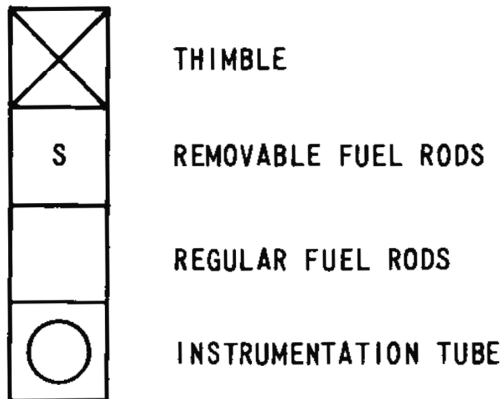
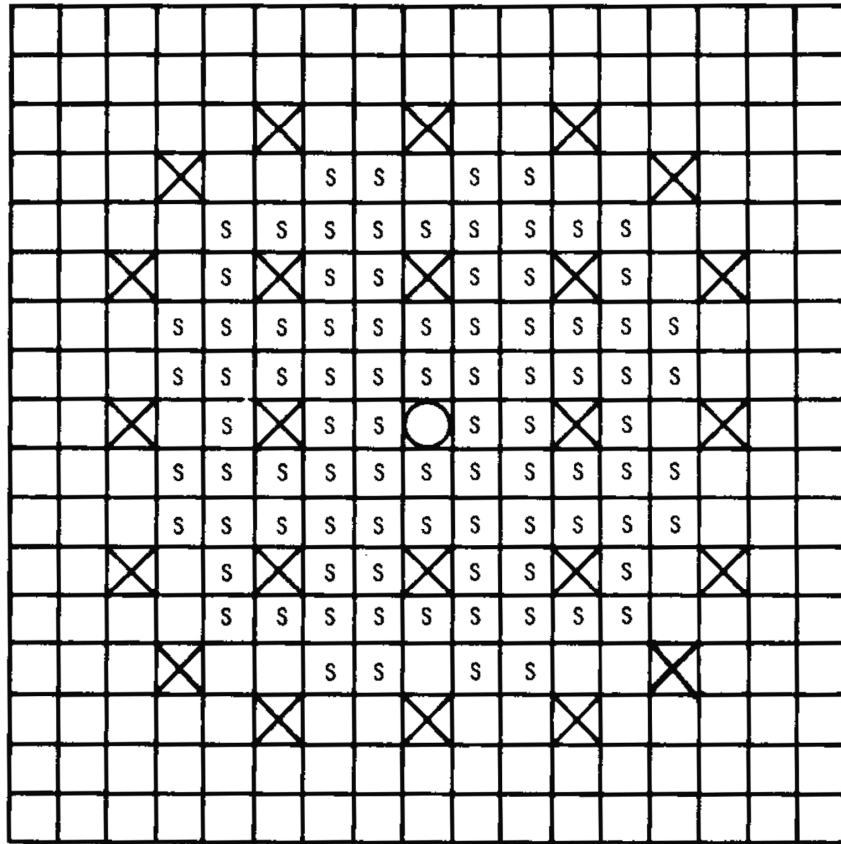


NON-REMOVABLE FUEL ROD
GROUP - 2

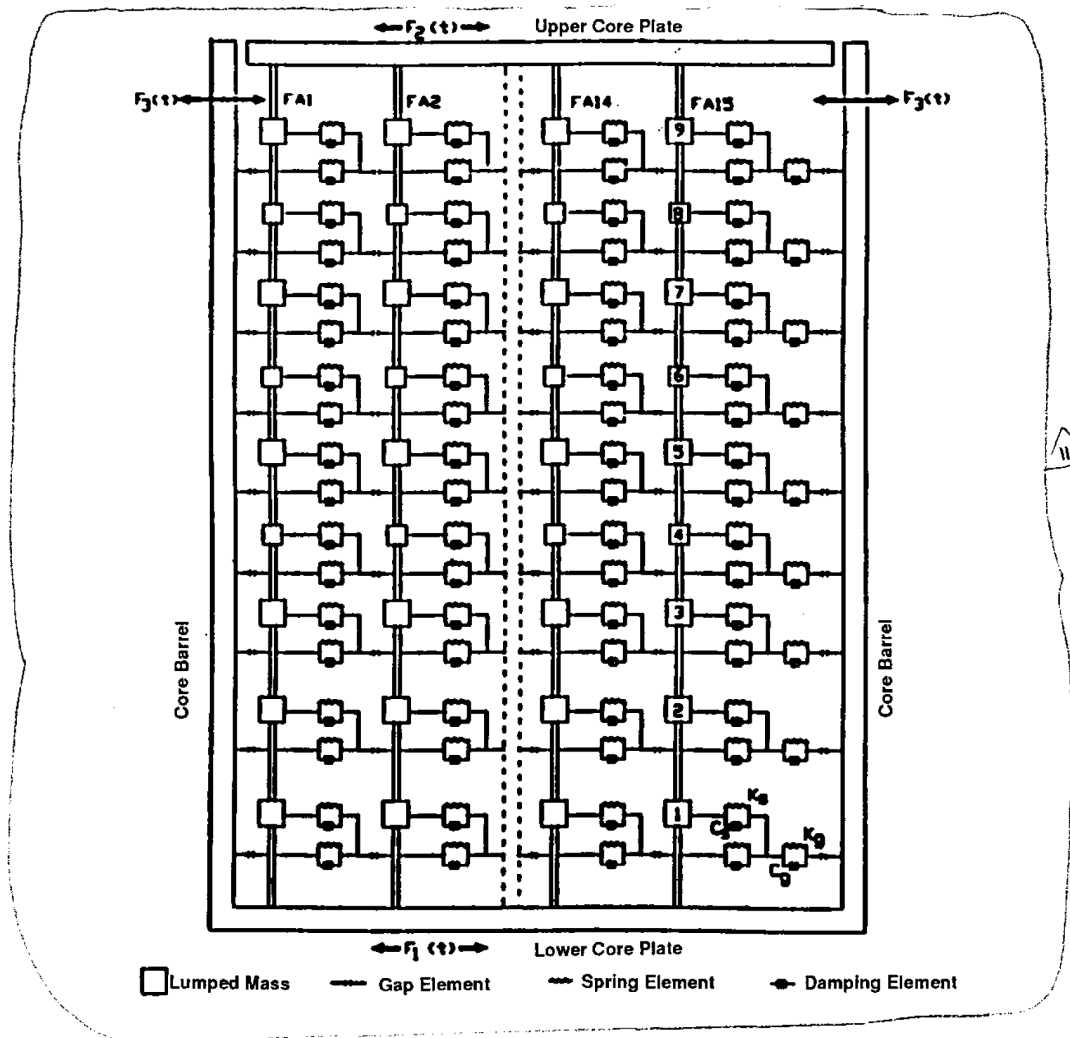
REV 21 5/08



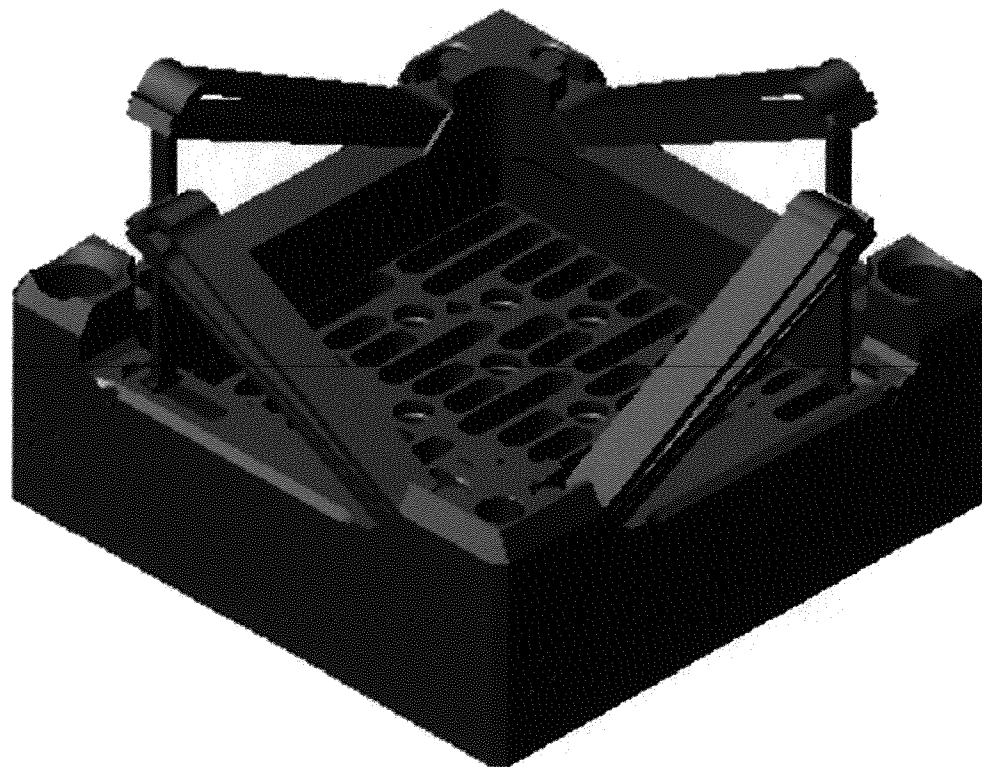
REV 21 5/08



REV 21 5/08



REV 21 5/08



REV 27 4/17



JOSEPH M. FARLEY
NUCLEAR PLANT
UNIT 1 AND UNIT 2

WESTINGHOUSE INTEGRAL NOZZLE (WIN)

FIGURE 4.2-29

4.3 **NUCLEAR DESIGN**

4.3.1 **DESIGN BASES**

This section describes the design bases and functional requirements used in the nuclear design of the fuel and reactivity control system and relates these design bases to the general design criteria (GDC) in 10 CFR 50 Appendix A. Where appropriate, supplemental criteria, such as the final acceptance criteria for emergency core cooling systems, are addressed. Before discussing the nuclear design bases, it is appropriate to briefly review the four major categories ascribed to conditions of plant operation.

The full spectrum of plant conditions is divided into four categories, in accordance with the anticipated frequency of occurrence and risk to the public:

- A. Condition I - Normal Operation
- B. Condition II - Incidents of Moderate Frequency
- C. Condition III - Infrequent Faults
- D. Condition IV - Limiting Faults

In general, the Condition I occurrences are accommodated with margin between any plant parameter and the value of that parameter which would require either automatic or manual protective action. Condition II incidents are accommodated with, at most, a shutdown of the reactor with the plant capable of returning to operation after corrective action.

Fuel damage^a is not expected during Condition I and Condition II events. It is not possible, however, to preclude a very small number of rod failures. These are within the capability of the chemical and volume control system (CVCS) and are consistent with the plant design basis.

Condition III incidents shall not cause more than a small fraction of the fuel elements in the reactor to be damaged, although sufficient fuel element damage might occur to preclude immediate resumption of operation. The release of radioactive material because of Condition III incidents is not sufficient to interrupt or restrict public use of those areas beyond the exclusion radius. Furthermore, a Condition III incident shall not, by itself, generate a Condition IV fault or result in a consequential loss of function of the reactor coolant system or reactor containment barriers.

Condition IV occurrences are faults that are not expected to occur, but are defined as limiting faults which must be designed against. Condition IV faults shall not cause a release of radioactive material that results in exceeding the limits of 10 CFR 100.

^aFuel damage as used here is defined as penetration of the fission product barrier; i.e., the fuel rod clad. The core design power distribution limits related to fuel integrity are met for Condition I occurrences through conservative design and maintained by the action of the control system.

The requirements for Condition II occurrences are met by providing an adequate protection system which monitors reactor parameters. The control and protection systems are described in chapter 7 and the consequences of Condition II, III, and IV occurrences are given in chapter 15.

4.3.1.1 Fuel Burnup

Basis

The fuel rod design basis is described in section 4.2. Fuel performance evaluations have been performed to extended burnup and have not identified any safety issues with operation to the burnup values given in reference 40.

A limitation on initial installed excess reactivity is not required other than as is quantified in terms of other design bases such as core negative reactivity feedback and shutdown margin discussed below.

Discussion

The above, along with the design basis 4.3.1.3, Control of Power Distribution, satisfies GDC 10.

Fuel burnup is a measure of fuel depletion, which represents the integrated energy output of the fuel (MWd/MTU). Fuel burnup is not safety related, but serves as a convenient means for quantifying fuel exposure criteria.

The core design lifetime, or design discharge burnup, is achieved by installing sufficient initial excess reactivity in each fuel region and by following a fuel replacement program (such as that described in subsection 4.3.2) that meets all safety-related criteria in each cycle of operation.

Initial excess reactivity installed in the fuel, although not a design basis, must be sufficient to maintain core criticality at full-power operating conditions throughout cycle life with equilibrium xenon, samarium, and other fission products present. The end of design-cycle life is defined to occur when the chemical shim concentration is essentially zero with control rods present to the degree necessary for operational requirements (e.g., the controlling bank at the "bite" position). In terms of chemical shim boron concentration this represents approximately 10 ppm with no control rod insertion.

4.3.1.2 Negative Reactivity Feedbacks (Reactivity Coefficient)

Basis

The fuel temperature coefficient will be negative and the moderator temperature coefficient of reactivity will be nonpositive at full power, thereby providing negative reactivity feedback characteristics at full power. The design basis meets GDC 11.

Discussion

When compensation for a rapid increase in reactivity is considered, there are two major effects. These are the resonance absorption effects (Doppler) associated with changing fuel temperature and the neutron spectrum and reactor composition change effects resulting from changing moderator density. These basic physics characteristics are often identified by

reactivity coefficients. The use of slightly enriched uranium ensures that the Doppler coefficient of reactivity is negative. This coefficient provides the most rapid reactivity compensation. The reload core is also designed to have an overall moderator temperature coefficient of reactivity which is $\leq +7.0$ pcm/°F for power levels up to 70% with a linear ramp to 0.0 pcm/°F at 100% power. At full power, reactor coolant temperature or void content provides another, slower compensatory effect. The moderator temperature coefficient is maintained at or below the above stated limit through the use of fixed BA rods, and/or integral fuel burnable absorbers (IFBAs) and/or control rods by limiting the reactivity held down by soluble boron.

BA content (quantity and distribution) is not stated as a design basis. However, for some reloads the use of BAs may be necessary for peaking factor limit control and for the accomplishment of a moderator temperature coefficient that is at or below the limit discussed above.

4.3.1.3 Control of Power Distribution

Basis

The nuclear design basis is that, with a 95% confidence level:

- A. The VANTAGE 5 fuel will not operate at > 13.9 kW/ft under normal operating conditions, including an allowance for calorimetric error.
- B. Under abnormal conditions, including the maximum overpower condition, the fuel peak power will not cause melting.
- C. The fuel will not operate with a power distribution that violates the departure from nucleate boiling (DNB) design basis (i.e., the departure from nucleate boiling ratio (DNBR) shall not be less than the design limit DNBR, as discussed in subsection 4.4.1) under Condition I and II events, including the maximum overpower condition.
- D. Fuel management will be such as to produce rod power and burnup consistent with the assumptions in the fuel rod mechanical integrity analysis of section 4.2. The above basis meets GDC-10.

Discussion

Calculation of extreme power shapes which affect fuel design limits is performed with proven methods and verified frequently with measurements on operating reactors. The conditions under which limiting power shapes are assumed to occur are chosen conservatively with regard to any permissible operating state.

Even though there is good agreement between calculated peak power and measurements, a nuclear uncertainty (see paragraph 4.3.2.2.1) is applied to calculated peak local power. Such a margin is provided both for the analysis of normal operating states and for anticipated transients.

4.3.1.4 Maximum Controlled Reactivity Insertion Rate

Basis

The maximum reactivity insertion rate caused by withdrawal of rod cluster control assemblies (RCCAs) at power or by boron dilution is limited. Maximum reactivity change rates of 78.75 pcm/s^b and 110 pcm/s for accidental withdrawal of control banks from a subcritical condition and at power, respectively, are set such that peak heat generation rate and DNBR do not exceed the maximum allowable at overpower conditions. This satisfies GDC 25.

The maximum reactivity worth of control rods and the maximum rates of reactivity insertion employing control rods are limited so as to preclude rupture of the coolant pressure boundary or disruption of the core internals to a degree which would impair core cooling capacity because of a rod withdrawal or ejection accident (see chapter 15).

Following any Condition IV event (rod ejection, steam line break, etc.) the reactor can be brought to the shutdown condition and the core will maintain acceptable heat transfer geometry. This satisfies GDC 28.

Discussion

Reactivity addition associated with an accidental withdrawal of a control bank (or banks) is limited by the maximum rod speed (or travel rate) and by the worth of the bank(s). For this reactor the maximum control rod speed is 45 in./min. The maximum rate of reactivity change considering two control banks moving from a subcritical condition is less than 78.75 pcm/s. During normal operation at power and with control rod overlap, the maximum reactivity change rate is less than 110 pcm/s.

4.3.1.5 Shutdown Margins

Basis

Minimum shutdown margin as specified in the Technical Specifications or Technical Requirements Manual is required in power operation startup, in hot standby, hot shutdown, and cold shutdown modes.

In all analyses involving reactor trip, the single, highest-worth RCCA is postulated to remain untripped in its full-out position (stuck rod criterion). This satisfies GDC 26.

Two independent reactivity control systems are provided, namely control rods and soluble boron in the coolant. The control rod system can compensate for the reactivity effects of the fuel and water temperature changes accompanying power level changes over the range from full load to no load. In addition, the control rod system provides the minimum shutdown margin under Condition I events and is capable of making the core subcritical rapidly enough to prevent

^b 1 pcm = 10^{-5} $\Delta\rho$ (see footnote table 4.3-2).

exceeding acceptable fuel damage limits, assuming that the highest-worth control rod is stuck out upon trip.

The boron system can compensate for all xenon burnout reactivity changes and will maintain the reactor in the cold shutdown. Thus, backup and emergency shutdown provisions are provided by a mechanical and a chemical shim control system which satisfies GDC 26.

When fuel assemblies are in the pressure vessel and the vessel lid is not in place, K_{eff} will be maintained at or below 0.95 with control rods and soluble boron. Further, the fuel will be maintained sufficiently subcritical that removal of all RCCAs will not result in criticality. No criterion is given for the refueling operation. However, a 5% margin, which is consistent with spent fuel storage and transfer and 3% below the new fuel storage, is adequate for the controlled and continuously monitored operations involved. The boron concentration required to meet the refueling shutdown is specified in the Core Operating Limits Report (COLR), which is referenced in the Technical Specifications. Verification that these shutdown criteria are met, including uncertainties, is achieved using standard design methods. The subcriticality of the core is continuously monitored as described in the Technical Specifications.

The Mode 6 boron concentration limit contained in the COLRs will ensure that a $K_{\text{eff}} \leq 0.95$ (5% shutdown margin) is maintained during the movement of fuel assemblies in the reactor vessel. This boron concentration limit takes credit for the worth of all rods (control and shutdown), less the worth of the highest worth rod, to ensure that K_{eff} will be maintained ≤ 0.95 during the movement fuel assemblies in the reactor vessel. This boron concentration limit also ensures subcriticality with all rods out (no credit for control and shutdown rods) during Mode 6.

4.3.1.6 Stability

Basis

The core will be inherently stable to power oscillations of the fundamental mode. This satisfies GDC 12.

Spatial power oscillations within the core, with a constant core power output, can be reliably and readily detected and suppressed, should they occur.

Discussion

Oscillations of the total power output of the core, from whatever cause, are readily detected by the loop temperature sensors and by the nuclear instrumentation. The core is protected by these systems and a reactor trip would occur if power increased unacceptably, preserving the design margins to fuel design limits. The stability of the turbine/steam generator/core systems and the reactor control system is such that total core power oscillations are not normally possible.

The redundancy of the protection circuits ensures an extremely low probability of exceeding design power levels.

The core is designed so that diametral and azimuthal oscillations caused by spatial xenon effects are self-damping and no operator action or control action is required to suppress them.

The stability of diametral oscillations is so great that this excitation is highly improbable. Convergent azimuthal oscillations can be excited by prohibited motion of individual control rods. Such oscillations are readily observable and alarmed, using the ex-core long ion chamber. Indications are also continuously available from incore thermocouples and loop temperature measurements. Moveable incore detectors can be activated to provide more detailed information. In all proposed cores these horizontal plane oscillations are self-damping by virtue of reactivity feedback effects designed into the core.

Axial xenon spatial power oscillations may occur in core life. The control bank and ex-core detectors are provided for control and monitoring of axial power distributions. Assurance that fuel design limits are not exceeded is provided by reactor overpower ΔT and overtemperature ΔT trip functions which use the measured axial power imbalance as an input.

4.3.1.7 Anticipated Transients Without Scram (ATWS)

The effects of anticipated transients with failure to scram were not considered in the original design basis of the plant because analysis indicated that the likelihood of such a hypothetical event was negligibly small. Furthermore, analysis of the consequences of a hypothetical failure to scram following anticipated transients showed that no significant core damage would result, system peak pressures would be limited to acceptable values, and no failure of the reactor coolant system would result.⁽¹⁾ As a result of subsequent analyses the NRC has required that Westinghouse PWRs install ATWS equipment independent of the RPS that will initiate turbine trip and auxiliary feedwater flow. The Farley system is described in section 7.8.

4.3.1.8 Long-Term Shutdown for Large Break Loss of Cooling Accident (LOCA)

Basis

The core will remain subcritical following a large-break LOCA (LBLOCA) without taking credit for the control rods dropping. This design basis is consistent with 10 CFR 50.46.

Discussion

Following a LBLOCA, the core must remain in a state amenable to long-term cooling. To fulfill the requirement, the core will remain subcritical following a LBLOCA. Credit for control rods is not taken. Water from all sources expected to contribute to a sump mixed-mean boron concentration is considered. BAs may be required in some reload designs to assure this design basis is met.

4.3.2 DESCRIPTION

4.3.2.1 Nuclear Design Description

The reactor core consists of a specified number of fuel rods which are held in bundles by spacer grids and top and bottom fittings. The fuel rods are constructed of zircaloy-4, ZIRLO, or Optimized ZIRLO cylindrical tubes containing UO_2 fuel pellets. The bundles, known as fuel assemblies, are arranged in a pattern which approximates a right circular cylinder.

Each fuel assembly contains a 17-x-17 rod array composed of 264 fuel rods, 24 rod cluster control (RCC) thimbles, and an incore instrumentation thimble. Figure 4.2-1 shows a cross-sectional view of a fuel assembly and the related RCC locations. Further details of the fuel assembly are given in subsection 4.2.1.

For initial core loading fuel rods within a given assembly have the same uranium enrichment in both the radial and axial planes.

(VANTAGE 5 fuel assemblies may have natural uranium axial blankets.) Fuel assemblies of three different enrichments are used in the initial core loading to establish a favorable radial power distribution. Figure 4.3-1, sheet 1 shows the fuel loading pattern used in the first core. Two regions consisting of the two lower enrichments are interspersed to form a checkerboard pattern in the central portion of the core. The third region is arranged around the periphery of the core and contains the highest enrichment. The enrichments for the first core are shown in table 4.3-1. The typical reloading pattern is a low leakage loading pattern with new fuel interspersed in the center of the core and depleted fuel on the core periphery as shown in figure 4.3-1, sheet 2. The reload cores normally operate approximately 18 months between refueling and accumulate approximately 20,000 MWD/MTU per cycle.

For reload cores, VANTAGE 5 fuel assemblies may be used. Detailed descriptions of the VANTAGE 5 fuel features are given in section 4.2. IFBAs in the central portion of the fuel stack may be used in reload cores to control excess reactivity. Axial blankets consisting of unenriched, mid-enriched, or fully-enriched solid or annular fuel pellets may be placed at the ends of the enriched pellet stack. The unenriched or mid-enriched axial blanket pellets are used in reload cores to reduce neutron leakage and to improve fuel utilization. The annular blanket pellets are used to increase the void volume for gas accommodation within the fuel rod.

The core average enrichment is determined by the amount of fissionable material required to provide the desired core lifetime and energy requirements. The physics of the burnout process are such that operation of the reactor depletes the amount of fuel available because of the absorption of neutrons by the U-235 atoms and their subsequent fission. The rate of U-235 depletion is directly proportional to the power level at which the reactor is operated. In addition, the fission process results in the formation of fission products, some of which readily absorb neutrons. As shown in figure 4.3-2, the depletion and the buildup of fission products are partially offset by the buildup of plutonium, which occurs because of the nonfission absorption of neutrons in U-238. Therefore, at the beginning of any cycle, a reactivity reserve equal to the depletion of the fissionable fuel and the buildup of fission product poisons over the specified cycle life must be "built" into the reactor. This excess reactivity is controlled by removable

neutron-absorbing material in the form of boron dissolved in the primary coolant and BA rods or boride-coated fuel pellets. The stack length of the coated pellets can vary for different core designs, with the optimum length determined on a design-specific basis.

The concentration of boric acid in the primary coolant is varied to provide control and to compensate for long-term reactivity requirements. The concentration of the soluble neutron absorber is varied to compensate for reactivity changes caused by fuel burnup; fission product poisoning, including xenon and samarium; BA depletion; and the cold-to-operating moderator temperature change. Using its normal makeup path, the CVCS is capable of inserting negative reactivity at a rate of approximately 30 pcm/min when the reactor coolant boron concentration is 1000 ppm and approximately 35 pcm/min when the reactor coolant boron concentration is 100 ppm. If the emergency boration path is used, the CVCS is capable of inserting negative reactivity at a rate of approximately 65 pcm/min when the reactor coolant boron concentration is 1000 ppm and approximately 75 pcm/min when the reactor coolant boron concentration is 100 ppm. The peak burnout rate for xenon is 25 pcm/min. (Paragraph 9.3.4.1.3 discusses the capability of the CVCS to counteract xenon decay.) Rapid transient reactivity requirements and safety shutdown requirements are met with control rods.

As the boron concentration is increased, the moderator temperature coefficient becomes less negative. High boron concentrations will cause the moderator temperature coefficient to be positive at beginning of life (BOL). Therefore, BAs are used to reduce the soluble boron concentration sufficiently to ensure that the moderator temperature coefficient is $\leq +7.0$ pcm/°F for power levels up to 70% with a linear ramp to 0.0 pcm/°F at 100% power. During operation the poison content in these BAs is depleted, thus adding positive reactivity to offset some of the negative reactivity from fuel depletion and fission product buildup. The depletion rate of the BAs is not critical, since chemical shim is always available and flexible enough to cover any possible deviations in the expected BA depletion rate. Figure 4.3-3 is a graph of core depletion for a typical reload with BAs in the form of boride-coated fuel pellets.

In addition to reactivity control, the BAs are strategically located to provide a favorable radial power distribution. Figure 4.3-4 shows typical BA patterns within a fuel assembly that may be used in the Farley core. The BA loading patterns used in the first cycle for each Farley core are shown in figures 4.3-5 and 4.3-6, sheet 1. Typical reload core BA loading patterns for discrete BAs and IFBAs are shown in figure 4.3-6, sheets 2 and 3.

Tables 4.3-1 through 4.3-3 contain a summary of reactor core design parameters, including reactivity coefficients, delayed neutron fraction, and neutron lifetimes. Sufficient information is included to permit an independent calculation of the nuclear performance characteristics of the core.

4.3.2.2 Power Distributions

The accuracy of power distribution calculations has been confirmed through approximately one thousand flux maps during some twenty years of operation under conditions very similar to those expected for the Farley plant. Details of this confirmation are given in reference 2 and in paragraph 4.3.2.2.7.

4.3.2.2.1 Definitions

Power distributions are quantified in terms of hot channel factors. These factors are a measure of the peak pellet power within the reactor core and the total energy produced in a coolant channel and are expressed in terms of quantities related to the nuclear or thermal design, namely:

Power density is the thermal power produced per unit volume of the core (kW/liter).

Linear power density is the thermal power produced per unit length of active fuel (kW/ft). Since fuel assembly geometry is standardized, this is the unit of power density most commonly used. For all practical purposes it differs from kW/liter by a constant factor which includes geometry effects and the fraction of the total thermal power which is generated in the fuel rod.

Average linear power density is the total thermal power produced in the fuel rods divided by the total active fuel length of all rods in the core.

Local heat flux is the heat flux at the surface of the cladding (Btu/ft²/h). For nominal parameters this differs from linear power density by a constant factor.

Rod power or rod integral power is the length-integrated linear power density in one rod (kW).

Average rod power is the total thermal power produced in the fuel rods divided by the number of fuel rods (assuming all rods have equal length).

The hot channel factors used in the discussion of power distributions in this section are defined as follows:

F_Q Heat Flux Hot Channel Factor, is defined as the maximum local heat flux on the surface of a fuel rod divided by the average fuel rod heat flux, allowing for manufacturing tolerances on fuel pellets and rods.

F_Q^N Nuclear Heat Flux Hot Channel Factor is defined as the maximum local fuel rod linear power density divided by the average fuel rod linear power density, assuming nominal fuel pellet and rod parameters.

F_Q^E Engineering Heat Flux Hot Channel Factor, is defined as the allowance on heat flux, required for manufacturing tolerances. The engineering factor allows for local variations in enrichment, pellet density and diameter, surface area of the fuel rod, and eccentricity of the gap between pellet and clad. Combined statistically, the net effect is a factor of 1.03 to be applied to fuel rod surface heat flux.

$F_{\Delta H}^N$ Nuclear Enthalpy Rise Hot Channel Factor, is defined as the ratio of the integral of linear power along the rod with the highest integrated power to the average rod power.

Manufacturing tolerances, hot channel power distribution, and surrounding channel power distributions are treated explicitly in the calculation of DNB ratio described in section 4.4.

FNP-FSAR-4

It is convenient for the purposes of discussion to define subfactors of F_Q ; however, design limits are set in terms of the total peaking factor.

$$\begin{aligned} F_Q &= \text{Total peaking factor (or heat flux hot channel factor)} \\ &= \frac{\text{Maximum kW/ft}}{\text{Average kW/ft}} \end{aligned}$$

$$\begin{aligned} F_Q &= F_Q^N \times F_Q^E \\ &= \max\{F_{xy}^N(Z) \times P(Z)\} F_U^N \times F_Q^E \end{aligned}$$

Where

F_Q^N and F_Q^E are defined above

$$F_U^N = \text{factor for measurement conservatism assumed to be 1.05, when using } \geq 38 \text{ detector thimbles, and is } [1.05 + [2\{3 - (T/12.5)\}]/100], \text{ where } T \text{ equals the number of detector thimbles (reference 58), when using } \geq 25 \text{ and } < 38 \text{ detector thimbles.}$$

$$P(Z) = \text{ratio of the power-per-unit core height in the horizontal plane at height } Z \text{ to the average value of power-per-unit core height.}$$

$$F_{xy}^N(Z) = \text{Ratio of peak power density to average power density in the horizontal plane of height } Z.$$

4.3.2.2.2 Radial Power Distributions

The power shape in horizontal sections of the core at full power is a function of the fuel assembly, the BA loading patterns, the control rod pattern, and the fuel burnup distribution. Thus, at any time in the cycle, any horizontal section of the core can be characterized as unrodded or with group D control rods. These two situations, combined with burnup effects, determine the radial power shapes which can exist in the core at full power. The effect on radial power shapes of power level, xenon, samarium, and moderator density effects are also considered, but these are quite small. The effect of nonuniform flow distribution is negligible. While radial power distributions in various planes of the core are often illustrated, the core radial enthalpy rise distribution, as determined by the integral of power up each channel, is of greater interest. Figures 4.3-7 through 4.3-11 show initial cycle and typical reload radial enthalpy rise distributions for one-eighth of the core (for initial cycle) and one-fourth of the core (for reload cycle) for representative operating conditions of the Farley plant. These conditions are (1) hot full power (HFP) at BOL - unrodded - no xenon; (2) HFP at BOL - unrodded - equilibrium xenon; (3) HFP at BOL - Bank D in - equilibrium xenon; (4) HFP at MOL - unrodded - equilibrium xenon, and (5) HFP at EOL - unrodded - equilibrium xenon.

Since the position of the hot channel varies from time to time, a single-reference, radial-design power distribution is selected for DNB calculations. This reference power distribution is chosen conservatively to concentrate power in one area of the core, minimizing the benefits of flow redistribution. Assembly powers are normalized to core average power.

4.3.2.2.3 Assembly Power Distributions

For the purpose of illustration, assembly power distributions from the BOL and EOL conditions corresponding to figures 4.3-8 and 4.3-11, respectively, are given for the same assembly in figures 4.3-12 and 4.3-13, respectively.

Since the detailed power distribution surrounding the hot channel varies from time to time, a conservatively flat (radial) assembly power distribution is assumed in the DNB analysis as described in section 4.4 with the rod of maximum integrated power artificially raised to the design value of $F_{\Delta H}^N$. Care is taken in the nuclear design of all fuel cycles and all operating conditions to ensure that a flatter assembly power distribution does not occur with limiting values of $F_{\Delta H}^N$.

4.3.2.2.4 Axial Power Distributions

The shape of the power profile in the axial or vertical direction is largely under the control of the operator through either manual operation of the control rods or automatic motion of full-length rods responding to manual operation of the CVCS. Nuclear effects which cause variations in the axial power shape include moderator density, Doppler effect on resonance absorption, spatial xenon, axial distribution of fuel enrichment and BA, and burnup.

Automatically controlled variations in total power output and full-length rod motion are also important in determining the axial power shape at any time. Signals are available to the operator from the ex-core ion chambers, which are long ion chambers outside the reactor vessel running parallel to the axis of the core. Separate signals are taken from the top and bottom halves of the chambers. The difference between top and bottom signals from each of four pairs of detectors is displayed on the control panel and called the Flux Difference, ΔI . Calculations of core average peaking factor for many plants and measurements from operating plants under many operating situations are associated with either ΔI or axial offset in such a way that an upper bound can be placed on the peaking factor. For these correlations axial offset is defined as:

$$\text{Axial offset} = \frac{\Phi_t - \Phi_b}{\Phi_t + \Phi_b}$$

and Φ_t and Φ_b are the top and bottom detector readings.

Representative axial power shapes from reference 3 for BOL, MOL, and EOL conditions are shown in figures 4.3-14 through 4.3-16. These figures cover a wide range of axial offset, including values not permitted at full power.

All of the power shapes in these figures, however, are allowed at some reduced power level. As noted in reference 3, these shapes could occur when a plant is following load. It is the intent of these figures to show axial power shapes which can result in large axial offsets.

4.3.2.2.5 Local Power Peaking

Fuel densification, which has been observed to occur under irradiation in several operating reactors, causes fuel pellets to shrink both axially and radially. The pellet shrinkage, combined with random hangup of fuel pellets, can result in gaps in the fuel column when the pellets below the hungup pellet settle in the fuel rod. Axial gaps greater than 0.5 in. can lead to cladding collapse which can then result in significant flux and power spiking. Therefore, a power spike factor allowance has been historically included in the determination of the total peaking factor, as a quantitative measure of the local power peaking which results from pellet densification.

Past creep collapse methods have assumed that pellet hangup occurs and an axial gap exists in all fuel rods within a reactor core. The size of the gap is estimated from conservative early-in-life fuel densification as determined from out-of-reactor sintering tests described in Regulatory Guide 1.126. The size of the axial gap also determines the magnitude of the power spike factor applied to Westinghouse fuel designs. In WCAP-13589-A⁽⁴⁵⁾, it has been demonstrated that no large axial gaps, i.e. > 0.3 in., form in current Westinghouse fuel designs. In this submittal, it was also shown that axial gaps less than 0.5 in. do not result in cladding collapse, and that these types of gaps are associated with relatively small power spikes of 1% or less. As a result, application of a power spike factor to account for fuel densification effects is no longer necessary for Westinghouse fuel designs.

4.3.2.2.6 Limiting Power Distributions

According to the American National Standards Institute (ANSI) Classification of Plant Conditions (see chapter 15), Condition I occurrences are those which are expected frequently or regularly in the course of power operation, maintenance, or maneuvering of the plant. As such, Condition I occurrences are accommodated with margin between any plant parameter and the value of that parameter that would require either automatic or manual protective action. Inasmuch as Condition I occurrences occur frequently or regularly, they must be considered from the point of view of affecting the consequences of fault conditions (Conditions II, III and IV). In this regard, analysis of each fault condition described is generally based on a conservative set of initial conditions corresponding to the most adverse set of conditions that can occur during Condition I operation. The list of steady-state and shutdown conditions, permissible deviations (such as one coolant loop out of service) and operational transients is given in chapter 15. Implicit in the definition of normal operation are proper and timely action by the reactor operator. That is, the operator follows recommended operating procedures for maintaining appropriate power distributions and takes any necessary remedial actions when alerted to do so by the plant instrumentation.

Thus, as stated above, the worst, or limiting, power distribution that can occur during normal operation is to be considered as the starting point for analysis of Conditions II, III and IV events.

Improper procedural actions or errors by the operator are assumed in the design as occurrences of moderate frequency (Condition II). Some of the consequences which might result are listed in chapter 15. Therefore, the limiting power shapes which result from such Condition II events are those power shapes that deviate from the normal operating condition at the recommended axial offset band, e.g., because of lack of proper action by the operator during a xenon transient following a change in power level brought about by control rod motion. Power shapes which fall into this category are used for determination of the reactor protection system setpoints so as to maintain margin to overpower or DNB limits.

The means for maintaining power distributions within the required hot channel factor limits are described in the COLR and the Technical Specifications. A complete discussion of power distribution control in Westinghouse PWRs is included in reference 4. Detailed information on the design constraints on local power density in a Westinghouse PWR, on the defined operating procedures, and on the measures taken to preclude exceeding design limits, is presented in the Westinghouse Topical Report on power distribution control and load following procedures.⁽²⁹⁾ The following paragraphs summarize these reports and describe the calculations used to establish the upper bound on peaking factors.

The calculations used to establish the upper bound on peaking factors, F_Q^N and $F_{\Delta H}^N$, include all of the nuclear effects which influence the radial and/or axial power distributions throughout core life for various modes of operation, including load follow, reduced power operation, and axial xenon transients.

Radial power distributions are calculated for the full-power condition. Fuel and moderator temperature feedback effects are included for the average enthalpy plane of the reactor. The steady-state design calculations are done for normal flow with the same mass flow in each channel. No credit is taken for flow redistribution effects. The nuclear effect of flow redistribution is calculated explicitly where it is important in the DNB analysis of accidents. The effect of xenon on radial power distribution is small (compare figures 4.3-7 and 4.3-8), but is included as part of the normal design process. Radial power distributions are relatively fixed and easily bounded with upper limits.

The core average axial profile, however, can experience significant changes which can occur rapidly as a result of rod motion and load changes and more slowly because of xenon distribution. For the study of points of closest approach to axial power distribution limits, several thousand cases are examined. Since the properties of the nuclear design dictate what axial shapes can occur, boundaries on the limits of interest can be set in terms of the parameters which are readily observed on the plant. Specifically, the nuclear design parameters which are significant to power distribution analysis are:

- A. Core power level.
- B. Core height.
- C. Coolant temperature and flow.
- D. Coolant temperature program as a function of reactor power.
- E. Fuel cycle lifetimes.
- F. Rod bank worths.

G. Rod bank overlaps.

Normal operation of the plant assumes compliance with the following conditions:

- A. Control rods in a single bank move together with no individual rod insertion differing by more than 12 steps (indicated) from the bank demand position.
- B. Control banks are sequenced with overlapping banks.
- C. The control full-length insertion limits are not violated.
- D. Axial power distribution procedures, which are given in terms of flux difference control and control bank position, are observed.

The axial power distribution procedures referred to above are part of the required operating procedures which are followed in normal operation. Limits placed on the axial flux difference are designed to assure that the heat flux hot channel factor F_Q is maintained within acceptable limits. The constant axial offset control (CAOC) operating procedures described in reference 29 require control of the axial flux difference at all power levels within a permissible operating band about a target value corresponding to the equilibrium full power value. The relaxed axial offset control (RAOC) procedures to be implemented in Unit 1 cycle 15 and Unit 2 cycle 12 and beyond, described in reference 44 were developed to provide wider control band widths and, consequently, more operating flexibility. These wider operating limits, particularly at lower power levels, can increase plant availability by allowing quicker plant startups and increased maneuvering flexibility without trip or reportable occurrences.

Further operating flexibility is achieved by combining RAOC operation with an F_Q surveillance technical specification. $F_{xy}(z)$ surveillance requires periodic plant surveillance on the height-dependent radial peaking factor, $F_{xy}(z)$, for partial verification that operation will not cause the $F_Q(z)$ limit to be exceeded. In the F_Q surveillance Technical Specification to be implemented in Unit 1 cycle 15 and Unit 2 cycle 12, $F_{xy}(z)$ surveillance will be replaced by $F_Q(z)$ surveillance. Monitoring $F_Q(z)$ and increasing the measured value for expected plant maneuvers provides a more convenient form of assuring plant operation below the $F_Q(z)$ limit while retaining the intent of using a measured parameter to verify Technical Specification compliance.

In standard CAOC analysis described in reference 29, the generation of the normal operation power distribution is constrained by the rod insertion limits (RIL) and the ΔI band limits. The purpose of RAOC is to find the widest permissible ΔI -power operating space by analyzing a wide range of ΔI . Therefore, the generation of normal operation power distributions is constrained only by the RIL for RAOC.

For a CAOC analysis, load-follow simulations are performed covering the allowed CAOC operating space to generate a typical range of allowed axial xenon distributions, which in turn are used to calculate axial power distributions in both normal operation and Condition II accident conditions. For a RAOC analysis, however, a reconstruction model described in reference 44 is used as a more practical method to create axial xenon distributions covering the wider ΔI -Power operating space allowed with RAOC operation. Each resulting power shape is analyzed to determine if LOCA constraints are met or exceeded. The total peaking factor, F_Q^T is determined using standard synthesis methods as described in reference 29.

The $F_Q(Z)$'s are synthesized from axial calculations combined with radial factors appropriate for rodded and unrodded planes, or are calculated directly using three-dimensional methods. In these calculations, the effects on the unrodded radial peak of xenon redistribution that occurs following the withdrawal of a control bank (or banks) from a rodded region are obtained. A factor to be applied on the unrodded radial peak is obtained from calculations in which xenon distribution is preconditioned by the presence of control rods and then allowed to redistribute for several hours. A detailed discussion of this effect may be found in reference 29. The calculated values have been increased by a factor of 1.05, when using ≥ 38 detector thimbles, and by $[1.05 + \{2\{3 - (T/12.5)\}/100\}]$, where T equals the number of detector thimbles (reference 58), when using ≥ 25 and < 38 detector thimbles for conservatism and a factor of 1.03 for the engineering factor F_Q^E .

The envelope drawn over the calculated maximum ($F_Q(Z) \times \text{power}$) points in figure 4.3-21 represents an upper-bound envelope on local power density versus elevation in the core. It should be emphasized that this envelope is a conservative representation of the bounding values of local power density.

Finally, as previously discussed, this upper-bound envelope is based on procedures on load follow which require the operator to operate within the allowed axial flux difference limits. Operation within this upper-bound envelope is ensured by limits contained in the Technical Specifications which rely only upon ex-core surveillance and is supplemented by the normal monthly full-core map requirement and by a computer-based alarm for deviation outside the allowed flux difference limits.

Allowing for fuel densification effects, the average kW/ft at 2821 MWt is 5.54. From figure 4.3-21, the conservative upper-bound values of normalized local power density, including densification effects, is 2.50 (VANTAGE 5 fuel), corresponding to peak local power density of 13.9 kW/ft (VANTAGE 5).

To determine reactor protection system setpoints with respect to power distributions, three categories of events are considered: rod control equipment malfunctions; operator errors of commission; and operator errors of omission. In evaluating these three categories of events, the core is assumed to be operating within the four constraints described above.

The first category comprises uncontrolled rod withdrawal (with rods moving in the normal bank sequence) for full-length banks. Also included are motions of the full-length banks below their insertion limits, which could be caused, for example, by uncontrolled dilution or primary coolant cooldown. Power distributions were calculated throughout these occurrences assuming short-term corrective action; that is, no transient xenon effects were considered to result from the malfunction. The event was assumed to occur from typical normal operating situations which did include normal xenon transients. It was further assumed in determining the power distributions that total power level would be limited by reactor trip to below 120%. Since the study is to determine protection limits with respect to power and axial offset, no credit was taken for trip setpoint reduction because of flux difference. Representative results are given on figure 4.3-22 in units of kW/ft. The peak power density that can occur in such events, assuming reactor trip at or below 120%, is less than that required for centerline melt.

FNP-FSAR-4

The second category, also appearing in figure 4.3-22, assumes that the operator mispositions the full-length rod bank in violation of the insertion limits and creates short-term conditions not included in normal operating conditions.

The third category assumes that the operator fails to take action to correct a flux difference violation. Representative results shown on figure 4.3-23. The figure shows that, provided the assumed error in operation does not continue for a period that is long compared to the xenon time constant, the maximum local power does not exceed fuel centerline melt limit, including the above factors.

Since the peak kW/ft is below the fuel centerline melt limit, no flux difference penalties are required for overpower protection.

It should be noted that a reactor overpower accident is not assumed to occur coincident with an independent operator error. Additional detailed discussion of these analyses is presented in reference 29.

The appropriate hot channel factors, F_Q and $F_{\Delta H}^N$ for peak local power density and for DNB analysis at full power, based on analyses of possible operating power shapes for the reactor described herein, are addressed in the COLR and the Technical Specifications.

The maximum allowable F_Q can be increased with decreasing power as shown in the Core Operating Limits Report and the Technical Specifications. Increasing $F_{\Delta H}^N$ with decreasing power is permitted by the DNB protection setpoints and allows radial power shape changes with rod insertion to the insertion limits as described in paragraph 4.4.3.2. The allowance for increased $F_{\Delta H}^N$ permitted is

$$F_{\Delta H}^N = 1.70 (1 + 0.3 (1-P)) \text{ VANTAGE 5 fuel.}$$

This becomes a design basis criterion which is used for establishing acceptable control rod patterns and control bank sequencing. Likewise, fuel loading patterns for each cycle are selected with consideration of this design criterion. The worst values of $F_{\Delta H}^N$ for possible rod configurations occurring in normal operation are used in verifying that this criterion is met. Typical radial factors and radial power distributions are shown in figures 4.3-7 through 4.3-11. The worst values generally occur when the rods are assumed to be at their insertion limits. Maintenance of constant axial offset control establishes rod positions which are above the allowed rod insertion limits, thus providing increasing margin to the $F_{\Delta H}^N$ criterion. It has been determined that, provided the above conditions are observed, the Technical Specification limits are met.

When a situation is possible in normal operation that could result in local power densities in excess of those assumed as the precondition for a subsequent hypothetical accident, but which would not itself cause fuel failure, administrative controls and alarms are provided for returning the core to a safe condition. These alarms are described in detail in chapter 7.

The independence of the various individual uncertainties constituting the uncertainty factor on F_Q enables the uncertainty (F_Q^U) to be calculated by statistically combining the individual uncertainties on the limiting rod. The standard deviation of the resultant distribution of F_Q^U is determined by taking the square root of the sum of the variances of each of the contributing distributions.⁽²⁾ The measurement uncertainty factor is 1.05 and is applicable when using ≥ 38 detector thimbles. Reference 58 evaluated using ≥ 25 and < 38 detector thimbles, and the measurement uncertainty factor is $[1.05 = [2\{3 - \{T/12.5\}\}]/100]$, where T equals the number of detector thimbles. The value for FEQ is 1.03. The value for the rod bow factor, F_Q^B , is 1.013, which accounts for the initial as-built rod bow.

4.3.2.2.7 Experimental Verification of Power Distribution Analysis

This subject is discussed in depth in reference 2. A summary of this report is given here. It should be noted that power distribution-related measurements are incorporated into the evaluation of calculated power distribution information, using an incore instrumentation processing code described in reference 30 or reference 48. The measured-versus-calculational comparison is normally performed periodically throughout the cycle lifetime of the reactor, as required by Technical Specifications.

In a measurement of peak local power density, F_Q , with the moveable detector system described in subsections 7.7.1 and 4.4.5, the following uncertainties have to be considered:

- A. Reproducibility of the measured signal.
- B. Errors in the calculated relationship between detector current and local flux.
- C. Errors in the calculated relationship between detector flux and peak rod power some distance from the measurement thimble.

The appropriate allowance for category A above has been quantified by repetitive measurements made with several intercalibrated detectors by using the common thimble features of the incore detector system. This system allows more than one detector to access any thimble. Errors in category B above are quantified to the extent possible by using the detector current measured at one thimble location to predict fluxes at another location, which is also measured. Local power distribution predictions are verified in critical experiments on arrays of rods with simulated guide thimbles, control rods, BAs, etc. These critical experiments provide quantification of errors in categories B and C above.

Reference 2 describes critical experiments performed at the Westinghouse Reactor Evaluation Center and measurements taken on two Westinghouse plants with incore systems of the same type as used in the Farley Nuclear Plant. The report concludes that the uncertainty associated with the peak nuclear heat flux factor, F_Q , is 4.58% at the 95% confidence level with only 5% of the measurements greater than the inferred value. This is the equivalent of a 1.645σ limit on a normal distribution and is the uncertainty to be associated with a full-core flux map with moveable detectors reduced with a reasonable set of input data incorporating the influence of burnup on the radial power distribution. The uncertainty is usually rounded up to 5%. In comparing measured power distributions (or detector currents) against the calculations for the

same situation, it is not possible to isolate the detector reproducibility. Thus, a comparison between measured and predicted power distributions has to include some measurement error. Such a comparison is given in figure 4.3-24 for one of the maps used in reference 2. Since the first publication of the report, hundreds of maps have been taken on these and other reactors. The results confirm the adequacy of the 5% uncertainty allowance on the calculated F_Q when using ≥ 38 detector thimbles. When using ≥ 25 and < 38 detector thimbles, the uncertainty allowance is increased by $[2\{3 - \{T/12.5\}\}]$, where T equals the number of detector thimbles (reference 58).

A similar analysis for the uncertainty in $F_{\Delta H}$ (rod integral power) measurements results in an allowance of 3.60% at the equivalent of a 1.645 σ confidence level. For historical reasons, an uncertainty factor is allowed in the nuclear design calculational basis; that is, the predicted rod integrals at full power must not exceed the design $F_{\Delta H}$ less 8%.

A measurement in the second cycle of a 121-assembly, 12-ft core is compared with a simplified one-dimensional core average axial calculated in figure 4.3-25. This calculation does not give explicit representation to the fuel grids.

The accumulated data on power distributions in actual operation are basically of three types:

- A. Much of the data is obtained in steady-state operation at constant power in the normal operating configuration.
- B. Data with unusual values of axial offset are obtained as part of the ex-core detector calibration exercise which is performed monthly.
- C. Special tests have been performed in load follow and other transient xenon conditions which have yielded useful information on power distributions.

These data are presented in detail in reference 5. Figure 4.3-26 contains a summary of measured values of F_Q as a function of axial offset for five plants from that report.

4.3.2.2.8 Testing

A very extensive series of physics tests was performed on the first core of the Farley Nuclear Plant. These tests and the criteria for satisfactory results are described in detail in chapter 14. Since not all limiting situations can be created at beginning of life, the main purpose of the tests is to provide a check on the calculational methods used in the predictions for the conditions of the test. Tests performed at the beginning of each reload cycle are limited to verification of the selected safety-related parameters of the reload design.

4.3.2.2.9 Monitoring Instrumentation

The adequacy of instrument numbers, spatial deployment, required correlations between readings and peaking factors, calibration and errors are described in references 2, 4, and 5. The relevant conclusions are summarized here in paragraph 4.3.2.2.7 and subsection 4.4.5.

Provided the limitations given in paragraph 4.3.2.2.6 on rod insertion and flux difference are observed, the ex-core detector system provides adequate monitoring of power distributions. Further details of specific limits on the observed rod positions and flux difference are given in the COLR and in the Technical Specifications, together with a discussion of their bases.

Limits for alarms, reactor trip, etc., are given in the Technical Specifications. Descriptions of the systems provided are given in section 7.7.

4.3.2.3 Reactivity Coefficients

The kinetic characteristics of the reactor core determine the response of the core to changing plant conditions or to operator adjustments made during normal operation, as well as the core response during abnormal or accidental transients. These kinetic characteristics are quantified in reactivity coefficients. The reactivity coefficients reflect the changes in the neutron multiplication because of varying plant conditions, such as power, moderator or fuel temperatures or, less significantly, because of a change in pressure or void conditions. Since reactivity coefficients change during the life of the core, ranges of coefficients are employed in transient analysis to determine the response of the plant throughout life. The results of such simulations and the reactivity coefficients used are presented in chapter 15. The reactivity coefficients are calculated on a core-wide basis by radial and axial diffusion theory methods. The effect of radial and axial power distribution on core average reactivity coefficients is implicit in those calculations and is not significant under normal operating conditions. For example, a skewed xenon distribution which results in changing axial offset by 5% changes the moderator and Doppler temperature coefficients by less than 0.01 pcm/°F and 0.03 pcm/°F, respectively. An artificially skewed xenon distribution which results in changing the radial $F_{\Delta H}^N$ by 3% changes the moderator and Doppler temperature coefficients by < 0.03 pcm/°F and 0.001 pcm/°F, respectively. The spatial effects are accentuated in some transient conditions (for example, in postulated rupture of the main steam line break and rupture of an RCCA mechanism housing described in subsections 15.1.5 and 15.4.8) and are included in these analyses. The analytical methods and calculational models used in calculating the reactivity coefficients are given in subsection 4.3.3. These models have been confirmed through extensive testing of more than thirty cores similar to those in the plant described herein. Results of these tests are discussed in subsection 4.3.3. Quantitative information for calculated reactivity coefficients, including fuel-Doppler coefficient, moderator coefficients (density, temperature, pressure, void) and power coefficient is given in the following sections.

4.3.2.3.1 Fuel Temperature (Doppler) Coefficient

The fuel temperature (Doppler) coefficient is defined as the change in reactivity per degree change in effective fuel temperature and is a measure of the Doppler broadening of U-238 and Pu-240 resonance absorption peaks. Doppler broadening of other isotopes such as U-236, Np-237, etc., is also considered, but their contributions to the Doppler effect are small. An increase in fuel temperature increases the effective resonance absorption cross-sections of the fuel and produces a corresponding reduction in reactivity.

The fuel temperature coefficient is calculated by performing two-group two- or three-dimensional calculations. Moderator temperature is held constant and the power level is varied on a core-wide basis. Spatial variation of fuel temperature is taken into account by calculating the effective fuel temperature as a function of power density as discussed in paragraph 4.3.3.1.

A typical Doppler temperature coefficient for a typical initial core is shown in figure 4.3-27 as a function of the effective fuel temperature (at BOL and EOL conditions). The effective fuel temperature is lower than the volume averaged fuel temperature since the neutron flux distribution is nonuniform through the pellet and gives preferential weight to the surface temperature.

A typical Doppler-only contribution to the power coefficient, defined later, is shown in figure 4.3-28 for a typical initial core as a function of relative core power. The integral of the differential curve on figure 4.3-28 is the Doppler contribution to the power defect and is shown in figure 4.3-29 as a function of relative power. The Doppler coefficient becomes more negative as a function of life as the Pu-240 content increases, thus increasing the Pu-240 resonance absorption; however, the overall value becomes less negative since the fuel temperature changes with burnup, as described in paragraph 4.3.3.1. The upper and lower limits of Doppler coefficient used in accident analyses are given in chapter 15.

4.3.2.3.2 Moderator Coefficient

The moderator coefficient is a measure of the change in reactivity because of a change in specific coolant parameters such as density, temperature, pressure, or void. The coefficients so obtained are moderator density, temperature, pressure, and void coefficients.

4.3.2.3.2.1 Moderator Density and Temperature Coefficients.

The moderator temperature (density) coefficient is defined as the change in reactivity per degree change in the moderator temperature. Generally, the effect of the change in moderator density as well as the temperature are considered together. Generally, a decrease in moderator density means less moderation which results in a negative moderator temperature coefficient. An increase in coolant temperature, keeping the density constant, leads to a hardened neutron spectrum and results in an increase in resonance absorption in U-238, Pu-240, and other isotopes. The hardened spectrum also causes a decrease in the fission-to-capture ratio in U-235 and Pu-239. Both of these effects make the moderator coefficient more negative. Since water density changes more rapidly with temperature as temperature increases, the moderator temperature (density) coefficient becomes more negative with increasing temperature.

The soluble boron used in the reactor as a means of reactivity control also has an effect on moderator density coefficient, since the soluble boron density as well as the water density is decreased when the coolant temperature rises. This decrease in the soluble boron density introduces a positive component in the moderator coefficient.

Thus, if the concentration of soluble boron is large enough, the net value of the coefficient may be positive. With the BAs present, however, the initial hot boron concentration is sufficiently low

that the moderator temperature coefficient is $\leq +7.0$ pcm/°F for power levels up to 70% power with a linear ramp to 0.0 pcm/°F at 100% power. The effect of control rods is to make the moderator coefficient more negative by reducing the required soluble boron concentration and by increasing the "leakage" of the core. With burnup, the moderator coefficient becomes more negative primarily as a result of boric acid dilution, but also to a significant extent from the effects of the buildup of plutonium and fission products.

The moderator coefficient is calculated for the various plant conditions discussed above by performing two-group two- or three-dimensional calculations, varying the moderator temperature (and density) by about $\pm 5^\circ\text{F}$ about each of the mean temperatures. The moderator coefficient for an initial cycle is shown as a function of core temperature and burnup boron concentration for the unrodded and rodded core in figures 4.3-30 through 4.3-32. The temperature range covered is from cold (68°F) to about 600°F . The contribution caused by Doppler coefficient (because of change in moderator temperature) has been subtracted from these results. Figure 4.3-33 shows the hot, full-power moderator temperature coefficient plotted as a function of first-cycle lifetime for the just-critical boron concentration condition based on the design boron letdown condition.

The moderator coefficients presented here are calculated on a core-wide basis, since they are used to describe the core behavior in normal and accident situations considered to affect the entire core.

4.3.2.3.2.2 Moderator Pressure Coefficient.

The moderator pressure coefficient relates the change in moderator density, resulting from a reactor coolant pressure change, to the corresponding effect on neutron production. This coefficient is of much less significance in comparison with the moderator temperature coefficient. A change of 50 psi in pressure has approximately the same effect on reactivity as a half-degree change in moderator temperature. This coefficient can be determined from the moderator temperature coefficient by relating change in pressure to the corresponding change in density. The moderator pressure coefficient is negative over a portion of the moderator temperature range at beginning of life (-0.004 pcm/psi, BOL), but is always positive at operating conditions and becomes more positive during life ($+0.3$ pcm/psi, EOL).

4.3.2.3.2.3 Moderator Void Coefficient.

The moderator void coefficient relates the change in neutron multiplication to the presence of voids in the moderator. In a PWR, this coefficient is not very significant because of the low void content in the coolant. The core void content is less than one-half of 1% and is caused by local or statistical boiling. The void coefficient varies from 50 pcm/percent void at BOL to -250 pcm/percent void at EOL and at operating temperatures. The void coefficient at operating temperature becomes more negative with fuel burnup.

4.3.2.3.3 Power Coefficient

The combined effect of moderator temperature and fuel temperature change as the core power level changes is called the total power coefficient and is expressed in terms of reactivity change per percent power change. The power coefficient at BOL and EOL for an initial cycle is given in figure 4.3-34. It becomes more negative with burnup, reflecting the combined effect of moderator and fuel temperature coefficients with burnup. The power defect (integral reactivity effect) at BOL and EOL for an initial cycle is given in figure 4.3-35.

4.3.2.3.4 Comparison of Calculated and Experimental Reactivity Coefficients

Subsection 4.3.3 describes the comparison of calculated and experimental reactivity coefficients in detail. Based on the data presented there, the accuracy of the current analytical model is as follows:

$\pm 0.2\% \Delta\rho$ for Doppler and power defect

± 2 pcm/°F for the moderator coefficient

Experimental evaluation of the calculated coefficients is done during the physics startup tests described in chapter 14.

4.3.2.3.5 Reactivity Coefficients Used in Transient Analysis

Table 4.3-2 gives the limiting values as well as the best-estimate values for the initial cycle reactivity coefficients. Limiting values are used as design limits in the transient analysis. The exact values of the coefficient used in the analysis depend on whether the transient of interest occurs at the beginning of life or end of life, whether the most negative or the most positive (least negative) coefficients are appropriate, and whether spatial nonuniformity must be considered in the analysis. Conservative values of coefficients, considering various aspects of analysis, are used in the transient analysis. This is completely described in chapter 15.

Limiting values of reactivity coefficients are chosen to encompass the best-estimate reactivity coefficients, including the uncertainties given in paragraph 4.3.3.3, over appropriate operating conditions. The most positive values, as well as the most negative, are selected to form the design basis range used in the transient analysis. A direct comparison of best estimate and design limit values can be misleading, since in many instances the most conservative combination of reactivity coefficients is used in the transient analysis even though the extreme coefficients assumed may not simultaneously occur at the conditions assumed in the analysis. The need for a reevaluation of any accident in a subsequent cycle is contingent upon whether or not the coefficients for that cycle fall within the identified range used in the analysis presented in chapter 15, with due allowance for the calculational uncertainties given in paragraph 4.3.3.3. Control rod requirements are given in table 4.3-3 for the initial cycle and for a hypothetical equilibrium cycle, since these are markedly different.

4.3.2.4 Control Requirements

To ensure the shutdown margin stated in the Technical Specifications or Technical Requirements Manual (TRM), as applicable, under conditions where a cooldown to ambient temperature is required, concentrated soluble boron is added to the coolant. Boron concentrations for several core conditions are listed in table 4.3-2 for the initial cycle. For all core conditions, including refueling, the boron concentration is well below the solubility limit. The RCCAs are employed to bring the reactor to the hot shutdown condition. The minimum required shutdown margin is given in the COLR, as referenced by the Technical Specifications and the TRM.

The ability to accomplish the shutdown for hot conditions is demonstrated in table 4.3-3 by comparing the difference between the RCCA reactivity, which is available with an allowance for the worst-struck rod, with that required for control and protection purposes. The shutdown margin includes an allowance of 10% for analytic uncertainties (see paragraph 4.3.2.4.9). The largest reactivity control requirement appears at the end of life when the moderator temperature coefficient reaches its peak negative value as reflected in the larger power defect.

The control rods are required to provide sufficient reactivity to account for the power defect from full power to zero power and to provide the required shutdown margin. The reactivity addition resulting from power reduction consists of contributions from Doppler effect, moderator temperature, flux redistribution, and reduction in void content, as discussed below.

4.3.2.4.1 Doppler Effect

The Doppler effect arises from the broadening of U-238 and Pu-240 resonance peaks with an increase in effective pellet temperature. This effect is most noticeable over the range of zero power to full power because of the large pellet temperature increase with power generation.

4.3.2.4.2 Variable Average Moderator Temperature

When the core is shutdown to the hot zero power condition, the average moderator temperature changes from the equilibrium full-load value determined by the steam generator and turbine characteristics (steam pressure, heat transfer, tube fouling, etc.) to the equilibrium no-load value, which is based on the steam generator shell-side design pressure. The design change in temperature is conservatively increased by 6°F to account for the control dead band and measurement errors.

When the moderator temperature coefficient is negative there is a reactivity addition with power reduction. The moderator temperature coefficient becomes more negative as the fuel depletes because the boron concentration is reduced. This effect is the major contributor to the increased requirement at end of life.

4.3.2.4.3 Redistribution

During full-power operation the coolant density decreases with core height and this, together with partial insertion of control rods, results in less fuel depletion near the top of the core. Under steady-state conditions, the relative power distribution will be slightly asymmetric towards the bottom of the core. On the other hand, at hot zero power conditions, the coolant density is uniform up the core, and there is no flattening because of the Doppler effect. The result will be a flux distribution which at zero power can be skewed toward the top of the core. The reactivity insertion, because of the skewed distribution, is calculated with an allowance for the effects of xenon distribution.

4.3.2.4.4 Void Content

A small void content in the core is caused by nucleate boiling at full power. The void collapse coincident with power reduction makes a small positive reactivity contribution.

4.3.2.4.5 Rod Insertion Allowance

At full power, the control bank is operated within a prescribed band of travel to compensate for small periodic changes in boron concentration, changes in temperature, and very small changes in the xenon concentration not compensated for by a change in boron concentration. When the control bank reaches either limit of this band, a change in boron concentration is required to compensate for additional reactivity changes. Since the insertion limit is set by a rod travel limit, a conservatively high calculation of the inserted worth is made which exceeds the normally inserted reactivity.

4.3.2.4.6 Installed Excess Reactivity For Depletion

Excess reactivity is installed at the beginning of each cycle to provide sufficient reactivity to compensate for fuel depletion and fission product buildup throughout the cycle. This reactivity is controlled by the addition of soluble boron to the coolant and by BA. The soluble boron concentration for several core configurations, the unit-boron worth, and BA worth are given in tables 4.3-1 and 4.3-2 for the initial cycle. Since the excess reactivity for burnup is controlled by soluble boron and/or BAs, it is not included in control rod requirements.

4.3.2.4.7 Xenon and Samarium Poisoning

Changes in xenon and samarium concentrations in the core occur at a sufficiently slow rate, even following rapid power level changes, that the resulting reactivity change can be controlled by changing the soluble boron concentration (also, see paragraph 4.3.2.5.5).

4.3.2.4.8 pH Effects

Changes in reactivity because of a change in coolant pH, if any, are sufficiently small in magnitude and occur slowly enough to be controlled by the boron system. Further details are available in reference 6.

4.3.2.4.9 Experimental Confirmation

Following a normal shutdown, the total core reactivity change during cooldown with a stuck rod has been measured on a 121-assembly, 10-ft high core and a 121-assembly, 12-ft high core. In each case, the core was allowed to cool down until it reached criticality simulating the steam line break accident. For the 10-ft core, the predicted result showed the core to be about 0.3% $\Delta\rho$ more reactive than measured. This represents an error of about 5% in the total reactivity change and is about half the uncertainty allowance for this quantity. For the 12-ft core, the difference between the measured and predicted reactivity change was an even smaller 0.2% $\Delta\rho$. These measurements and others demonstrate the ability of the methods described in subsection 4.3.3 to accurately predict the total shutdown reactivity of the core.

4.3.2.5 Control

Core reactivity is controlled by means of a chemical shim dissolved in the coolant, RCCAs, and BAs as described above.

4.3.2.5.1 Chemical Shim

Boron in solution as boric acid is used to control relatively slow reactivity changes associated with:

- A. The moderator temperature defect in going from cold shutdown at ambient temperature to the hot operating temperature at zero power.
- B. The transient xenon and samarium poisoning, such as that following power changes or changes in rod cluster control position.
- C. The reactivity effects of fissile inventory depletion and buildup of long-life fission products.
- D. The BA depletion.

The boron concentrations for various core conditions are presented in table 4.3-2 for the initial cycle.

4.3.2.5.2 Rod Cluster Control Assemblies

The number of full-length assemblies is shown in table 4.3-1. The full-length RCCAs are used for shutdown and control purposes to offset fast reactivity changes associated with:

- A. The required shutdown margin in the hot zero power, stuck-rods condition.
- B. The reactivity compensation as a result of an increase in power above hot zero power (power defect including Doppler effect and moderator reactivity changes).
- C. Unprogrammed fluctuations in boron concentration, coolant temperature, or xenon concentration (with rods not exceeding the allowable rod insertion limits).
- D. Reactivity ramp rates resulting from load changes.

The allowed control bank reactivity insertion is limited at full power to maintain shutdown capability. As the power level is reduced, control rod reactivity requirements are also reduced and more rod insertion is allowed. The control bank position is monitored and the operator is notified by an alarm if the limit is approached. Determination of the insertion limits uses conservative xenon distributions and axial power shapes. In addition, the RCCA withdrawal pattern determined from these analyses is used in determining power distribution factors and in determining the maximum worth of an inserted RCCA ejection accident. For further discussion, refer to the Technical Specifications on rod insertion limits.

Power distribution, rod ejection, and rod misalignment analyses are based on the arrangement of the shutdown and control groups of the RCCAs shown in figure 4.3-36. All shutdown RCCAs are assumed to be withdrawn before withdrawal of the control banks is initiated. The limits of rod positions and further discussion on the basis for rod-insertion limits are provided in the Technical Specifications, Technical Specification Bases, and COLR.

4.3.2.5.3 Burnable Absorbers

Either the standard, wet annular BA rods and/or integral fuel BAs may be used to provide partial control of the excess reactivity available during any fuel cycle. In doing so, these BAs control peaking factors and prevent the moderator temperature coefficient from exceeding the Technical Specification limits. They perform this function by reducing the requirement for soluble boron in the moderator at the beginning of the fuel cycle as described previously. The BA rod pattern in the core for cycle 1, together with the number of rods per assembly, is shown in figure 4.3-5 for Unit 1 and 4.3-6, sheet 1 for Unit 2. Figure 4.3-4 shows typical within-assembly configurations for discrete BAs and integral fuel BAs. Figure 4.3-6, sheets 2 and 3, show typical reload core BA loading patterns for discrete BAs and integral fuel BAs, respectively. The boron in the BAs is depleted with burnup, but at a sufficiently slow rate so that the resulting critical concentration of soluble boron is such that the peaking factor limits are not exceeded and the moderator temperature coefficient remains within the limits at all times for power operating conditions.

In addition, BAs may be required in some reload designs to assure that the core will remain subcritical without taking credit for the control rods dropping following a large break LOCA.

4.3.2.5.4 Peak Xenon Startup

Compensation for the peak xenon buildup is accomplished using the boron control system. Startup from the peak xenon condition is accomplished with a combination of rod motion and boron dilution. The boron dilution may be made at any time, including during the shutdown period, provided the shutdown margin is maintained.

4.3.2.5.5 Load Follow Control and Xenon Control

During load follow maneuvers power changes are accomplished using control rod motion and dilution or boration by the boron system as required. Control rod motion is limited by the control rod insertion limits provided in the Technical Specifications and the COLR and discussed in paragraph 4.3.2.5.2. The power distribution is maintained within acceptable limits through the location of the bank D control rods. Reactivity changes caused by the changing xenon concentration can be controlled by rod motion and/or changes in the soluble boron concentration.

4.3.2.5.6 Burnup

Control of the excess reactivity for burnup is accomplished using soluble boron and/or BA. The boron concentration must be limited during operating conditions to ensure that the moderator temperature coefficient does not exceed the COLR and the Technical Specification limits. Sufficient BAs are installed at the beginning of a cycle to give the desired cycle lifetime without exceeding the boron concentration limit. The practical minimum boron concentration is in the range of 0 to 10 ppm.

4.3.2.6 Control Rod Patterns And Reactivity Worth

The full-length RCCAs are designated by function as the control groups and the shutdown groups. The terms "group" and "bank" are used synonymously throughout this report to describe a particular grouping of control assemblies.

The rod cluster assembly pattern is displayed in figure 4.3-36, which is not expected to change during the life of the plant. The control banks are labeled A, B, C, and D and the shutdown banks are labeled SA, SB, etc. Each bank, although operated and controlled as a unit, is comprised of two subgroups. The axial position of the full-length RCCAs may be controlled manually or automatically. These RCCAs are all dropped into the core following actuation of reactor trip signals.

Two criteria have been employed for selection of the control groups. First, the total reactivity worth must be adequate to meet the requirements specified in table 4.3-3. Second, in view of the fact that these rods may be partially inserted at power operation, the total power-peaking factor should be low enough to ensure that the power capability requirements are met. Analyses indicate that the first requirement can be met either by a single group or by two or

more banks whose total worth equals at least the required amount. The axial power shape would be more peaked following movement of a single group of rods worth 3 to 4% $\Delta\rho$; therefore, four banks (described as A, B, C, and D in figure 4.3-36) each worth approximately 1% $\Delta\rho$ have been selected.

The position of control banks for criticality under any reactor condition is determined by the concentration of boron in the coolant. On an approach to criticality, boron is adjusted to ensure that criticality will be achieved with control rods above the insertion limit set by shutdown and other considerations. (See the COLR and the Technical Specifications.) Early in the cycle there may also be a withdrawal limit necessary to maintain a moderator temperature coefficient that is $\leq +7.0$ pcm/ $^{\circ}\text{F}$ for power levels up to 70% with a linear ramp to 0.0 pcm/ $^{\circ}\text{F}$ at 100% power. Usual practice is to adjust boron to ensure that the rod position lies within the so-called maneuvering band, that is, such that an escalation from zero power to full power does not require further adjustment of boron concentration.

Ejected rod worths are given in subsection 15.4.6 for several different conditions. Experimental confirmation of these worths can be found by reference to startup test reports such as reference 7.

Allowable deviations because of misaligned control rods are discussed in the plant Technical Specifications.

A representative differential rod worth calculation for two banks of control rods withdrawn simultaneously (rod withdrawal accident) is given in figure 4.3-37.

Calculation of the control rod reactivity worth versus time-after-trip involves knowledge of the circuit delays, rod velocity, and differential reactivity worth. The rod position versus time-of-travel assumed is given in figure 4.3-38. For nuclear design purposes, the reactivity worth versus rod position is calculated by a series of steady-state calculations at various control rod positions, assuming all rods out at the time of trip since this is conservative with respect to the initial rate of reactivity insertion. Also, to be conservative, the rod of highest worth is assumed stuck out of the core and the flux distribution (and, thus, reactivity importance) is assumed to be skewed towards the bottom of the core. Figure 4.3-39 shows the results of these calculations.

The shutdown groups provide additional negative reactivity to assure an adequate shutdown margin. Shutdown margin is defined as the amount by which the core would be subcritical at hot shutdown if all RCCAs are tripped, but assumes that the highest-worth assembly remains fully withdrawn and no changes in xenon or boron concentration occur. With any RCCA not capable of being fully inserted, the reactivity worth of the RCCA must be accounted for in the determination of SDM; and in Modes 1 and 2, the fuel and moderator temperatures are changed to the hot zero power temperatures. The loss of control rod worth because of the depletion burnup of the absorber material is negligible, since only bank D rods may be in the core under normal operating conditions (near full power).

The values given in table 4.3-3 show that the available reactivity in withdrawn RCCAs provides the design-basis minimum-shutdown margin allowing for the highest-worth cluster to be at its fully withdrawn position. An allowance for uncertainty in the calculated worth of N-1 rods is made before determination of the shutdown margin.

4.3.2.7 Criticality of the Reactor During Refueling

Criticality of fuel assemblies outside of the reactor is precluded by adequate design of fuel transfer and fuel storage facilities and by administrative control procedures. This section identifies those criteria important to criticality safety analyses.

All enrichments discussed in this section are nominal enrichments. Nominal enrichments, when increased by the manufacturing uncertainty of 0.05 wt%, yield maximum enrichments.

4.3.2.7.1 New Fuel Storage

New fuel is stored in 21-in. center-to-center spaced racks in the new fuel storage facilities in a dry condition. This spacing is sufficient to maintain a subcritical array for the dry condition and for a postulated flooding event with unborated water. For the flooded condition with unborated water, assuming new fuel with the highest anticipated enrichment in place, the effective multiplication factor does not exceed 0.95. For the normally dry condition, the effective multiplication factor does not exceed 0.98 with fuel of the highest anticipated enrichment in place and assuming optimum moderation conditions (for example, because of the presence of aqueous foam or mist).

Westinghouse 17-x-17 OFA and VANTAGE 5 fuel assemblies with nominal enrichments up to 4.80 wt% can be safely stored in the new fuel rack utilizing all locations. Storage of fuel assemblies with nominal enrichments above 4.80 wt% and up to 5.00 wt% is also acceptable by taking credit for the same IFBAs required for storage in the spent-fuel rack (see Technical Specification Figure 4.3-1 and Technical Specification Table 4.3-5). Westinghouse 17-x-17 LOPAR fuel assemblies with nominal enrichments of up to 4.25 wt% can be safely stored in the new fuel rack utilizing all locations. No IFBA is required for LOPAR fuel.

Verification that the 21-in. center-to-center spaced new fuel storage racks meet the design criteria for normally dry storage, assuming possible sources of optimum moderation, or for the flooded condition, with fresh nonborated water has been determined by the Monte-Carlo transport model KENO-IV/AMPX.^(31, 32) The assumptions utilized in the analysis were as follows:

- A. The fuel assembly is modeled at its most reactive point in life, and no credit is taken for any natural enrichment axial blankets.
- B. All fuel rods contain uranium dioxide at a maximum enrichment of 4.85 wt% over the entire length of each rod. This maximum enrichment corresponds to a nominal enrichment of 4.80 wt%. Nominal enrichments above 4.80 wt% are also allowed by taking credit for IFBAs (see discussion below).
- C. The fuel pellets are modeled at 96% of theoretical density without dishing or chamfering to bound the maximum fuel assembly loading.
- D. No credit is taken for any U234 or U236 in the fuel, nor is any credit taken for the buildup of fission product poison material.
- E. No credit is taken for any spacer grids or spacer sleeves.

- F. All racks were modeled in the stainless-steel corner configuration rather than the stainless-steel canister configuration. This is more conservative because the neutron absorption effects of the stainless-steel corner design would be less than the stainless-steel canister.
- G. For the fully flooded condition, a value of 1.0 g/cc was used for the density of water. The rack was modeled as an infinite in lateral (x and y) and axial (vertical) extent which precludes any neutron leakage from the array. This is conservative since the number of fuel assemblies modeled is infinite and the absorption effects of surrounding structure and walls are ignored.
- H. For the low-water density (optimum moderation) condition, various water densities were examined in the range of 0.06 g/cc to 0.12 g/cc to show that the optimum moderation reactivity peak satisfied the criticality criteria. The rack was modeled as an infinitely long double row of fuel assemblies with a nominal pitch of 21 in. Concrete walls and floor were modeled. Under low-water density conditions, the presence of concrete is conservative because neutrons are reflected back into the fuel array more efficiently than they would be with just low density water. The area above the fresh fuel rack is filled water at the optimum moderation density.

With the above assumptions, the analysis confirmed that the criticality acceptance criteria were satisfied for OFA and VANTAGE-5 fuel assemblies with nominal enrichments up to 4.80 wt%. Based on comparison of the non-IFBA nominal enrichment limits of the new fuel rack (4.80 wt%) and spent-fuel rack (3.90 wt%), it was concluded that application of the spent-fuel rack IFBA requirements limit (Technical Specification Figure 4.3-1 and Technical Specification Table 4.3-5) to the new fuel rack was conservative. Therefore, storage of OFA and VANTAGE-5 fuel assemblies in the new fuel rack with nominal enrichments above 4.80 wt% and up to 5.00 wt% is acceptable, provided the IFBA requirements of the spent-fuel rack IFBA-credit limit are satisfied.

Under normal conditions, the new fuel racks are maintained in a dry environment. The introduction of water into the new fuel rack area is the worst case accident scenario. The full density and low density optimum moderation cases are bounding accident situations which result in the most conservative fuel rack K_{eff} .

Other accidents can be postulated which would cause some reactivity increase (i.e., dropping a fuel assembly between the rack and wall or on top of the rack). For these other accident conditions, the double contingency principle is applied. This states that one is not required to assume two unlikely, independent, concurrent events to ensure protection against a criticality accident. Thus, for these other accident conditions, the absence of a moderator in the new fuel storage racks can be assumed as a realistic initial condition since assuming its presence would be a second unlikely event.

The results of all analyses verify that the NRC acceptance criteria continue to be met. That is, there is a 95% probability at a 95% confidence level (including uncertainties) that K_{eff} of the new fuel storage racks will be ≤ 0.95 when fully loaded and dry or flooded with unborated water and ≤ 0.98 for optimum moderation conditions or postulated accidents, as recommended in ANSI N18.3-1973.

4.3.2.7.2 Wet Spent-Fuel Storage

The following information describes the design criteria and analysis techniques for storage of spent fuel in the Unit 1 and Unit 2 spent-fuel racks and for cask loading operations. The Unit 1 and Unit 2 spent-fuel racks were analyzed in accordance with the methodology contained in WCAP-18414⁽⁴⁶⁾, which credits the soluble boron contained in the spent-fuel pool water. Cask loading operations were analyzed in accordance with the methodology contained in Westinghouse Calculation Note CN-CRIT-207⁽⁴⁹⁾, which also credits soluble boron in the spent-fuel pool water.

4.3.2.7.2.1 Storage of Spent-Fuel Assemblies in the Spent-Fuel Storage Racks. The spent-fuel storage pool contains high-density poison racks, designed by PaR Systems, which have a center-to-center spacing of 10.75 in. They are designed to store Westinghouse 17-x-17 fuel assemblies with a maximum nominal enrichment of 5.0 wt% U-235, in the following configurations:

Westinghouse 17-x-17 fuel assemblies are stored according to their fuel type (STD/RFA or OFA), decay time since last operation, nominal enrichment and burnup. Westinghouse 17-x-17 fuel assemblies with nominal enrichments less than or equal to 5 wt% ²³⁵U can be stored in Array A as Fuel Category 1 as shown in Technical Specification Figure 4.3-1. In the Array A checkerboard storage arrangement, 2 fuel assemblies can be stored face adjacent to an empty storage location.

Westinghouse 17-x-17 fuel assemblies can be stored in a burned/fresh checkerboard arrangement (Array B, Fuel Categories 4 and 2) of a 2-x-2 matrix of storage cells as shown in Figure 4.3-1 of the Technical Specifications. In the Array B checkerboard arrangement, assemblies must satisfy the minimum burnup and enrichment requirements of Fuel Category 2 and Fuel Category 4 assemblies as shown in Figure 4.3-1 and Tables 4.3-1, 4.3-3, and 4.3-4 of the Technical Specifications. Fresh Fuel Category 2 assemblies must also meet the Integral Fuel Burnable Absorber requirements of Table 4.3-5 of the Technical Specifications.

Westinghouse 17-x-17 fuel assemblies can be stored in a uniform "all-cell" arrangement (Array C) of a 2-x-2 matrix of storage cells as shown in Figure 4.3-1 of the Technical Specifications. In the Array C all cell arrangement, assemblies must satisfy the minimum burnup and enrichment requirements of Fuel Category 4 assemblies as shown in Figure 4.3-1 and Tables 4.3-1, 4.3-3, and 4.3-4 of the Technical Specifications.

Eleven damaged Westinghouse 17-x-17 fuel assemblies (F02, F05, F06, F15, F17, F18, F19, F20, F30, F31, and F32) can be stored (in the Unit 1 spent-fuel pool) in a 12-storage cell configuration surrounded by empty cells as shown in Technical Specification Figure 4.3-2. (The eleven fuel assemblies contain a nominal enrichment of 3.0 w/o U-235.)

The design basis for wet spent-fuel storage criticality analyses is that there is a 95% confidence level that the effective multiplication factor of the fuel storage array (K_{eff}), including uncertainties and biases, will be < 0.95 in accordance with ANSI Standard N57.2-1983. The criticality analyses include a calculational bias, mechanical uncertainties, consideration of 0.05 wt%

enrichment variability temperature bias, burnup measurement uncertainty, depletion uncertainty, consideration of grid growth during irradiation, fission product and actinide worth bias, eccentric positioning bias, and operational uncertainty.

For the spent-fuel storage criticality analysis⁽⁴⁶⁾, the fuel is assumed to be a mixture of fresh and spent fuel, with the potential for IFBA credit for fresh fuel. The spent fuel pool moderator is pure water at 20°C with a temperature bias incorporated within the spent-fuel pool limits which yields the maximum reactivity. Credit for soluble boron and burnup credit for spent fuel is discussed below. Spent fuel storage racks are assumed to be infinite in lateral extent (x and y) and reflective in the vertical extent (z direction). Reactivity impact is explicitly calculated for the stainless-steel structural material of the spent-fuel racks, and some of the structural materials of the fuel assemblies. Reactivity credit is not taken for spacer grids or spacer sleeves, the neutron absorption by the control poison material (Boraflex), or natural enrichment axial blankets (if any).

The criticality calculation method and cross-section values are verified by comparison with critical experiment data for fuel assemblies similar to those for which the racks are designed. These benchmarking data are sufficiently diverse to establish that the method bias and uncertainty will apply to rack conditions which include strong neutron absorbers and large water gaps.

The design method which ensures the criticality safety of fuel assemblies in the spent-fuel storage rack uses the Scale Version 6.2.3 package⁽³³⁾ system of codes for cross-section generation and KENO V.a⁽³³⁾ for reactivity determination.

The SCALE CSAS5 control sequence with the parm=centrm option is utilized in the analysis, indicating that CSAS5 implements the modern material and cross section processing module XSProc⁽³³⁾ to process material input using the BONAMI, CENTRM and PMC routines in SCALE for generation of problem dependent self-shielded cross-sections from the base 238 group ENDB/B-VII cross-sections. The problem dependent multigroup cross-sections are then used as input to KENO V.a⁽³³⁾. KENO V.a provides reliable and efficient means of performing k_{eff} calculations for systems that are routinely encountered in engineering practice, especially in the calculation of k_{eff} of 3-D system models.

An extensive set of critical experiments has been analyzed using the SCALE CSAS5 control sequence to demonstrate its applicability to criticality analysis and to establish the methodology bias and bias uncertainty. The experiments range from water moderated, oxide fuel arrays separated by various materials (B₄C, steel, water, etc.) that simulate light water reactor (LWR) fuel storage conditions⁽⁴⁶⁾ including critical benchmarks designed to represent burned fuel that demonstrate the wide range of applicability of the method.

The two dimensional transport theory computer code, PARAGON Version 1.2.0⁽⁵⁶⁾ and its cross-section library based on ENDF/B-VI.3 are used to simulate in-reactor fuel assembly depletion to generate burnup-specific, depleted fuel isotopics for burnup credit for use in SCALE/KENO V.a Monte Carlo⁽³³⁾ spent fuel pool reactivity and tolerance models.

FNP-FSAR-4

The methodology to calculate spent fuel pool biases and uncertainties which lead to the creation of burnup vs. enrichment requirements given in Technical Specifications 4.3.1.1 are discussed in Reference 46. This analysis provides burnup requirements such that the Farley Units 1 & 2 SFP remains subcritical in unborated conditions at a 95% probability at a 95% confidence level.

To ensure that the burnup requirements generated are appropriate, a target k_{eff} value is created for each array at different enrichments (maximum fresh, 3, 4, and 5 wt%, ^{235}U). The target k_{eff} value accounts for the reactivity effect of applicable biases and uncertainties and includes administrative margin to ensure safety as shown below.

$$\text{Target } k_{eff} = \text{Acceptance Criterion} - \text{Admin Margin} - \Sigma (\text{Biases \& Uncertainties})$$

where,

Acceptance Criterion	=	the maximum allowable k_{eff} for a storage array (1.0 without soluble boron and 0.95 with soluble boron)
Admin Margin	=	the administrative margin (0.005 Δk) taken to provide additional certainty of safe operation
Σ (Biases & Uncertainties)	=	the amount of reactivity that accounts for biases and uncertainties in the reactivity calculation for each storage array

The sum of biases are simply additive while the sum of uncertainties are statistically added as the root sum square of the individual reactivity uncertainties. Uncertainties account for allowable variations within the real model whether they are physical (manufacturing tolerances), analytical (depletion uncertainty and validation bias uncertainty), or measurement related (burnup measurement uncertainty). Biases have a greater impact due to their direct addition to the total sum of bias and uncertainty.

Technical Specifications Tables 4.3-1 through 4.3-5 were generated using the above method for generation of burnup vs. enrichment requirements using bias and uncertainty calculations for each of the Farley Units 1 & 2 Spent Fuel Pool storage configurations.

Soluble boron credit for normal operating conditions and postulated accident has been calculated for Farley Units 1 & 2. Additional pertinent details for modeling each storage array conservatively for the normal and accident operating condition soluble boron determination are found in WCAP-18414⁽⁴⁶⁾.

To determine the maximum soluble boron concentration for normal operating conditions to meet a 95/95 k_{eff} of < 0.95 including biases and uncertainties, where 95/95 k_{eff} is defined as:

$$\text{KENO } k_{eff} + 2\sigma_{keff} < \text{Target } k_{eff}$$

where:

KENO k_{eff} = The simulated accident condition k_{eff}

σ_{keff} = The simulated accident condition k_{eff} Monte Carlo simulation standard deviation

The minimum soluble boron concentration to maintain $k_{eff} < 0.95$ for the limiting normal condition including biases, uncertainties, and administrative margin is 320 ppm. This value meets the Technical Specification value of 400 ppm soluble boron for normal operating conditions.

Spent fuel pool soluble boron concentration required to mitigate the most limiting accident is confirmed. Accidents can be postulated for each storage configuration which would increase reactivity beyond the analyzed condition. The first being a loss of spent fuel pool cooling capability through various means. The second accident would be dropping an assembly onto an already loaded cell or into a non-fuel location. The third would be a misload of an assembly or multiple assemblies into a cell for which the restrictions on location, enrichment, or burnup are not satisfied. The final postulated accident would be an inadvertent dilution of soluble boron within the spent fuel pool.

In the event of failure of a spent-fuel pool cooling pump, or loss of cooling to a spent-fuel pool heat exchanger, the second spent-fuel pool cooling train provides 100% backup capability, thus ensuring continued cooling of the spent-fuel pool. Therefore, a loss of spent-fuel pool cooling event is not part of FNP's licensing basis. However, even if a loss of spent-fuel pool cooling were to occur, there is sufficient soluble boron to prevent k_{eff} from exceeding 0.95. For the loss of fuel pool cooling system accident, the potential increase in SFP reactivity will be bounded by the multiple assembly misload accident.

During placement of the fuel assemblies in the racks, it is possible to drop the fuel assembly from the fuel handling machine. The dropped assembly could land horizontally on top of the other fuel assemblies in the rack. In this case, there is significant separation between the dropped fuel assembly and the active regions of the rest of the fuel assemblies due to the top nozzle, fuel rod plenum, fuel rod end plug, and the separation between the fuel rod and the top nozzle. Due to the large physical separation between the active region of the fuel and the dropped assembly, it is clear that the multiple misloaded fresh fuel assembly described below is more limiting than a single assembly lying horizontally on top of other assemblies in the rack.

It is possible to misplace a fuel assembly in a location not intended for fuel. Misloading a single fuel assembly between the storage rack and pool wall is bounded by the multiple misloading of fresh 5 wt% ^{235}U fuel assemblies inside the racks. This is because it is a single misload, and will have increased leakage due to the presence of the pool wall. A fresh unpoisoned 5 wt% ^{235}U fuel assembly bounds all assembly enrichments and burnup combinations currently licensed for use at Farley.

Reference 46 addresses both the misload of a single assembly into an unacceptable storage location and multiple assemblies being misloaded in series into unacceptable storage locations. The soluble boron required to maintain a total k_{eff} of 0.95 when a 5 wt% ^{235}U fresh fuel assembly is misplaced into a SFP storage cell is much less reactive than the misloading of multiple fresh 5 wt% ^{235}U assemblies in any configuration. This accident is bounded by the multiple misload event.

A multiple assembly misload is a postulated accident where fresh 5 wt% ^{235}U assemblies are misloaded in series due to a common cause. Reference 46 calculates that this limiting accident requires 1710 ppm of boron to maintain k_{eff} below 0.95. The current technical specification limit for pool soluble boron concentration of 2000 ppm is therefore confirmed as adequate and significant margin is available.

The results of all analyses verify that there is a 95% probability at a 95% confidence level (including uncertainties) that k_{eff} of the spent-fuel storage racks will be < 0.95 when flooded with water borated to a concentration of 2000 ppm. Only the most limiting of these accidents is considered to establish the boron concentration limit required for accidents, since each accident is independent, and two accidents do not have to be assumed to occur simultaneously (ANSI/ANS 8.1-1983).

A spent-fuel pool boron dilution evaluation was previously performed to determine the volume necessary to dilute the spent-fuel pool from the Technical Specification limit of 2000 ppm to 400 ppm (the boron concentration required to maintain $K_{\text{eff}} < 0.95$). The boron dilution evaluation determined that approximately 480,000 gal of water would be required to dilute the spent-fuel pool from 2000 ppm to 400 ppm (which is greater than the normal operating condition soluble boron concentration of 320 ppm). A dilution event that would result in this large volume of water would require the transfer of a large quantity of water from the dilution source and a significant increase in the spent-fuel pool level, which would ultimately overflow the pool. This large volume of water would be readily detected and terminated by plant personnel. A spent-fuel pool dilution event of this magnitude is not a credible event.

4.3.2.7.2.2 Storage of Loose Fuel Pellets and Rod Debris. A criticality analysis was done to evaluate the loose pellet transport container stored in the spent-fuel racks. The transport container is comprised of five pellet canisters. Each canister has the dimension of 7 in. by 5 in. and is 20 in. long. The canister can hold up to a maximum of 1000 pellets. Farley may have up to a total of five canisters capable of storing up to 5000 loose pellets. These five canisters may be stored in the spent-fuel rack cell, one on top of the other, occupying only one rack cell in the spent-fuel pool.

The following assumptions are used to develop the KENO-Va model for storage of the loose pellet transport container in the spent-fuel storage racks:

1. The fuel pellet parameters relevant to the criticality analysis are based on the Westinghouse 17-x-17 OFA and STD designs.
2. Westinghouse 17-x-17 OFA and STD fuel pellets contain uranium dioxide at a nominal enrichment of 5.0 w/o ^{235}U over the entire length of each stack.
3. The fuel pellets are modeled assuming a conservative theoretical density of 98.0% and a zero dishing fraction.
4. No credit is taken for any natural or reduced enrichment axial blankets.
5. No credit is taken for any ^{234}U or ^{236}U in the fuel, nor is any credit taken for the buildup of fission product poison material.
6. No credit is taken for any BA on the fuel pellets.
7. No credit is taken for the presence of spent-fuel rack Boraflex poison panels. The Boraflex volume is replaced with water.

8. The moderator is water with 0-ppm soluble boron at a temperature of 68°F. A water density of 1.0 gm/cm³ is used.
9. The fuel stack array is conservatively modeled as infinite in lateral (x and y) extent and infinite in axial (vertical) extent.

From the criticality analysis, the reactivity of the loose pellet container problem is considerably less than the nominal KENO-Va reference reactivities of all the other storage configurations in the Farley spent-fuel rack. Because the loose pellet container is smaller than the rack cell, the asymmetric placement of the container was also considered. From the analysis performed, it was demonstrated that the reactivity of an asymmetric configuration with the loose pellet container is lower than the reactivity of the all cell asymmetric configuration. Therefore, it is concluded that the five loose pellet canisters, with up to 1000 pellets in each, can be safely stored in one spent-fuel pool rack cell in place of an assembly in any of the Farley approved configurations.

Since a transport canister with five completely filled pellet canisters will contain a smaller number of fuel pellets than a fuel assembly, it will be less limiting than a fuel assembly from a spent-fuel pool bulk temperature standpoint. Thus, no thermal analysis is required to demonstrate compliance with spent-fuel pool bulk temperature limits. However, a thermal analysis was performed by Southern Company Services which demonstrated that no local boiling would occur in a pellet canister trap which contained up to 1000 fuel pellets. For this analysis, five pellet canisters each containing 1000 fuel pellets were assumed to be placed in the transport canister in the spent-fuel pool rack 150 h after reactor shutdown following infinite operation. Additionally, the spent-fuel pool was assumed to be at its maximum allowable temperature of 180°F and natural convection was assumed to be the only mode of heat transfer.

4.3.2.7.2.3 Spent-Fuel Cask Loading Operations. The cask storage area is connected to the spent-fuel pool and is used to facilitate cask loading operations using the Holtec HI-STORM 100 Cask System Multi-Purpose Canister (MPC)-32. The spent-fuel cask contains storage locations for 32 fuel assemblies. Westinghouse 17-X-17 fuel assemblies with initial enrichments ≤ 5.0 wt% U-235 can be stored in any location in the spent-fuel cask provided the fuel burnup-enrichment combinations are within the limits specified in Figure 3.7.18-1 of the Technical Specifications. Westinghouse Calculation Note CN-CRIT-207, "MPC-32 Criticality Analysis for the J. M. Farley Nuclear Plant,"⁽⁴⁹⁾ provides the basis for acceptability to conduct cask loading operations in the cask storage area assuming a postulated boron dilution event.

The primary objectives of the criticality analysis are as follows:

- Determine the design basis fuel assembly for spent-fuel cask loading configuration.
- Determine the average assembly burnup versus initial enrichment limits required for safe loading of fuel assemblies in the spent-fuel cask.
- Determine the amount of soluble boron required to maintain $K_{\text{eff}} \leq 0.95$, including all biases and uncertainties, assuming the most limiting plausible reactivity accident.

The criticality analysis approach and criteria are as follows:

- Determine the fresh and spent-fuel storage requirements using no soluble boron conditions such that the 95/95 upper tolerance limit value of K_{eff} , including applicable biases and uncertainties, is < 0.970 . Note that the NRC limit for this condition is unity, yet the calculations analyze to this reduced limit to later minimize the amount of soluble boron that is required to maintain $K_{\text{eff}} < 0.95$. The analysis was performed with a spent-fuel cask model loaded with either fresh or spent-fuel assemblies.
- Determine the amount (ppm) of soluble boron necessary to reduce the K_{eff} value in the canister by at least $0.025 \Delta K_{\text{eff}}$ units. Since the unborated calculations are limited to a $K_{\text{eff}} < 0.970$, this reduction will ensure that the soluble boron maintains the K_{eff} value < 0.945 . Note that the NRC limit for this condition is 0.95. Therefore, an additional margin of $0.005 \Delta K_{\text{eff}}$ units is included in the analysis results.
- Determine the amount of soluble boron necessary to compensate for 5% of the maximum burnup credited in the analysis. In addition, determine the amount of soluble boron necessary to account for a reactivity depletion uncertainty equal to $1.0\% \Delta K_{\text{eff}}$ per 30,000 MWD/MTU of credited assembly burnup.
- Determine the largest increase in reactivity caused by postulated accidents and the corresponding amount of soluble boron needed to offset this reactivity increase.

The Soluble Boron Credit Methodology ⁽⁴⁹⁾ provides additional reactivity margin in the multipurpose canister loading analysis which is then used to implement added flexibility in the storage criteria. The storage configuration modeled in this analysis employs the nominal representation of the pitch between storage locations. The square storage cell pitch modeled is 9.218 in.

The selection of the design basis fuel assembly type is based on an evaluation of the variety of fuel assemblies possibly employed in the reactor to date and selecting the most reactive type for the spent-fuel cask configuration. The candidate fuel assembly types include the Westinghouse 17-x-17 Standard (STD), Optimized (OFA), and Robust (RFA) fuel assembly designs. The Westinghouse 17-x-17 Standard fuel assembly has been evaluated to be the design basis fuel assembly to represent fuel assemblies in this analysis. The design basis fuel assembly bounds the other fuel assembly designs for all calculations except postulated accident cases. When considering a misload of fresh reactive fuel, the misloaded fuel is conservatively modeled as OFA. The most reactive spent-fuel pool temperature is employed for the fuel assembly storage configuration such that the analysis results are valid over the nominal spent-fuel temperature range (up to 180 °F). The reactivity characteristics of the spent-fuel cask are evaluated using a finite model that accounts for leakage; this environment is employed in all evaluations.

The analysis methodology employs:

- SCALE version 4.4⁽⁵⁰⁾ with the SCALE version 4.4 versions of the 44 and 238 group ENDF/B-V neutron cross-section libraries, and
- The two-dimensional integral transport code DIT⁽⁵¹⁾ with an ENDF/B-VI neutron cross-section library.

SCALE is used for calculations involving the representation of the entire spent-fuel cask to evaluate the reactivity characteristics. SCALE, used in both the benchmarking and multipurpose canister storage configurations, includes the control module CSAS25 and the following functional modules: BONAMI, NITAWL-II, and KENO V.a. All references to KENO in the text to follow should be interpreted as referring to the KENO V.a module. The DIT code is used for simulation of in-reactor fuel assembly depletion.

Validation of SCALE for purposes of fuel storage rack and canister analyses is based on the analysis of selected critical experiments from two experimental programs. The first program is the Babcock & Wilcox (B&W) experiments carried out in support of close proximity storage of power reactor fuel⁽³⁴⁾. The second program is the Pacific Northwest Laboratory (PNL) program carried out in support of the design of fuel shipping and storage configurations; the experiments of current interest to this effort are documented in reference 52. Reference 53, as well as several of the relevant thermal experiment evaluations in reference 54, is found to be useful in updating pertinent experimental data for the PNL experiments.

Nineteen experimental configurations are selected from the B&W experimental program; these consist of the following experimental cores: Core X, the seven measured configurations of Core XI, Cores XII through XXI, and Core XIII A. These analyses employ measured critical data, rather than the extrapolated configurations to a fixed critical water height reported in reference 34 so as to avoid introducing possible biases or added uncertainties associated with the extrapolation techniques. In addition to the active fuel region of the core, the full environment of the latter region, including the dry fuel above the critical water height, is represented explicitly in the analyses.

The B&W group of experimental configurations employs variable spacing between individual rod clusters in the nominal 3-x-3 array. In addition, the effects of placing either SS-304 or borated aluminum plates of different boron contents in the water channels between rod clusters are measured.

Eleven experimental configurations were selected from the PNL experimental program. These experiments include unpoisoned uniform arrays of fuel pins and 2-x-2 arrays of rod clusters with and without interposed SS-304 or B/Al plates of different blackness. As in the case of the B&W experiments, the full environment of the active fuel region is represented explicitly.

The approach employed for the determination of the mean calculational bias and the mean calculational variance is based on Criterion 2 of reference 55. For a given KENO calculated value of K_{eff} and associated one sigma uncertainty, the magnitude of $K_{95/95}$ is computed. Accordingly, the mean calculational bias, the mean calculational variance, and the 95/95 confidence level multiplier are determined.

As noted above, the CSAS25 control module is employed to execute the functional modules within SCALE. The CSAS25 control module is used to analyze either infinite arrays of single or multiple storage cells or a full spent-fuel storage configuration. In this analysis, the entire spent-fuel cask is considered.

The DIT code performs a heterogeneous multigroup transport calculation for an explicit representation of a fuel assembly. The neutron transport equations are solved in integral form

within each pin cell. The cells retain full heterogeneity throughout the discrete integral transport calculations. The multigroup spectra are coupled between cells through the use of multigroup interface currents. The angular dependence of the neutron flux is approximated at cell boundaries by a pair of second order Legendre polynomials. Anisotropic scattering within the cells, together with the anisotropic current coupling between cells, provides an accurate representation of the flux gradients between dissimilar cells.

The multigroup cross-sections are based on the Evaluated Nuclear Data File Version 6 (ENDF/B-VI). Cross-sections have been collapsed into an 89-group structure which is used in the assembly spectrum calculation. Following the multigroup spectrum calculation, the region-wise cross-sections within each heterogeneous cell are collapsed to a few groups (usually four broad groups), for use in the assembly flux calculation. A B_1 assembly leakage correction is performed to modify the spectrum according to the assembly in- or outleakage. Following the flux calculation, a depletion step is performed to generate a set of region-wise isotopic concentrations at the end of a burnup interval. An extensive set of depletion chains are available, containing 33 actinide nuclides in the thorium, uranium, and plutonium chains; 171 fission products; the gadolinium, erbium, and boron depletable absorbers; and all structural nuclides. The spectrum-depletion sequence of calculations is repeated over the life of the fuel assembly. Several restart capabilities provide the temperature, density, and boron concentration dependencies needed for three-dimensional calculations with full thermal-hydraulic feedback effects.

The DIT code and its cross-section library are employed in the design of initial and reload cores and have been extensively benchmarked against operating reactor history and test data. For the purpose of spent-fuel criticality analysis calculations, the DIT code is used to generate the detailed fuel isotopic concentrations as a function of fuel burnup and initial feed enrichment. Each complete set of fuel isotopics is reduced to a smaller set of depleted fuel isotopics at specified time points after discharge. The latter depleted fuel representation includes the following nuclides: ^{235}U , ^{236}U , ^{238}U , ^{239}Pu , ^{240}Pu , ^{241}Pu , ^{149}Sm , ^{16}O , and ^{10}B . The DIT code lists the ^{149}Sm isotopics for both ^{149}Sm and $^{149\text{D}}\text{Sm}$ (a metastable isomer). Since ^{149}Sm is a stable isotope, the concentration of this Samarium isotope is the sum of the individual concentration of these two isomers.

The isotopic number densities from the DIT calculation are based upon pin cell averaged values. The input to KENO calculations requires that the number densities be specified for the fuel pellet. Therefore, the number densities from the DIT calculations are scaled by the ratio of area of the cell to the area of the fuel pellet for use in the KENO calculations. The concentration of ^{10}B supplied to KENO is such that the KENO and DIT assembly k_∞ values (at room temperature and unborated conditions) agree to within one sigma of the KENO calculation.

The total soluble boron credit requirement is defined as the sum of three quantities:

$$SBC_{TOTAL} = SBC_{95/95} + SBC_{RE} + SBC_{PA}$$

where,

SBC_{TOTAL} is the total soluble boron credit requirement (ppm),

$SBC_{95/95}$ is the soluble boron requirement for 95/95 $K_{eff} \leq 0.95$ (ppm),

FNP-FSAR-4

SBC_{RE} is the soluble boron required to account for burnup and reactivity uncertainties (ppm),
 SBC_{PA} is the soluble boron required for $K_{eff} \leq 0.95$ under accident conditions (ppm).

The initial enrichment and assembly burnup chosen to represent the storage configuration is based upon minimizing the soluble boron worth. The soluble boron worth decreases as assembly burnup increases, so the uniform burnup model at 5 w/o ^{235}U and 35,000 MWD/MTU is utilized. The reactivity worth, ΔK_{eff} , of the soluble boron is determined by subtracting the K_{eff} value, for a given soluble boron concentration, from the K_{eff} value for zero soluble boron. The soluble boron concentration and reactivity worth data are then fit to a third-degree polynomial. This polynomial is then employed to determine the amount of soluble boron required to reduce K_{eff} by 0.025 ΔK_{eff} units, which is 232 ppm ($SBC_{95/95}$).

The soluble boron credit required for reactivity uncertainties is determined by converting the uncertainty in fuel assembly reactivity and the uncertainty in absolute fuel assembly burnup values to a soluble boron concentration, in units of ppm, necessary to compensate for these two uncertainties. By applying the same third-degree polynomial, the soluble boron concentration necessary to compensate for this reactivity is found to be 158 ppm (SBC_{RE}).

The soluble boron concentration required to maintain $K_{eff} < 0.95$ under accident condition was determined by evaluating all credible events which increase the K_{eff} value of the spent-fuel cask. The accident event which produces the largest increase in the spent-fuel cask K_{eff} value is employed to determine the required soluble boron concentration necessary to mitigate this and all less severe accident events. The list of accident cases considered includes:

- Dropped fresh fuel assembly on top of the spent-fuel cask.
- Misloaded fresh fuel assembly outside of the spent-fuel cask.
- Spent-fuel cask assembly-to-assembly pitch reduction due to seismic event.
- Spent-fuel cask water temperature $> 180^{\circ}\text{F}$.
- Misloaded fresh fuel assembly into a spent-fuel cask location.

It is possible to drop a fresh fuel assembly on top, or immediately outside, of the spent-fuel cask. In this case the physical separation (approximately 20 in.) between the fuel assemblies loaded inside the spent-fuel cask and the assembly lying on top or outside is sufficient to neutronically decouple the accident. This accident will produce a very small positive reactivity increase. This small increase will not be as limiting as the reactivity increase associated with a fuel misloading event inside the spent-fuel cask.

For the accident due to a seismic event the assembly-to-assembly pitch is reduced such that the condition can be approximated by that of the off-center assembly case (performed as part of the uncertainty analysis). An increase of 0.00304 ΔK_{eff} (not accounting for uncertainties) is determined for this case, and this is significantly less than the reactivity increase due to a fuel misloading event inside the spent-fuel cask.

The nominal water temperature range addressed for the spent-fuel cask in this analysis is 50°F to 180°F . It is possible to increase the spent-fuel cask water temperature above 180°F .

However, an increase to 180°F is determined to actually decrease reactivity (as part of the uncertainty analysis). Based on the response of the reactivity to increasing temperature up to 180°F, any increase in reactivity above 180°F will be minimal as compared to the fuel mishandling event. Therefore, at higher temperatures, the fuel mishandling event remains limiting.

The fuel assembly misloading accident represents the most severe postulated event for reactivity increase in K_{eff} and involves the placement of a fresh Westinghouse OFA fuel assembly enriched to 5.0 wt% (containing no burnable poisons) into a cask center cell storage location. This misload would result in a positive reactivity addition increasing K_{eff} toward 0.95. The amount of soluble boron required to compensate for the positive reactivity added is 269 ppm (SBC_{PA}).

Accordingly, the individual contributions and total soluble boron requirement are summarized below:

$$SBC_{95/95} = 232 \text{ ppm}$$

$$SBC_{RE} = 158 \text{ ppm}$$

$$SBC_{PA} = 269 \text{ ppm}$$

$$SBC_{TOTAL} = 659 \text{ ppm}$$

Therefore, a total of 659 ppm of soluble boron is required to maintain $K_{\text{eff}} \leq 0.95$ (including all biases and uncertainties) assuming the most limiting single accident (since each accident is independent, two accidents do not have to be assumed to occur simultaneously per ANSI/ANS 8.1-1983) which is well below the spent-fuel pool boron concentration limit of 2000 ppm in the cask storage area.

Table 4.3-13 contains the 95/95 K_{eff} values for the spent-fuel cask storage configuration.

During cask loading operations, the active volume of the spent-fuel pool will be increased by the volume of the transfer canal and cask storage area when the transfer canal gate and cask storage gate are open. This has the effect of reducing the rate of dilution of the pool. Therefore, the dilution evaluation for the spent-fuel pool discussed in paragraph 4.3.2.7.2.1 remains bounding for cask loading operations. As an added precaution to assure the boron dilution evaluation remains bounding, the spent-fuel transfer canal gate and the cask storage area gate will be kept open during cask loading operations, except during the brief period that the spent-fuel cask is moved into and out of the cask storage area. During that time, at least one gate must be closed as an added defense-in-depth measure to protect against a postulated heavy load cask drop to preclude a breach of the spent-fuel pool, even though the cask crane is a single-failure proof design and a cask drop event is not considered credible.

4.3.2.8 Stability

4.3.2.8.1 Introduction

The stability of the PWR cores against xenon-induced spatial oscillations and the control of such transients are discussed extensively in references 4, 8, 9, and 10. A summary of these reports is given in the following discussion and the design bases are given in paragraph 4.3.1.6.

In a large reactor core, xenon-induced oscillations can take place with no corresponding change in the total power of the core. The oscillation may be caused by a power shift in the core which occurs rapidly by comparison with the xenon-iodine time constants. Such a power shift occurs in the axial direction when a plant load change is made by control rod motion and results in a change in the moderator density and fuel temperature distributions. Such a power shift could occur in the diametral plane of the core as a result of abnormal action.

Because of the negative power coefficient of reactivity, PWR cores are inherently stable to oscillations in total power. Protection against total power instabilities is provided by the control and protection system as described in section 7.7. Hence, the discussion on the core stability will be limited here to xenon-induced spatial oscillations.

4.3.2.8.2 Stability Index

Power distributions, either in the axial direction or in the X-Y plane, can undergo oscillations because of perturbations introduced in the equilibrium distributions without changing the total core power. The overtones in the current PWRs, and the stability of the core against xenon-induced oscillations, can be determined in terms of the Eigenvalues of the first flux overtones. Writing the Eigenvalue, ζ , of the first flux harmonic as

$$1. \quad \zeta = b + ic,$$

then b is defined as the stability index and $T = \frac{2\pi}{c}$ as the oscillation period of the first

harmonic. The time dependence of the first harmonic $\delta\phi$ in the power distribution can now be represented as:

$$2. \quad \delta\phi(t) = Ae^{\zeta t} = ae^{bt} \cos ct,$$

where A and a are constants. The stability index can also be obtained approximately by:

$$3. \quad b = \frac{1}{T} \ln \frac{A_{n+1}}{A_n}$$

where A_n , A_{n+1} are the successive peak amplitudes of the oscillation and T is the time period between the successive peaks.

4.3.2.8.3 Prediction Of The Core Stability

The stability of the Farley core against xenon-induced spatial oscillations is comparable to that of earlier designs. The prediction is based on a comparison of the parameters which are significant in determining the stability of the core against the xenon-induced oscillations, namely (a) the overall core size is unchanged and spatial power distributions will be similar; (b) the moderator temperature coefficient is expected to be similar at full power, and (c) the Doppler coefficient of reactivity is expected to be equal or slightly more negative at full power.

Analysis of both the axial and X-Y xenon transient rests, discussed in paragraph 4.3.2.8.5, shows that the calculational model is adequate for the prediction of core stability.

[HISTORICAL]

[4.3.2.8.4 Stability Measurements

1. Axial Measurements

Two axial xenon transient tests conducted in a PWR with a core height of 12 ft and 121 fuel assemblies are reported in reference 11, and will be briefly discussed here. The tests were performed at approximately 10% and 50% of cycle life.

Both a free-running oscillation test and a controlled test were performed during the first test. The second test at mid-cycle consisted of a free-running oscillation test only. In each of the free-running oscillation tests, a perturbation was introduced to the equilibrium power distribution through an impulse motion of the Control Bank D and the subsequent oscillation was monitored to measure the stability index and the oscillation period. In the controlled test conducted early in the cycle, the part-length (P/L) rods were used to follow the oscillations to maintain an axial offset (AO) within the prescribed limits. The AO of power was obtained from the ex-core ion chamber readings (which had been calibrated against the incore flux maps) as a function of time for both of the tests, as shown in figure 4.3-40.

The total core power was maintained constant during these spatial xenon tests, and the stability index and the oscillation period were obtained from a least square fit of the AO data in the form of Eq. (2). The AO of power is the quantity that properly represents the axial stability, in the sense that it essentially eliminates any contribution from even-order harmonics including the fundamental mode. The conclusions of the tests are:

- a. The core was stable against induced axial xenon transients both at the core-average burnups of 1550 MWD/MTU and 7700 MWD/MTU. The measured stability indices are 0.041 h⁻¹ for the first test (curve 1 of figure 4.3-40) and -0.014 h⁻¹ for the second test (curve 2 of figure 4.3-40). The corresponding oscillation periods are 32.4 h and 27.2 h, respectively.*

- b. *The reactor core becomes less stable as fuel burnup progresses and the axial stability index was essentially zero at 12,000 MWD/MTU. However, the moveable control rod systems can control axial oscillations, as described in paragraph 4.3.2.8.*

2. *Measurements in the X-Y Plane*

Two X-Y xenon oscillation tests were performed at a PWR plant with a core height of 12 ft and 157 fuel assemblies. The first test was conducted at a core- average burnup of 1540 MWD/MTU and the second at a core average burnup of 12,900 MWD/MTU. Both of the X-Y xenon tests show that the core was stable in the X-Y plane at both burnups. The second test shows that the core became more stable as the fuel burnup increased and all Westinghouse PWRs with 121 and 157 assemblies are expected to be stable throughout their burnup cycles.

In each of the two X-Y tests, a perturbation was introduced to the equilibrium power distribution through an impulse motion of one RCC unit located along the diagonal axis. Following the perturbation, the uncontrolled oscillation was monitored using the moveable detector and thermocouple system and the ex-core power range detectors. The quadrant tilt difference is the quantity that properly represents the diametral oscillation in the X-Y plane of the reactor core in that the differences of the quadrant average powers over two symmetrically opposite quadrants essentially eliminates the contribution to the oscillation from the azimuthal mode. The quadrant tilt difference (QTD) data was fitted in the form of Eq. (2) through a least square method. A stability index of -0.076-h^{-1} with a period of 29.6 h was obtained from the thermocouple data shown in figure 4.3-41.

It was observed in the second X-Y xenon test that the PWR core with 157 fuel assemblies had become more stable because of an increased fuel depletion and the stability index was not determined.

4.3.2.8.5 *Comparison of Calculations with Measurements*

The analysis of the axial xenon transient tests was performed in an axial slab geometry using a flux synthesis technique. The direct simulation of the AO data was carried out using the PANDA Code⁽¹³⁾. The analysis of the X-Y xenon transient tests was performed in an X-Y geometry using a modified TURTLE⁽¹⁴⁾ code. Both the PANDA and TURTLE codes solve the two-group time dependent neutron diffusion equation with time-dependent xenon and iodine concentrations. The fuel temperature and moderator density feedbacks are limited to a steady-state model. All the X-Y cancellations were performed in an average enthalpy plane.

The basic nuclear cross-sections used in this study were generated from a unit cell depletion program which evolved from the codes LEOPARD⁽¹⁵⁾ and CINDER⁽¹⁶⁾. The detailed experimental data during the tests, including the reactor power level, enthalpy rise, and the impulse motion of the control rod assembly, as well as the plant follow burnup data, were closely simulated in the study.

The results of the stability calculation for the axial tests are compared with the experimental data in table 4.3-4. The calculations show conservative results for both of the axial tests with a margin of approximately 0.01 h^{-1} in the stability index.

An analytical simulation of the first X-Y xenon oscillation tests shows a calculated stability index of -0.081 h^{-1} , in good agreement with the measured value of -0.076 h^{-1} . As indicated earlier, the second X-Y xenon test showed that the core had become more stable compared to the first test and no evaluation of the stability index was attempted. This increase in the core stability in the X-Y plane because of increased fuel burnup is caused mainly by the increased magnitude of the negative moderator temperature coefficient.

Previous studies of the physics of xenon oscillation, including three-dimensional analysis, are reported in the series of topical reports, references 8, 9, and 10. A more detailed description of the experimental results and analysis of the axial and X-Y xenon transient tests is presented in references 11 and section 1 of reference 12.]

4.3.2.8.6 Stability Control and Protection

The ex-core detector system is utilized to provide indications of xenon-induced spatial oscillations. The readings from the ex-core detectors are available to the operator and also form part of the protection system.

A. Axial Power Distribution

For maintenance of proper axial power distributions, the operator is instructed to maintain an axial offset within a prescribed operating band, based on the ex-core detector readings. Should the axial offset be permitted to move far enough outside this band, the protection limit will be reached thereby reducing the OTΔT trip setpoint to provide protection consistent with core safety limits.

As fuel burnup progresses, 12-ft PWR cores become less stable to axial xenon oscillations. However, free xenon oscillations are not allowed to occur, except for special tests. The full-length control rod banks are sufficient to dampen and control any axial xenon oscillations present. Should the axial offset be inadvertently permitted to move far enough outside the control band because of an axial xenon oscillation for any other reason, the protection limit on axial offset will be reached, thereby reducing the OTΔT trip setpoint to provide protection consistent with core safety limits.

B. Radial Power Distribution

The Farley core is calculated to be stable against X-Y xenon-induced oscillations at all times in life.

The X-Y stability of large PWRs will be further verified as part of the startup physics test program at a PWR core with 193 fuel assemblies. The measured X-Y stability of the PWR cores with 157 assemblies was in good agreement with the

calculated stability as discussed in paragraphs 4.3.2.8.4 and 4.3.2.8.5. In the unlikely event that X-Y oscillations occur, backup actions are possible and would be implemented, if necessary, to increase the natural stability of the core. This is based on the fact that several actions could be taken to make the moderator temperature coefficient more negative, which will increase the stability of the core in the X-Y plane.

Provisions for protection against nonsymmetrical perturbations in the X-Y power distribution that could result from equipment malfunctions are made in the protection system design. This includes control rod drop, rod misalignment, and asymmetric loss-of-coolant flow.

A more detailed discussion of the power distribution control in PWR cores is presented in reference 4.

4.3.2.9 Vessel Irradiation

A brief review of the methods and analyses used in determination of neutron and gamma flux attenuation between the core and the pressure vessel is given below. A more complete discussion on the pressure vessel irradiation and surveillance program is given in paragraph 5.4.3.6.

The primary shielding material that serves to attenuate high-energy neutron and gamma flux originating in the core consists primarily of the core baffle, core barrel, the neutron pads, and associated water annuli, all of which are within the region between the core and the pressure vessel.

In general, few group-neutron diffusion-theory codes are used to determine flux and fission power density distributions within the active core, and the accuracy of these analyses is verified by incore measurements on operating reactors. Region and rod-wise power-sharing information from the core calculations is then used as source data in the dimensional SN transport calculations which compute the flux distributions throughout the reactor.

The neutron flux distribution and spectrum in the various structural components varies significantly from the core to the pressure vessel. Representative values of the neutron flux distribution and spectrum are presented in table 4.3-5. The values listed are based on time-averaged, equilibrium-cycle, reactor-core parameters and power distributions and, thus, are suitable for long-term nvt projections and for correlation with radiation damage estimates.

As discussed in paragraph 5.4.3.6, the irradiation surveillance program utilizes actual test samples to verify the accuracy of the calculated fluxes at the vessel.

4.3.3 ANALYTICAL METHODS

Calculations required in nuclear design consist of three distinct types, which are performed in sequence:

- A. Determination of effective fuel temperatures.
- B. Generation of macroscopic few-group parameters.
- C. Space-dependent, few-group diffusion calculations.

These calculations are carried out by computer codes which can be executed individually. However, at Westinghouse, most of the codes required have been linked to form an automated design sequence which minimizes design time, avoids errors in transcription of data, and standardizes the design methods.

4.3.3.1 Fuel Temperature Doppler Calculations

Temperatures vary radially within the fuel rod, depending on the heat-generation rate in the pellet; the conductivity of the materials in the pellet, gap, and clad; and the temperature of the coolant.

The fuel temperatures for use in most nuclear design Doppler calculations are obtained from a simplified version of the Westinghouse fuel-rod design code described in section 4.2, which considers the effect of radial variation of pellet conductivity, expansion coefficient and heat generation rate, elastic deflection of the clad, and a gap conductance which depends on the initial fill gas, the hot open gap dimension, and the fraction of the pellet over which the gap is closed. The fraction of the gap assumed closed represents an empirical adjustment used to produce good agreement with observed reactivity data at BOL. Further gap closure occurs with burnup and accounts for the decrease in Doppler defect with burnup, which has been observed in operating plants.

Radial power distributions in the pellet as a function of burnup are obtained from LASER⁽¹⁷⁾ calculations.

The effective U-238 temperature for resonance absorption is obtained from the radial temperature distribution by applying a radially-dependent weighting function. The weighting function was determined from REPAD⁽¹⁸⁾ Monte Carlo calculations of resonance escape probabilities in several steady-state and transient-temperature distributions. In each case a flat pellet temperature was determined which produced the same resonance escape probability as the actual distribution. The weighting function was empirically determined from these results.

The effective Pu-240 temperature for resonance absorption is determined by a convolution of the radial distribution of Pu-240 number densities from LASER burnup calculations and the radial weighting function. The resulting temperature is burnup dependent, but the difference between U-238 and Pu-240 temperatures, in terms of reactivity effects, is small.

The effective pellet temperature for pellet dimensional change is that value which produces the same outer-pellet radius in a virgin pellet as that obtained from the temperature model. The effective clad temperature for dimensional change is its average value.

The temperature calculational mode has been validated by plant Doppler-defect data as shown in table 4.3-6 and Doppler coefficient data as shown in figure 4.3-42. Stability index measurements also provide a sensitive measure of the Doppler coefficient near full power (see paragraph 4.3.2.8). It can be seen that Doppler-defect data are typically within 0.2% $\Delta\rho$ of prediction.

4.3.3.2 Macroscopic Group Constants

There are two lattice codes which have been used for the generation of macroscopic group constants needed in the spatial, few-group diffusion codes. One is PHOENIX-P which has historically been the sources of the macroscopic group constants. The other is PARAGON, which will be used in forthcoming reload designs. Following is a detailed description of each.

PHOENIX-P has been approved by the NRC as a lattice code for the generation of macroscopic and microscopic few-group cross-sections for PWR analysis (reference 42). PHOENIX-P is a two-dimensional, multigroup, transport-based lattice code capable of providing all necessary data for PWR analysis. Since it is a dimensional lattice code, PHOENIX-P does not rely on predetermined spatial/spectral interaction assumptions for the heterogeneous fuel lattice and can provide a more accurate multigroup flux solution.

The solution for the detailed spatial flux and energy distribution is divided into two major steps in PHOENIX-P (reference 42). First, a two-dimensional fine energy group nodal solution is obtained, coupling individuals sub-cell regions (pellet, clad, and moderator) as well as surrounding pins, using a method based on Carlvik's collision probability approach and heterogeneous response fluxes which preserve the heterogeneity of the pin cells and their surroundings. The nodal solution provides an accurate and detailed local flux distribution, which is then used to homogenize the pin cells spatially to fewer groups. Then, a standard S4 discrete ordinates calculation solves for the angular distribution, based on the group-collapsed and homogenized cross-sections from the first step. These S4 fluxes normalize the detailed spatial and energy nodal fluxes, which are then used to compute reaction rates and power distributions and to deplete the fuel and burnable absorbers. A standard B1 calculation evaluates the fundamental mode critical spectrum, providing an improved fast diffusion coefficient for the core spatial codes.

PHOENIX-P employs a 70 energy group library derived from the ENDF/B-6 basic data. This library was designed to capture the integral properties of the multigroup data properly during group collapse and to model important resonance parameters properly. It contains all neutronics data necessary for modeling fuel, fission products, cladding and structural materials, coolant, and control and burnable absorber materials present in PWRs. Group constants for burnable absorber cells, control rod cells, guide thimbles and instrumentation thimbles, or other nonfuel cells, can be obtained directly from PHOENIX-P without any adjustments such as those required in the cell or 1D lattice codes.

PARAGON has been approved by the NRC as the new generation of Westinghouse lattice code (reference 47). PARAGON is a replacement for PHOENIX-P and its primary use will be to provide the same types of input data that PHOENIX-P generates for use in three dimensional core simulator codes. This includes macroscopic cross-sections, microscopic cross-sections for feedback adjustments to the macroscopic cross-sections, pin factors for pin power reconstruction calculations, discontinuity factors for a nodal method solution, and other data needed for safety analysis or other downstream applications.

PARAGON is based on collision probability-interface current cell coupling methods. PARAGON provides flexibility in modeling that was not available in PHOENIX-P including exact cell geometry representation instead of cylinderization, multiple rings and regions within the fuel pin and the moderator cell geometry, and variable cell pitch. The solution method permits flexibility in choosing the quality of the calculation through both increasing the number of regions modeled within the cell and the number of angular current directions tracked at the cell interfaces.

The calculation scheme in PARAGON is based on the conventional lattice modules: resonance calculation, flux solution, leakage correction, and depletion. The detailed theory of these modules is described in reference 56. The cross-section resonance calculation module is based on the space dependent Dancoff method (reference 56). It is a generalization of the PHOENIX-P methodology that permits to subdivide the fuel pin into many rings and therefore generates space dependent self-shielded isotopic cross-sections. The flux solution module uses the interface current collision probability method and permits a detailed representation of the fuel cells (reference 56). The other two modules (leakage and depletion) are similar to the ones used in PHOENIX-P.

The current PARAGON cross-section library is a 70-group library, based on the ENDF/B basic nuclear data, with the same group structure as the library currently used with PHOENIX-P. The PARAGON qualification library has been improved through the addition of more explicit fission products and fission product chains (reference 56). PARAGON is, however, designed to employ any number of energy groups.

The new NEXUS cross-section generation system uses PARAGON as the lattice code (reference 57).

4.3.3.3 Spatial Few-Group Diffusion Calculations

Spatial few-group diffusion calculations are performed using the Advanced Nodal Code (ANC) (reference 26).

The three-dimensional nature of this code provides both radial and axial power distributions. For some applications, the updated version of the PANDA will continue to be used for axial calculations, and a two-dimensional collapse of 3D ANC that properly accounts for the three-dimensional features of the fuel will be used for X-Y calculations.

FNP-FSAR-4

Nodal calculations (four radial mesh per assembly) are carried out to determine the critical boron concentrations and power distributions. The moderator coefficient is evaluated by varying the inlet temperature in the same kind of calculations as those used for power distribution and reactivity predictions.

Discrete X-Y calculations (1 mesh per cell) were carried out to determine critical boron concentrations and power distributions in the X-Y plane. An axial average in the X-Y plane was obtained by synthesis from unrodded and rodded planes. Axial effects in unrodded depletion calculations were accounted for by the axial buckling, which varies with burnup and is determined by radial depletion calculations which are matched in reactivity to the analogous R-Z depletion calculation. The moderator coefficient is evaluated by varying the inlet temperature in the same X-Y calculations used for power distribution and reactivity predictions.

Validation of the reactivity calculations is associated with the validation of the group constants themselves, as discussed in paragraph 4.3.3.2. Validation of the Doppler calculations is associated with the fuel temperature validation discussed in paragraph 4.3.3.1. Validation of the moderator coefficient calculation is obtained by comparison with plant measurements at hot zero power conditions as shown in table 4.3-11.

Present designs primarily use ANC for two-dimensional and three-dimensional calculations. ANC can be used in safety analysis calculations, critical boron concentrations, control rod worth, reactivity coefficients, etc.

Axial calculations are used to determine differential control rod worth curves (reactivity versus rod insertion) and axial power shapes during steady-state and transient xenon conditions (flyspeck curve). Group constants are obtained from the three-dimensional nodal model by flux-volume weighting on an axial slicewise basis. Radial bucklings are determined by varying parameters in the buckling model while forcing the one-dimensional model to reproduce the axial characteristics (axial offset, mid-plane power) of the three-dimensional model.

Validation of the spatial codes for calculating power distributions involves the use of incore and ex-core detectors and is discussed in paragraph 4.3.2.2.7.

Based on comparison with measured data, it is estimated that the accuracy of current analytical methods is as follows:

- $\pm 0.2\text{-}\% \Delta\rho$ for Doppler defect.
- $\pm 2 \times 10^{-5} \Delta\rho/^{\circ}\text{F}$ for moderator coefficient.
- ± 50 ppm for critical boron concentration with depletion.
- $\pm 3\%$ for power distributions.
- $\pm 0.2\% \Delta\rho$ for rod bank worth.
- ± 4 pcm/step for differential rod worth.
- ± 0.5 pcm/ppm for boron worth.
- $\pm 0.1\% \Delta\rho$ for moderator defect.

REFERENCES

1. Gangloff, W. C. and Loftus, W. D., "Westinghouse Anticipated Transients Without Reactor Trip Analysis," WCAP-8330, August 1974.
2. Spier, E. M., "Evaluation of Nuclear Hot Channel Factor Uncertainties," WCAP-7308-L-P-A (Proprietary) and WCAP-7308-L-A, (Nonproprietary), June 1988.
3. McFarlane, A. F., "Core Power Capability in Westinghouse PWRs," WCAP-7809, December 1971.
4. Moore, J. S., "Power Distribution Control of Westinghouse Pressurized Water Reactors," WCAP-7811, December 1971.
5. McFarlane, A. F., "Power Peaking Factors," WCAP-7912, March 1972.
6. Cermak, J. O., et al., "Pressurized Water Reactor pH-Reactivity Effect," Final Report, WCAP-3696-8 (EURAEC-2074), October 1968.
7. Outzs, J. E., "Plant Startup Test Report, H. B. Robinson Unit No. 2," WCAP-7844, January 1972.
8. Poncelet, C. G. and Christie, A. M., "Xenon-Induced Spatial Instabilities in Large PWRs," WCAP-3680-20 (EURAEC-1974), March 1968.
9. Skogen, F. B. and McFarlane, A. F., "Control Procedures for Xenon-Induced X-Y Instabilities in Large PWRs," WCAP-3680-21, (EURAEC-2111), February 1969.
10. Skogen, F. B. and McFarlane, A. F., "Xenon-Induced Spatial Instabilities in Three Dimensions," WCAP-3680-22 (EURAEC-2116), September 1969.
11. Lee, J. C., et al., "Axial Xenon Transient Tests at the Rochester Gas and Electric Reactor," WCAP-7964, June 1971.
12. Kubit, C. J., "Safety-Related Research and Development for Westinghouse Pressurized Water Reactors, Program Summaries, Winter 1977-Summer 1978," WCAP-8768 (Revision 2), October 1978.
13. Barry, R. F., et al., "The PANDA Code," WCAP-7758, September 1971.
14. Altomare, S. and Barry, R. F., "The TURTLE 24.0 Diffusion Depletion Code," WCAP-7756-A, February 1975.
15. Barry, R. F., "LEOPARD - A Spectrum-Dependent Non-Spatial Depletion Code for the IBM-7094," WCAP-3269-26, September 1963.
16. England, T. R., "CINDER - A One-Point Depletion and Fission Product Program," WAPD-TM 334, August 1962.

FNP-FSAR-4

17. Poncelet, C. G., "LASER - A Depletion Program for Lattice Calculations Based on MUFT and THERMUS," WCAP-6073, April 1966.
18. Olheoft, J. E., "The Doppler Effect for a Nonuniform Temperature Distribution in Reactor Fuel Elements," WCAP-2048, July 1962.
19. Nodvik, R. J., et al., "Supplementary Report on Evaluation of Mass Spectrometric and Radiochemical Analyses of Yankee Core I Spent Fuel, Including Isotopes of Elements Thorium Through Curium," WCAP-6086, August 1969.
20. Drake, M. K., ed., "Data Formats and Procedure for the ENDF Neutron Cross Section Library," BNL-50274, ENDF-102, Vol. I, 1970.
21. Suich, J. E. and Honeck, H. C., "The HAMMER System, Heterogeneous Analysis by Multigroup Methods of Exponentials and Reactors," DP-1064, January 1967.
22. Flatt, H. P. and Buller, D. C., "AIM-5, A Multigroup, One-Dimensional Diffusion Equation Code," NAA-SR-4694, March 1960.
23. Moore, J. S., "Nuclear Design of Westinghouse Pressurized Water Reactors with Burnable Poison Rods," WCAP-7806, December 1971.
24. Deleted
25. Thomas, J. T., "Critical Three-Dimensional Arrays of U (93.2)-Metal Cylinders," Nuclear Science and Engineering, Vol. 52, pp 350-359, 1973.
26. Liu, Y. S., et al., "ANC: A Westinghouse Advanced Nodal Computer Code," WCAP-10965-P-A, September 1986.
27. Deleted
28. Deleted
29. Morita, T., Radcliffe, R. E., et al., "Power Distribution Control and Load Following Procedures," WCAP-8403, September 1974.
30. Meyer, C. E. and Stover, R. L., "In-Core Power Distribution Determination In Westinghouse Pressurized Water Reactors," WCAP-8498, July 1975.
31. Greene, N. M., "AMPX: A Modular Code System For Generating Coupled Multigroup Neutron-Gamma Libraries From ENDF/B," ORNL/TM-3706, March 1976.
32. Petrie, L. M. and Landers, N. F., "KENO Va - An Improved Monte Carlo Criticality Program with Supergrouping," NUREG/CR-0200, Vol. 2, Section F11, November 1993.
33. SCALE Code System, ORNL/TM-2005/39, Version 6.2.3, March 2018.

FNP-FSAR-4

34. Baldwin, M. N., "Critical Experiments Supporting Close Proximity Water Storage of Power Reactor Fuel," BAW-1484-7, July 1979.
35. Thomas, J. T., "Critical Three-Dimensional Arrays of U (93.2) Metal Cylinders," Nuclear Science and Engineering, Volume 52, pp 350-359, 1973.
36. Leamer, R. D., et al., "PuO-UO Fueled Critical Experiments," WCAP-3726-1, July 1967.
37. Nodvic, R. J., "Saxton Core II Fuel Performance Evaluation," WCAP-3385-56, Part II, "Evaluation of Mass Spectrometric and Radiochemical Material Analyses of Irradiated Saxton Plutonium Fuel," July 1970.
38. Harris, A. J., "A Description of the Nuclear Design and Analysis Programs for Boiling Water Reactors," WCAP-10106, June 1982.
39. Not used
40. Davidson, S. L., ed., et al., "Extended Burnup Evaluation of Westinghouse Fuel," WCAP-10125-P-A, December 1985.
41. Not Used
42. Nguyen, T. Q., et al., "Qualification of the PHOENIX-P/ANC Nuclear Design System for Pressurized Water Reactor Cores," WCAP-11596-P-A, June 1988.
43. Mildrum, C. M., Mayhue, L. T., Baker, M. M., and Isaac, P. G., "Qualification of the PHOENIX/POLCA Nuclear Design and Analysis Program for Boiling Water Reactors," WCAP-10841 (Proprietary), and WCAP-10842 (Nonproprietary), June 1985.
44. Miller, R. W., et al., "Relaxation of Constant Axial Offset Control; Fq Surveillance Technical Specification," WCAP-10216-P-A Revision 1A (Proprietary), and WCAP-10217-A Revision 1A (Nonproprietary), February 1994.
45. Kersting, P. J., et al., "Assessment of Clad Flattening and Densification Power Spike Factor Elimination in Westinghouse Nuclear Fuel," WCAP-13589-A, March 1995.
46. Wenner, M. T., "J.M. Farley Units 1 and 2 Spent Fuel Pool Criticality Safety Analysis," WCAP-18414, September 2019.
47. Yarbrough, M. B., et al., "APOLLO - A One-Dimensional Neutron Theory Program," WCAP-13524-P-A, Revision 1-A, September 1997.
48. Beard, C. L. and Morita, T., "BEACON Core Monitoring and Operations Support System," WCAP-12472-P-A Addendum 1-A, January 2000.
49. CN-CRIT-207, MPC-32 Criticality Analysis for the J. M. Farley Nuclear Plant.

50. "SCALE: A Modular Code System for Performing Standardized Computer Analyses for Licensing Evaluation," NUREG/CR-0200, distributed by the Radiation Shielding Information Center, Oak Ridge National Laboratory, Oak Ridge, Tennessee, September 1998.
51. "DIT: Discrete Integral Transport Assembly Design Code," CE-CES-11, Revision 4-P, April 1994.
52. Bierman, S. R. and Clayton, E. D., "Critical Experiments with Subcritical Clusters of 2.35 Wt% ²³⁵U Enriched UO₂ Rods in Water at a Water-to-Fuel Volume Ratio of 1.6," NUREG/CR-1547, PNL-3314, July 1980.
53. Bierman, S. R. and Clayton, E. D., "Criticality Experiments with Subcritical Clusters of 2.35 and 4.31 Wt% U-Enriched UO₂ Rods in Water with Steel Reflecting Walls," Nuclear Technology, Vol. 54, p. 131, August 1981.
54. International Handbook of Evaluated Criticality Safety Benchmark Experiments, Nuclear Energy Agency and Organization for Economic Cooperation and Development.
55. Marshall, W., et al., "Criticality Safety Criteria," TANS Vol. 35, p. 278, 1980.
56. Ouisloumen, M., et al., "Qualification of the Two-Dimensional Transport Code PARAGON," WCAP-16045-P-A, Westinghouse, 2004.
57. Zhang, B., et al., "Qualification of the NEXUS Nuclear Data Methodology," WCAP-16045-P-A, Addendum 1, Westinghouse, 2005.
58. FNP RER SNC799923-01, "Farley Unit 1 & 2 Movable Incore Detector System Thimble Reduction Study."

FNP-FSAR-4

TABLE 4.3-1 (SHEET 1 OF 3)

REACTOR CORE DESCRIPTION

	<u>LOPAR</u>	<u>VANTAGE 5</u>
Active Core		
Equivalent diameter (in.)	119.7	119.7
Active fuel height (in.)	143.7	143.7
Height-to-diameter ratio	1.20	1.20
Total cross-section area (ft ²)	78.14	78.14
H ₂ O/U molecular ratio, lattice (cold)	2.41	2.73
Reflector Thickness and Composition		
Top - water plus steel (in.)	~10	~10
Bottom - water plus steel (in.)	~10	~10
Side - water plus steel (in.)	~15	~15
Fuel Assemblies		
Number	157	157
Rod array	17 x 17	17 x 17
Rods per assembly	264	264
Rod pitch (in.)	0.496	0.496
Overall transverse dimensions (in.)	8.426 x 8.426	8.426 x 8.426
Fuel weight (as UO ₂) (lb)	181,205 ^(a)	166,111 ^(d)
Zircaloy-4/ZIRLO/Optimized ZIRLO weight (active core) (lb)	41,416	37,350
Number of grids per assembly	8-R type	2-non-mixing vane type 6-mixing vane type 3-IFM 1-Protective grid
Composition of grids		
	Inconel-718	2 Inconel-718 end grids 6 Zircaloy-4/ZIRLO™ spacer grids 3 Zircaloy-4/ZIRLO™ IFM grids 1 Inconel-718 Protective grid
Weight of grids in active core (lb)		
	Inconel-718-1885	Inconel-718-270 Zircaloy-4/ZIRLO™ 2885
Number of guide thimbles per assembly		
Composition of guide thimbles	24 Zircaloy 4	24 Zircaloy 4/ZIRLO™
Diameter of guide thimbles (upper part) (in.)	0.450 ID x 0.482 OD	0.442 ID x 0.474 OD
Diameter of guide thimbles (lower part) (in.)	0.397 ID x 0.430 OD	0.397 ID x 0.430 OD
Diameter of instrument guide thimbles (in.)	0.450 ID x 0.482 OD	0.442 ID x 0.474 OD
Fuel Rods		
Number	41,448	41,448
Outside diameter (in.)	0.374	0.360
Diameter gap (in.)	0.0065	0.0062
Clad thickness (in.)	0.0225	0.0225
Clad material	Zircaloy 4	Zircaloy-4, ZIRLO, or Optimized ZIRLO

FNP-FSAR-4

TABLE 4.3-1 (SHEET 2 OF 3)

	<u>LOPAR</u>	<u>VANTAGE 5</u>
Fuel Pellets		
Material	UO ₂ sintered	UO ₂ sintered
Density (percent of theoretical)	95	95
<i>[HISTORICAL] [Fuel enrichments w/o (first core)]</i>		
Region 1	2.10	
Region 2	2.60	
Region 3	3.10	
Diameter (in.)	0.3225	0.3088(c)
Length (in.)	0.387(b)	0.370/0.462 or 0.500 (blanket pellet)
Mass of UO ₂ per ft of fuel rod (lb/ft)	0.364	0.334(a)
Rod Cluster Control Assemblies		
Neutron absorber	Ag-In-Cd	
Composition	80%, 15%, 5%	
Diameter (in.)	0.341	
Density (lb/in. ³)	0.367	
Cladding material	Type 304, cold-worked stainless steel	
Clad thickness (in.)	0.0185	
Number of clusters		
Full-length	48	
Number of absorber rods per cluster	24	
Full-Length assembly weight (dry) (lb)	157	
Standard Burnable Absorber Rods		
Number (First Core)	1072	
Material	Borosilicate glass	
Outside diameter (in.)	0.381	
Inner tube, OD (in.)	0.1805	
Clad material	Stainless steel	
Inner tube material	Stainless steel	
Boron loading (w/o B ₂ O ₃ in glass rod)	12.5	
Initial reactivity worth (% Δρ) (First Core)	7.0 (hot), ~5 (cold)	
Wt. of boron - 10 ft of rod (lb/ft)	0.000419	
WABA Rods		
Material	A1 ₂ O ₃ - B ₄ C	
Outside tube OD (in.)	0.381	
Outside tube clad thickness (in.)	0.026	
Inner tube OD (in.)	0.267	
Inner tube clad thickness (in.)	0.021	
Outer tube material	Zircaloy 4	
Inner tube material	Zircaloy 4	
Boron loading (w/o B ₄ C in A1 ₂ O ₃ -B ₄ C)	14.0	
Weight of Boron -10 (g/cm)	0.006	
Integral Fuel Burnable Absorber material	Boride coated	
Typical Boron-10 content (mg/in.)	1.50 to 2.25 (1.0X to 1.5X)	

FNP-FSAR-4

TABLE 4.3-1 (SHEET 3 OF 3)

	<u>LOPAR</u>	<u>VANTAGE 5</u>
Excess Reactivity		
Maximum fuel assembly k_{eff} (cold, clean, unborated water)	< 1.6	
Maximum core k_{eff} (cold, zero power, beginning of cycle)	1.25	

-
- a. Without chamfered pellet. Chamfered pellet design increases indicated fuel weight by less than 1 percent.
 - b. Farley 1 Cycle 9 and Farley 2 Cycle 7 and following. Pellet length prior to Farley 1 Cycle 9 and Farley 2 Cycle 7 is 0.530 in.
 - c. Without IFBA. IFBA coated fuel pellets have a thin boride coating on the pellet cylindrical surface.
 - d. The decrease in fuel weight due to annular pellets is not considered.

FNP-FSAR-4

[HISTORICAL] [TABLE 4.3-2 (SHEET 1 OF 2)]

NUCLEAR DESIGN PARAMETERS (FIRST CYCLE)

Core Average Linear Power, kW/ft, including Densification Effects	5.20	
Total Heat Flux Hot Channel Factor, F_Q	2.32	
Nuclear Enthalpy Rise Hot Channel Factor, $F_{\Delta H}^N$	1.55	
<u>Reactivity Coefficients</u>	<u>Design Limits</u>	<u>Best Estimate</u>
Doppler-only power, Coefficients, pcm/% power ^(b) (upper limit)	-19.4 to -12.6	-12.2 to -8.1
Lower limit	-10.2 to -6.7	-11.8 to -7.9
Doppler temperature coefficient (pcm/°F) ^(b)	-2.9 to -1.4	-2.2 to -1.4
Moderator temperature coefficient (pcm/°F) ^(b)	0	-1 to -40
Boron coefficient (pcm/ppm) ^(b)	-16 to -8	-13 to -9
Rodded moderator density (pcm/g/cm ³) ^(b)	$\leq 0.43 \times 10^5$	$\leq 33 \times 10^5$
<u>Delayed Neutron Fraction and Lifetime</u>		
β_{eff} , BOL, (EOL)		0.0075, (0.0048)
ℓ , BOL, (EOL) μ s		19.9 (18.1)
<u>Control Rods</u>		See table 4.3-3
Rod requirements		
Maximum bank worth, pcm ^(b)	< 2300	
Maximum ejected rod worth		See chapter 15
<u>Radial Factor (BOL to EOL)</u>		
Unrodded		1.37 to 1.25
D bank		1.58 to 1.42
D + C		1.63 to 1.42
D + C + B		1.80 to 1.55

FNP-FSAR-4

[HISTORICAL] [TABLE 4.3-2 (SHEET 2 OF 2)]

	<u>Design Limits</u>	<u>Best Estimate</u>
<u>Boron Concentrations</u>		
Zero power, $K_{eff} = 1.00$ cold rod cluster control assemblies out (1% $\Delta\rho$ uncertainty included) ^(a)		1429
Zero power, $K_{eff} = 1.00$ hot rod cluster control assemblies out (1% $\Delta\rho$ uncertainty included) ^(a)		1419
Design basis refueling boron concentration		2000
Zero power, $K_{eff} 0.95$, cold rod cluster control assemblies in (1% $\Delta\rho$ uncertainty included) ^(a)		1196
Full power, no xenon, $K_{eff} = 1.0$, hot rod cluster control assemblies out		1195
Full power, equilibrium xenon, $K_{eff} = 1.0$, hot rod cluster control assemblies out		906
<u>Reduction with fuel burnup</u>		
First cycle (ppm/GWd/Mtu) ^(c)		~60
Reload cycle (ppm/GWd/Mtu) ^(c)		~85

a. Uncertainties are given in paragraph 4.3.3.3.

b. $1 \text{ pcm} = (\text{percent milli rho}) = 10^{-5} \Delta\rho$ where $\Delta\rho$ is calculated from two statepoint values of K_{eff} by $\ln(k_2/k_1)$.

c. Gigawatt day (GWd) = 1000 megawatt day (1000 MWd). During the first cycle, fixed BA rods are present which significantly reduce the boron depletion rate compared to reload cycles.]

TABLE 4.3-3

REACTIVITY REQUIREMENTS FOR ROD CLUSTER CONTROL ASSEMBLIES

<u>Reactivity Effects, Percent</u>	<u>[HISTORICAL]</u>		<u>End of Life (Equilibrium Cycle)</u>
	<u>[BOL</u>	<u>EOL</u>	
	<u>(First Cycle)</u>		
Control requirements			
Fuel temperature (Doppler)(% $\Delta\rho$)	1.26	1.05	1.11
Moderator temperature (% $\Delta\rho$)	0.23	1.07	1.20
Void (% $\Delta\rho$)	0.05	0.05	0.05
Redistribution (% $\Delta\rho$)	0.50	0.85	1.00
Rod Insertion Allowance (% $\Delta\rho$)	0.50	0.50	0.50
(1) Total control (% $\Delta\rho$)	2.54	3.52	3.86
Estimated rod cluster control assembly worth (48 rods)			
a. All full-length assemblies inserted (% $\Delta\rho$)	9.88	9.57	8.50
b. All but one (highest worth) assemblies inserted (% $\Delta\rho$)	7.85	7.81	7.65
(2) Estimated rod cluster control assembly credit with 10-percent adjustment to accommodate uncertainties (3 to 10 percent) (% $\Delta\rho$)	7.06	7.03	6.88
Shutdown margin available (2-1) (% $\Delta\rho$)	4.52	3.51]	3.02 ^(a)

a. The design basis minimum shutdown is 1.77 percent.

[HISTORICAL] [TABLE 4.3-4***AXIAL STABILITY INDEX PWR CORE WITH A 12-FT HEIGHT***

<u>Burnup (MWD/T)</u>	<u>F_z</u>	<u>C_B (ppm)</u>	<u>Stability Index (hr^{-1})</u>	
			<u>Exp</u>	<u>Calc</u>
1550	1.34	1065	-0.041	-0.032
7700	1.27	700	-0.014	-0.006
5090 ^(a)			-0.0325	-0.0255
<u>Radial Stability Index</u>				
2250 ^(b)	-0.068		0.07	

a. 4-loop plant, 12-foot core in cycle 1, axial stability test.

b. 4-loop plant, 12-foot core in cycle 1, radial (X-Y) stability test.]

TABLE 4.3-5**TYPICAL NEUTRON FLUX LEVELS (n/cm² -s) AT FULL POWER**

	<u>E > 1.0 Mev</u>	<u>5.53 Kev < E ≤ 01.0 Mev</u>	<u>0.625 ev ≤ E ≤ 5.53 Kev</u>	<u>E < .625 ev (hardened spectrum)</u>
Core center	6.51×10^{13}	1.12×10^{14}	8.50×10^{13}	3.00×10^{13}
Core outer radius at midheight	3.23×10^{13}	5.74×10^{13}	4.63×10^{13}	8.60×10^{12}
Core top, on axis	1.53×10^{13}	2.42×10^{13}	2.10×10^{13}	1.63×10^{12}
Core bottom, on axis	2.36×10^{13}	3.94×10^{13}	3.50×10^{13}	1.46×10^{13}
Pressure vessel inner wall, azimuthal peak, core midheight	2.77×10^{10}	5.75×10^{10}	6.03×10^{10}	8.38×10^{10}

TABLE 4.3-6**COMPARISON OF MEASURED AND CALCULATED DOPPLER DEFECTS**

<u>Plant</u>	<u>Fuel Type</u>	<u>Core Burnup (MWD/MTU)</u>	<u>Measured (pcm)</u>	<u>Calculated (pcm)^(a)</u>
1	Air and helium-filled	8460	1200	1210
2	Helium-filled	0	1130	1220
3	Helium-filled	0	1180	1220

a. $\text{pcm} = 10^5 \times \ln \frac{k_1}{k_2}$

[HISTORICAL] [TABLE 4.3-7 (SHEET 1 OF 2)]**BENCHMARK CRITICAL EXPERIMENTS (26,34,35) LEOPARD COMPARISONS**

<u>Description of Experiments^(a)</u>	<u>No. of Experiments</u>	<u>LEOPARD K_{eff} Using Experimental Bucklings</u>
<i>UO₂</i>		
<i>Al clad</i>	14	1.0012
<i>SS clad</i>	19	0.9963
<i>Borated H₂O</i>	7	0.9989
<i>Total</i>	40	0.9985
<u><i>U-Metal</i></u>		
<i>Al clad</i>	43	0.9995
<i>Unclad</i>	20	0.9990
<i>Total</i>	61	0.9993
<i>All above</i>	101	0.9990

a. Reported in reference 25.

FNP-FSAR-4

TABLE 4.3-7 (SHEET 2 OF 2)

AMPX - KENO COMPARISONS

	<u>General Description</u>	<u>Enrichment w/o U235</u>	<u>Reflector</u>	<u>Separating Material</u>	<u>Characterizing Separation (cm)</u>
1.	UO ₂ rod lattice	2.35	water	water	11.92
2.	UO ₂ rod lattice	2.35	water	water	8.39
3.	UO ₂ rod lattice	2.35	water	water	6.39
4.	UO ₂ rod lattice	2.35	water	water	4.46
5.	UO ₂ rod lattice	2.35	water	Stainless steel	10.44
6.	UO ₂ rod lattice	2.35	water	Stainless steel	11.47
7.	UO ₂ rod lattice	2.35	water	Stainless steel	7.76
8.	UO ₂ rod lattice	2.35	water	Stainless steel	7.42
9.	UO ₂ rod lattice	2.35	water	boral	6.34
10.	UO ₂ rod lattice	2.35	water	boral	9.03
11.	UO ₂ rod lattice	2.35	water	boral	5.05
12.	UO ₂ rod lattice	4.29	water	water	10.64
13.	UO ₂ rod lattice	4.29	water	Stainless steel	9.76
14.	UO ₂ rod lattice	4.29	water	Stainless steel	8.08
15.	UO ₂ rod lattice	4.29	water	boral	6.72
16.	U metal cylinders	93.2	bare	air	15.43
17.	U metal cylinders	93.2	paraffin	air	23.84
18.	U metal cylinders	93.2	bare	air	19.97
19.	U metal cylinders	93.2	paraffin	air	36.47
20.	U metal cylinders	93.2	bare	air	13.74
21.	U metal cylinders	93.2	paraffin	air	23.48
22.	U metal cylinders	93.2	bare	plexiglas	15.74
23.	U metal cylinders	93.2	paraffin	plexiglas	24.43
24.	U metal cylinders	93.2	bare	plexiglas	21.74
25.	U metal cylinders	93.2	paraffin	plexiglas	27.94
26.	U metal cylinders	93.2	bare	steel	14.74
27.	U metal cylinders	93.2	bare	plexiglas, steel	16.67]

FNP-FSAR-4

[HISTORICAL] [TABLE 4.3-8

SAXTON CORE II ISOTOPICS ROD MY+, AXIAL ZONE 6

<u>Atom Ratio</u>	<u>Measured^(a)</u>	<u>2 Precision (%)</u>	<u>LEOPARD Calculation</u>
<i>U-234/U</i>	4.65×10^{-5}	± 29	4.60×10^{-5}
<i>U-235/U</i>	5.74×10^{-3}	± 0.9	5.73×10^{-3}
<i>U-236/U</i>	3.55×10^{-4}	± 5.6	3.74×10^{-4}
<i>U-238/U</i>	0.99386	± 0.01	0.99385
<i>Pu-238/Pu</i>	1.32×10^{-3}	± 2.3	1.222×10^{-3}
<i>Pu-239/Pu</i>	0.73971	± 0.03	0.74497
<i>Pu-240/Pu</i>	0.19302	± 0.2	0.19102
<i>Pu-241/Pu</i>	6.014×10^{-2}	± 0.3	5.74×10^{-2}
<i>Pu-242/Pu</i>	5.81×10^{-3}	± 0.9	5.38×10^{-3}
<i>Pu/U^(b)</i>	5.938×10^{-2}	± 0.7	5.970×10^{-2}
<i>Np-237/U-238</i>	1.14×10^{-4}	± 15	0.86×10^{-4}
<i>Am-241/Pu-239</i>	1.23×10^{-2}	± 15	1.08×10^{-2}
<i>Cm-242/Pu-239</i>	1.05×10^{-4}	± 10	1.11×10^{-4}
<i>Cm-244/Pu-239</i>	1.09×10^{-4}	± 20	0.98×10^{-4}

a. Reported in reference 37.

b. Weight ratio.]

[HISTORICAL] [TABLE 4.3-9***CRITICAL BORON CONCENTRATIONS (ppm), HZP, BOL***

<u><i>Plant Type</i></u>	<u><i>Measured</i></u>	<u><i>Calculated</i></u>
<i>2-Loop, 121 assemblies 10-foot core</i>	<i>1583</i>	<i>1589</i>
<i>2-Loop, 121 assemblies 12-foot core</i>	<i>1625</i>	<i>1624</i>
<i>2-Loop, 121 assemblies 12-foot core</i>	<i>1517</i>	<i>1517</i>
<i>3-Loop, 157 assemblies 12-foot core</i>	<i>1169</i>	<i>1161</i>
<i>3-Loop, 157 assemblies 12-foot core</i>	<i>1344</i>	<i>1319</i>
<i>4-Loop, 193 assemblies 12-foot core</i>	<i>1370</i>	<i>1355</i>
<i>4-Loop, 193 assemblies 12-foot core]</i>	<i>1321</i>	<i>1309</i>

[HISTORICAL] [TABLE 4.3-10]***COMPARISON OF MEASURED AND CALCULATED AG-IN-CD ROD WORTH***

<u><i>2-Loop Plant, 121 Assemblies, 10-foot core</i></u>	<u><i>Measured (pcm)</i></u>	<u><i>Calculated (pcm)</i></u>
<i>Group B</i>	<i>1885</i>	<i>1893</i>
<i>Group A</i>	<i>1530</i>	<i>1649</i>
<i>Shutdown group</i>	<i>3050</i>	<i>2917</i>
 <i>ESADA Critical^(a), 0.69" Pitch, 2 w/o PuO₂, 8% Pu²⁴⁰, 9 Control Rods</i>		
<i>6.21" rod separation</i>	<i>2250</i>	<i>2250</i>
<i>2.07" rod separation</i>	<i>4220</i>	<i>4160</i>
<i>1.38" rod separation</i>	<i>4100</i>	<i>4010</i>

a. Reported in reference 36.]

TABLE 4.3-11

**COMPARISON OF MEASURED AND CALCULATED MODERATOR
COEFFICIENTS AT HZP, BOL**

<u>Plant Type/ Control Bank Configuration</u>	<u>Measured $\alpha_{iso}^{(a)}$ (pcm/°F)</u>	<u>Calculated $\alpha_{iso}^{(a)}$ (pcm/°F)</u>
3-loop, 157 assemblies, 12-foot core		
D at 160 steps	- 0.50	- 0.50
D in, C at 190 steps	- 3.01	- 2.75
D in, C at 28 steps	- 7.67	- 7.02
B, C, and D in	- 5.16	- 4.45
2-loop, 121 assemblies, 12-foot core		
D at 180 steps	+ 0.85	+ 1.02
D in, C at 180 steps	- 2.40	- 1.90
C and D in, B at 165 steps	- 4.40	- 5.58
B, C, and D in, A at 174 steps	- 8.70	- 8.12
4-loop, 193 assemblies, 12-foot core		
ARO	- 0.52	- 1.2
D in	- 4.35	- 5.7
D and C in	- 8.59	-10.0
D, C, and B in	-10.14	-10.55
D, C, B, and A in	-14.63	-14.45

a. Isothermal coefficients, which include the Doppler effect in the fuel.

$$\alpha_{iso} = 10^5 \ln \frac{k_2}{k_1} / \Delta T^{\circ}F$$

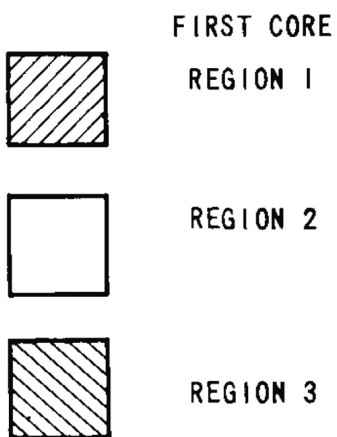
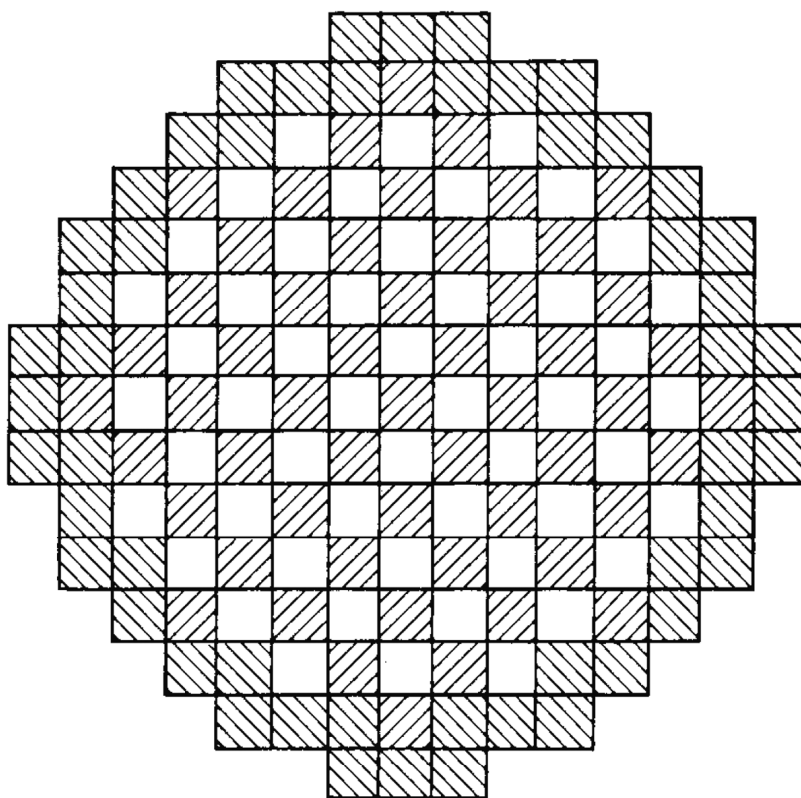
TABLE 4.3-12**95/95 K_{eff} FOR SPENT FUEL RACK STORAGE CONFIGURATIONS**

<u>Configuration</u>	Nominal Enrichment <u>w/o U-235</u>	No Soluble Boron <u>95/95 K_{eff}</u>	Soluble Boron <u>Credit 95/95 K_{eff}</u>
All Cell	2.15	0.99201	0.93741
2-out-of-4 Checkerboard	5.0	0.94285	0.N/A*
Burned/Fresh Checkerboard	1.6/3.9	0.99415	0.94025

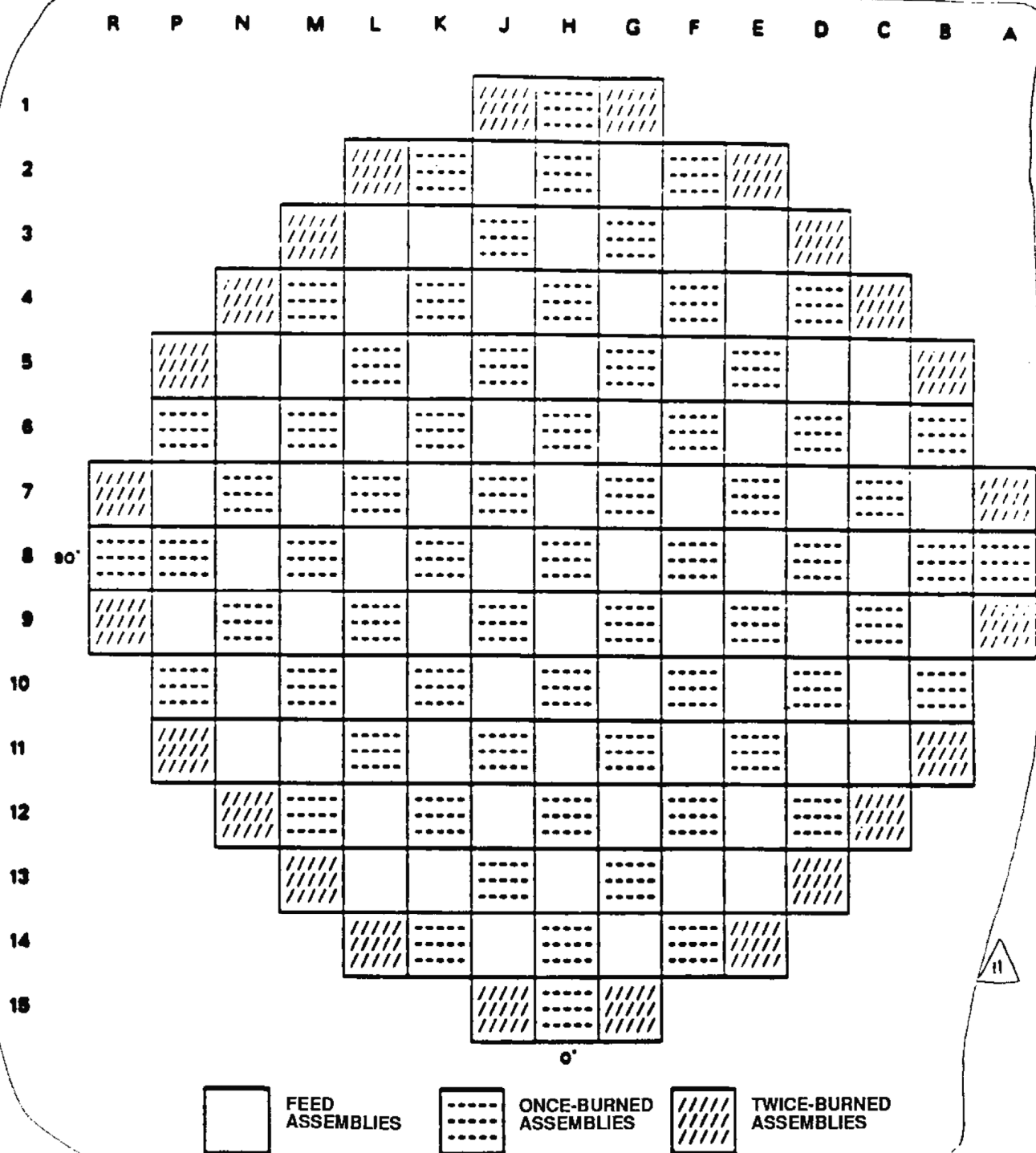
*No soluble boron credit is necessary for the 2-out-of-4 checkerboard to maintain $K_{eff} \leq 0.95$.

TABLE 4.3-13**95/95 K_{eff} FOR SPENT FUEL CASK LOADING OPERATIONS**

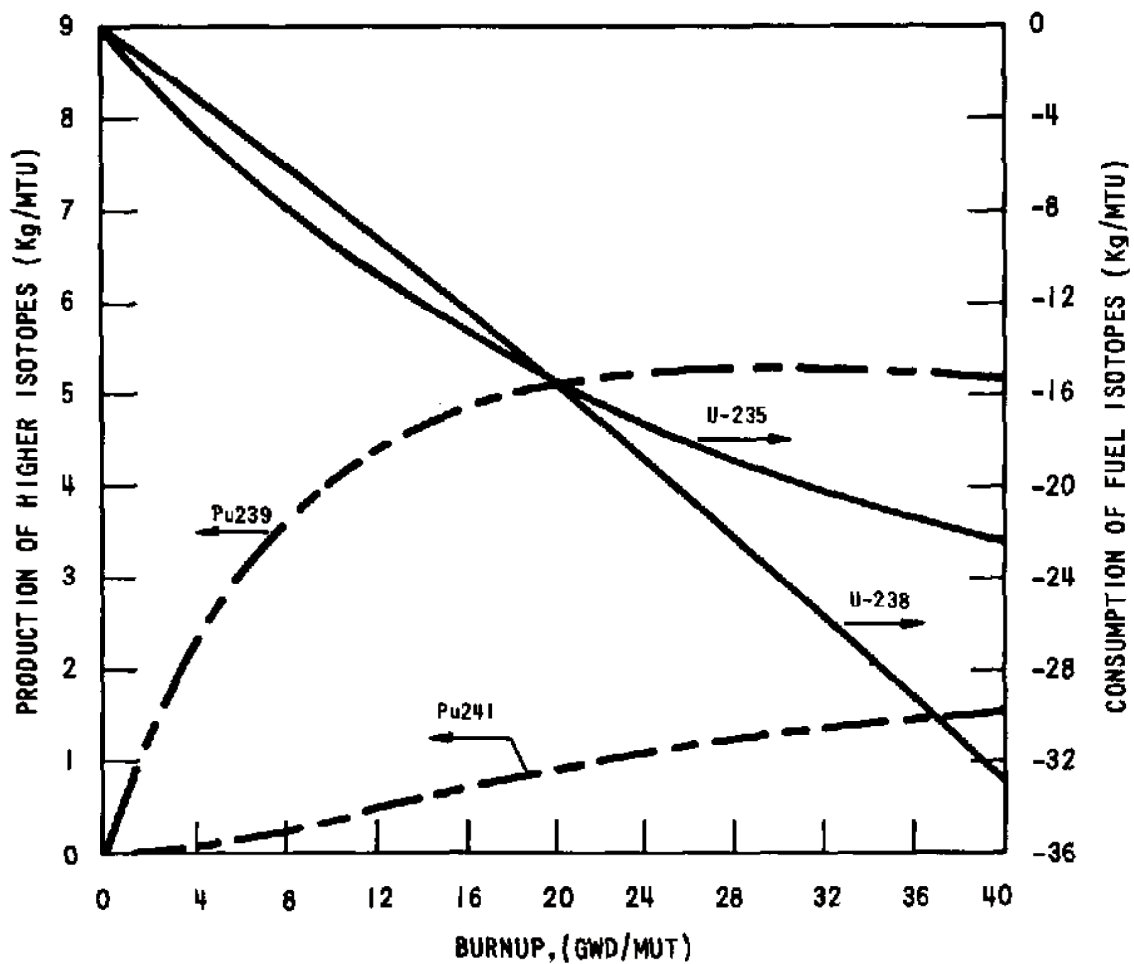
<u>Configuration</u>	Nominal Enrichment <u>w/o U-235</u>	No Soluble Boron <u>95/95 K_{eff}</u>	Soluble Boron <u>Credit 95/95 K_{eff}</u>
Cask Storage	2.09	0.970	0.945



REV 21 5/08



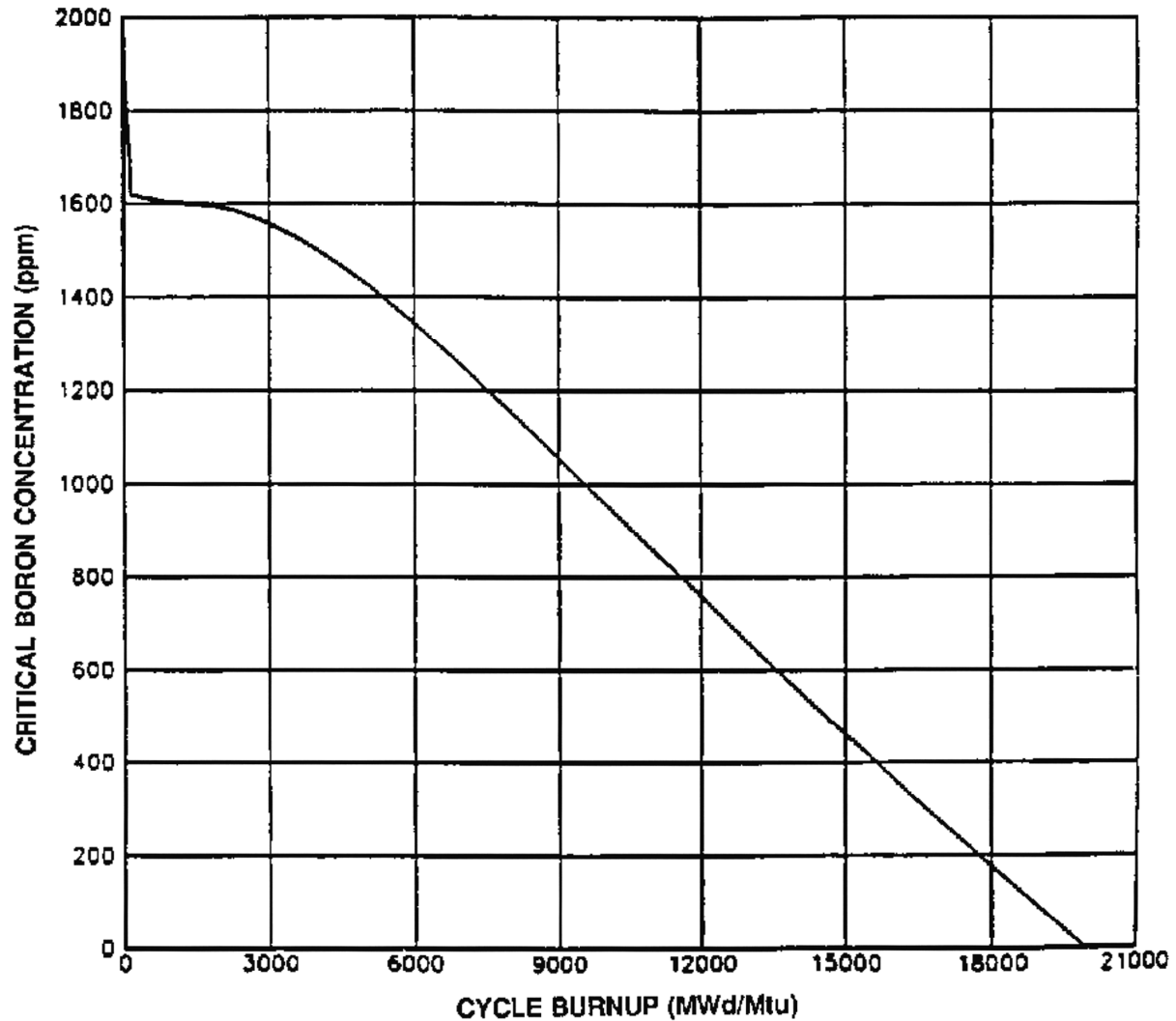
REV 21 5/08



15

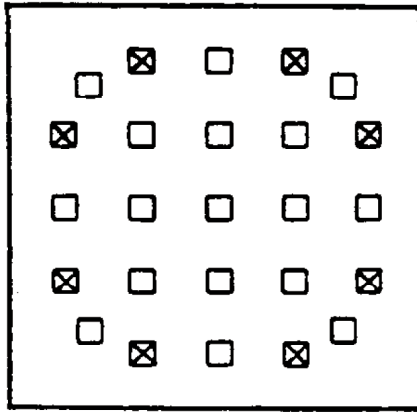
REV 21 5/08

NOTE: HOT FULL POWER ALL RODS OUT

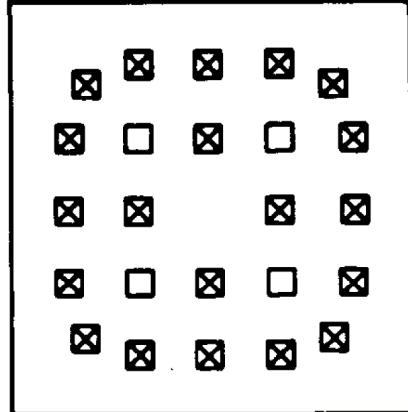


15

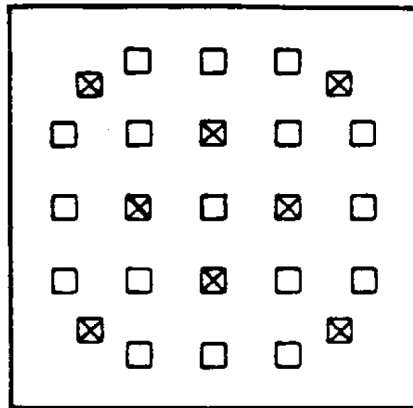
REV 21 5/08



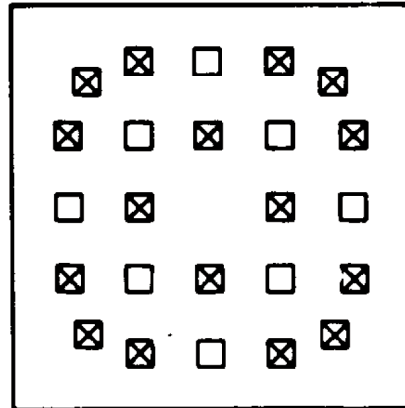
8 BA s



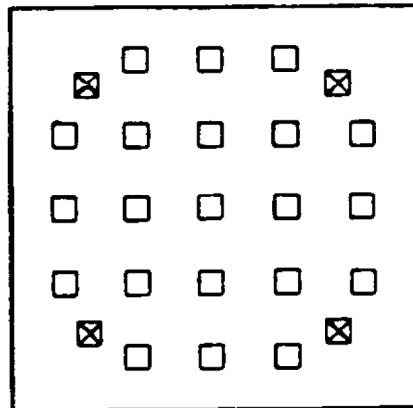
20 BA s



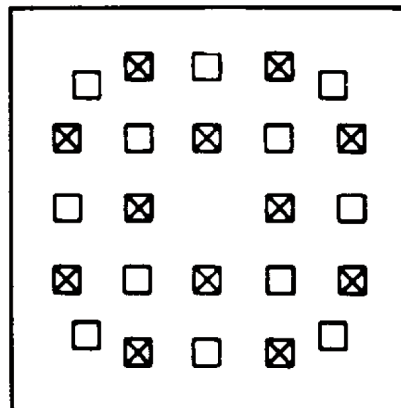
8 BA s



16 BA s

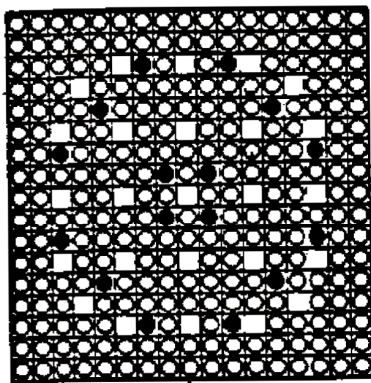


4 BA s

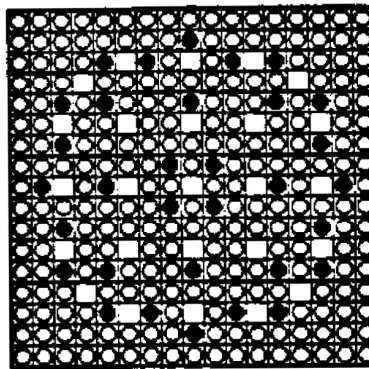


12 BA s

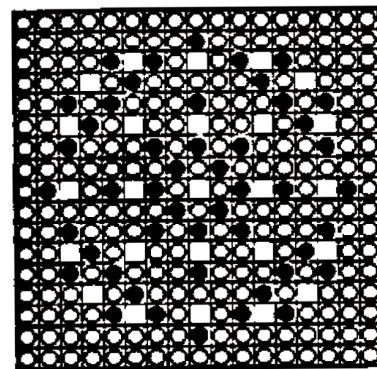
REV 21 5/08



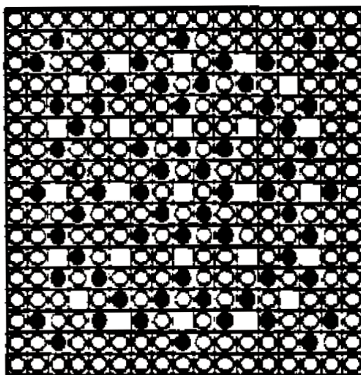
16 IFBA Rod Assembly



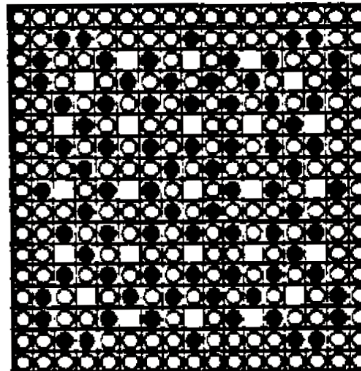
32 IFBA Rod Assembly



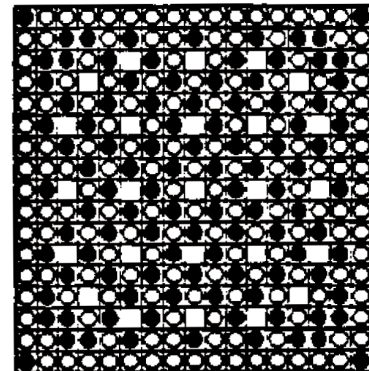
48 IFBA Rod Assembly



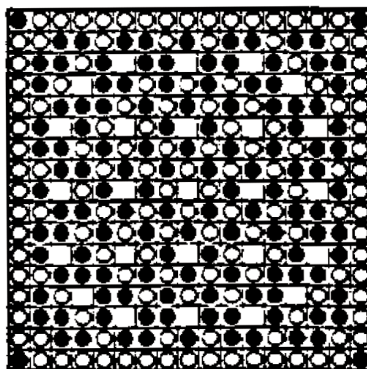
64 IFBA Rod Assembly



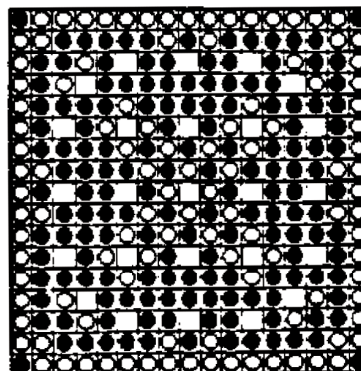
80 IFBA Rod Assembly



104 IFBA Rod Assembly



128 IFBA Rod Assembly



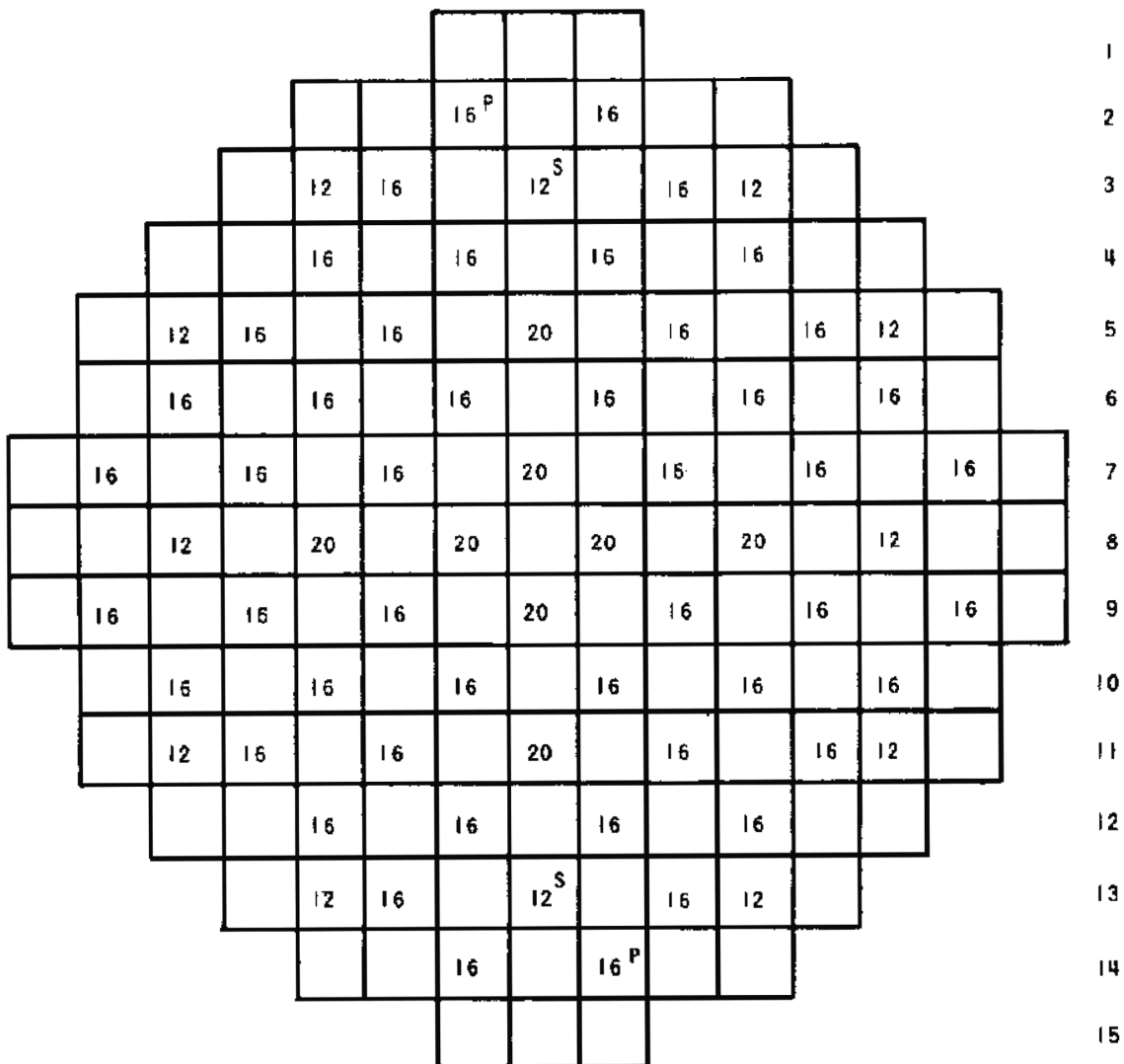
156 IFBA Rod Assembly

- Fuel Rod
- Fuel Rod with IFBA
- Guide Tube/Inst. Tube



REV 21 5/08

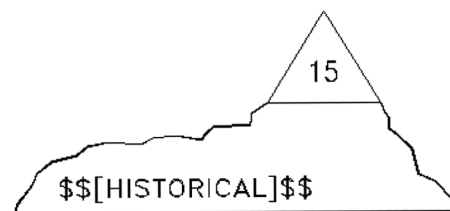
R P N M L K J H G F E D C B A



NUMBER INDICATES NUMBER OF BURNABLE ABSORBER RODS

S INDICATES SECONDARY SOURCE RODS

P INDICATES PRIMARY SOURCE RODS



REV 21 5/08

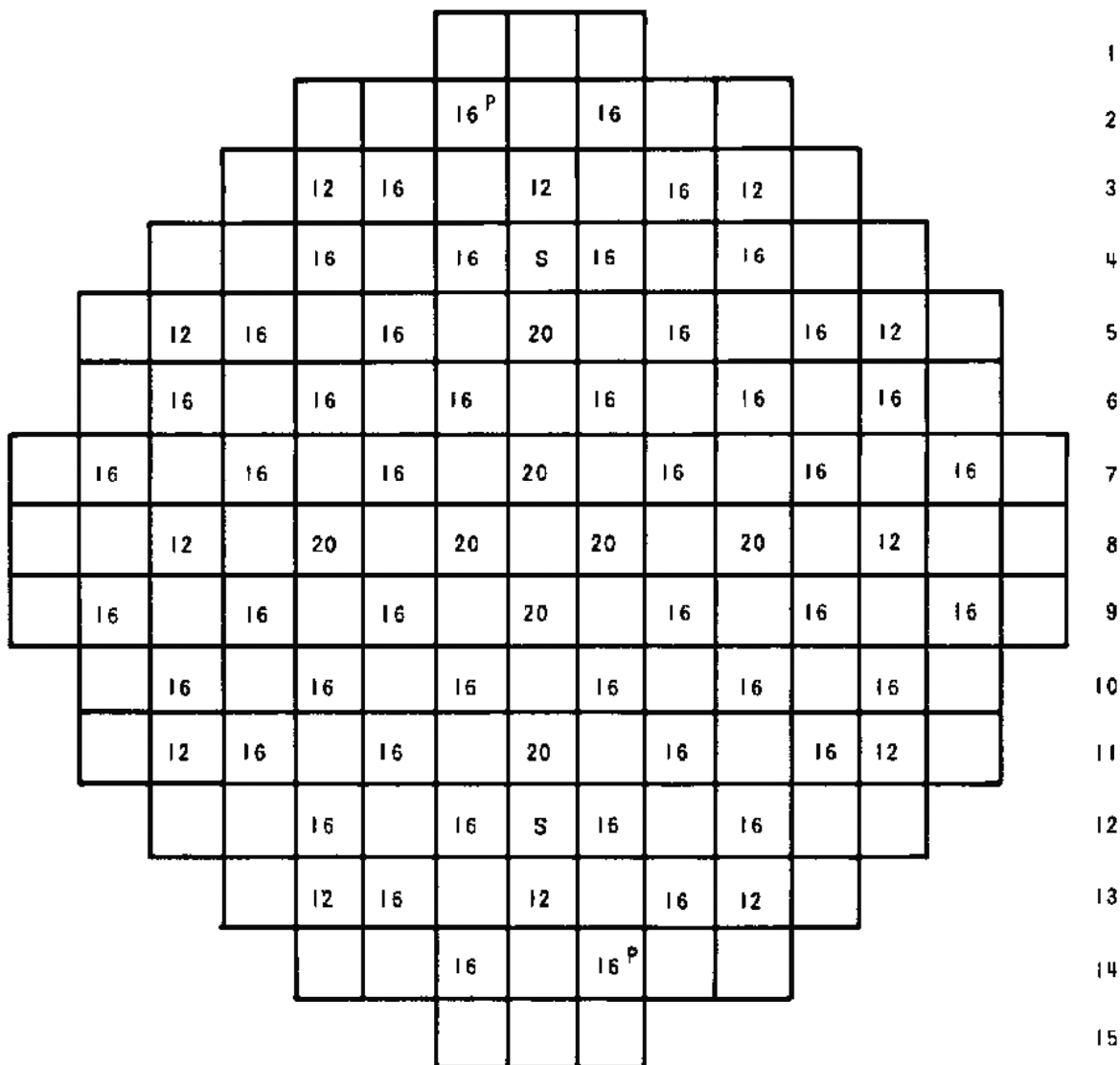


JOSEPH M. FARLEY
NUCLEAR PLANT
UNIT 1 AND UNIT 2

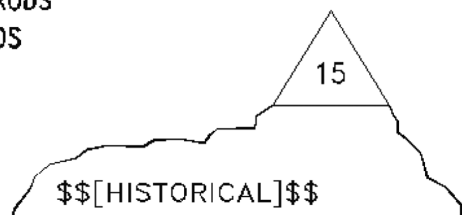
[UNIT 1 CYCLE 1
BURNABLE ABSORBER LOADING PATTERN

FIGURE 4.3-5]

R P N M L K J H G F E D C B A



NUMBER INDICATES NUMBER OF BURNABLE ABSORBER RODS
 S INDICATES SECONDARY SOURCE RODS
 P INDICATES PRIMARY SOURCE RODS



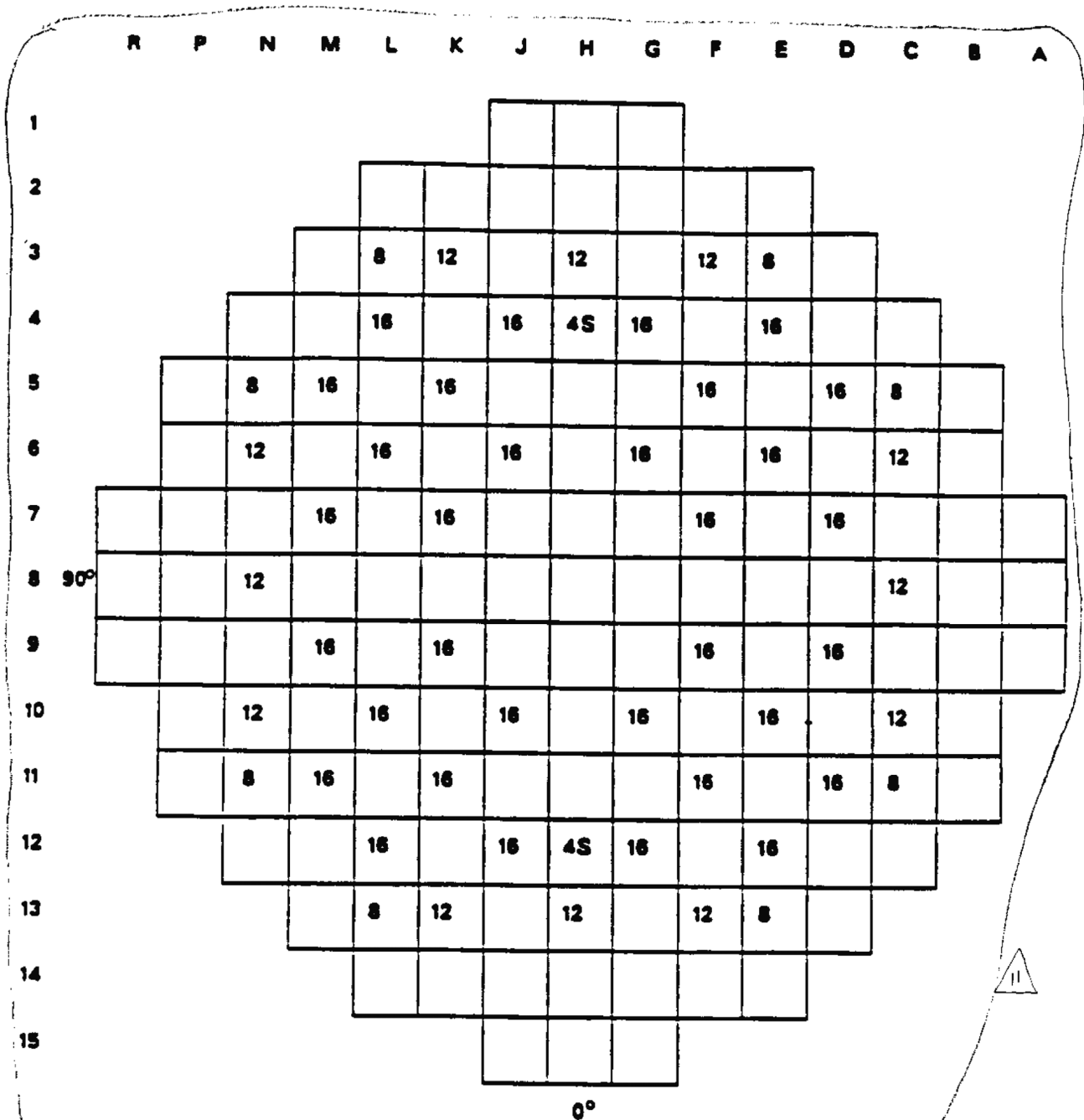
REV 21 5/08



JOSEPH M. FARLEY
 NUCLEAR PLANT
 UNIT 1 AND UNIT 2

UNIT 2 CYCLE 1 BURNABLE ABSORBER
 LOADING PATTERN

FIGURE 4.3-6 (SHEET 1 OF 3)



#S

Number of Discrete BA's
Number of Secondary Source Rods

REV 21 5/08

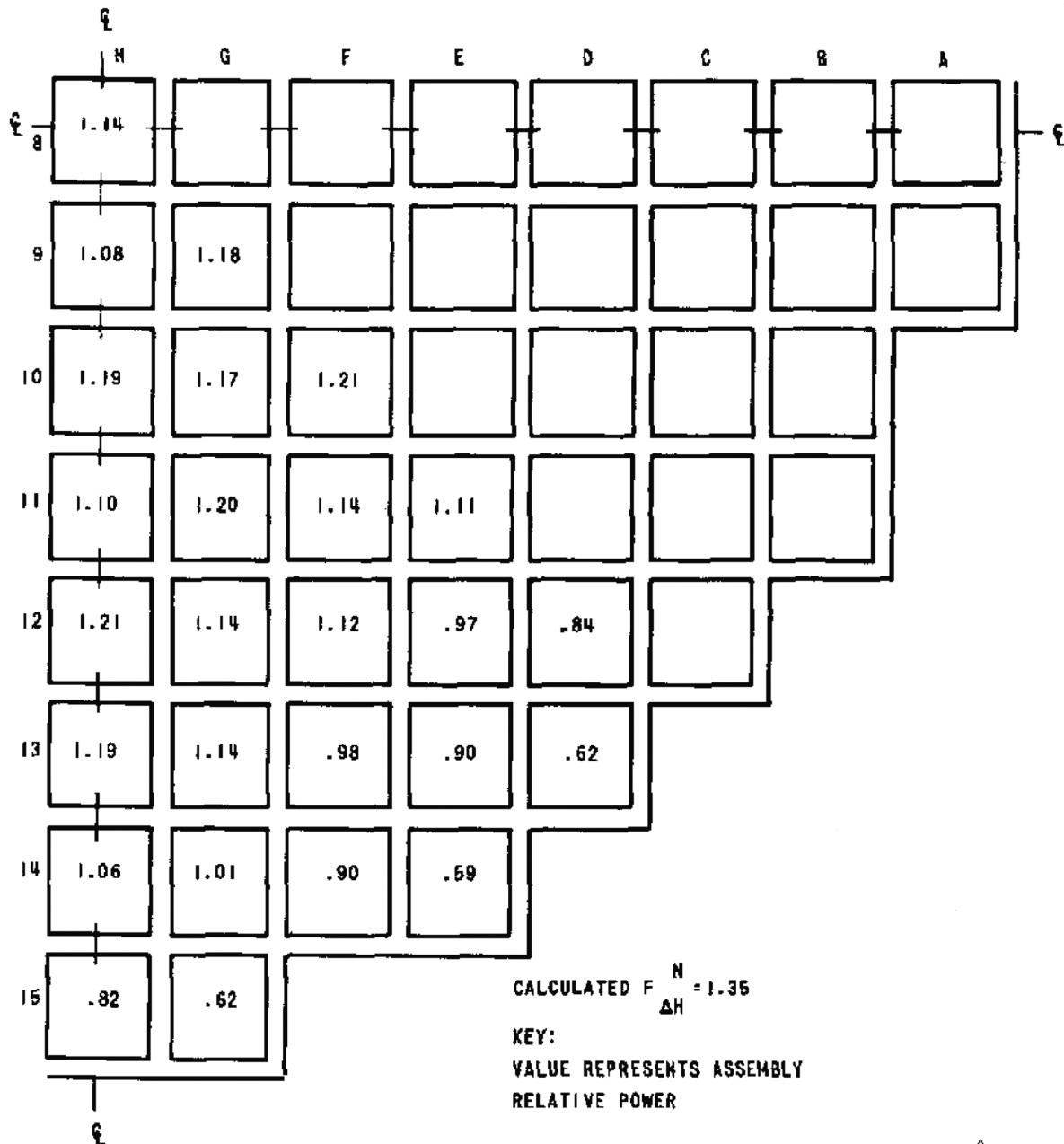
R P N M L K J H G F E D C B A

1
2
3
4
5
6
7
8
9
10
11
12
13
14
15

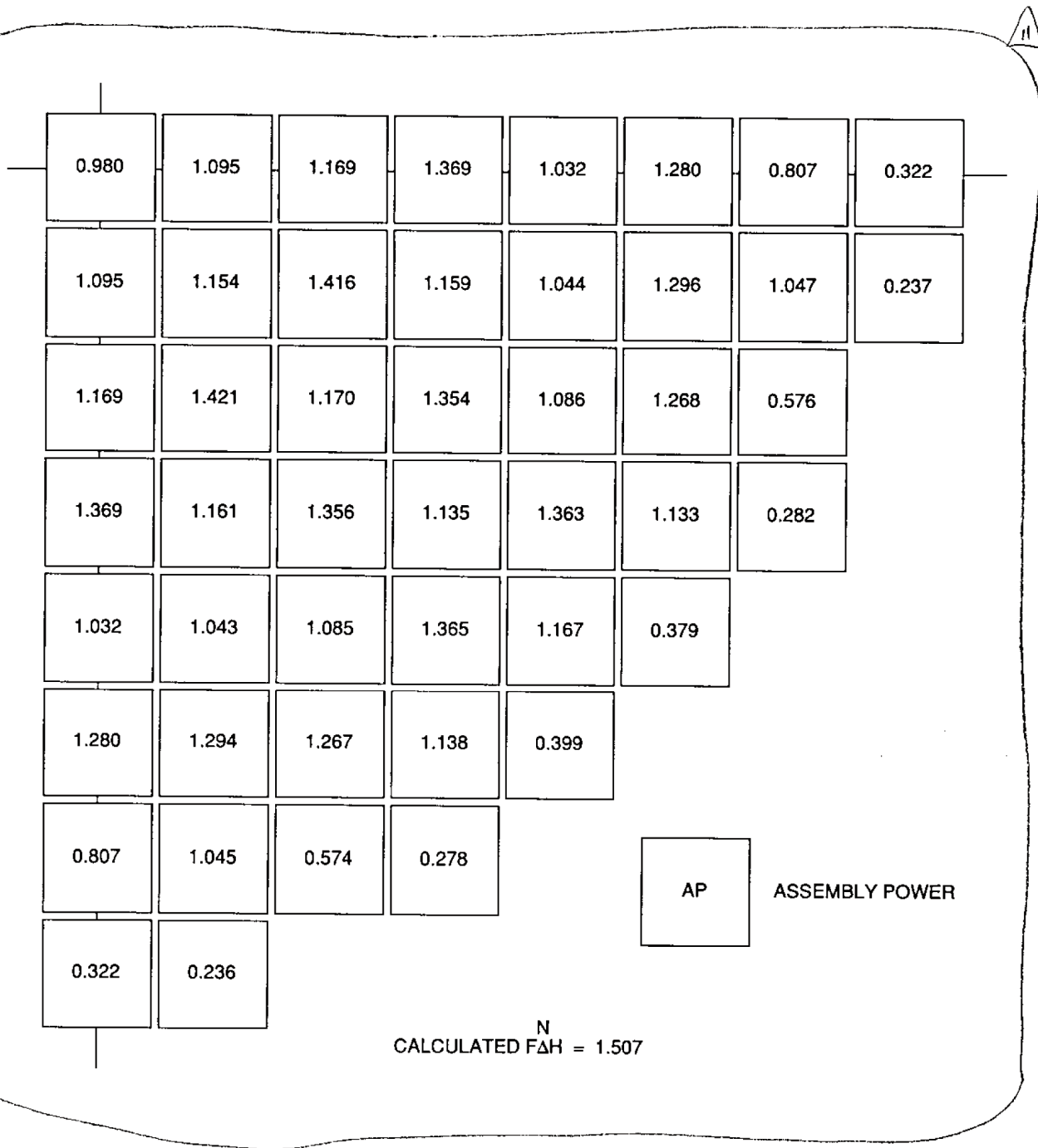
				32		32								
		32	104	104	104	104	104	32						
		32	128			4S			128	32				
	32	128		104		128		104		128	32			
	104		104		128		128		104		104			
	32	104			128			128			104	32		
		104		128					128		104			
	32	104			128			128			104	32		
	104		104		128		128		104		104			
	32	128		104		128		104		128	32			
		32	128			4S			128	32				
		32	104	104	104	104	104	32						
				32		32								

Number of IFBA
#S Number of Secondary Source Rods

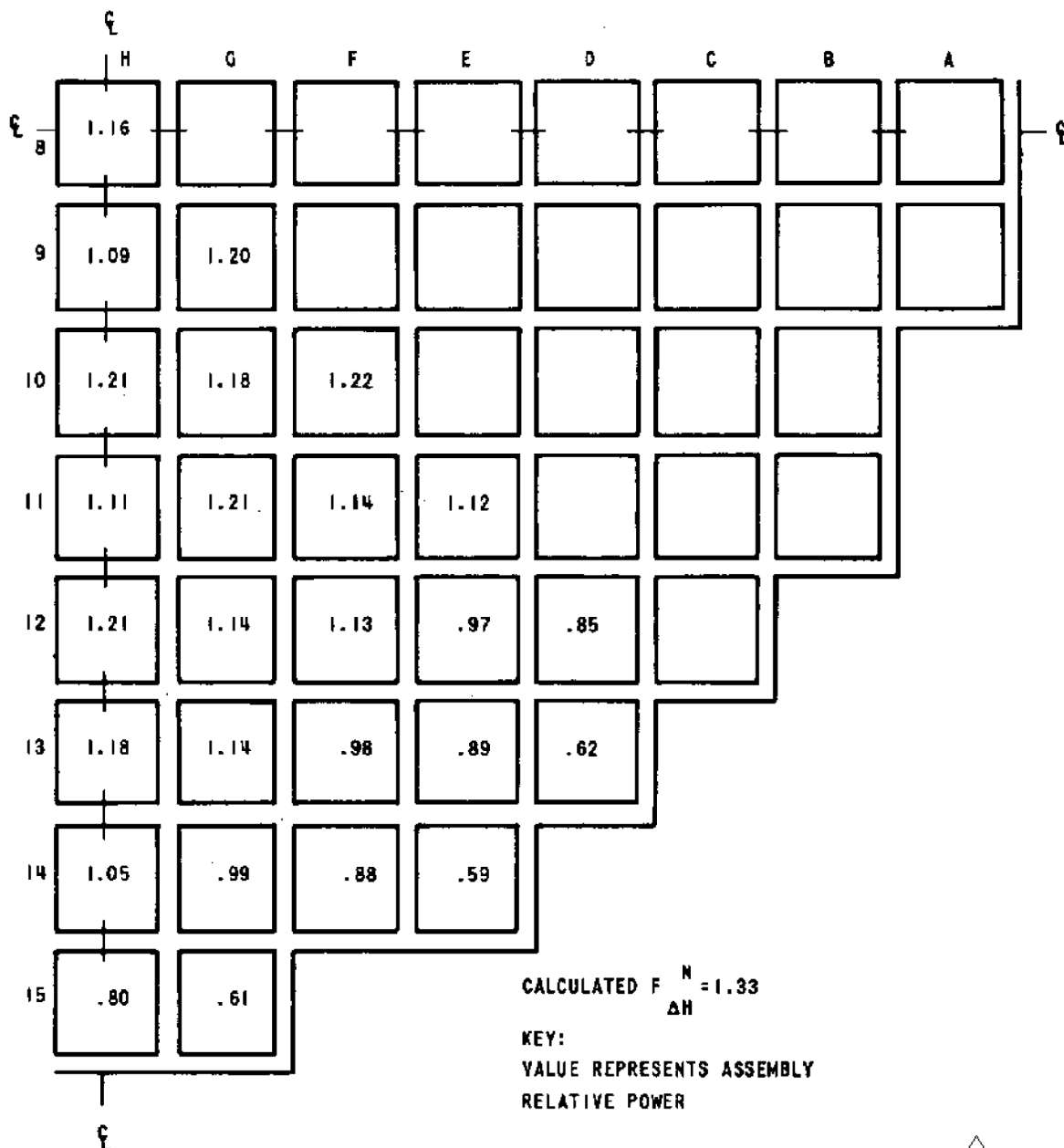
REV 21 5/08



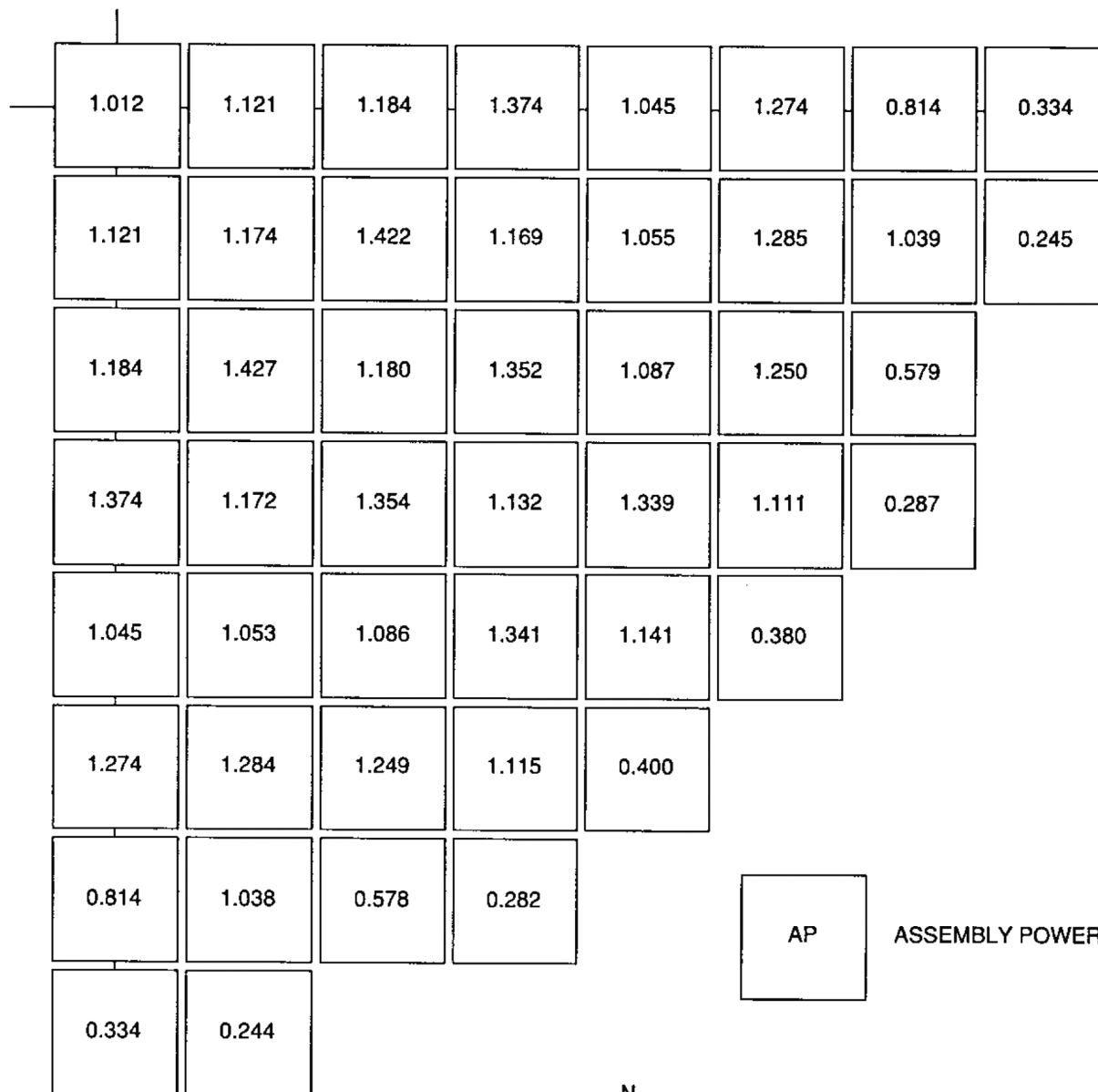
REV 21 5/08



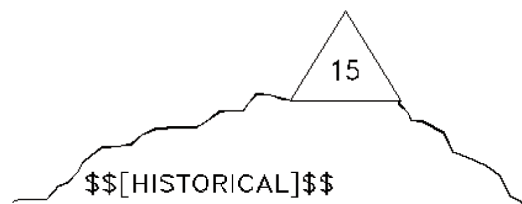
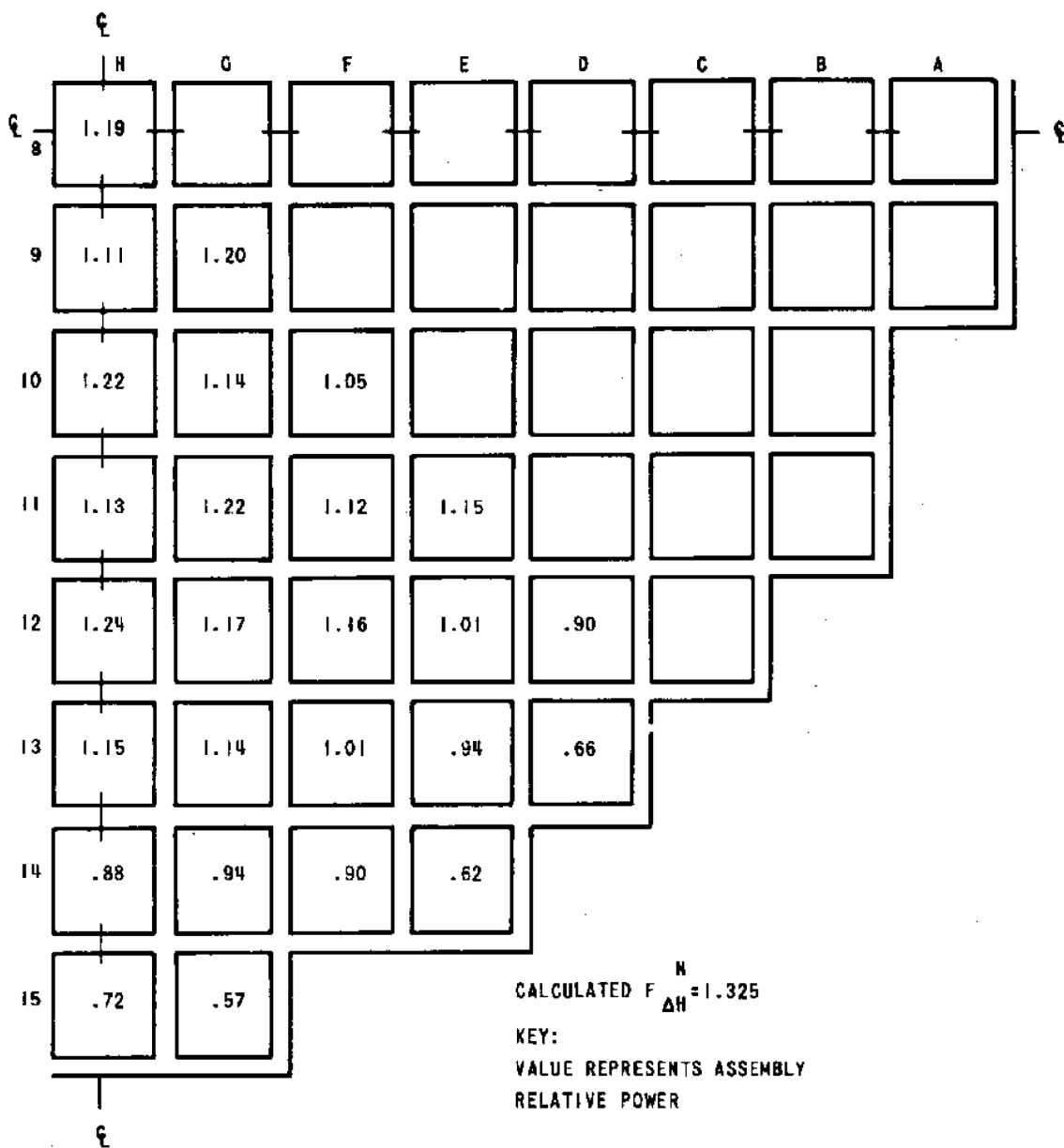
REV 21 5/08



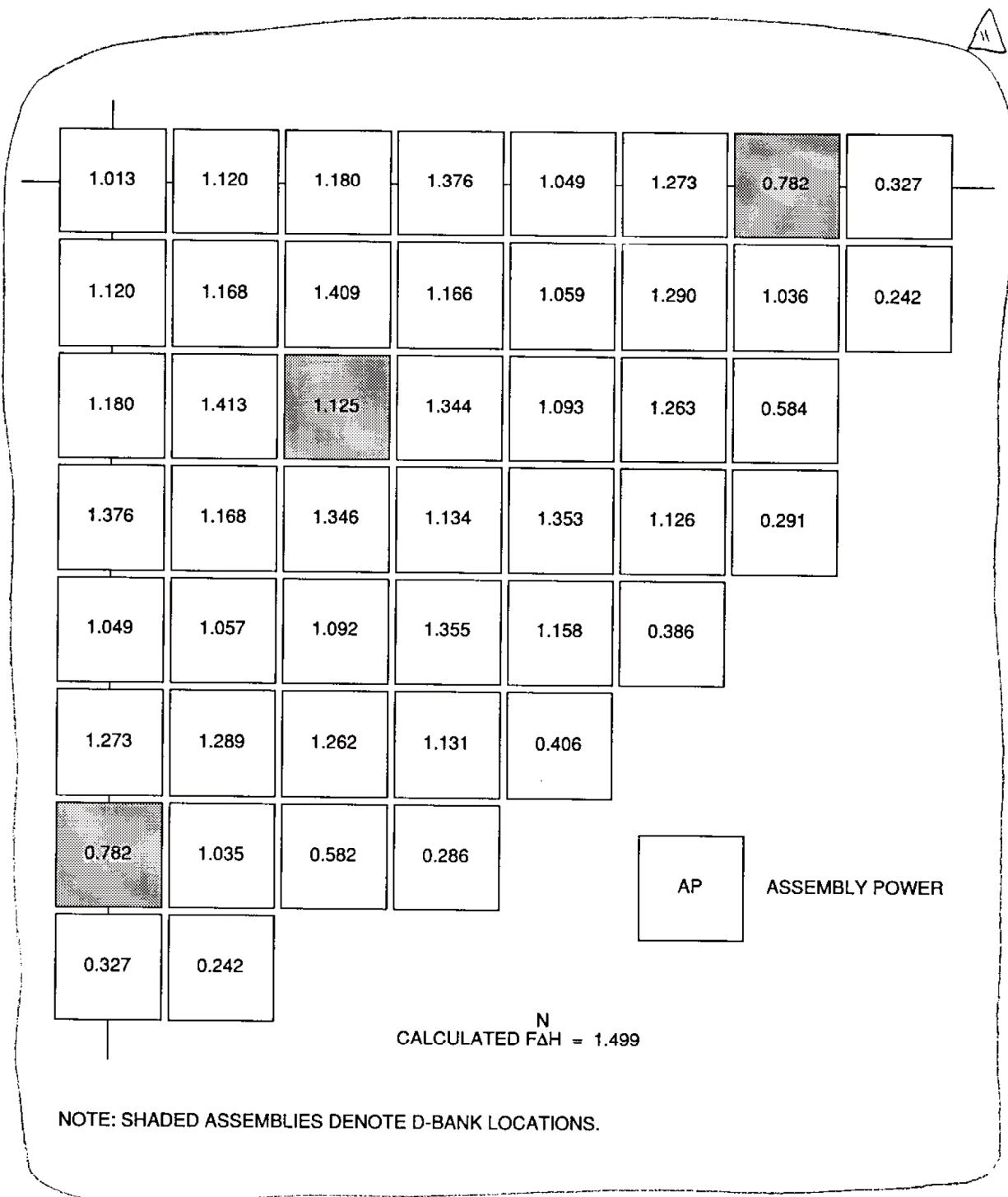
REV 21 5/08



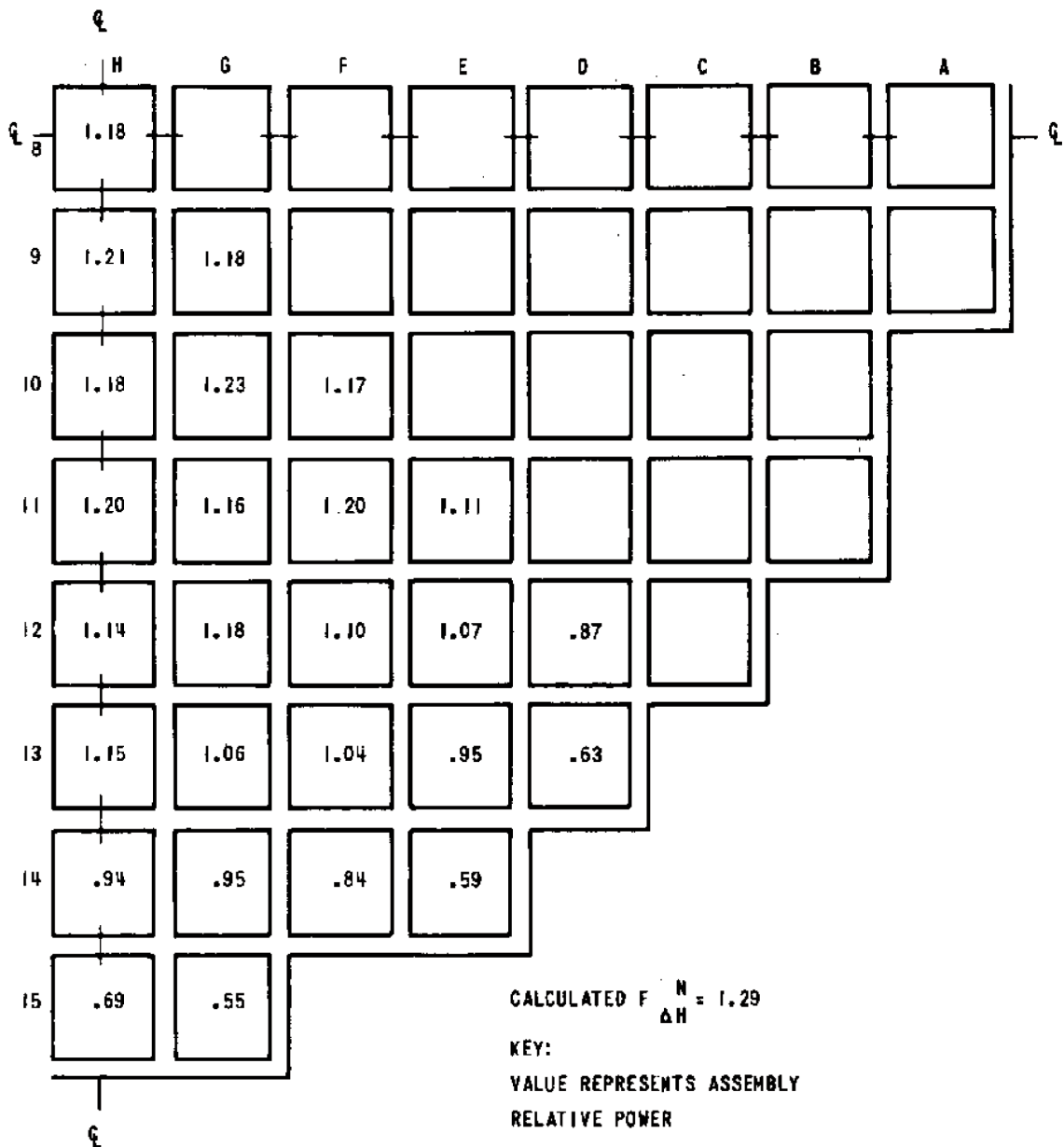
REV 21 5/08



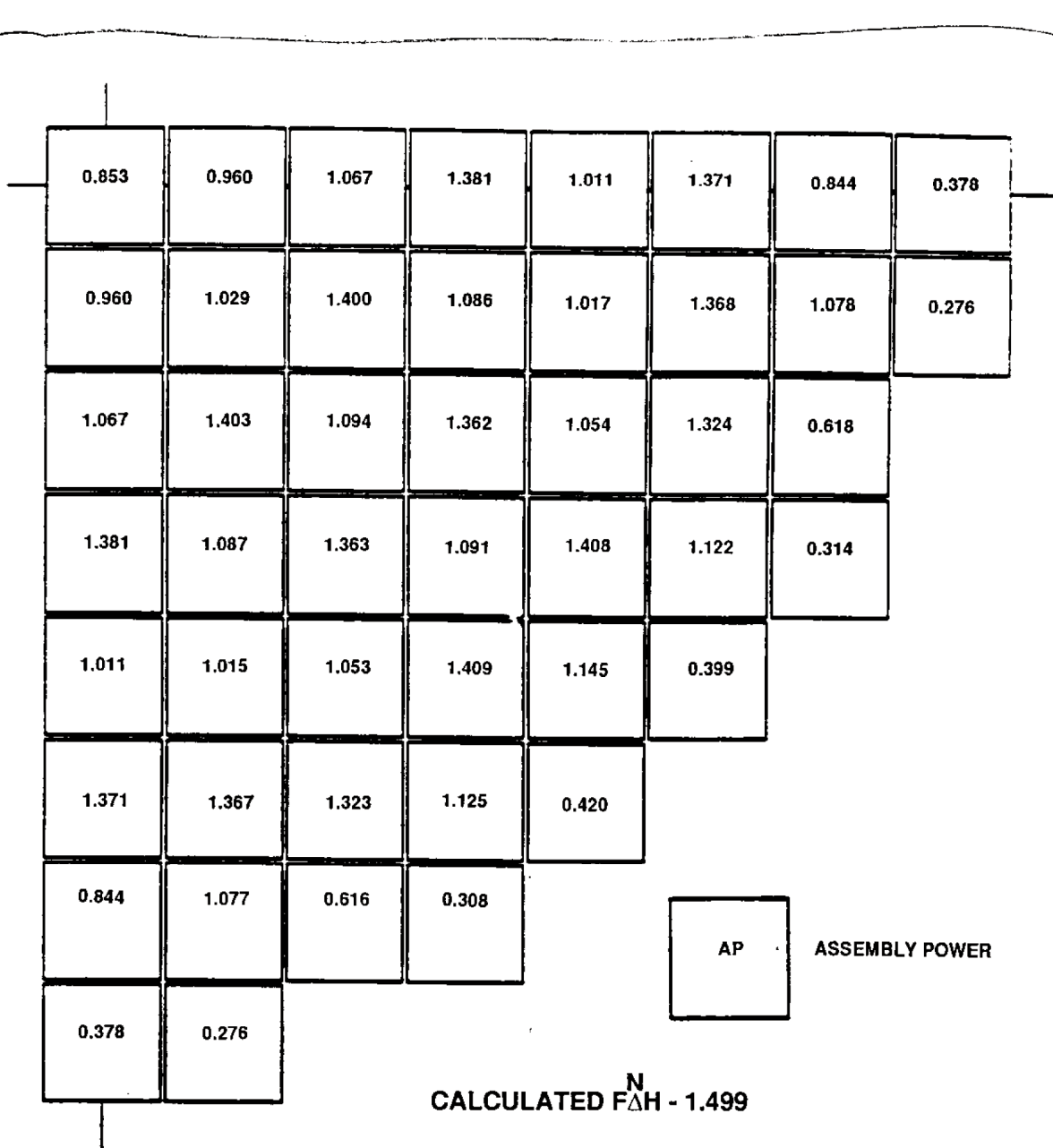
REV 21 5/08



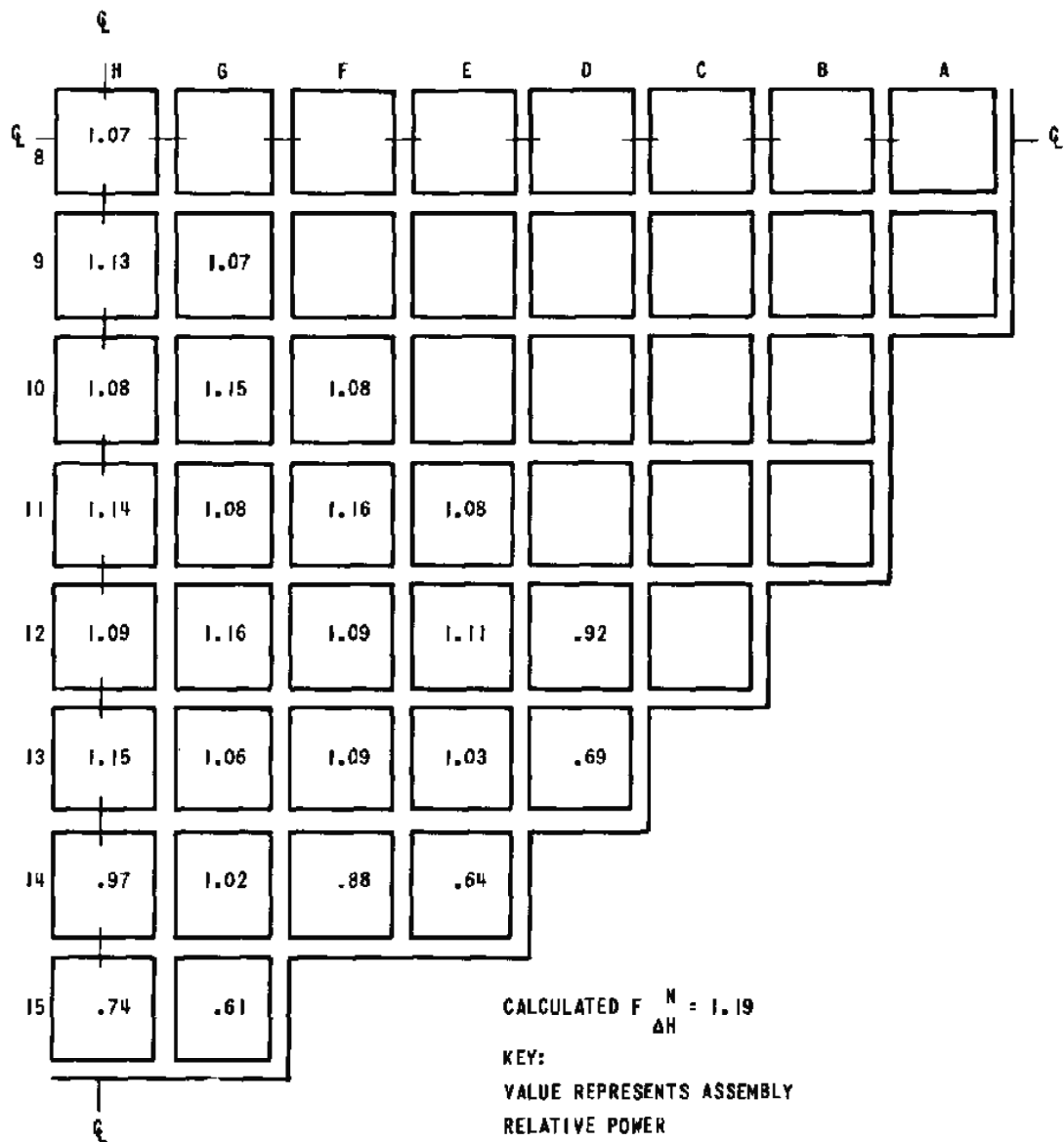
REV 21 5/08



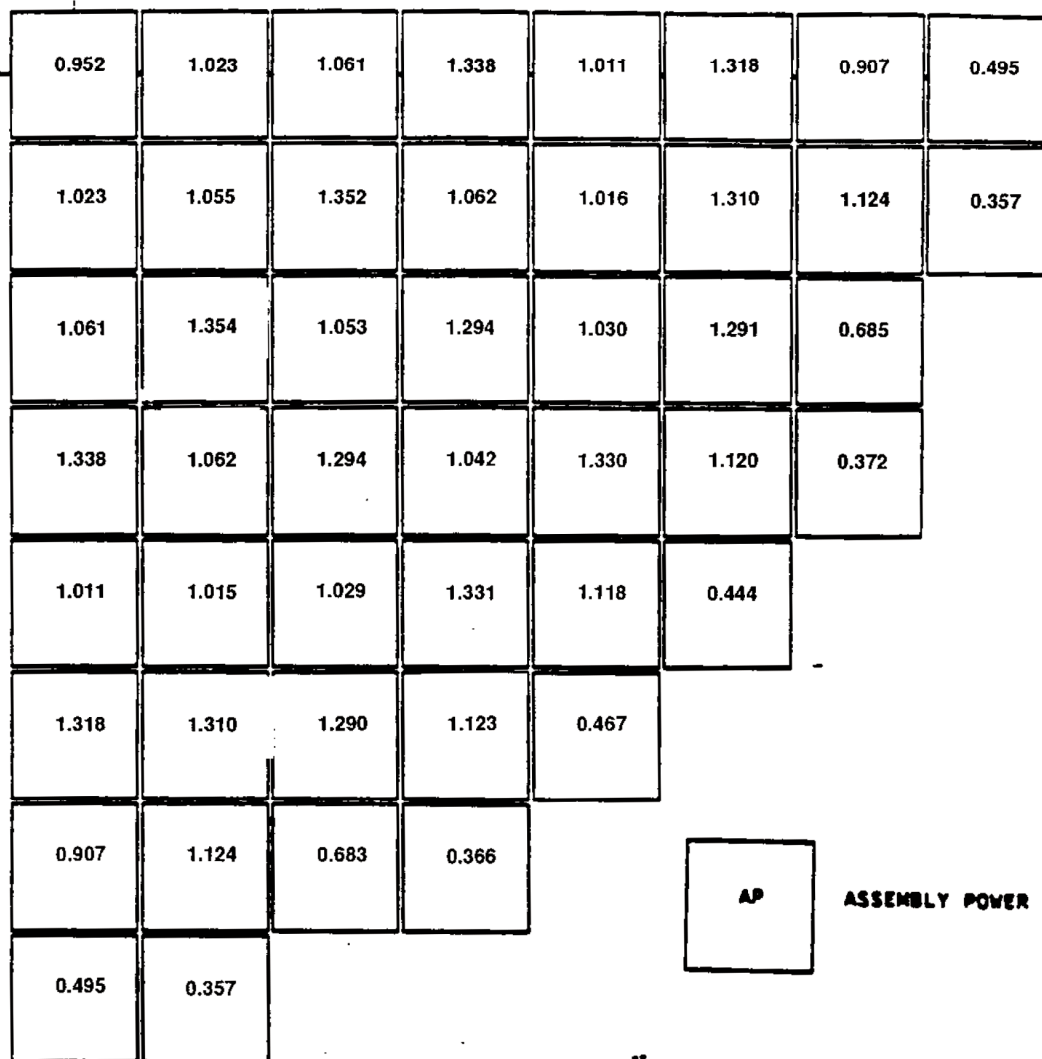
REV 21 5/08



REV 21 5/08



REV 21 5/08



CALCULATED F_{AH}^N = 1.399

REV 21 5/08

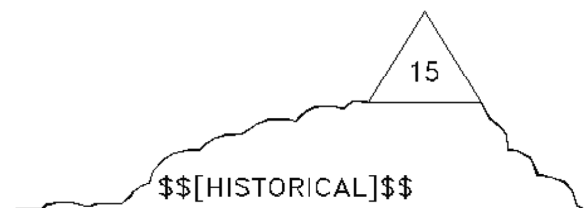


FIGURE 4.3-12 (SHEET 1 OF 2)

11

1.32	1.35	1.35	1.36	1.38	1.39	1.39	1.38	1.37	1.37	1.36	1.34	1.32	1.29	1.27	1.25	1.22
1.36	1.32	1.27	1.29	1.37	1.35	1.38	1.39	1.35	1.37	1.35	1.31	1.31	1.22	1.19	1.22	1.25
1.36	1.27	1.29	1.40	1.38	X	1.36	1.42	X	1.40	1.34	X	1.33	1.34	1.22	1.19	1.26
1.37	1.30	1.41	X	1.45	1.38	1.38	1.33	1.40	1.32	1.35	1.34	1.40	X	1.33	1.22	1.28
1.40	1.38	1.39	1.46	1.38	1.44	1.34	1.37	1.34	1.36	1.32	1.40	1.34	1.40	1.32	1.30	1.31
1.41	1.37	X	1.39	1.44	X	1.42	1.35	X	1.35	1.40	X	1.40	1.33	X	1.30	1.32
1.41	1.40	1.38	1.39	1.34	1.42	1.33	1.37	1.35	1.36	1.32	1.40	1.31	1.34	1.32	1.34	1.34
1.42	1.41	1.44	1.34	1.38	1.36	1.37	1.33	1.40	1.32	1.36	1.34	1.35	1.30	1.38	1.35	1.34
1.41	1.38	X	1.42	1.36	X	1.35	1.41	X	1.40	1.34	X	1.33	1.38	X	1.32	1.34
1.41	1.41	1.43	1.34	1.38	1.36	1.37	1.33	1.40	1.32	1.36	1.34	1.35	1.30	1.39	1.36	1.35
1.41	1.40	1.37	1.38	1.34	1.42	1.33	1.37	1.35	1.36	1.32	1.40	1.31	1.35	1.33	1.37	1.35
1.40	1.36	X	1.38	1.43	X	1.42	1.36	X	1.35	1.41	X	1.41	1.35	X	1.32	1.35
1.39	1.37	1.38	1.45	1.38	1.43	1.33	1.37	1.35	1.36	1.32	1.41	1.35	1.42	1.34	1.33	1.34
1.36	1.28	1.39	X	1.45	1.37	1.37	1.33	1.40	1.32	1.36	1.36	1.42	X	1.36	1.25	1.32
1.35	1.26	1.28	1.39	1.37	X	1.36	1.42	X	1.41	1.35	X	1.35	1.37	1.25	1.22	1.31
1.34	1.30	1.25	1.28	1.36	1.35	1.38	1.39	1.36	1.39	1.37	1.34	1.34	1.26	1.23	1.27	1.30
1.31	1.32	1.34	1.35	1.38	1.39	1.39	1.39	1.38	1.39	1.38	1.37	1.36	1.33	1.32	1.31	1.27

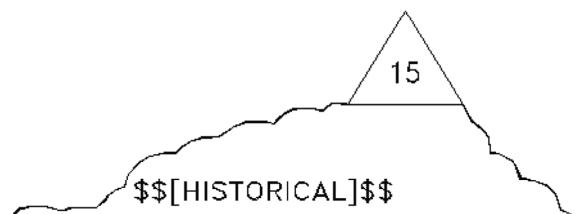
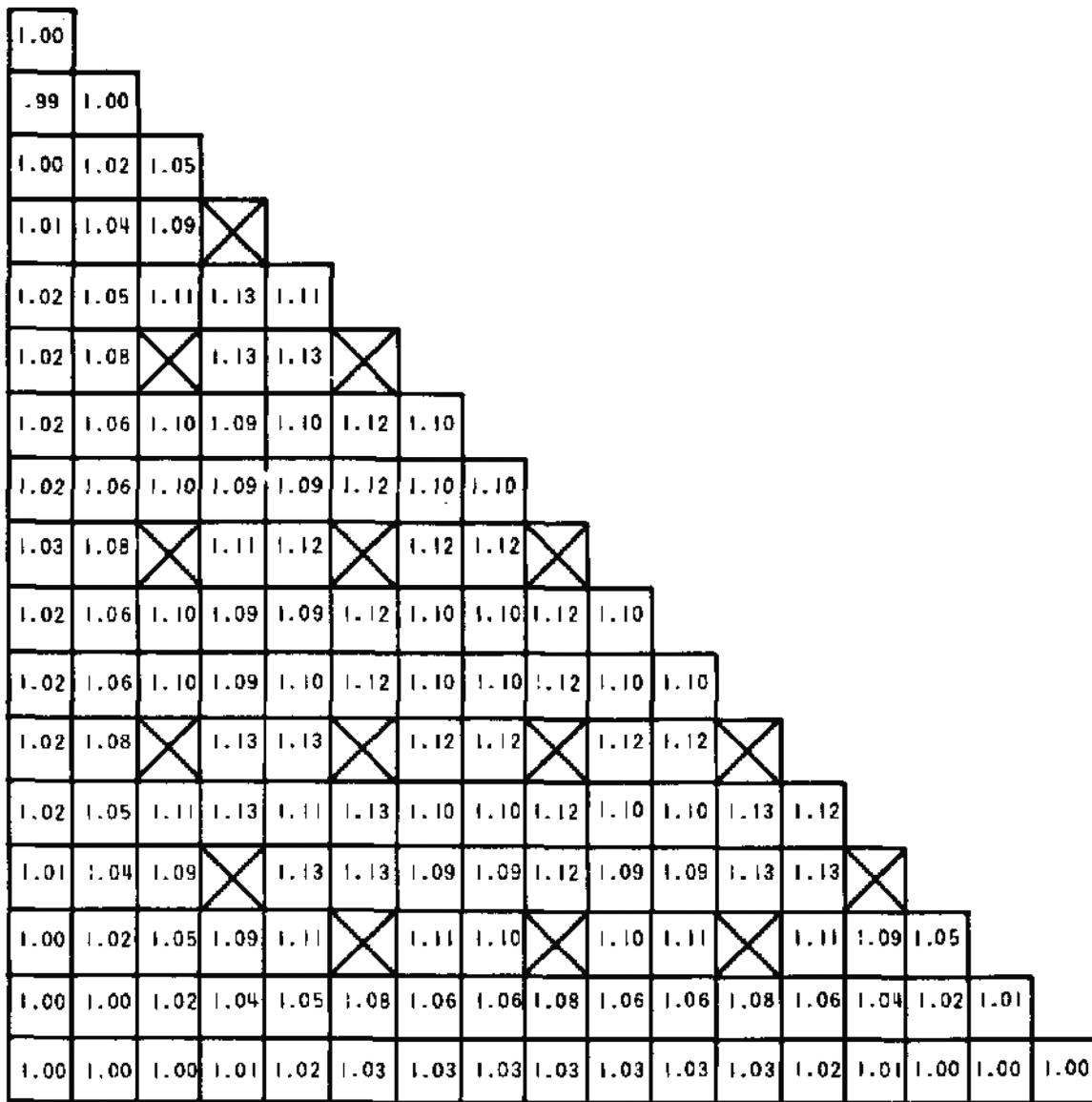
REV 21 5/08



JOSEPH M. FARLEY
NUCLEAR PLANT
UNIT 1 AND UNIT 2

TYPICAL RELOAD RODWISE POWER DISTRIBUTION IN A
TYPICAL ASSEMBLY (ASSEMBLY E-10) NEAR BEGINNING
OF LIFE, HOT FULL POWER, EQUILIBRIUM XENON,
UNRODDED CORE

FIGURE 4.3-12 (SHEET 2 OF 2)



REV 21 5/08



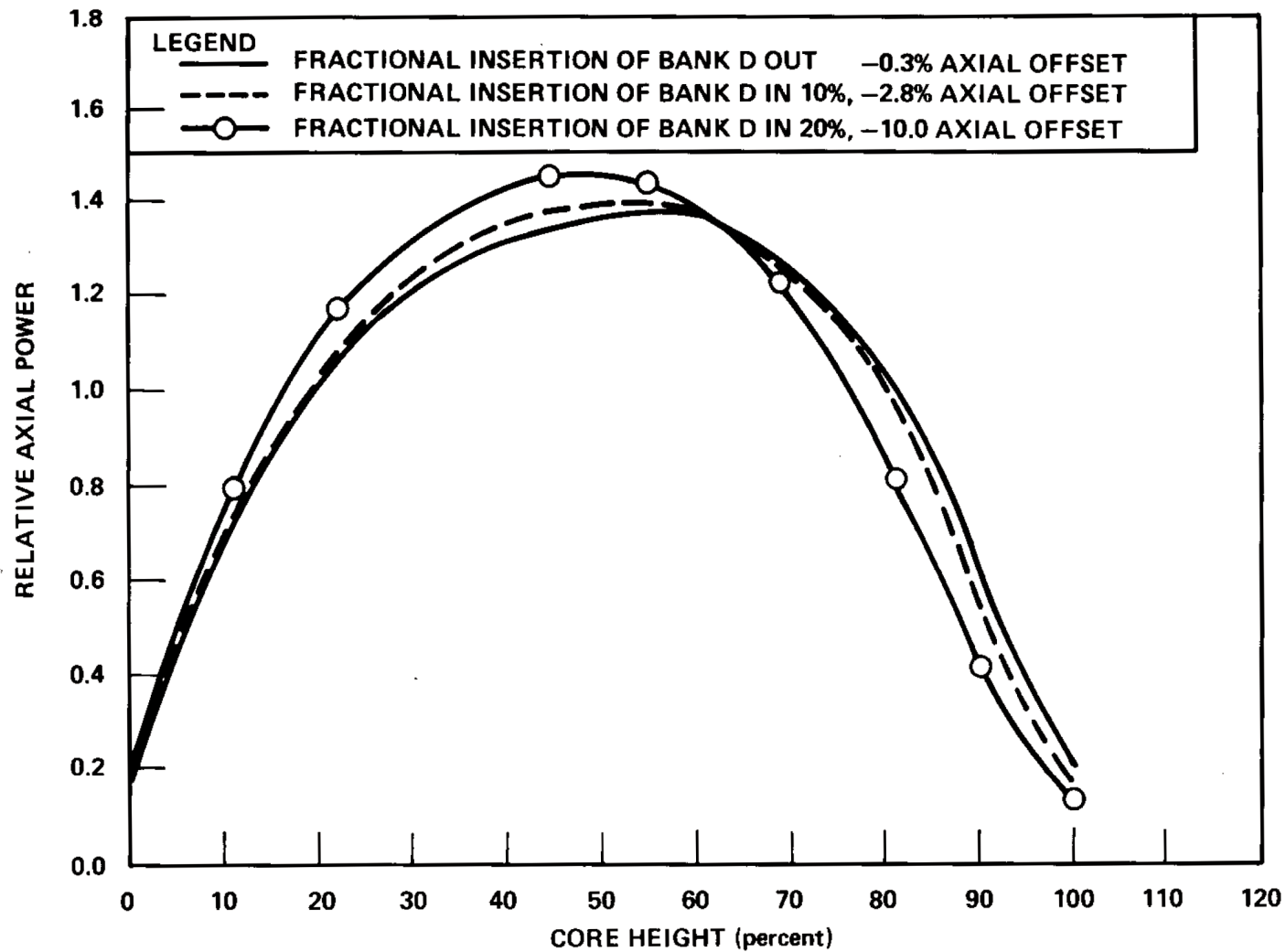
JOSEPH M. FARLEY
NUCLEAR PLANT
UNIT 1 AND UNIT 2

[CYCLE 1 RODWISE POWER DISTRIBUTION IN A TYPICAL
ASSEMBLY (ASSEMBLY G-9) NEAR END OF LIFE,
HOT FULL POWER, EQUILIBRIUM XENON,
UNRODDED CORE

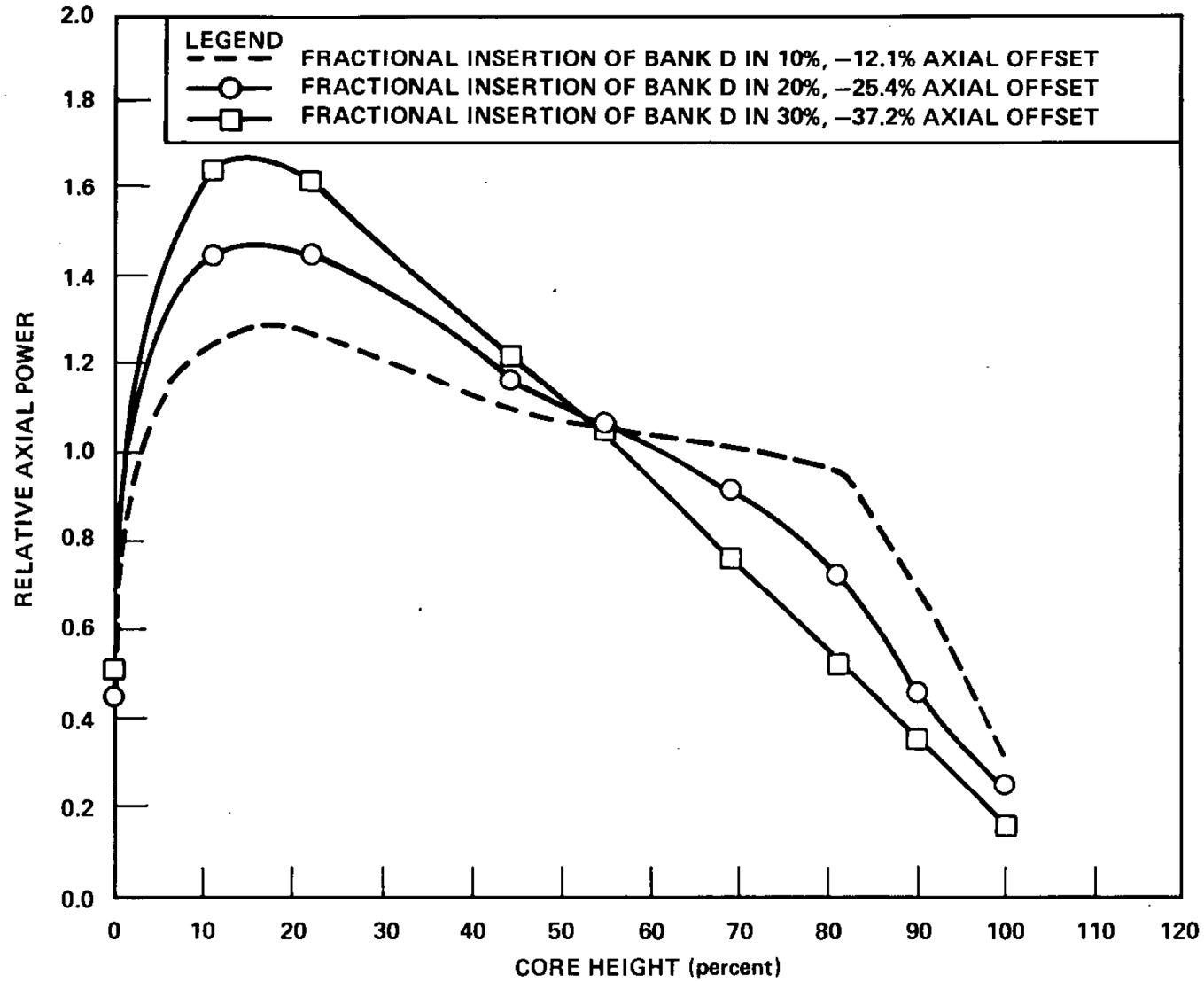
FIGURE 4.3-13 (SHEET 1 OF 2)]

1.30	1.28	1.28	1.28	1.29	1.30	1.29	1.28	1.28	1.29	1.28	1.28	1.27	1.25	1.24	1.23	1.25
1.28	1.24	1.25	1.27	1.28	1.31	1.28	1.27	1.29	1.27	1.27	1.29	1.25	1.23	1.21	1.19	1.23
1.28	1.26	1.27	1.30	1.32	X	1.31	1.30	X	1.30	1.30	X	1.30	1.27	1.23	1.21	1.23
1.29	1.27	1.31	X	1.33	1.33	1.29	1.29	1.31	1.29	1.28	1.31	1.31	X	1.27	1.23	1.25
1.30	1.28	1.33	1.33	1.32	1.33	1.30	1.29	1.31	1.29	1.29	1.31	1.30	1.31	1.30	1.25	1.26
1.31	1.32	X	1.34	1.33	X	1.32	1.32	X	1.32	1.32	X	1.31	1.31	X	1.29	1.27
1.31	1.29	1.32	1.30	1.31	1.33	1.30	1.30	1.32	1.30	1.30	1.32	1.29	1.28	1.30	1.26	1.27
1.31	1.29	1.32	1.30	1.30	1.33	1.30	1.30	1.32	1.30	1.30	1.32	1.29	1.29	1.30	1.27	1.28
1.30	1.31	X	1.32	1.32	X	1.33	1.32	X	1.32	1.32	X	1.31	1.30	X	1.29	1.28
1.31	1.29	1.32	1.30	1.30	1.33	1.30	1.30	1.32	1.30	1.30	1.32	1.29	1.28	1.30	1.27	1.28
1.31	1.29	1.32	1.30	1.30	1.33	1.30	1.30	1.33	1.30	1.30	1.32	1.29	1.29	1.31	1.27	1.29
1.31	1.31	X	1.33	1.33	X	1.33	1.33	X	1.33	1.32	X	1.32	1.32	X	1.30	1.29
1.30	1.28	1.33	1.33	1.32	1.33	1.30	1.30	1.32	1.30	1.30	1.33	1.31	1.32	1.32	1.27	1.29
1.29	1.27	1.30	X	1.33	1.33	1.30	1.30	1.31	1.30	1.30	1.33	1.33	X	1.30	1.26	1.28
1.28	1.25	1.26	1.30	1.32	X	1.32	1.31	X	1.31	1.32	X	1.32	1.30	1.26	1.25	1.27
1.27	1.24	1.25	1.26	1.28	1.31	1.28	1.28	1.31	1.28	1.28	1.31	1.28	1.26	1.25	1.23	1.27
1.30	1.27	1.28	1.28	1.30	1.30	1.30	1.30	1.29	1.30	1.30	1.30	1.30	1.28	1.28	1.27	1.30

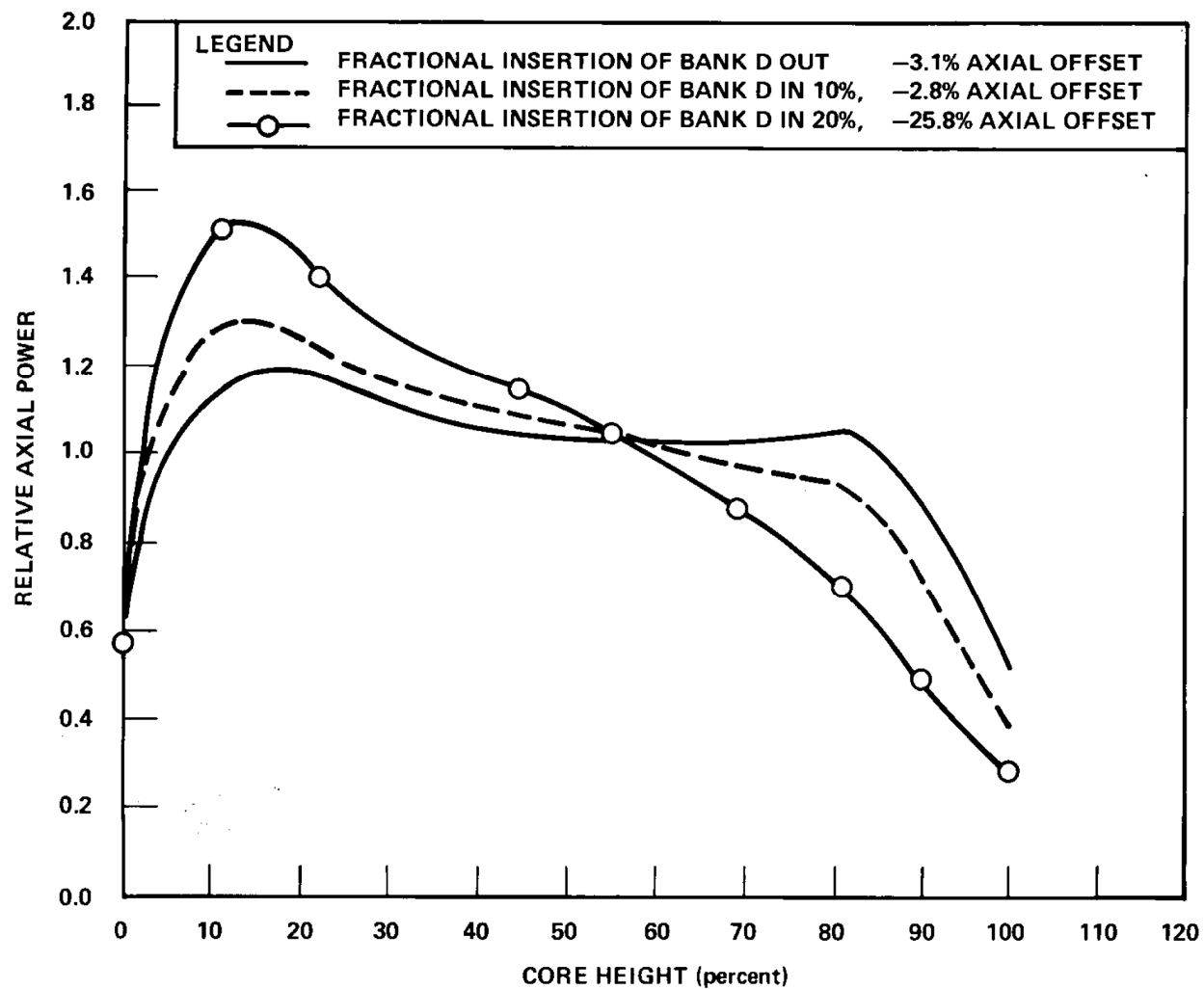
REV 21 5/08



REV 21 5/08



REV 21 5/08



REV 21 5/08

THIS FIGURE HAS BEEN DELETED.



REV 21 5/08



**JOSEPH M. FARLEY
NUCLEAR PLANT
UNIT 1 AND UNIT 2**

**A TYPICAL COMPARISON OF
ASSEMBLY AXIAL POWER DISTRIBUTION WITH
CORE AVERAGE AXIAL DISTRIBUTION
BANK "D" SLIGHTLY INSERTED**

FIGURE 4.3-17

THIS FIGURE HAS BEEN DELETED

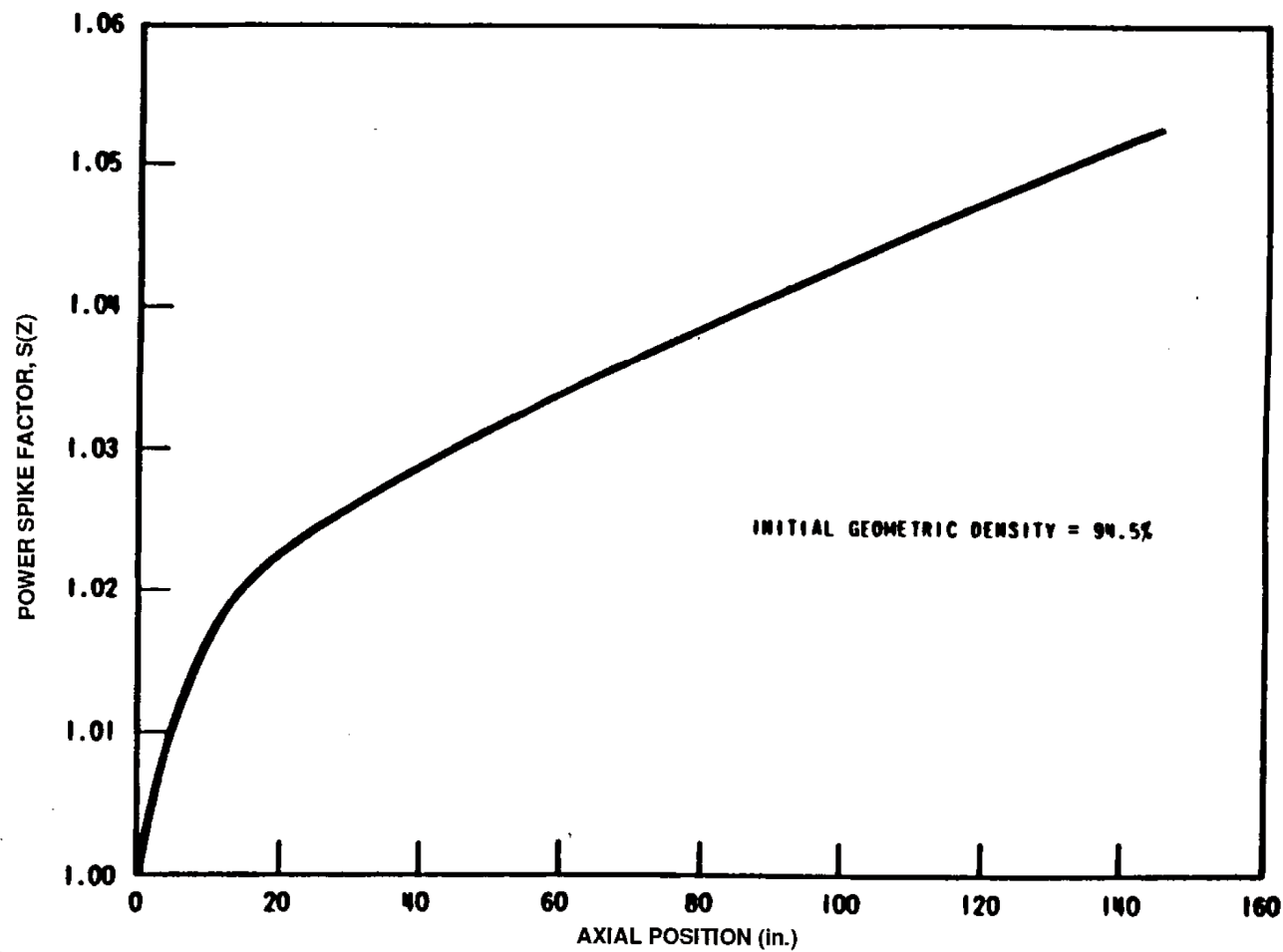
14

REV 21 5/08

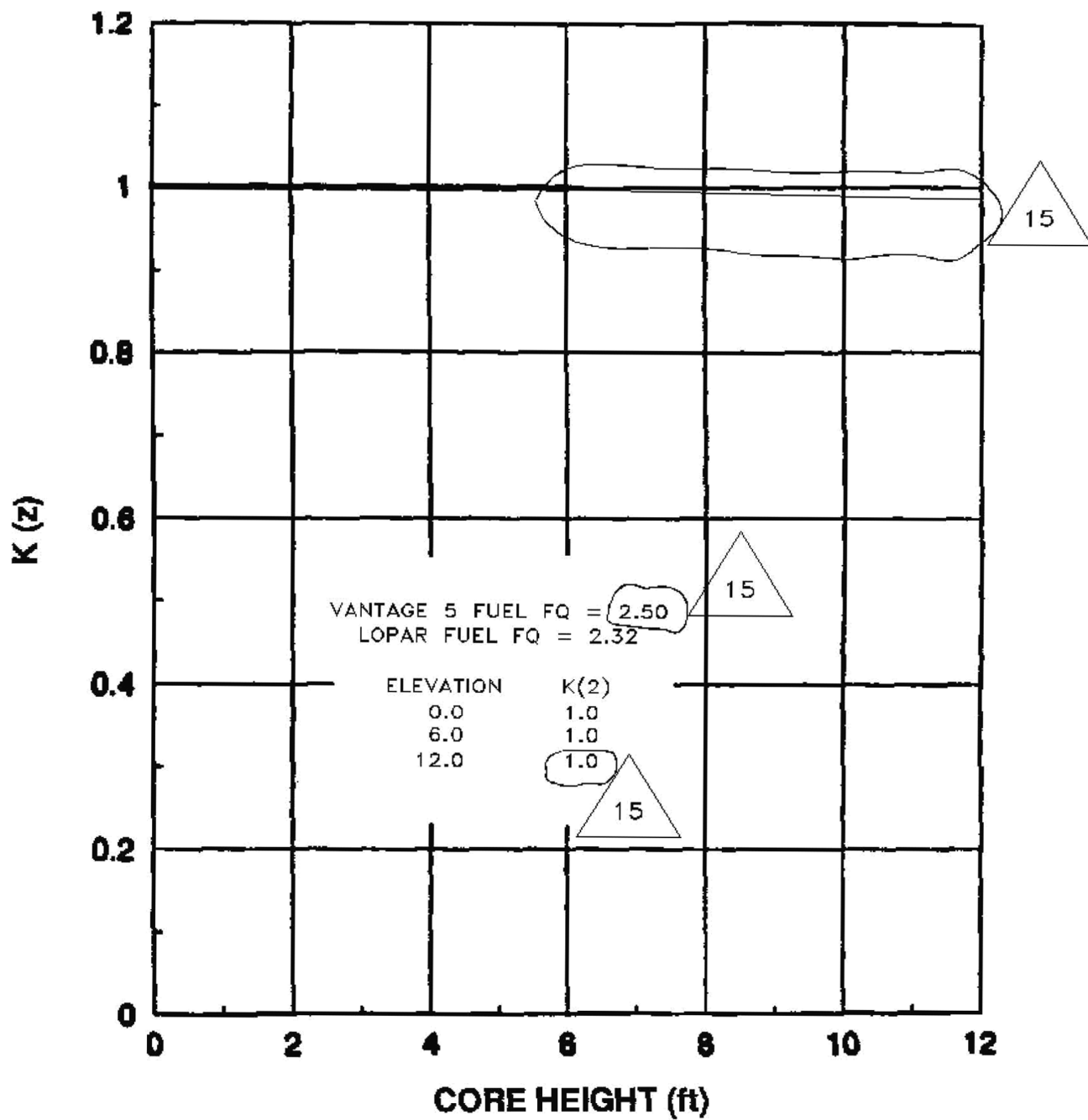
THIS FIGURE HAS BEEN DELETED

14

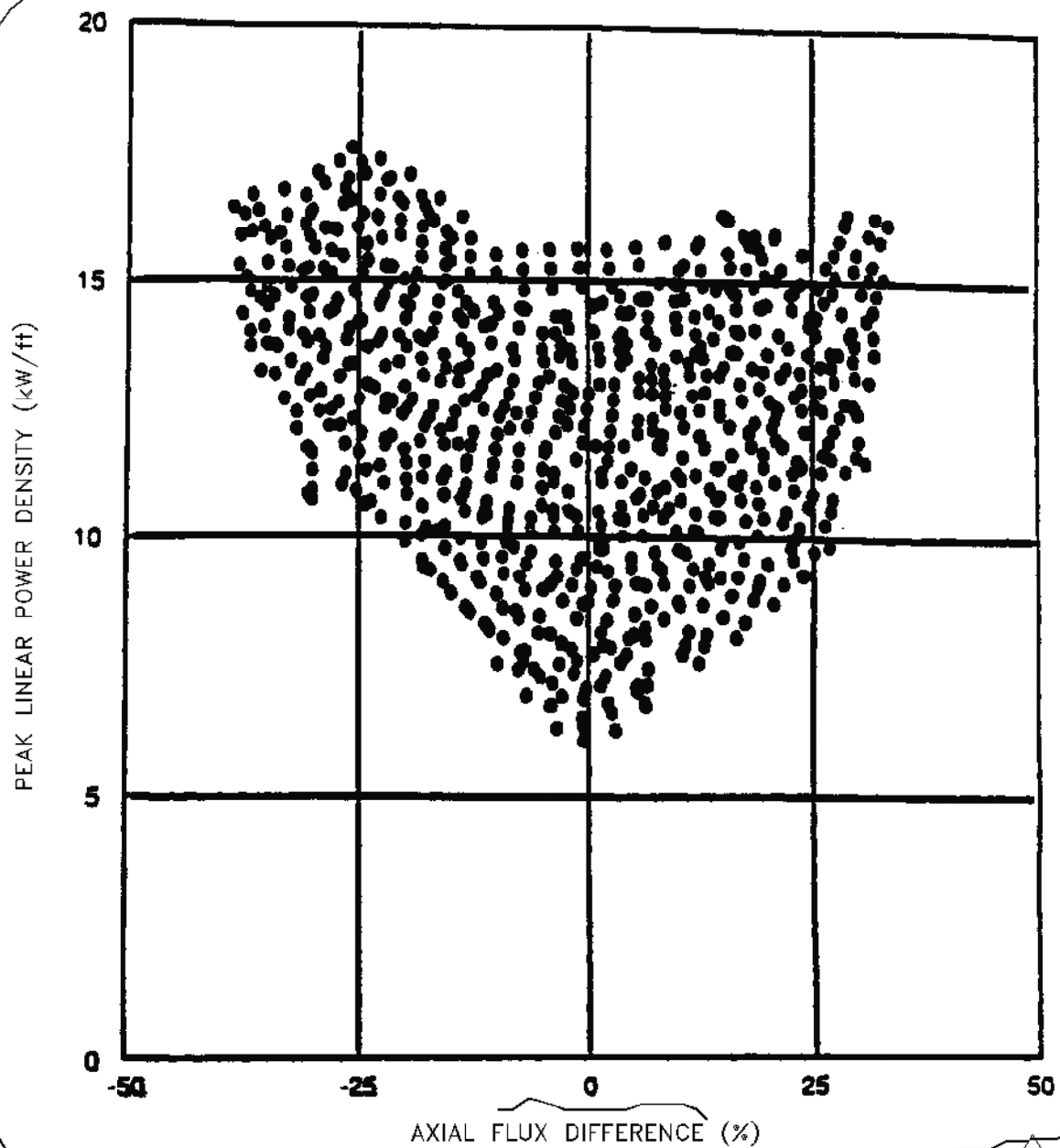
REV 21 5/08



REV 21 5/08

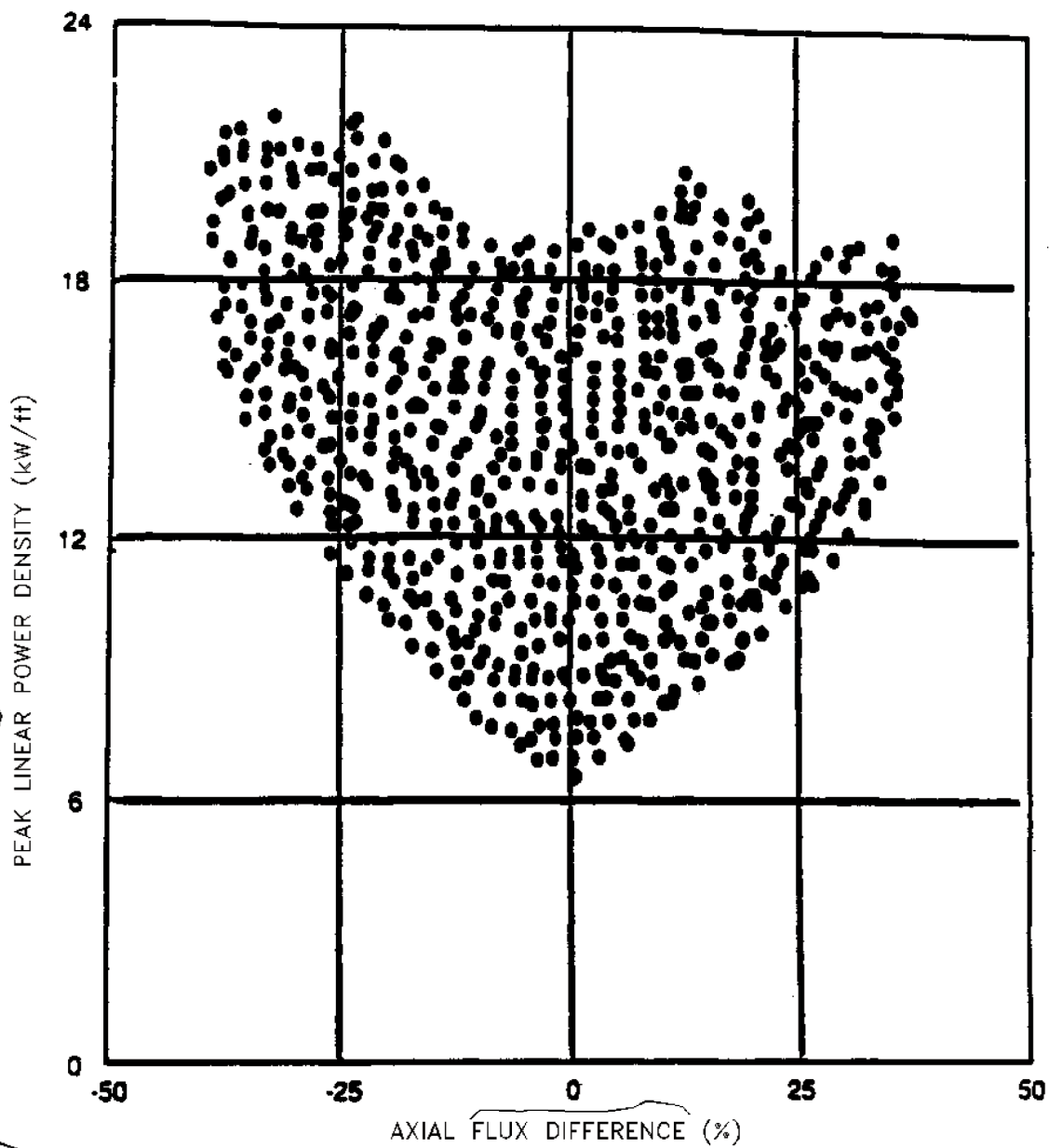


REV 21 5/08



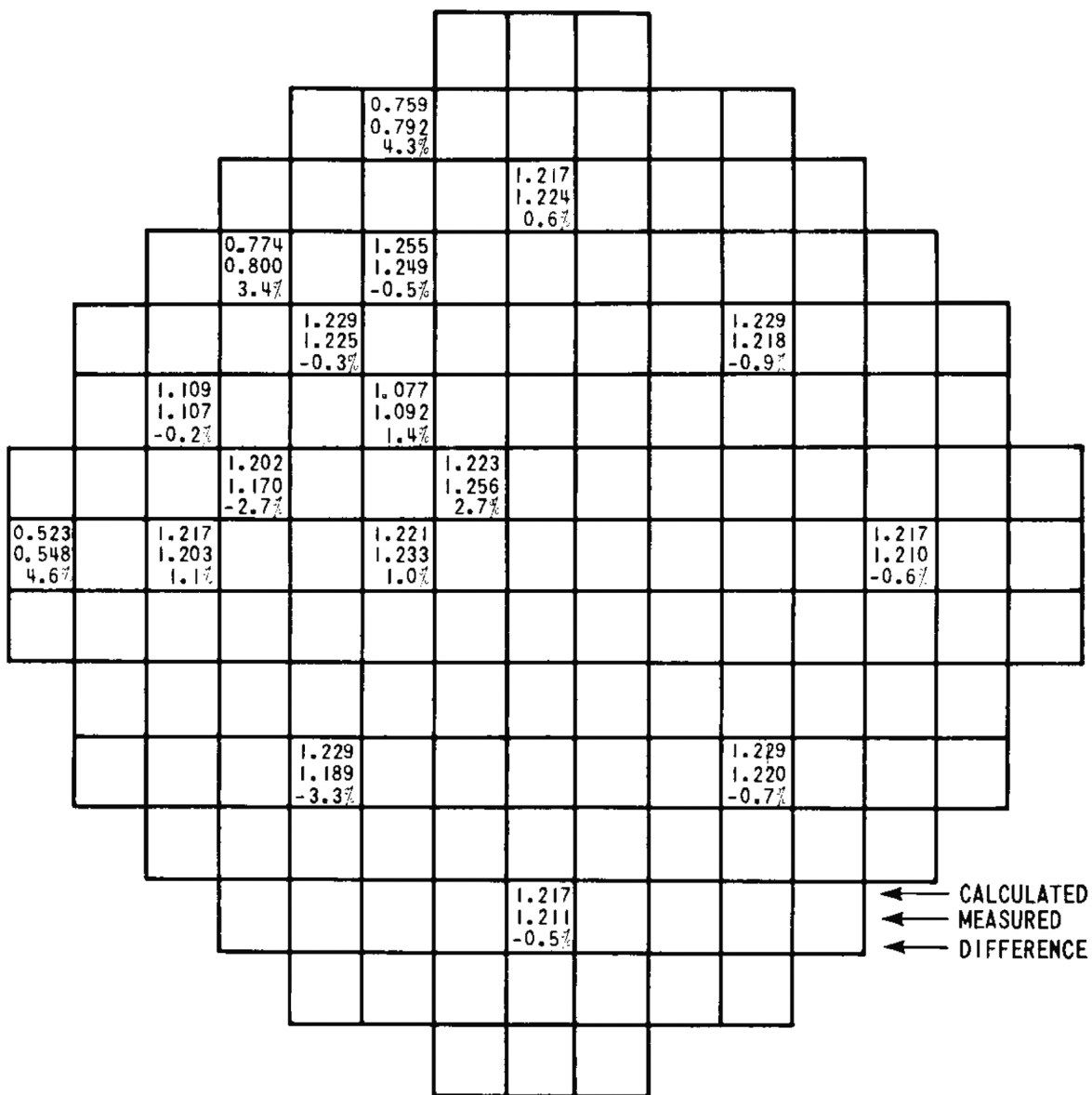
14

REV 21 5/08



14

REV 21 5/08



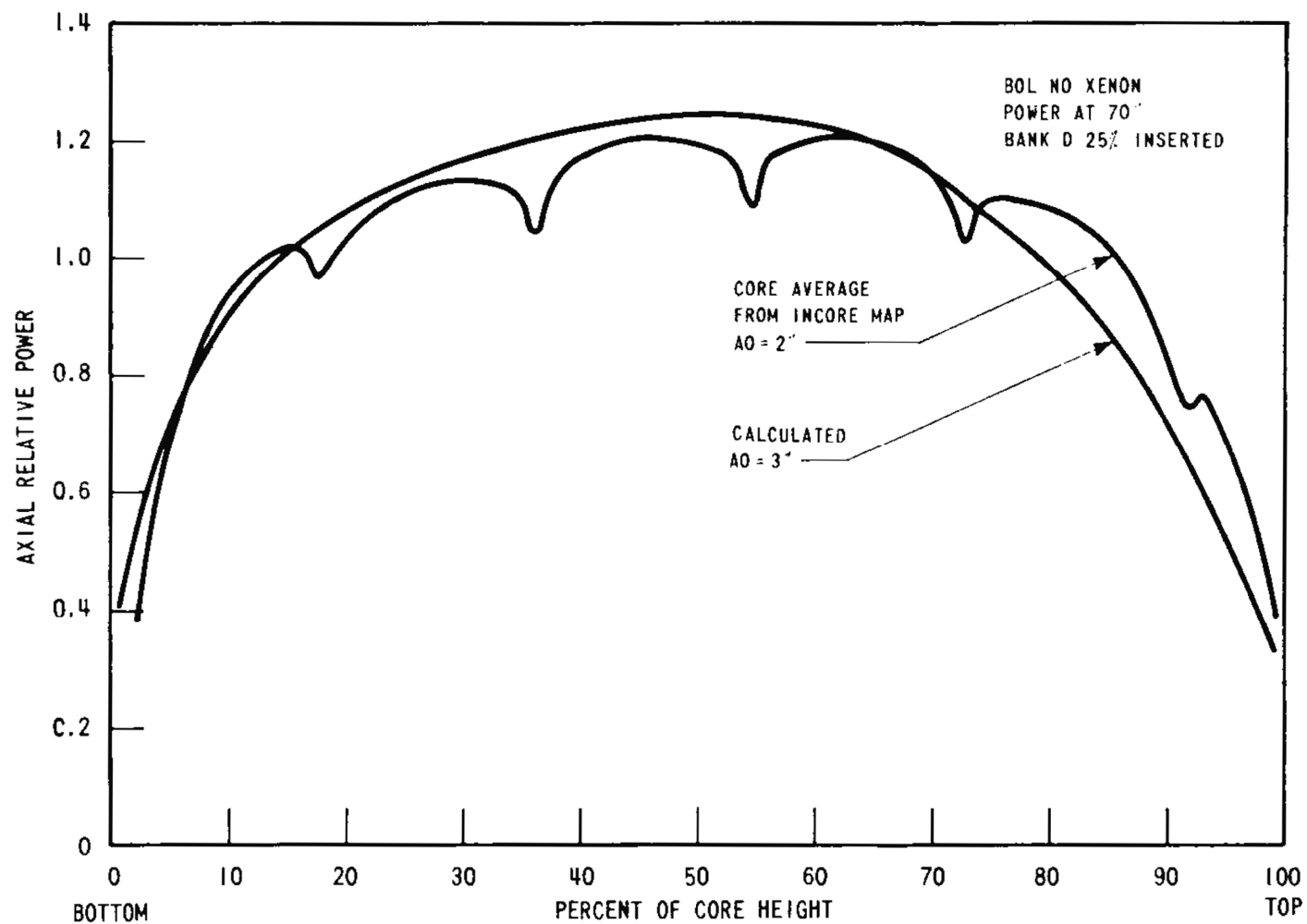
PEAKING FACTORS

$\bar{F}_z = 1.5$

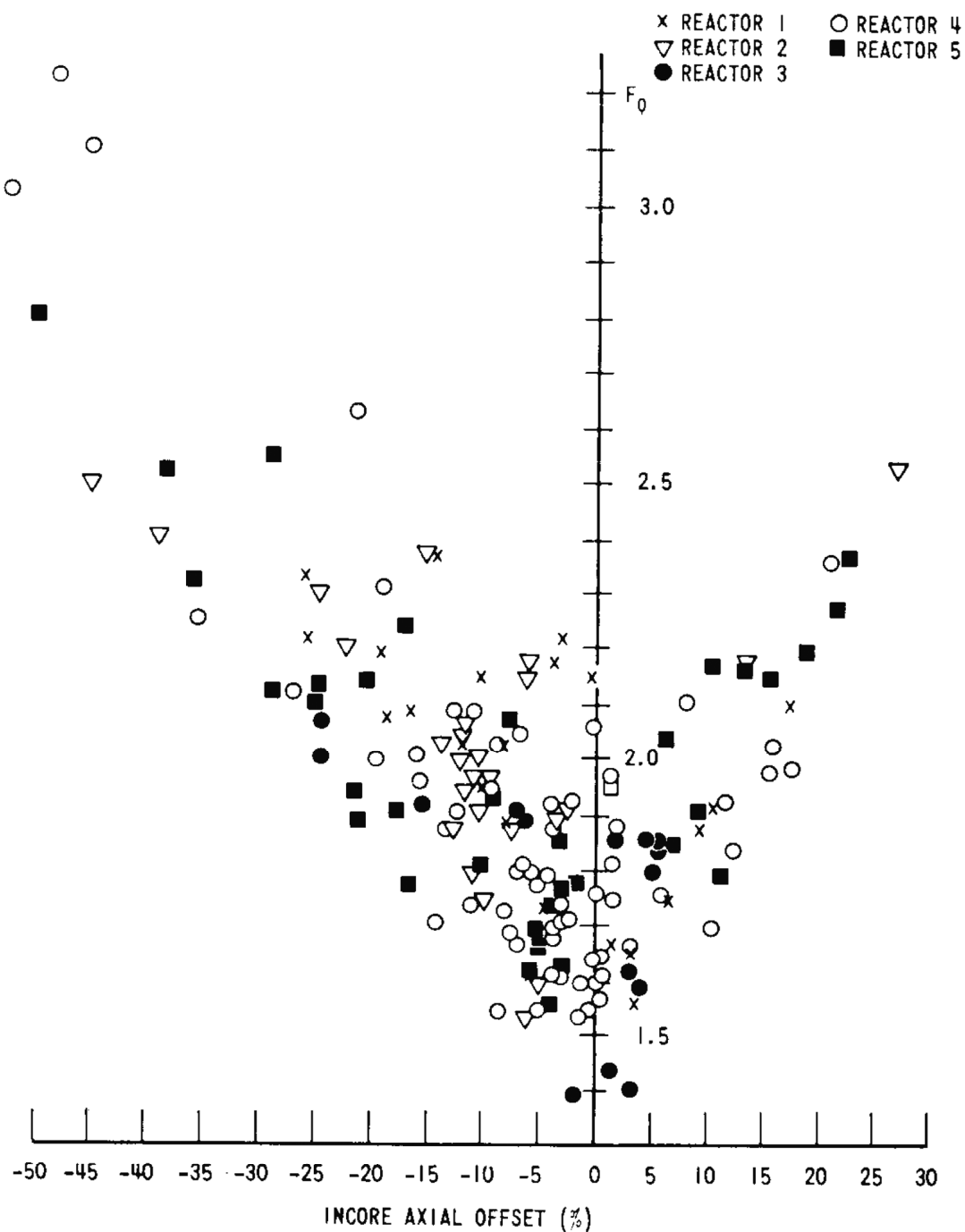
$F_{\Delta H}^N = 1.357$

$F_Q^N = 2.07$ LOCATED AT
M-8 SOUTH

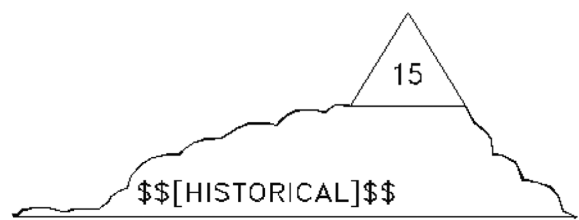
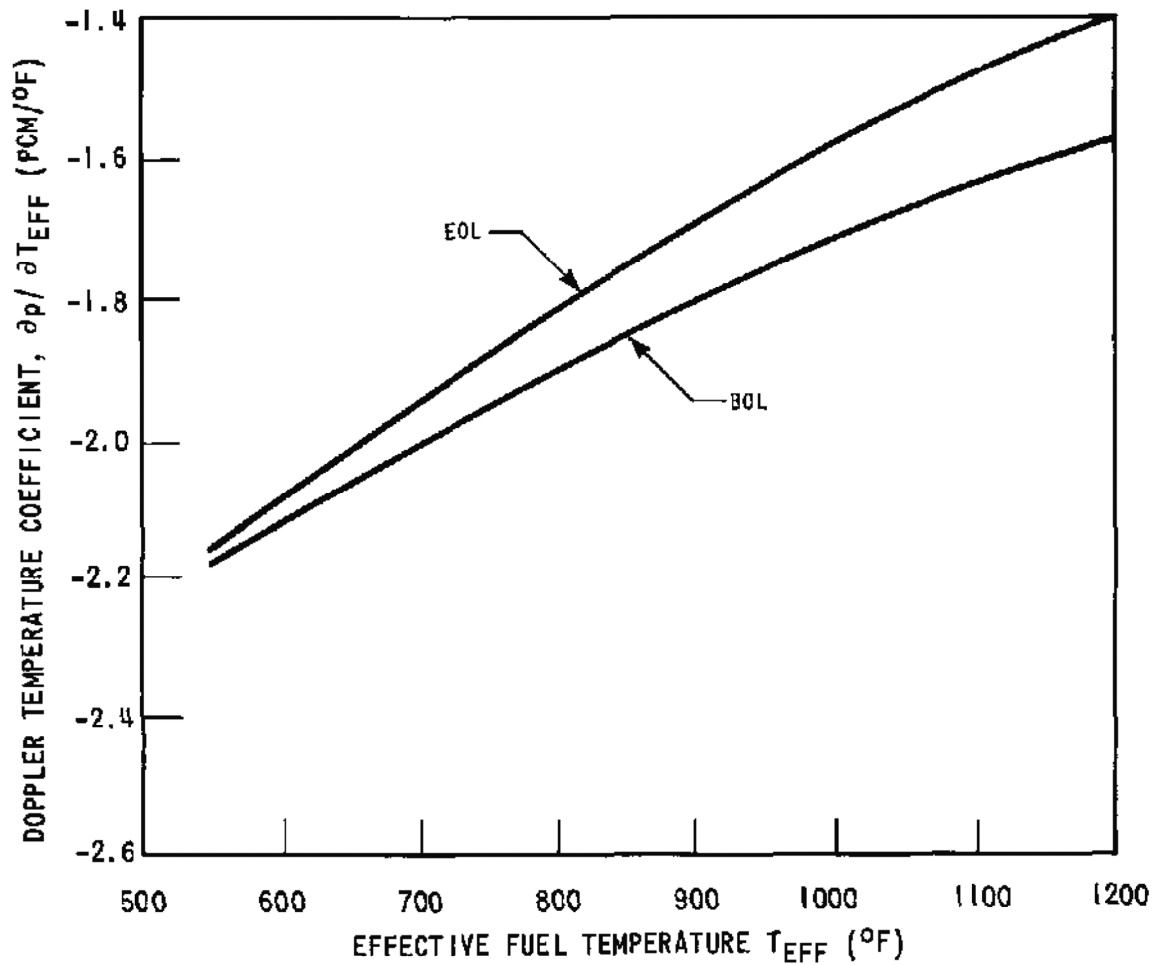
REV 21 5/08



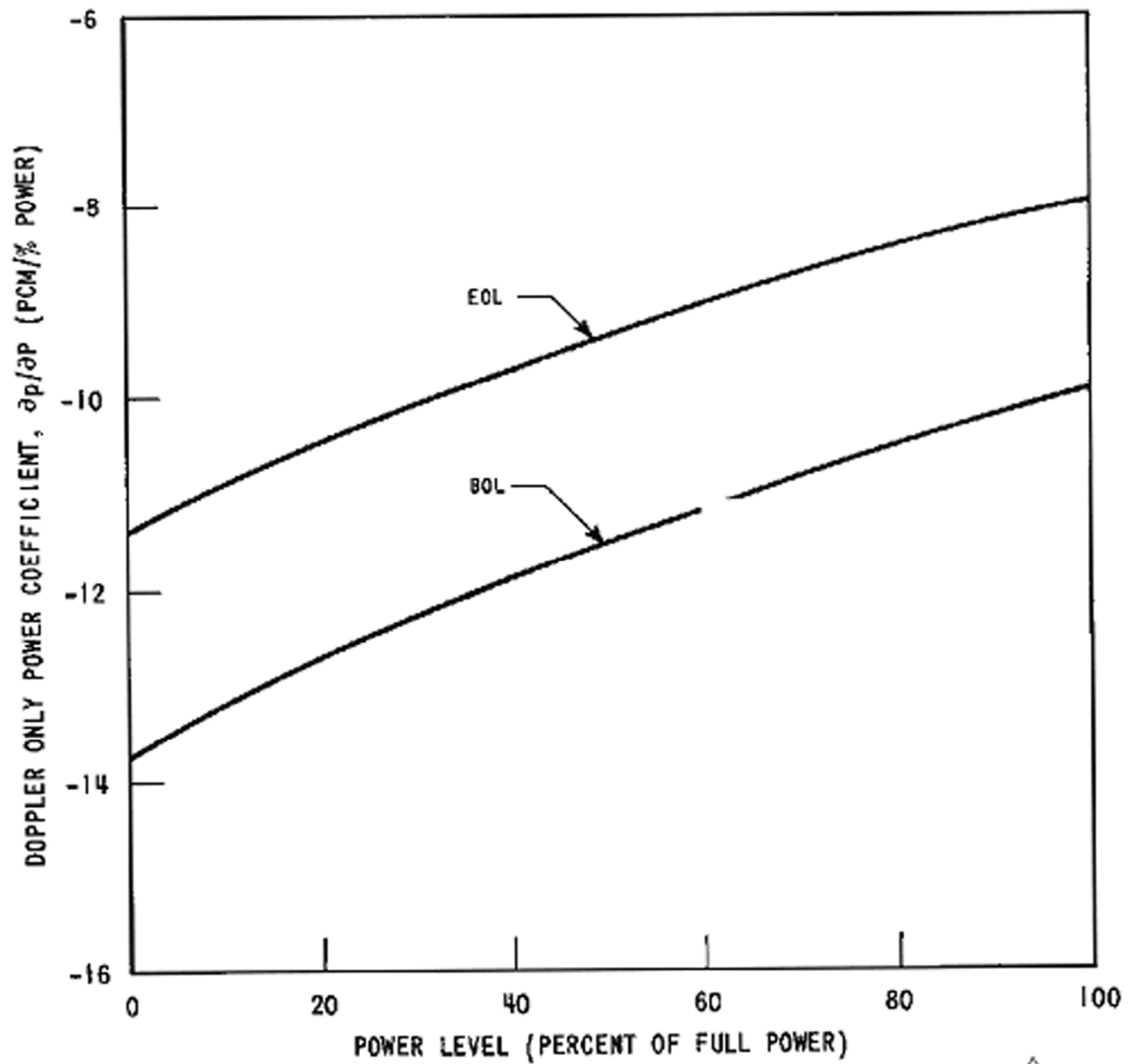
REV 21 5/08



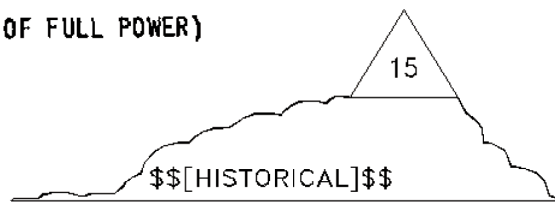
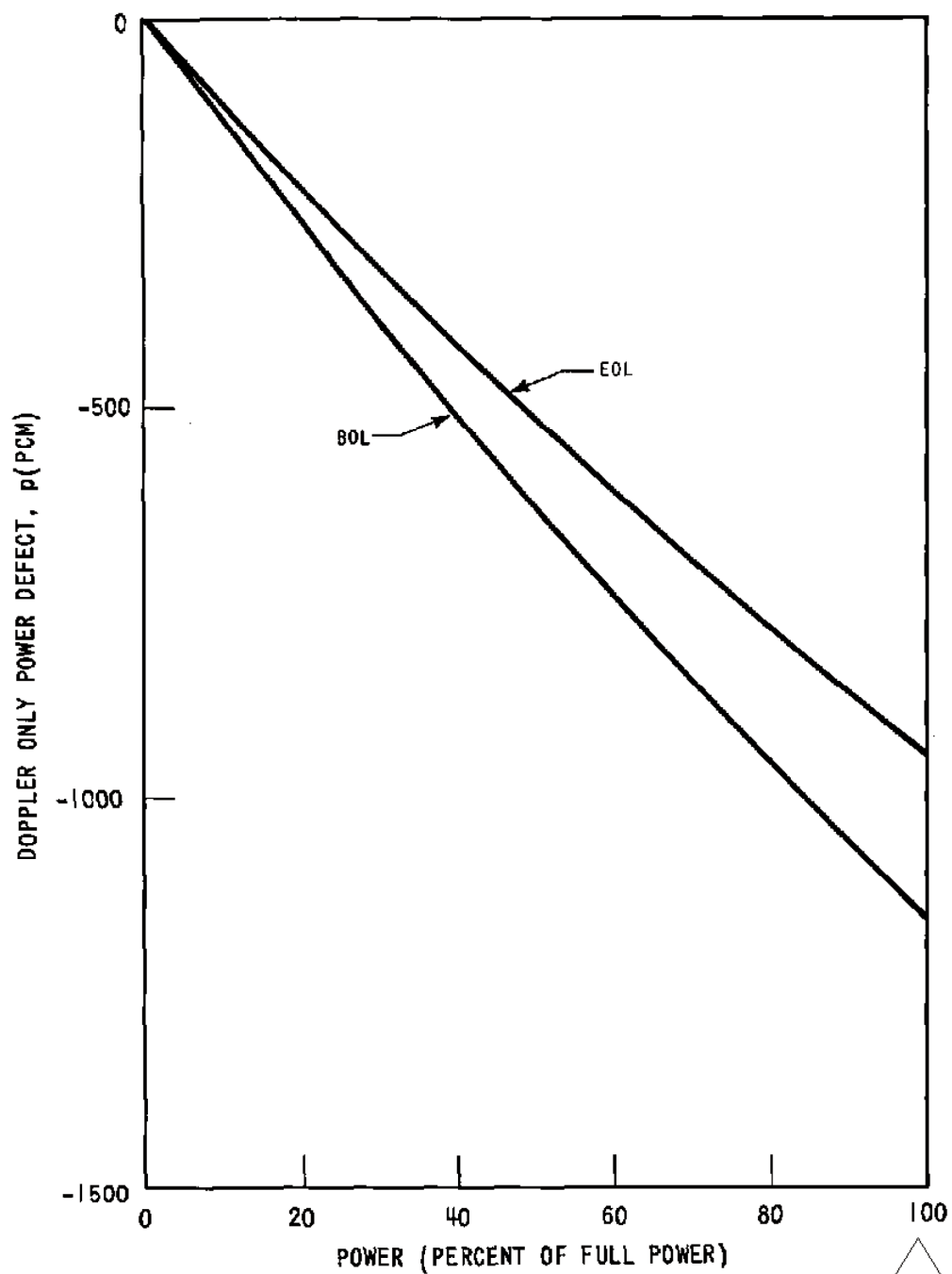
REV 21 5/08



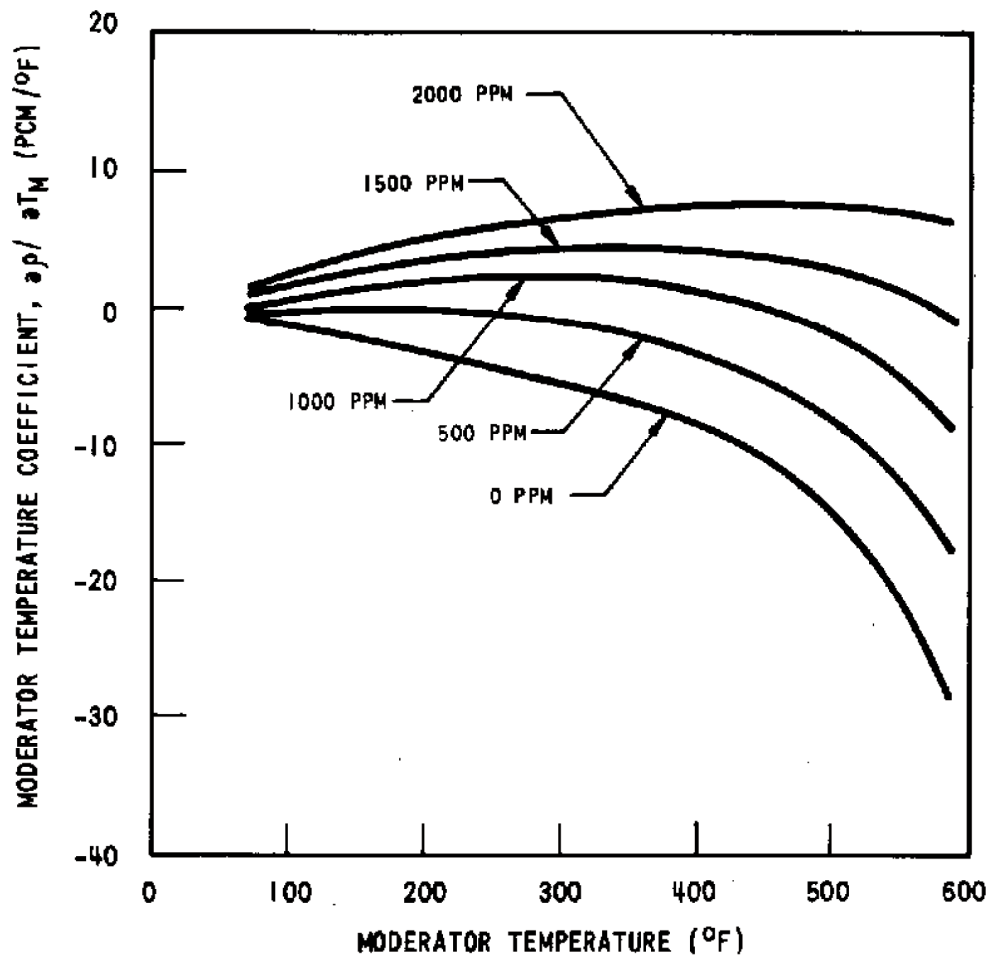
REV 21 5/08



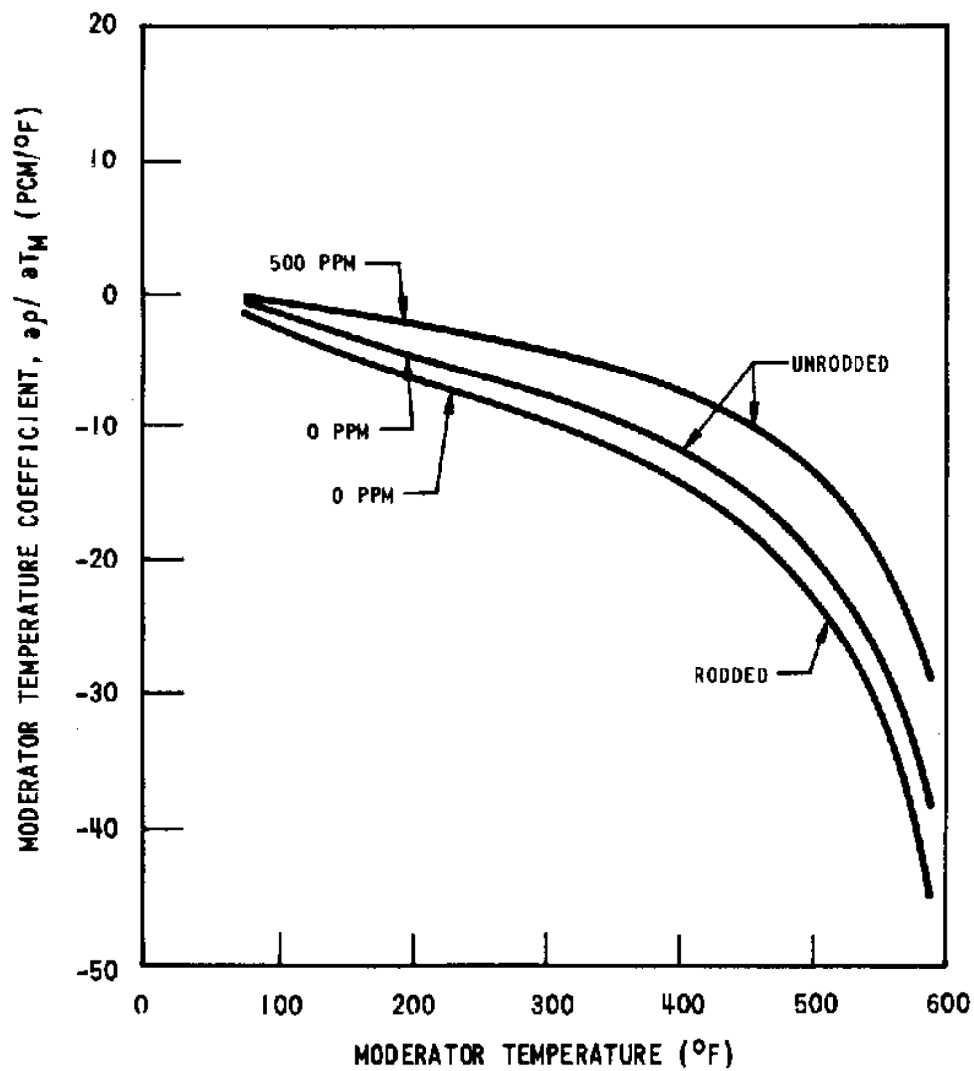
REV 21 5/08



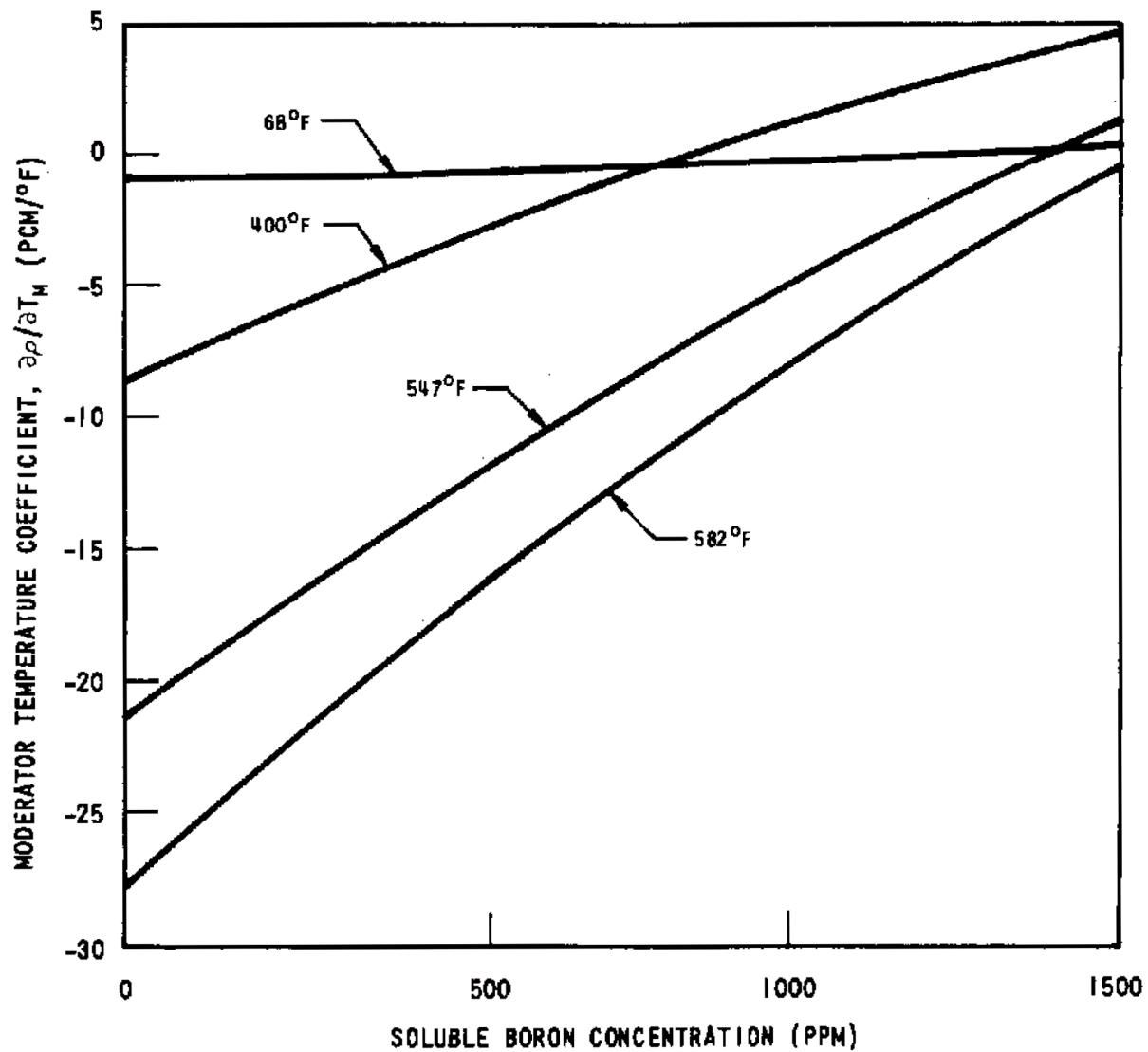
REV 21 5/08



REV 21 5/08

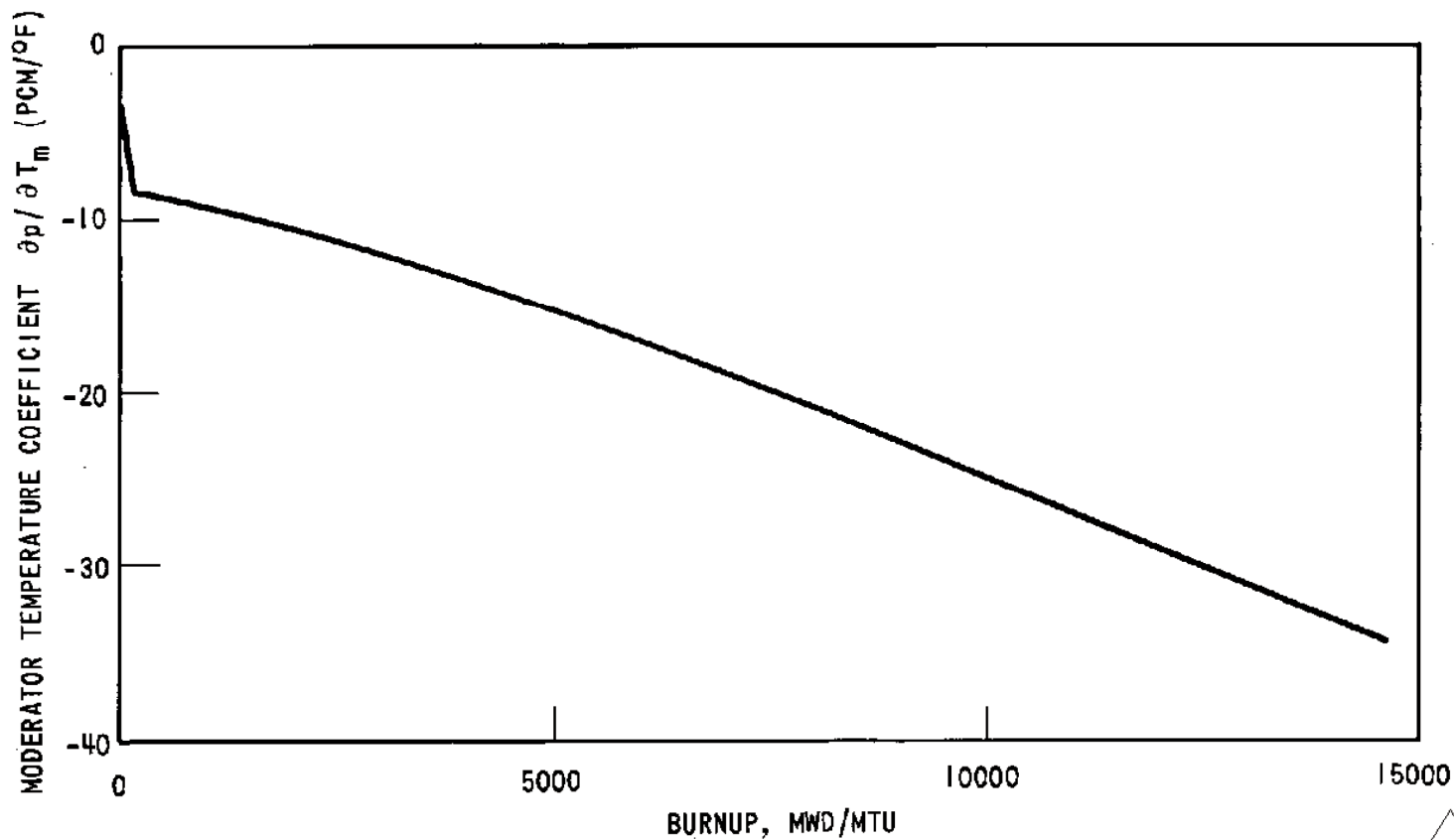


REV 21 5/08



REV 15 \triangle 15
 \$\$\$[HISTORICAL]\$\$\$

REV 21 5/08



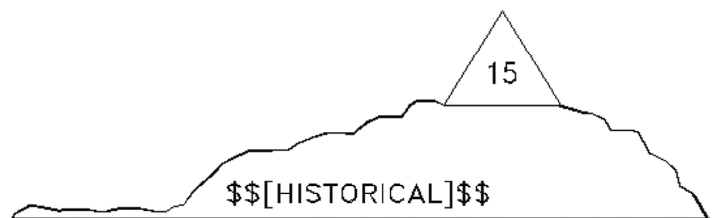
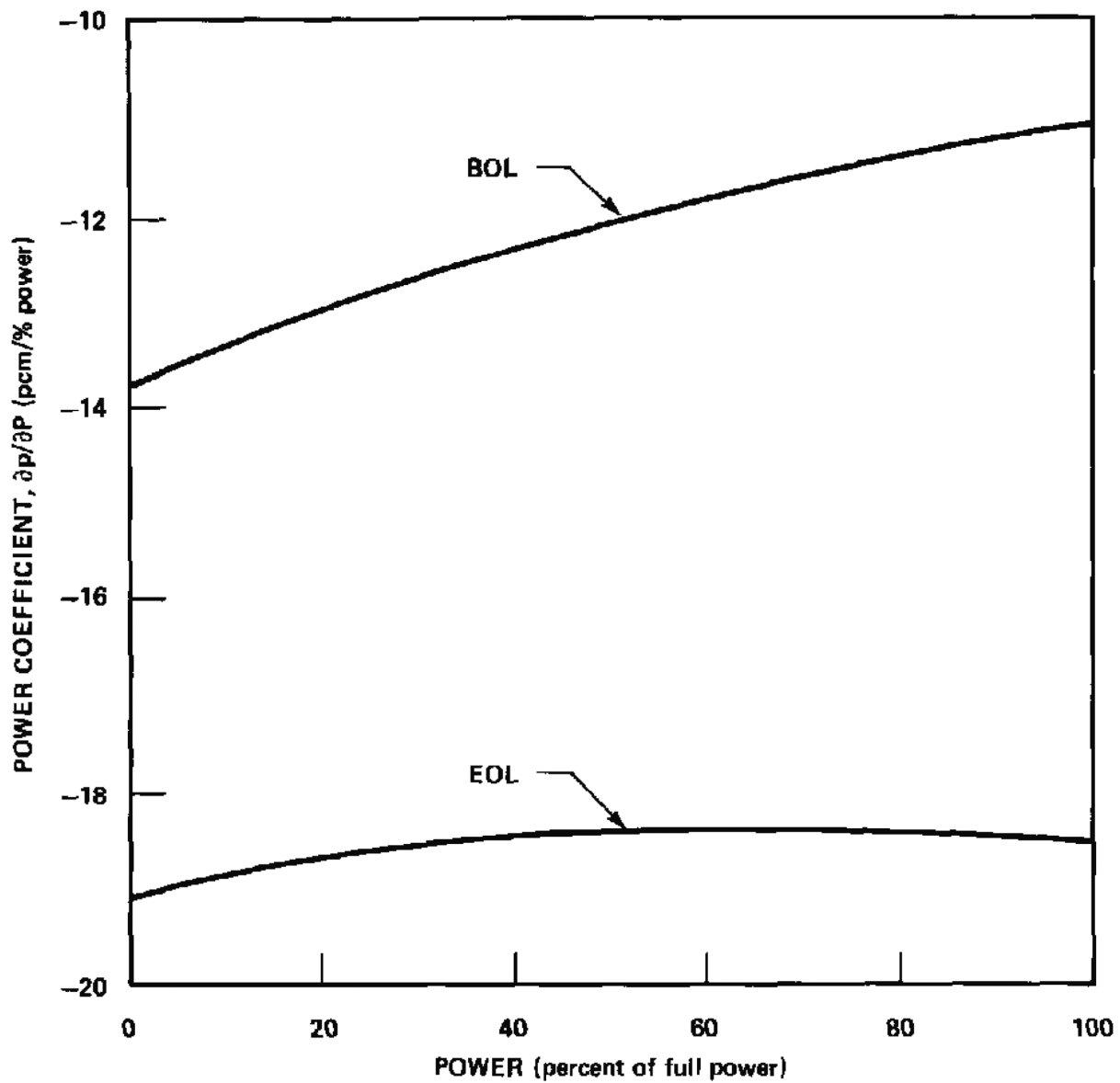
REV 21 5/08



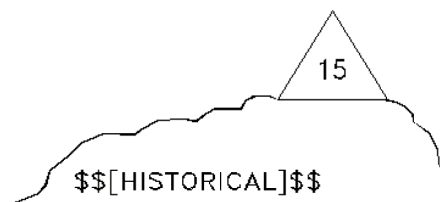
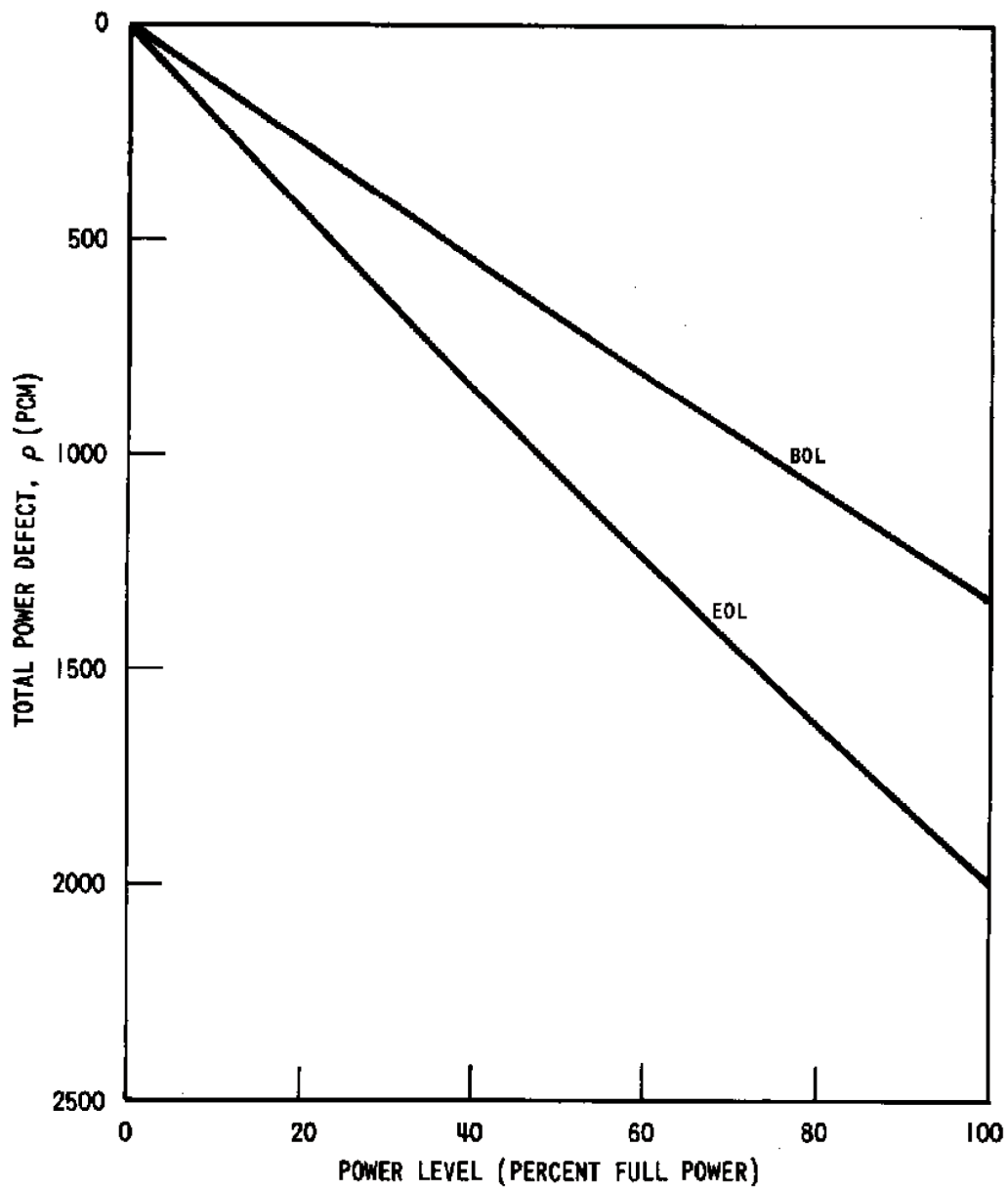
JOSEPH M. FARLEY
NUCLEAR PLANT
UNIT 1 AND UNIT 2

[HOT FULL POWER MODERATOR
TEMPERATURE COEFFICIENT DURING CYCLE 1 FOR THE
CRITICAL BORON CONCENTRATION

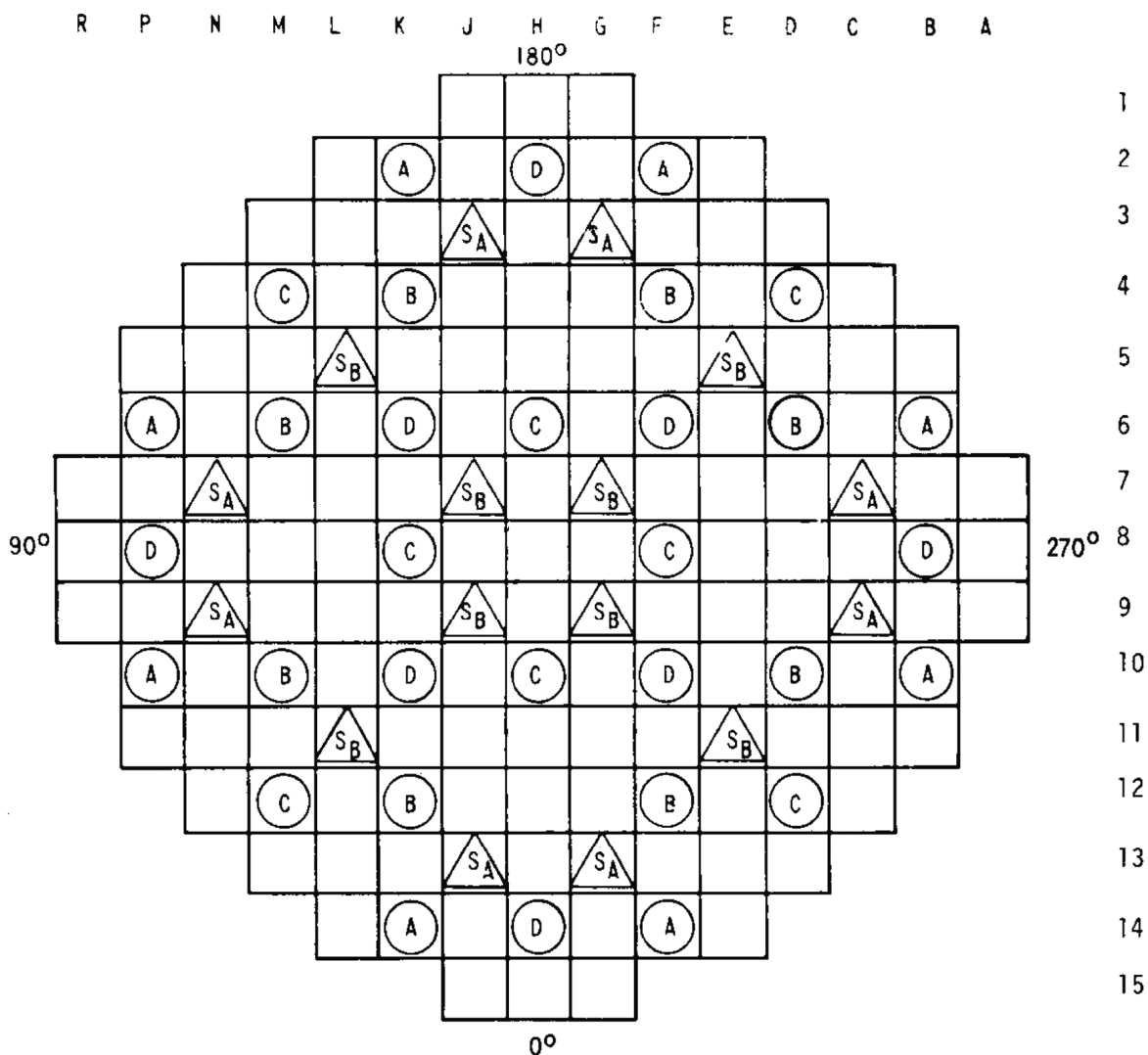
FIGURE 4.3-33]



REV 21 5/08

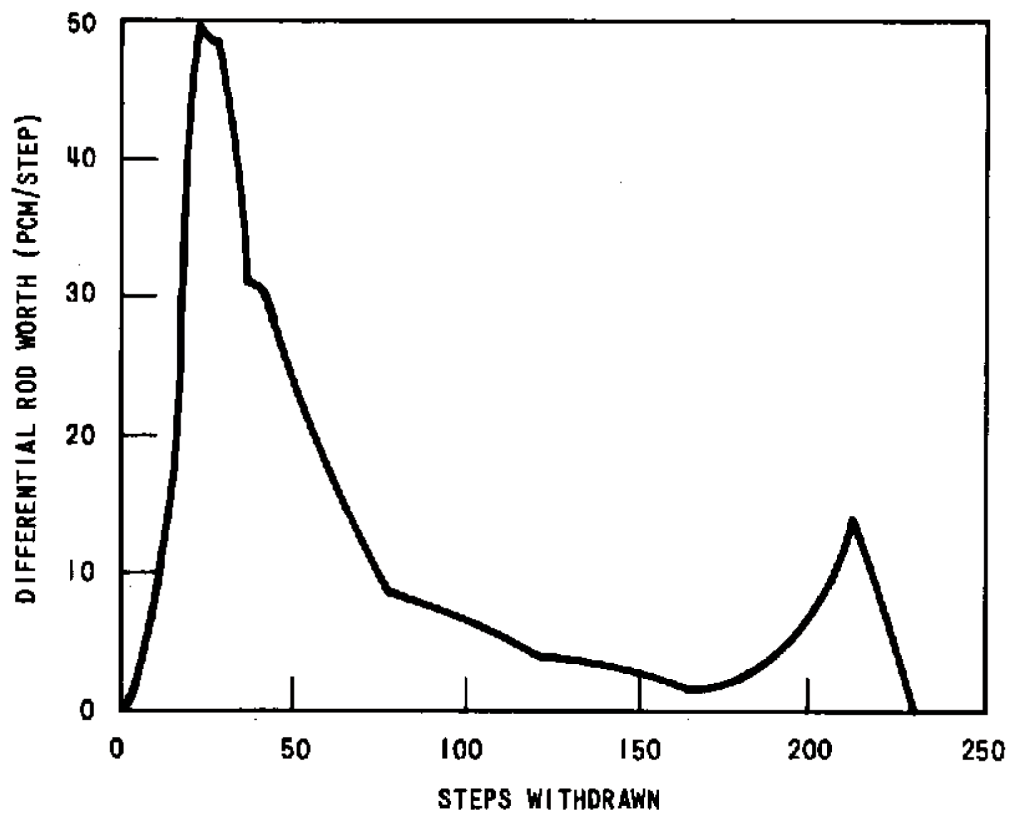


REV 21 5/08



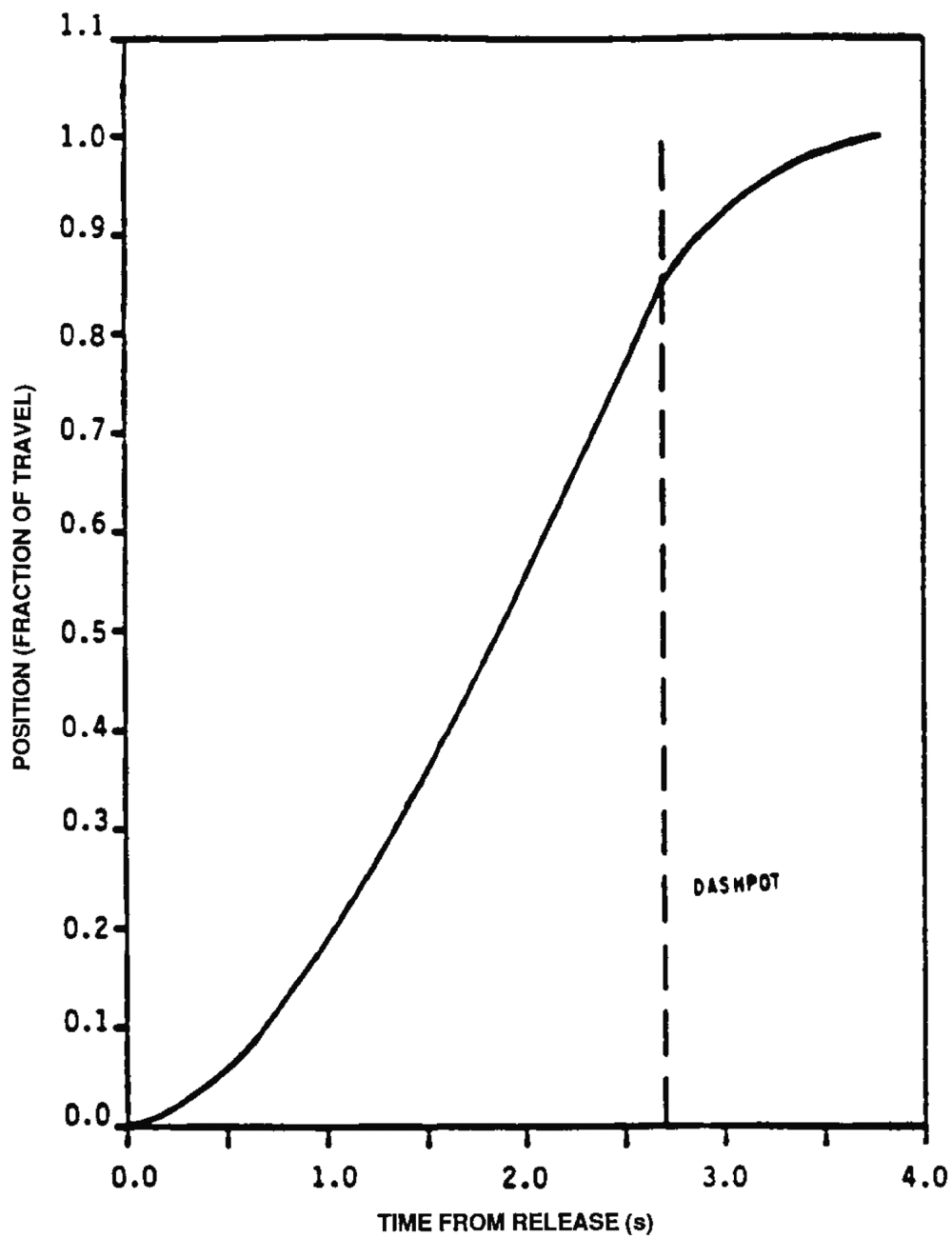
FUNCTION	NUMBER OF CLUSTERS
CONTROL BANK D	8
CONTROL BANK C	8
CONTROL BANK B	8
CONTROL BANK A	8
SHUTDOWN BANK S _B	8
SHUTDOWN BANK S _A	8

REV 21 5/08

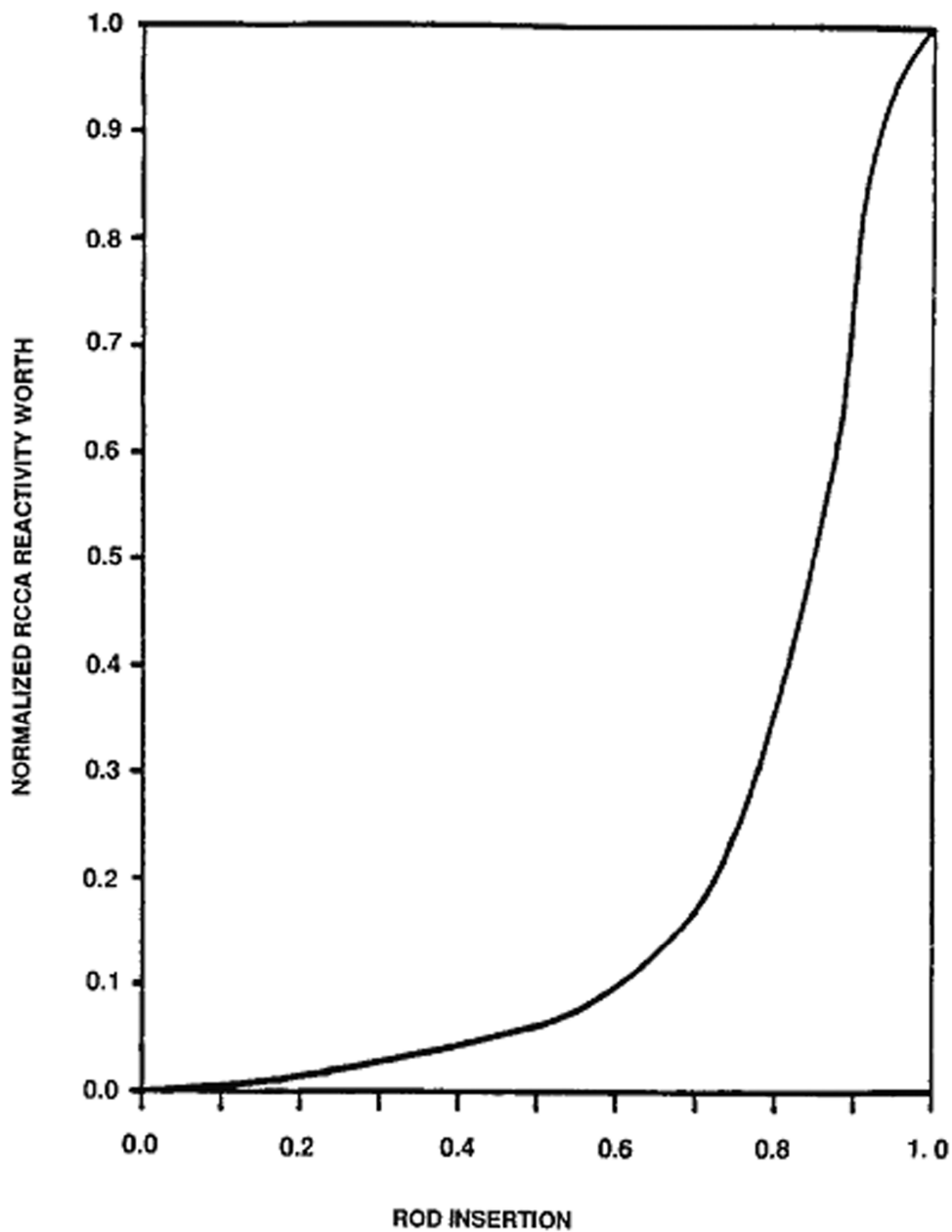


15

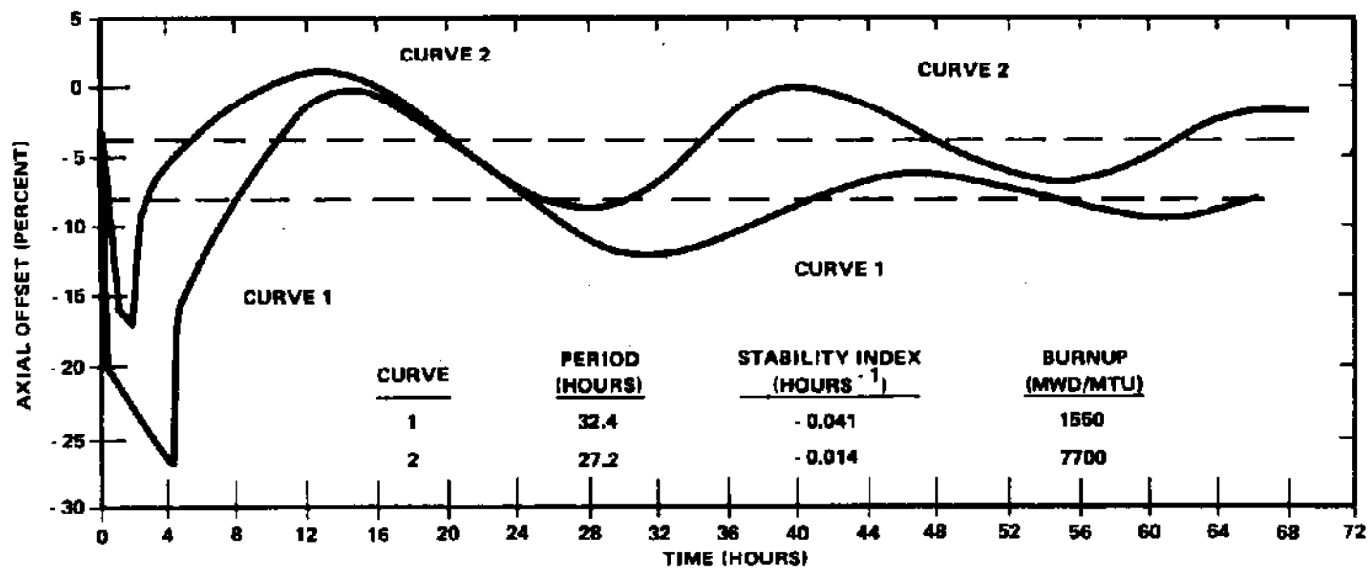
REV 21 5/08



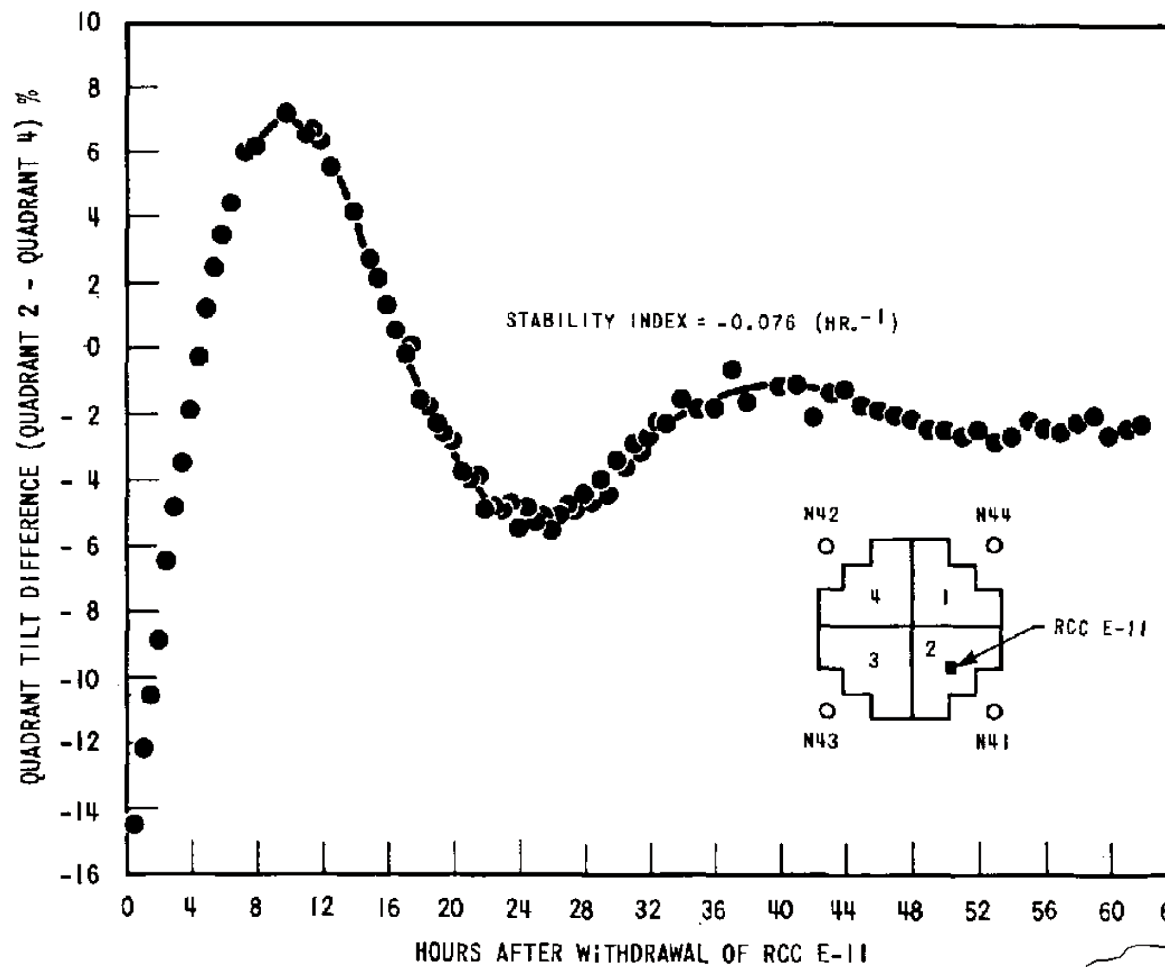
REV 21 5/08



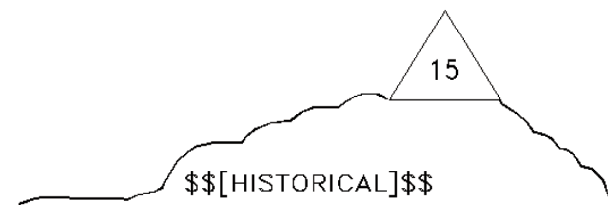
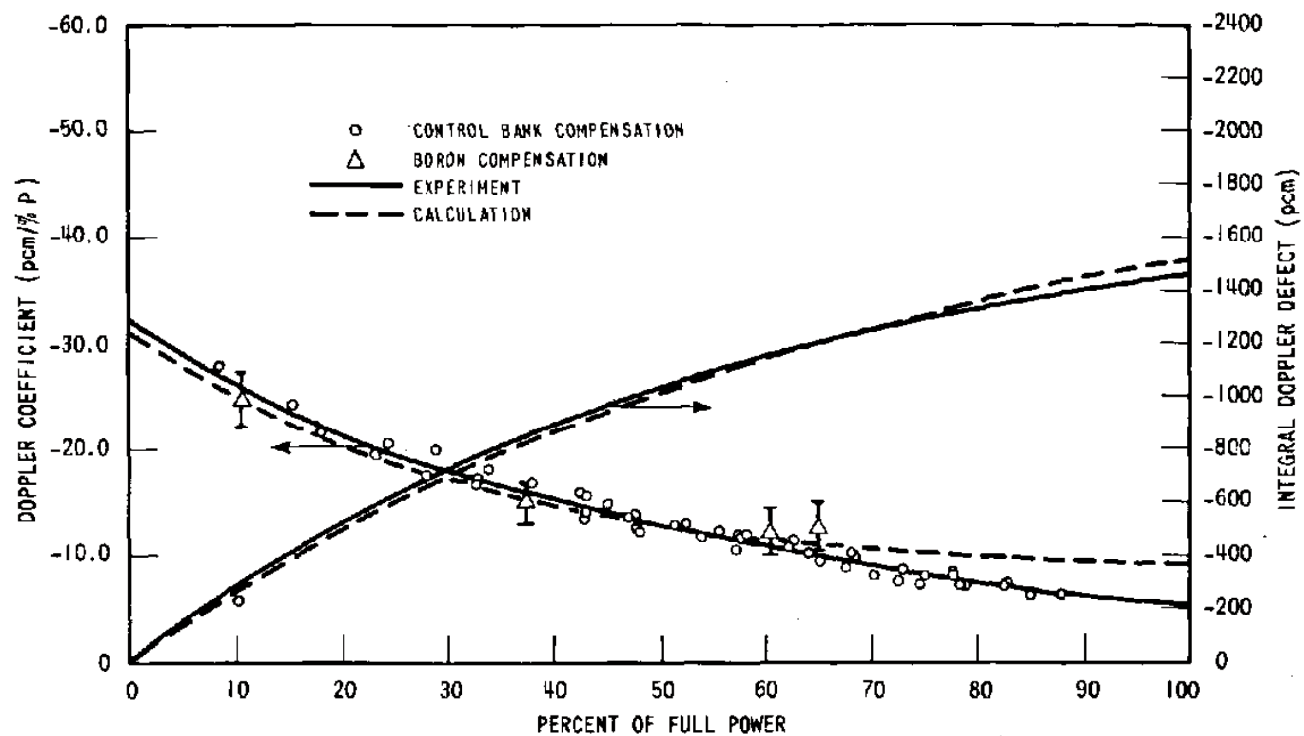
REV 21 5/08



REV 21 5/08



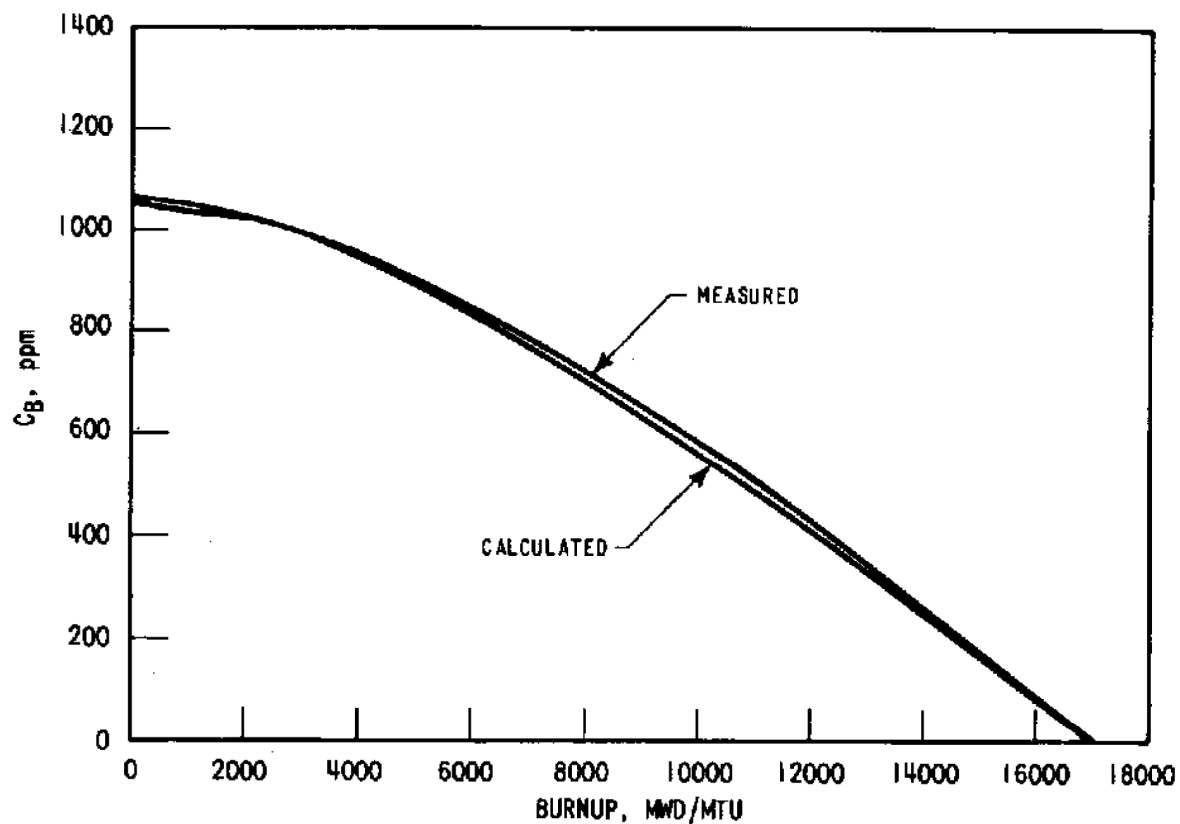
REV 21 5/08



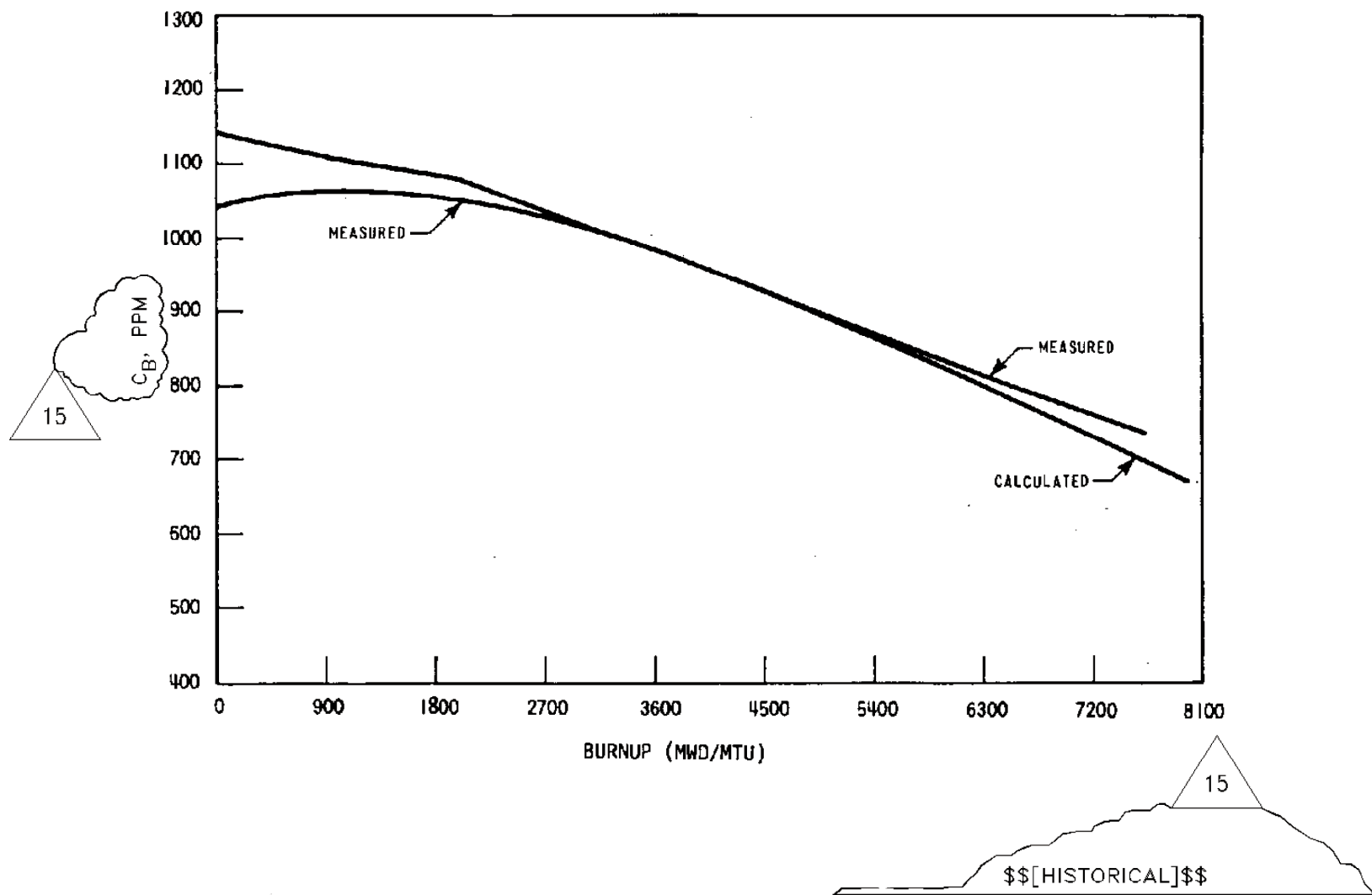
REV 21 5/08

[CALCULATED AND MEASURED DOPPLER DEFECT AND COEFFICIENTS AT BOL TWO-LOOP PLANT, 121 ASSEMBLIES, 12-FOOT CORE

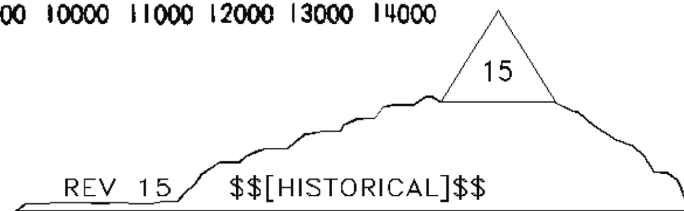
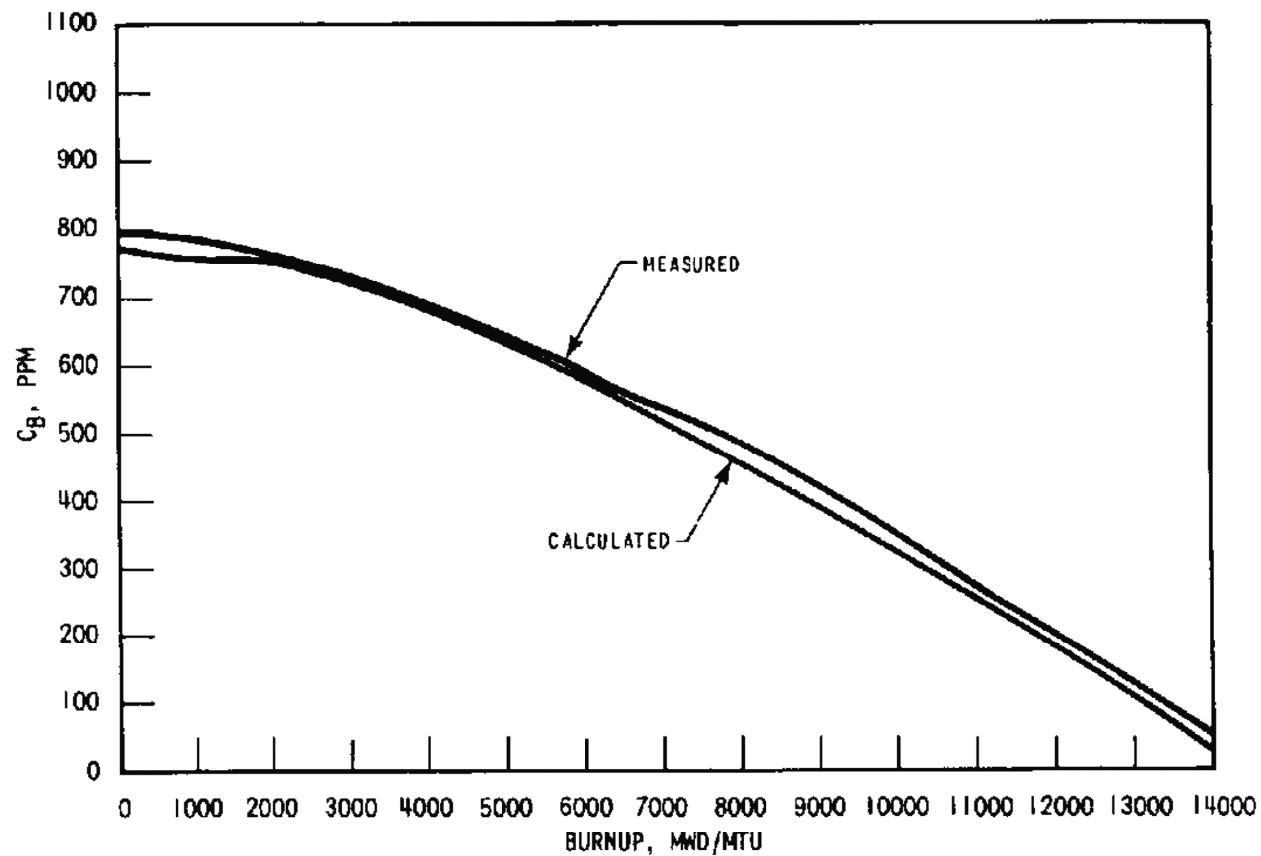
FIGURE 4.3-42]



REV 21 5/08



REV 21 5/08



REV 21 5/08

DELETED

REV 30 10/21

4.4 **THERMAL AND HYDRAULIC DESIGN**

4.4.1 **DESIGN BASES**

The overall objective of the thermal and hydraulic design of the reactor core is to provide adequate heat transfer which is compatible with the heat generation distribution in the core, such that heat removal by the reactor coolant system (RCS) or the emergency core cooling system (ECCS), when applicable, assures that the following requirements are met:

- A. Fuel damage^a is not expected during normal operation and operational transients (Condition I) or any transient conditions arising from faults of moderate frequency (Condition II). It is not possible, however, to preclude a very small number of rod failures. These will be within the capability of the plant cleanup system and are consistent with the plant design bases.
- B. The reactor can be brought to a safe state following a Condition III event with only a small fraction of fuel rods damaged^a, although sufficient fuel damage might occur to preclude resumption of operation without considerable outage time.
- C. The reactor can be brought to a safe state and the core can be kept subcritical with acceptable heat transfer geometry following transients arising from Condition IV events.

In order to satisfy the above requirements the following design bases have been established for the thermal and hydraulic design of the reactor core.

4.4.1.1 **Departure from Nucleate Boiling (DNB) Design Basis**

Basis

There will be at least a 95-percent probability that DNB will not occur on the limiting fuel rods during normal operation and operational transients and any transient conditions arising from faults of moderate frequency (Condition I and II events) at a 95-percent confidence level.

Discussion

The design method employed to meet the DNB design basis for the VANTAGE+/VANTAGE 5 and LOPAR fuel assemblies is the revised thermal design procedure (RTDP), reference 2. With the RTDP methodology, uncertainties in plant operating parameters, nuclear and thermal parameters, fuel fabrication parameters, computer codes, and DNB correlation predictions are considered statistically to obtain DNB uncertainty factors. Based on the DNB uncertainty factors, RTDP design limit DNBR values are determined such that there is at least a 95-percent probability at a 95-percent confidence level that DNB will not occur on the most limiting fuel rod during normal operation and operational transients and during transient conditions arising from faults of moderate frequency (Condition I and II events as defined in ANSI N18.2).

^a Fuel damage as used here is defined as penetration of the fission product barrier (i.e. the fuel rod clad).

Uncertainties in the plant operating parameters (pressurizer pressure, primary coolant temperature, reactor power, and reactor coolant system flow) have been evaluated for the Farley Units 1 and 2 for RTD bypass loops eliminated (references 3 and 4). In the departure from nucleate boiling ratio (DNBR) analyses with RTDP, a set of plant operating parameter uncertainties was used as bounding for operation with RTD bypass loops eliminated. Only the random portion of the plant operating parameter uncertainties is included in the statistical combination. Instrumentation bias is treated as a direct DNBR penalty. Since the parameter uncertainties are considered in determining the RTDP design limit DNBR values, the plant safety analyses are performed using input parameters at their nominal values.

The RTDP design limit DNBR value for the WRB-2 correlation is 1.24 for the typical and thimble cells in the mixing vane region of the VANTAGE+/VANTAGE 5 fuel. The RTDP design limit DNBR value for the ABB-NV correlation is 1.18 for the typical and thimble cells below the mixing vane region of the VANTAGE+/VANTAGE 5 fuel.

The design limit DNBR values are used as a basis for the technical specifications and for consideration of the applicability of items requiring NRC approval as defined in 10 CFR 50.59.

To maintain DNBR margin to offset DNB penalties such as those due to fuel rod bow (paragraph 4.4.2.2.7) and transition core (paragraph 4.4.2.2.8), the safety analyses were performed to DNBR limits higher than the design limit DNBR values. The difference between the design limit DNBRs and the safety analysis limit DNBRs results in available DNBR margin. The net DNBR margin, after consideration of all penalties, is available for operating and design flexibility.

The option of thimble plug removal has been included in all of the DNBR analyses performed for the VANTAGE+/VANTAGE 5 and LOPAR fuel. The primary impact of thimble plug removal on the thermal-hydraulic analysis is an increase in the core bypass flow. Bypass flow is assumed to be ineffective for core heat removal. The increased bypass flow is included in all of the flow and DNBR values presented in table 4.4-1.

Operation with thimble plugs in place reduces the core bypass flow through the fuel assembly thimble tubes. The reduction in core bypass flow for operation with the thimble plugs in place is a DNBR benefit. The increased margin associated with the use of a full complement of thimble plugs can be used to offset DNBR penalties.

The standard thermal design procedure (STDP) is used for those analyses where RTDP is not applicable. In the STDP method, the parameters used in analysis are treated in a conservative way from a DNBR standpoint. The parameter uncertainties are applied directly to the plant safety analyses input values to give the lowest minimum DNBR. The DNBR limit for STDP is the appropriate DNB correlation limit increased by sufficient margin to offset the applicable DNBR penalties.

Discussion

By preventing departure from nucleate boiling, adequate heat transfer is assured between the fuel cladding and the reactor coolant, thereby preventing fuel damage as a result of inadequate cooling. Maximum fuel rod surface temperature is not a design basis, as it will be within a few

degrees of coolant temperature during operation in the nucleate boiling region. Limits provided by the nuclear control and protection systems are such that this design basis will be met for transients associated with Condition II events, including overpower transients. There is an additional large DNBR margin at rated power operation and during normal operating transients.

4.4.1.2 Fuel Temperature Design Basis

Basis

During modes of operation associated with Condition I and Condition II events, the maximum fuel temperature shall be less than the melting temperature of UO_2 . The maximum peak local power for Condition I and Condition II events will have a 95% probability with a 95% confidence of being less than melt limit defined in Reference 105. By precluding UO_2 melting, the fuel geometry is preserved and possible adverse effects of molten UO_2 are eliminated.

Discussion

Fuel rod thermal evaluations are performed at rated power, maximum overpower, and during transients at various burnups. These analyses assure that this design basis, as well as the fuel integrity design bases given in section 4.2, are met. They also provide input for the evaluation of Condition III and IV faults given in chapter 15.

4.4.1.3 Core Flow Design Basis

Basis

A minimum of 92.9 percent of the thermal flowrate will pass through the fuel rod region of the core and will be effective for fuel rod cooling. Coolant flow through the thimble tubes, as well as the leakage from the core barrel baffle region into the core, are not considered effective for heat removal.

Discussion

Core cooling evaluations are based on the thermal flowrate (minimum flow) entering the reactor vessel. A maximum of 7.1 percent of this value is allotted as bypass flow. This includes rod cluster control (RCC) guide thimble cooling flow, head cooling flow, baffle leakage, and leakage to the vessel outlet nozzle.

The maximum bypass flow fraction of 7.1 percent assumes no plugging devices, burnable absorbers, or secondary source rods in the RCC guide thimble tubes which do not contain RCC rods.

4.4.1.4 Hydrodynamic Stability Design Bases

Basis

Modes of operation associated with Condition I and II events shall not lead to hydrodynamic instability.

4.4.1.5 Other Considerations

The above design basis, together with the fuel clad and fuel assembly design bases given in paragraph 4.2.1.1, are sufficiently comprehensive so that additional limits are not required.

Fuel rod diametral gap characteristics, moderator-coolant flow velocity and distribution, and moderator void are not inherently limiting. Each of these parameters is incorporated into the thermal and hydraulic models used to ensure that the above mentioned design criteria are met. For instance, the fuel rod diametral gap characteristics change with time (see paragraph 4.2.1.3.1) and the fuel rod integrity is evaluated on that basis. The effect of the moderator flow velocity and distribution (see paragraph 4.4.2.3) and moderator void distribution (see paragraph 4.4.2.5) are included in the core thermal evaluation and thus affect the design bases.

Meeting the fuel clad integrity criteria covers possible effects of clad temperature limitations. As noted in paragraph 4.2.1.3.1, the fuel rod conditions change with time. A single clad temperature limit for Condition I or Condition II events is not appropriate, since it would of necessity be overly conservative. A clad temperature limit is applied to the loss-of-coolant accident (LOCA) (subsection 15.4.1), and locked rotor accident.

4.4.2 DESCRIPTION

4.4.2.1 Summary Comparison

Table 4.4-1 provides a comparison of the design parameters for the 17 x 17 LOPAR fuel and the VANTAGE+/VANTAGE 5 fuel.

The LOPAR fuel is not analyzed for use at the power uprate (2821 MWt). The LOPAR design parameters at 2775 MWt are retained in Table 4.4-1 for historical purposes.

4.4.2.2 Fuel and Cladding Temperatures (Including Densification)

Consistent with the thermal hydraulic design bases described in subsection 4.4.1, the following discussion pertains mainly to fuel pellet temperature evaluation. A discussion of fuel clad integrity is presented in paragraph 4.2.1.3.1.

The thermal hydraulic design ensures that the maximum fuel temperature is below the melting point of UO_2 (Reference 105). The temperature distribution within the fuel pellet is predominantly a function of the local power density and the UO_2 thermal conductivity. However, the computation of radial fuel temperature distributions combines crud, oxide, clad, gap, and pellet conductances. The factors that influence these conductances, such as gap size (or

contact pressure), internal gas pressure, gas composition, pellet density, and radial power distribution within the pellet, etc., have been combined into a semi-empirical thermal model (See References 100 and 105). Reference 100 is used for the basis of LOCA inputs, while Reference 105 is used for all other analyses, which include a model for time dependent fuel densification as given in references 5, 100, and 105 for this section. This thermal model enables the determination of these factors and their net effects on temperature profiles. The temperature predictions have compared to online fuel temperature measurements and/or melt radius data as part of the generic approval of the fuel performance model (References 100 and 105).

Effect of Fuel Densification on Fuel Rod Temperatures

Fuel densification results in fuel pellet shrinkage. This affects the fuel temperatures in the following ways:

- A. Pellet radial shrinkage increases the pellet diametral gap, which results in increased thermal resistance of the gap and, thus, higher fuel temperatures (see paragraph 4.2.1.3.1).
- B. Pellet axial shrinkage may produce pellet-to-pellet gaps resulting in local power spikes and, thus, higher total heat flux hot channel factor, F_Q , and local fuel temperatures. Application of a local power spike factor is no longer necessary for Westinghouse fuel designs, as described in paragraph 4.3.2.2.5.
- C. **As described in reference 5, 100, and 105, fuel rod thermal evaluations (fuel centerline, average, and surface temperatures) are determined throughout the fuel rod lifetime with consideration of time-dependent densification and burnup related phenomena.**

4.4.2.2.1 Treatment of Peaking Factors

The total heat flux hot channel factor, F_Q , is defined by the ratio of the maximum to core average heat flux. As presented in table 4.3-2 and discussed in paragraph 4.3.2.2.1, F_Q for normal operation is 2.32 for LOPAR fuel and 2.50 for VANTAGE 5 fuel. This results in a peak local power of 12.63 kW/ft for LOPAR fuel and 13.85 kW/ft for VANTAGE 5 fuel. The peak linear power for determination of protection setpoint is less than that defined by the centerline melt temperature (Reference 105).

The centerline temperature at this kW/ft must be below the UO_2 melt temperature over the lifetime of the rod, including allowances for uncertainties.

4.4.2.2.2 Effects of Rod Bow on DNBR

The phenomenon of fuel rod bowing⁽³⁷⁾ must be accounted for in the DNBR safety analysis of Condition I and Condition II events for each plant application. Applicable generic credits for margin resulting from retained conservatism in the evaluation of DNBR and/or margin obtained from measured plant operating parameters (such as $F_{\Delta H}^N$ or core flow), which are

less limiting than those required by the plant safety analysis, can be used to offset the effect of rod bow.

For the safety analysis of the Farley units, sufficient DNBR margin was maintained (paragraph 4.4.1.1) to accommodate the full and low flow rod bow DNBR penalties which are based on the methodology in reference 38. The rod bow DNBR penalties that are applicable to LOPAR fuel assembly analyses using the WRB-1 DNB correlation and to VANTAGE+/VANTAGE 5 fuel assembly analyses using the WRB-2 DNB correlation were determined using the methodology in reference 38.

The maximum rod bow penalties accounted for in the design safety analysis are based on an assembly average burnup of 24,000 MWd/Mtu. At burnups greater than 24,000 MWd/Mtu, credit is taken for the effect of $F_{\Delta H}^N$ burndown, due to the decrease in fissionable isotopes and the buildup of fission product inventory, and no additional rod bow penalty is required (reference 39).

In the upper spans of the VANTAGE+/VANTAGE 5 fuel assembly, additional restraint is provided with the intermediate flow mixer (IFM) grids such that the grid-to-grid spacing in those spans with IFM grids is approximately 10 in. compared to approximately 20 in. in the other spans. Using the NRC approved scaling factor results in predicted channel closure in the limiting 10-in. spans of less than 50% closure; therefore, no rod bow DNBR penalty is required in the 10-in. spans in the VANTAGE+/VANTAGE 5 safety analyses.

4.4.2.2.3 Transition Core DNB Methodology

The LOPAR and VANTAGE 5 designs have been shown to be hydraulically compatible in reference 40.

The Westinghouse transition core DNB methodology is given in references 41, 42, and 43. Using this methodology, transition cores are analyzed as if the entire core consisted of one assembly type (full LOPAR or full VANTAGE 5). The resultant DNBRs are then reduced by the appropriate transition core penalty.

The VANTAGE 5 fuel assembly has a higher mixing vane grid loss coefficient relative to the LOPAR mixing vane grid loss coefficient. In addition, the VANTAGE 5 fuel assembly has IFM grids located in spans between mixing vane grids, where no grid exists in the LOPAR assembly. The higher loss coefficients and the additional grids introduce localized flow redistribution from the VANTAGE 5 fuel assembly into the LOPAR assembly at the axial zones near the mixing vane grid and the IFM grid position in a transition core. Between the grids, the tendency for velocity equalization in parallel open channels causes flow to return to the VANTAGE 5 fuel assembly. The localized flow redistribution described above actually benefits the LOPAR assembly. This benefit more than offsets the slight mass flow bias due to velocity equalization at nongridded locations. Thus, the analysis for a full core of LOPAR is appropriate for that fuel type in a transition core. There is no transition core DNBR penalty for the LOPAR fuel.

The transition core penalty is a function of the number of VANTAGE 5 fuel assemblies in the core based on the methodology of reference 44. Modifications to the magnitude of the DNBR transition core penalty for a VANTAGE 5/LOPAR transition are given in reference 45. Sufficient DNBR margin is maintained in the VANTAGE 5 safety analysis to completely offset this transition core penalty.

4.4.2.3 Critical Heat Flux Ratio or Departure from Nucleate Boiling Ratio and Mixing Technology

The minimum DNBRs for the rated power, design overpower, and anticipated transient conditions are given in table 4.4-1. The minimum DNBR in the limiting flow channel is typically downstream of the peak heat flux location (hot spot) because of the increased downstream enthalpy rise.

DNBRs are calculated by using the correlation and definitions described in paragraphs 4.4.2.3.1 and 4.4.2.3.2. The VIPRE computer code (discussed in paragraph 4.4.3.4.1) is used to determine the flow distribution in the core and the local conditions in the hot channel for use in the DNB correlation. The use of hot channel factors is discussed in paragraph 4.4.3.2.1 (nuclear hot channel factors) and in paragraph 4.4.2.3.4 (engineering hot channel factors).

4.4.2.3.1 Departure from Nucleate Boiling Technology

The primary DNB correlation that was used for the analysis of the 17 x 17 LOPAR fuel was the WRB-1 correlation (reference 46). The primary DNB correlation used for the analysis of the VANTAGE+/VANTAGE 5 fuel is the WRB-2 correlation (reference 40).

The WRB-1 correlation was developed based exclusively on the large bank of mixing vane grid rod bundle critical heat flux (CHF) data (over 1100 points) that Westinghouse has collected. The WRB-1 correlation, based on local fluid conditions, represents the rod bundle data with better accuracy over a wide range of variables than the previous correlation used in design. This correlation accounts directly for both typical and thimble cold wall cell effects, uniform and nonuniform heat flux profiles, and variations in rod heated length and in grid spacing.

The applicable range of parameters for the WRB-1 correlation is as follows:

Pressure	$1440 \leq P \leq 2490$ psia
Local Mass Velocity	$0.9 \leq G_{loc}/10^6 \leq 3.7$ lb/ft ² -h
Local Quality	$-0.2 \leq X_{loc} \leq 0.3$
Heated Length, Inlet to CHF Location	$L_h \leq 14$ ft
Grid Spacing	$13 \leq g_{sp} \leq 32$ in.
Equivalent Hydraulic Diameter	$0.37 \leq d_e \leq 0.60$ in.
Equivalent Heated Hydraulic Diameter	$0.46 \leq d_h \leq 0.59$ in.

FNP-FSAR-4

Figure 4.4-5, sheet 1 shows measured CHF plotted against predicted critical heat flux using the WRB-1 correlation.

A correlation limit DNBR of 1.17 for the WRB-1 correlation has been approved by the NRC for 17 x 17 LOPAR fuel.

The WRB-2 DNB correlation was developed to take credit for the VANTAGE+/VANTAGE 5 intermediate flow mixer (IFM) grid design. A limit of 1.17 is also applicable for the WRB-2 correlation. Figure 4.4-5, sheet 2 shows measured critical heat flux (CHF) plotted against predicted CHF using the WRB-2 correlation.

Use of this correlation has been conservatively modified to utilize a penalty above a certain high quality threshold within the approved ranges (reference 101).

The applicable range of parameters for the WRB-2 correlation is as follows:

Pressure	$1440 \leq P \leq 2490$ psia
Local Mass Velocity	$0.9 \leq G_{loc}/10^6 \leq 3.7$ lb/ft ² -h
Local Quality	$-0.1 \leq X_{loc} \leq 0.3$
Heated Length, Inlet to CHF Location	$L_h \leq 14$ ft
Grid Spacing	$10 \leq g_{sp} \leq 26$ in.
Equivalent Hydraulic Diameter	$0.33 \leq d_e \leq 0.5101$ in.
Equivalent Heated Hydraulic Diameter	$0.45 \leq d_h \leq 0.66$ in.

Prior to the Measurement Uncertainty Recapture Power Uprate (MUR-PU) the W-3 DNB correlation (references 47 and 48) was used for both fuel types where the primary DNBR correlations were not applicable. The WRB-1 and WRB-2 correlations were developed based on mixing vane data and, therefore, are only applicable in the heated rod spans above the first mixing vane grid. The W-3 correlation, which does not take credit for mixing vane grids, was used to calculate DNBR value in the heated region below the first mixing vane grid. In addition, the W-3 correlation was applied in the analysis of accident conditions where the system pressure is below the range of the primary correlations. For system pressures in the range of 500 to 1000 psia, the W-3 correlation limit is 1.45 (reference 49). For system pressures greater than 1000 psia, the W-3 correlation limit is 1.30. A cold wall factor (CWF) (reference 50) is applied to the W-3 DNB correlation to account for the presence of the unheated thimble surfaces.

For the DNB analyses supporting the MUR-PU, the W-3 Alternative correlations have been implemented. The W-3 Alternative correlations, consisting of ABB-NV and WLOP, are based exclusively on DNB data from rod bundle tests, have a wider applicable range, and are more accurate than the W-3 correlation for prediction of margin to DNB. The two correlations are used for DNBR calculations as an alternative to the W-3 correlation, in supplement to the primary DNB correlation, WRB-2.

The ABB-NV correlation was originally developed for fuel designs in Combustion Engineering designed Pressurized Water Reactors (PWR) based on a linear relationship between CHF and local quality. The correlation includes the following parameters: pressure, local mass velocity, local equilibrium quality, distance from grid to CHF location, heated length from inlet to CHF

location, and heated hydraulic diameter of the subchannel. Supplemental rod bundle data evaluation confirms that ABB-NV with the 95/95 correlation limit of 1.13 is applicable to the fuel region below the first mixing vane grid of the fuel designs for Westinghouse designed PWRs (Reference 104). Figure 4.4-5 Sheet 3 shows measured critical heat flux plotted against predicted heat flux using the ABB-NV correlation.

The applicable range of the ABB-NV correlation is:

Pressure (psia):.....	:	1750 to 2415
Local Mass Velocity (106 lbm/hr-ft ²):.....	:	0.8 to 3.16
Local Quality (fraction)	:	< 0.22
Heated Length, inlet to CHF location (in.).....	:	48 (minimum) to 150
Heated Hydraulic Diameter Ratio	:	0.679 to 1.08
Grid Distance (in.)	:	7.3 to 24

The WLOP correlation is a modified ABB-NV correlation specifically developed for low pressure conditions and extended flow range to cover low pressure/low flow conditions. Modifications to ABB-NV were made based on test data from rod bundles containing non-mixing vane grids. The WLOP correlation with a 95/95 DNBR limit of 1.18 has also been validated with test data from rod bundles containing mixing vane grids (Reference 104). Figure 4.4-4 sheet 4 shows measured critical heat flux plotted against predicted heat flux using the WLOP correlation.

The applicable range of the WLOP correlation is:

Pressure (psia)	:	185 to 1800
Local Mass Velocity (106 lbm/hr-ft ²)	:	0.23 to 3.07
Local Quality (fraction)	:	< 0.75
Heated Length, inlet to CHF location (in.)	:	48 (minimum) to 168
Heated Hydraulic Diameter Ratio	:	0.679 to 1.00
Grid Spacing Term (Reference 104)	:	27 to 115

4.4.2.3.2 Definition of Departure from Nucleate Boiling Ratio

The DNB heat flux ratio (DNBR) as applied to typical cells (flow cells with all walls heated) and thimble cells (flow cells with heated and unheated walls) is defined as:

$$\text{DNBR} = \frac{q''_{\text{DNB,N}}}{q''_{\text{loc}}} \quad (4.4-4)$$

where

$$q''_{\text{DNB,N}} = \frac{q''_{\text{DNB,EU}}}{F} \quad (4.4-5)$$

$q''_{\text{DNB,EU}}$ is the uniform DNB heat flux as predicted by the WRB-1 DNB correlation, WRB-2 DNB correlation, or the W-3 DNB correlation (typical cell only), or the alternative correlations (ABB-NV and WLOP).

F is the flux shape factor to account for nonuniform axial heat flux distributions (reference 51) with the "C" term modified as in reference 48.

q''_{loc} is the actual local heat flux.

The DNBR as applied to the W-3 DNB correlation when a cold wall is present is as follows:

$$\text{DNBR} = \frac{q''_{\text{DNB,N,CW}}}{q''_{\text{loc}}}$$

where

$$q''_{\text{DNB,N,CW}} = \frac{q''_{\text{DNB,EU,D}_h} \times \text{CWF}}{F}$$

$q''_{\text{DNB,EU,D}_h}$ is the uniform DNB heat flux as predicted by the W-3 cold wall DNB correlation (reference 48) when not all flow cell walls are heated (thimble cold wall cell).

$$\text{CWF (reference 52)} = 1.0 - \text{Ru} \left\{ 1.376 - 1.372e^{1.78X} - 4.732 \left(\frac{G}{10^6} \right)^{-0.0535} - 0.0619 \left(\frac{P}{1000} \right)^{0.14} - 8.509 D_h^{0.107} \right\}$$

$$\text{and } \text{Ru} = 1 - \frac{De}{D_h}$$

4.4.2.3.3 Mixing Technology

The rate of heat exchange by mixing between flow channels is proportional to the difference in the local mean fluid enthalpy of the respective channels, the local fluid density, and flow velocity. The proportionalism is expressed by the dimensionless thermal diffusion coefficient, TDC, which is defined as:

$$\text{TDC} = \frac{W'}{pVa} \quad (4.4-12)$$

where:

$$W' = \text{flow exchange rate per unit length, lbm/ft-s.}$$

FNP-FSAR-4

P	=	fluid density, lbm/ft ³ .
V	=	fluid velocity, ft/s.
a	=	lateral flow area between channels per-unit-length, ft ² /ft.

The application of the TDC in the THINC analysis for determining the overall mixing effect or heat exchange rate is presented in reference 53. The application of the TDC in the VIPRE-01 analysis is presented in Reference 102.

Westinghouse has also sponsored and directed mixing tests at Columbia University.⁽⁵⁴⁾ These series of tests using the "R" mixing vane grid design on 13-, 26-, and 32-in. grid spacings were conducted in pressurized water loops at Reynolds numbers similar to that of a PWR core under the following single- and two-phase (subcooled boiling) flow conditions:

Pressure	1500 to 2400 psia
Inlet Temperature	332°F to 642°F
Mass Velocity	1.0 to 3.5 x 10 ⁶ lb/h ft ²
Reynolds Number	1.34 to 7.45 x 10 ⁵
Bulk Outlet Quality	-52.1 to -13.5 percent

TDC was determined by comparing the THINC code predictions with the measured subchannel exit temperatures. Data for 26-in. axial grid spacing are presented in figure 4.4-6 where the thermal diffusion coefficient is plotted versus the Reynolds number. TDC is found to be independent of the Reynolds number, mass velocity, pressure, and quality over the ranges tested. The two-phase data (local, subcooled boiling) fell within the scatter of the single-phase data.

The effect of two-phase flow on the value of TDC has been demonstrated by Cadek,⁽⁵⁴⁾ Rowe and Angle,^(55, 56) and Gonzalez-Santalo and Griffith.⁽⁵⁷⁾ In the subcooled boiling region the values of TDC were indistinguishable from the single-phase values. In the quality region, Rowe and Angle show that in the case with rod spacing similar to that in PWR reactor core geometry, the value of TDC increased with quality to a point and then decreased, but never below the single-phase value.

Gonzalez-Santalo and Griffith showed that the mixing coefficient increased as the void fraction increased.

The data from these tests on the "R" grid showed that a design TDC value of 0.038 (for 26-in. grid spacing) can be used in determining the effect of coolant mixing in the THINC or VIPRE-01 analysis.

A mixing test program similar to the one described above was conducted at Columbia University for the 17 x 17 geometry and mixing vane grids on 26-in. spacing.⁽⁵⁸⁾ The mean value of TDC

obtained from these tests was 0.051, and all data were well above the current design value of 0.038.

Since the actual grid spacing of 17 x 17 LOPAR fuel is approximately 20 in., additional margin is available for this design, as the value of TDC increases as grid spacing decreases.⁽⁵⁴⁾

The inclusion of three IFM grids in the upper spans of the VANTAGE+/VANTAGE 5 fuel assembly results in a grid spacing of approximately 10 in. Per reference 40, a design TDC value of 0.038 was chosen as a conservatively low value for use in VANTAGE+/VANTAGE 5 to determine the effect of coolant mixing in the core thermal performance analysis.

4.4.2.3.4 Hot Channel Factors

The total hot channel factors for heat flux and enthalpy rise are defined as the maximum-to-core average ratios of these quantities. The heat flux hot channel factor considers the local maximum linear heat generation rate at a point (the "hot spot"), and the enthalpy rise hot channel factor involves the maximum integrated value along a channel (the "hot channel").

Each of the total hot channel factors is the product of a nuclear hot channel factor (see table 4.3-2 and paragraph 4.4.3.2) describing the neutron power distribution and an engineering hot channel factor, which allows for variations in flow conditions and fabrication tolerances. The engineering hot channel factors are made up of subfactors which account for the influence of the variations of fuel pellet diameter, density, enrichment, and eccentricity; inlet flow distribution; flow redistribution; and flow mixing.

Heat Flux Engineering Hot Channel Factor, F_Q^E

The heat flux engineering hot channel factor is used to evaluate the maximum linear heat generation rate in the core. This subfactor is determined by statistically combining the fabrication variations for fuel pellet diameter, density, and enrichment and has a value of 1.03 at the 95-percent probability level with 95-percent confidence. As shown in reference 59, no DNB penalty need be taken for the short, relatively low-intensity heat flux spikes caused by variations in the above parameters, as well as fuel pellet eccentricity and fuel rod diameter variation.

Enthalpy Rise Engineering Hot Channel Factor, $F_{\Delta H}^E$

The effect of variations in flow conditions and fabrication tolerances on the hot channel enthalpy rise is directly considered in the VIPRE-01 subchannel analysis (paragraph 4.4.3.4.1) under any reactor operating condition. The items considered contributing to the enthalpy rise engineering hot channel factor are discussed below:

A. Pellet diameter, density, and enrichment:

Variations in pellet diameter, density, and enrichment are considered statistically in establishing the limit DNBRs (paragraph 4.4.1.1) for the RTDP (reference 2)

employed in this application. Uncertainties in these variables are determined from sampling manufacturing data.

B. Inlet Flow Maldistribution:

The consideration of inlet flow maldistribution in core thermal performances is discussed in paragraph 4.4.3.1.2. A design basis of 5-percent reduction in coolant flow to the hot assembly is used in the VIPRE-01 analysis.

C. Flow Redistribution:

The flow redistribution accounts for the reduction in flow in the hot channel because of the local or bulk boiling. The effect of the nonuniform power distribution is inherently considered in the VIPRE-01 analysis for every operating condition which is evaluated.

D. Flow Mixing:

The subchannel mixing model incorporated in the VIPRE-01 code and used in reactor design is based on experimental data⁽⁶⁰⁾ discussed in paragraph 4.4.3.4.1. The mixing vanes incorporated in the spacer grid design induce additional flow mixing between the various flow channels in a fuel assembly, as well as between adjacent assemblies. This mixing reduces the enthalpy rise in the hot channel resulting from local power peaking or unfavorable mechanical tolerances.

4.4.2.4 Flux Tilt Considerations

Significant quadrant power tilts are not anticipated during normal operation since this phenomenon is caused by some asymmetric perturbation. A dropped or misaligned RCCA could cause changes in hot channel factors. However, these events are analyzed separately in chapter 15. This discussion will be confined to flux tilts caused by x-y xenon transients, inlet temperature mismatches, enrichment variations within tolerances, and so forth.

The design value of the enthalpy rise hot channel factor $F_{\Delta H}^N$, which includes an 8-percent uncertainty (as discussed in paragraph 4.3.2.2.7), is assumed to be sufficiently conservative that flux tilts up to, and including, the alarm point (see technical specifications) will not result in values of $F_{\Delta H}^N$ greater than that assumed in this submittal. The design value of F_Q does not include a specific allowance for quadrant flux tilts.

4.4.2.5 Void Fraction Distribution

The VIPRE-01 calculated core average and the hot subchannel maximum and average void fractions are presented in table 4.4-2 for operation at full power. The void fraction distribution in

the core at various radial and axial locations is presented in reference 61. The void models used in the VIPRE-01 computer code are described in paragraph 4.4.2.8.3.

4.4.2.6 Core Coolant Flow Distribution

Assembly average coolant mass velocity and enthalpy at various radial and axial core locations are given in figures 4.4-7 through 4.4-9. Coolant enthalpy rise and flow distributions are shown for the 4-ft elevation (1/3 of core height) in figure 4.4-7 and 8-ft elevation (2/3 of core height) in figure 4.4-8, and at the core exit in figure 4.4-9. These distributions are representative of a Westinghouse 3-loop plant. The THINC code analysis for this case utilized a uniform core inlet enthalpy and inlet flow distribution.

4.4.2.7 Core Pressure Drops and Hydraulic Loads

4.4.2.7.1 Core Pressure Drops

The analytical model and experimental data used to calculate the pressure drops shown in table 4.4-1 are described in paragraph 4.4.2.8. The core pressure drop includes the fuel assembly, lower core plate, and upper core plate pressure drops. The full power operation pressure drop values shown in table 4.4-1 are the unrecoverable pressure drops across the vessel, including the inlet and outlet nozzles, and across the core. These pressure drops are based on the best-estimate flow for actual plant operating conditions as described in subsection 5.5.1. This subsection also defines and describes the thermal design flow (minimum flow) which is the basis for reactor core thermal performance and the mechanical design flow (maximum flow) which is used in the mechanical design of the reactor vessel internals and fuel assemblies. Since the best-estimate flow is that flow which is most likely to exist in an operating plant, the calculated core pressure drops in table 4.4-1 are based on this best-estimate flow rather than the thermal design flow.

Uncertainties associated with the core pressure drop values are discussed in paragraph 4.4.2.10.2.

4.4.2.7.2 Hydraulic Loads

The fuel assembly holddown springs (figure 4.2-2) are designed to keep the fuel assemblies in contact with the lower core plate under all Condition I and II events with the exception of the turbine overspeed transient associated with a loss of external load. The holddown springs are designed to tolerate the possibility of an over-deflection associated with fuel assembly liftoff for this case and provide contact between the fuel assembly and the lower core plate following this transient. More adverse flow conditions occur during a LOCA. These conditions are presented in subsection 15.4.1.

Hydraulic loads at normal operating conditions are calculated based on the mechanical design flow, which is described in section 5.1, and accounting for the minimum core bypass flow based

on manufacturing tolerances. Core hydraulic loads at cold-plant startup conditions are also based on this flow, but are adjusted to account for the coolant density difference. Conservative core hydraulic loads for a pump overspeed transient, which create flowrates 20 percent greater than the mechanical design flow, are evaluated to be greater than twice the fuel assembly weight.

The hydraulic verification tests for the LOPAR fuel assembly and the VANTAGE 5 fuel assembly are discussed in references 62 and 40, respectively.

4.4.2.8 Correlation and Physical Data

4.4.2.8.1 Surface Heat Transfer Coefficients

Forced convection heat transfer coefficients are obtained from the familiar Dittus-Boelter correlation⁽⁶³⁾, with the properties evaluated at bulk fluid conditions:

$$\frac{hD_e}{K} = 0.023 \left(\frac{(D_e G)^{0.8}}{\mu} \right) \frac{(C_p \mu)^{0.4}}{K} \quad (4.4-12)$$

where

- h = heat transfer coefficient, Btu/h-ft²-°F.
- D_e = equivalent diameter, ft.
- K = thermal conductivity, Btu/h-ft-°F.
- G = mass velocity, lb/h-ft².
- μ = dynamic viscosity, lb/ft-h.
- C_p = heat capacity, Btu/lb-°F.

This correlation has been shown to be conservative⁽⁶⁴⁾ for rod bundle geometries with pitch-to-diameter ratios in the range used by PWRs. The onset of nucleate boiling occurs when the clad wall temperature reaches the amount of superheat predicted by Thom's⁽⁶⁵⁾ correlation. After this occurrence, the outer clad wall temperature is determined by:

$$\Delta T_{\text{sat}} = \left[0.072 \exp \left(-\frac{P}{1260} \right) \right] (q'')^{0.5}$$

where

- ΔT_{sat} = wall superheat, $T_w - T_{\text{sat}}$.

q''	=	wall heat flux, Btu/h-ft ² .
p	=	pressure, psia.
T_w	=	outer clad wall temperature, °F.
T_{sat}	=	saturation temperature of coolant at P, °F.

4.4.2.8.2 Total Core and Vessel Pressure Drop

Unrecoverable pressure losses occur as a result of viscous drag (friction) and/or geometry changes (form) in the fluid flow path. The flow field is assumed to be incompressible, turbulent, single-phase water. These assumptions apply to the core and vessel pressure drop calculation for the purpose of establishing the primary loop flowrate. Two-phase considerations are neglected in the vessel pressure drop evaluation because the core-average void is negligible (paragraph 4.4.2.5 and table 4.4-2). Two-phase flow considerations in the core thermal subchannel analyses are considered and the models are discussed in paragraph 4.4.3.1.3. Core and vessel pressure losses are calculated by equations of the form:

$$\Delta P_L = \left(K + F \frac{L}{D_e} \right) \frac{\rho V^2}{2g_c(144)} \quad (4.4-14)$$

where:

ΔP_L	=	unrecoverable pressure drop, lb _f /in ² .
ρ	=	fluid density, lb/ft ³ .
L	=	length, ft.
D_e	=	equivalent diameter, ft.
V	=	fluid velocity, ft/s.
g_c	=	32.174, $\frac{\text{lb}_m - \text{ft}}{\text{lb}_f - \text{s}^2}$
K	=	form loss coefficient, dimensionless.
F	=	friction loss coefficient, dimensionless.

Fluid density is assumed to be constant at the appropriate value for each component in the core and vessel. Because of the complex core and vessel flow geometry, precise analytical values

for the form and friction loss coefficients are not available. Therefore, experimental values for these coefficients are obtained from geometrically similar models.

Values are quoted in table 4.4-1 for unrecoverable pressure loss across the reactor vessel, including the inlet and outlet nozzles, and across the core. The results of full-scale tests of core components and fuel assemblies were utilized in developing the core pressure loss characteristic. The pressure drop for the vessel was obtained by combining the core loss with correlation of 1/7th-scale model hydraulic test data on a number of vessels^(66, 67) and form loss relationships.⁽⁶⁸⁾ Moody⁽⁶⁹⁾ curves were used to obtain the single-phase friction factors.

Tests of the primary coolant loop flowrates will be made (paragraph 4.4.4.1) prior to initial criticality to verify that the flowrates used in the design, which were determined in part from the pressure losses calculated by the method described here, are conservative.

4.4.2.8.3 Void Fraction Correlation

VIPRE-01 considers two-phase flow in two steps. First, a quality model is used to compute the flowing vapor mass fraction (true quality) including the effects of subcooled boiling. Then, given the true quality, a bulk void model is applied to compute the vapor volume fraction (void fraction).

VIPRE-01 uses a profile fit model (Reference 103) for determining subcooled quality. It calculates the local vapor volumetric fraction in forced convection boiling by: 1) predicting the point of bubble departure from the heated surface, and 2) postulating a relationship between the true local vapor fraction and the corresponding thermal equilibrium value.

4.4.2.9 Thermal Effects of Operational Transients

DNB core safety limits are generated as a function of coolant temperature, pressure, core power, and axial power imbalance. Steady-state operation within these safety limits ensures that the DNB design basis is met. Figure 15.1-1 shows the DNBR limit lines and the resulting overtemperature ΔT trip lines (which become part of the technical specifications), plotted as ΔT vs. T_{avg} for various pressures.

This system provides adequate protection against anticipated operational transients that are slow with respect to fluid transport delays in the primary system. In addition, for fast transients, e.g., uncontrolled rod bank withdrawal at power incident (subsection 15.2.2), specific protection functions are provided as described in section 7.2, and the uses of these protection functions are described in chapter 15. (See table 15.1-3.)

The thermal response of the fuel rod is discussed in paragraph 4.4.3.7.

4.4.2.10 Uncertainties in Estimates

4.4.2.10.1 Uncertainties in Pressure Drops

Core and vessel pressure drops based on the best-estimate flow, described in section 5.1, are quoted in table 4.4-1. The uncertainties quoted are based on the uncertainties in both the test results and the analytical extension of these values to the reactor application. A major use of the core and vessel pressure drops is to determine the primary system coolant flowrates. In addition, as discussed in paragraph 4.4.4.1, tests on the primary system prior to initial criticality will be made to verify that a conservative primary system coolant-flowrate has been used in the design and analyses of Farley Nuclear Plant.

4.4.2.10.2 Uncertainties Caused by Inlet Flow Maldistribution

The effects of uncertainties in the inlet flow maldistribution criteria used in the core thermal analyses are discussed in paragraph 4.4.3.1.2.

4.4.2.10.3 Uncertainty in DNB Correlation

The uncertainty in the DNB correlation (paragraph 4.4.2.3) can be written as a statement on the probability of not being in DNB based on the statistics of the DNB data. This is discussed in paragraph 4.4.2.3.2.

4.4.2.10.4 Uncertainties in DNBR Calculations

The uncertainties in the DNBRs calculated by VIPRE-01 analysis (see paragraph 4.4.3.4.1) because of uncertainties in the nuclear peaking factors are accounted for by applying conservatively high values of the nuclear peaking factors and including measurement error allowances in the statistical evaluation of the limit DNBR (paragraph 4.4.1.1) using the RTDP (reference 2).

In addition, conservative values for the engineering hot channel factors are used as discussed in paragraph 4.4.2.3.4.

The results of a sensitivity study⁽⁶¹⁾ with THINC-IV show that the minimum DNBR in the hot channel is relatively insensitive to variations in the core-wide radial power distribution (for the same value of $F_{\Delta H}$). VIPRE-01 was demonstrated to be equivalent to THINC-IV in Reference 102.

The ability of the VIPRE computer code to accurately predict flow and enthalpy distributions in rod bundles is discussed in Subsection 4.4.4.5 and in Reference 102. Studies have been performed (References 102 and 103) to determine the sensitivity of the minimum DNBR in the hot channel to void fraction correlation (Subsection 4.4.2.7.3) and the inlet flow distributions. The results of these studies show that the minimum DNBR is relatively insensitive to variation in

these parameters. Furthermore, the VIPRE flow field model for predicting conditions in the hot channels is consistent with that used in the derivation of the DNB correlation limits, including void/quality modeling, turbulent mixing and crossflow, and two-phase friction (Reference 102).

4.4.2.10.5 Uncertainties in Flowrates

The uncertainties associated with loop flowrates are discussed in section 5.1. A thermal design flow is defined for use in core thermal performance evaluations which accounts for both prediction and measurement uncertainties. In addition, another 7.1 percent of the thermal design flow is assumed to be ineffective for core heat removal capability because it bypasses the core through the various available vessel flow-paths described in paragraph 4.4.3.1.1.

4.4.2.10.6 Uncertainties in Hydraulic Loads

As discussed in paragraph 4.4.2.7.2, hydraulic loads on the fuel assembly are evaluated for a pump overspeed transient which creates flowrates 20 percent greater than the mechanical design flow. The mechanical design flow as stated in section 5.1 is greater than the best estimate or most likely flowrate value for the actual plant operating condition.

4.4.2.10.7 Uncertainty in Mixing Coefficient

The value of the mixing coefficient, TDC, used in VIPRE-01 analyses for this application is 0.038 for LOPAR fuel and VANTAGE+/VANTAGE 5 fuel.

The results of the mixing tests done on 17 x 17 LOPAR geometry, as discussed in paragraph 4.4.2.3.3, had a mean value of TDC of 0.059 and standard deviation of $\sigma = 0.007$. Hence the current design value of TDC is almost three standard deviations below the mean for 26-in. grid spacing.

4.4.2.11 Plant Configuration Data

Plant configuration data for the thermal hydraulic and fluid systems external to the core are provided in the appropriate chapters 5, 6, and 9. Implementation of the emergency core cooling system is discussed in chapter 15. Some specific areas of interest are the following:

- A. Total coolant flowrates for the reactor coolant system and each loop are provided in table 5.1-1. Flowrates employed in the evaluation of the core are presented in section 4.4.
- B. Total RCS volume, including pressurizer and surge line and RCS liquid volume (including pressurizer water at steady-state power conditions), are given in table 5.1-1.
- C. The flowpath length through each volume may be calculated from physical data provided in the above-referenced sections.

- D. The height of fluid in components of the RCS may be determined from the physical data presented in section 5.5. The components of the RCS are water filled during power operation, with the pressurizer being approximately 60-percent water filled.
- E. The elevation of components of the RCS relative to the reactor containment are shown in figures 1.2-6 and 1.2-7. Components of the ECCS are to be located in a manner which meets the criteria for NPSH described in section 6.3, and provide the minimum emergency flow as discussed in sections 15.3 and 15.4.
- F. Line lengths and sizes for the safety injection system are determined in a manner which guarantees a total system resistance which provides, as a minimum, the fluid delivery rates assumed in the safety analyses described in chapter 15.
- G. The minimum flow areas for components of the RCS are presented in section 5.5, Component and Subsystem Design.
- H. The steady-state pressure and temperature distributions through the RCS are presented in table 5.1-1.

4.4.3 EVALUATION

4.4.3.1 Core Hydraulics

4.4.3.1.1 Flowpaths Considered in Core Pressure Drop and Thermal Design

The following flowpaths for core bypass flow are considered:

- A. Flow through the spray nozzles into the upper head for head cooling purposes.
- B. Flow entering into the RCC guide thimbles to cool the core component rods.
- C. Leakage flow from the vessel inlet nozzle directly to the vessel outlet nozzle through the gap between the vessel and the barrel.
- D. Flow introduced between the baffle and the barrel for the purpose of cooling these components and not considered available for core cooling.
- E. Flow entering into the core from the barrel baffle region through the gaps between the baffle plates.

The above contributions are evaluated to confirm that the design basis value of ≤ 7.1 -percent core bypass flow is met. This design bypass value is also used in the evaluation of the core pressure drops quoted in table 4.4-1 and the determination of reactor flowrates in section 5.1.

Flow model test results for the flowpath through the reactor are discussed in paragraph 4.4.2.8.2.

4.4.3.1.2 Inlet Flow Distribution

Data have been considered from several 1/7-scale hydraulic reactor model tests⁽⁶⁶⁾⁽⁶⁷⁾⁽⁷⁴⁾ in arriving at the core inlet flow maldistribution criteria to be used in the THINC analyses (see paragraph 4.4.3.4.1). THINC I analyses made using these data have indicated that a conservative design basis is to consider a 5-percent reduction in the flow to the hot assembly.⁽⁵³⁾ The same design basis of 5-percent reduction to the hot assembly inlet is used in the VIPRE-01 analyses.

The experimental error estimated in the inlet velocity distribution has been considered as outlined in reference 61, where the sensitivity of changes in inlet velocity distributions to hot channel thermal performance is shown to be small. Studies⁽⁶¹⁾ made with the THINC-IV model show that it is adequate to use the 5-percent reduction in inlet flow to the hot assembly for a loop out of service, based on the experimental data in references 66 and 67. VIPRE-01 was demonstrated to be equivalent to THINC-IV in Reference 102.

The effect of the total flowrate on the inlet velocity distribution was studied in the experiments of reference 66. As was expected, on the basis of the theoretical analysis, no significant variation could be found in inlet velocity distribution with reduced flowrate.

4.4.3.1.3 Empirical Friction Factor Correlations

Empirical friction factor correlations are used in the VIPRE-01 computer code (described in paragraph 4.4.3.4.1).

The friction factor in the axial direction, parallel to the fuel rod axis, is evaluated using a correlation for the smooth tube (Reference 102). The effect of two-phase flow on the friction loss is expressed in terms of the single-phase friction pressure drop and a two-phase friction multiplier. The multiplier is calculated directly using the homogeneous equilibrium flow model.

The flow in the lateral directions, normal to the fuel rod axis, views the reactor core as a large tube bank. Thus, the lateral friction factor proposed by Idel'chik⁽⁶⁸⁾ is applicable. This correlation is of the form

$$FL = A Re_L^{-0.2} \quad (4.4-15)$$

where:

A = is a function of the rod pitch and diameter as given in reference 68.

Re_L = is the lateral Reynolds number based on the rod diameter.

Extensive comparisons of VIPRE-01 predictions using these correlations to THINC-IV predictions are given in reference 102 and verify the applicability of these correlations in PWR design.

4.4.3.2 Influence of Power Distribution

The core power distribution, which is largely established at beginning of life by fuel enrichment, loading pattern, and core power level, is also a function of variables such as control rod worth and position and fuel depletion throughout lifetime. Radial power distributions in various planes of the core are often illustrated for general interest. However, the core radial enthalpy rise distribution as determined by the integral of power up each channel is of greater importance for DNB analyses. These radial power distributions, characterized by $F_{\Delta H}^N$ (defined in paragraph 4.3.2.2.2), as well as axial heat flux profiles, are discussed in the following two sections.

4.4.3.2.1 Nuclear Enthalpy Rise Hot-Channel Factor, $F_{\Delta H}^N$

Given the local power density q' (kW/ft) at point x, y, z in a core with N fuel rods and height H ,

$$F_{\Delta H}^N = \frac{\text{hot rod power}}{\text{average rod power}} = \frac{\text{Max} \int_0 Hq'(x_0, y_0, z) dz}{\frac{1}{N} \sum_{\text{all rods}} \int_0 Hq'(x, y, z) dz}$$

The way in which $F_{\Delta H}^N$ is used in the DNB calculation is important.

It is obvious that the location of minimum DNBR will depend on the axial profile and the value of DNBR will depend on the enthalpy rise to that point. Basically, the maximum value of the rod integral is used to identify the most likely rod for minimum DNBR. An axial power profile is obtained which, when normalized to the design value of $F_{\Delta H}^N$, recreates the axial heat flux along the limiting rod. The surrounding rods are assumed to have the same axial profile with rod average powers which are typical of distributions found in hot assemblies. In this manner, worst-case axial profiles can be combined with worst-case radial distributions for reference DNB calculations.

It should be noted again that $F_{\Delta H}^N$ is an integral and is used as such in the DNB calculations. Local heat fluxes are obtained by using hot channel and adjacent channel explicit power shapes which take into account variations in horizontal power shapes throughout the core. The sensitivity of the DNB calculations to radial power shapes is discussed in reference 61. The VIPRE analyses were based on the design radial power distribution discussed in Reference 61. For operation at a fraction P of full power, the design $F_{\Delta H}^N$, used is given by:

$$F_{\Delta H}^N = 1.30 [1 + 0.3(1 - P)] \text{ for LOPARfuel}$$

$$F_{\Delta H}^N = 1.70 [1 + 0.3(1 - P)] \text{ for VANTAGE5 fuel}$$

It should be noted that the maximum value of the analysis of record $F_{\Delta H}^N$ for both Unit 1 and Unit 2 is 1.70 as indicated above.

The permitted relaxation of $F_{\Delta H}^N$ is included in the DNB protection setpoints and allows radial power shape changes with rod insertion to the insertion limits,⁽⁷⁷⁾ thus allowing greater flexibility in the nuclear design.

4.4.3.2.2 Axial Heat Flux Distributions

As discussed in paragraph 4.3.2.2, the axial heat flux distribution can vary as a result of rod motion, power change, or because of spatial xenon transients which may occur in the axial direction. Consequently, it is necessary to measure the axial power imbalance by means of the ex-core nuclear detectors (as discussed in paragraph 4.3.2.2.7) and protect the core from excessive axial power imbalance. The reactor trip system provides automatic reduction of the trip setpoint in the overtemperature ΔT channels on excessive axial power imbalance; that is, when an extremely large axial offset corresponds to an axial shape which could lead to a DNBR which is less than that calculated for the reference DNB design axial shape.

The reference DNB design axial shape used in the automatic reduction of the overtemperature ΔT setpoint is a chopped cosine shape with a peak-to-average of 1.70.

4.4.3.3 Core Thermal Response

A general summary of the steady-state thermal hydraulic design parameters is provided in table 4.4-1 for all loops in operation.

As stated in subsection 4.4.1, the design bases of the application are to prevent departure from nucleate boiling and to prevent fuel melting for Condition I and II events. The protective systems described in chapter 7 (Instrumentation and Controls) are designed to meet these bases. The response of the core to Condition II transients is given in section 15.

4.4.3.4 Analytical Techniques

4.4.3.4.1 Core Analysis

The objective of reactor core thermal design is to determine the maximum heat removal capability in all flow subchannels and show that the core safety limits, as presented in technical specifications, are not exceeded including the effects of engineering and nuclear hot channel factors. The thermal design takes into account local variations in dimensions, power generation, flow redistribution, and mixing.

Prior to the MUR power uprate to 2831 MWt, the THINC-IV code (References 61, 73, and 78) was used for the core thermal design. Commencing with the MUR power uprate, the VIPRE-01 code is used for the core thermal design. VIPRE-01 is a three-dimensional subchannel code that has been developed to account for hydraulic and nuclear effects on the enthalpy rise in the core and hot channels (Reference 103). VIPRE-01 modeling of a PWR core is based on onepass modeling approach (Reference 102). In the one-pass modeling, hot channels and their adjacent channels are modeled in detail, while the rest of the core is modeled simultaneously on a relatively coarse mesh. The behavior of the hot assembly is determined by superimposing the power distribution upon inlet flow distribution while allowing for flow mixing and flow distribution between flow channels. Local variations in fuel rod power, fuel rod and pellet fabrication, and turbulent mixing are also considered in determining conditions in the hot channels. Conservation equations of mass, axial and lateral momentum, and energy are solved for the fluid enthalpy, axial flow rate, lateral flow, and pressure drop.

Steady-State Analysis

The VIPRE-01 core model as approved by the NRC, Reference 102, is used with the applicable DNB correlations to determine DNBR distributions along the hot channels of the reactor core under all expected operating conditions. The VIPRE-01 code is described in detail in Reference 103, including discussions on code validation with experimental data. The VIPRE-01 modeling method is described in Reference 102, including empirical models and correlations used.

The effect of crud on the flow and enthalpy distribution in the core is not directly accounted for in the VIPRE-01 evaluations. However, conservative treatment by the VIPRE-01 modeling method has been demonstrated to bound this effect in DNBR calculations (Reference 102). The VIPRE-01 model has been demonstrated in Reference 102 to be equivalent to the THINCIV code for steady-state analyses.

Extensive experimental verification of VIPRE-01 is presented in reference 103.

The VIPRE-01 analysis is based on a knowledge and understanding of the heat transfer and hydrodynamic behavior of the coolant flow and the mechanical characteristics of the fuel elements. The use of the VIPRE-01 analysis provides a realistic evaluation of the core performance and is used in the thermal analysis as described above.

Transient Analysis

VIPRE-01 is capable of transient DNB analysis. The conservation equations in the VIPRE-01 code contain the necessary accumulation terms for transient calculations. The input description can include one or more of the following time dependent arrays:

1. Inlet flow variation,
2. Core heat flux variation,
3. Core pressure variation,
4. Inlet temperature or enthalpy variation.

At the beginning of the transient, the calculation procedure is carried out as in the steady state analysis. The time is incremented by an amount determined either by the user or by the time step control options in the code itself. At each new time step the calculations are carried out with the addition of the accumulation terms which are evaluated using the information from the previous time step. This procedure is continued until a preset maximum time is reached.

At time intervals selected by the user, a complete description of the coolant parameter distributions as well as DNBR is printed out. In this manner the variation of any parameter with time can be readily determined.

The methods for evaluating fuel rod thermal response are described in Section 15.1.14.

4.4.3.4.2 Fuel Temperatures

As discussed in paragraph 4.4.2.2, the fuel rod behavior is evaluated utilizing a semiempirical thermal model which considers, in addition to the thermal aspects, such items as clad creep, fuel swelling, time-dependent densification, fission gas release, release of absorbed gases, cladding corrosion and elastic deflection, and helium solubility.

A detailed description of the thermal model can be found in references 5, 100 and 105.

4.4.3.4.3 Hydrodynamic Instability

The analytical methods used to assess hydraulic instability are discussed in paragraph 4.4.3.5.

4.4.3.5 Hydrodynamic and Flow Power Coupled Instability

Boiling flow may be susceptible to thermohydrodynamic instabilities (reference 85). These instabilities are undesirable in reactors since they may cause a change in thermohydraulic conditions that may lead to a reduction in the DNB heat flux relative to that observed during a steady flow condition, or to undesired forced vibrations of core components. Therefore, a thermohydraulic design criterion was developed which states that modes of operation under Condition I and II events shall not lead to thermohydrodynamic instabilities.

Two specific types of flow instabilities are considered for Westinghouse PWR operation. These are the Ledinegg or flow excursion-type of static instability and the density wave-type of dynamic instability.

A Ledinegg instability involves a sudden change in flowrate from one steady state to another. This instability occurs (reference 85) when the slope of the reactor coolant system pressure drop-flowrate curve $\left(\frac{\partial \Delta p}{\partial G}\right)_{\text{INTERNAL}}$ becomes algebraically smaller than the loop supply (pump head) pressure drop-flowrate curve $\left(\frac{\partial \Delta p}{\partial G}\right)_{\text{EXTERNAL}}$. The criterion for stability is thus

$\frac{\partial \Delta p}{\partial G} \Big|_{\text{INTERNAL}} \geq - \frac{\partial \Delta p}{\partial G} \Big|_{\text{EXTERNAL}}$. The W pump head curve has a negative slope $\left(\frac{\partial \Delta p}{\partial G}\right)_{\text{EXTERNAL}} < 0$,

whereas the reactor coolant system pressure drop-flow curve has a positive slope $\left(\frac{\partial \Delta p}{\partial G}\right)_{\text{INTERNAL}} > 0$ over the Condition I and Condition II operational ranges. Thus, the Ledinegg instability will not occur.

The mechanism of density wave oscillations in a heated channel has been described by Lahey and Moody (reference 86). Briefly, an inlet flow fluctuation produces an enthalpy perturbation. This perturbs the length and the pressure drop of the single-phase region and causes quality or void perturbations in the two-phase regions which travel up the channel with the flow. The quality and length perturbations in the two-phase region create two-phase pressure drop perturbations. However, since the total pressure drop across the core is maintained by the characteristics of the fluid system external to the core, then the two-phase pressure drop perturbation feeds back to the single-phase region. These resulting perturbations can be either attenuated or self-sustained.

A simple method has been developed by Ishii (reference 87) for parallel, closed-channel systems to evaluate whether a given condition is stable with respect to the density wave-type of dynamic instability. This method had been used to assess the stability of typical Westinghouse reactor designs (references 88, 89, 90) under Condition I and II operation. The results indicate that a large margin to density wave instability exists, e.g., increases on the order of 150 percent of rated reactor power would be required for the predicted inception of this type of instability.

The application of the method of Ishii (reference 87) to Westinghouse reactor designs is conservative because of the parallel open-channel feature of Westinghouse PWR cores. For such cores, there is little resistance to lateral flow leaving the flow channels of high power density. There is also energy transfer from channels of high power density to lower-power density channels. This coupling with cooler channels has led to the opinion that an open-channel configuration is more stable than the above closed-channel analysis under the same boundary conditions. Flow stability tests (reference 91) have been conducted where the closed-channel systems were shown to be less stable than when the same channels were cross-connected at several locations. The cross-connections were such that the resistance to channel crossflow and enthalpy perturbations would be greater than that which would exist in a PWR core which has a relatively low resistance to crossflow.

Flow instabilities which have been observed have occurred almost exclusively in closed-channel systems operating at low pressure relative to the Westinghouse PWR operating pressures. Kao, Morgan, and Parker (reference 92) analyzed parallel closed-channel stability experiments simulating a reactor core flow. These experiments were conducted at pressures up to 2200 psia. The results showed that for flow and power levels typical of power reactor conditions, no flow oscillations could be induced above 1200 psia.

Additional evidence that flow instabilities do not adversely affect thermal margin is provided by the data from the rod bundle DNB tests. Many Westinghouse rod bundles have been tested over wide ranges of operating conditions with no evidence of premature DNB or of inconsistent data which might be indicative of flow instabilities in the rod bundle.

In summary, it is concluded that thermohydrodynamic instabilities will not occur under Condition I and II modes of operation for Westinghouse PWR reactor designs. A large power margin

exists to predicted inception of such instabilities. Analysis has been performed which shows that minor plant-to-plant differences in Westinghouse reactor designs such as fuel assembly arrays, core power flow ratios, fuel assembly length, etc., will not result in gross deterioration of the above power margins.

4.4.3.6 Temperature Transient Effects Analysis

Waterlogging damage of a fuel rod could occur as a consequence of a power increase on a rod after water has entered the fuel rod through a cladding defect. Water entry will continue until the fuel rod internal pressure is equal to the reactor coolant pressure. A subsequent power increase raises the temperature and, hence, could raise the pressure of the water contained within the fuel rod. The increase in hydrostatic pressure within the fuel rod then drives a portion of the water from the fuel rod through the water entry defect. Cladding distortion and/or rupture can occur if the fuel rod internal pressure increase is excessive because of insufficient venting of water to the reactor coolant. This occurs when there is both a rapid increase in the temperature of the water within the fuel rod and small defect. Zircaloy-clad fuel rods which have failed because of waterlogging^(93, 94) indicate that very rapid power transients are required for fuel failure. Normal operational transients are limited to about 40 cal/g-min (peak rod) while the Spert tests⁽⁹³⁾ indicate that 120- to 150-cal/g is required to rupture the cladding even with very short transients (5.5 ms period). Release of the internal fuel rod pressure is expected to have minimal effect on the reactor coolant system⁽⁹³⁾ and is not expected to result in failure of additional fuel rods.⁽⁹⁴⁾ Ejecting of fuel pellet fragments into the coolant stream is not expected.^(93, 94) A cladding breach because of waterlogging is thus expected to be similar to any fuel rod failure mechanism which exposes fuel pellets to the reactor coolant stream. Waterlogging has not been identified as the mechanism for cladding distortion or perforation of any Westinghouse Zircaloy-4/ZIRLO/Optimized ZIRLO clad fuel rods.

4.4.3.7 Potentially Damaging Temperature Effects During Transients

The fuel rod experiences many operational transients (intentional maneuvers) during its residency in the core. A number of thermal effects must be considered when analyzing the fuel rod performance.

The clad can be in contact with the fuel pellet at some time in the fuel lifetime. Clad pellet interaction occurs if the fuel pellet temperature is increased after the clad is in contact with the pellet. Clad pellet interaction is discussed in paragraph 4.2.1.3.1.

The potential effects of operation with waterlogged fuel are discussed in paragraph 4.4.3.6, which concluded that waterlogging is not a concern during operational transients.

Clad flattening, as noted in paragraph 4.2.1.3.1, has been observed in some operating power reactors. Thermal expansion (axial) of the fuel rod stack against a flattened section of clad could cause failure of the clad. This is no longer a concern because clad flattening is precluded during the fuel residence in the core. (See paragraph 4.2.1.3.1.)

There can be a differential thermal expansion between the fuel rods and the guide thimbles during a transient. Excessive bowing of the fuel rods could occur if the grid assemblies did not allow axial movement of the fuel rods relative to the grids. Thermal expansion of the fuel rods is considered in the grid design so that axial loads imposed on the fuel rods during a thermal transient will not result in excessively-bowed fuel rods (see paragraph 4.2.1.3.2).

4.4.3.8 Energy Release During Fuel Element Burnout

As discussed in paragraph 4.4.3.3, the core is protected from going through DNB over the full range of possible operating conditions. At full power nominal operating conditions, the minimum DNBR is 2.15 for the VANTAGE+/VANTAGE 5 fuel as compared to the DNBR limit 1.24. This means that at nominal conditions, the probability of a rod going through DNB is negligible based on the statistics used with RTDP to determine the DNBR limit. In the extremely unlikely event that DNB should occur, the clad temperature will rise because of the steam blanketing at the rod surface and the consequent degradation in heat transfer. During this time there is a potential for a chemical reaction between the cladding and the coolant. However, because of the relatively good film-boiling heat transfer following DNB, the energy release resulting from this reaction is insignificant compared to the power produced by the fuel.

DNB With Physical Burnout - Westinghouse⁽⁹⁵⁾ has conducted DNB tests in a 25-rod bundle where physical burnout occurred with one rod. After this occurrence, the 25-rod test section was used for several days to obtain more DNB data from the other rods in the bundle. The burnout and deformation of the rod did not affect the performance of neighboring rods in the test section during the burnout or the validity of the subsequent DNB data points as predicted by the W-3 correlation. No occurrences of flow instability or other abnormal operation were observed.

DNB With Return to Nucleate Boiling - Additional DNB tests have been conducted by Westinghouse⁽⁹⁶⁾ in 19- and 21-rod bundles. In these tests, DNB without physical burnout was experienced more than once on a single rod in the bundles for short periods of time. Each time, a reduction in power of approximately 10 percent was sufficient to reestablish nucleate boiling on the surface of the rod. During these and subsequent tests, no adverse effects were observed on this rod or any other rod in the bundle as a consequence of operating in DNB.

4.4.3.9 Energy Release or Rupture of Waterlogged Fuel Elements

A full discussion of waterlogging, including energy release, is contained in paragraph 4.4.3.6. It is noted that the resulting energy release is not expected to affect neighboring fuel rods.

4.4.3.10 Fuel Rod Behavior Effects from Coolant Flow Blockage

Coolant flow blockages can occur within the coolant channels of a fuel assembly or external to the reactor core. The effects of fuel assembly blockage within the assembly on fuel rod behavior is more pronounced than external blockages of the same magnitude. In both cases, the flow blockages cause local reductions in coolant flow. The amount of local flow reduction, where it occurs in the reactor, and how far along the flow stream the flow reduction persists are

considerations which will influence the fuel rod behavior. The effects of coolant flow blockages, in terms of maintaining rated core performance, are determined both by analytical and experimental methods. The experimental data are usually used to augment analytical tools. Inspection of the DNB correlations (paragraph 4.4.2.3 and references 40, 46, 47, 48, and 51) shows that the predicted DNBR is dependent upon the local values of quality and mass velocity.

The VIPRE-01 code is capable of predicting the effects of local flow blockages on DNBR within the fuel assembly on a subchannel basis, regardless of where the low blockage occurs. In reference 103, it is shown that for a fuel assembly similar to the Westinghouse design, VIPRE-01 accurately predicts the flow distribution within the fuel assembly when the inlet nozzle is completely blocked. Full recovery of the flow was found to occur about 30 in. downstream of the blockage. With the reactor operating at the nominal full power conditions specified in table 4.4-1, the effects of an increase in enthalpy and decrease in mass velocity in the lower portion of the fuel assembly would not result in a minimum DNBR below the DNBR limit.

From a review of the literature, it is concluded that flow blockage in "open-lattice cores" similar to the Westinghouse cores causes flow perturbations which are local to the blockage. For instance, A. Oktsubo, et al.⁽⁹⁷⁾ show that the mean bundle velocity is approached asymptotically about 4 in. downstream from a flow blockage in a single flow cell. Similar results were also found for 2 and 3 cells completely blocked. Basmer⁽⁹⁸⁾, et al., tested an open-lattice fuel assembly in which 41 percent of the subchannels were completely blocked in the center of the test bundle between spacer grids. Their results showed that the stagnant zone behind the flow blockage essentially disappears after 1.65 L/De, or about 5 in. for their test bundle. They also found that leakage flow through the blockage tended to shorten the stagnant zone or, in essence, the complete recovery length. Thus, local flow blockages within a fuel assembly have little effect on subchannel enthalpy rise. The reduction in local mass velocity is then the main parameter which affects the DNBR. If the Farley reactor were operating at full power and nominal steady-state conditions, as specified in table 4.4-1, a significant reduction in local mass velocity (60 percent in the VANTAGE+/VANTAGE 5 fuel and 85 percent in the LOPAR fuel) would be necessary to reduce the DNBR to the DNBR limit based on the assumption of fully developed flow along the full channel length. In reality, a local flow blockage is expected to promote turbulence and, thus, would likely not effect DNBR at all.

Coolant flow blockages induce local crossflows as well as promote turbulence. Fuel rod behavior is changed under the influence of a sufficiently high crossflow component. Fuel rod vibration could occur, caused by this crossflow component, through vortex shedding or turbulent mechanism. If the crossflow velocity exceeds the limit established for fluid elastic stability, large-amplitude whirling results. The limits for a controlled vibration mechanism are established from studies of vortex shedding and turbulent pressure fluctuations. The crossflow velocity required to exceed fluid elastic stability limits is dependent on the axial location of the blockage and the characterization of the crossflow (jet flow or not). These limits are greater than those for vibratory fuel rod wear.

4.4.4 TESTING AND VERIFICATION

4.4.4.1 Tests Prior to Initial Criticality

A reactor coolant flow test is performed following fuel loading, but prior to initial criticality. Coolant loop pressure drop data are obtained in this test. These data, in conjunction with coolant pump performance information, allow determination of the coolant flowrates at reactor operating conditions. This test verifies that proper coolant flowrates were used in the core thermal and hydraulic analysis.

Following initial criticality, periodic testing in accordance with the technical specification DNB surveillance for RCS flow will ensure that actual core flowrates are bounded by the assumptions found in the core thermal and hydraulic analysis.

4.4.4.2 Initial Power and Plant Operation

Core power distribution measurements are made at several core power levels (see paragraph 4.3.2.2.7). These tests are used to ensure that conservative peaking factors are used in the core thermal and hydraulic analysis.

Additional demonstration of the overall conservatism of the THINC analysis was obtained by comparing THINC predictions to incore thermocouple measurements. These measurements were performed on the Zion reactor.⁽⁹⁹⁾ No further inpile testing is planned. VIPRE-01 was demonstrated to be equivalent to THINC-IV in Reference 102.

An additional test is provided which measures how the N35 and N36 detector currents are affected by Control Bank D insertions at a constant power level between 30 and 35 percent. The results of this rod shadowing test are used to optimize the calibration of the IR instruments.

4.4.4.3 Component and Fuel Inspections

Inspections performed on the manufactured fuel are delineated in paragraph 4.2.1.4. Fabrication measurements critical to thermal and hydraulic analysis are obtained to verify that the engineering hot channel factors employed in the design analyses (paragraph 4.4.2.3.4) are met.

4.4.5 INSTRUMENTATION APPLICATION

4.4.5.1 Incore Instrumentation

The movable neutron detector with the fixed thermocouple system is used to provide information on the radial, axial, and azimuthal core characteristics for all core quadrants.

The incore instrumentation system is comprised of thermocouples positioned to measure fuel assembly coolant outlet temperatures at preselected positions and fission chamber detectors, positioned in guide thimbles, which run the length of selected fuel assemblies to measure the neutron flux distribution. Figures 4.4-16 and 4.4-17 show the number and location of instrumented assemblies in the core for Units 1 and 2, respectively.

The movable incore neutron detector system is the primary means for monitoring core power distribution. Routine collection of incore data is used to determine fission power density distribution, coolant enthalpy distribution, and fuel burnup distribution.

The core exit thermocouples provide an independent means for monitoring radial core power distribution. The core exit thermocouples are also utilized as post-accident instrumentation for monitoring of adequacy of core cooling.

The incore instrumentation can be used to obtain data from which fission power density distribution in the core, coolant enthalpy distribution in the core, and fuel burnup distribution may be determined.

4.4.5.2 Overtemperature and Overpower ΔT Instrumentation

The overtemperature ΔT trip protects the core against low DNBR. The overpower ΔT trip protects against excessive power (fuel rod rating protection).

As discussed in paragraph 7.2.1.1.2, factors included in establishing the overtemperature ΔT and overpower ΔT trip setpoints include the reactor coolant temperature in each loop and the axial distribution of core power through the use of the two-section, ex-core neutron detectors.

4.4.5.3 Instrumentation to Limit Maximum Power Output

The output of the three ranges (source, intermediate, and power) of detectors, with the electronics of the nuclear instruments, are used to limit the maximum power output of the reactor within their respective ranges.

A total of eight neutron flux detectors are installed in six locations around the reactor in the primary shield. Two proportional counters for the source range are installed on opposite "flat" portions of the core containing the primary startup sources at an elevation approximately one-quarter of the core height. Two compensated ionization chambers for the intermediate range, located in the same instrument wells and detector assemblies as the source range detectors, are positioned at an elevation corresponding to one-half of the core height; four dual-section, uncompensated ionization chamber assemblies for the power range are installed vertically at the four corners of the core and located equidistant from the reactor vessel at all points and, to minimize neutron flux pattern distortions, within 1 ft of the reactor vessel. Each power range detector provides two signals corresponding to the neutron flux in the upper and in the lower sections of a core quadrant. The three ranges of detectors are used as inputs to monitor

neutron flux from a completely shutdown condition to 120 percent of full power, with the capability of recording overpower excursions up to 200 percent of full power.

The difference in neutron flux between the upper and lower sections of the power range detectors is used to limit the overtemperature- ΔT and overpower- ΔT trip setpoints and to provide the operator with an indication of the core power axial offset. In addition, the outputs of the power range channels are used for:

- A. The rod speed control function.
- B. To alert the operator to an excessive power imbalance between the quadrants.
- C. Protecting the core against the consequences of rod ejection accidents.
- D. Protecting the core against the consequences of adverse power distributions resulting from dropped rods.

Details of the neutron detectors and nuclear instrumentation design and the control and trip logic are given in chapter 7. The limits on neutron flux operation and trip setpoints are given in subsection 16.2.3.

4.4.5.4 Instrumentation to Measure Reactor Vessel Head Plenum Coolant Temperature

On Unit 1 there will be 13 thermocouples positioned at preselected positions to measure the coolant temperatures in the reactor vessel head plenum and two stanchions installed on the internals upper support plate as shown on figures 4.4-18 and 4.4-19. Up to four additional thermocouples will also be installed on the outside surface of the reactor vessel head to obtain additional information above fluid temperatures in this region. Data collected with this instrumentation will be provided to Westinghouse for use in a generic program. The conclusions from this program will be reported to the NRC by Westinghouse.

4.4.5.5 Instrumentation to Measure Reactor Coolant Inventory

The heated junction thermocouple (HJTC) system is part of an inadequate core cooling monitoring system (ICCMS). This section addresses the HJTC reactor coolant inventory measurement capability. The remainder of the system is described in subsection 7.5.4.

The HJTC probe assembly in each ICCMS channel consists of eight HJTC sensors, a separator tube, a seal plug, and electrical connectors. The sensors are physically independent and located at key level points from the reactor vessel head to the fuel alignment plate.

As pictured in figure 4.4-20, an HJTC sensor consists of a Chromel-Alumel thermocouple near a heater (or heated junction) and another Chromel-Alumel thermocouple positioned away from the heater (or unheated junction or reference junction). In a fluid with relatively good heat transfer properties, the temperature difference between the adjacent thermocouples is very small. In a

fluid with relatively poor heat transfer properties, the temperature difference between the thermocouples is large.

The heated and unheated thermocouples in the HJTC probes are connected as shown in figure 4.4-21. When water surrounds the thermocouples, their voltage outputs are approximately equal. Therefore V_T is low.

In the absence of liquid, the heated thermocouple temperature increases in relation to the unheated thermocouple, causing V to rise. When V_T passes a predetermined setpoint, the system considers the sensor uncovered, changing the display level.

Another determination of the absence of liquid is when the absolute temperature of the sensor (V_{TR}) rises beyond the normal maximum coolant temperature. Then, the system will consider the sensor uncovered.

Two design features ensure proper operation under saturation conditions. First, each HJTC is shielded to avoid overcooling due to direct water contact during two-phase fluid conditions. The HJTC probe with the splash shield is referred to as the HJTC sensor. Second, a string of HJTC sensors is enclosed in a tube that separates the liquid and gas phases that surround it.

The separator tube creates a collapsed liquid level that the HJTC sensors measure. This collapsed liquid level is directly related to the average liquid fraction of the fluid in the reactor head volume above the fuel alignment plate. The mode of direct in-vessel sensing reduces spurious effects due to pressure, fluid properties, and nonhomogeneities of the fluid medium.

The probe assembly is housed in a stainless steel structure that protects the sensors from flow loads and serves as the guide path for the sensors.

The equipment required to install the HJTC consists of a probe holder shroud assembly and a head port adapter.

There are two probe holder shroud assemblies in the upper internals assembly at core locations N-5 and C-11. The probe holder shroud assembly is similar in design to control rod drive mechanism guide tubes. The probe holder shrouds support, vent, and shroud the Combustion Engineering (CE) HJTC probe and probe holder.

The shroud consists of a lower and upper assembly that are bolted together. A probe holder, provided by CE, is inserted into the center of the probe holder shroud. The probe holder is held in place at four locations. A guide plate assembly is located at three elevations on the inside of the lower assembly of the probe holder shroud assembly. An interference fit exists between the probe holder shroud and each guide plate assembly. The probe holder is bolted to the upper flange of the upper assembly of the probe holder shroud. The shroud, with the CE supplied probe holder, is installed into the upper internals in a manner similar to the CRDM guide tubes. The shroud is bolted to the upper support plate and has a support pin type arrangement at the bottom.

The head port adapter is compatible with the reactor vessel head penetration on one end and is provided with an integrally machined "Grayloc" hub feature on the other end. The head port

adapter is machined from a single homogenous piece of metal. The head port adapter is part of the primary pressure boundary and extends approximately 164 in. above the reactor vessel mating surface. The head port adapter provides the HJTC probe access into the vessel.

The only ASME Section III item is the head port adapter. The applicable code for this item is ASME III, 1998 Edition through 2000 Addenda. The applicable material specification is SA-182, Type 316 Stainless Steel.

REFERENCES

1. Cristensen, J. A., Allio, R. J., and Biancheria, A., "Melting Point of Irradiated UO_2 ," WCAP-6065, February 1965.
2. Friedland, A. J. and Ray, S., "Revised Thermal Design Procedure," WCAP-11397-P-A, April 1989.
3. Andre', S. V., et al., "RCS Flow Verification Using Elbow Taps at Westinghouse 3-Loop PWRs," WCAP-14750-P-A (Proprietary), Rev. 1, September 1999.
4. Phillips, B. T., et al., "Westinghouse Revised Thermal Design Procedure Instrument Uncertainty Methodology for Alabama Power Farley Nuclear Plant Units 1 and 2 Power (Model 54F Steam Generators and 2785 MWt and NSSS Power)," WCAP-12771-P, Rev. 3, (Proprietary), December 2011.
5. Weiner, R. A., et al., "Improved Fuel Performance Models for Westinghouse Fuel Rod Design and Safety Evaluations," WCAP-10851-P-A, August 1988.
6. Kjaerheim, G. and Rolstad, E., "Inpile Determination of UO_2 Thermal Conductivity, Density Effects and Gap Conductance," HPR-80, December 1967.
7. Kjaerheim, G., Inpile Measurements of Centre Fuel Temperatures and Thermal Conductivity Determination of Oxide Fuels, paper IFA-175 presented at the European Atomic Energy Society Symposium on Performance Experience of Water Cooled Power Reactor Fuel, Stockholm, Sweden, October 21-22, 1969.
8. Cohen, I., Lustman, B., and Eichenberg, J. D., "Measurements of the Thermal Conductivity of Metal-Clad Uranium Oxide Rods During Irradiation," WAPD 228, 1960.
9. Clough, D. J. and Sayers, J. B., "The Measurement of the Thermal Conductivity of UO_2 under Irradiation in the Temperature Range 150-1600°C," AERE-R-4690, UKAEA Research Group, Harwell, December 1964.
10. Stora, J. P., DeBernardy DeSigoyer, B., Delmas, R., Deschamps, P., Ringot, C., and Lavaud, B., "Thermal Conductivity of Sintered Uranium Oxide under Inpile Conditions," EURAE-1095, 1964.

11. Devold, I., "A Study of the Temperature Distribution in UO_2 Reactor Fuel Elements," AE-318, Aktiebolaget Atomenergi, Stockholm, Sweden, 1968.
12. Balfour, M. G., Christensen, J. A., and Ferrari, H. M., "Inpile Measurement of UO_2 Thermal Conductivity," WCAP-2923, 1966.
13. Leech, W. J., et al., "Revised PAD Code Thermal Safety Model," WCAP-8720, Addendum 2, October 1982.
14. Duncan, R. N., "Rabbit Capsule Irradiation of UO_2 ," CVTR Project, CVNA-142, June 1962.
15. Nelson, R. C., Coplin, D. H., Lyons, M. F., and Weidenbaum, B., "Fission Gas Release from UO_2 Fuel Rods with Gross Central Melting," GEAP-4572, July 1964.
16. Hellman, J. M., ed., "Fuel Densification Experimental Results and Model for Reactor Application," WCAP-8219, October 1973.
17. Howard, V. C. and Gulvin, T. G., "Thermal Conductivity Determinations on Uranium Dioxide by a Radial Flow Method," UKAEA IG-Report 51, November 1960.
18. Lucks, C. F. and Deem, H. W., "Thermal Conductivity and Electrical Conductivity of UO_2 ," in Progress Reports Relating to Civilian Applications, BMI-1448 (Rev.) for June 1960; BMI-1489 (Rev.) for December 1960; and BMI-1518 (Rev.) for May 1961.
19. Daniel, J. L., Matolich, J., Jr., and Deem, H. W., "Thermal Conductivity of UO_2 ," HW-69945, September 1962.
20. Feith, A. D., "Thermal Conductivity of UO_2 by a Radial Heat Flow Method," TID-21668, 1962.
21. Vogt, J., Grandell, L., and Runfors, U., "Determination of the Thermal Conductivity of Unirradiated Uranium Dioxide," AB Atomenergi Report RMB-527, quoted by IAEA Report on Thermal Conductivity of Uranium Dioxide, 1964.
22. Nishijima, T., Kawada, T., and Ishihata, A., "Thermal Conductivity of Sintered UO_2 and Al_2O_3 at High Temperatures," J. American Ceramic Society, 48, pp 31-34, 1965.
23. Ainscough, J. B. and Wheeler, M. F., "The Thermal Diffusivity and Thermal Conductivity of Sintered Uranium Dioxide," in Proceedings of the Seventh Conference on Thermal Conductivity, p. 467, National Bureau of Standards, Washington, 1968.
24. Godfrey, T. G., Fulkerson, W., Killie, T. G., Moore J. P., and McElroy, D. L., "Thermal Conductivity of Uranium Dioxide and Armco Iron by an Improved Radial Heat Flow Technique," ORNL-3556, June 1964.
25. Stora, J. P., et al., "Thermal Conductivity of Sintered Uranium Oxide Under Inpile Conditions," EURAE-1095, August 1964.

26. Bush, A. J., "Apparatus for Measuring Thermal Conductivity to 2500°C," Westinghouse Research Laboratories Report 64-1P6-401-R3, (Westinghouse Proprietary), February 1965.
27. Asamoto, R. R., Anselin, F. L., and Conti, A. E., "The Effect of Density on the Thermal Conductivity of Uranium Dioxide," GEAP-5493, April 1968.
28. Kruger, O. L., Heat Transport Properties of Uranium and Plutonium Dioxide, paper presented at the fall meeting of Nuclear Division of the American Ceramic Society, Pittsburgh, PA, September 1968.
29. Gyllander, J. A., "Inpile Determination of the Thermal Conductivity of UO₂ in the Range 500-2500°C," AE-411, January 1971.
30. Lyons, M. F., et al., "UO₂ Powder and Pellet Thermal Conductivity During Irradiation," GEAP-5100-6, 1966.
31. Coplin, D. H., et al., "The Thermal Conductivity of UO₂ by Direct In-Reactor Measurements," GEAP-5100-1, March 1968.
32. Bain, A. S., "The Heat Rating Required to Produce Center Melting in Various UO₂ Fuels," ASTM Special Technical Publication, No. 306, p 30.
33. Stora, J. P., "In-Reactor Measurements of the Integrated Thermal Conductivity of UO₂ - Effect of Porosity," Trans. ANS, 13, p 137, June 1970.
34. International Atomic Energy Agency, "Thermal Conductivity of Uranium Dioxide," Report of the Panel held in Vienna, April, 1965, IAEA Technical Reports Series, No. 59, Vienna, The Agency, 1966.
35. Poncelet, C. G., "Burnup Physics of Heterogeneous Reactor Lattices," WCAP-6069, June 1965.
36. Nodvick, R. J., "Saxton Core II Fuel Performance Evaluation," WCAP-3386-56. Part II, Evaluation of Mass Spectrometric and Radiochemical Analyses of Irradiated Saxton Plutonium Fuel, July 1970.
37. Skaritka, J., ed., "Fuel Rod Bow Evaluation, WCAP-8691, Revision 1, July 1979.
38. Partial Response to Request Number 1 for Additional Information on WCAP-8691, Revision 1, letter NS-EPR-2515, E. P. Rahe, Jr., (Westinghouse) to J. R. Miller (NRC), October 9, 1981 and Remaining Response to Request Number 1 for Additional Information on WCAP-8691, Revision 1, letter NS-EPR-2572, E. P. Rahe, Jr., to R. J. Miller, March 16, 1982.

FNP-FSAR-4

39. Letter from C. Berlinger (NRC) to E. P. Rahe Jr. (W), Subject: "Request for Reduction in Fuel Assembly Burnup Limit for Calculation of Maximum Rod Bow Penalty, June 18, 1986.
40. Davidson, S. L. and Kramer, W. R., ed. "Reference Core Report VANTAGE 5 Fuel Assembly," WCAP-10444-P-A, September 1985.
41. Davidson, S. L. and Iorij, J. A., "Reference Core Report - 17 x 17 Optimized Fuel Assembly," WCAP-9500-A, May 1982.
42. Letter from E. P. Rahe (W) to Miller (NRC), NS-EPR-2573, WCAP-9500, and WCAPS-9401/9402 NRC SER Mixed Core Compatibility Items, March 19, 1982.
43. Letter from C. O. Thomas (NRC) to Rahe (W) - "Supplement Acceptance No. 2 for Referencing Topical Report WCAP-9500," January 1983.
44. Schueren, P. and McAtee, K. R., "Extension of Methodology for Calculating Transition Core DNBR Penalties," WCAP-11837-P-A, January 1990.
45. Not Used
46. Motley, F. E., et al., "New Westinghouse Correlation WRB-1 for Predicting Critical Heat Flux in Rod Bundles with Mixing Vane Grids," WCAP-8762-P-A, July 1984.
47. Tong, L. S., "Critical Heat Fluxes in Rod Bundles, Two Phase Flow and Heat Transfer in Rod Bundles," Annual Winter Meeting ASME, p 3146, November 1968.
48. Tong, L. S., "Boiling Crisis and Critical Heat Flux," NRC Critical Review Series, TID-25887, 1972.
49. Letter from A. C. Thadani (NRC) to W. J. Johnson (Westinghouse), Subject: Acceptance for Referencing of Licensing Topical Report, WCAP-9226-P/9227-NP, "Reactor Core Response to Excessive Secondary Steam Releases," January 31, 1989.
50. Motley, F. E. and Cadek, F. F., "DNB Test Results for R-Grid Thimble Cold Wall Cells," WCAP-7695-L, Addendum 1, October 1972.
51. Tong, L. S., "Prediction of Departure from Nucleate Boiling for an Axially Nonuniform Heat Flux Distribution," J. Nucl. Energy, 21, pp 241-248, 1967.
52. Motley, F. E. and Cadek, F. F., "DNB Tests Results for New Mixing Vane Grids (R)," WCAP-7695-L, (Westinghouse Proprietary), July 1972 and WCAP-7958-A, January 1975.
53. Shefcheck, J., "Application of the THINC Program to PWR Design," WCAP-7359-L, August 1969 (Westinghouse Proprietary), and WCAP-7838, January 1972.

54. Cadek, F. F., Motley, F. E., and Dominicis, D. P., "Effect of Axial Spacing on Interchannel Thermal Mixing with the R Mixing Vane Grid," WCAP-7941-P-A, (Westinghouse Proprietary), June 1972 and WCAP-7959-A (Nonproprietary), October 1972.
55. Rowe, D. S. and Angle, C. W., "Crossflow Mixing Between Parallel Flow Channels During Boiling," Part II, "Measurement of Flow and Enthalpy in Two Parallel Channels," BNWL-371, Part 2, December 1967.
56. Rowe, D. S. and Angle, C. W., "Crossflow Mixing Between Parallel Flow Channels During Boiling," Part III, "Effect of Spacers on Mixing Between Two Channels," BNWL-371, Part 3, January 1969.
57. Gonzalez-Santalo, J. M., and Griffith, P., "Two-Phase Flow Mixing in Rod Bundle Subchannels," ASME Paper 72-WA/NE-19.
58. Motley, F. E., Wenzel, A. H., and Cadek, F. F., "The Effect of 17 x 17 Fuel Assembly Geometry on Interchannel Thermal Mixing," WCAP-8299-A, January 1975.
59. Hill, K. W., Motley, F. E., and Cadek, F. F., "Effect of Local Heat Flux Spikes on DNB in Nonuniform Heated Rod Bundles," WCAP-P-A, (Westinghouse Proprietary), February 1975 and WCAP-8202-A February 1975.
60. Cadek, F. F., "Interchannel Thermal Mixing with Mixing Vane Grids," WCAP-7667-P-A, (Westinghouse Proprietary), February 1975 and WCAP-7755-A, February 1975.
61. Hochreiter, L. E., "Application of the THINC-IV Program to PWR Design," WCAP-8054-P-A, (Westinghouse Proprietary), and WCAP-8195-A, (Non-Proprietary) February 1989.
62. Nakazato, S. and DeMario, E. E., "Hydraulic Flow Test of the 17 x 17 Fuel Assembly," WCAP-8279, February 1974.
63. Dittus, F. W. and Boelter, L. M. K., "Heat Transfer in Automobile Radiators of the Tubular Type," Calif. Univ. Publication in Eng., 2, No. 13, pp 443-461, 1930.
64. Weisman, J., "Heat Transfer to Water Flowing Parallel to Tube Bundles," Nucl. Sci. Eng., 6, pp 78-79, 1959.
65. Thom, J. R. S., Walker, W. M., Fallon, T. A., and Reising, G. F. S., "Boiling in Subcooled Water During Flowup-Heated Tubes or Annuli," Proc. Instn. Mech. Engrs., 180, Pt. C, pp 226-246, 1965-66.
66. Hetsroni, G., "Hydraulics Tests of the San Onofre Reactor Model," WCAP-3269-8, June 1964.
67. Hetsroni, G., "Studies of the Connecticut-Yankee Hydraulic Model," NYO-3250-2, June 1965.

FNP-FSAR-4

68. Idel'chik, I. E., Handbook of Hydraulic Resistance, NRC-TR-6630, 1960.
69. Moody, L. F., "Friction Factors for Pipe Flow," Transaction of the American Society of Mechanical Engineers, 66 pp 671-684, 1944.
70. Not Used |
71. Not Used |
72. Not Used |
73. Hochreiter, L. E., Chelemer, H., and Chu, P. T., "THINC-IV, An Improved Program for Thermal Hydraulic Analysis of Rod Bundle Cores," WCAP-7956, February 1989. |
74. Carter, F. D., "Inlet Orificing of Open PWR Cores," WCAP-9004 (Westinghouse Proprietary), January 1969 and WCAP-7836, January 1972.
75. Not Used |
76. Not Used |
77. McFarlane, A. F., "Power Peaking Factors," WCAP-7912-P-A (Westinghouse Proprietary), January 1975 and WCAP-7912-A, January 1975. |
78. Friedland, A. J. and Ray, S., "Improved THINC IV Modeling for PWR Core Design," WCAP-12330-A, September 1991. |
79. Not Used |
80. Not Used |
81. Not Used |
82. Not Used |
83. Not Used |
84. Deleted
85. Boure, J. A., Bergles, A. E., and Tong, L. S., "Review of Two-Phase Flow Instability," Nucl. Eng. Design 25, pp 165-192, 1973.
86. Lahey, R. T. and Moody, F. J., "The Thermal Hydraulics of a Boiling Water Reactor," American Nuclear Society, 1977.

87. Saha, P., Ishii, M., and Zuber, N., "An Experimental Investigation of the Thermally-Induced Flow Oscillations in Two-Phase Systems," J. of Heat Transfer, pp 616-622, November 1976.
88. Summer, V. C., FSAR, Docket No. 50-395.
89. Byron/Braidwood, FSAR, Docket No. 50-456.
90. South Texas, FSAR, Docket No. 50-498.
91. Kakac, S., Veziroglu, T. N., Akyuzlu, K., Berkol, O., Sustained and Transient Boiling Flow Instabilities in a Cross-Connected Four-Parallel-Channel Upflow System, Proc. of 5th International Heat Transfer Conference, Tokyo, September 3-7, 1974.
92. Kao, H. S., Morgan, T. D., and Parker, W. B., "Prediction of Flow Oscillation in Reactor Core Channel," Trans. ANS, Vol. 16, pp 212-213, 1973.
93. Stephan, L. A., "The Effects of Cladding Material and Heat Treatment on the Response of Water-logged UO₂ Fuel Rods to Power Bursts," IN-ITR-111, January 1970.
94. Western New York Nuclear Research Center Correspondence with the NRC on February 11 and August 27, 1971, Docket 50-57.
95. Weisman, J., Wenzel, A. H., Tong, L. S., Fitzsimmons, D., Thorne, W., and Batch, J., "Experimental Determination of the Departure from Nucleate Boiling in Large Rod Bundles at High Pressures," Chem. Eng. Prog. Symp. Ser. 64, No. 82, pp 114-125, 1968.
96. Tong, L. S., et al., Critical Heat Flux (DNB) in Square and Triangular Array Rod Bundles, presented at the Japan Society of Mechanical Engineers Semi-International Symposium held at Tokyo, Japan, pp 25-34, September 4-8, 1967.
97. Ohtsubo, A. and Uruwashi, S., "Stagnant Fluid Due to Local Flow Blockage," J. Nucl. Sci. Technol. 9, No. 7, pp 433-434, 1972.
98. Basmer, P., Kirsh, D., and Schultheiss, G. F., "Investigation of the Flow Pattern in the Recirculation Zone Downstream of Local Coolant Blockages in Pin Bundles," Atomwirtschaft, 17, No. 8, pp 416-417, 1972. (In German).
99. Burke, T. M., Meyer, C. E., Shefcheck, J., "Analysis of Data from the Zion (Unit 1) THINC Verification Test," WCAP-8453-A (Non-proprietary), May 1976.
100. Foster, J. P., et al., "Westinghouse Improved Performance Analysis and Design Model (PAD 4.0)," WCAP-15063-P-A, Revision 1, with Errata, July 2000.
101. Westinghouse letter ALA-15-97, dated December 8, 2015, "Westinghouse Resolution Plan and Technical Basis for NSAL-14-5, 'Lower than Expected Critical Heat Flux Results Obtained During DNB Testing.'"

FNP-FSAR-4

102. Sung, Y. X., et al., "VIPRE-01 Modeling and Qualification for Pressurized Water Reactor Non-LOCA-Thermal Hydraulic Safety Analysis," WCAP-14565-P-A (Proprietary) and WCAP-14565-A (Non-Proprietary), October 1999
103. Stewart, C. W., et al., "VIPRE-01 A Thermal Hydraulic Code for Reactor Core", Volume 1 -3 (Revision 3, August 1989) Volume 4 (April 1987), NP-2511-CCM-A, Electric Power Research Institute
104. Joffrey, P. F., et al., "Addendum 2 to WCAP-14565-P-A Extended Application of ABB-NV Correlation and Modified ABB-NV Correlation WLOP for PWR Low Pressure Applications," WCAP-14565-P-A Addendum 2-P-A (Proprietary) / WCAP-15306-NP-A Addendum 2-NP-A (Non-Proprietary), April 2008
105. Linsuain, O., et al., "Westinghouse Performance Analysis and Design Model (PAD 5), "WCAP-17642-P-A, Revision 1, November 2017

TABLE 4.4-1 (SHEET 1 OF 3)

THERMAL AND HYDRAULIC COMPARISON TABLE FOR FNP UNITS 1 AND 2

Design Parameters

Reactor core heat output (MWt)	2821
Reactor core heat output (10^6 Btu/h)	9626
Heat generated in fuel (%)	97.4
System pressure, nominal (psia)	2250
System pressure, minimum steady-state (psia)	2200

Coolant temperature

Nominal inlet (°F)	530.0 – 540.5
Average rise in core (°F)	79.4 – 78.3
Average rise in vessel (°F)	74.4 – 73.4
Average in core (°F)	571.8 - 572
Average in vessel (°F)	567.2 - 577.2
Nominal core outlet (°F)	609.4 – 618.8
Nominal vessel outlet (°F)	604.4 – 613.9

Coolant conditions^(b)

Vessel minimum measured flowrate (MMF) ^(c)	
10^6 lbm/h	105.4 - 104
gal/min	273,900 ^(k)

Vessel Thermal Design flowrate (TDF)	
10^6 lbm/h	99.5 – 98.2
gal/min	258,000

Effective flowrate for heat transfer (based on TDF)	
10^6 lbm/h	92.5 – 91.2
gal/min	239,680

	<u>LOPAR^(l)</u>	<u>VANTAGE5+/ VANTAGE 5</u>
Minimum DNBR at nominal conditions		
Typical flow channel	3.20	2.23
Thimble (cold wall) flow channel	3.02	2.153
Minimum DNBR for design transients		
Typical flow channel	1.25	1.24
Thimble (cold wall) flow channel	1.24	1.24

TABLE 4.4-1 (SHEET 2 OF 3)

<u>Design Parameters</u>	<u>VANTAGE5+/ VANTAGE 5</u>	
	WRB-1	WRB-2
DNB correlation ^(a)		
Effective flow area for heat transfer (ft ²) ^(d)	41.55	44.04
Average velocity along fuel rods (ft/s) ^(d)	13.5	12.8
Average mass velocity 10 ⁶ lbm/h-ft ² (based on TDF) ^(d)	2.22 - 2.19	2.10 - 2.07
Heat transfer		
Active heat transfer, surface area (ft ²) ^(d)	48,598	46,779
Average heat flux (Btu/h-ft ²) ^(d)	189,820	200,426
Maximum heat flux for normal operation (Btu/h-ft ²) ^(d,e)	440,380	501,065
Average linear power (kW/ft) ^(f)	5.45	5.54
Peak linear power for normal operation (kW/ft) ^(e,f)	12.63	13.85
Power density (kW/l of core) ⁽ⁱ⁾	104.5	106.2
Specific power (kW/kg uranium) ^(d,i)	37.3	42.6
Pressure drop		
Across Core (psi)		23.8 ± 2.4 ^(j)
Across Vessel, Including Nozzle (psi)		42.3 ± 4.2
		See Table 5.1-1

TABLE 4.4-1 (SHEET 3 OF 3)

- a. See paragraph 4.4.1.1 for the use of the W-3 correlation.
- b. Flowrates are based on 15-percent average and 20-percent peak steam generator tube plugging.
- c. Inlet temperature (°F) = 532.0 – 542.5.
- d. Assumes all LOPAR or VANTAGE5+/VANTAGE-5 core.
- e. Based on 2.32 FQ peaking factor for LOPAR and 2.50 FQ peaking factor for VANTAGE5+/VANTAGE-5.
- f. Based on densified active fuel length.
- g. See paragraph 4.3.2.2.6.
- h. See paragraph 4.4.2.2.6.
- i. Based on cold dimensions and 95 percent of theoretical density fuel.
- j. Maximum core pressure drop is based on 0% SGTP, thimble plugging devices installed and the Best Estimate Reactor Flow Rate of 98,600 gpm/loop for Unit 1 (bounds Unit 2).
- k. Value includes a 2.1-percent flow uncertainty (0.1-percent feedwater venturi fouling bias included). The minimum measured flow (MMF) rate is the flow used in the reactor core DNB analyses which were performed with the Revised Thermal Design Procedure. The DNB analyses also bound a MMF of 274,800 gpm which reflects a flow measurement uncertainty of 2.4-percent (0.1-percent feedwater venturi fouling bias included).
- l. The LOPAR fuel is not analyzed for the power uprate. The LOPAR values at 2775 MWt are retained for historical purposes.

TABLE 4.4-2**VOID FRACTIONS AT NOMINAL REACTOR CONDITIONS**

		<u>Average (percent)</u>	<u>Maximum (percent)</u>
Core	(LOPAR [Unit 1])	0.12	--
	(VANTAGE5+/VANTAGE 5 [Unit 2])	<0.1%	
Hot subchannel	(LOPAR [Unit 1])	0.4	0.9
	(VANTAGE5+/VANTAGE 5 [Unit 2])	1.4%	6.4%

FNP-FSAR-4

TABLE 4.4-3

DELETED

DELETED

REV 30 10/21



JOSEPH M. FARLEY
NUCLEAR PLANT
UNIT 1 AND UNIT 2

LOPAR PEAK FUEL AVERAGE AND SURFACE
TEMPERATURES DURING FUEL ROD LIFETIME
VS. LINEAR POWER

FIGURE 4.4-1 (SHEET 1 OF 2)

DELETED

REV 30 10/21



JOSEPH M. FARLEY
NUCLEAR PLANT
UNIT 1 AND UNIT 2

ZIRLO CLAD VANTAGE-5 PEAK FUEL AVERAGE AND
SURFACE TEMPERATURES DURING FUEL ROD
LIFETIME VS. LINEAR POWER

FIGURE 4.4-1 (SHEET 2 OF 2)

DELETED

REV 30 10/21



JOSEPH M. FARLEY
NUCLEAR PLANT
UNIT 1 AND UNIT 2

LOPAR PEAK FUEL CENTERLINE TEMPERATURE DURING
FUEL ROD LIFETIME VS. LINEAR POWER

FIGURE 4.4-2 (SHEET 1 OF 2)

DELETED

REV 30 10/21



JOSEPH M. FARLEY
NUCLEAR PLANT
UNIT 1 AND UNIT 2

ZIRLO CLAD VANTAGE-5 PEAK FUEL
CENTERLINE TEMPERATURE DURING
FUEL ROD LIFETIME VS. LINEAR POWER

FIGURE 4.4-2 (SHEET 2 OF 2)

DELETED

REV 30 10/21



JOSEPH M. FARLEY
NUCLEAR PLANT
UNIT 1 AND UNIT 2

THERMAL CONDUCTIVITY OF UO_2
(DATA CORRECTED TO 95% THEORETICAL DENSITY)

FIGURE 4.4-3

DELETED

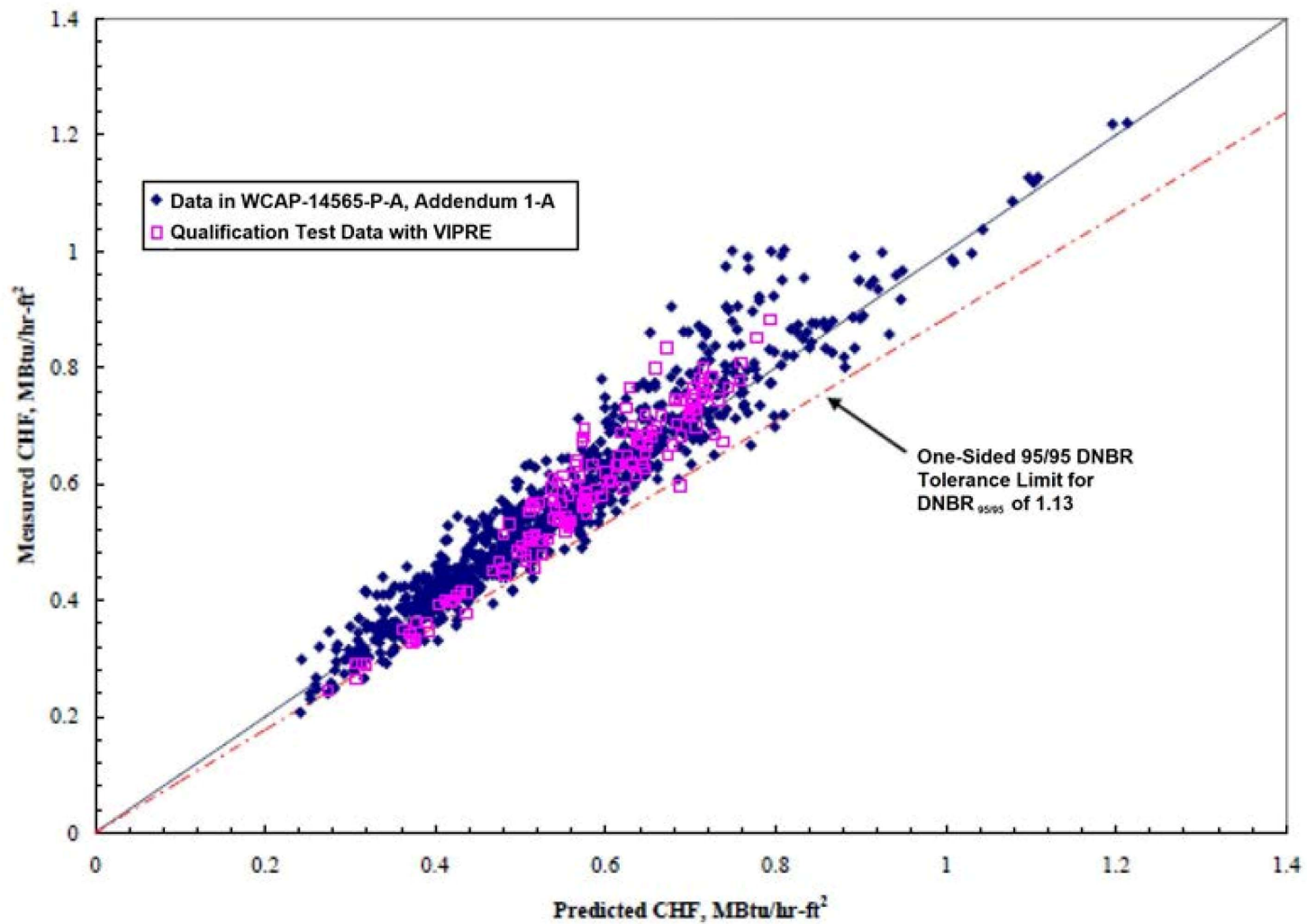
REV 30 10/21



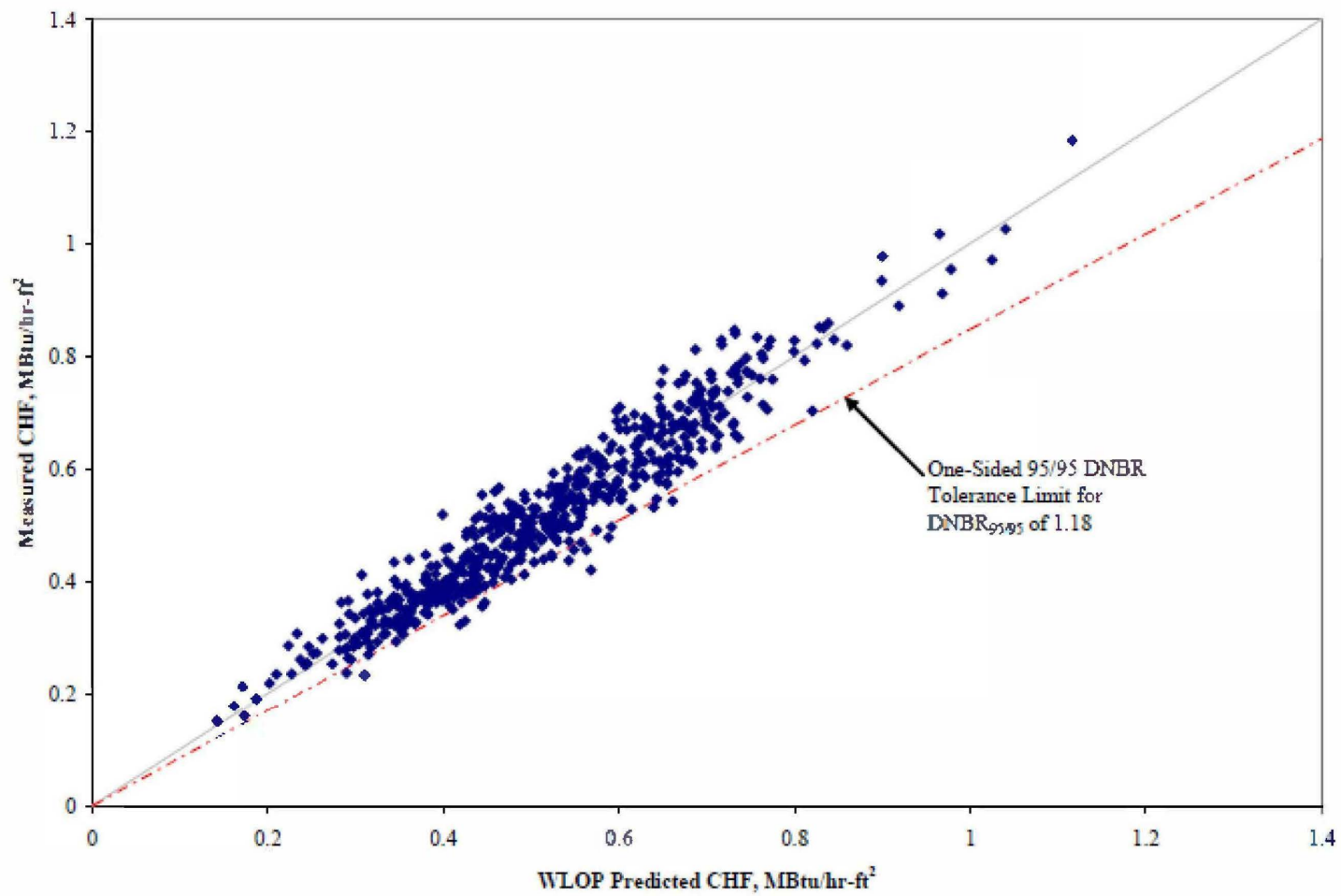
JOSEPH M. FARLEY
NUCLEAR PLANT
UNIT 1 AND UNIT 2

TYPICAL AXIAL VARIATION OF AVERAGE CLAD
TEMPERATURE FOR ROD OPERATING AT 5.43 kW/ft

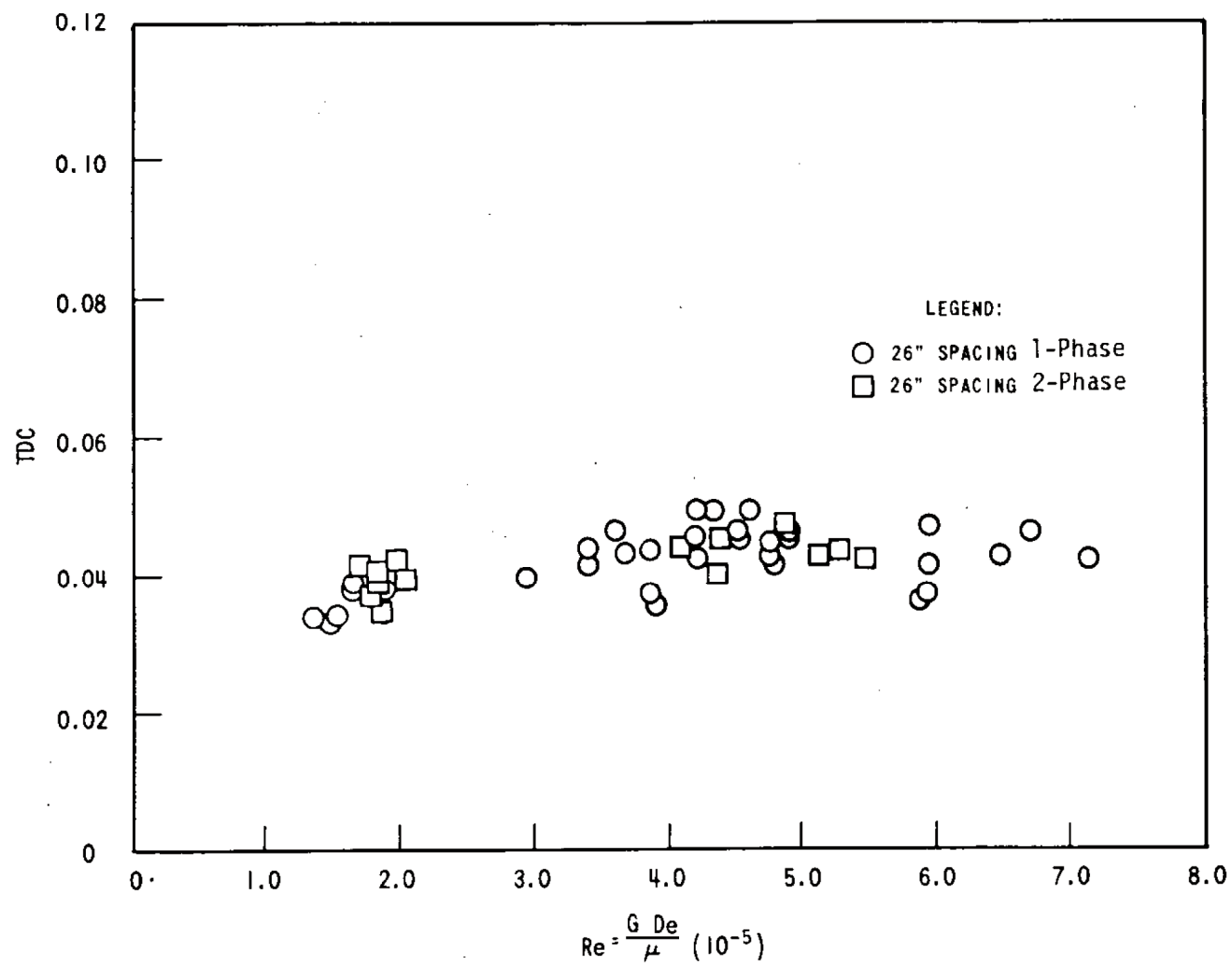
FIGURE 4.4-4



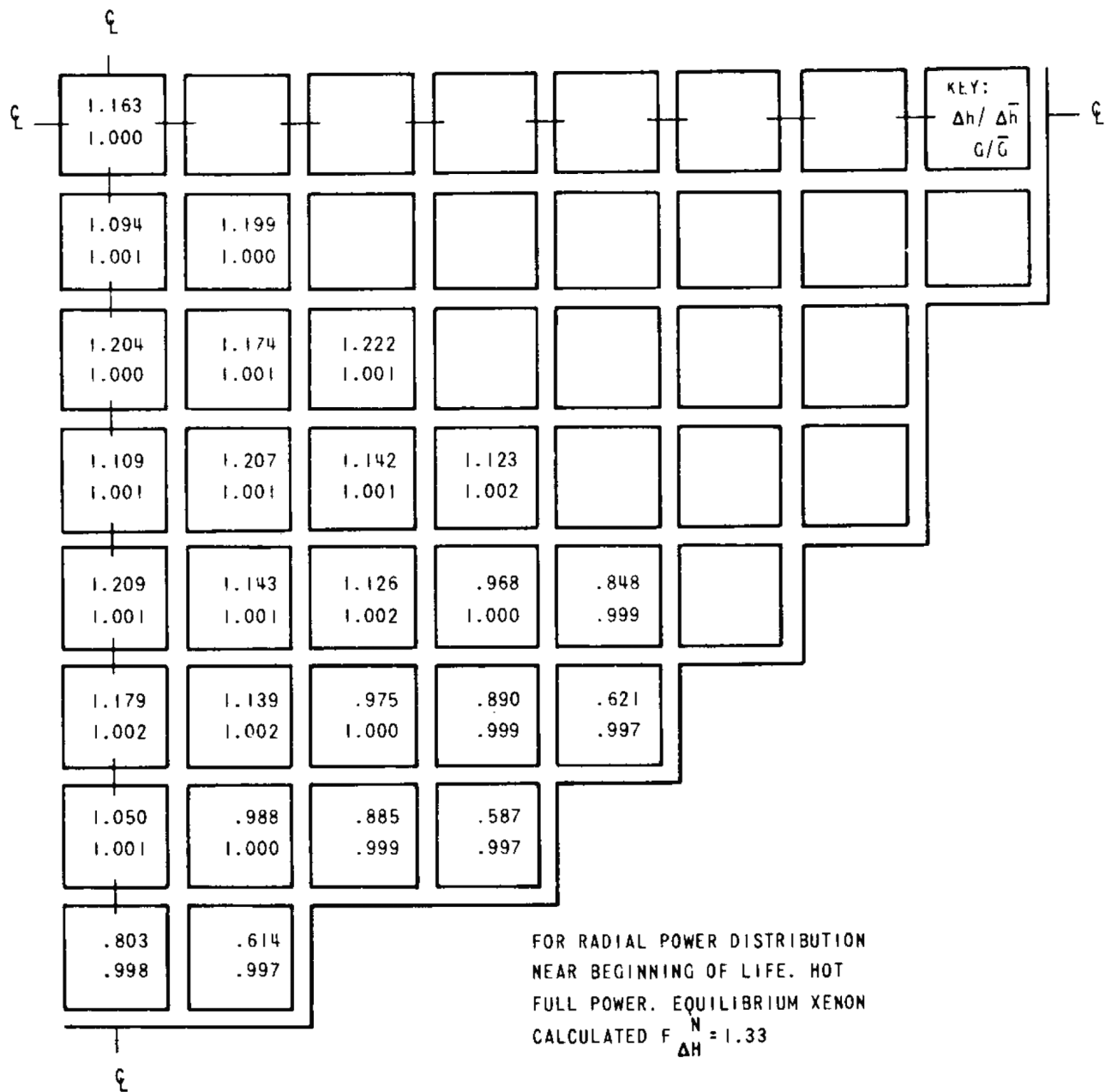
REV 30 10/21



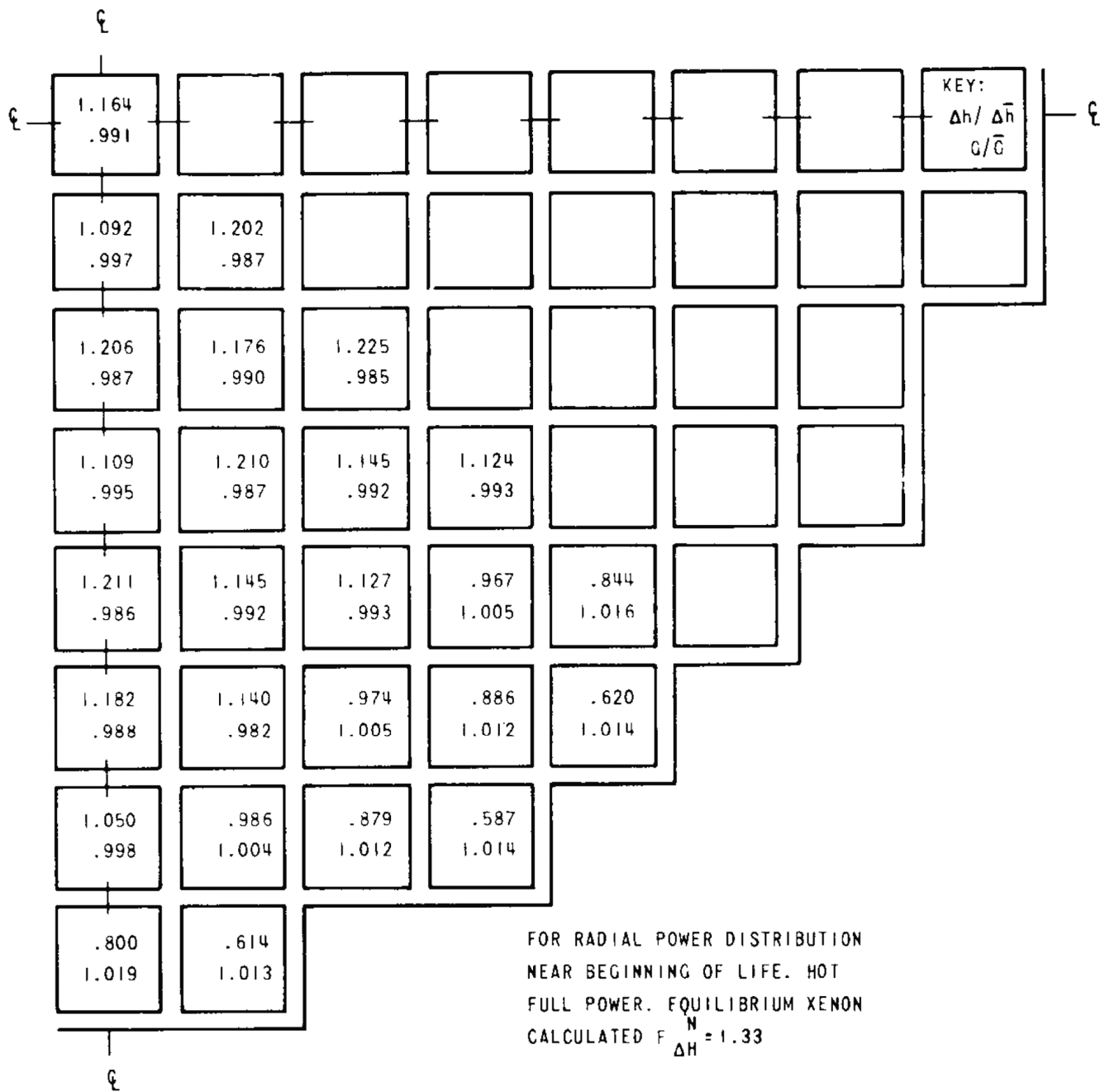
REV 30 10/21



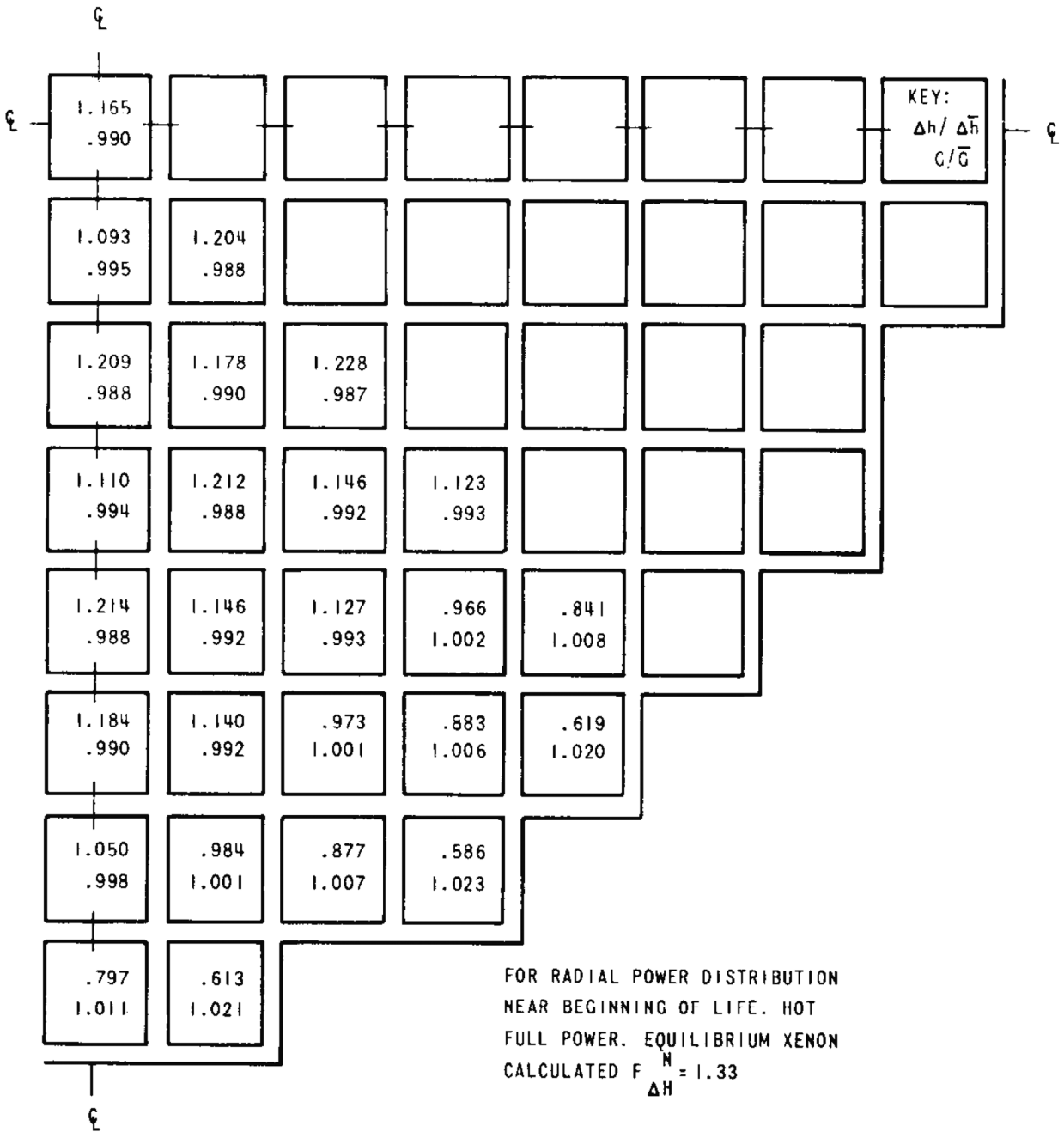
REV 21 5/08



REV 21 5/08



REV 21 5/08



REV 21 5/08

DELETED

REV 30 10/21



JOSEPH M. FARLEY
NUCLEAR PLANT
UNIT 1 AND UNIT 2

VOID FRACTION VERSUS THERMODYNAMIC QUALITY
 $H-H_{SAT}/H_g-H_{SAT}$

FIGURE 4.4-10

DELETED

REV 30 10/21



JOSEPH M. FARLEY
NUCLEAR PLANT
UNIT 1 AND UNIT 2

PWR NATURAL CIRCULATION TEST

FIGURE 4.4-11

DELETED

REV 30 10/21



JOSEPH M. FARLEY
NUCLEAR PLANT
UNIT 1 AND UNIT 2

COMPARISON OF A REPRESENTATIVE
W TWO-LOOP REACTOR INCORE THERMOCOUPLE
MEASUREMENTS WITH THINC-IV PREDICTIONS

FIGURE 4.4-12

DELETED

REV 30 10/21



JOSEPH M. FARLEY
NUCLEAR PLANT
UNIT 1 AND UNIT 2

COMPARISON OF A REPRESENTATIVE W
THREE-LOOP INCORE THERMOCOUPLE
MEASUREMENTS WITH THINC-IV PREDICTIONS

FIGURE 4.4-13

DELETED

REV 30 10/21



JOSEPH M. FARLEY
NUCLEAR PLANT
UNIT 1 AND UNIT 2

HANFORD SUBCHANNEL TEMPERATURE DATA
COMPARISON WITH THINC-IV

FIGURE 4.4-14

DELETED

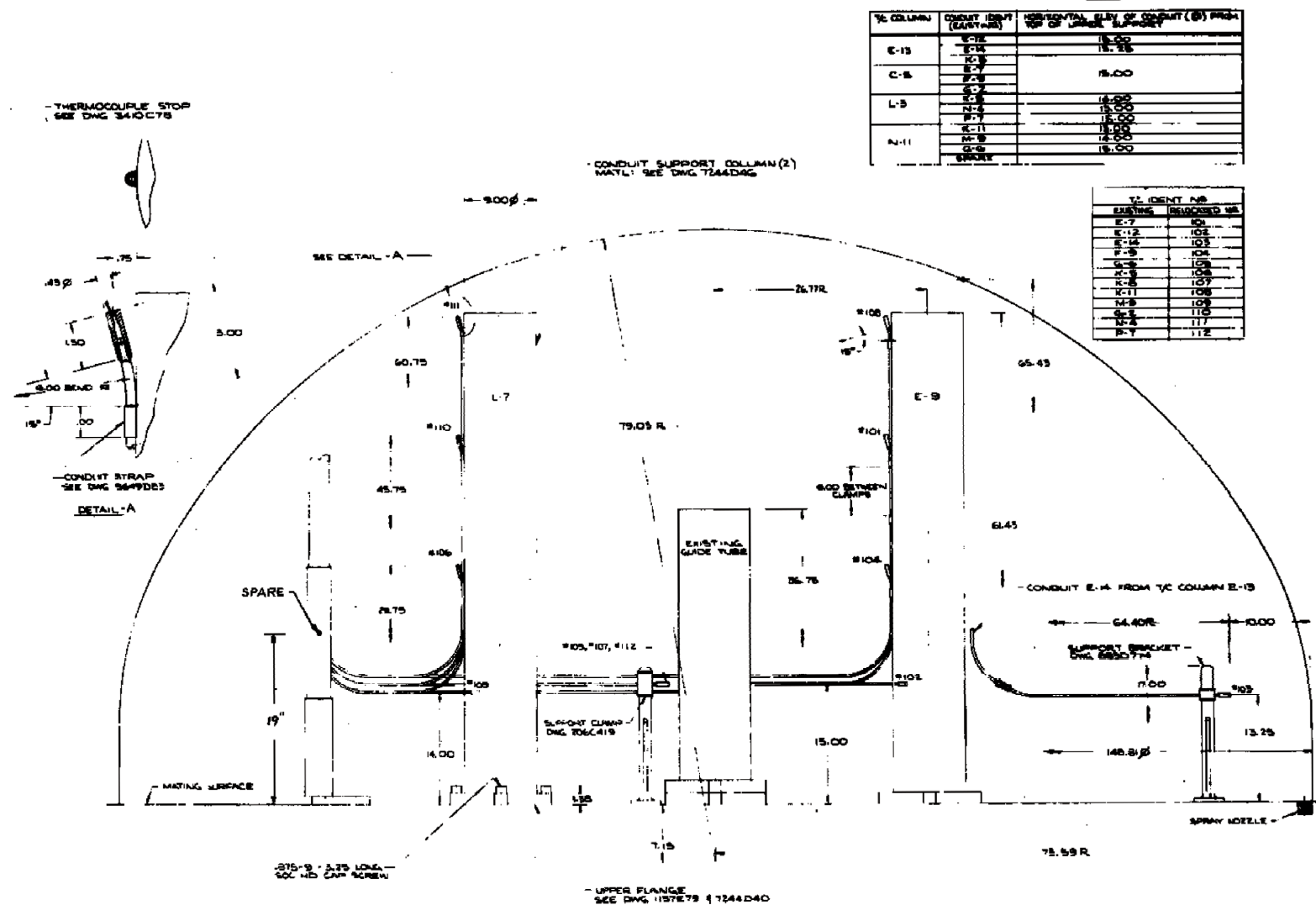
REV 30 10/21



JOSEPH M. FARLEY
NUCLEAR PLANT
UNIT 1 AND UNIT 2

HANFORD SUBCIRITICAL TEMPERATURE DATA
COMPARISON WITH THINC-IV

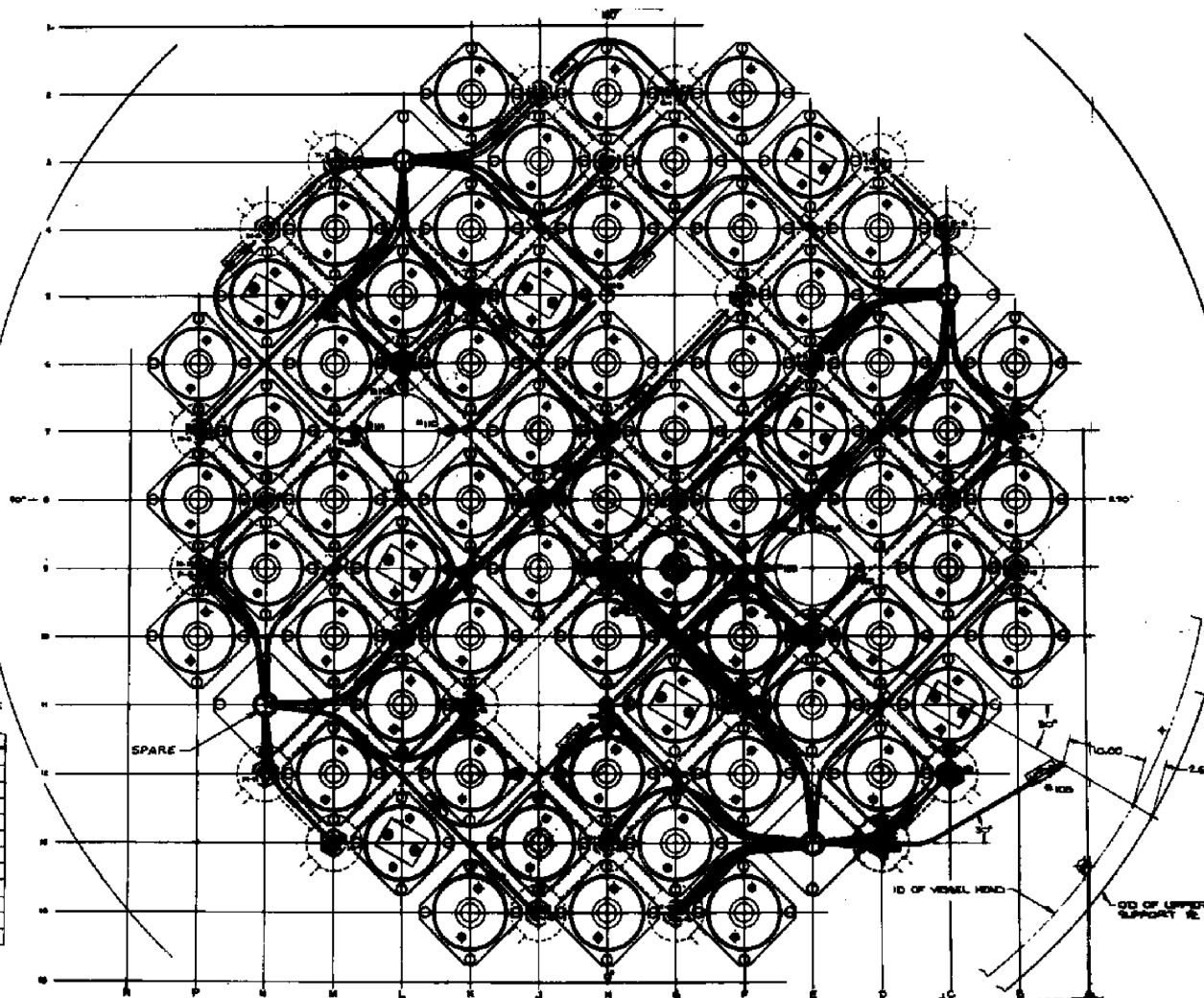
FIGURE 4.4-15



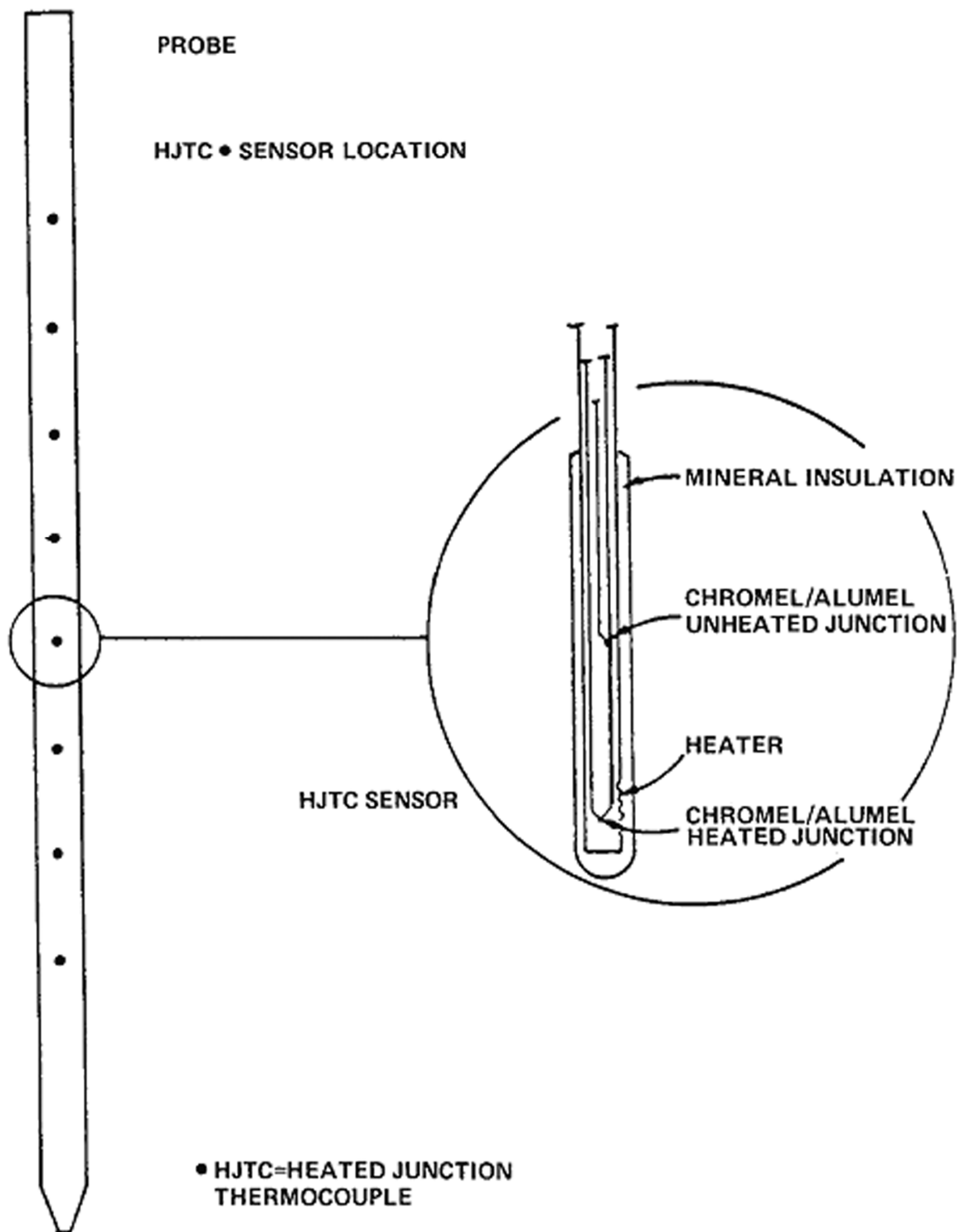
REV 21 5/08

THE CONDUITS IDENTIFIED
IN THIS BLOCK BELOW ARE
TO BE DRAINED BY TOP
OF UPPER SUPPORT R.

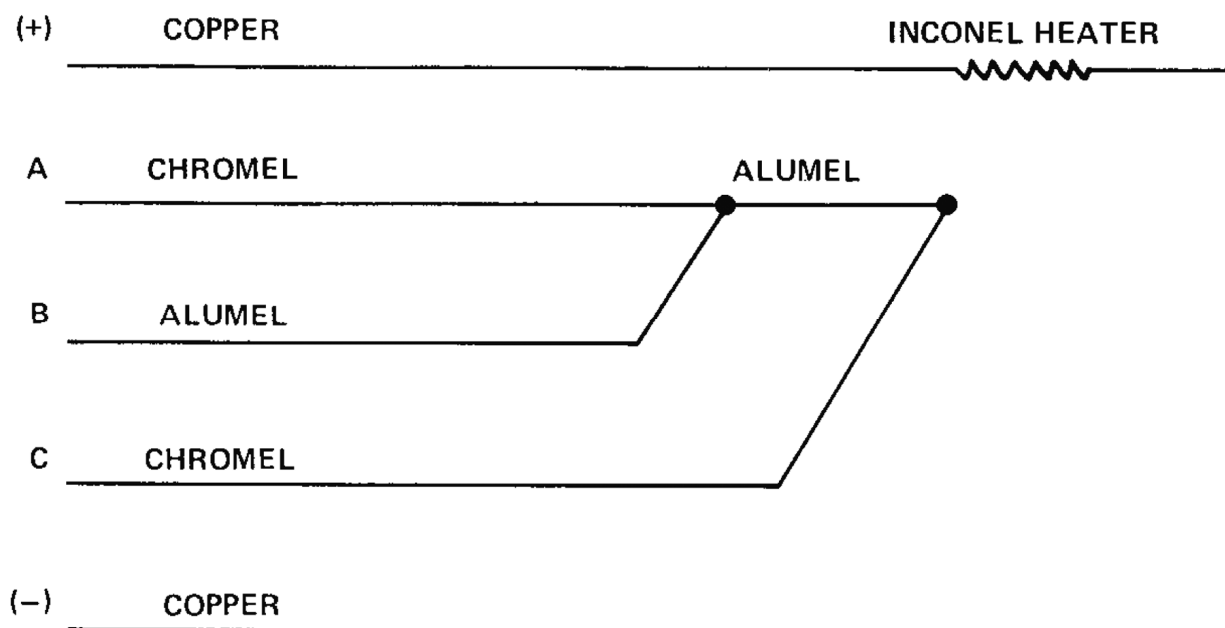
IDENT NO.	COORDINATE
E-7	E-8
E-12	F-11
E-14	D-18
F-9	E-10
G-6	F-5
K-5	K-5
K-8	J-8
M-11	K-11
N-9	V-10
G-8	G-8
N-4	N-4
P-7	P-7



REV 21 5/08



REV 21 5/08



$V(A-B)$ = Absolute Temperature, Unheated Junction
 $V(C-B)$ = Absolute Temperature, Heated Junction
 $V(A-C)$ = Differential Temperature

REV 21 5/08